CHARACTERISATION OF THE METAMORPHIC, FLUID AND MINERALISATION HISTORY OF THE ZINKGRUVAN Zn-Pb-Ag DEPOSIT, SWEDEN

VICTORIA KIRSTEN GUNN

SCHOOL OF OCEAN AND EARTH SCIENCE
UNIVERSITY OF SOUTHAMPTON

MAY 2002

UNIVERSITY OF SOUTHAMPTON

ABSTRACT

FACULTY OF SCIENCE
SCHOOL OF OCEAN AND EARTH SCIENCE

Doctor of Philosophy

CHARACTERISATION OF THE METAMORPHIC, FLUID AND MINERALISATION HISTORY OF THE ZINKGRUVAN Zn-Pb-Ag DEPOSIT, SWEDEN

by Victoria Kirsten Gunn

The stratiform Zinkgruvan Zn-Pb(-Ag) deposit of south-central Sweden is hosted in an early Proterozoic (~1.9 – 1.84 Ga) sequence of high temperature quartzofeldspathic gneisses, calc-silicate rocks and migmatites, interpreted as original volcanics, carbonate rocks and pelitic sediments respectively, deposited in a subsiding back-arc basin or an intracontinental incipient rift environment.

Geochemical and petrological investigations show the rhyolitic-dacitic volcanic rocks of the mine area have been intensely enriched in potassium and depleted in sodium as a result of sub-seafloor hydrothermal alteration associated with a mineralising system. Geochemistry, petrology and Sr isotopic analyses demonstrate that the overlying metamorphosed shallow marine carbonates contain admixed volcanic detritus, which was also selectively K-enriched. A regional, but heterogenous dolomitisation event occurred during diagenesis. Dolomitic marbles in the mine area are enriched in Fe and Mn as well as being silicified during hydrothermal activity.

Mineral assemblages (especially the associations Qtz + Kfs + Sil + Bt, and Cal + Dol + Fo) indicate that upper amphibolite facies metamorphism related to the Svecofennian orogeny (2.0 - 1.75 Ga) reached a peak of 750 ±50°C and 5 ±1 kbar in the mine area, decreasing to lower amphibolite facies 10 km further south. Metamorphism was 'open system' and accompanied by an aqueous (low XCO_2) fluid throughout, despite significant decarbonation during calc-silicate mineral formation. Two retrogressive events have been identified at ~550°C and ~250°C, with mineral assemblages indicative of aqueous fluid infiltration.

Mineralisation is Zn-Pb rich and Fe-poor, with pyrrhotite forming the main Fe-bearing phase. The main Zn-Pb ore horizons are underlain by semi-concordant Cu-rich mineralisation in the western part of the deposit, which may represent the feeder zone for mineralising fluids. Ore fluids are interpreted to be hot (~250°C), acidic (pH = ~4), weakly reducing ($aH_2S > aSO_4$) and saline. The precise ore-forming mechanisms remain unclear due to recrystallisation of textures in both the ore and host rocks, but expulsion of metalliferous brines via a structurally-controlled fluid conduit in a submarine setting is recognised.

Zinkgruvan is shown to have much in common with the giant Broken Hill Zn-Pb deposit in Australia. Both areas contain features common to volcanogenic massive sulphide (VMS) and sedimentary-exhalative (SEDEX) base metal deposits. This hybrid type of deposit is assigned to a separate group known as Broken Hill-type (BHT), characterised by their Proterozoic age, high metamorphic grade, distinctive stratigraphic and tectonic setting, and laterally extensive mineralisation. This fits well with local and regional features at Zinkgruvan.

ACKNOWLEDGEMENTS

This project was initiated and funded by North Ltd (now part of Rio Tinto Plc), to whom I am grateful for financial sponsorship and for providing me with the opportunity to undertake such challenging and stimulating geological research.

My supervisors, Andy Barker, Leigh Schmidt and Bob Nesbitt have provided guidance and advice throughout the duration of this project. My thanks in particular to Andy for providing endless enthusiasm, motivation and encouragement, and for his expertise on all things metamorphic and fluid-related. I am grateful to Leigh for guidance during and after fieldwork, critical review (and extensive de-waffling) of chapters, and for adding a wealth of Australian expletives to my vocabulary. Thanks also to Bob for providing advice on geochemical and isotopic matters.

I am indebted to the geologists at North Exploration, Ammeberg (as was) and at Zinkgruvan mine for their assistance during fieldwork – thanks to Lena Albrecht for her help navigating the underground maze at Zinkgruvan, and to Ulrika, Virginia and Roger for making my visits to Sweden entertaining and enjoyable. I am particularly grateful to Stefan Sädbom for his unending enthusiasm, cheerfulness and good humour (not to mention geological expertise and local knowledge), without whom the second field season would have been all work and no play. Thanks also to Dianne Schmidt for numerous hot dinners, BBQ's, paperbacks and entertainment during my visits to Sweden.

At SOC, thanks must go to Bob Jones and John Ford for preparing in excess of 250 thin sections over the three years. Barbara Cressey and Richard Pearce assisted with SEM work, Andy Milton helped with LA-ICPMS, Ian Croudace provided XRF advice and Posy Boella carried out strontium analyses. Hand specimen photography and other photographic support was provided by Barry Marsh. I am also particularly grateful to Challenger Division for allowing me time during work hours to finish writing up.

Thanks to all my friends and colleagues at SOES who have made the past three and a half years entertaining and enjoyable. In particular, Ian Harding and Ross McGowan who have been co-conspirators of mischief and mayhem both at home in Southampton and on several field trips...long may it continue!! Fellow geology postgrads Fran, Evans, Moss, Frank, KT, Reeder, Paul, Thorsten and Kev (and Kim!), who have all already escaped but without whom the School would have been a much duller place. Also the Tea Club to whom I am eternally grateful for providing essential twice-daily distraction, banter, gossip and much needed chocolate biscuits.

Finally, to my long-suffering boyfriend Russell, who has endured a lot of grumpiness and bad temper (particularly in the last few months), thank you for your support and encouragement – I couldn't have done it without your nagging!

CONTENTS

LIST OF FIGURES

LIST OF TABLES

CHAPTER 1

INTRODUCTION

CHAPTER 1: INTRODUCTION

1.1 RATIONALE

This project was initiated to address some fairly basic questions about the geology and mineralisation at the Zinkgruvan Mine, Sweden. Although the mine has been in operation for over 140 years and is one of the largest zinc producers in northern Europe, there has been little laboratory study of the orebody and its enclosing rock package, and no comprehensive recent study. Understanding is hampered by the intense chemical alteration and high grade metamorphic overprint that has destroyed the majority of the primary lithological characteristics of the host sequence. Correlation of rock units, even between closely spaced drill holes, is difficult due to lateral mineralogical/chemical facies variations.

A variety of geological and geochemical data for Zinkgruvan has been amassed over the years as part of numerous exploration programmes, research initiatives and individual studies. This research aims to synthesise, consolidate and, in some cases, reinterpret existing data and combine it with new data in order to present a comprehensive assessment of the geological and chemical evolution of the mine package. The main objective of this research is to establish a more complete picture of the geological history of the mine area. In particular, the research is focused on the metamorphic-fluid-mineralisation history to improve understanding of the mineralisation and its enclosing host package. This knowledge will be used to refine near-mine exploration and to help develop strategies for exploration elsewhere.

1.2 OBJECTIVES

Unravelling the geological history of the Zinkgruvan mine package requires careful analysis of the pattern and consequences of deformation, metamorphic and metasomatic events on the mineralisation and the host rocks.

To achieve this the following objectives must be fulfilled:

1) Detailed definition of the various pre-metamorphic and prograde metamorphic mineral assemblages to determine which features of the mine package are pre-metamorphic in origin, and which features result from metamorphism and alteration. Study is focused on the metacarbonate units, as these present the most sensitive indicators of metamorphic and chemical change.
2) Identification of retrograde and alteration events, and their effect on the pre-existing rocks.
3) Use the prograde and retrograde mineral assemblages together with whole-rock geochemistry to define the various stages in the metamorphic and fluid history of the sequence and to gain an understanding of the timing and composition of fluid infiltration events.

4) Improve understanding of the sulphide ores in relation to the above events, and define the nature of the fluids responsible for mineralisation.

1.3 METHODOLOGY OF RESEARCH

The project entailed fieldwork at Zinkgruvan Mine and laboratory studies carried out at the University of Southampton. During two field seasons the following work was completed:

Field season 1 (July-August 1998): Detailed underground mapping of the mine package to the south of the ore body to clarify stratigraphy and key marker horizons, and to guide sampling for thin section and XRF analysis. Reconnaissance mapping was carried out around Zinkgruvan to gain familiarity with the regional geology.

Field season 2 (April-July 1999): Remapping of key areas covered in the first field season to refine stratigraphy, examination of alteration fronts and small-scale variations in banded skarn units, and mapping of other key areas within the sequence to the south of the orebody. Selected areas were resampled after thin section observations of the first sample set. Approximately 18 km of core from drill holes throughout the mine was logged to clarify understanding of the mine package to the north of the mineralisation. Several holes from subsidiary orebodies were logged for comparison with the main ore body. Sampling for thin section and geochemical analysis focused on marbles and calc-silicate skarns as these are the lithologies most sensitive to physical and chemical changes through time. However, a wide range of lithologies was collected for laboratory study.

A regional carbonate sampling program provided material for comparison with mine package lithologies. These samples represent less altered varieties of lithologies present in the mine package. Regional samples were collected to enable identification of chemical/fluid events specific to the mine environment that may reflect the mineralising process.

Laboratory studies were dominated by petrographic analysis of thin sections in transmitted and reflected light to identify the mineral assemblages and determine the metamorphic evolution of the various lithologies, the effects of fluid events, textural relationships, and the relationship of ore minerals to the silicate host. Compositions of individual mineral phases in prograde and retrograde assemblages were determined using the Scanning Electron Microscope (SEM). Data collected from these methods were used to construct estimates of pressure-temperature conditions prevailing at various stages during the metamorphic evolution of the mine package, and to define the chemistry of fluids present at various stages in the evolution of the rock package. SEM analysis was used to detail the sub-microscopic textural relationships between different mineral phases, to help with reconstructing the relative timing of events.

Whole rock and trace element analyses obtained by X-Ray Fluorescence (XRF) methods were used in conjunction with petrological observations to resolve fluid-related alteration events and

products. Laser Ablation Inductively-Coupled Plasma Mass Spectrometry (LA-ICPMS) and SEM element mapping techniques were applied to garnet crystals to refine the rare earth element (REE) characteristics of fluids present during alteration events.

1.4 INTRODUCTION TO THE STUDY AREA

Zinkgruvan (meaning 'zinc mine') village is located in the southwestern part of the Bergslagen Province of central Sweden, approximately 50 km south east of Örebro (Fig. 1.1). The town has built up around the mine and has a population of approximately 750 people. The topography of the surrounding area is gently undulating, reaching elevations of around 220 m above sea level, with small rocky protrusions concealed by thick undergrowth and moss. The landscape surrounding the mine comprises 80% Scandinavian pine forest, 10% agricultural land and 10% lakes. Summer seasons are mild and fairly wet, while the winters are harsh, with widespread snow and temperatures falling below -10°C.

Bedrock exposure varies from abundant in elevated topographic positions to none in lowland positions where it is obscured by till or lacustrine deposits. For the most part, bedrock is covered by a thick mat of moss which can be peeled back to reveal fresh surfaces polished by glaciation. In other cases, rocks are exposed as small cliffs and protrusions. Lake shores occasionally provide some good exposure, but access can be limited by water levels. Old mine workings and shallow pits also allow limited access to rock exposure.

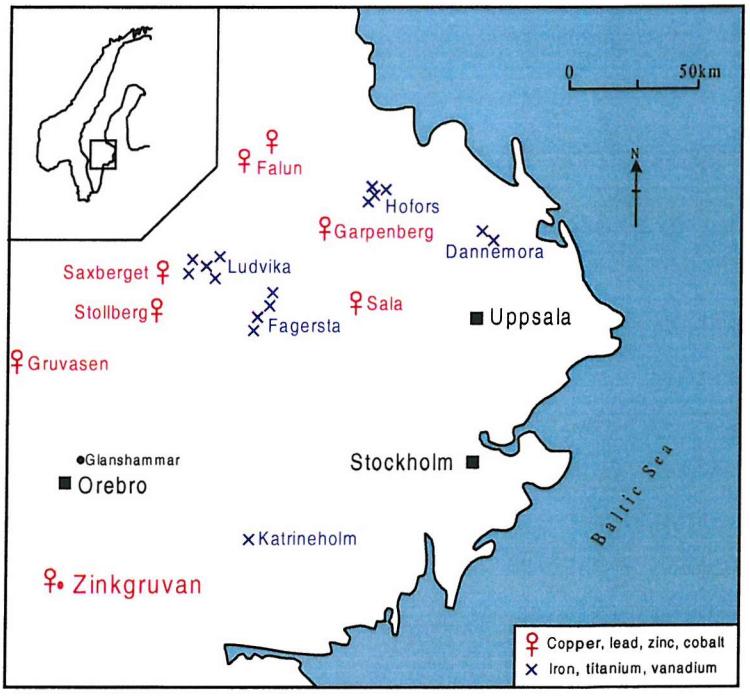

Figure 1.1: Map to show location of Zinkgruvan and other major metal deposits in Bergslagen.

The region surrounding Zinkgruvan is host to a number of small, sub-economic deposits of cobalt, copper, iron and other base metals. Extensive iron mining and smelting took place from at least the early 14th Century until the 19th Century. Local cobalt deposits were important suppliers to the local ceramic industry in the 18th Century, and minor copper deposits have been worked. As a result, small excavations, shafts and pits are common in the countryside around the mine.

Mineralisation has been known at Zinkgruvan since the 16th Century, and mining in the Bergslagen region dates back to Prehistoric times. However, mining on a commercial scale at Zinkgruvan started in 1857, when the Vielle Montagne company took over the working of the lead-zinc orebodies. Since then, production has steadily increased. The current proven plus probable reserve of 11.9 Mt at 10.0% Zn, 4.4% Pb and 90g/t Ag will support the current 800,000 tons per year production for a further 14 years (North Ltd 1999/Rio Tinto Plc 2000 Annual Report).

1.5 PREVIOUS WORK

The first major research on the Zinkgruvan orebodies was published by Johanssen (1910), providing a comprehensive description of the lithologies and mineralisation in the district. Based on the apparent 'close genetic relationship' between the ores and the host rock package, Johanssen concluded a syngenetic origin for the mineralisation, considering there to be no evidence for an epigenetic origin. However, he was unable to decide on either a sedimentary or a magmatic source for the ores and the enclosing rock package: *"....the blende and other sulphide impregnations of this ore field must be regarded as formed at essentially the same time as the other rocks of the gray granulite belt, and they should be regarded as either of magmatic or of sedimentary origin, according to which hypothesis is preferred for the latter rocks".*

Lindroth (1925) inferred a pneumatolytic-metasomatic origin for the mineralisation. He envisaged a supracrustal pile of tuffaceous rocks infiltrated by ore-bearing fluids of magmatic origin, resulting in carbonate-rich layers within the pile being metasomatised and replaced by zinc ore. This study concluded a magmatic origin for the quartzofeldspathic gneisses and migmatites of the host package.

Magnusson (1950) discarded the syngenetic theory in favour of an epigenetic model, whereby the ore formed as part of the migmatisation process during orogenesis and metamorphism. This model involved removal of metals from the migmatite mass and their transport to the present ore position, where zinc and lead ore replaced carbonate horizons.

Henriques (1964) published a detailed description of the ore body and its host rocks. After much discussion and weighing up of the stratigraphic, petrologic and geochemical evidence, he favoured a syngenetic model, suggesting that ore formation was a result of submarine hydrothermal exhalations related to nearby volcanism, a theory which has become popular for

many of the Bergslagen base metal deposits. Hedström *et al.* (1989) described the geology of the Zinkgruvan deposit in detail, and concluded a syngenetic hydrothermal exhalative genesis for the ore, with deposition proximal to a vent located in a distal volcanic setting.

More recent research has focused on specific aspects of the deposit. Billström (1985, 1990) studied lead and sulphur isotopes from galena in Zinkgruvan ore and concluded that the metal was sourced predominantly from the underlying volcanic sequence, having been leached out by ore-forming fluids. However, extensive studies by Sundblad (1994) on sulphide deposits throughout Bergslagen showed that ore lead from southern Bergslagen has a different origin to that from deposits elsewhere in the province, with lead in southern Bergslagen partly sourced from a more primitive reservoir than lead in sulphide deposits further to the north. Sundblad (1994) concluded that the lead isotopic signature at Zinkgruvan resulted from mixing of lead derived from supracrustal metabasalts and metasediments.

Kumpulainen *et al.* (1996) carried out research on the Sm-Nd isotope systematics within the host sequence and attempted a stratigraphic classification for the rocks of the Zinkgruvan deposit and the surrounding district. This paper supports a fluvial origin for some of the metasediments present in the Bergslagen Supracrustal Sequence, based on the observation of cross bedding and other sedimentary structures in psammitic units.

Numerous reports and papers have been compiled on the more regional aspects of Bergslagen geology. Of these, the most useful is Allen *et al.* (1996), who undertook a detailed investigation of the volcanic facies and associated mineralisation found within the province. Several publications on the hydrothermal alteration patterns within the host volcanic sequence are available. The most comprehensive of these are Freitsch (1982a), Lagerblad & Gorbatschev (1985), Hellingwerf (1988) and Rickard (1988). These workers attribute the hydrothermal alteration patterns in the volcanics to warm seawater circulating through the volcanic pile, causing metasomatism and alteration. Rickard (1988) suggested that these hydrothermal fluids were then expelled onto the seafloor and were responsible for mineralisation.

1.6 Introduction to Broken Hill-type deposits

The Zinkgruvan deposit displays several features that are common to a group of orebodies known as Broken Hill-type (BHT) deposits (Beeson, 1990; Parr & Plimer, 1993; Walters, 1996; Large *et al.*, 1996; Cooke *et al.*, 1999). Broken Hill-type deposits share a number of characteristics with volcanogenic-hosted massive sulphide (VMS) deposits and stratiform, sediment-hosted exhalative (SEDEX) deposits. As such, BHT deposits may be considered to be transitional between these two end members.

The majority of BHT deposits are of early to middle Proterozoic age (most can be dated at 1600–1900 Ma), but the common uniting factor between them is the host-rock stratigraphy. The main characteristic features of such a sequence are as follows:

1) Base metal mineralisation occurs in a transition zone between a lower felsic volcanic-dominated sequence and an upper clastic-dominated sequence. This transition zone often contains carbonates and calc-silicate lithologies intercalated with minor volcanics and sedimentary units.
2) Iron formations are common in the sequence below the level of base metal mineralisation.
3) The overall sequence often contains complex chemical sediments, including exhalites, garnetites, iron formations and a variety of skarn lithologies.
4) Lithologies tend to be oxidised rather than reduced and pyrite-bearing.
5) The sequence has been subject to high temperature, low pressure metamorphism of upper amphibolite or granulite facies, and the surrounding terrain has a long and complex history of deformation, metamorphism and metasomatism.
6) Many deposits are interpreted to have formed in an intracontinental rift setting, during a period of waning volcanic activity.

Well-known examples of BHT deposits are the type area Broken Hill deposit, New South Wales, Australia; the Aggeneys/Gamsberg deposits of South Africa; and the Cannington deposit of NW Queensland, Australia. The Bergslagen Province of Sweden has many features in common with Broken Hill-type terrains, and Zinkgruvan could be considered part of the BHT group. However, Zinkgruvan has several characteristics that set it slightly apart from the other BHT deposits, and these are considered in more detail in Chapter 8. Table 1.1 summarises the features of the Bergslagen Province which are considered characteristic of a Broken Hill-type terrain.

Criteria	Present at Zinkgruvan?
Lower to mid-Proterozoic age	Yes: Volcanics dated at 1.9 – 1.85Ga
High grade metamorphism	Yes: Upper amphibolite facies
Rift-related tectonic setting	Yes: Continental rift/back arc setting
Stratigraphy dominated by volcanics in lower part and pelitic sediments in upper part.	Yes
Mineralisation concentrated at transition zone between lower and upper sequences	Yes
Thin exhalites present	Possibly. Metamorphism and alteration obscures original characteristics.
Banded Iron Formations present	No
Skarns common	Yes: Skarns present both above and below the orebody.
Ore mineralogy dominated by Zn + Pb, with subordinate Po + Mgt and low Py.	Yes
No obvious focused footwall feeder zone with intense alteration	Yes
Sillimanite and garnet common in qtz-fsp rocks, forming an alteration halo	Yes

Table 1.1: Summary of some of the main characteristics of Broken Hill-type deposits and their presence/absence at Zinkgruvan.

CHAPTER 2

REGIONAL GEOLOGY

CHAPTER 2: REGIONAL GEOLOGY

2.1 THE BERGSLAGEN PROVINCE WITHIN THE BALTIC SHIELD

Sweden forms part of the Baltic Shield, which formed through progressive accretion in a southwesterly direction around an Archaean nucleus during the period 3.5 - 1.5 Ga. The shield evolved through a series of four orogenic episodes: the Saamian orogeny (>3.1 – 2.9 Ga), the Lopian orogeny (2.9 – 2.6 Ga), the Svecofennian orogeny (2.0 – 1.75 Ga) and the Gothian orogeny (1.75 – 1.50 Ga). The western margin of the shield was subsequently affected by the Grenvillian (1.25 – 0.9 Ga) and Caledonian (0.6 – 0.4 Ga) orogenies.

The Baltic shield can be divided into three distinctly different domains (Fig. 2.1), which become progressively younger from north-east to south-west:

1) Archaean domain (north eastern part of shield)
2) Svecofennian domain (central part of shield)
3) SW Scandinavian domain (south western part of shield)

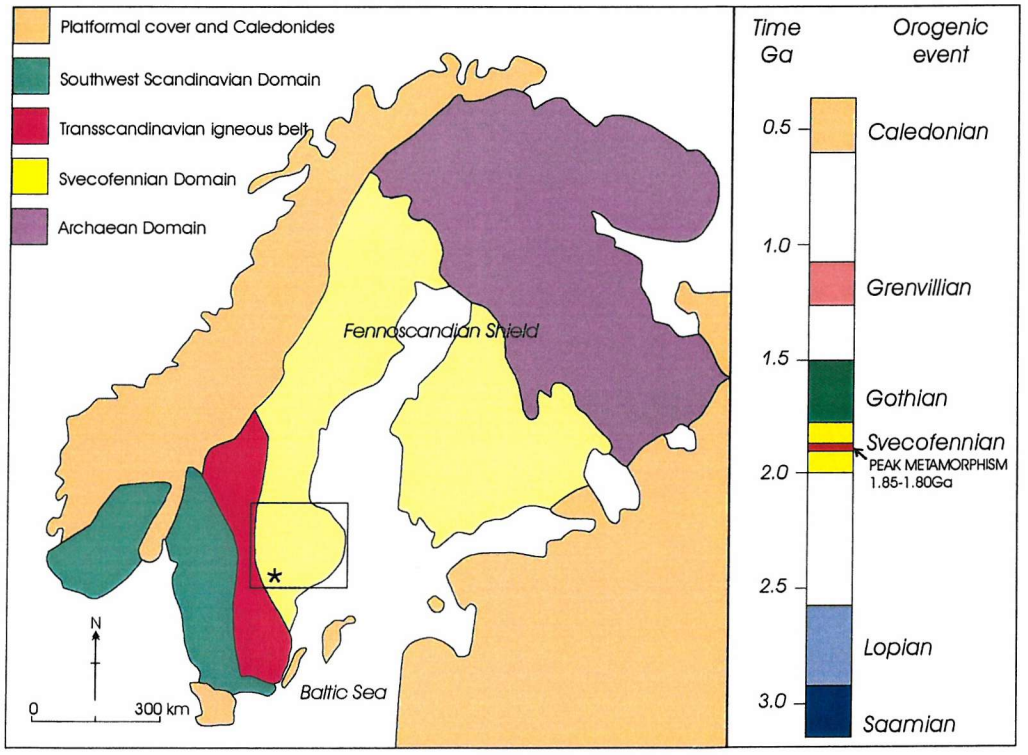

*Figure 2.1: Sketch map showing the different tectonic domains of the Baltic Shield. The box outline shows the location of the Bergslagen Province (detail shown in Fig. 2.3). * marks the approximate location of Zinkgruvan. Adapted from Kumpulainen et al. (1996). Column on right hand side illustrates the time scale for shield evolution.*

2.1.1 The Svecofennian Domain

The Bergslagen Province lies within the Svecofennian domain, which is divided into the Northern, Central and Southern Svecofennian Provinces. The Northern and Southern provinces are characterised by 1.9 – 1.87 Ga calc-alkaline rhyolitic and dacitic volcanic rocks interbedded with thin carbonate horizons and clastic metasediments. The Central Svecofennian Province comprises the Bothnian Basin, containing over 10 km of metagreywackes and metapelites. Geochemical evidence from the volcanic rocks and the presence of greywackes at the base of the volcanic sequences suggest the Svecofennian Province formed part of an active continental margin environment (Gaal & Gorbatschev, 1987).

Granitoid plutonism is widespread throughout the Svecofennian domain, and is divided into three different phases:

1) ***Early orogenic (1.89 – 1.85 Ga) granitoids:*** These are characterised by large calcic and calc-alkaline I-type granitoid plutons ranging widely in composition from gabbro to granite. These magmas are probably genetically related to the volcanic sequences (Vivallo, 1985), and Allen *et al.* (1996) identify some of these bodies as synvolcanic intrusives. Late stage dolerite dyke swarms are associated with this phase of plutonism.
2) ***Late orogenic (1.85 – 1.75 Ga) granitoids:*** This suite of granites differs significantly from the early orogenic rocks, comprising crustal, anatectic S-type granites associated with migmatites and pegmatites. Little granodioritic material is associated with this phase, which mainly forms small massifs and fault-related dyke networks, although larger masses occur in the Bothnian Basin.
3) ***Post-orogenic granitoids:*** These isolated, minor granites occur within NE-SW fault-controlled belts, and include a period of bimodal gabbro and anorthosite-rapakivi granite intrusion between 1.70 – 1.54 Ga.

Metamorphism associated with the Svecofennian orogeny was widespread, reaching the highest grades of 600-800°C and up to 8 kbar in areas of intense deformation and faulting (Gaal & Gorbatschev, 1987). Most areas, however, suffered only lower greenschist or amphibolite facies metamorphism at lower pressures. In some places, two main periods of deformation and metamorphism can be identified which roughly coincide with the early and late orogenic granitoid intrusions. The early granitoid phase was intruded during localised folding, but larger-scale regional compressive stresses caused extensive deformation throughout the area. Late Svecofennian deformation resulted in folding of incompetent supracrustal rocks and resistive granite masses in response to E-W compression. Peak metamorphism and migmatisation is estimated to have occurred between 1.85 – 1.80 Ga (Kumpulainen *et al*, 1996; Welin & Stålhös, 1987).

2.1.2 The Bergslagen Province

The Bergslagen Province is traditionally thought of in geological terms as the mineralised district stretching from Falun in the northern part of the province, to Zinkgruvan in the south (Fig 1.1). To the south and west it is bordered by the younger (1.85 – 1.77 Ga), highly magnetic granitoids of the Transscandinavian Igneous Belt, and to the east by the Baltic Sea (Fig. 2.1). This ore belt can be traced eastwards into SW Finland and NE Estonia, where the mineralisation and host lithologies share similar characteristics with those found in Bergslagen.

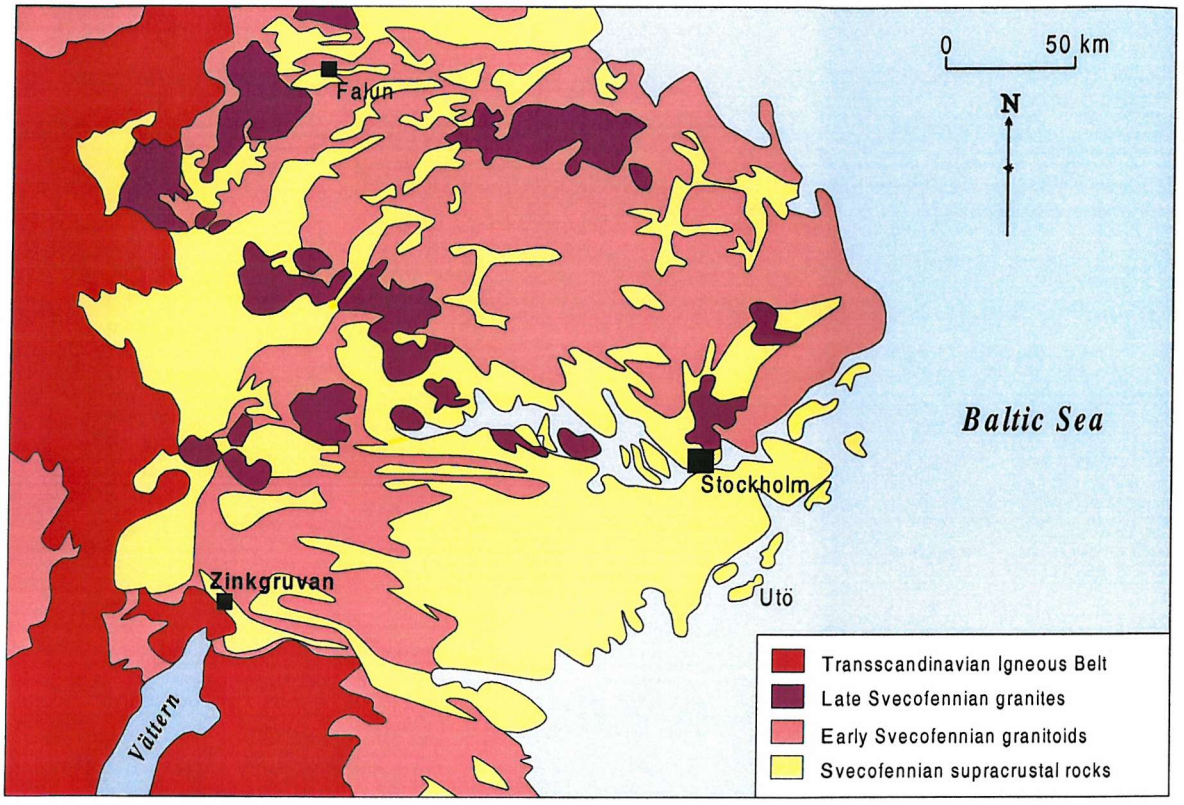

Figure 2.2: Regional geology of the Bergslagen Province. Adapted from Kumpulainen et al. (1996).

2.2 REGIONAL STRATIGRAPHY OF BERGSLAGEN

The regional geology of Bergslagen comprises a 10 km thick sequence of early Proterozoic (*ca.* 1.9 – 1.84 Ga) felsic metavolcanics and epiclastic metasediments, commonly referred to as the 'supracrustal sequence' in the literature, intruded by a series of pre- to post-tectonic granitoids (Fig 2.2). Regional trends show that metavolcanic rocks dominate the lower part of the sequence and metasediments become prevalent towards the top. Minor basic volcanics occur intercalated with the acidic rocks, locally increasing in frequency and volume towards the top of the sequence. Hydrothermal alteration is widespread throughout the province, the most consistent feature being K/Na alkali metasomatism in the volcanic sequence. Mineralisation is abundant and varied; where base metal mineralisation occurs, it is usually situated within the transition zone between the volcanics and the sediments.

The Bergslagen supracrustal sequence has experienced middle to upper amphibolite facies metamorphism, although greenschist facies rocks are found locally. Deformation is variable over the province, with the most intense deformation occurring around and south of Lake Mälaren, NW of Stockholm (Lundström, 1987). E-W trending isoclinal folds dominate the eastern part of the province, whilst more open N-S folds are more common in the west (Lundström, 1988).

2.2.1 Basement

Basement is not exposed in the Bergslagen Province, but detrital zircons dated at >2.20 Ga (Åberg, 1978; Åberg & Persson, 1984) and 2.70 Ga (Kumpulainen *et al.*, 1996) present within supracrustal metaquartzite units suggest the presence of underlying felsic bedrock. Welin (1987) suggested derivation of zircons from 2.90 – 2.50 Ga Archaean orthogneiss, and Johanssen & Rickard (1985) inferred a pre-Svecofennian crust from Pb isotope data. The presence of an underlying continental basement can also be inferred by the volume of felsic volcanics. Due to their bimodal basaltic-rhyolitic nature, it is reasonable to invoke evolution of a basaltic magma by crustal assimilation and contamination by felsic basement material to produce the large volumes of felsic volcanics rather than fractionation and evolution of a rhyolitic lava from an original intermediate melt. Allen *et al.* (1996) provided a discussion of these models. A felsic basement is also supported by the presence of quartz-rich turbidites underlying the oldest known volcanic rocks in the eastern parts of the province. Following a comprehensive study of Sm-Nd isotopic ratios in all components of the Svecofennian terrain in Sweden and Finland, Patchett *et al.* (1987) argued that there is no underlying Archaean basement as such, but that Archaean material was introduced into the Bergslagen area in the form of turbiditic sediments.

2.2.2 Metavolcanic rocks

The metavolcanic rocks comprise a series of felsic lavas, tuffs and pyroclastic rocks and their reworked equivalents. Locally, fine grained quartz-feldspar rocks are traditionally known as 'leptites', a term that describes a range of lithologies but has no strict geological meaning, although in essence can be regarded as metarhyolite or metafelsite (see Chapter 3 for definitions).

In most areas, the base of the main volcanic suite is not exposed. However, at Utö in the eastern part of the province (Fig. 2.2), quartzitic metasediments underlie the metavolcanic rocks. Zircons in the early metavolcanic rocks here have been dated at 1904 ± 4 Ma by U-Pb methods (Lundström *et al.*, 1998). U-Pb dating carried out on zircons from the metavolcanics throughout the region give a range of ages up to 1862 Ma at the top of the volcanic sequence (Lundström, 1987). A comprehensive review of radiometric dates for the Bergslagen metavolcanics is found in Lundström *et al.* (1998).

The volcanic rocks are dominantly rhyolitic, although minor volumes of dacite and andesite appear in eastern areas. Geochemical analyses of least-altered non-reworked volcanic rocks from a number of different facies carried out by Allen *et al.* (1996) revealed a spectrum of sub-alkaline to calc-alkaline compositions (Fig. 2.3).

Basic volcanic rocks occur in small amounts: as sills and dykes at lower stratigraphic levels, and as flows and lavas higher up. These metabasites form part of a bimodal volcanic sequence in western Bergslagen.

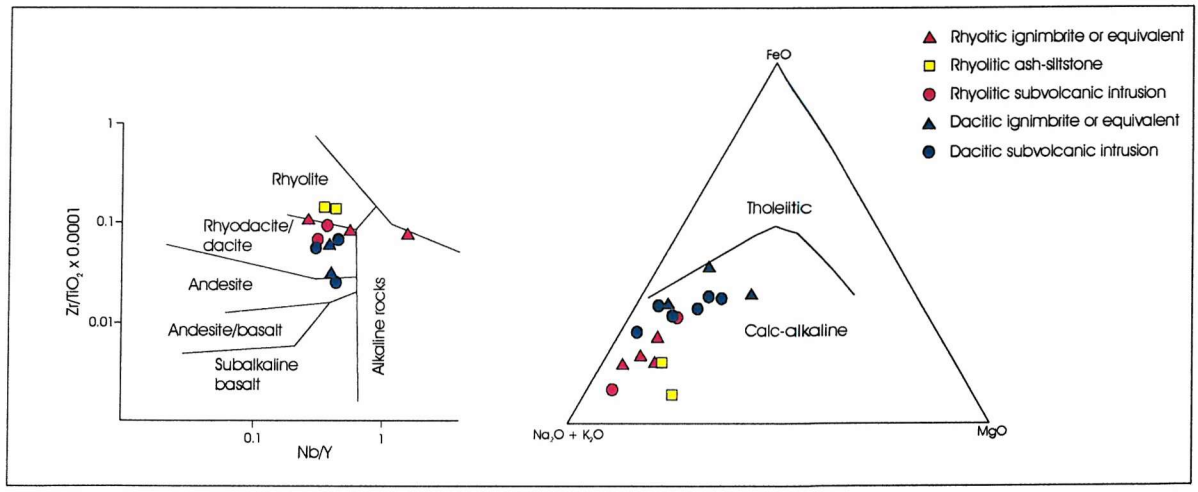

Figure 2.3: a) Immobile element rock classification diagram, and b) Geochemical discrimination diagram for Bergslagen volcanic rocks and subvolcanic intrusions. After Allen et al. (1996).

Regional distribution

There are distinct compositional and stratigraphic variations in the supracrustal sequence across the Bergslagen region. Although the volcanites are dominantly rhyolitic, Allen *et al.* (1996) identified at least three dacitic centres in eastern parts of Bergslagen. In western areas, occurrences of gabbro and basalt sills and lavas suggest that volcanism here may have been bimodal (Van der Velden *et al.*, 1982). In eastern areas, basic igneous bodies are not uncommon but they do not appear to be linked to the felsic volcanism.

Lundström (1987) compared the stratigraphy from the Lindesberg-Filipstad area in the west with that from the Uppsala-Nyköping area in the east to highlight the differences between the two successions (Fig. 2.4). The western sequence comprises an estimated 8 km of rhyolitic metavolcanics resting on an unknown basement. The lowermost volcanics are felsic, subaqueous pyroclastics conformably overlain by rhyolitic tuffites with frequent intercalations of limestone (now marble) and metasediments. Minor basic volcanics increase in frequency towards the top of the volcanic succession, which is capped by a thick unit of epiclastic metasediments.

The eastern sequence (Uppsala-Nyköping) comprises a lowermost unit of cross-bedded, graded greywackes overlain by rhyolitic-dacitic tuffites containing interbedded limestone (marble), calc-silicate rocks and metasediments. This volcanic unit may correlate with the upper part of the metavolcanics in the western succession. The volcanics are capped by epiclastic greywackes and meta-argillites. The lowermost metavolcanics in the east of the region are apparently significantly older than those from the west of the region, dated at 1904 Ma ± 4 Ma, compared to an average of 1891 Ma ± 4 Ma from western volcanics (Lundström *et al.*, 1998).

Freitsch (1982a) suggested that these differences in volcanic composition across the region may be due to silicification during hydrothermal alteration. He suggested that rhyolitic volcanics in the western, ore-rich part of the province were originally also dacitic/andesitic but were silica-enriched during hydrothermal alteration to form felsic rocks of apparently rhyolitic composition. He argued that if the volcanics formed in an island arc setting, the magma would have to pass through a considerable thickness of acidic crust before achieving a rhyolitic composition and this scenario could only be feasible if the magma erupted as intermediate in composition, and was altered to a felsic composition at a later date. However, the trace element data of Allen *et al.* (1996) (Fig. 2.3a), and the interpretation of the region as an active continental margin rather than an oceanic island arc has disproved this theory. The variations in volcanic composition and texture are now considered a primary feature (Allen *et al.*, 1996).

The differences in the supracrustal succession in western and eastern Bergslagen are summarised in Table 2.1 and Fig. 2.4.

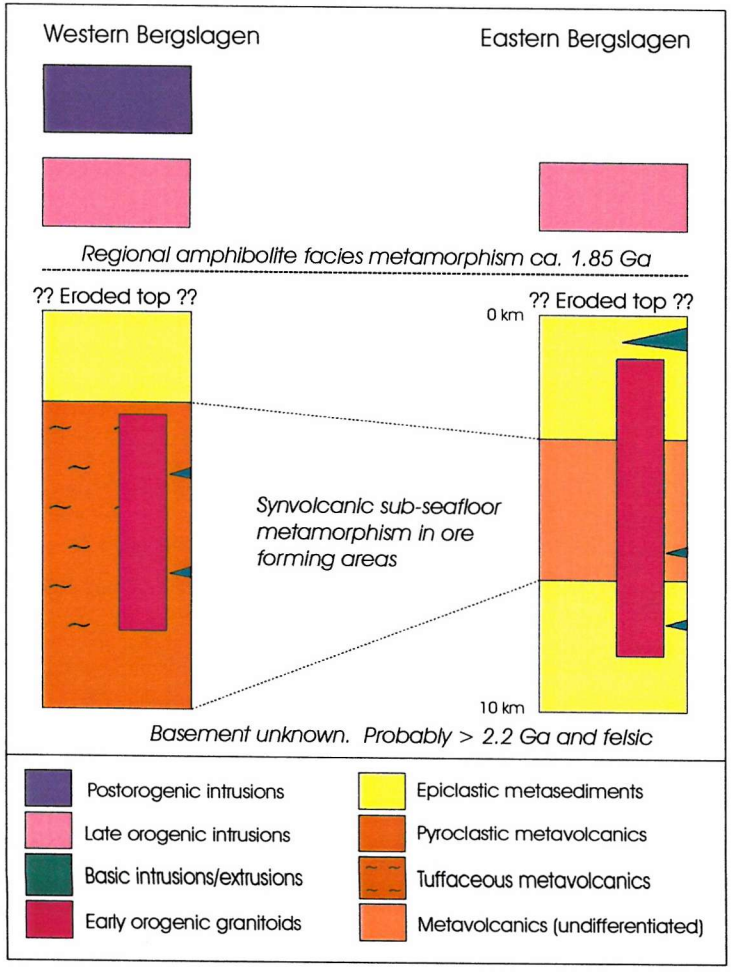

Figure 2.4: Summary diagram to show the main lithostratigraphic differences between sequences in western and eastern Bergslagen. After Lundström (1987).

	Western Bergslagen	*Eastern Bergslagen*
Stratigraphy	Metavolcanics dominate Metavolcanics overlain by metasediments	Metasediments dominate Metavolcanics sandwiched between metasediments
Volcanism	Oldest volcanics dated at ?1891Ma Rhyolite-dominated Bimodal volcanism evident Basic volcanics scarce	Oldest volcanics dated at 1904Ma Rhyolitic-dacitic/calc-alkaline No bimodal distribution Basic volcanics more frequent
Mineralisation	Ore deposits varied and widespread	Ore deposits scarce
Metamorphism	Greenschist to amphibolite facies	Upper amphibolite facies

Table 2.1: Summary of the lithological differences in the supracrustal sequences of western and eastern Bergslagen.

Depositional Environment

Despite strong hydrothermal and metamorphic overprints, Allen *et al.* (1996) identified 21 different volcanic, sedimentary and shallow intrusive facies around the Bergslagen district on the basis of primary textural evidence. The facies vary from primary eruptive and syneruptive facies (ignimbrites, pyroclastics, lavas and shallow intrusions) to reworked, posteruptive facies. Thick bedding, poor stratification and abundant pumice and glass shards in welded tuffs are considered to be indicative of rapid emplacement of the volcanics. The presence of accretionary lapilli in tuffites and other textural evidence points to widespread subaqueous deposition from shallow marine to subaerial volcanic centres. Radiometric dating suggests that the main eruptive phase may have been as short as 15 Ma (Allen *et al.*, 1996).

The lithological characteristics of the Bergslagen volcanic sequence suggest eruption in an extensional continental setting. Oen *et al.* (1982) suggested a continental rift setting, whereas Allen *et al.* (1996) favour a continental margin back-arc environment.

2.2.3 Metasediments

Limestones and their metamorphosed equivalents are commonly interbedded with volcanic units in the transition zone between the volcanic and sedimentary sequences. Stromatolitic structures have been recognised in the limestone units near Grythyttan (Boekschoten *et al.*, 1988), and are reported from Dannemora and Hällefors (Lager, 1986; Lundqvist, 1979). Oen *et al.* (1986) described skarns containing possible microbial fossils from metasediments in the same area, and convincing stromatolitic structures are observed at Glanshammar and Sala (L. Schmidt, pers. comm.). Stable isotope data generated by De Groot & Sheppard (1988) and Fischer (2000) show that $^{13}C/^{12}C$ ratios for stratabound carbonates interbedded with volcanics are consistent with formation in a shallow marine environment.

As shown in Fig. 2.4, metasediments occur in the upper portion of the western Bergslagen supracrustal sequence, whereas they occur both above and below the volcanics in eastern Bergslagen. In western Bergslagen the sediments comprise mainly metamorphosed quartz-feldspar sandstones and greywackes, although pelitic precusors are also identified at the top of the sequence in many places, including Zinkgruvan. Relict cross-stratification, ripple marks and graded bedding have been reported from some localities, as well as localised breccia and conglomerate horizons (Kumpulainen *et al.* 1996). Nd isotope data suggest that much of the sediment was sourced from Archaean (possibly granitic) basement to the north and transported southwards into tectonic basins in the Bergslagen area (Sundblad *et al.*, 1993; Kumpulainen, 1994; Kumpulainen *et al.*, 1996).

Original metasediment characteristics are largely obscured or obliterated in areas of high grade metamorphism. They now occur as quartzofeldspathic gneisses, migmatites and marbles.

Reaction skarns are common in the sequence, particularly along the boundaries between carbonate and quartzofeldspathic units. Some calc-silicate skarns and garnet-bearing quartzites have been interpreted as exhalite lithologies (e.g., Parr & Rickard, 1987; Vivallo & Rickard, 1990), but syn-orogenic fluid events and/or metamorphic reactions are likely to produce similar lithologies.

2.2.4 Stratigraphic classification

Some effort has been made to divide the Bergslagen supracrustal sequence into lithostratigraphic units. Oen *et al.* (1982) interpreted Bergslagen as a continental rift area, subdividing the volcanics and sediments in relation to various stages of rifting. Early volcanism is represented by the Lower Leptite Group, comprising large volumes of predominantly acid pyroclastic volcanics erupted onto subsiding crustal basement in a shallow sea environment. An initial rifting stage produced the acid volcanics, limestones, pelites and iron formations of the Middle Leptite Group, deposited in small N-S basins located between the volcanic centres and the main rift basins. The main rifting phase is characterised by the Upper Leptite-Hälleflinta and Slate Group, composed of siltstones, greywackes and limestones with rhyolitic tuff horizons, ignimbrites and agglomerates. Following rifting, the region was uplifted and conglomerates and other sediments were deposited in localised post-rift basins. This sequence is summarised in Fig. 2.5.

Kumpulainen *et al.* (1996) attempted a more detailed classification of the regional strata, based on the sequence observed in Zinkgruvan area. In this interpretation, the supracrustal sequence belongs to the Emme Group, which is further divided into eight lithostratigraphic units based on the volcanic or sedimentary nature of the rocks. This classification is summarised in Fig. 2.6.

GEOCHRONOLOGY		PHASE	LITHOSTRATIGRAPHY	
	Late uplift			
1650	*Younger granite intrusion*	**Younger Granite Series**	Younger Svecokarelian Granite Suite	
1730	*Subsidence, metamorph-ism and plutonism*	**Middle Granite Series**	Middle Svecokarelian Granite Suite	
1830	*Supracrustal development*	**Post-rift Stage**	Main phase of deformation and regional metamorphism	
			Volcano-sedimentary sequence	Conglomerates
1860		**Rift Stage**	*Upper Leptite-halleflinta and Slate Group*	Grey Slate Formation, Black Slate, tuffites, greywackes,limestones. Basic dykes, sheets & flows
		Initial Rift Stage	*Middle Leptite Group*	Acid volcanics, limestones, banded pelitic,calcareous, and siliceous sediments,iron formations
1900		**Early Volcanic Stage**	*Lower Leptite Group*	Predominantly acid volcanics
Ma				

Figure 2.5: Stratigraphic division of regional stratigraphy related to continental rifting phases. After Oen et al. (1982).

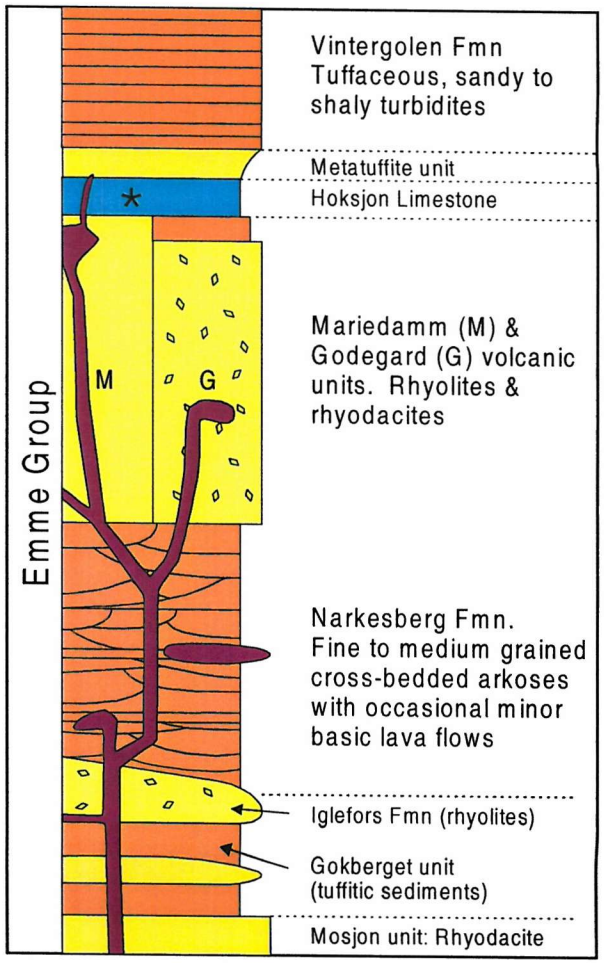

*Figure 2.6: Classification of regional stratigraphy based on the sequence observed in the Zinkgruvan area. * marks the approximate stratigraphic position of the Zinkgruvan base metal mineralisation. After Kumpulainen et al. (1996).*

2.2.5 Hydrothermal alteration patterns

Alkali metasomatism

An elevated geothermal gradient and high heat flow during Proterozoic times produced regional hydrothermal alteration dominated by K-Na alkali metasomatism in the metavolcanic rocks.

On a regional scale, the metavolcanics show a well-defined trend from Na-enriched rocks in the lower part of the stratigraphy, to K-enriched rocks towards the upper part of the sequence (Sundius, 1923; Magnusson, 1925, 1940; Hjelmqvist, 1937). The altered rocks typically contain ~6% Na_2O or K_2O, and on a regional scale, rocks containing intermediate levels of alkali metals are rare (Freitsch, 1982a). Alteration is most intense in rhyolites associated with base metal mineralisation in the western part of the province, although all areas show some evidence of K-Na alteration. On a local scale, the division of the volcanics into a lower Na-rich unit and an upper K-rich unit is less clear, with frequent alternations between K and Na-rich extremes although the general overall trend is still apparent.

Early interpretations of this geochemical pattern ascribed it to a primary variation in magma composition during volcanic activity (Johanssen, 1906, 1907; Sundius, 1923). However, later geochemical investigation revealed minor regular variations in the distribution of immobile elements and major irregular variations in the distribution of mobile elements that could not be ascribed to primary magmatic processes. This, combined with the observation that the alteration is more pronounced in the western, ore-rich part of the province, led to the conclusion that the variations are due to seawater-rock interaction in a sub-seafloor environment (Arvanitidis & Rickard, 1981; Freitsch, 1982a, b; Lagerblad & Gorbatschev, 1985). However, it should be noted that these alterations could also be due to later pre- or synmetamorphic fluid events (Hellingwerf, 1997).

Arvanitidis & Rickard (1981) suggested that this K-Na pattern reflects the different parts of a circulating sub-seafloor hydrothermal system, with Na-rich rocks representing the warmer lower parts of the system, and the K-rich rocks representing the cooler upper parts. This concept was developed further by Lagerblad & Gorbatschev (1985) following an extensive investigation into the geochemistry of the altered volcanics. This detailed work demonstrated that metavolcanics enriched in Na are markedly depleted in Fe, Mn, K, Rb, Ba, Zn and Pb, but commonly have high SiO_2. Rocks enriched in K also have high Rb but are depleted in Na, Ca and Sr.

There is a close spatial relationship between strongly alkali-metasomatised volcanics and the occurrence of base metal mineralisation. Base metal mineralisation and manganiferous Fe skarn ores usually occur in the upper, K-enriched part of the volcanic stratigraphy. With the exception of non-manganiferous Fe skarn ores, the Na-enriched part of the sequence is essentially barren of

mineralisation. This suggestion of a genetic link between hydrothermal alteration and mineralisation is further strengthened by the apparent leaching of ore metals from the lower parts of the system, and their concentration in the upper parts. Lagerblad & Gorbatschev (1985) presented a model where seawater, heated by waning volcanism, circulated through the volcanic pile, causing potassic enrichment in the upper, cooler parts of the system and sodic enrichment in the deeper, warmer parts. During early stages of this hydrothermal circulation, Mg sourced from the seawater is filtered out, creating Mg-metasomatism in the volcanic rocks at various stratigraphic levels. Na is retained in the fluid which becomes progressively hotter and acidic as it descends through the volcanic pile. The acidic fluid causes leaching of K, Rb, Fe, Mn, Ba, Pb and Zn from the lower parts of the volcanic sequence and simultaneous enrichment of Na. At this stage, the hydrothermal fluids may have reacted with carbonate layers in the sequence to form non-manganiferous Fe skarn ores. As the hot fluids rise towards the surface and start to cool, K, Rb, Ba and Sr are enriched in the surrounding volcanic rocks. Eventually, as the hydrothermal solutions reach the seafloor and are expelled, interaction with the cold seawater causes precipitation of base metal sulphides. The environment around the venting site becomes heated, causing Mg to precipitate directly from seawater to form a Mg-enriched alteration halo around the base metal mineralisation. This model is summarised in Table 2.2 and Fig. 2.7.

Hellingwerf (1988) suggested that the relative stabilities of K-feldspar and albite in seawater may accommodate the K-Na enrichment: at temperatures below 140°C K-feldspar is stable, whereas albite is unstable. At temperatures above 140°, albite takes the place of K-feldspar as the dominant stable feldspar.

Freitsch (1982a), Vivallo & Rickard (1984) and Rickard (1988) also supported a sub-seafloor hydrothermal origin for the regional K-Na metasomatism.

	Na-enriched volcanics	***K-enriched volcanics***
Stratigraphic position	Lower level	Upper level
Enriched	Na, Mg, SiO_2	K, Rb, Cs, Ba, ore metals
Depleted	Fe, Mn, K, Rb, Ba, Zn, Pb	Ca, Na, Sr
Associated mineralisation	Non-Mn Fe skarn ores	Base metal sulphides Manganiferous Fe skarns
Common textures	Massive (primary textures destroyed)	Flow banded Ignimbritic textures

Table 2.2: Summary of the differences in the K- and Na-enriched volcanics.

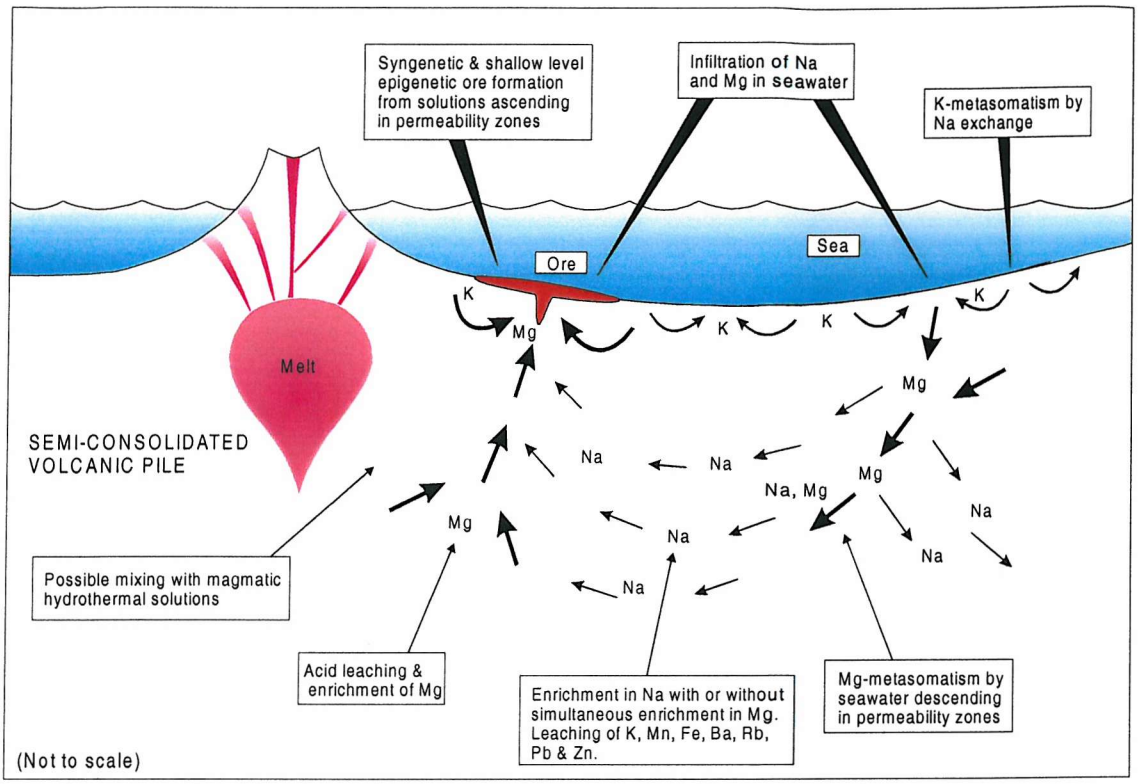

Figure 2.7: Model for hydrothermal alteration and related mineralisation according to Lagerblad & Gorbatschev (1985). The symbols Na, Mg and K indicate sites of enrichment of these elements in the volcanic rocks. Large arrows indicate rapid transport of downgoing alkaline infiltrating solutions and upgoing acidic ore-forming solutions in permeability zones. Smaller arrows indicate slow hydrothermal percolation in the rest of the volcanic pile. After Lagerblad & Gorbatschev (1985).

Potassic enrichment

Detailed work on potassic alteration in Bergslagen by Hellingwerf (1988) identified two separate styles of potassic alteration, first documented by Baker (1985):

1. Regional, low-temperature hydrothermal potassium enrichment dominates; here much of the original rock texture is preserved with little modification apart from what is interpreted to be replacement of plagioclase phenocrysts by K-feldspar.
2. Local high-temperature hydrothermal alteration commonly associated with mineralisation is dominated by sericitisation, biotitisation and microclinisation.

The two styles cannot normally be distinguished in the field. However, trace element analysis shows that regionally-altered rocks show little variation in their Ti/Zr ratio due to the restricted mobility of these elements at low temperatures. Hellingwerf (1988) considered that localised intensely K-altered rocks show enrichment in TiO_2 as a result of the higher mobility of Ti during high temperature alteration (Fig. 2.8).

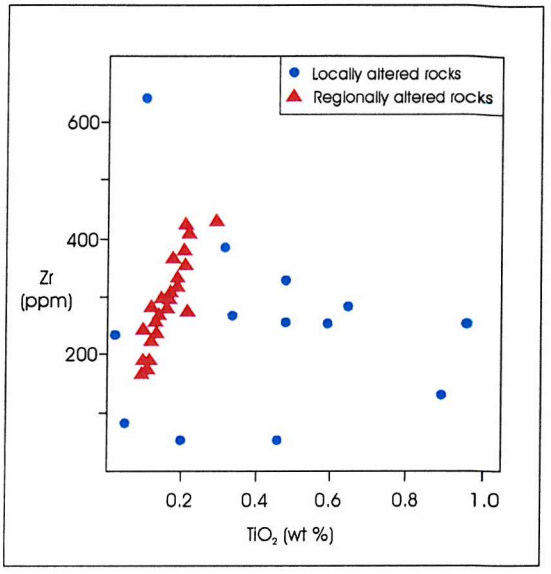

Figure 2.8: TiO_2 -Zr diagram showing the distinction between regionally altered rocks (which show the original magmatic Ti/Zr ratio) and locally-altered rocks. After Hellingwerf (1998).

Boron metasomatism

Research conducted by Hellingwerf *et al.* (1994) suggested that boron metasomatism may have played a role in the hydrothermal evolution of the district. The distribution of tourmaline in Bergslagen shows no particular spatial relationship with granite masses but instead appears to be associated with some ore horizons, zones of leaching and areas of hydrothermal alteration. Tourmaline occurs in a variety of forms, ranging from primary tourmalinites (rocks containing > 20% tourmaline, (Fig. 2.9A) and chemical sediment-hosted tourmaline, through to tourmaline-quartz veins (Fig. 2.9B), metasomatic tourmaline-bearing schists and late-stage tourmaline pegmatites and remobilised fracture infills. Field relationships indicate that the tourmaline may have formed by recrystallisation of clay minerals and micas with an original high boron content (Hellingwerf *et al.*, 1994). The source of the boron is enigmatic, but it is most likely to have originated from hydrothermal fluids fed by Proterozoic seawater, or possibly from evaporite horizons. The spatial association of tourmaline and mineralisation suggests a common source for metals and boron, and this is strengthened by enrichment of tourmalines in metals found in nearby orebodies (Hellingwerf *et al.*, 1994).

A

B

Figure 2.9: A) Photograph of tourmalinite layer (dark grey) in fine grained quartzofeldspathic gneiss, Blackfärdsmossen. B) Tourmaline vein in metasediments near Höksjön (Photograph B courtesy of A. Barker). See Appendix B for locations.

2.3 MINERALISATION WITHIN THE BERGSLAGEN PROVINCE

2.3.1 Introduction

A wide variety of mineral deposit types, styles and size are present in Bergslagen, ranging from small, subeconomic Fe-(Mn) deposits to large stratiform base metal deposits and skarn ores. Localised occurrences of tungsten and molybdenum are related to granitic intrusions. Of these deposit types, Fe-(Mn) mineralisation is by far the most common. Base metal sulphide mineralisation generally occurs at the top of the metavolcanic part of the supracrustal sequence, in a transitional zone containing mixed metavolcanics, metasediments and calc-silicate rocks.

Mineralisation is commonly divided into seven types, detailed in Table 2.3 (Parr & Rickard, 1987; Allen *et al.*, 1996):

Mineralisation type	*Deposit style*	*Description*	*Origin*
Fe-Mn ores	Quartz-banded iron ores	Metamorphosed banded iron formations.	Sedimentary-exhalative
	Skarn iron ores	Irregular to tabular bodies of Fe and magnetite within Px-Am-And-Ep skarn.	Synvolcanic
	Apatite iron ores	Localised occurrence in high grade terranes. Mgt-Ap-Act assemblage.	Magmatic or hydrothermal.
	Mn oxide-silicates		
Base metal sulphides	Falun-type Cu-Zn-Pb ores	Stratiform/stratabound tabular orebodies often hosted in metavolcanic/metasediment transition zone. See below for explanation.	Sedimentary exhalative??
	Ämmeberg-type Pb-Zn ores (Zinkgruvan)		
Tungsten/ molybdenum	Skarn/vein ores	Scheelite skarns and veins associated with granitoids and pegmatites.	Magmatic/ hydrothermal

Table 2.3: Summary of the main mineralisation styles in Bergslagen.

The 'Falun-type' and 'Åmmeberg-type' subdivisions of base metal sulphide deposits were originally based on perceived genetic differences. Falun-type deposits were genetically linked with the early Svecofennian granitoids, comprising Zn-Pb-Cu deposits with abundant Fe sulphides. In contrast, the Fe sulphide-poor Åmmeberg-type Zn-Pb-Ag deposits were believed to be related

to the intrusion of late Svecofennian granitoids. However, it is now generally accepted that all the sulphide ores in the Bergslagen region formed through volcanogenic processes as proposed by Henriques (1964), Vivallo (1985), and Hedström *et al.* (1989) amongst others, so a distinction based on a perceived granite association is no longer valid.

2.3.2 Ore "stratigraphy"

Allen *et al.* (1996) described a regional ore 'stratigraphy' for Bergslagen, whereby skarn ores and marble-hosted mineralisation occur at the base of the sequence, passing upwards into BIF's and associated deposits, and finally into base metal sulphide deposits at the top of the sequence. In subdividing the base metal sulphide deposits at the top of the 'ore stratigraphy', these authors used a classification very similar to the Åmmeberg-type/Falun-type system used by previous workers. However, instead of attributing the two different groups of mineralisation to separate genetic events, classification is based on physical lithological and mineralogical characteristics and it is suggested that the two deposit types form end members of a common volcanogenic process. 'Stratiform Ash-Siltstone' (SAS) mineralisation corresponds roughly to the Åmmeberg-type classification, comprising sheetlike Zn-Pb-Ag-rich ores poor in Cu and Fe, as at the Zinkgruvan deposit. Mineralisation is hosted within rhyolitic ash-siltstone with a variety of associated skarn rocks and what are interpreted to be chemical sediments. Footwall alteration is dominantly potassic, although some Mg enrichment and siliceous alteration may also be present. The host ash-siltstone is interpreted by Allen *et al.* (1996) to have originated from phreomagmatic eruptions at shallow water vents. Associated clastic sediments and limestones indicate deposition in shallow water (~5-20m depth) in nearby basins after sediment was stripped from land and shallow subaqueous slopes.

'Stratabound, Volcanic-Associated Limestone-Skarn' (SVALS) deposits comprise the former Falun-type ores, with irregular lenses and pods of massive and disseminated stratabound Zn-Pb-Ag-Cu-Au replacement mineralisation hosted in metamorphosed limestones and skarns. Footwall alteration is characterised by Mg enrichment.

2.3.3 Mineralisation styles

Fe-Mn mineralisation

A variety of Fe-Mn mineralisation styles are found throughout Bergslagen. Apatite-bearing iron ores, accounting for approximately one third of the iron ores found in the province, are found in a NNE-trending belt running across the NW corner of the region. A further 30% of the ores occur in a parallel band to the SE of the apatite-bearing ores (Grip, 1978). The remainder are scattered throughout the province, occurring as either individual deposits or associated with base metal sulphides as discussed below. Fe-Mn ore types include stratabound Fe oxides hosted in

metavolcanics, Fe skarn deposits, banded iron formations (BIF's) which are often referred to as quartz-banded ores, carbonate-hosted Mn-Fe ores and banded Mn ores.

Genesis

Sundius (1923) suggested synvolcanic metasomatic replacement of limestone beds as the origin for the iron skarn deposits, whilst Magnusson (1970) concluded that Fe ores were deposited coevally with limestone precipitation, with the skarn forming through reactions between the two components. Freitsch (1982b) considered the BIF ores, Fe skarns, and Fe-Mn silicate rocks to be exhalative-sedimentary in origin, enclosed within the host metavolcanics and carbonates, with the skarns forming through reactions during regional metamorphism. A volcanogenic sedimentary-exhalative origin for the iron ores is now widely accepted.

Freitsch (1982b) and Zakrzewski (1982) attribute the distribution of the various Fe-Mn ores to a facies change controlled by water depth, hence redox potential and pH in a marine basin. The physiochemical change from shallow, oxygenated water at the basin margin to successively more reducing and alkaline facies towards the basin centre are responsible for controlling the precipitation of metals to form ore bodies.

O_2 rich areas $\rightarrow$ Banded iron formation deposition

CO_2 rich areas $\rightarrow$ Mn/Fe and Fe skarn ores

H_2S rich areas $\rightarrow$ Graphitic slates and FeS deposition

This concept is illustrated in 2.10.

Zakrzewski (1982) identified four main geomorphological facies in the Grythyttan-Hällefors area ranging from marginal facies through to carbonate and sulphide facies based on similar principles. Both Freitsch (1982b) and Zakrzewski (1982) infer a common volcanogenic source for the metals, with the different deposit types forming as a result of precipitation controlled by varying physiochemical conditions in the basin, giving a spatial distribution of ore minerals according to redox potential and pH.

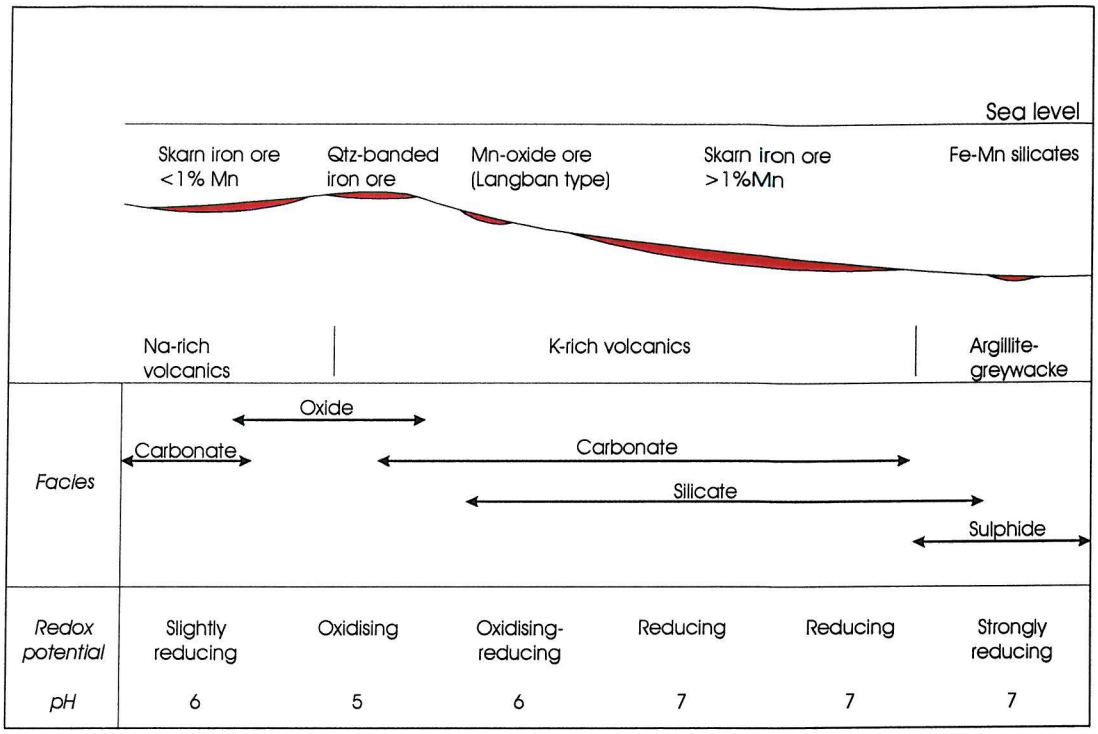

Figure 2.10: Schematic diagram showing possible relationships between the environment of deposition and style of Fe-Mn mineralisation in the Bergslagen region. After Freitsch (1982b).

Base metal sulphide deposits

Sulphide ores are concentrated within a belt approximately 30km wide, stretching from Falun in the NW of the province southeastwards through Garpenberg to Sala and on to the coast in the east (Grip, 1978). NE of this sulphide belt, base metal sulphide deposits are found associated with iron ores; in the main sulphide belt these stratabound Fe (-Mn) ores are subordinate to the main sulphide ores. In the SW of the province is the economically-important sulphide deposit at Zinkgruvan, which is still under active exploitation today.

Most base metal sulphides occur near the top of the metavolcanics and can be considered stratabound. The ore bodies are typically surrounded by alteration zones containing disseminated sulphides, and are commonly hosted within banded or layered strata that contain unusual calc-silicate and skarn mineralogies. These deposits are generally accepted to be volcanogenic sedimentary-exhalative in origin, with ore deposition taking place coeval with sedimentation. Deposits are commonly underlain by a pipe-like Cu-rich stockwork or alteration zone, interpreted as ancient feeder conduits for mineralising fluids.

Each sulphide deposit, although sharing many characteristics with other base metal deposits in the region, varies in mineralogy, chemistry, host lithologies and other associated mineralisation. Individual description of deposits is beyond the scope of this study, but the principal features of the major base metal deposits are presented in Table 2.4.

Deposit	*Mineralisation*	*Host rocks*	*Tonnage*	*Grades*
Falun	Zn Pb Ag Cu Au + Py/Po	Felsic volcanics Lst-dol skarn	28.1 Mt	2-4% Cu, 4% Zn, 1.5% Pb, 13-24g/t Ag, 2-4g/t Au
Garpenberg	Zn Pb Ag Cu Au + Py	Lst-dol skarn Felsic volcanics	21.5 Mt	5.3% Zn, 3.3% Pb, 0.3%Cu, 98g/t Ag, 0.65g/t Au
Sala	Zn Pb Ag Cu Au	Lst-dol skarn	5.0 Mt	150->1000g/t Ag, 12%Zn, 1-2%Pb
Saxberget	Zn Pb Ag Cu Au	Lst-dol skarn	6.8 Mt	7.1% Zn, 2.2%Pb, 0.9% Cu, 0.4g/t Au, 42g/t Ag
Zinkgruvan	Zn Pb Ag	Felsic volcanics	> 43.0	10% Zn, 1.5% Pb, 45g/t Ag

Table 2.4: Main features of some of the major base metal deposits in Bergslagen. Modified after Allen et al. (1996). Locations of the deposits are shown in Fig 1.1.

Tungsten and molybdenum deposits

The most important tungsten resources in Scandinavia occur in the Ludvika area in NW Bergslagen. Most deposits occur in clusters, although some isolated deposits related to late Svecokarelian granitoid emplacement are known.

Ohlsson (1979) identified four main styles of tungsten deposit:

1) Skarn deposits adjacent to late Svecofennian granites
2) Skarn deposits adjacent to pegmatites
3) Skarn deposits formed at a distance to Svecofennian granites
4) Vein deposits.

The skarn deposits reach in excess of 20m thick and several hundred metres long. Scheelite is the most economically important mineral. Ohlsson (1979) concluded that the majority of tungsten deposits formed from H_2O-rich residual fluids generated by late Svecofennian granites, with the tungsten possibly sourced from the incorporation of W-rich sediments into the melt. However, Oen *et al.* (1982), Baker & Hellingwerf (1988) and Oen (1987) reinterpreted some of the late Svecofennian W-Mo-mineralised granites as early Svecofennian high level intrusives. Sundblad *et al.* (1993) proposed a model whereby two generations of rock and ore-forming processes are responsible for the occurrence of different ore types:

1) Phase 1 (1890-1850 Ma): Coeval with felsic volcanism and originating from volcanogenic exhalations on the sea floor. This phase produced stratiform base metal sulphide deposits and Fe-Mn ores.
2) Phase 2 (late to post-Svecofennian): W and Mo-mineralisation and greisen vein deposits.

2.3.4 Metal sources

Several studies have been carried out on the lead isotopic compositions of the various base metal deposits around Bergslagen to determine the origin of the metals. Rickard (1978) and Johansson & Rickard (1985) showed that the lead isotopic composition of galena is remarkably similar across the province, suggesting that the vast majority of these ores formed through similar large-scale processes with lead derived from a large, well-mixed metal source. The authors believe the data are consistent with an active continental margin tectonic setting and an exhalative-sedimentary origin for the mineralisation. Hallberg (1989) suggested that Pb was sourced from supracrustal rocks, with homogenisation of Pb isotopes during deposition, thus creating large areas of uniform Pb chemistry. Billström (1990) examined galena from two deposits in the Bergslagen district, and found that the data fit with that of Johansson & Rickard (1985), as well as with data from deposits at Långban, Sala and Utö. Billström (1990) also suggested that the supracrustal metavolcanics may have provided the lead for the ore fluids, based on their distribution and homogeneous nature.

Most recently, Sundblad (1994) used more accurate mass spectrometry techniques to highlight subtle isotopic differences, concluding that Bergslagen Pb is sourced from several different reservoirs. Sampling around the province showed that most of the base metal deposits in interior Bergslagen are sourced from a major, well-mixed, homogenous reservoir. In contrast, ore deposits from the Stockholm archipelago in eastern Bergslagen and those from the southern margin of the province show significantly different isotopic signatures.

Galena in sulphide ores from interior Bergslagen give average Pb isotope ratios of: $^{206}Pb/^{204}Pb$ = 15.715; $^{207}Pb/^{204}Pb$ = 15.342 and $^{208}Pb/^{204}Pb$ = 35.234, consistent with the bulk Pb isotope signature of the felsic metavolcanics at the time of their deposition (Sundblad, 1994). In contrast, Pb isotopes of galena in sulphide ores from the sediment-dominated Stockholm archipelago display a significantly more radiogenic or evolved character due to input from Svecofennian epiclastic sediments (Fig. 2.11).

Sulphide deposits from the southern margin of the province, including Zinkgruvan, show a spread of Pb isotopic ratios that defines a linear mixing trend between highly primitive Pb and evolved, radiogenic Pb. Sundblad (1994) believed the primitive Pb to be sourced from tholeiitic basalts that are more abundant in southern Bergslagen than elsewhere in the province, while the more radiogenic Pb originated from epiclastic metasediments.

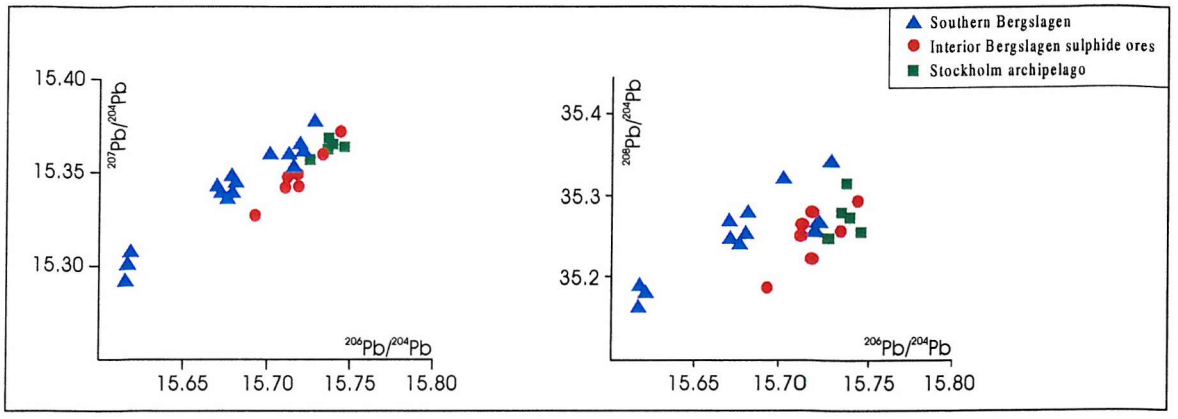

Figure 2.11: Pb isotope plots from galena in various ores from interior Bergslagen, southern Bergslagen and the Stockholm archipelago. Modified after Sundblad (1994).

2.4 METAMORPHISM AND DEFORMATION

2.4.1 Deformation

Rocks were deformed and regionally metamorphosed during the Svecofennian Orogeny from 2.0 – 1.75 Ga, peaking at 1.85 - 1.80 Ga. Metamorphic facies and deformation intensity is somewhat variable over the province, with highest grade areas occurring in the east where isoclinal folding is strongly developed (Lundström, 1988). The intensity of deformation and metamorphic grade decreases westwards. Parr & Rickard (1987) suggested that metamorphic grade is dependent on the relative positions of late orogenic granitoids.

Initial east-west compression in the eastern high-grade area produced N-S trending, west-verging F_1 isoclinal folds (Lundström, 1988). A major change in stress regime to regional N-S compression resulted in E-W trending F_2 structures that can be observed over most of Bergslagen.

2.4.2. Metamorphism

The detailed metamorphic history of the province remains unresolved. Magnusson (1936) suggested two metamorphic events: an initial episode associated with intrusion of synorogenic granitoids, and a second, more intense event which resulted in localised incipient melting. Stålhös (1969) preferred a single metamorphic event that increased in intensity over time, whereas Lundström (1983) and Vivallo (1984) identified multi-stage metamorphic histories for the Lindesberg and Garpenberg areas. Both authors identified a low-pressure/high-temperature (amphibolite facies) event preceded by early hydrothermal metasomatism, and followed by a later pervasive retrograde (greenschist facies) phase. Rickard (1988) related metamorphism to the infilling and subsequent burial of a subsiding basin, with variations in metamorphic grade as a direct consequence of sedimentation rate and burial depth. This is illustrated in Fig. 2.12.

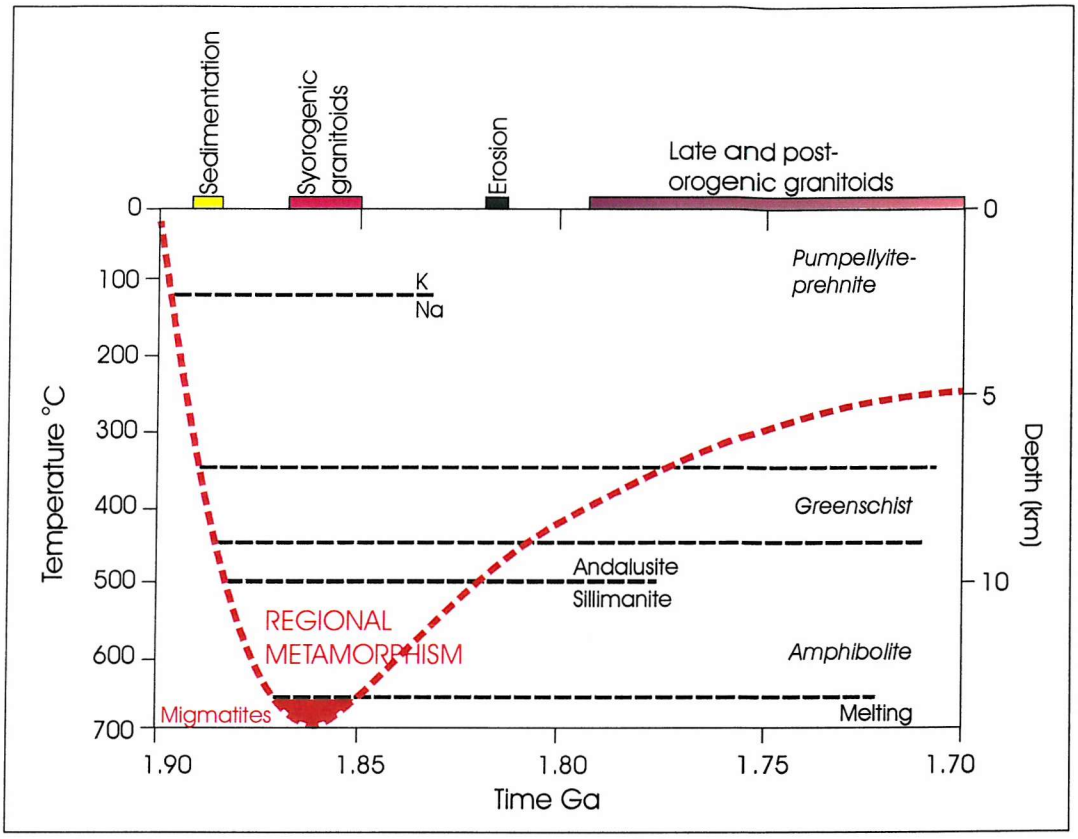

Figure 2.12: Estimated average P-T-t path for Bergslagen rocks in the early Proterozoic. Peak amphibolite facies metamorphism preceded an extended period of greenschist facies retrogression followed by pumpellyite-prehnite facies alteration caused by long, shallow burial. After Rickard (1988).

Elevated temperatures continued beyond peak deformation to produce a strong granoblastic recrystallisation texture that overprints much of the tectonic fabric in areas of amphibolite facies metamorphism. Metamorphic isograds frequently crosscut fold structures (Rickard, 1988; Lundström, 1988). Allen *et al.* (1996) observed faint relict primary textures in rocks of lower amphibolite facies metamorphism, but noted that in areas of higher grade, strong granoblastic recrystallisation has coarsened grain size and obliterated phenocrysts, leaving little evidence of primary structures. There is no evidence to suggest that regional metamorphism continued beyond 1840 Ma (Rickard, 1988).

Metamorphic grade across the region is variable. Some areas in the west experienced only greenschist facies metamorphism, whilst rocks at the same stratigraphic level in other areas have undergone amphibolite facies metamorphism (Rickard, 1988; Lundström, 1987). As there is apparently no evidence of major structural discontinuity between the areas of different facies, it is assumed that the changes in alteration are due to variation in pressure-temperature conditions due to differing levels of burial or heat flow.

Mineral assemblages in the supracrustal sequence are dominated by quartz, mica, feldspar and Al_2SiO_5 polymorphs. Andalusite and sillimanite are common in the province, with sillimanite

dominant in areas of upper amphibolite facies metamorphism and zones of migmatisation. Kyanite is generally absent in Bergslagen, and staurolite is rare (Rickard, 1988). Localised migmatisation is common in the metasedimentary part of the sequence, characterised by the disappearance of muscovite, which breaks down in the presence of quartz by the reaction:

$$\mathbf{Ms + Qtz \rightarrow Al_2SiO_5 + Kfs + H_2O}$$

The water liberated by this reaction plays an important role in the migmatisation process by increasing XH_2O and lowering the melting point of the rock (Chapter 5). The importance of the muscovite reaction in Bergslagen was first recognised by Stålhös (1969). Hellingwerf (1995) suggests that boron present in tourmaline may also have acted as a flux in the melting of the metasediments during peak metamorphism.

Melting is also dependent on heat flow and geothermal gradient. Several estimates of the geothermal gradient for Bergslagen have been made, most recently by Rickard (1988) who calculated a minimum gradient of 50°C km^{-1} based on metamorphic mineral assemblages, particularly the Al_2SiO_5 polymorphs. This figure is in agreement with previous estimates made by Karlsson (1980) and Stålhös (1972).

CHAPTER 3

LOCAL GEOLOGY AND STRATIGRAPHY

CHAPTER 3: LOCAL GEOLOGY

3.1 THE ZINKGRUVAN BASIN

The stratigraphy at Zinkgruvan is consistent with the regional pattern of early Proterozoic felsic metavolcanic rocks grading upwards into metasediments (Allen *et al.*, 1996; see Chapter 2). Base metal mineralisation at Zinkgruvan lies in the transition zone between the metavolcanic and the metasedimentary rocks.

An area informally known as the Zinkgruvan Basin encompasses the sequence of metavolcanic and metasedimentary rocks from north of the mine through to south of Lake Höksjön (Fig. 3.1). Within this 'basin', the metavolcanics underlie and pass into metasediments through a transitional sequence containing metacarbonate rocks and calc-silicate skarns.

The simplest interpretation of the stratigraphic repetition is a synform with an E-W trending axis through the metasediments (Fig. 3.2). Unpublished mapping by mine personnel shows this picture is simplistic, but the structure remains unresolved. The axial trace is slightly off-centre, and an overturned northern limb means that the stratigraphy in the mine area is inverted. However, as there are no way-up indicators, this model is still debatable. Note that major base metal mineralisation is not known in the southern part of the basin.

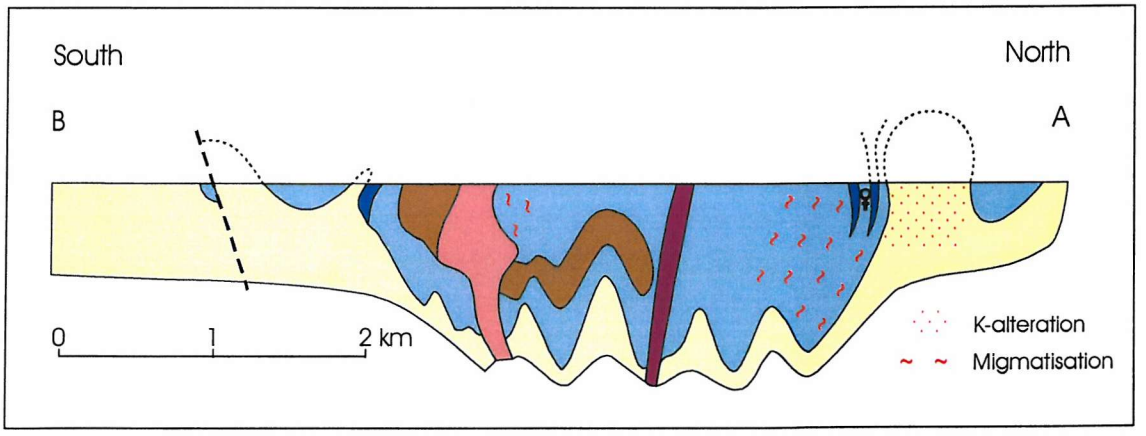

Figure 3.2: N-S schematic cross section through the geology of the Zinkgruvan Basin. Key and line of section as shown in Figure 3.1. Modified from the SGU Series Af No. 165, 9F Finspång SV 1:50 000 map.

Metamorphic grade in the south of the district is lower temperature and pressure (andalusite grade) than that of the mine area (sillimanite grade). Lower metamorphic grade in the south means that some remnant sedimentary and volcanic textures are preserved, and these rocks provide useful mineralogical and chemical comparisons to the higher grade and altered lithologies found at the mine. The sequence that hosts the mineralisation at Zinkgruvan shows distinct geochemical and mineralogical characteristics linked to the mineralisation process. These include intense K-enrichment, Fe-Mn enrichment and silicification.

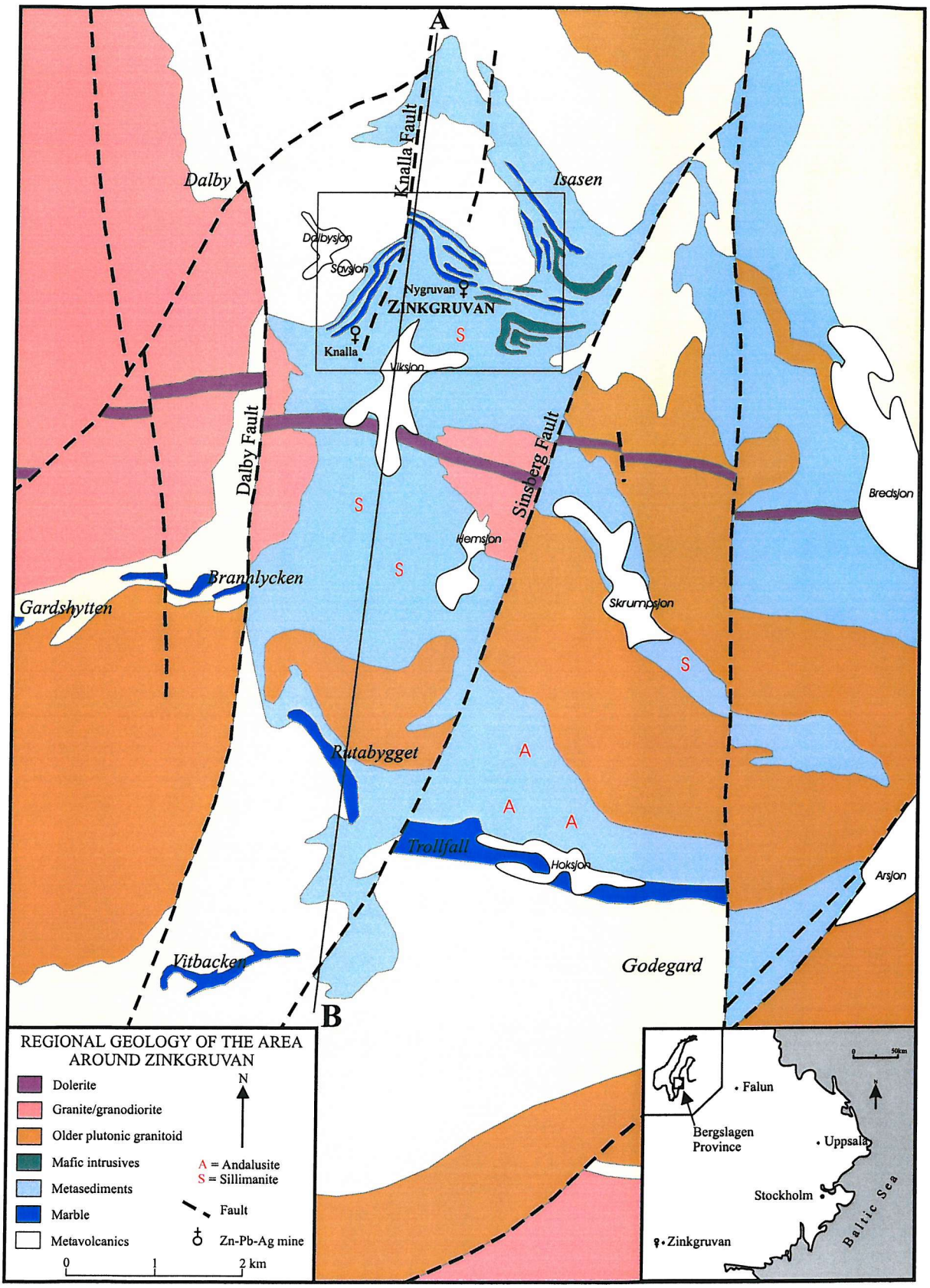

Figure 3.2: Simplified geological map of the Zinkgruvan Basin area.
Adapted from the SGU Series Af Number 165, 9F Finspang SV 1:50 000 geological map. The line A-B shows the position of the cross- section given in Figure 3.2
Box shows the location of the map given in Figure 3.4.

3.2 LOCAL GEOLOGY AND STRATIGRAPHY

Zn-Pb(-Ag) mineralisation at Zinkgruvan is hosted within a sequence of metavolcanics and metasediments comprising quartzofeldspathic gneisses, carbonates, calc-silicate skarns and minor basic igneous rocks (figs 3.3 & 3.4). Mineralisation consists of laterally extensive sphalerite-galena-bearing horizons with minor pyrrhotite and chalcopyrite. The sequence has been affected by high temperature, low pressure amphibolite facies metamorphism which caused localised migmatisation (see Chapter 5 for detail).

Zinkgruvan mine personnel informally divide the stratigraphy into three distinct units (Fig. 3.3). The stratigraphic terminology used here is consistent with mine terminology, and comprises (from youngest to oldest):

3. ***Viksjön Formation:*** comprises migmatites and gneisses interpreted as equivalent to less metamorphosed sediments outcropping north of lake Höksjön.
2. ***Zinkgruvan Formation:*** represents the transition zone between the metavolcanic sequence and the overlying metasediments. The sequence of interbedded and reworked metavolcanics, marble horizons and calc-silicate skarns is well exposed in mine workings and numerous drill holes. Major base metal mineralisation occurs in the upper part of the formation.
1. ***Isåsen Formation:*** comprises metamorphosed and hydrothermally altered volcanic rocks of mainly dacitic composition. The formation is believed to be chronostratigraphically equivalent to the uppermost part of a rhyolitic volcanic sequence in the south of the district, informally termed the Godegård Formation by Kumpulainen *et al.* (1996).

Strata at Zinkgruvan dip 70-80° to the north (Fig. 3.2), and are interpreted to be inverted on the basis of regional (Chapter 2) and circumstantial evidence. Way-up indicators observed in areas of lower grade metamorphism show the metasediments to overlie the metavolcanics. To the east of the mine the Zinkgruvan Formation is offset by the NNE-SSW trending Sinsberg Fault, and to the west by the N-S trending Dalby Fault. The sequence is intruded by several minor granitoid suites (Fig. 3.1).

The stratigraphy at the mine is difficult to establish in detail due to alteration, deformation and metamorphism. Abundant faulting has disrupted the sequence such that in places it is difficult to make detailed correlation between closely spaced drill holes. Surface mapping provides limited information; exposure of the relatively soft Zinkgruvan Formation is particularly poor due to selective erosion during glaciation.

Data collection

The stratigraphic sequence and lithological descriptions presented in this chapter have been compiled through underground mapping and drill core logging. The majority of the underground observations were made in the Nygruvan (eastern) part of the mine as this provides the best exposed and least disturbed section through the stratigraphy. As most mine development is located in the structural footwall (stratigraphic hangingwall) of the ore horizon, descriptions of this sequence were made by underground mapping complemented by thin section analysis. The stratigraphic footwall is not exposed underground, so this part of the sequence was investigated using drill core. Samples have also been collected from lower grade areas in the south of the basin.

The local stratigraphy is summarised in Fig. 3.3. Detailed mineralogy and chemistry of the stratigraphic units is discussed in Chapter 4.

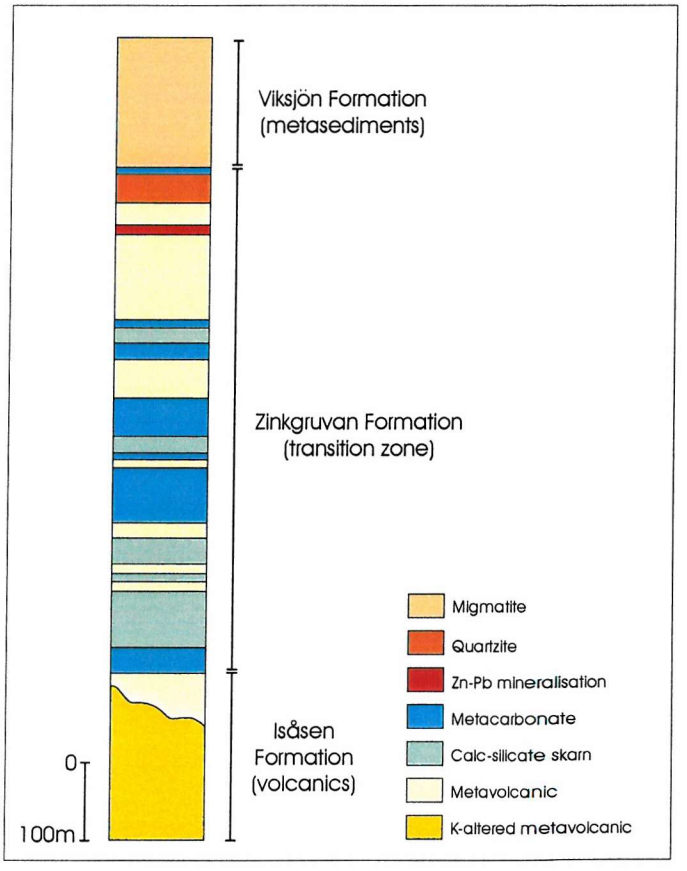

Figure 3.3: Simplified stratigraphic column for the Nygruvan part of the mine. Modified after Hedström et al. (1989).

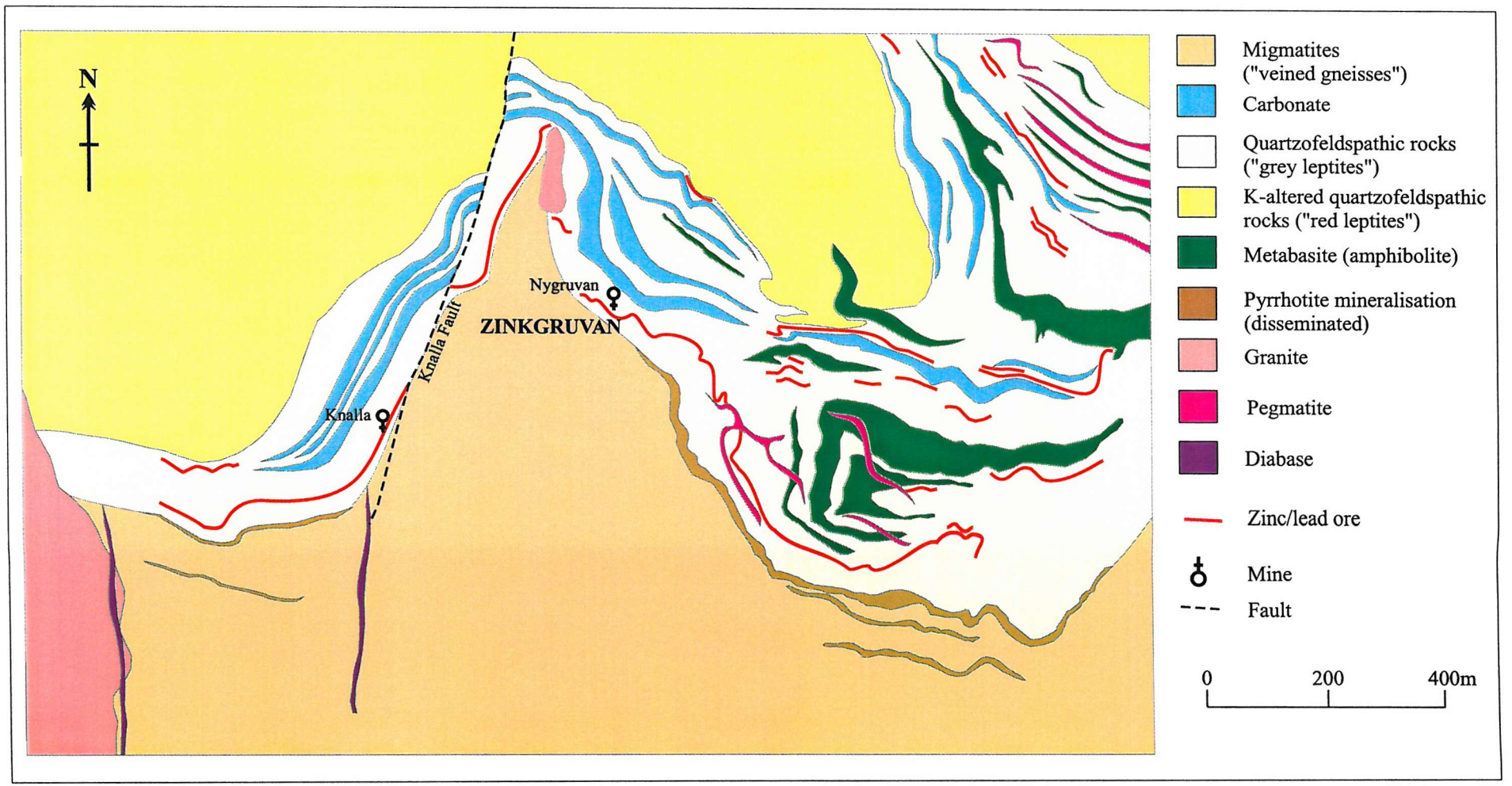

Figure 3.4: Geology of the area surrounding the Zinkgruvan mine. Modified after Henriques (1964). For location of map are see Figure 3.1.

3.2.1 Isåsen Formation

Quartzofeldspathic gneisses, interpreted as metavolcanic rocks, dominate the lower part of the stratigraphy, outcropping approximately 500 metres north of the ore horizon at Zinkgruvan. Following Swedish geological convention, these rocks are referred to as 'leptites' by the local geologists and in the literature (e.g., Hedström *et al.*, 1989 and Oen *et al.*, 1982). The term was first introduced by Hummel (1875), and was widely adopted in Swedish geological literature following the International Geological Congress in 1910. Högbom (1910) defines leptites as *"...dense, fine grained metamorphic rocks in which their chemical and mineralogical composition agree with the gneisses. Micas are generally present, though mostly subordinately; garnet occurs in some varieties, but is seldom a prominent ingredient"*. However, the concept of 'leptite' as a geological term has changed over time. Geijer & Magnusson (1944) gave the following definition: *"By the term leptite, we now mean a metamorphic (recrystallised) supracrustal rock, with approximately granitic composition, which has a secondary grain size between 0.03 and 0.05mm as a lower limit and 0.5-1mm, excluding phenocrysts which may be present"*.

At Zinkgruvan, the 'leptites' are interpreted to be a metamorphosed sequence of rhyolitic-dacitic volcanic rocks and associated tuff deposits (Hedström *et al.*, 1989; Allen *et al.*, 1996, Hellingwerf, 1997). The term 'leptite' is not used in this investigation.

The Isåsen Formation comprises approximately 500 m of metadacites with a metarhyolite unit near the top and minor metabasic (amphibolite) bodies throughout (described in section 3.2.2). The Isåsen Formation is correlated with the upper part of the 4 km-thick rhyolitic Godegård Formation at the southern margin of the basin (Allen *et al.*, 1996). The Isåsen Formation may represent the stratigraphic top of the Godegård Formation, but exact stratigraphic relationships are difficult to determine.

Hellingwerf (1988, 1997) discussed regional-scale alteration where the upper part of the metavolcanic sequence is typically weakly to moderately potassic altered and lower parts typically exhibit sodic alteration (see Chapter 2). In the Zinkgruvan area, mainly the upper, potassic-altered part of the ~8 km-thick volcanic pile is exposed, although Hedström *et al.* (1989) report that to the north and stratigraphically downwards, the K-altered rocks pass into metavolcanics with higher Na_2O/K_2O ratios. This is consistent with regional trends (see Chapter 2).

Local intense potassic metasomatism at Zinkgruvan has produced a massive, pink to grey fine to medium grained quartz-microcline rock with <15% biotite, informally termed 'quartz-microcline rock' or 'potassic leptite'. Most of the quartz-microcline rocks are weakly to strongly foliated but compositional layering present in the non-altered metavolcanics of the overlying Zinkgruvan Formation (section 3.2.2) is not observed here, although subtle variations in grain size can produce faint banding. Porphyritic varieties containing euhedral crystals of plagioclase and

quartz have been reported in the district (Henriques, 1964), and in places lapilli and pyroclastic textures are preserved (Fig. 3.5).

Mineralogy and whole-rock geochemistry of these rocks is presented in Chapter 4 (section 4.2.1).

A

B

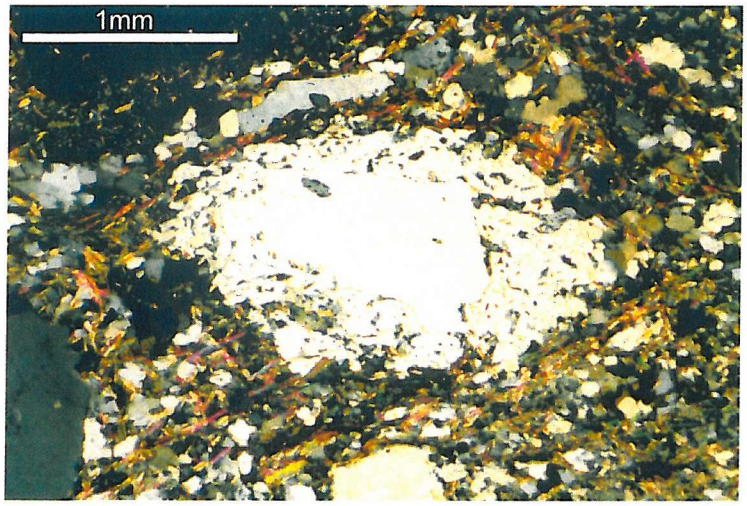

C

Figure 3.5: Textures of metavolcanic rocks from the Zinkgruvan district
A) Pyroclastic texture in metavolcanic rock near Godegard.
B) Close up of picture A, showing detail of pyroclastic texture. Outcrop near Godegard.
C) Remnant quartz phenocryst in metavolcanic rock. Sample ZV4922, south of Lake Hoksjon. Cross polarised light, x2.5 magnification.

3.2.2 Zinkgruvan Formation

The Zinkgruvan Formation represents the transition from volcanic facies to sedimentary facies, and comprises a sequence of interbedded metavolcanics, quartzites and metacarbonate units, with calc-silicate skarns developed between them as a result of metamorphism. Major base mineralisation occurs in the upper part of this formation.

Unaltered volcanic rocks

The potassic-altered volcanics of the Isåsen Formation pass stratigraphically upwards into variably altered metavolcanics interbedded with calc-silicate and metacarbonate horizons. The less altered metavolcanics are fine to medium grained quartzofeldspathic rocks, with the assemblage Qtz + Kfs (microcline) + Bt + Pl (andesine), and variable quantities of calc-silicate minerals (diopside, tremolite, etc.), garnet and Fe-oxides. Muscovite is a common overprinting (retrogressive) phase. The mineralogy and geochemistry of these rocks is discussed in Chapter 4.

The Zinkgruvan Formation metavolcanic rocks commonly show compositional layering (S_1) believed to be bedding-parallel, defined by relative concentrations of quartz + feldspar and biotite, and enhanced by subtle grain size variation. Layering is often accentuated by the presence of calc-silicate minerals, particularly near boundaries with marble or massive calc-silicate skarn units. In high concentrations, the calc-silicate minerals give a green, highly banded appearance to the rock locally known as 'skarn-banded leptite'. In thin section, mm-scale banding defined by changes in grain size or mineralogy is common. The skarn-banded metavolcanics have achieved their banded appearance through the development of 'reaction zones' between interlayered silica-rich (quartzofeldspathic) layers and carbonate horizons during prograde and retrograde metamorphism (see Chapter 5).

Texturally, the metavolcanic rocks range from very fine grained (< 0.1mm), dark, granoblastic rocks to paler grey, slightly coarser grained rocks with planar foliation. Gneissic textures are also common, where mafic and felsic minerals have segregated into bands that are locally folded and contorted. In places, a distinct 'augen' texture is present (where the 'augen' are represented by neoblasts of K-feldspar), and more plastic textures indicative of either higher metamorphic grade or higher strain rates are observed in several drill holes. Within the gneissic varieties, aluminous horizons containing finely braided colourless or milky white masses of fibrolitic sillimanite aligned parallel to the foliation are common, and are a distinctive feature of the Zinkgruvan Formation metavolcanic rocks.

The sulphide content of the metavolcanics is highly variable. Horizons showing weak to moderate sphalerite dissemination are locally common, and strong sphalerite impregnation occurs in a few discrete layers within the sequence. Pyrrhotite and minor chalcopyrite are common accessories. Sphalerite usually occurs as fine grained disseminations concentrated into foliation-

parallel layers, but is also occasionally observed in fractures and cracks. Pyrrhotite can also occur as fine disseminations, but more often appears as a fracture infill or along the margins of thin quartz veins within the metavolcanic rocks. This minor mineralisation is most commonly associated with the quartz-rich metavolcanics, and often with garnet-bearing horizons that occur in close proximity to the ore horizon.

In some areas of the mine, particularly in eastern Nygruvan, intervals of dark green, magnetite-rich skarn up to 8 m thick occur within the volcanic sequence. These highly magnetic skarn bodies are dominated by green Fe-rich biotite, hedenbergite and often contain large quantities of pink garnets (Mn-rich almandine) and minor pyrrhotite and ilmenite.

Garnet-bearing quartzite

Garnetiferous quartzites occur as distinctive layers of several metres thickness within the metavolcanics, often associated with disseminated sphalerite mineralisation. The quartzite is very fine grained (< 0.1 mm) and contains minor plagioclase, K-feldspar and biotite. Almandine garnets form rounded pink porphyroblasts and have two modes of occurrence:

1) Very fine grained garnets occurring within the foliation (S_1) of the rock, often forming distinct thin layers up to 20-30 mm thick.
2) Larger aggregates of pink garnet, scattered throughout the rock, apparently overprinting the foliation. Individual aggregates can reach 30-40 mm in diameter. In some garnet-bearing horizons, the garnet aggregates appear concentrated along darker, more biotite-rich areas and in a few places the garnets occur solely within ~100 mm thick intervals of massive, green Fe-rich biotite.

Stratigraphically below the ore horizon, garnet horizons (particularly type 1) are often host to ZnS mineralisation, with sphalerite and garnets forming alternate foliation-parallel layers within the quartzite. A distinct garnetiferous horizon often occurs a few metres below the Main Ore zone. These garnet-bearing horizons sometimes give a moderate magnetic signature due to the presence of minor pyrrhotite.

On 650 m and 500 m levels in Nygruvan, approximately 45-60 m stratigraphically above the ore body, a 9-12 m thick unit of garnetiferous quartzite occurs. This unit is dark grey, fine grained, and can include thin units of calc-silicate material, particularly at the boundary with the underlying skarn. Fine grained garnets are common through the quartzite, but coarser grained aggregates are scarce. The unit is usually massive, although some parts may show a rough S_1 foliation or banding.

Amphibolites (metabasites)

Occurring sporadically in the Zinkgruvan Formation, amphibolites are more common in the westerly parts of Nygruvan, becoming thinner and scarcer towards the east. The amphibolites form apparently concordant massive, dark green bodies, usually enriched in calc-silicate minerals at the margins due to fluid infiltration and reaction processes. The margins have a paler green colouration compared to the pristine dark grey-green hornblende-dominated cores. Small tabular biotite porphyroblasts are present, typically aligned to define a rough fabric (S_1) within the rock, and plagioclase can account for up to 25% of the assemblage.

The origin of these rocks is uncertain. A pre-metamorphic age is indicated by their foliation and mineralogy. Their occurrence in the volcanic sequences of the Isåsen and Zinkgruvan Formations, and their apparent absence from the Viksjön Formation metasediments suggests they may be a component of the main volcanic phase.

Metacarbonate rocks

The Zinkgruvan Formation contains a variety of CaO-rich rocks, whose classification and terminology requires some explanation. In essence, this group of rocks spans three end-member lithologies:

1) ***Marbles:*** Strictly speaking, marbles (*s.s.*) should contain > 80% carbonate minerals. However, metamorphism of slightly impure limestones or low grade marbles will as a matter of course produce a rock which, with increasing metamorphic grade, will evolve an increasing proportion of calc-silicate minerals and subsequently less carbonate. Continuous reaction between silica-bearing and carbonate phases will continue to produce calc-silicate phases until one of the parent components is exhausted. Due to high grade metamorphism at Zinkgruvan, limestones which may have originally contained only a small amount of impurities now contain up to 40% calc-silicate minerals. For the purposes of this investigation, the term ***marble*** refers to metacarbonate rocks containing >50% carbonate minerals.
2) ***Calc-silicate marbles:*** Within the mine area, some metacarbonate units contain a higher level of impurities than the marbles described above. As such, they often contain 50% or more calc-silicate minerals, although calcite or dolomite remain the single dominant mineral phase within the assemblage. For the purposes of this investigation, the term ***calc-silicate marble*** refers to metacarbonate units containing < 50% carbonate minerals, but where a carbonate phase (calcite or dolomite) is still the dominant single phase within the rock.
3) ***Calc-silicate skarns:*** This term refers to rock units composed of either:
   i) Massive calc-silicate material, usually dominated by diopside.
   ii) Bands (< 30cm) of alternating calc-silicate minerals, quartzofeldspathic rock and metacarbonate rock.

Carbonate minerals are usually subordinate in these rock types.

In this investigation, the term ***metacarbonate*** collectively refers to marbles and calc-silicate marbles. Metacarbonate units form an important part of the Zinkgruvan Formation, mostly occurring stratigraphically below the ore horizon. Above the mineralised horizon the metacarbonates are generally < 1m thick and mainly occur within banded skarn units. Below the ore zone the metacarbonate units are up to tens of metres thick, increasing in frequency and thickness towards the eastern side of the deposit.

Marbles

Within the Zinkgruvan district, marbles range in composition from calcite-rich rocks with <15% calc-silicate minerals, to more siliceous varieties containing up to 40% calc-silicates and dolomitic marbles containing forsterite.

Calcitic marbles are fine to medium grained, and tend to be pale cream to faintly green depending on the degree of calc-silicate mineral development. Marbles in lower grade areas in the south of the basin contain less calc-silicate minerals than those in higher grade areas around the mine. Diopside and tremolite are the most common calc-silicate phases, but their occurrence and distribution is dependent on bulk rock chemistry and metamorphic grade (Chapter 5). Phlogopite, microcline and quartz are common products of contaminants in the original protolith. Some samples show compositional banding, defined by varying proportions of carbonate and calc-silicate phases and accentuated by the alignment of micas.

Dolomitised marbles are also fine to medium grained and foliated, with a mottled blue-grey colouration. The carbonate component is usually a mixture of dolomite and subordinate calcite. Dolomites that have undergone sufficient metamorphism contain forsterite (commonly altered to serpentine), pleonaste spinel and variable quantities of phlogopite and clinochlore, depending on bulk rock composition. In a few samples, the forsterite has been altered to saponite (a Mg-rich clay mineral). Relationships between bulk rock composition, mineral chemistry and metamorphic grade are investigated in chapters 4 & 5.

Calc-silicate marbles

Metacarbonate rocks falling into this category have similar mineralogy to the marbles described above, but contain >50% silicate and calc-silicate minerals. In eastern Nygruvan, calcitic calc-silicate marbles contain up to 30% quartz and lesser quantities of microcline, plagioclase and diopside, which may be a function of the impurities in the original rock and/or the influx of an externally-derived fluid (see Chapter 5).

During metamorphism, calc-silicate reaction skarns are developed between carbonates and the surrounding silicate-dominated lithologies. These skarn units can reach thicknesses of 5 metres or

more, comprising either massive diopside skarns, or finely banded layers of calcite-dominated carbonate, calc-silicate minerals and quartzofeldspathic gneiss.

Whole-rock analyses of typical calcitic/dolomitic marbles and calc-silicate marbles are given in Table 3.1.

	Dolomitic marble (W. Nygruvan)	***Calcitic calc-silicate marble (E. Nygruvan)***	***Calcitic carbonate (Regional)***
	Dol + Cal + Fo/Serp + Phl	Cal + Qtz + Di (+ Pl)	Cal + Qtz + Di
SiO_2	5.60	35.09	5.67
TiO_2	0.02	0.13	0.00
Al_2O_3	0.54	5.46	0.10
Fe_2O_3 (total)	2.25	2.51	0.25
MnO	0.35	0.25	0.00
MgO	24.51	4.76	0.86
CaO	35.42	33.42	64.03
Na_2O	0.10	0.05	0.12
K_2O	0.15	2.59	0.04
P_2O_5	0.01	0.05	0.01
SO_3	0.11	0.14	0.05
LOI (CO_2)	29.92	14.35	28.87
Total	98.78	101.44	100.00

Table 3.1: Comparison of whole-rock analyses (XRF) for dolomitic carbonate (Sample 555/17) and calcitic, siliceous carbonate (451/17) from the mine package, and a carbonate sampled away from the area of mineralisation (Sample ZR04). Data in weight %. LOI accounts for loss of CO_2 (and minor water vapour) during sample ignition. Original XRF data and laboratory procedures in Appendix E.

Distribution

In the mine area, limestones (now marbles) have been dolomitised and silicified, although dolomitisation is not exclusive to areas of mineralisation. Within the Nygruvan part of the mine, a compositional variation within the metacarbonate rocks is observed. In the east of the mine, calcitic calc-silicate marbles containing up to 35% quartz dominate. Moving westwards, dolomite and forsterite-bearing marbles occur. The trends associated with this change are explored in chapters 4 and 5.

Calc-silicate skarns

Throughout the Zinkgruvan Formation, calc-silicate skarns are common, although like the metacarbonate units they tend to be thicker below the ore horizon than above. The skarn units range from occasional bands <500 mm thick to numerous mm-scale layers within the metavolcanics (the so-called 'skarn-banded leptites'), to massive, uninterrupted diopside-dominated units of 8-10 m thick. It is usual to find sections of finely interbedded quartzofeldspathic and calc-silicate material at the margins of these massive units, and 100-150 mm bands of calc-silicate rich metavolcanic material within the skarn up to two metres from the contact. Boundaries with the metavolcanic rocks are usually sharp, with the transition from quartzofeldspathic rock to calc-silicate skarn occurring over a 10-20 mm interval.

The massive calc-silicate skarns are green and usually fine grained. Mineral assemblages are characteristically dominated by diopside, accompanied by varying quantities of tremolite, garnet, zoisite, sphene, quartz, microcline, phlogopite and calcite/dolomite. Some skarns show intricate, 5-10 mm scale layering of pale green diopside-dominated assemblages, pale pink quartz/garnet-rich assemblages and cream coloured calcitic marble. These bands are often discontinuous and contorted, and usually appear at the margins of fairly thick (1-2 m) massive diopside skarn units. Wollastonite skarns occur locally as massive, colourless or white units of relatively coarse grained, acicular wollastonite. Diopside-wollastonite skarns also occur, where an intimate mix of green diopside and cream-coloured wollastonite phases produce a "plastic" texture. Opaques are generally scarce within the massive skarns, but banded calc-silicate skarns may contain up to 5-10% disseminated sphalerite and galena.

A distinctive, 5-10 m thick, laterally persistent banded calc-silicate skarn unit occurs just above the ore horizon at Nygruvan. The 10-20 mm to 300-400 mm wide bands have a varied composition, including dark grey quartzitic material; green diopside skarn comprising 70-80% diopside; pink garnet-rich bands; thin carbonate layers; polymineralic skarn bands and the typical Qtz-Fsp-Bt metavolcanic material. Small scale folding commonly deforms the skarn bands, and localised boudinage occurs. Isoclinal folds up to 2 m amplitude are sometimes observed.

The fine grained, polymineralic skarn layers are composed of varying quantities of quartz, diopside and garnet, accompanied by lesser plagioclase, zoisite, vesuvianite (idocrase) and sphene. The zoisite commonly shows well-developed zoning, and is likely to have developed as a retrograde product after garnet or plagioclase (Chapter 5). Sub-mm scale internal layering within individual bands is defined by changes in grain size and the relative abundance of quartz, garnet and diopside. Some bands are highly quartz-rich with few accessory phases, whereas other layers are a mix of all components listed above. Both galena and sphalerite are common, occurring as widespread disseminations or as fracture infills.

Zn-Pb mineralisation

Zinkgruvan mine comprises several tabular to lenticular, apparently stratiform ore bodies separated by thin and sub-economic mineralisation. The mine is divided into two sections by the Knalla Fault (Figs 3.2 & 3.5); to the east lies the dominant Nygruvan orebody, and to the west are Knalla, Burkland, Cecilia and several other subsidiary orebodies. Mine geometry is discussed in detail in section 3.3.

The bulk of the Zn-Pb mineralisation occurs in the Main Ore horizon with a subsidiary tonnage in the underlying Parallel Ore. Mineralisation ranges from disseminations of sphalerite and galena in a calc-silicate bearing quartzite host rock, to near-massive sulphide layers intercalated with quartzites and calc-silicate layers. The stratigraphic upper boundary of mineralisation at Nygruvan and parts of Knalla is marked by a distinct unit of green (diopside-rich), finely banded calc-silicate skarn, known locally as the 'hangingwall skarn'.

The distribution of mineralisation and detailed characteristics of the various orebodies are discussed in section 3.3. Ore petrography is presented in Chapter 7.

Pyrrhotite horizon

A quartzofeldspathic gneiss unit containing abundant disseminated pyrrhotite lies approximately 100 m stratigraphically above the Main Ore zone. The pyrrhotite horizon is considered to mark the base of the Viksjön Formation.

The thickness of this horizon is highly variable: underground at Nygruvan it is 5-15 m thick, but Henriques (1964) reported it to range up to 50 m, and to pinch out completely in places. In the mine and on surface it is easily identified by the rusty weathered appearance of the exposed pyrrhotite. The presence of pyrrhotite yields a strong response to magnetic surveys.

Perthitic feldspars and myrmekitic intergrowths are evidence of high-temperature metamorphism in this horizon. Pyrrhotite occurs as an interstitial phase between grains of quartz, K-feldspar, plagioclase and biotite, although some has been remobilised into small fractures within K-feldspar grains. Textural relationships between sulphide and silicate phases suggest that the pyrrhotite was present in the rock prior to peak metamorphism.

3.2.3 Viksjön Formation

This unit comprises a series of schists, gneisses and migmatites, correlated with the metasedimentary rocks described by Kumpulainen *et al.* (1996) to the south. High grade metamorphism caused partial melting, thought to be triggered by their higher water content compared to surrounding rocks. These rocks have been previously described as veined gneisses by Johanssen (1910) and Henriques (1964).

Schist and quartzite samples from areas of lower grade metamorphism around lake Höksjön (Fig. 3.1) contain quartz, plagioclase, biotite and muscovite with large porphyroblasts of andalusite and abundant phyllosilicates in the schist. In some areas, the schist has a 'knotted' appearance due to the development of muscovite aggregates. S_1 foliation is created by the alignment of biotite in most samples. Tourmaline and extensively pinitised cordierite are present in some samples.

The migmatites are well exposed underground at Nygruvan, where the main P1 hoisting shaft has been sunk near the lower boundary of the Viksjön Formation. At Zinkgruvan, high grade metamorphism means that much of the primary muscovite has reacted out (Chapter 5), and sillimanite is the dominant aluminous phase. The stratigraphic base of the metasediments is marked by the appearance of gneisses and pelitic schists, which grade into migmatites approximately 50 metres up section. Locally, remnants of highly altered staurolite porphyroblasts occurring alongside sillimanite in some of the schists and gneisses are evidence of earlier, moderate temperature stages of metamorphism. Some samples show small rounded garnet porphyroblasts included within the assemblage, but cordierite has not been recognised.

The transition from metapelitic gneisses and schists to the migmatites is often marked by an irregular body of granite generated by partial melting of metasediments during anatexis, particularly in the area around the P1 shaft in Nygruvan. This melt product comprises medium to coarse grained, equigranular quartz, plagioclase, K-feldspar and minor biotite, and has sharp contacts with the surrounding migmatites.

Within the migmatites, two main textures are observed: the stratigraphically lower migmatites are dark (biotite-rich) and massive with white K-feldspar (microcline) porphyroblasts ranging 3-30mm in diameter. The second type of migmatite occurs slightly further south (stratigraphically higher) and shows a more typical migmatitic appearance with planar segregations of felsic material (leucosome) surrounded by black selvages of biotite (Figs 3.6A & B). The fabric (S_1) in these migmatites is frequently contorted and folded, and rafts of fine grained quartzite or metabasite up to 1m in diameter are common (Fig. 3.6C). These represent unmelted blocks of metasedimentary and metavolcanic material with higher melting points than the surrounding material. Elsewhere in the mine, pods of calc-silicate material form rafts within the migmatites, indicating that the skarns formed prior to the migmatisation event. These inclusions often cause deviation of the

surrounding migmatitic fabric, and alteration of their margins due to reaction with the surrounding migmatite is common.

The characteristic assemblage of the pelitic metasediments is Qtz + Bt + Kfs + Pl (andesine) + Sil. Primary muscovite is absent, which has important implications for P-T determinations (see Chapter 5). Sillimanite is commonly developed as fibrolitic layers, interspersed with biotite-rich and quartzofeldspathic layers. Perthitic textures and myrmekitic intergrowths are common, indicative of high temperatures during peak metamorphism. Samples that are strongly foliated show the biotite and sillimanite enveloping large masses of quartz and feldspar.

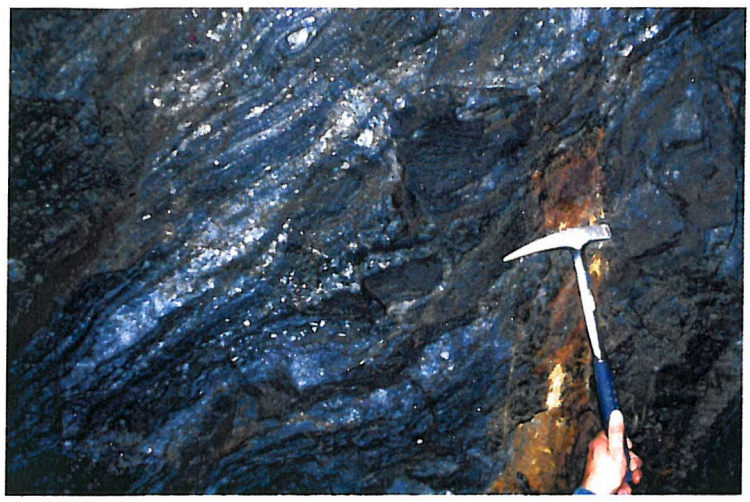

A

B

C

Figure 3.6: Textures observed in migmatites, 650m level, Nygruvan
A) Planar segregations of felsic leucosome (white) surrounded by biotite-rich material.
B) Contortion of planar fabric illustrated in A.
C) Large mafic inclusion within migmatites. Inclusion measures approximately 60cm across.

3.2.4 Pegmatites

Pegmatites are common throughout the mine package, and usually form massive bodies running sub-parallel to the foliation of the rocks, although small irregular bodies also occur. Several generations of pegmatite are present. The earliest bodies intruded prior to or during peak metamorphism are irregular in shape and may be related to the migmatisation event which has affected the strata to the south of the orebody. Many of these pegmatites have clear spatial relationships to areas of migmatisation. Later generation pegmatites have more planar, dyke-like morphology suggesting intrusion into relatively cold, rigid, fractured crust.

The pegmatites comprise quartz, K-feldspar, plagioclase, biotite, minor muscovite and accessory tourmaline. Early pegmatites show a rough foliation (S_1) with aggregates of biotite aligned parallel to each other, particularly near the margins of the body. Garnet clusters sometimes occur along the pegmatite margins, especially where the pegmatite has intruded a calc-silicate lithology. Pyrrhotite and (less commonly) chalcopyrite form later-stage fracture infills, again particularly around the margins of the pegmatite body.

In pegmatites near Zn-Pb mineralisation, the K-feldspar is typically green due to contamination with lead to form the variety amazonite. Other pegmatites show a purplish discolouration caused by alteration of feldspars, possibly by lead-rich fluids or by contamination of feldspars crystallising from a melt which has passed through a pre-existing Pb-rich rock (i.e., the ore zone). This discolouration has been formerly referred to as "amphoedolite" by mine geologists, after an entry in the 1932 edition of Dana's Handbook of Mineralogy, but no modern references confirm this as a recognisable mineral. Johanssen (1910) and Henriques (1964) mis-identified this mineral as fluorite. The most likely explanation of the purple colouration is the presence of submicroscopic Pb phases trapped as micro-inclusions in the feldspar lattice. Contamination of feldspars by high concentrations of Pb indicates that mineralisation must pre-date some phases of pegmatite generation.

3.2.5 Dolerite dykes

Several generations of dolerite dykes occur in the Zinkgruvan district and post-date the regional S_1 fabric and peak metamorphism. West of lake Viksjön, two ~15 m thick dykes trending N-S intrude the metasediments of the Viksjön Formation. Towards the south of lake Viksjön, a 250 m wide E-W trending dolerite dyke of the Breven swarm postdates late orogenic granitoid intrusions, but is dissected by the NNE-trending faults (Fig. 3.1). Henriques (1964) describes the mineralogy of the N-S dolerite dykes as mainly plagioclase and secondary hornblende, sometimes with plagioclase phenocrysts. The larger E-W trending dyke contains ophitic plagioclase and pyroxene, with accessory chlorite and magnetite.

3.3 MINERALISATION

Major base metal mineralisation is confined to the Zinkgruvan mine, although sub-economic base metal occurrences are scattered throughout the area. Major base metal mineralisation is shown as a red line in Fig. 3.4.

Economic production at Zinkgruvan commenced in 1857 from a pre-production resource now estimated at 48 Mt at 10.4% Zn, 3.2% Pb and 69g/t Ag, making it the largest known Zn-Pb accumulation in the Fennoscandian Shield (Allen *et al.*, 1996). Zinkgruvan is one of only two operational mines in Bergslagen, exploiting Pb and Zn sulphides from several orebodies (Fig. 3.7). At December 2000, proven plus probable reserves stood at 11.9Mt at 10.0% Zn, 4.4% Pb and 90g/t Ag, which is sufficient to maintain production at the current extraction rate for a further 14 years (North Ltd Annual Report 1999/Rio Tinto Annual Report 2000). Base metal mineralisation extends as intermittent horizons in the area west of the mine, where continuing exploration is focused. At present, underground development at Zinkgruvan reaches a depth of around 950m, although mineralisation is known to extend below 1000 m.

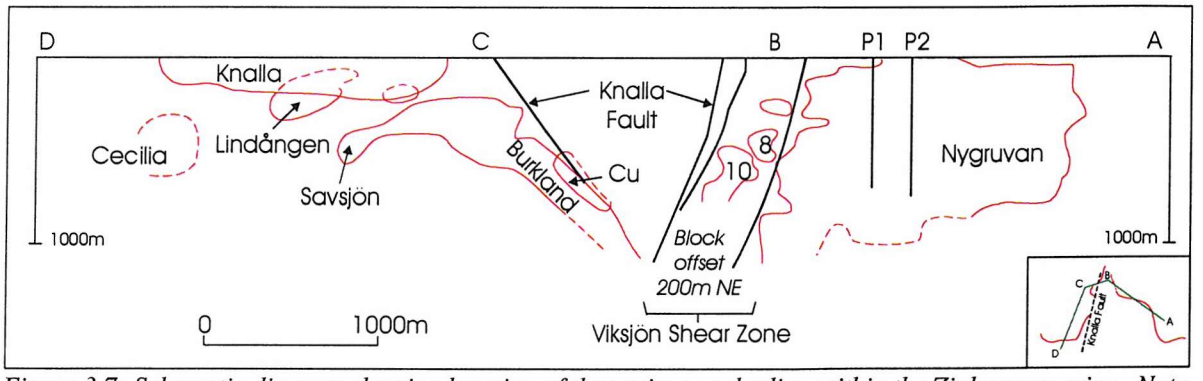

Figure 3.7: Schematic diagram showing location of the various orebodies within the Zinkgruvan mine. Note that the section has been unfolded so that the Knalla Fault appears twice. Line of section shown in inset. After Schmidt et al. (2000).

3.3.1 The Nygruvan orebody

Mineralisation at Nygruvan is exploited from the Main Ore and, locally, the underlying Parallel Ore. The thickness of the ore zone as a whole varies from a few metres in the west to 20-25m in the east, and the Parallel Ore is better developed where the ore zone is thickest (Hedström *et al.*, 1989). The Nygruvan orebody is divided by a fault passing through the P1 shaft area (Fig. 3.7). The ore horizons are separated by a 3-8 m thick quartzofeldspathic gneiss unit.

The Parallel Ore is up to 4 m thick and comprises thin layers of Pb and Zn sulphides hosted in a skarny quartzofeldspathic unit, interpreted by Hedström *et al.* (1989) as a metatuffite. Ore grade increases stratigraphically upwards towards the Main Ore zone, but in comparison with the Main Ore, the Parallel Ore has distinctly lower Zn/Pb ratios.

The Main Ore can be divided into two parts. The lower part consists of concentrations of galena and sphalerite interlayered with garnet-bearing quartzite. Ore layers are approximately 1 m thick, but contain internal laminations defined by varying proportions of sulphides and silicate minerals. This lower section of ore is persistent throughout the eastern part of the Nygruvan orebody, but grades laterally into so-called quartzitic metatuffite to the west (Hedström *et al.*, 1989). The stratigraphic upper part of the Main Ore comprises a thick (up to 8 m) horizon of massive Zn-Pb ore containing up to 45% Zn and 10% Pb. This part of the orebody is laterally persistent and can be traced for almost 2 km through the mine area, along with an interbanded barren skarny quartzofeldspathic layer <0.5 m thick, locally known as the 'Long Snake'.

Metal content varies laterally within the Nygruvan orebody, with Zn/Pb ratios increasing eastwards, away from the Knalla Fault zone (Fig. 3.8). Both the Main Ore and Parallel Ore show an increase in Pb + Zn grades stratigraphically upwards.

The hangingwall skarn immediately above the Main Ore zone contains minor quantities of disseminated sphalerite and galena, particularly near the contact with the ore, and abundant disseminated pyrrhotite.

3.3.2 The Knalla orebody

Immediately to the west of the Knalla fault lies the Knalla orebody, which although linked underground to the Nygruvan development, is served by a separate shaft (marked on Fig. 3.4). Here, the Main Ore zone varies between 1-10 m thick, but the Parallel Ore is indistinct or absent. The hangingwall skarn is present, but more variable in width and composition than at Nygruvan. Mineralisation at Knalla is generally more Pb-rich than at Nygruvan (Fig. 3.8), and native silver occurs as fracture infills.

3.3.3 The Burkland orebody

The Burkland orebody is located directly adjacent to the Knalla Fault, just NE of the Knalla orebody (Fig. 3.7). Chalcopyrite-dominated copper mineralisation hosted in serpentine marble underlies the Zn-Pb ore horizon. Minor cubanite, pyrrhotite, magnetite and an array of accessory Ni and Co-Fe-As-Sb-S minerals are present. A resource of 2.7 Mt at 3.0% Cu and 52g/t Ag is estimated (Rio Tinto Annual Report, 2000). Hedström *et al.* (1989) interpreted this copper mineralisation as the stockwork feeder zone to the main Zn-Pb-Ag ore horizon.

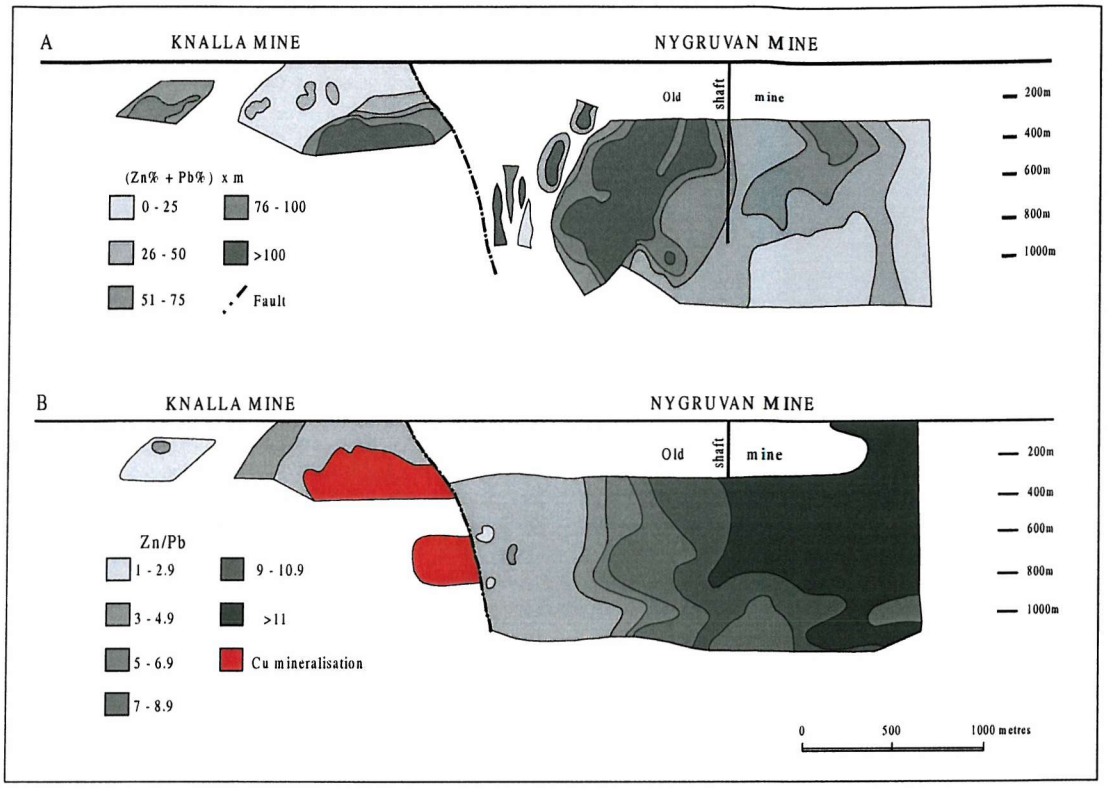

Figure 3.8: Cross section through Zinkgruvan to show variation in metal content. A: Amount of deposited metal in the Main Ore horizon, represented as % Zn + Pb multiplied by width of mineralised zone. B: Zn/Pb ratio of the Main Ore horizon and distribution of Cu mineralisation at Burkland. Orientation of sections as in Fig. 3.7. After Hedström et al. (1989).

3.4 STRUCTURE

The main phase of deformation (D_1) affecting the rocks of the Zinkgruvan Basin occurred during the Svecofennian orogeny around 2.0-1.75Ga. Peak metamorphism is shown to have outlasted deformation in the region by the development of a strong granoblastic overprint in many of the rock units. This is a common phenomenon over much of Bergslagen. In the Zinkgruvan Basin, peak metamorphic isograds do not appear to follow the F_1 deformation pattern, so it is assumed that the main thermal event continued after the rocks were deformed into the F_1 synformal structure. Metamorphic isograds are displaced by later-stage faulting.

3.4.1 Folding

The Zinkgruvan Basin is interpreted as a broadly E-W striking isoclinal synform (F_1) with a partially overturned northern limb (Fig. 3.2), created by N-S D_1 compression during the Svecofennian orogeny. Most rocks in the basin show a strong S_1 foliation, generally sub-parallel to bedding (S_0). This foliation is likely to be axial planar to the main E-W striking synform, but appears to be parallel to bedding as strata are near-vertical in most parts of the basin.

D_2 deformation due to E-W compression, possibly related to intrusion of post-orogenic granites (Hedström *et al.*, 1989) produced open folding of strata near Zinkgruvan. The S_1 fabric in the migmatites appears to have deformed in a relatively ductile manner, so D_2 deformation is likely to have occurred whilst the rocks were still relatively warm and ductile ($\geq 350°C$) following peak metamorphism. In the mine, strata are folded and contorted on a smaller scale. These structures are most easily identified in the ore zone, with the Knalla orebody and western Nygruvan showing the most intense deformation. At Knalla, pronounced F_2 isoclinal folding about a west-dipping, undulating fold axis has produced intense contortion and disruption of the mineralised horizon (Fig. 3.10A) (Hedström *et al.*, 1989). This folding pattern is also recognised in western Nygruvan, and in minor structural disruptions throughout the mine.

An oblique S_2 cleavage is recognised in some places where D_2 deformation is intense, such as areas of Knalla, but in most places identifying later foliations is difficult and it is suspected that later deformation events did not give rise to fabric development (L. Schmidt, pers. comm.). Development of a secondary cleavage can be observed in some exposures of gneiss/migmatite where crenulation cleavage has been further deformed to produce a faint S_2 cleavage (Fig. 3.9).

Figure 3.9: Spaced cleavage (orientation indicated by yellow line) developed in crenulated quartzofeldspathic gneiss. Sample taken from surface outcrop south of P2 shaft.

3.4.2 Faulting

The supracrustal sequence in the Zinkgruvan Basin is cut by several major steeply dipping NNE-trending fault zones (Fig. 3.1). The faults (?D_4) post-date the main phases of folding. The lateral and vertical offset along these discontinuities, both laterally and vertically, is variable but several show northward displacement of the eastern (structural hangingwall) block. The ore horizon is downthrown 100 m and displaced 400 m northwards on the eastern side of the Knalla Fault. The Sinsberg Fault shows more substantial disruption, with the eastern block displaced approximately 1500 m northwards. Vertical displacement is unknown. Offset on the Dalby fault is poorly defined, and the fault plane dips westwards rather than eastwards.

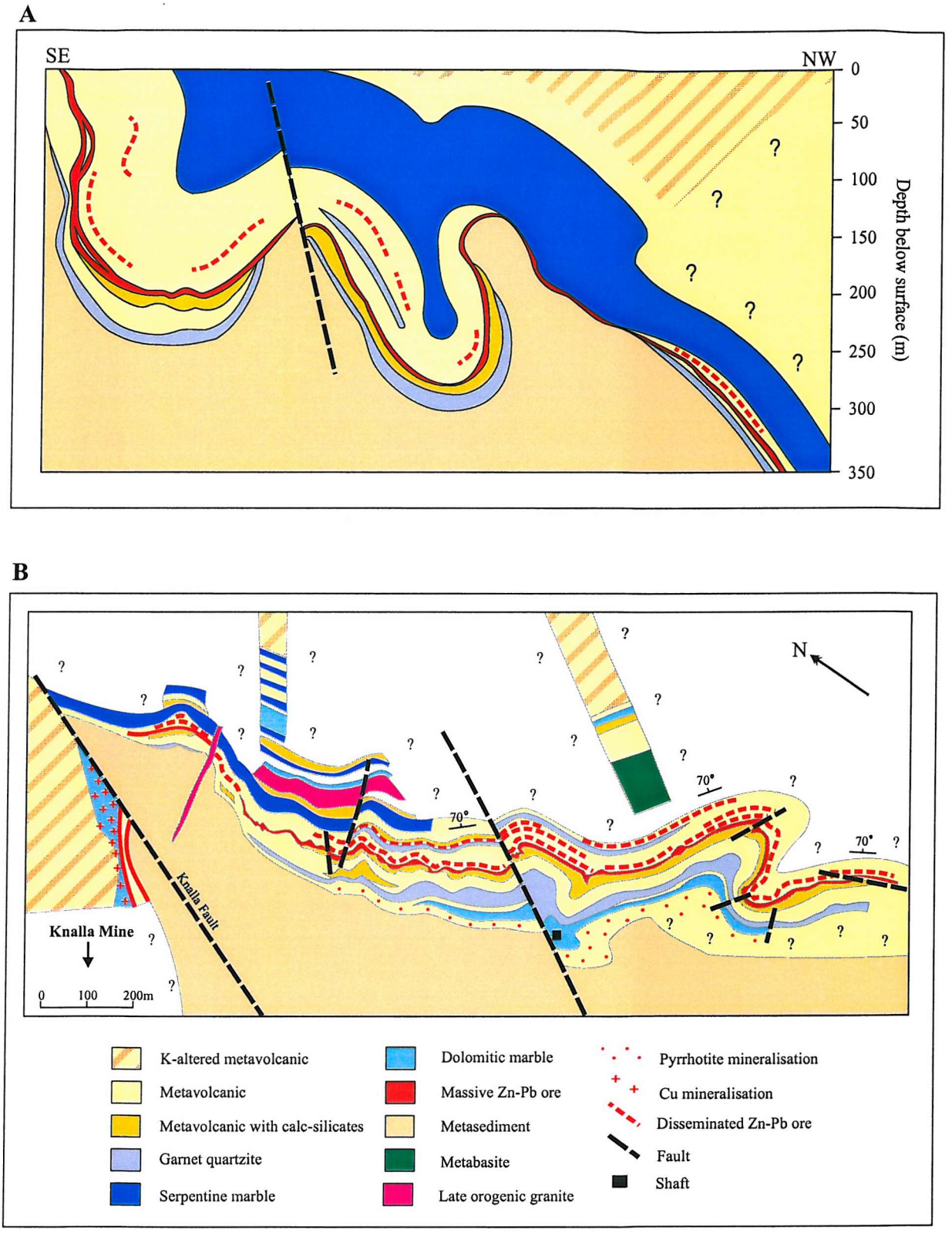

Figure 3.10: Geological sections through Zinkgruvan mine
A) Vertical section through Knalla to show F_2 folding. Legend as Fig 3.10B.
B) Geological plan of 650m level, Nygruvan.
Both diagrams modified after Hedstrom et al (1989).

CHAPTER 4

GEOCHEMISTRY AND PETROLOGY

CHAPTER 4: GEOCHEMISTRY & PETROLOGY

4.1 INTRODUCTION

The geochemistry and petrology of the metavolcanic and metacarbonate units from the mine area and surrounding district are examined in this chapter. These studies provide evidence for hydrothermal fluid events and alteration episodes, and aid the identification and interpretation of anomalous or unusual lithologies. Knowledge of the above is crucial to understanding the chemical evolution of the host rock package and defining some of the chemical processes which contributed to the ore-forming event.

The metavolcanic rocks of the Isåsen and Zinkgruvan formations are considered in relatively broad terms because they provide important information on the source of silica and other non-carbonate components in the metacarbonate units, but are not the main thrust of this study. The metacarbonate and calc-silicate units of the Zinkgruvan Formation are the main focus of this chapter because they are sensitive indicators of chemical change. The Viksjön Formation metasediments are not investigated as they do not show any evidence of large-scale hydrothermal alteration or genetic links to the mineralisation.

The relationships between whole-rock geochemistry and mineralogy provide a key tool for identifying fluid events and their relative timing. Metacarbonate rock mineral assemblages provide constraints on the chemistry of infiltrating fluids and alteration events, and textural relationships provide information on the timing of such episodes. Full descriptions of the mineralogical variations of the major lithological units in the mine package have been presented in the previous chapter; this chapter examines mineralogy and mineral chemistry in relation to bulk rock geochemistry.

Whole-rock XRF geochemical data used in this chapter were provided by North Ltd with additional analyses performed at the University of Southampton by the author. Sample preparation methods and analytical results are given in Appendix E. Whilst good quality controls are implemented on the new data (see sample preparation methods and operating conditions in the appropriate appendices), there is little information for the older data provided by the mine. There is less certainty regarding the reliability of older data for some elements and the two data types may not be directly comparable. However, most of the geochemistry utilises elemental ratios and trends rather than absolute values, which minimises the impact of absolute errors.

Petrological observations were made using standard 30μm thin sections and polished thin sections under polarising transmitted and reflected light. Individual semi-quantitative mineral analyses were obtained using a JEOL JSM 6400 scanning electron microscope (SEM) at the University of Southampton for a count time of 100 seconds per analysis. SEM mineral analyses carried out by Bengtsson (2000) and Lundstam (1998) are also included. Laser ablation

inductively-coupled plasma mass spectrometry (LA-ICPMS) techniques were used to investigate rare earth element zonation in garnet crystals from selected samples in order to identify the chemical signature of the fluid event responsible for their formation, and the relative timing of that event.

Details of thin section preparation and SEM procedures are given in appendices D and F respectively. Methodology and results of LA-ICPMS work are in Appendix G.

Terminology

In this chapter, **FeO*** refers to 'non-sulphide Fe', calculated from original whole-rock Fe_2O_3 data using the method outlined in Appendix E. For whole-rock XRF analyses, FeO (Tot) refers to the total amount of Fe oxide present in the sample. This is also the case for SEM mineral analyses, although for some mineral groups the proportion of Fe_2O_3 has been stoichiometrically calculated and is detailed in Appendix F.

Mine marbles are situated mainly in the stratigraphic footwall of the orebody, with few samples from the stratigraphic hangingwall. Samples are taken from drill core and underground exposure.

Near-mine marbles are arbitrarily defined as surface or drillcore samples from within ~1.5 km of the mine.

District marbles are those found within the boundaries of the Zinkgruvan Basin, as defined in Chapter 2, but are remote from known mineralisation. Most samples are taken from surface outcrop.

Regional marbles refer to metacarbonate rocks in the Bergslagen Province outside the Zinkgruvan Basin. In this study, regional marble samples are sourced from Glanshammar, approximately 70 km NNE of Zinkgruvan. All samples are sourced from surface outcrop.

4.2 METAVOLCANIC ROCKS

The Isåsen and Zinkgruvan formations contain metavolcanic rocks interpreted on geochemical grounds as having initial rhyolitic to dacitic composition (Hellingwerf, 1997). Upper amphibolite facies metamorphism (Chapter 5) and potassic alteration, especially in the Isåsen Formation, has destroyed original textures and modified the composition of these units. The composition of these rocks is shown in Fig. 4.1.

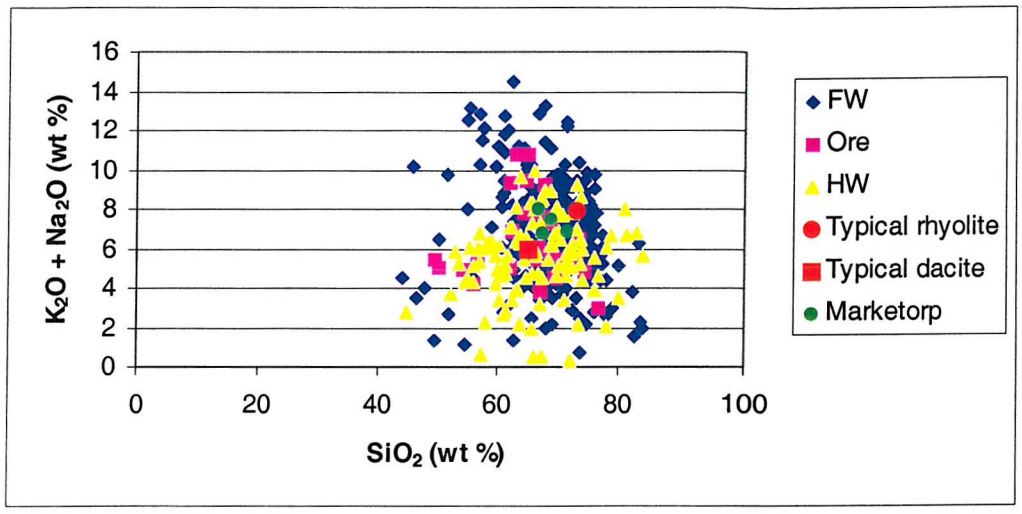

Figure 4.1: Classification of metavolcanic rocks of the Isåsen and Zinkgruvan formations using whole-rock XRF data. Samples are grouped according to their stratigraphic position relative to the orebody: FW = footwall; Ore = in the ore zone; HW = hangingwall. Scatter of data towards the low-silica end of the diagram is mainly due to dilution by relatively small quantities of calc-silicate minerals. Relatively unaltered metavolcanic rocks from Marketorp (30 km east of Zinkgruvan) and typical rhyolite and dacite are plotted for comparison (data from Cox et al., 1979). Original data and laboratory procedures in Appendix E.

4.2.1 Isåsen Formation metavolcanic rocks

Alkali metasomatism is widespread in metavolcanic sequences of the Bergslagen region (Chapter 2), with K-altered metavolcanics containing up to 6 wt% K_2O (Freitsch, 1982a). However, the K-enrichment displayed by the Isåsen Formation is much more intense, indicating a localised alteration event. Potassic alteration in the Zinkgruvan area has been briefly discussed by Hedström *et al.* (1989) and Hellingwerf (1997), and K-altered rocks were described by Henriques (1964).

K_2O contents can reach as high as 14 wt%, although most rocks contain around 9-11 wt% K_2O. Na_2O contents are correspondingly very low, typically less than 0.7 wt%. K_2O contents in these rocks are abnormally high, even compared to regionally K-altered rocks elsewhere in Bergslagen. Al_2O_3 is usually around 12-14 wt%, although some samples contain up to 17 wt %. Whole-rock geochemical analyses and mineralogical compositions of typical metavolcanic rocks from the Isåsen Formation are given in Table 4.1.

	454/36 (Isåsen Fmn)	*ZV4924 (Isåsen Fmn)*	*ZV4922 (Zinkgruvan Fmn)*	*898/4 (Zinkgruvan Fmn)*	*454/11 (Zinkgruvan Fmn)*
SiO_2	65.09	67.80	72.60	72.10	69.66
TiO_2	0.43	0.42	0.27	0.30	0.38
Al_2O_3	16.19	13.90	12.50	13.20	13.26
Fe_2O_3 (total)	0.80	2.85	3.89	2.32	3.09
MnO	0.02	0.05	0.03	-	0.15
MgO	0.41	0.77	1.39	2.91	1.73
CaO	0.56	1.17	0.09	0.23	0.80
Na_2O	0.77	0.95	0.17	0.53	0.89
K_2O	13.55	10.90	7.07	6.36	8.75
P_2O_5	0.07	0.08	0.06	0.03	0.08
Total	98.00	98.89	98.07	97.98	98.79
Quartz	40	50	60	45	45
K-fsp	50	35	-	25	30
Plagioclase	-	-	-	-	-
Biotite	8	10	15	15	15
Muscovite	-	-	20	-	-
Others	2	5	5	15	10

Table 4.1: Whole-rock geochemistry (XRF) and mineralogy of typical metavolcanic rocks from the Isåsen and Zinkgruvan formations. 454/36 = quartz-microcline rock, Nygruvan; ZV4924 = pink quartz-microcline rock, near Mariedamm; ZV4922 = quartzofeldspathic gneiss with remnant quartz phenocrysts, Höksjön; 898/4 = quartzofeldspathic gneiss, Cecilia; 454/11 = quartzofeldspathic gneiss, Nygruvan. Chemical data in weight %; mineralogical data in estimated volume %. Original data and XRF laboratory procedure in Appendix E.

The iron content is variable; the majority of samples contain 1.5 - 3.0 wt % total Fe oxide, which is within the normal range for acidic volcanic rocks. However, many strongly K-altered samples contain <1 wt% total Fe oxide, indicating Fe removal during or after the K-enrichment process. In most areas, quartz-microcline dominant rocks are stained pink by haematite inclusions developed along K-feldspar cleavage planes as a result of Fe release from original plagioclase during K-Na exchange (Kinnaird, 1985).

Potassic enrichment

K-enrichment is reflected by the development of K-feldspar (microcline) at the expense of plagioclase. As a result, K-altered metavolcanic rocks of the Isåsen Formation are pale in appearance, consisting almost entirely of quartz and microcline.

Potassic alteration involves replacement of Na, originally held in alkali feldspar, by K. The dominance of K_2O over Na_2O is illustrated in Fig. 4.2, which also shows that potassic alteration is more pronounced in the footwall of the orebody. Almost all samples are K-enriched relative to typical acid to intermediate volcanics (Fig. 4.2, red symbols). The scatter of samples away from the main K-enrichment trend not only identifies samples less affected by the alteration, but also identifies those apparently depleted in alkalis. This may be due to the inclusion of metavolcanic samples with a more basic composition, or signifies an alkali leaching event. The former possibility seems more likely, given the number of samples plotting below 60 wt% SiO_2 in Fig. 4.1. The close spatial link on a regional scale between exceptionally potassic-altered rocks and economic mineralisation suggests that the alteration event is linked to the ore-forming process.

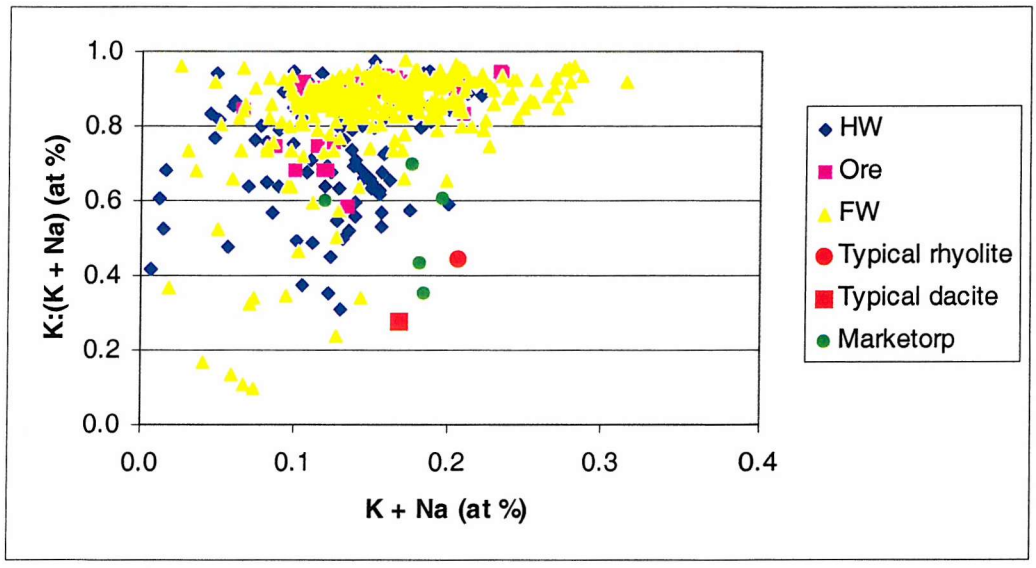

Figure 4.2: Graph to show dominance of K over Na in metavolcanic rocks from the Zinkgruvan and Isåsen formations. Samples with a K: (K + Na) ratio of near to 1 indicate replacement of Na by K. Relatively unaltered metavolcanic rocks from Marketorp (30km east of Zinkgruvan), plus a typical rhyolite and dacite are plotted for comparison (data from Cox et al., 1979). Samples are classified according to their position relative to the main ore horizon: FW = footwall; Ore = orezone; HW = hangingwall. Note that samples from the footwall show much stronger replacement of Na by K compared to many hangingwall samples. Original XRF data and laboratory procedures in Appendix E.

Mass/volume change considerations

Apparent geochemical enrichment trends can be also caused by loss of components from a rock as well as through addition. The potential for apparent K-enrichment as a function of mass and volume loss (e.g., through loss of silica) is investigated here. Removal of one or more

elements without replacement by another element can create a systematic and proportional increase in the other elements in the rock, so that they appear to be enriched.

This effect can be measured using various mass balance techniques such as those described by Gresens (1967), Grant (1986), MacLean & Kranidiotis (1987) and MacLean (1990). All these techniques are based on the fundamental assumption that some chemical components have remained immobile during the alteration process. If these immobile components are identified (commonly Ti, Zr and/or Al) they can serve to establish the relative loss or gain of other components, as they become concentrated during net mass loss and diluted during net mass gain. Mass changes can be calculated from the concentration levels of an immobile element in altered samples and their precursors.

At Zinkgruvan, the use of mass balance techniques to resolve the nature and origin of the highly potassic rocks present in the Isåsen and Zinkgruvan formations is somewhat restricted due to the relative lack of geochemical data for pristine, unaltered volcanic material. In addition, the primary geochemical variability of the volcanic sequence is difficult to assess due to the intense potassic and metamorphic overprints. In fact, it is known (section 3.2) that the volcanic sequence becomes increasingly acidic stratigraphically upwards. Therefore, the use of a least-altered sample sourced away from the mine area, if not a stratigraphic equivalent, may not be an ideal precursor for mass balance calculations involving the highly potassic samples from the mine area, but it is the best comparison available.

Geochemical data published by Allen *et al.* (1996) for an unaltered sample of syneruptive volcaniclastic rock from Godegård is used here as a comparison to K-altered metavolcanic samples from the Isåsen and Zinkgruvan formations in the mine area (Table 4.2). The pumice breccia has a fairly typical rhyolitic composition, and shows no evidence of the K-enrichment which affects most metavolcanic rocks in the Zinkgruvan Basin. A sample of porhyritic rhyolite, also from the Godegård area, shows moderately elevated levels of K_2O and slightly depleted Na_2O (Table 4.2), but no change in SiO_2 or Al_2O_3 relative to the unaltered sample.

Wt %	*Unaltered volcaniclastic sample from Godegård*	*Least altered porphyritic rhyolite from Godegård*	*K-altered sample from Zinkgruvan Fmn (454/11)*	*K-altered sample from Isåsen Fmn (454/36)*
SiO_2	74.70	74.40	69.66	65.09
TiO_2	0.20	0.22	0.38	0.43
Al_2O_3	13.00	13.20	13.26	16.19
Fe_2O_3	1.97	1.11	3.09	0.80
MgO	1.28	0.73	1.73	0.41
CaO	0.56	0.11	0.80	0.56
MnO	0.02	0.03	0.15	0.02
Na_2O	4.05	2.73	0.89	0.77
K_2O	3.14	6.46	8.75	13.55
P_2O_5	0.04	0.06	0.08	0.07
Total	98.96	99.05	98.79	98.00

Table 4.2: Comparison of unaltered and least-altered volcanic samples from the Godegård area (data from Allen et al., 1996) with K-altered volcanic samples from the Isåsen and Zinkgruvan formations in the mine area.

Comparison of the major elements from the least-altered Godegård samples with the K-altered sample from the Zinkgruvan Formation (454/11) reveals significant depletion in Na_2O and enrichment in K_2O in the altered sample, but no variation in Al_2O_3 and only minor decrease in SiO_2. Significant mass changes due, for example, to net loss of silica, would be reflected in a proportional increase **in all the other elements**, not just the K_2O component. Similar effects would be caused by volume changes, whereby the proportions of all chemical components would vary uniformly. The loss of silica is not supported by the chemical analyses of metavolcanic samples from either the Zingruvan or the Isåsen Formation.

Application of the isochon diagram described by Grant (1986), a modification of Gresens (1967) technique, shows that the best-fit line through the data equates to a zero change in mass, and also correlates to constant Al_2O_3 (Fig. 4.3A). It is apparent that there has been a small amount of silica loss (~5 wt% SiO_2), which is balanced by a proportional increase in all other elements except Al, Na and K. The shaded grey area represents the expected range of values that would be produced in other elements due to loss or gain of 5 wt% SiO_2, which equates to a proportional loss or gain of 6.3%. This trend can be attributed to alteration processes; if the decrease in silica was the result of primary igneous variation, an increase in Al_2O_3 would be expected. The depletion in Na and enrichment in K are far more pronounced, and do not fall into the shaded grey area representing the expected shift in elemental values due to the silica loss. This implies that silica loss alone cannot be responsible for these trends, although it may have contributed slightly to K increase.

The more intensely K-altered sample from the Isåsen Formation shows further depletion in SiO_2 with significant increase in Al_2O_3 and K_2O (Fig. 4.3B). However, the proportional increases in the other elements that would be expected if the lowered values of SiO_2 were due to silica loss are not observed. This, coupled with the significant increase in $^{*}Al_2O_3$ (which was shown to be immobile in the alteration of sample 454/11, Fig. 4.3A), suggests this rock has a primary dacitic character, and therefore comparisons with a rhyolitic precursor are inappropriate. The expected decrease in K_2O, which would be expected when comparing rhyolitic and dacitic rock types, is not observed due to the potassic enrichment.

In summary, the data show that the K-enrichment trends displayed by metavolcanic rocks in the mine area are most likely the result of bulk potassium addition through alkali (K-Na) exchange, rather than through mass loss of components such as silica. Apparent loss of SiO_2 and increase of Al_2O_3 in the more K-enriched samples of the Isåsen Formation are attributed to a more dacitic precursor, rather than to alteration processes. A minor amount of silica loss may have occurred during alteration as indicated by the data in Fig. 4.3A, but the geochemical variability of the original volcanic sequence is poorly constrained, so SiO_2 changes of a few per cent may also be part of the original igneous sequence.

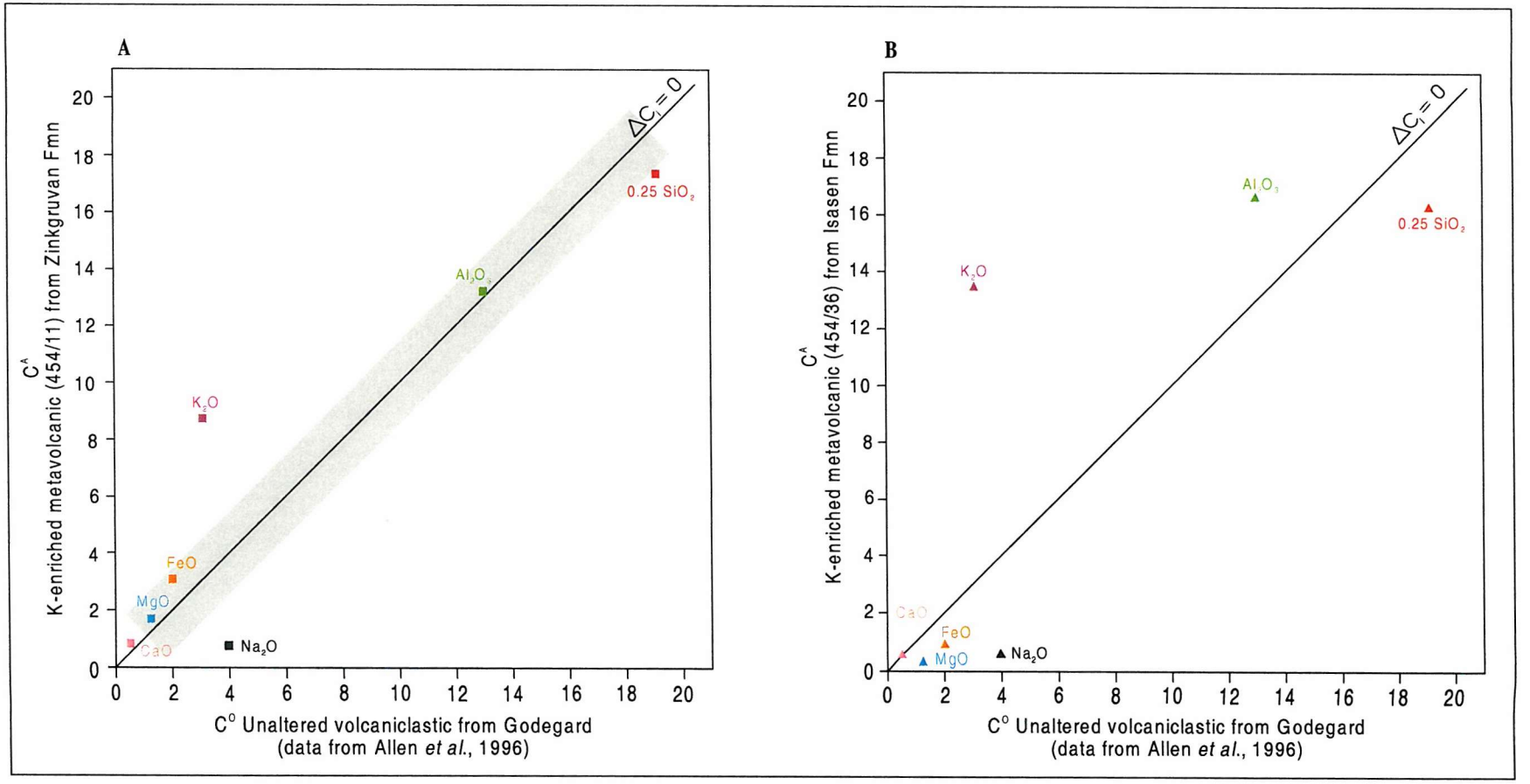

Figure 4.3: Isochon diagrams (Grant, 1986) comparing altered samples(C^A) with an unaltered volcaniclastic precursor sample (C^O) from Godegård (data from Allen et al., 1996). A) Comparison of unaltered Godegård sample and moderately K-altered metavolcanic (sample 454/11) from the Zinkgruvan Fmn in the mine area. Shaded area shows the expected range of elemental values if a loss of 5 wt% SiO_2 occurred. B) Comparison of the unaltered Godegård sample with an intensely K-altered metavolcanic sample from the Isåsen Fmn in the mine area. Depletion in SiO_2 may be partly due to loss during alteration, but is more likely a function of the more dacitic character of this sample, as is the apparent enrichment in Al_2O_3. Black line in both diagrams equates to zero mass change. See text for explanation.

The maximum K content of the metavolcanic rocks in the Isåsen and Zinkgruvan formations is ultimately limited by the Al_2O_3 content, as all K-rich minerals present (microcline + biotite) are aluminium silicates. Potassium introduced to the rock via a fluid may only be accommodated if there is sufficient Al_2O_3 to form such aluminosilicates.

Mechanisms of K-alteration are generally poorly understood. The introduction of large amounts of potassium to dacitic volcanic rocks could be accommodated in two ways, depending on physiochemical conditions at the alteration site:

i) Simple 1:1 replacement of Na by K in alkali feldspar (albite), with formation of microcline and removal of Na in solution. However, microcline is unlikely to be stable in a sub-seafloor environment unless pH is high, water activity is low and aK^+ and $aSiO_2$ are both high (Fig. 4.4). Given that hydrothermal fluids are most likely responsible for the K-alteration, low aH_2O is unlikely and the pH of the fluid is likely to be low due to fluid-rock interactions at depth.

ii) Breakdown of albite to sericite/muscovite and removal of Na in solution. Probable high water activity in the system favours formation of mica over K-feldspar (Fig. 4.4), with microcline formed later through breakdown of muscovite during prograde metamorphism (Chapter 5). A similar mechanism was suggested by Plimer (1979) for the K-alteration at Broken Hill, Australia.

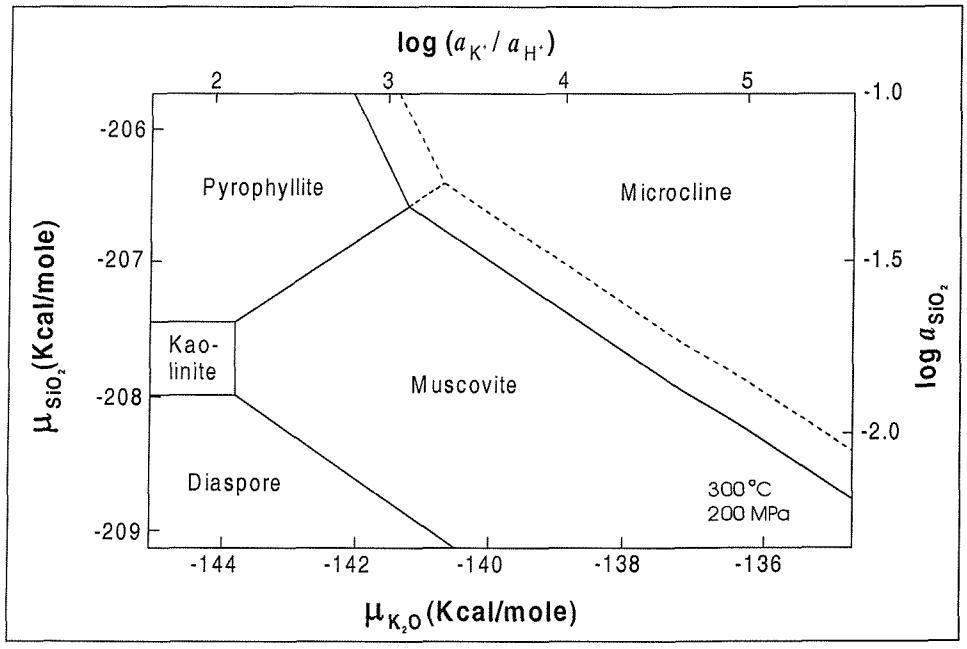

Figure 4.4: Chemical potential diagram showing the relationships between chemical potential (μ) and aqueous activity (a) in the system K_2O-Al_2O_3-SiO_2-H_2O-HCl. Note that microcline is stable under conditions of lower H^+ activity and higher silica activity relative to muscovite. Dashed line shows the expansion of the muscovite stability field under stress. Modified after Wintsch (1985).

Introduction of an aqueous fluid to the original biotite-bearing metavolcanic rocks at sub-seafloor temperatures will also cause biotite to become unstable and break down to chlorite, releasing potassium which is consumed by formation of muscovite/sericite or K-feldspar. Biotite may have re-formed during prograde metamorphism by reversal of this reaction, but the low proportion of biotite in the peak assemblage and evidence for bulk Fe loss indicates partial removal of Fe and Mg, probably at the same time as K-enrichment.

Hellingwerf (1988) suggested that localised, intense potassic alteration in the Bergslagen region took place via sericitisation, biotitisation and microclinisation processes.

Mineralogy

As a result of intense potassic alteration and amphibolite facies metamorphism, most Isåsen metavolcanic rocks consist of Qtz + Kfs (± Bt). Biotite is minor or absent in strongly K-altered samples, but is a common accessory mineral in less altered rocks, usually forming small laths aligned to define a weak foliation. Other accessory phases include tourmaline, apatite and minor opaque material. Chlorite has formed locally (usually <10 vol% of the assemblage) by late-stage alteration of biotite. Metavolcanics from areas of lower metamorphic grade usually contain muscovite in addition to microcline, and often contain heavily altered remnants of plagioclase.

Many samples show overprinting by calc-silicate minerals, particularly near the upper stratigraphic boundary with the Zinkgruvan Formation. Typical calc-silicate minerals are garnet, diopside and tremolite. Cross-cutting tremolite and/or epidote veins are a common late-stage feature.

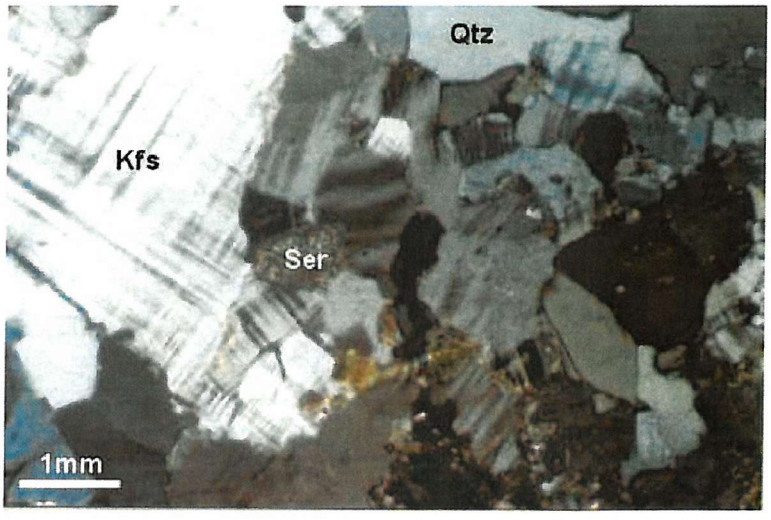

Figure 4.5: Typical Qtz + Kfs assemblage in a K-altered Isåsen Formation metavolcanic rock. Sample 454/38, Nygruvan. Cross polarised light.

4.2.2 Zinkgruvan Formation metavolcanic rocks

Variable potassic alteration, admixed carbonate material and calc-silicate alteration make these rocks more heterogeneous than the Isåsen Formation. K_2O content is typically 5-7 wt% and tends to be greater stratigraphically below the orebody. Locally, and especially near the Isåsen Formation, K_2O contents reach 12 wt%. Higher SiO_2 and lower Al_2O_3 (12-13 wt% rather than 13-16 wt%, Table 4.1) than the Isåsen Formation probably reflect a more rhyolitic (rather than dacitic) protolith. MgO and FeO (total) also tend to be slightly higher in Zinkgruvan Formation metavolcanic rocks, reflected in the greater abundance of biotite which is scarce or absent from the intensely K-altered rocks of the Isåsen Formation. This may be due to large-scale mobilisation of Fe and Mg during intense K-alteration.

Metavolcanic rocks affected by calc-silicate skarn development (as described in section 3.2.2) typically show increased levels of CaO and MgO, contributed by diffusion of chemical components from adjacent metacarbonate units.

Mineralogy

A typical metavolcanic rock from the Zinkgruvan Formation contains the assemblage Qtz + Kfs + Pl + Bt ± Sil ± Grt (Figs 4.6A & B). Sillimanite is a common component, usually developed due to low K_2O and Na_2O rather than excess Al_2O_3. Its general absence from Isåsen Formation metavolcanic rocks is due to formation of microcline where K is abundant. Garnets occur scattered throughout the rocks, usually as isolated crystals, but siliceous garnet-rich horizons and magnetite skarns as described in section 3.2.2 are common in Nygruvan.

K-feldspar (microcline) is common, with muscovite occurring in lower grade regions and as a retrograde overprint. Where calc-silicate minerals are developed diopside is dominant, with lesser garnet, zoisite, wollastonite and tremolite. A gradation in mineralogy and geochemistry is observed between 'pure' metavolcanic material and 'pure' calc-silicate skarn, described in sections 4.5 and 4.6.

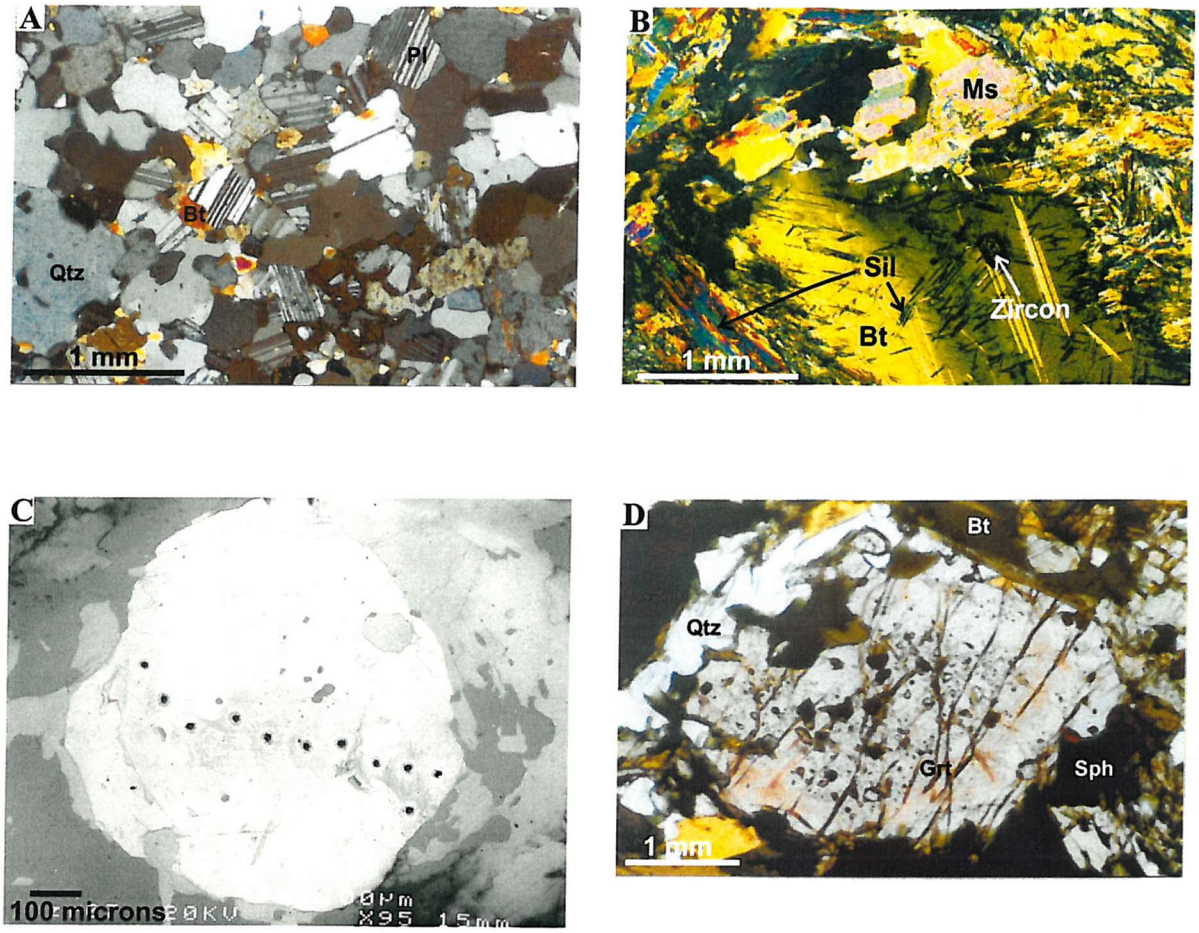

Figure 4.6: Mineralogical features of metavolcanic rocks from the Zinkgruvan Formation

A) Typical Qtz + Pl + Bt (+ Kfs) assemblage in relatively unaltered metavolcanic rock. Sample 454/08, Nygruvan. Cross polarised light.
B) Sil-bearing metavolcanic assemblage containing retrogressive Ms. Sample 454/01, Nygruvan. Cross polarised light.
C) SEM EDS image showing ablation pits caused by LA-ICPMS traverse. Note deviation to avoid quartz inclusions (darker grey patches). Sample 1557/09, Burkland.
D) Garnet with inclusions of Qtz and Bt. Note concentration of inclusions towards centre of garnet, and lack of inclusions near rim. Biotite in this sample is unusually Fe-rich and green. Sample 454/13 (garnet-biotite horizon), Nygruvan. Plane polarised light.

Garnet-rich horizons

Garnets are locally common, occurring as isolated, scattered crystals and concentrated horizons. Horizons of intense garnet nucleation commonly contain disseminated sphalerite. Rare earth element (REE) and yttrium (Y) profiling of garnet crystals carried out using laser ablation inductively-coupled plasma mass spectrometry (LA-ICPMS) combined with major element mapping suggests that these garnets developed at or shortly after peak metamorphism.

Major element zonation is a well-documented feature in metamorphic and igneous garnets (e.g., Atherton & Edmonds, 1966; Hollister, 1966; Yardley, 1977). Research shows that high temperature metamorphism (>600°C) causes homogenisation of major element zonation due to increased diffusion rates for most major divalent cations (Woodsworth, 1977; Yardley, 1977; Cygan & Lasaga, 1985; Spear & Kohn, 1996). However, several studies (e.g. Hickmott *et al.*, 1987; Lanzirotti, 1995; Bea *et al.*, 1994; Bea *et al.*, 1997) have found that REE and trace element zonation patterns are preserved under these conditions, despite major element homogenisation. In addition, Bea *et al.* (1997) showed that the Gd/Dy ratio in zoned garnets can be correlated with increasing metamorphic pressure, and is apparently independent of temperature, bulk rock composition and whole rock REE abundance.

In natural systems, HREE's and yttrium are preferentially partitioned into garnets over other major silicate mineral phases (Yang *et al.*, 1999; Lanzirotti, 1995) and accessory minerals such as xenotime, monazite, apatite and zircon also form HREE sinks. Consequently, trace element zonation in garnet is highly sensitive to changes in the accessory mineral assemblage and to changes in bulk rock or fluid chemistry. This means that garnets often preserve a detailed record of the reaction history of the rock.

Zonation of yttrium in metamorphic garnets has been studied in depth by Jaffe (1951), Lanzirotti (1995) and Pyle & Spear (1999). Yttrium is almost exclusively accommodated in garnet and xenotime (YPO_4), with lesser amounts in the other accessory phases listed above. The mechanisms responsible for yttrium zonation in garnets are poorly understood and may be attributed to several processes, including fluid infiltration, growth zoning, resorption, changes in growth rate and the breakdown of yttrium-rich phases (Lanzirotti, 1995). Pyle & Spear (1999) showed that the degree of yttrium zonation in garnets is strongly related to the amount of xenotime in the rock matrix and as inclusions within the garnet itself.

Backscattered electron imagery and X-ray element mapping techniques on the SEM detected no variation in major element concentration, and SEM spot analyses revealed only very minor variation in MnO, MgO and FeO across individual garnet crystals from garnetiferous horizons (Figs 4.7B & C). The flat major element profile is consistent with crystallisation or homogenisation at high metamorphic temperatures. Overprinting textures demonstrate that the majority of garnet growth in these horizons post-dates the main S_1 fabric-forming phase, hence the

peak thermal phase of metamorphism outlasted the main fabric-forming event (see chapters 2 & 3).

The distribution patterns of rare earth elements across the same garnet crystals display distinct zonation (Figs 4.7A & 4.8A), commonly showing a higher abundance of heavy rare earth elements in the core (Fig. 4.8B). In some samples the ratio of HREE:LREE oscillates in symmetric zones across the crystal (Fig. 4.8A), often mirrored by the yttrium concentrations. The presence of such HREE-rich bands is representative of a change in the physiochemical conditions at that time in the garnet's growth history; either a change in the abundance of HREE and Y, or a change in their distribution coefficients.

Garnet crystals in these horizons consistently show a pronounced negative Eu^{2+} anomaly (Fig. 4.8B). This not unusual for many metamorphic garnets (Hickmott & Spear, 1992; Schwandt *et al.*, 1993; Bea *et al.*, 1997), but it does indicate probable oxidising conditions at the time of garnet growth, which may explain the unusual dominance of Fe^{3+} over Fe^{2+} in stoichiometric calculations for many garnets from these horizons (Table 4.3; Appendix F). Similar studies on garnets from garnetite horizons at Broken Hill, Australia have shown that the Eu anomaly varies with proximity to mineralisation (Schwandt *et al.*, 1993), with positive Eu anomalies occurring proximal to the ore, and negative anomalies in more distal locations. However, Schwandt *et al.* (1993) concluded that the REE patterns were more likely inherited from the pre-metamorphic protolith rather than hydrothermal fluids.

A

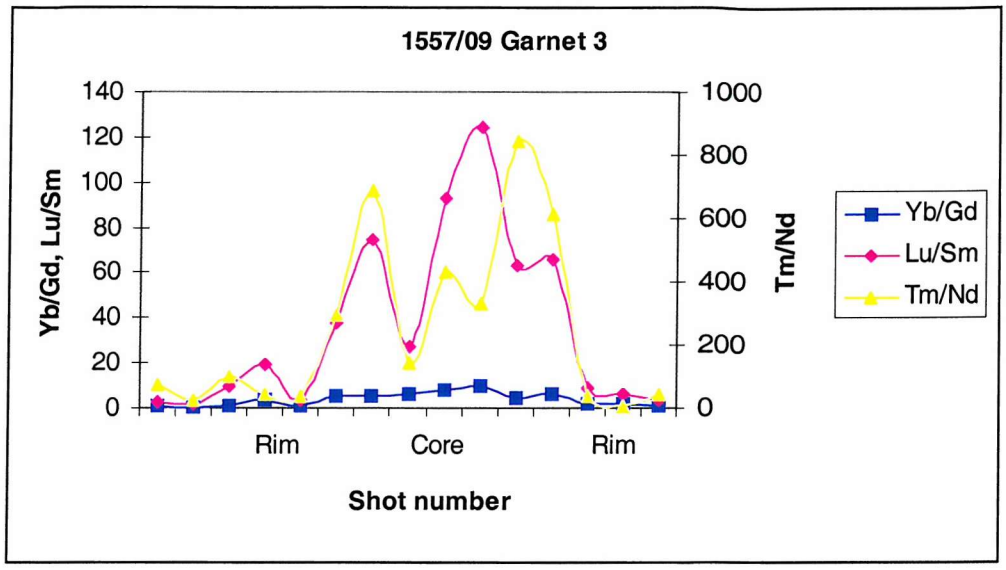

B

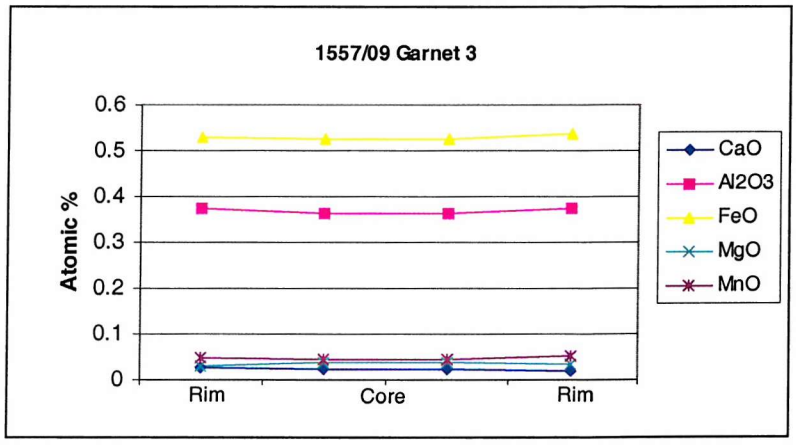

C

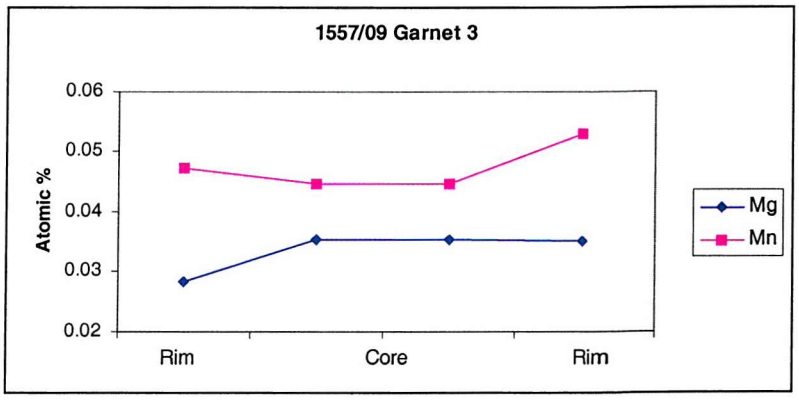

Figure 4.7: A) LA-ICPMS rare earth element profile across a garnet crystal from sample 1557/09. Values are plotted as a ratios of HREE:LREE. Note the high abundance of the heavy rare earth elements in the core relative to the rims. See Appendix G for method and original data.. B) Plot to show flat major element profiles across the same garnet crystal, using SEM analyses (Appendix F). C) Enlarged view of Mg and Mn variations to show the slight variation in concentration from core to rim.

A

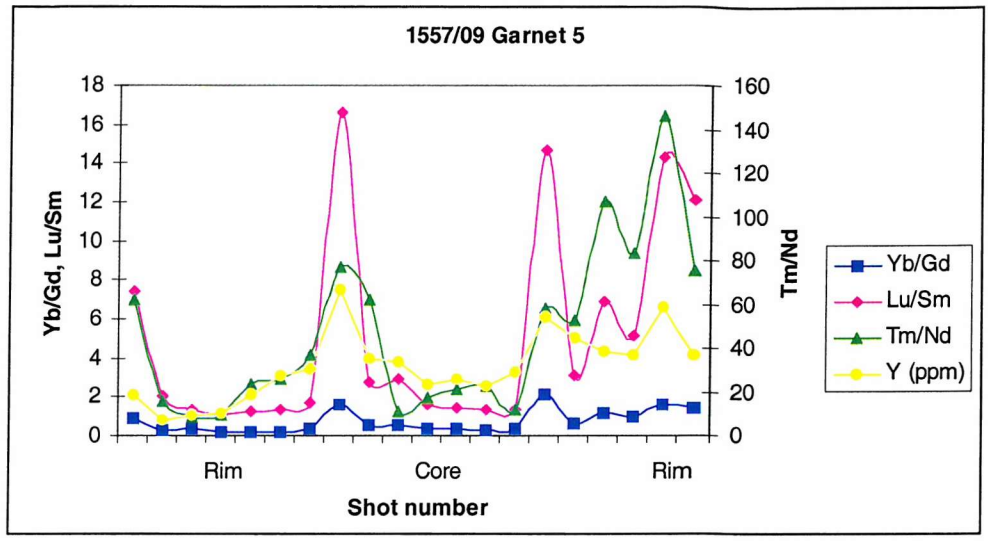

B

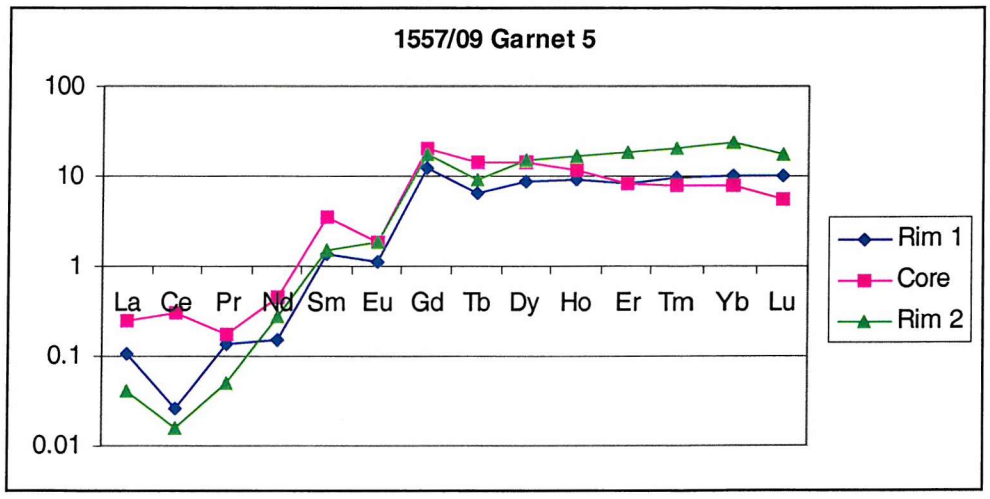

Figure 4.8: A) REE profile across a garnet from sample 1557/09 showing oscillatory zoning of HREE:LREE ratios and yttrium values. Note the presence of an HREE-enriched band adjacent to the core of the crystal. B) Logarithmic plot (normalised to Y) showing the increased abundance of HREE relative to LREE in the same garnet crystal for analyses taken at the core and rims. Note the negative Eu anomaly and somewhat flattened profile at the HREE end, which is typical of garnet formation at high temperatures.

Garnetiferous horizons contain Fe-rich almandines (Table 4.3) with minor Mn, and are usually accompanied by abundant dark green biotite containing around 35 wt% Fe oxide (Fig. 4.6D). Most garnet crystals comprise a core with abundant quartz and biotite inclusions surrounded by an inclusion-free rim (Fig 4.6D). This pattern is most likely to have been caused by rapid growth in the early stages of development, followed by a slower growth phase or change in growth mechanism.

	Garnet		***Green biotite***	
Sample No.	**1557/09** ***(n = 8)***		**670/04** ***(n = 4)***	
	wt % oxide	S.D	wt % oxide	S.D
SiO_2	37.55	1.22	35.27	0.61
TiO_2	-	-	0.68	0.08
Al_2O_3	18.39	0.91	12.58	0.34
FeO (total)	38.05	1.23	34.83	0.30
MnO	3.00	0.75	0.30	0.08
MgO	1.97	0.86	5.33	0.26
CaO	1.09	0.20	0.09	0.05
Na_2O	-	-	-	-
K_2O	-	-	8.38	0.45
H_2O	-	-	3.00	0.00
Total	100.05		100.46	
Si	3.03	0.08	5.77	0.06
Al	1.86	0.09	2.22	0.06
Al	-	-	0.20	0.06
Ti	-	-	0.08	0.01
Fe2+	1.12	1.33	4.77	0.07
Fe3+	1.54	0.07	-	-
Mn	0.21	0.05	0.04	0.01
Mg	0.24	0.10	1.30	0.07
Ca	0.09	0.02	0.02	0.01
Na	-	-	-	-
K	-	-	1.75	0.08
OH	-	-	3.28	0.03
O	12.00	0.00	24.00	0.00

Table 4.3: SEM geochemical analyses and stoichiometry of minerals found in garnet-rich horizons within the Zinkgruvan Formation metavolcanic sequence. Chemical data in weight %; stoichiometry in ionic proportions. Fe^{3+} not calculated for biotite as it is a hydrous phase. S.D = standard deviation. Original data in Appendix F.

The garnets in these horizons range in size up to >3 cm in diameter, although most are between 0.3-0.6 mm in diameter. The abundance, anhedral shape and internal structure of these garnet crystals suggests rapid nucleation and growth at or shortly after peak metamorphism. However, the cause of growth is enigmatic: influx of a silica-bearing fluid is necessary, either containing high concentrations of Fe, or infiltrating an exceptionally Fe-rich horizon. There is no unequivocal evidence to prove one theory over the other, although given the spatially restricted nature of these garnetiferous horizons, a siliceous fluid exploiting a pre-existing Fe-rich layer is more plausible. The concentration of sphalerite along these horizons may be due to remobilisation by fluid, but is equally likely to be a primary feature. A late-stage fluid event occurring at elevated temperatures is supported by the overprinting texture, flattened REE profiles and homogenised major element distribution. The timing of this event is likely to be at peak or shortly after peak metamorphism.

Garnets from magnetite skarn horizons (DDH 451, eastern Nygruvan) show similar REE zonation patterns (figs 4.9 & 4.10) and textural relationships, indicating that these horizons are also likely to have formed as a result of fluid infiltration. However, garnets from these skarn horizons show REE concentrations of an order of magnitude greater than those measured from garnetiferous horizons in the metavolcanic sequence (sample 1557/09). Elevated REE concentrations may reflect higher REE levels in the fluid accompanying skarn formation, but may have been inherited from the protolith, as the bulk mineralogy and major element chemistry of the garnets from the skarns are greatly different from those of the garnetiferous horizons found within the metavolcanic sequence.

A

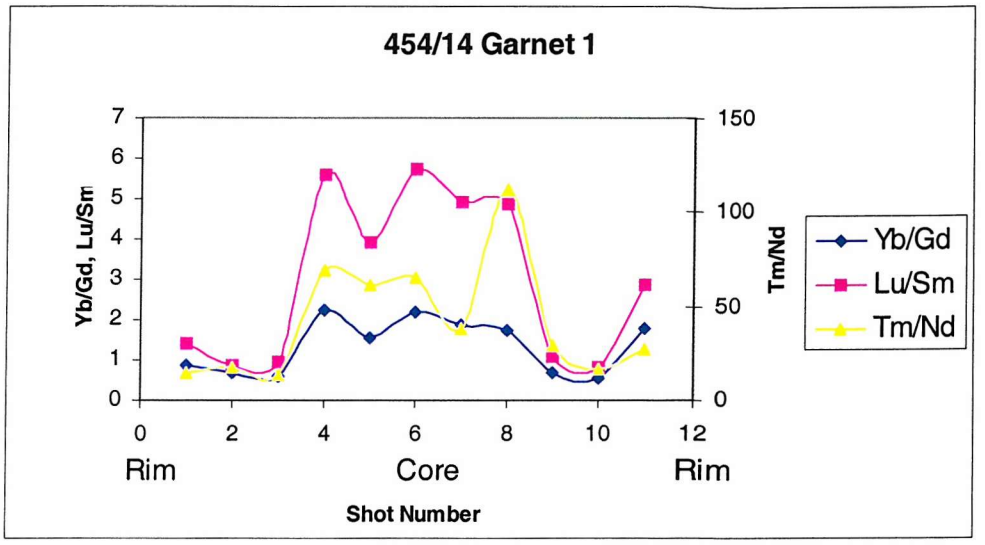

B

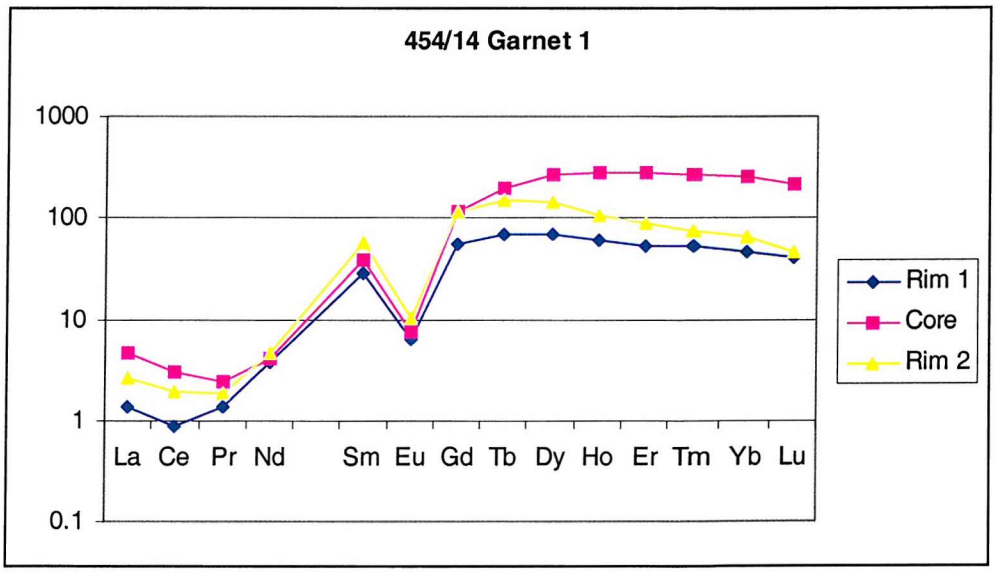

Figure 4.9: A) REE profile across a garnet from sample 454/14 (Fe skarn) showing zoning of HREE:LREE ratios B) Plot (Normalised to Y) showing the increased abundance of HREE relative to LREE in the same garnet crystal for analyses taken at the core and rims. Note the pronounced negative Eu anomaly and somewhat flattened profile at the HREE end, which is typical of garnet formation at high temperatures.

A

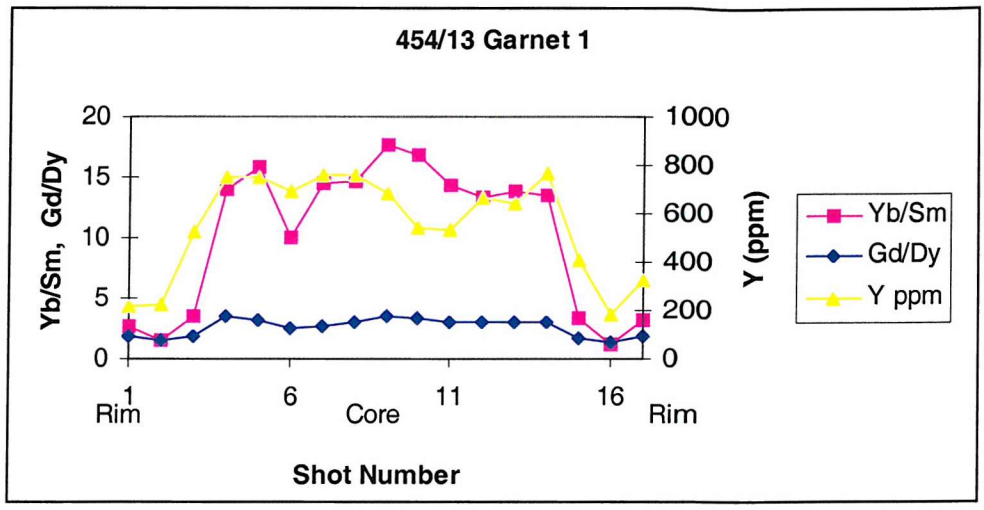

B

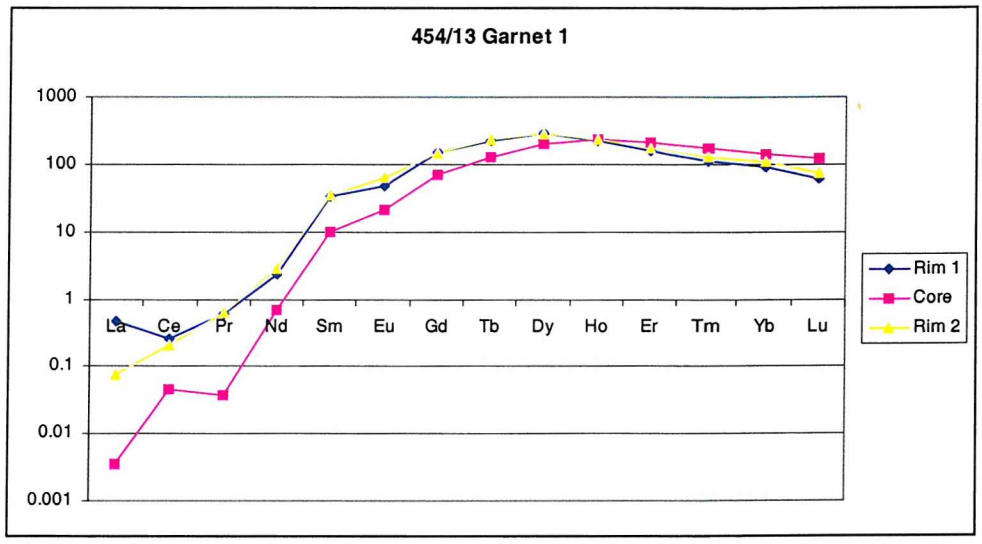

Figure 4.10: A) REE profile across a garnet from sample 454/13 (Fe skarn) showing zoning of HREE:LREE ratios and yttrium levels B) Plot (normalised to Y) showing the increased abundance of HREE relative to LREE in the same crystal. Note the lack of negative Eu anomaly and the shape of the profile at the HREE end, which is typical of garnet formation at high temperatures.

4.2.3 Summary of geochemistry of metavolcanic rocks

- Metavolcanic rocks of the Isåsen and Zinkgruvan formations are intermediate to acidic in composition. Isåsen Formation volcanics appear to be more dacitic than the stratigraphically higher Zinkgruvan Formation.
- Isåsen Formation metavolcanic rocks have been subject to intense early-stage potassic alteration (probably sub-seafloor), resulting in the removal of biotite and plagioclase, and the widespread development of K-feldspar. Stratigraphically equivalent areas of lower metamorphic grade away from the mine also contain muscovite.
- Metavolcanic rocks of the Zinkgruvan Formation are variably enriched in potassium.
- Potassic alteration is most pronounced in the footwall of the orebody, although most metavolcanic samples from Zinkgruvan and the surrounding area are enriched in potassium relative to typical acidic and intermediate volcanic rocks.
- Potassic alteration took place by alkali exchange, with the majority of K-altered samples showing significant or total depletion in Na_2O.
- REE and major element zonation in almandine garnets from garnetiferous horizons within the Zinkgruvan metavolcanic sequence shows that they formed at or shortly after peak metamorphism as a result of fluid influx, either Fe-rich or exploiting a pre-existing Fe-rich layer. Negative Eu^{2+} anomalies in most samples indicate that the fluid was probably oxidising.

4.3 GEOCHEMISTRY OF METACARBONATE ROCKS

4.3.1 Dolomitisation and Fe-Mn enrichment

The metacarbonate units comprise a combination of carbonate and calc-silicate minerals, the relative proportions of which define a simple classification scheme outlined in section 3.2.2. Regardless of the quantity of calc-silicate minerals present in the rock, the metacarbonate rocks can be divided according to the relative proportions of Ca to Mn, Mg and Fe* (Fig. 4.11):

a) Calcite-normative marbles: Whole rock Ca:Ca+Mn+Mg+Fe* molar ratio is > 0.5
b) Dolomite-normative marbles: Whole rock Ca:Ca+Mn+Mg+Fe* molar ratio is ~ 0.5.

These terms are used independently of the carbonate content of the rocks, which varies from 100% in pure marbles to zero in pure calc-silicate rocks. Although most calcite-normative marbles do contain calcite as the dominant carbonate phase, dolomite-normative marbles are not now usually dominated by dolomite. This is due to the consumption of dolomite through prograde metamorphic reactions (Chapter 5) to leave calcite as the dominant carbonate, with Mg, Mn and Fe originally contained in the dolomite now forming calc-silicate minerals within the marble assemblage.

Fig. 4.11 shows the geochemistry of marble samples from around the Zinkgruvan district, plus a number of samples taken from elsewhere in the Bergslagen Province to act as an unaltered comparison. The X-axis in Fig. 4.11 shows the percentage of Ca+Mn+Mg+Fe* present in non-carbonate form. Non-carbonate metal is mostly contained within calc-silicate minerals with a minor amount in sulphides and oxides. Fig. 4.11 uses calculated non-sulphide Fe* (see Appendix E), and the small amount of Fe now forming magnetite was originally contained within forsterite so it is considered a valid part of the non-carbonate metal budget. Formation of calc-silicates in a pure metacarbonate rock requires the presence of silica, so the spread of data along the X-axis is an indication of silica content.

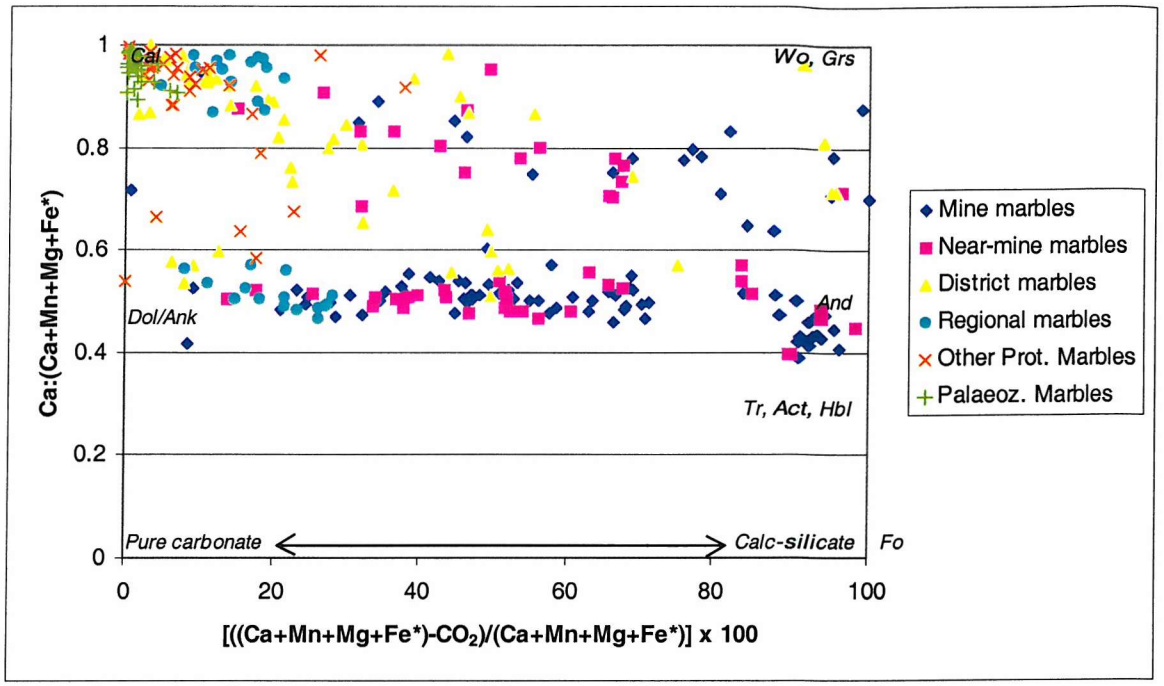

Figure 4.11: Geochemistry of marbles and calc-silicate rocks from the Zinkgruvan Basin. Samples fall into two trends: calcite-normative (Cal) marbles with a Ca:(Ca+Mn+Mg+Fe) ratio of around 1.0, and dolomite-normative (Dol/Ank) marbles with a ratio of 0.5. Horizontal linear trends are created by the variable quantity of silica in the samples, expressed as % calc-silicate minerals following metamorphism. Other Proterozoic and Palaeozoic marbles from Bergslagen are plotted for comparison. Typical compositions for common calc-silicate minerals are marked for reference. Data are expressed as atomic %. See Appendix E for original XRF data.

Two clear geochemical trends are apparent in Fig. 4.11. Calcite-normative marbles contain Ca:(Ca+Mn+Mg+Fe*) ratios of 0.65 to 1.0 (pure calcite plots in the top left corner), and dolomite-normative marbles have ratios of around 0.5 (pure dolomite plots at 0.5 on the Y-axis). Marble samples from the mine area are dominantly dolomite-normative, whilst district samples are dominantly calcite-normative. Approximately 75% of mine samples are dolomitised, and most of these are stratigraphically below the ore. Approximately 25% of district and regional marbles are dolomitic. Both calcitic and dolomitic marble samples from the mine contain more calc-silicate minerals than district samples and regional samples (as shown by the spread of data to the right in Fig. 4.11). Almost all metacarbonate rocks from the mine area contain more FeO* + MnO than district and regional samples (Figs 4.12 & 4.13).

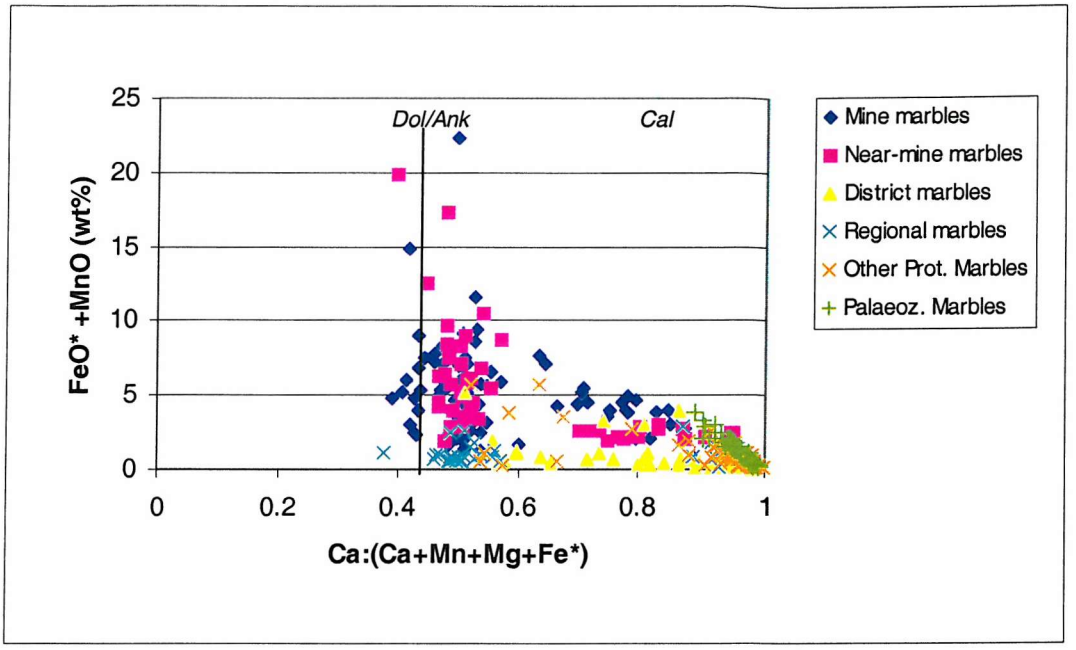

Figure 4.12: Fe-Mn enrichment in marbles in the mine area relative to district and regional marble samples. Dolomite-normative marbles are generally more enriched in FeO + MnO than calcite-normative samples. Note the clear segregation of mine (blue), near-mine (pink) and district (yellow) calcitic samples in terms of Fe-Mn enrichment. Other Bergslagen Proterozoic and Palaeozoic marbles are plotted for reference. Original data presented in Appendix E.*

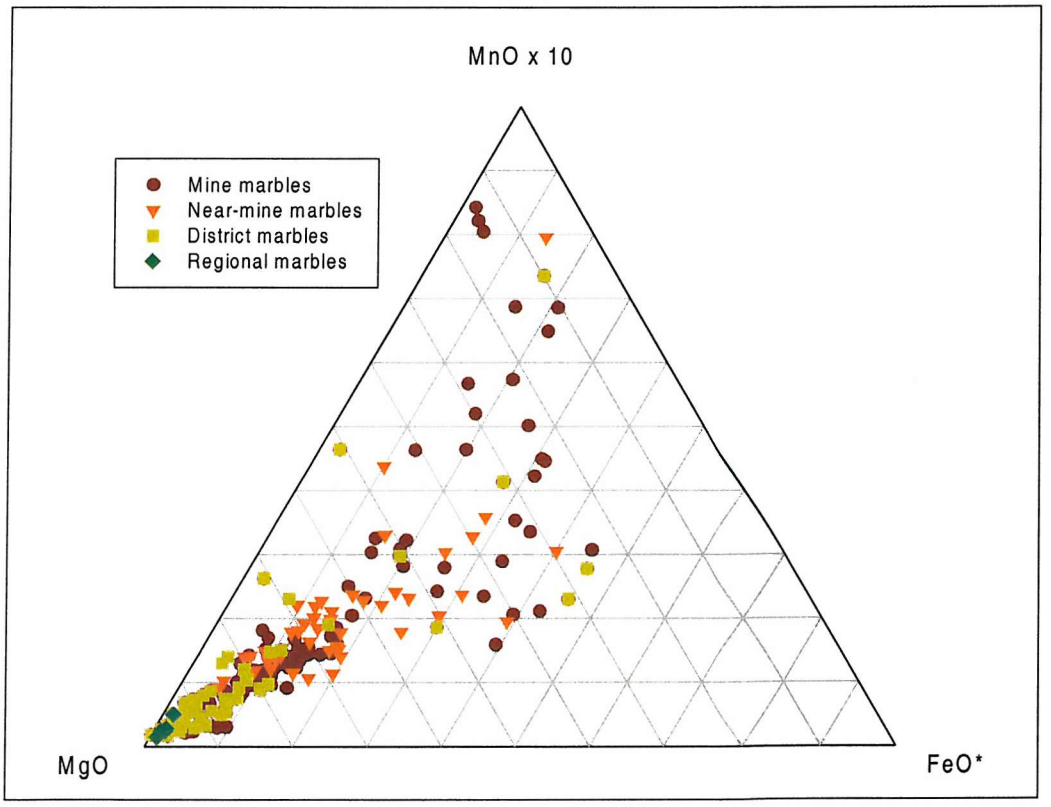

Figure 4.13: Relative proportions of MgO:MnO:FeO in marbles from the Zinkgruvan Basin. All values plotted are molar values. Mn contents are x10 to enhance trend. Original data in Appendix E.*

Most district samples and all regional samples show little Fe-Mn enrichment and represent a background against which altered samples can be compared. Most district and all regional metacarbonate rocks contain <1 wt% FeO* + MnO (Fig. 4.12), regardless of the dominant carbonate phase. In contrast, marbles from the mine area display significantly different degrees of Fe-Mn enrichment. Calcite-normative marbles contain up to 5 wt% FeO* + MnO (held in tremolite/diopside), whereas dolomite-normative samples contain up to 10 wt% FeO* + MnO (held in diopside, dolomite & forsterite), with a few samples extending to 20 wt%. This difference is due to the limited substitution of Fe and Mn for Ca in calcite compared to the ease of replacing Mg in dolomite. The FeO* + MnO content in calcite-normative marbles in the mine area may be accounted for by their minor dolomite component.

Fe*-Mn enrichment was probably accommodated by the development of ankerite (Ca(Mg, Fe, Mn)$(CO_3)_2$), which is distinguished from dolomite by a Mg:Fe (+ Mn) ratio of ≤ 4:1 (Deer *et al.*, 1992). Ankerite and dolomite both contain Ca: (Ca+Mn+Mg+Fe*) ratios of 0.5, so in figs 4.11 and 4.12, dolomite and ankerite plot along the same line. In thin section, ankerite is not observed, having broken down during prograde metamorphic reactions (Chapter 5). However, in several samples calcite and dolomite are still ferroan in composition (determined through thin section staining and supported by SEM analyses; Appendices D and F). Most Mg, Mn and Fe originally forming ankerite is now contained within calc-silicate minerals such as tremolite, diopside, forsterite etc.

The relative timing of the dolomitisation and Fe-Mn enrichment events is very difficult to ascertain. It is possible that only one dolomitisation event is responsible for both Mg and Fe-Mn enrichment, with normal dolomitisation occurring over most of the Zinkgruvan district except in the mine area, where fluids were anomalously high in Fe and Mn. Given the localised occurrence of the Fe-Mn enrichment, it is likely to be linked to the mineralisation event. However, hydrothermal fluids that have circulated through the crust are usually depleted in Mg, having lost it through fluid-rock reactions (e.g., chloritisation) at an early stage of hydrothermal circulation. It is more likely that regional dolomitisation occurred in the upper parts of the hydrothermal system via down-pull of seawater, which then may have been incorporated into the larger-scale, deep-seated hydrothermal circulation which generated alkali metasomatism and mineralisation. Fe-Mn enrichment then occurred via expulsion of mineralised fluids either at the surface (forming Fe-Mn-rich carbonate precipitates) prior to the main stage of Zn-Pb mineralisation, or below the surface by replacement of Mg by Fe and Mn in dolomites. This issue is discussed further in Chapter 8.

4.3.2 Silica addition

Marbles at Zinkgruvan show variable silica content (Fig. 4.14). The addition of silica to a carbonate rock prior to or during metamorphism results in the development of calc-silicate minerals during prograde metamorphism (Chapter 5), with silica derived from admixed detrital quartz or introduced in solution. Silica may also be introduced via short-distance transport from adjacent or enclosing metavolcanic or siliclastic units.

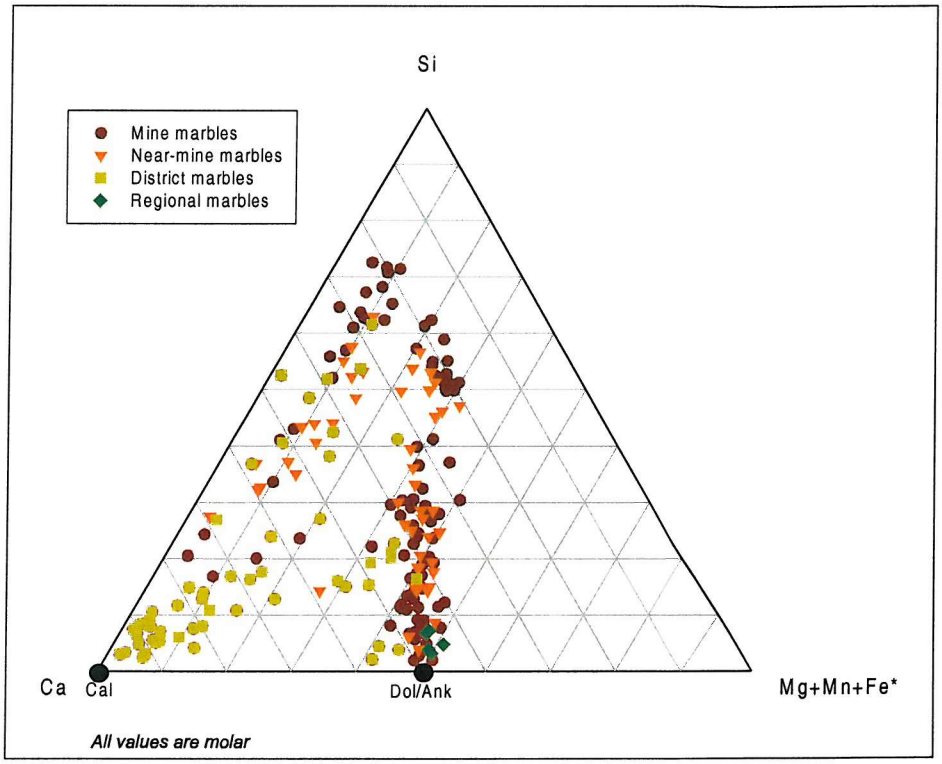

Figure 4.14: Ternary plot showing the silica content in mine and near-mine marble samples relative to district and regional samples. Ratios used are molar ratios. XRF laboratory procedures and original data in Appendix E.

Most calcite-normative and dolomite-normative marbles in the mine area contain more silica than the majority of district and all regional samples (Figs 4.14 & 4.15). District samples contain up to 20 wt% SiO_2. A continuum exists between originally near-pure carbonate rocks and carbonate-free metavolcanics and their metamorphosed equivalents.

In some samples, high silica content has produced free quartz in mineral assemblages where the silica exceeds the quantity of metals required to form calc-silicate minerals. In these cases, the rocks cannot be considered to be true marbles. The apparently strongly silicified samples (>52 wt% SiO_2, Fig. 4.15) represent calc-silicate skarn reaction zones between metacarbonate units and adjacent quartzofeldspathic units (discussed further below).

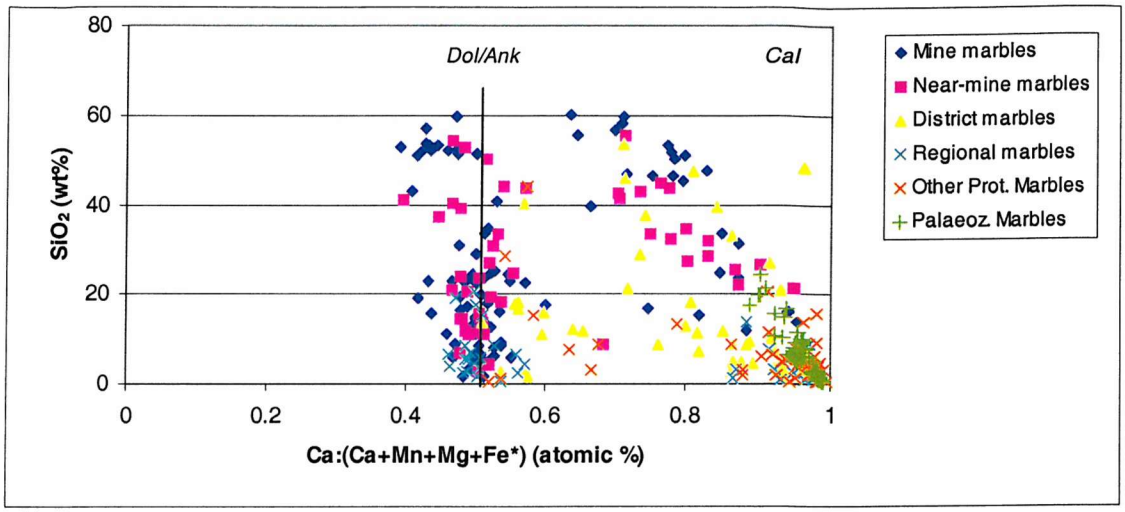

Figure 4.15: Silica enrichment trends in mine area metacarbonate samples relative to district and regional samples. Samples containing >50 wt% SiO_2 are calc-silicate rocks mainly comprising massive diopside. Other Bergslagen Proterozoic and Palaeozoic marbles are plotted for comparison. Laboratory procedures and original data in Appendix E.

Silica source

The 0-15 wt% SiO_2 content in most district samples suggests it was an original component of the carbonate sediment. The two most likely silica sources are primary or reworked volcanic material, and pelitic sediment, which are difficult to distinguish geochemically. Given the regional setting (Chapter 2), the proximity of the Godegård volcanic centre (Allen *et al.*, 1996), the widespread occurrence of thin volcanic layers in marble units, and the apparent lack of significant metasedimentary units in this part of the stratigraphic sequence, it is most likely that the silica was sourced from volcanic ash. The regional marble samples from Glanshammar are very clean, mostly containing <10 wt % SiO_2.

If the silica present in the marbles is sourced from volcanic ash, affected samples should show some chemical characteristics similar to the metavolcanic rocks of the underlying Isåsen and enclosing Zinkgruvan formations. The two main chemical components of these volcanic rocks are Si and Al, so if silica in marbles is wholly sourced from ash input and/or reworked volcanic material, the Si:Al ratios in the marbles should be similar to those observed in the metavolcanic rocks.

Metavolcanic rocks around the region contain an average Si:Al ratio between 4 and 7 (Fig. 4.16), which can be considered as the background level for the Zinkgruvan district. The majority of marble samples are consistent with this, but some contain silica levels far in excess of the background value.

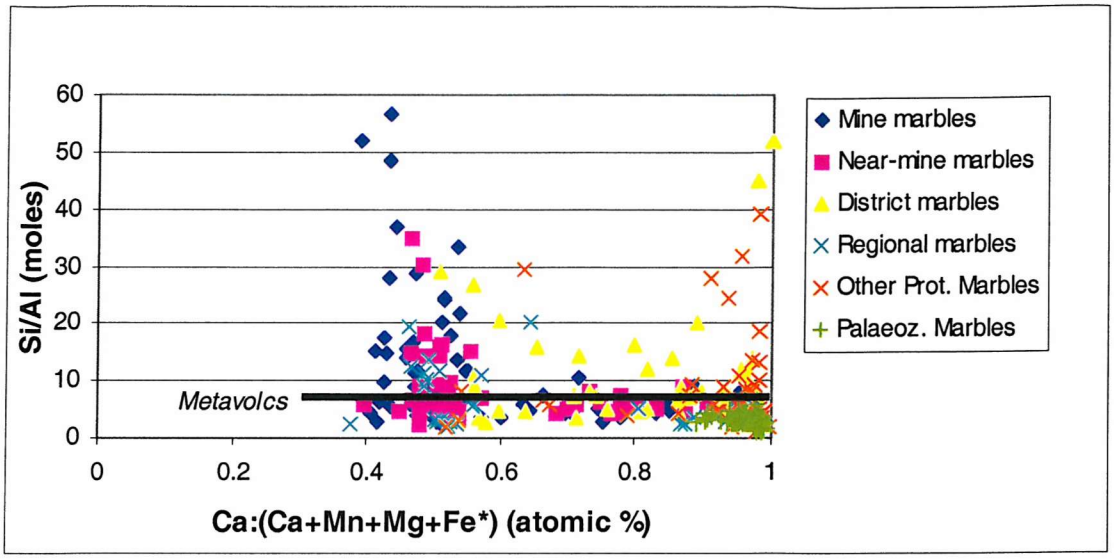

Figure 4.16: Plot to show molar Si:Al ratios in marbles. Black line shows typical Si:Al ratios in Isåsen and Zinkgruvan Formation volcanics. Note that although Si:Al ratios in the regional samples from Glanshammar appear to be higher than the metavolcanics, the absolute values are very low. See Appendix E for laboratory procedure and original data.

Fig. 4.16 shows that the majority of the district samples contain Si:Al ratios similar to the local metavolcanic rocks, suggesting a volcanic ash component. Regional samples from Glanshammar are variably enriched, but most samples plot below the metavolcanic Si/Al ratio.

District samples with Si:Al ratios >20 are from the band of metacarbonate rock running E-W near Lake Höksjön and an outcrop at Tybble (see Fig. 3.1 and Appendix B). In these areas, increased SiO_2 content without corresponding Al_2O_3 increase indicates an additional silica source unrelated to volcanic ash input. In both areas, the marble outcrop occurs close to K-altered volcanics. K-rich metasomatic fluids may be responsible for the silica input into marbles in this area, although potassium is only slightly increased in these samples. Detrital quartz is also a possibility.

The bulk of marble samples containing higher than background Si:Al ratios are dolomite-normative rocks in the mine area, although many mine and near-mine samples contain Si:Al ratios consistent with the volcanic material. All available thin sections have been checked to confirm that all samples plotted are marbles and not calc-silicate rocks, but some data supplied by the mine do not have accompanying mineralogical data. Geochemically, calc-silicate skarns can be separated from silica-enriched marbles using the absolute content of SiO_2, which is higher in calc-silicate rocks than in true marbles (Fig. 4.17). Even discounting the rocks which are shown to be calc-silicate skarns rather than marbles, many marble samples still show anomalously high Si:Al ratios relative to the district background level (Fig. 4.16), indicating localised SiO_2 enrichment in the mine area.

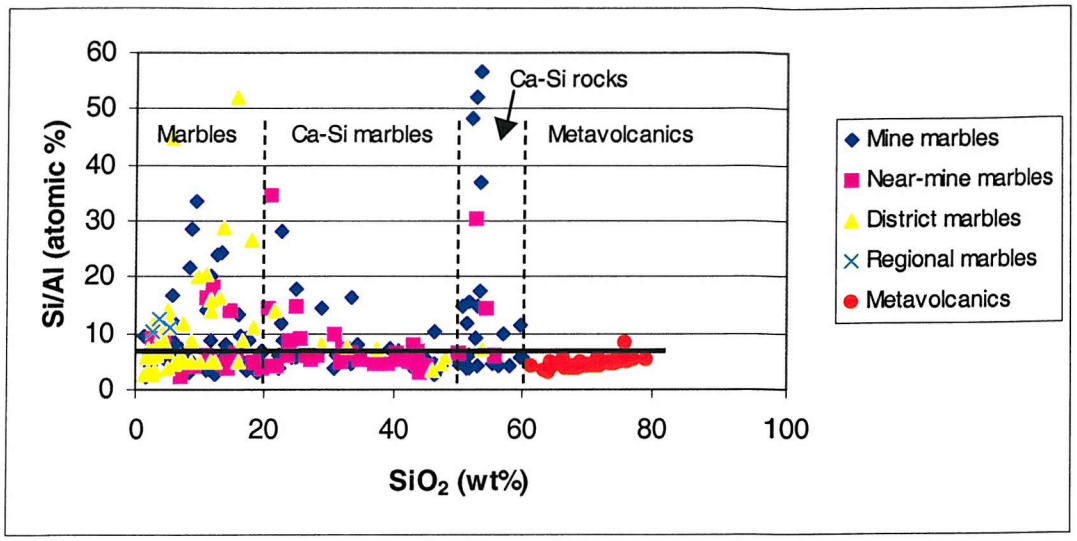

Figure 4.17: Plot of SiO_2 (wt%) vs Si/Al (atomic %) to discriminate between marbles containing volcanic ash (plotting below black line), Si-enriched marbles (plotting above black line) and calc-silicate skarns which form a vertical linear trend at ~50 wt% SiO_2. Metavolcanic rocks (red circles) are plotted for reference. A compositional continuum exists between near-pure marbles and metavolcanic rocks as a result of mixing of volcanic ash and carbonate at the time of deposition, and interaction between adjacent units during metamorphism. Original data and laboratory procedure in Appendix E.

At Brännlycken (Fig. 3.1), the metamorphic interaction of carbonate rock with thin siliceous bands (probably volcanic ash layers) is clearly illustrated in the development of numerous green calc-silicate bands (Fig. 4.18).

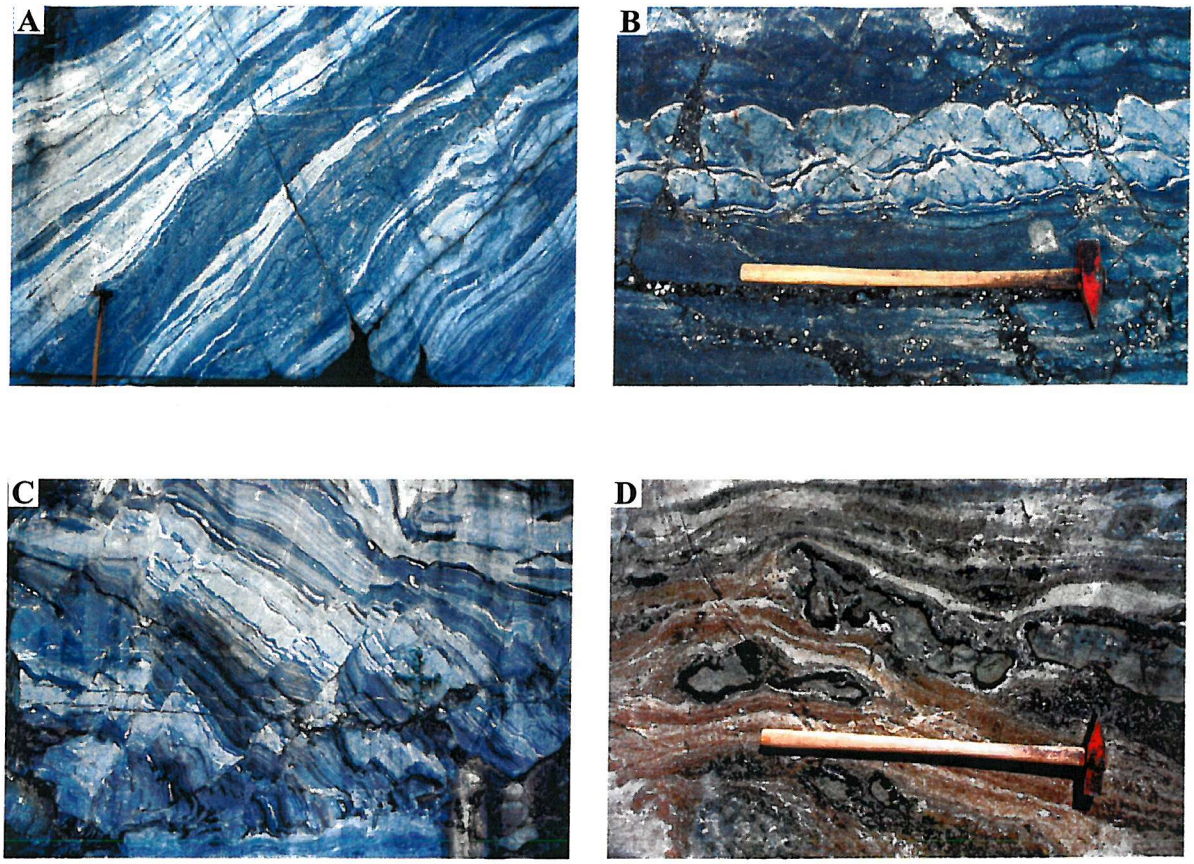

Figure 4.18: Calc-silicate marble at Brannlycken quarry
A) Parallel bands of calc-silicate material (grey-green) and marble (white), developed t hrough metamorphic interaction between carbonate and silicate layers during prograde metamorphism. Geological hammer is approx. 60 cm long.

B) Close-up view of calc-silicate layers developed in marble. Darkest material is serpentine/forsterite-rich, palest material is calcite-dolomite with diopside. Note the apparent boundinage of the upper, thinner calc-silicate layers with dark serpentine-rich enclosing the individual boudins. Geological hammer is approximately 60 cm long.

C) Multiple calc-silicate layers developed in marble, affected by late-stage brittle faulting which has caused offset of calc-silicate bands. Field of view is ~2.5 metres across.

D) Close-up view of forsterite/serpentine-rich band (green-black areas) developed in dolomitic marble (brown-white colour). Black rims around forsterite-diopside-rich masses are dominated by serpentine. Note how the fabric in marble layer deviates around the calc-silicate mass, probably due to localised extensional stress causing boudinage. Geological hammer is approx. 60 cm long.

Volcanic ash component

The amount of ash in marbles can be estimated based on the following assumptions:

a) Volcanic ash input is the dominant source of Al in the marbles.

b) Al is relatively immobile. Zr and TiO_2 are also useful indicators of volcanic components. Si, K and Na are unsuitable for use in this calculation due to their high mobility in fluids.

c) The Al_2O_3 content of the volcanic ash is the same as the metavolcanic rocks in the Isåsen and Zinkgruvan formations with an average 14 wt% Al_2O_3.

d) The bulk Al_2O_3 content of the metavolcanic rocks and marbles has remained largely unaffected by metamorphism or metasomatism.

The quantity of ash in the marbles is estimated by dividing % Al_2O_3 in marble by 14%. District marbles contain an average of 1.4 wt % Al_2O_3, indicating approximately 10% ash content. This can be considered as the district 'background' level. Ash content at this level also introduces small amounts of K, Na, Fe and Mg, as well as significant Al and Si. The Zr:Al_2O_3 ratios support a volcanic origin for the non-carbonate component in the marbles (Fig. 4.19), and illustrate the continuum between near-pure marbles, calc-silicate skarns and pure volcanic rocks.

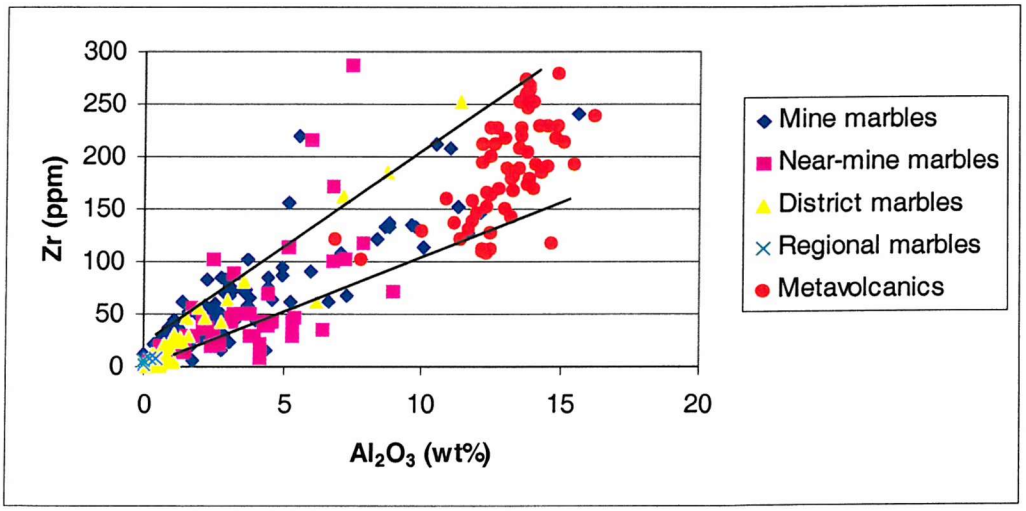

Figure 4.19: Zr vs Al_2O_3 for marble and metavolcanic samples in the mine area. Black lines show the mixing trend between pure carbonate and pure metavolcanic material. Original data in Appendix E.

4.3.3 Potassic enrichment

The potassic enrichment observed in the metavolcanic rocks of the Isåsen and Zinkgruvan formations is also evident in the Zinkgruvan Formation metacarbonate rocks (Fig. 4.20). The spread of data in Fig. 4.20 demonstrates the mixing of carbonate and volcanic components. However, it is clear that the mixing trend lies between near-pure carbonate and intensely K-altered metavolcanic rocks (between solid black lines), **not** unaltered acidic volcanic rocks (dashed black

line). During the potassic alteration event, hydrothermal fluids altered the volcanic component of ash-contaminated marbles by alteration of Na-feldspar (section 4.2.1). Subsequent metamorphism has homogenised the composition of K-altered admixed volcanic-carbonate rocks, with phlogopite being the main peak metamorphic K-bearing mineral.

The majority of regional samples are clean marbles, although some show evidence for a minor admixed volcanic component. However, the trend for these samples is more characteristic of mixing with unaltered rhyolite rather than K-altered volcanics. Most district samples show a small amount of admixture (~10% ash), and their trend along the bottom of the data spread indicates that their volcanic component was not as strongly K-altered as that present in mine area samples.

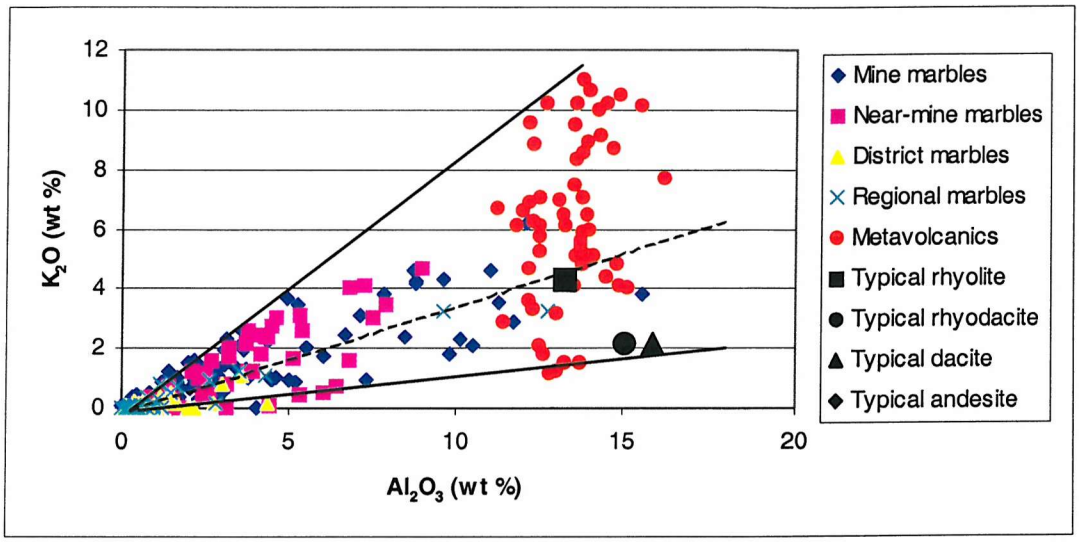

Figure 4.20: Comparison of K_2O and Al_2O_3 contents in metavolcanic and metacarbonate rocks. Typical values for acidic-intermediate rocks taken from Cox et al. (1979). Solid black lines show the range of compositions produced by mixing carbonate with variably K-altered volcanic material. Dashed line shows upper compositional limit of mixing with typical non-altered rhyolitic material. Samples containing Al and K purely sourced from volcanic ash should fall between the two solid black mixing lines. All samples lying below the lower mixing line are not affected by ash input. Note that the volcanic component in district and regional marbles appears to be substantially less K-enriched than that in mine area samples.

Sr and Rb contents in the metacarbonate units show that the mine area rocks are depleted in Sr and variably enriched in Rb relative to district samples (Fig. 4.21). Mine area marbles contain <50 ppm Sr (most are <25 ppm) and 0-150 ppm Rb, whereas district marbles contain up to 300 ppm Sr, but rarely contain more than 50ppm Rb (Fig. 4.21). Regional samples contain <30 ppm Sr and <5 ppm Rb.

Variable Rb enrichment in the mine area marbles is linked to the potassic enrichment event. Lagerblad & Gorbatschev (1985) proposed a hydrothermal model for the Bergslagen alkali metasomatism whereby K-enriched rocks also become enriched in Rb but depleted in Sr (Chapter 2, section 2.2.5). The data in Fig. 4.21 show that although Sr has clearly been leached from the

mine area samples, Rb enrichment is variable, probably due to a combination of mineralogical factors, patchy permeability of carbonate units and distance from the alteration front. Although they were probably caused by the same event, Sr depletion and Rb enrichment occurred via different mechanisms. Straightforward replacement of Sr by Rb is not indicated by the data distribution in Fig. 4.21, and is not mineralogically likely. Sr in the original carbonate sediment is likely to be mostly contained within carbonates, whereas incoming Rb will most likely be hosted in micas and feldspars. Slight enrichment of Rb in the district samples is probably caused by the background volcanic ash component, which would be expected to contribute approximately 15-20 ppm Rb at 10% contamination levels. Sr contribution from this source is minimal, around 3-6 ppm.

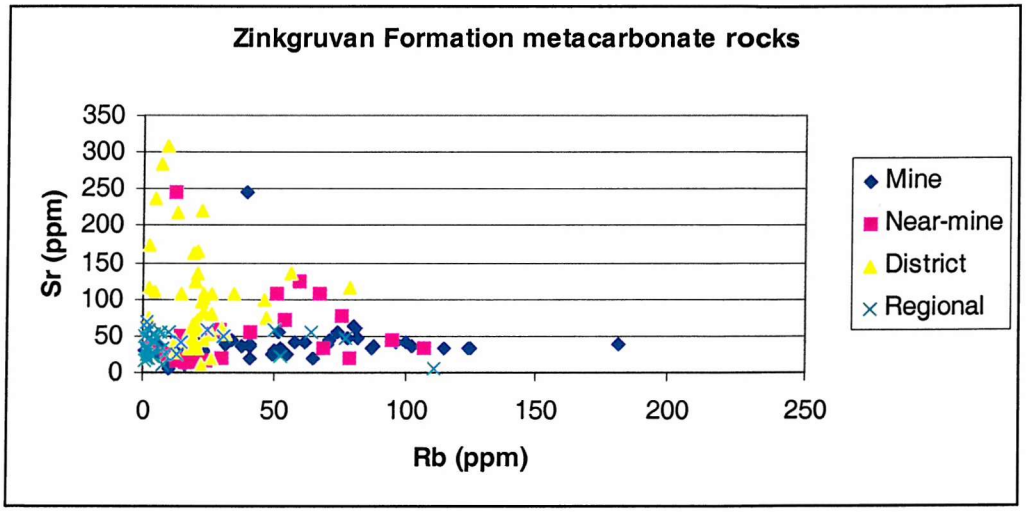

Figure 4.21: Rb and Sr contents for metacarbonate rocks at Zinkgruvan and the surrounding area. Regional samples from Glanshammar are plotted for comparison.

The low concentrations of both Rb and Sr in the majority of regional samples may be attributed to localised processes in the Glanshammar area. Whilst low Rb levels are to be expected in relatively unaltered carbonate rocks (Veizer (1990) quoted values of around 3 ppm for typical marine limestones), the average marine limestone contains around 600 ppm Sr (Veizer, 1990), suggesting that significant Sr depletion has also occurred throughout the district.

Potassic enrichment of volcanic rocks in the Zinkgruvan area is well documented (Henriques, 1964; Hedström *et al.*, 1989; Hellingwerf, 1996; section 4.2), and alkali metasomatism is a common phenomenon in the Bergslagen region (see Chapter 2). The potassic enrichment affecting the local metavolcanic rocks was also responsible for K-enrichment in the marbles, and was a pre-metamorphic fluid (hydrothermal) event. This is a key event in the evolution of the region and will be discussed further in relation to mineralisation in Chapter 8.

4.4 MINERALOGY OF METACARBONATE ROCKS

The mineral assemblages observed are the products of moderate to high grade metamorphism (see Chapter 5). For the regional and district samples, the bulk rock chemistry was apparently little altered prior to metamorphism, save for localised dolomitisation. In view of this, the present-day assemblage should closely reflect the original bulk rock chemistry. Conversely, the carbonate component of marbles in the mine area have undergone dolomitisation, ankeritisation, silicification and the volcanic component has suffered variable degrees of K-enrichment during fluid infiltration prior to peak metamorphism. Therefore, the assemblages observed in these samples do not represent the original carbonate chemistry.

4.4.1 Regional marbles from Glanshammar

As demonstrated in section 4.3, marble samples from the Glanshammar region appear to be unaltered apart from dolomitisation. Volcanic ash is minor or absent in the samples. All samples comprise coarse grained dolomite with subordinate calcite and very minor quantities of phlogopite and clinochlore. Two samples contain well-developed talc crystals up to 15 mm long (Fig. 4.22) overprinting the main assemblage. Phlogopite and clinochlore are absent in talc-bearing samples.

The minor amount of silica and aluminium available to form talc, phlogopite and clinochlore is probably sourced from minor detrital or volcanic contamination at the time of deposition. There is no evidence for hydrothermal activity in these samples. A representative whole-rock geochemical analysis for a talc-bearing marble sample is given in Table 4.4.

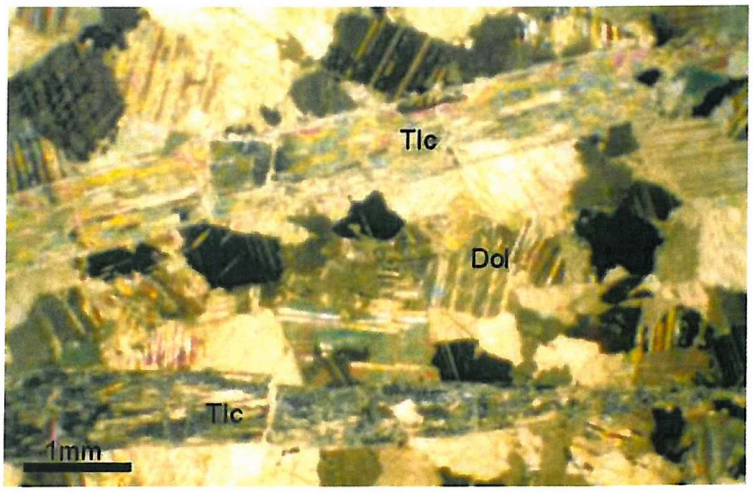

Figure 4.22: Large, elongate crystals of talc overprinting the peak Dol-dominant assemblage. Sample ZV3048, Glanshammar. Cross polarised light.

4.4.2 Zinkgruvan district marbles

Most metacarbonate samples away from the mine are calcite-normative with Ca:(Ca+Mg+Mn+Fe*) typically ≥ 0.85. Some parts of the district such as the area south of lake Bredsjön and the Rutabygget quarry areas (see Appendix B for locations) are dolomitised. District marbles contain a minor silicate component, likely to be volcanic ash added at the time of deposition. The ash component is estimated at approximately ≤10% (section 4.3.2) of the rock, but it has contributed significant amounts of SiO_2, Al_2O_3 and K_2O and minor FeO, MgO, CaO and Na_2O, which is reflected in the mineralogy. These marbles do not show any evidence of the ankeritisation or K-enrichment that has affected marbles in the mine area.

Calcite-normative marbles

Calcite is the dominant carbonate phase, usually accompanied by 15-25% tremolite and/or diopside, and minor (≤ 5%) phlogopite. The amount of tremolite and diopside in the assemblage is limited by the quantity of SiO_2 and metamorphic grade. Samples with low SiO_2 form a limited amount of calc-silicate minerals. Metamorphic grade in many areas limits calc-silicate generation to tremolite, but diopside appears in higher temperature areas closer to the mine. In many cases, a high percentage of SiO_2 enables quartz to remain stable in the mineral assemblage at moderate metamorphic grades. Whole-rock XRF analyses of representative calcite-normative district marbles are given in Table 4.3.

The low phlogopite content in these samples is consistent with a ~10% rhyolitic volcanic ash input, which contributed approximately 0.4 wt% K_2O and 1.4 wt% Al_2O_3 to the rock. A phlogopite with 10 wt% K_2O would form approximately 4% of the mineral assemblage. Excess of aluminium over that required to form phlogopite is usually accommodated in the development of minor (~2%) anorthite or zoisite. There is usually insufficient Al_2O_3 to form grossular except near quartzofeldspathic rock types which can contribute the necessary Al (± Fe, Mg and Mn) to calc-silicate skarns developed at the contact between the two lithologies.

The typical mineral assemblage for calcite-normative district marbles is Cal + Qtz + Tr/Di (± Phl). Wollastonite is not observed in this sample set. Fig. 4.23A shows the key mineralogical features of a typical calcite-normative district marble assemblage.

Dolomite-normative district marbles

Locally, as at Gardshyttan and Bredsjön (Fig. 3.1), carbonate rocks are completely dolomitised. The proportions of calcite and dolomite are variable, with calcite regenerated through the breakdown of dolomite during prograde metamorphism (Chapter 5). Whole-rock geochemistry for typical rocks is given in Table 4.4.

The contribution of silica, aluminium and potassium from the volcanic ash component is manifested in the development of calc-silicate minerals, phlogopite and clinochlore. Diopside is the dominant calc-silicate phase, although metamorphic grade has been high enough to permit the growth of forsterite, which has subsequently retrogressed to serpentine + magnetite in some areas (e.g., sample ZR08, Table 4.5). Potassium and aluminium are hosted in phlogopite, and the remaining aluminium is taken up in the formation of minor clinochlore rather than anorthite/zoisite. District marbles do not usually contain sufficient aluminium to generate the pleonaste spinel observed in samples from the mine area. Free quartz is very rarely observed in dolomite-normative samples, with all silica reacting to form calc-silicate phases.

The typical assemblage found in dolomite-normative marbles is Cal + Dol + Di ± Fo ± Serp + Phl ± Chl, and is illustrated in Fig. 4.23B.

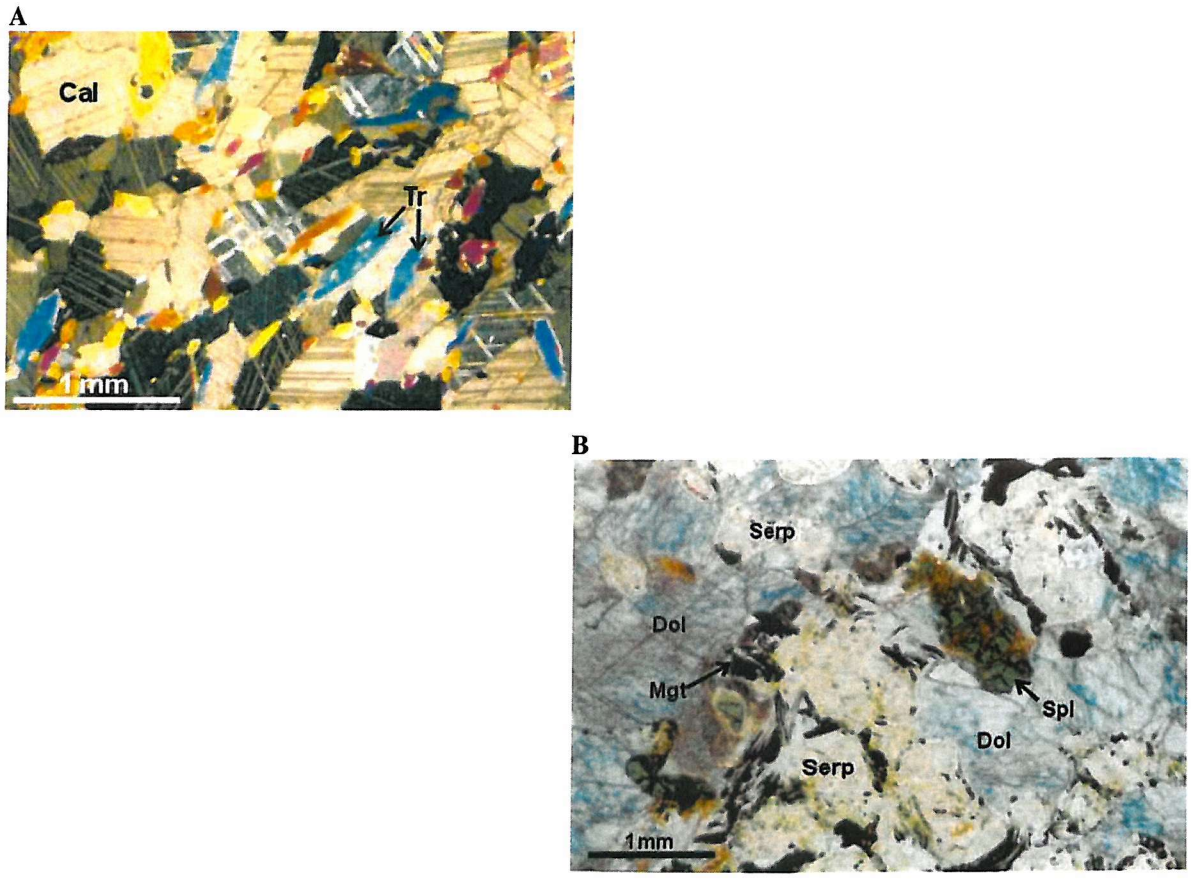

Figure 4.23: District marble assemblages

A) Calcite-normative assemblage containing Cal + Tr (+ Qtz). Sample ZR09, Tybble. Cross polarised light.

B) High-T dolomite-normative assemblage containing Dol + Serp + Spl + Mgt. Serp and Mgt are products of serpentisation of forsterite. Sample ZR19, East Broängen. Plane polarised light.

	Mine area			*District*	
Sample No.	**451/15**	**451/16**	**451/17**	**ZR04**	**ZR09**
SiO_2	32.07	33.34	34.69	5.72	20.96
TiO_2	0.09	0.12	0.14	0.00	0.00
Al_2O_3	3.78	4.46	5.40	0.11	0.13
Fe_2O_3	2.64	2.34	2.77	0.28	0.47
FeO*	1.84	1.64	1.94	-	0.44
MnO	0.34	0.21	0.25	0.00	0.13
MgO	5.76	6.12	4.71	0.87	2.19
CaO	34.14	29.68	33.04	64.49	49.61
Na_2O	0.79	0.42	0.91	0.13	0.22
K_2O	2.58	2.71	2.56	0.04	0.02
P_2O_5	0.05	0.05	0.05	0.01	0.01
CO_2	16.02	16.81	14.19	29.08	25.39
Calcite	40	40	40	85	45
Diopside	25	25	30	7	15
Quartz	10	15	25	8	25
K-feldspar	15	15	5	-	-
Dolomite	5	5	-	-	-
Tremolite	-	-	-	-	15

*Table 4.4: Comparison of whole-rock (XRF) geochemical data and mineralogy of selected **calcite-normative** marbles from the **mine area** (samples 451/15, 451/16 & 451/17) and from the **Zinkgruvan district** (SE part of the Zinkgruvan Basin - samples ZR04 & ZR09). Chemical data in weight %; mineralogy in volume %. Original data and laboratory procedure in Appendix E.*

	Mine area		*District*		*Regional*
Sample No.	**555/07**	**454/04**	**ZV3018**	**ZR08**	**ZV3048**
SiO_2	22.35	23.96	7.35	13.60	2.37
TiO_2	0.19	0.08	0.02	0.02	0.00
Al_2O_3	5.24	2.29	0.52	0.40	0.00
Fe_2O_3	7.57	8.48	0.27	4.70	0.60
FeO*	5.30	5.93	0.19	4.44	0.50
MnO	0.55	0.47	0.07	0.68	0.10
MgO	12.06	17.39	7.15	19.93	24.45
CaO	28.28	26.69	46.21	32.84	32.32
Na_2O	0.31	0.24	0.00	0.11	0.01
K_2O	3.43	1.02	0.07	0.23	0.02
P_2O_5	0.07	0.05	0.02	0.04	0.01
CO_2	16.39	17.29	35.17	25.51	40.18
Calcite	45	30	55	35	5
Dolomite	5	5	4	10	75
Diopside	-	5	12	-	-
Forsterite	5	-	1	-	-
Serpentine	(15)	30 (+10)	20	35	-
Phlogopite	20	15	8	10	5
Clinochlore	-	-	-	-	5
Pleonaste	-	-	-	-	-
Talc	-	-	-	-	10
Opaques	10	5	-	10	-

Table 4.5: Comparison of whole-rock (XRF) geochemical data and mineralogy of selected ***dolomite-normative*** *marbles and calc-silicate marbles from the* ***mine area*** *(samples555/07 and 454/04),* ***district*** *marbles from Vinnern (ZV3018), Bredsjön (ZR08), and* ***regional*** *marble from Glanshammar (ZV3048). Figures in brackets refer to saponite as an alteration product after serpentine. Chemical data in weight %; mineralogy in volume %. Original data and laboratory procedure in Appendix E.*

4.4.3 Mine and near-mine marbles

Marbles in the mine area have been subject to silicification, ankeritisation and K-enrichment, and contain a significant volcanic ash component. In addition, metamorphic grade is known to be higher in the mine area relative to most parts of the surrounding basin (see Chapter 5). This has resulted in slightly different mineralogies to district samples, with differing proportions of mineral phases and different mineral chemistries.

Dolomite-normative marbles in the stratigraphic footwall of the orebody grade into calcite-normative rocks at the SE extremity of the Nygruvan orebody and beyond. Most rocks in the hangingwall are calcite-normative, irrespective of lateral position.

Calcite-normative marbles

The normal assemblage in these rocks is Cal + Di ± Qtz ± Wo ± Kfs. The extent of calc-silicate mineral development is governed by the quantity of detrital/original and introduced silica in the sample. Table 4.4 shows the whole-rock geochemistry for typical calcite-normative mine and district marble samples.

Calcite contains < 2 wt% MgO and little FeO, and is usually coarse grained (up to 2 mm diameter), indicative of re-equilibration to lower P and T following metamorphism (see section 5.6.2). Dolomite is sometimes present, but rarely accounts for more than 5% of the total assemblage. Diopside is the main calc-silicate mineral and hosts the bulk of the Fe+Mg+Mn in the rock. Diopside can account for up to 35% of the assemblage, usually occurring as prismatic crystals or massive aggregates (Fig. 4.24A). The high-temperature calc-silicate phase wollastonite is developed where physiochemical conditions were suitable (see section 5.4), forming aggregates or layers of prismatic to acicular crystals, usually aligned with the dominant fabric of the rock. Table 4.6 shows typical chemical analyses of diopside and wollastonite occurring in calcite-normative marbles from the mine area.

Potassium is contained within K-feldspar (usually microcline), which remains stable through metamorphism due to the lack of Mg and Fe required to form biotite or phlogopite. Calcite-normative mine marbles average approximately 3 wt% K_2O, resulting in up to 15-20% K-feldspar. Table 4.6 shows a typical chemical analysis for K-feldspar in calcite-normative mine area marbles.

The excess aluminium in many mine samples is sufficient to form grossular and/or anorthite. However, most garnet-bearing metacarbonate samples contain enough calc-silicate phases to be classified as calc-silicate marbles (see section 3.2.2 for carbonate classification). These phases are discussed in section 4.5 (calc-silicate skarns).

A

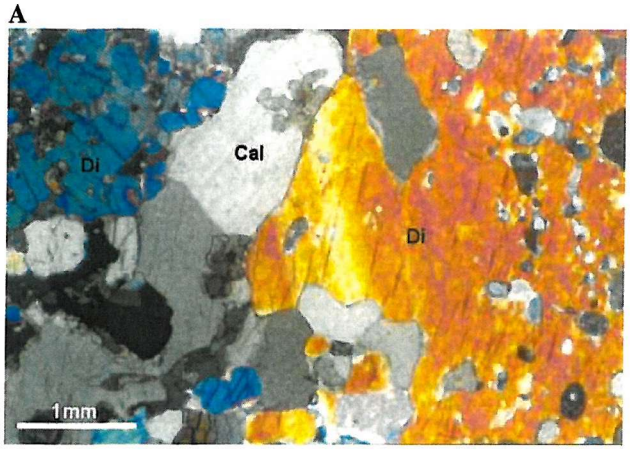

B

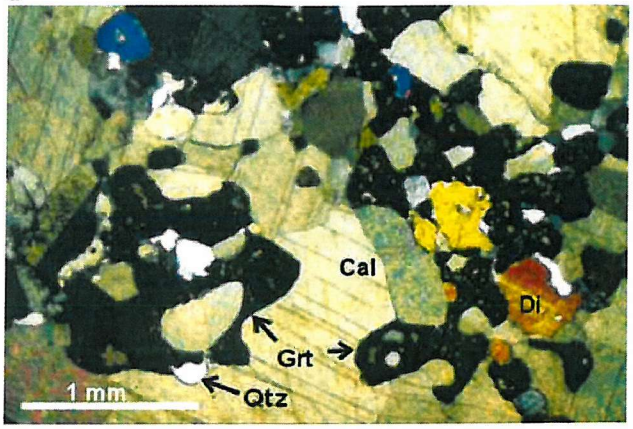

Figure 4.24: Mine & near-mine marble assemblages (cal-normative)

A) Typical Cal + Di (+ Qtz) assemblage. Sample 454/28, Nygruvan. Cross polarised light.

B) Skarny calcite-normative marble containing abundant garnet. Sample 454/24, Nygruvan. Cross polarised light.

	Diopside		*Wollastonite*		*Microcline*	
Sample No.	**451/19** *(n = 3)*		**451/19** *(n = 1)*		**451/19** *(n = 1)*	
	wt % oxide	S.D	wt % oxide	S.D	wt % oxide	S.D
SiO_2	52.48	0.36	48.16	-	62.74	-
TiO_2	0.06	0.11	0.06	-	-	-
Al_2O_3	-	-	-	-	18.08	-
FeO (total)	8.38	0.51	-	-	-	-
MnO	0.82	0.19	0.23	-	-	-
MgO	13.19	0.12	-	-	-	-
CaO	24.76	0.29	51.20	-	0.26	-
Na_2O	-	-	-	-	-	-
K_2O	-	-	0.02	-	17.40	-
P_2O_5	-	-	-	-	-	-
SO_3	0.10	0.12	-	-	0.05	-
CuO	0.08	0.12	-	-	0.20	-
ZnO	0.12	0.21	-	-	-	-
PbO	-	-	-	-	1.28	-
Total	99.99		100.01		100.00	
Si	1.97	0.01	0.93	-	2.93	-
Ti	-	-	-	-	-	-
Al	-	-	-	-	1.00	-
Fe2+	0.06	0.04	-	-	-	-
Fe3+	0.21	0.02	-	-	-	-
Mn	0.03	0.01	-	-	-	-
Mg	0.74	0.01	-	-	-	-
Ca	1.00	0.01	1.06	-	0.01	-
Na	-	-	-	-	-	-
K	-	-	-	-	1.04	-
OH	-	-	-	-	-	-
O	6.00	0.00	3.00		8.00	

Table 4.6: Typical average SEM chemical analyses and stoichiometry for key mineral phases present in ***calcite-normative*** *marbles from the mine area. Chemical data in wt% oxide; stoichiometry in ionic proportions. Original data in Appendix F.*

Dolomite-normative marbles

Whole-rock geochemical data for typical dolomite-normative mine marbles are given in Table 4.5.

Calcite is usually the dominant carbonate phase due to the breakdown of dolomite during prograde metamorphism (Chapter 5). Residual ferroan dolomite forms approximately 5-10% of the assemblage and co-exists with Fe-free calcite containing 1-2 wt% MgO.

In these samples, forsterite is the most common calc-silicate phase (figs 4.25A & B), sometimes occurring with diopside. However, peak metamorphic conditions have exceeded the stability field for diopside in most parts of the mine so it is usually absent from the assemblage. A full discussion of stable mineral assemblages with respect to metamorphic grade is covered in Chapter 5.

Most forsterite contains approximately 4-7 wt% FeO(total), representing a composition of $Fo_{90}Fa_{10}$. A maximum 13 wt% FeO(total) was recorded, but the growth of very fine grained magnetite along fractures as a by-product of serpentinisation can cause analytical errors. Forsterite also usually contains around 1 wt% MnO. In some samples (e.g., 555/07 from Nygruvan), the Mn-rich olivine knebelite is present as rounded blebs within forsterite which appear to be unaffected by serpentinisation (Fig. 4.25C). The manganese required to form this mineral is presumably sourced from the Fe-Mn enrichment event which occurred prior to metamorphism. The knebelite is rarely seen in thin section due to its small size, and the extensive serpentinisation of forsterite masses. Table 4.6 shows typical chemical analyses for knebelite and forsterite found in dolomite-normative mine marbles.

Potassium is held in phlogopite, which is present in most samples and forms up to 25% of the mineral assemblage. Remaining aluminium is usually contained in clinochlore. Silica-poor (or highly Al-rich) marbles commonly develop a small amount of pleonaste spinel (Fig. 4.25D). Pleonaste is transitional between hercynite ($FeAl_2O_4$) and true spinel ($Mg_2Al_2O_4$) (see Table 4.7), and occurs as small, square to rounded crystals often displaying zonation from emerald green on the crystal margins to almost black in the centre, probably due to magnetite inclusions.

High magnification SEM analysis has revealed sub-microscopic inclusions of galena in pleonaste spinels in marbles containing, or close to, zinc mineralisation. The 1-2μm inclusions are roughly square-shaped and appear to be crystallographically controlled (Fig. 4.25E). Spinel also occurs as thin lamellae in large crystals of exsolved magnetite (Fig. 4.25F), produced through re-equilibration of Fe-rich spinel to lower temperatures (Lindsley, 1991).

The presence of clinohumite in some near-mine samples is an indicator of fluorine either in the original rock chemistry or (more usually) introduced via a fluid prior to or during metamorphism. Clinohumite is rare, occurring as small crystals intergrown with forsterite in samples from DDH 1350 (to the NW of the mine area) (Fig. 4.25G & H). However, extensive serpentinisation of

forsterite masses in the majority of samples may obscure the clinohumite, and it may be more common than observed in thin section.

Serpentinisation of forsterite is extensive in marbles in the mine area, varying from partial to total replacement. Fine grained clinochlore is commonly intergrown with serpentine (Fig 4.25I). Magnetite is a by-product of the serpentinisation process and is concentrated along fractures and around the rims of the serpentine pseudomorphs. Saponite/iddingsite intergrowths, and occasionally fine grained carbonate, have replaced serpentine during a late retrogressive event (figs 4.25J to L). In all cases, the original forsterite crystal shape is preserved.

Figure 4.25: Mineralogical features of dolomite-normative mine and near-mine marbles

A) Typical Cal + Dol + Fo (+ Phl) assemblage, with rounded crystals of unaltered forsterite and lath-like crystals of phlogopite. Sample 555/28, Nygruvan. Cross polarised light.

B) Close-up view of forsterite crystals. Note the thin rim of alteration, and alteration to fine grained serpentine along fractures. Sample 555/28, Nygruvan. Cross-polarised light.

C) SEM backscattered electron image of a forsterite crystal containing blebs of knebelite (pale grey). Note the concentric rings in the forsterite caused by partial alteration to serpentine, which do not appear to affect the knebelite inclusions. Sample 555/07, Nygruvan.

D) Large zoned pleonaste crystal in Fo-bearing marble. Colour zonation is caused by inclusions of magnetite. Sample ZR21. Plane polarised light.

E) SEM backscattered electron image of sub-microscopic square inclusions of galena (pale grey) in pleonaste spinel (dark grey). Note the strong crystallographic control over the distribution of the inclusions. Sample 1557/26, forsterite marble, Burkland.

F) SEM backscattered electron image of spinel lamellae (dark grey) in magnetite (pale grey). Note the crystallographic control over the distribution of the lamellae. Sample 1557/26, forsterite marble, Burkland.

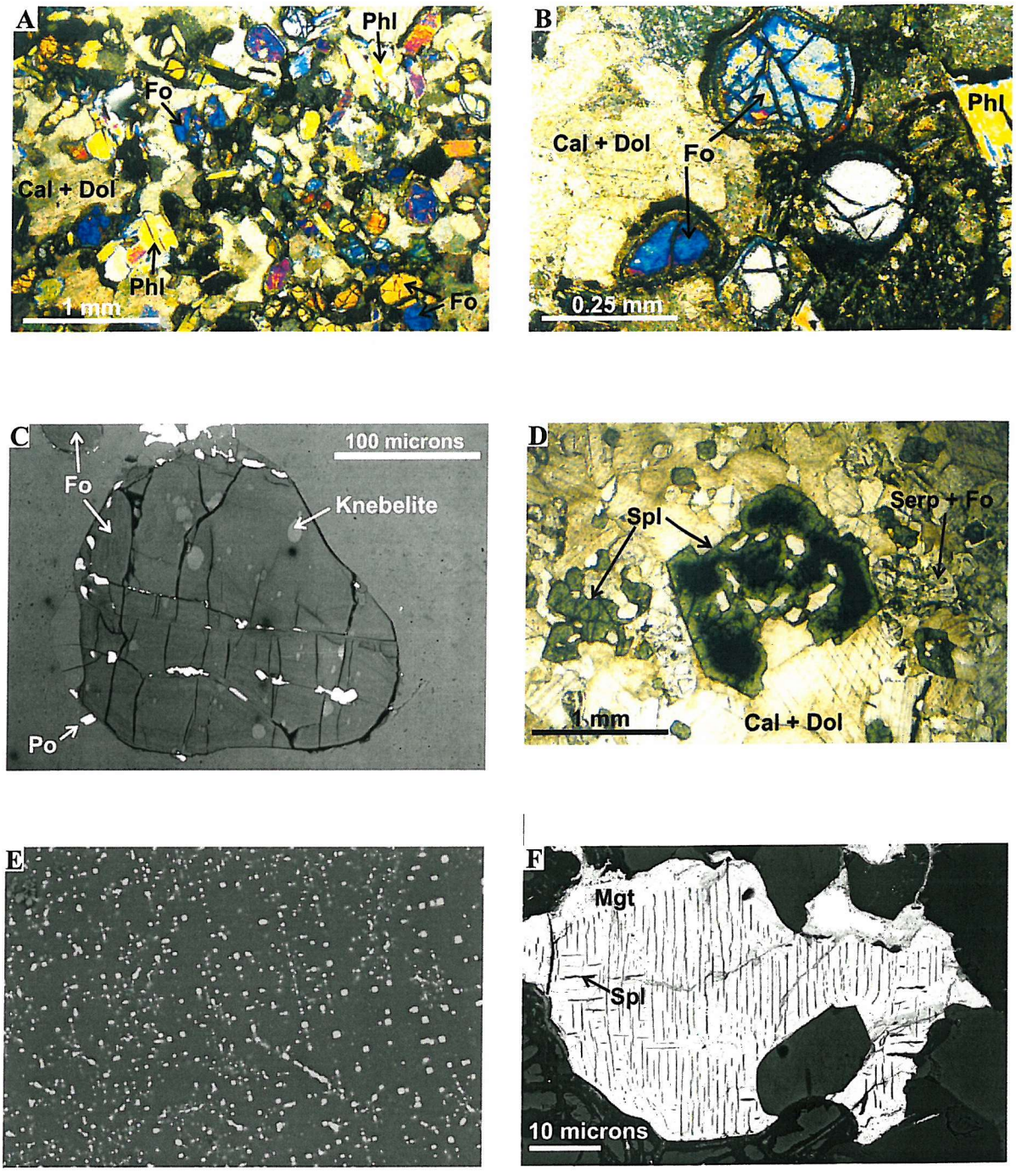

Figure 4.25: Mineralogical features of dolomite-normative marbles from the mine area

Figure 4.25 (cont): Mineralogical features of dolomite-normative mine and near-mine marbles.

G) Large, twinned clinohumite crystal in forsterite-bearing marble. Sample ZV3027, DDH1350 Cecilia. Cross polarised light.

H) Clinohumite crystals and magnetite in forsterite-bearing marble. Sample ZV3027, DDH 1350 Cecilia. Plane polarised light.

I) Clinochlore overprint in serpentinised marble. Clinochlore forms elongate laths (white) overprinting the peak metamorphic phases and the serpentinite forming pseudomorphs after forsterite. Sample ZR06, Isåsen. Cross polarised light.

J) Replacement of serpentine (originally after forsterite) by saponite-iddingsite material (orange). Assemblage also includes magnetite (black) and phlogopite (pale yellow-brown). Sample 555/07, Nygruvan. Cross polarised light, x2.5 magnification.

K) *Enlarged view of saponite-iddingsite pseudomorphs after serpentine/forsterite. Note magnetite developed around the rims and in the cracks of the pseudomorphs (probably remnants of the serpentinisation process). Sample 555/07, Nygruvan. Cross polarised light.*

L) *Late-stage replacement of serpentine by fine grained carbonate material. Note serpentine rims around alteration masses. Sample ZV3030, Nyhytten. Cross polarised light.*

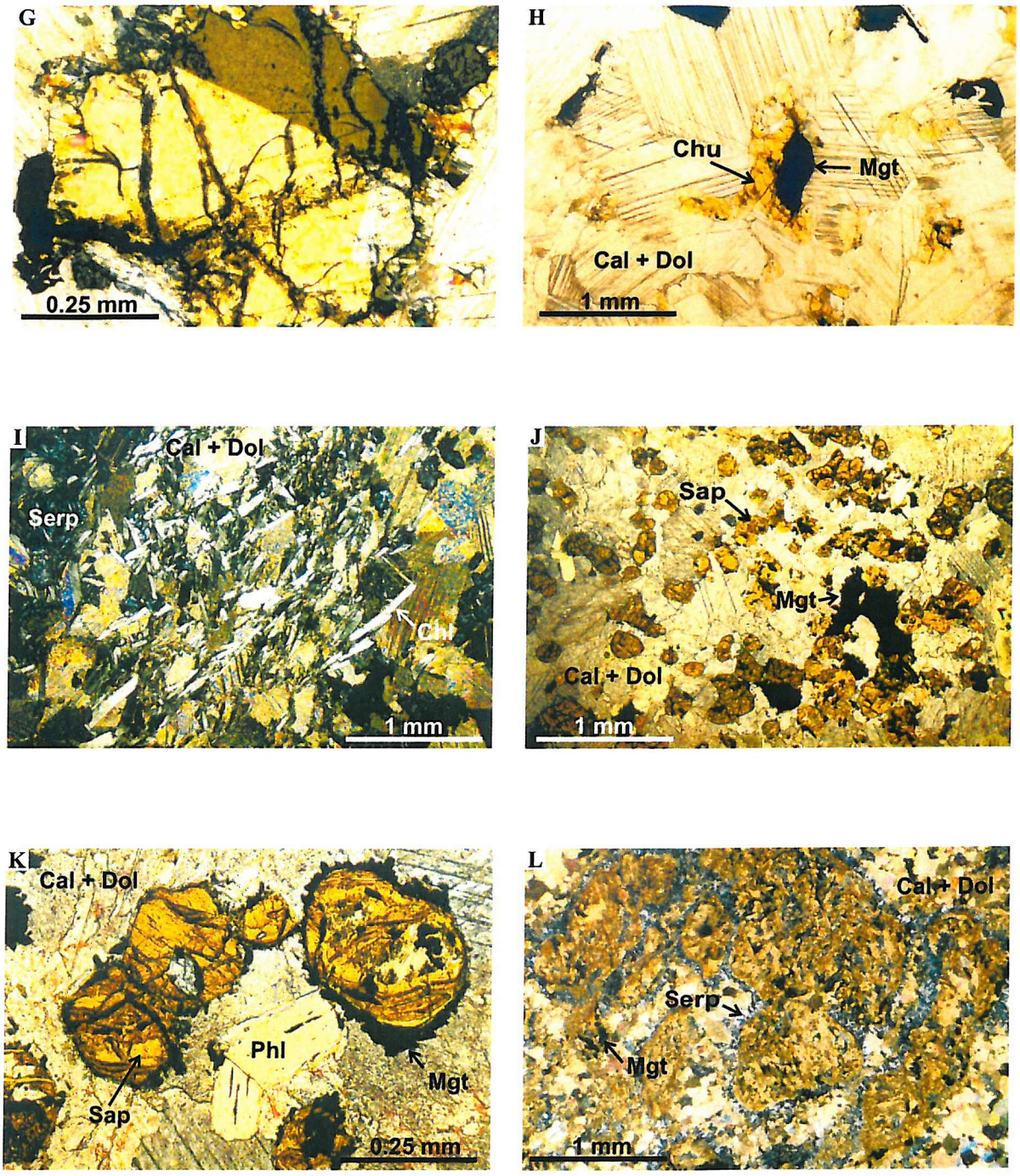

Figure 4.25 (cont): Mineralogical features of dolomite-normative marbles from the mine area.

	Forsterite		*Knebelite*		*Pleonaste*		*Clinochlore*		*Phlogopite*	
Sample No.	**ZR06** *(n = 1)*		**555/07** *(n = 6)*		**555/06 ZR06** *(n = 5)*		**ZR06** *(n = 1)*		**555/07 555/11** *(n = 4)*	
	wt % oxide	S.D	wt % oxide	S.D	wt % oxide	S.D	wt % oxide		wt % oxide	S.D
SiO_2	47.19	-	35.18	2.56	-	-	34.49	-	39.50	0.71
TiO_2	-	-	0.07	0.09	0.10	0.14	-	-	0.49	0.10
Al_2O_3	3.97	-	0.05	0.10	64.03	1.10	20.21	-	14.02	0.66
FeO (total)	3.36	-	16.29	1.25	16.21	0.68	1.51	-	7.62	0.42
MnO	-	-	30.31	2.67	0.27	0.37	0.03	-	0.19	0.07
MgO	45.48	-	10.64	0.75	19.20	1.71	30.65	-	22.14	0.48
CaO	-	-	5.47	0.53	0.01	0.02	0.10	-	0.30	0.06
Na_2O	-	-	-	-	-	-	-	-	-	-
K_2O	-	-	0.13	0.09	0.02	0.05	-	-	10.66	0.13
P_2O_5	-	-	-	-	-	-	-	-	-	-
H_2O	-	-	-	-	-	-	13.00	-	5.00	0.00
PbO	-	-	-	-	-	-	-	-	-	-
CuO	-	-	-	-	-	-	-	-	-	-
ZnO	-	-	-	-	-	-	-	-	-	-
SO_3	-	-	-	-	-	-	-	-	-	-
Total	99.99		98.15		99.84		99.99		99.91	
Si	1.14		1.10	-	-	-	6.36	-	5.65	0.09
Ti	0.00		-	-	-	-	-	-	2.37	0.14
Al	0.15		-	-	1.74	0.44	4.40	-	0.01	0.02
Al	-		-	-	-	-		-	0.05	0.01
Fe^{3+}	-		-	-	0.22	0.05	-	-		
Fe^{2+}	0.15		0.43	-	0.13	0.14	0.23	-	0.91	0.05
Mn	-		0.78	-	-	-	0.01	-	0.02	0.01
Mg	1.57		0.49	-	0.89	0.41	8.43	-	4.72	0.10
Ca	-		0.18	-	-	-	0.02	-	0.05	0.01
Na	-		-	-	-	-	-	-	-	-
K	-		-	-	-	-	-	-	1.70	0.47
OH	6.00		-	-	-	-	16.00	-	4.17	1.19
O	-		6.00		4.00	0.00	36.00		24.00	0.00

Table 4.7: Typical average SEM chemical analyses and stoichiometry of key mineral phases found in dolomite-normative marbles from the mine area. Chemical data are wt% oxide; stoichiometry in ionic proportions. S.D = standard deviation. Original data in Appendix F.

4.5 GEOCHEMISTRY OF CALC-SILICATE SKARNS

The metacarbonate rock types grade geochemically and mineralogically from pure calcite/dolomite marbles representing the system $CaO\text{-}MgO\text{-}CO_2$, up to calc-silicate marbles representing the broader system $CaO\text{-}MgO\text{-}SiO_2\text{-}Al_2O_3\text{-}FeO\text{-}MnO\text{-}K_2O\text{-}H_2O\text{-}CO_2$ (+ other minor components), containing appreciable amounts of calc-silicate minerals. Calc-silicate skarns are a continuation of this trend, with calc-silicate minerals strongly dominant over carbonate minerals.

Calc-silicate skarns observed in the Zinkgruvan Formation originate from metamorphic interaction between carbonate and quartzofeldspathic rocks, so their geochemistry is transitional between these two lithologies, depending on the proximity of the sample to either lithology. The variation in the chemistry of the rock type is directly reflected in its mineralogy (section 4.6).

A calc-silicate skarn from roughly mid-way between the metacarbonate unit and the metavolcanic unit contains substantial quantities of aluminium and silica from the metavolcanics, as well as retaining a distinctly calcic signature from the metacarbonate source. Interaction of metavolcanic material with calcite-normative and dolomite-normative marbles produces slightly different skarn chemistries. Calc-silicate skarns developed adjacent to dolomite-normative marbles tend to be slightly richer in Mg and Fe than those developed adjacent to calcite-normative marbles.

Typical calc-silicate skarns contain around 3-8 wt% Al_2O_3 (max. 13 wt%), and 45-55 wt% SiO_2. K_2O varies from <0.5 to >6 wt%, depending on the extent of alteration in the adjacent rock types. Most samples contain 3-6 wt% FeO (total), and MgO commonly exceeds 12 wt% (Appendix E). Table 4.8 shows typical whole rock XRF analyses and modal mineralogies for selected calc-silicate samples from the mine area.

The highly variable geochemistry and mineralogy of these rocks makes characterisation of fluid events considerably more difficult than for metacarbonate and metavolcanic rock types.

	555/32	*454/03*	*454/31*	*UZ20*
Adjacent marble	D	D	Mixed	C
Distance from nearest metavolcanic	2.15 m	0.88 m	7.38 m	~1.50 m
Distance from nearest metacarbonate	- (skarn is likely to represent complete alteration of a thin carbonate layer within the metavolcanic unit)	0.41 m	3.17 m	~2.50 m
SiO_2	50.70	48.42	52.79	49.59
TiO_2	0.16	0.27	0.12	0.25
Al_2O_3	3.26	13.55	6.31	9.47
FeO (Tot)	5.54	4.50	4.53	3.95
MnO	0.43	0.28	0.37	0.58
MgO	16.25	11.07	6.43	5.29
CaO	20.84	16.94	23.57	21.80
Na_2O	0.16	0.63	0.16	0.72
K_2O	0.66	1.41	3.63	3.80
P_2O_5	0.08	0.12	0.06	0.69
CO_2	2.04	2.86	2.05	3.57
Total	100.11	100.04	100.04	99.08
Qtz	-	-	15	35
Kfs	-	-	8	15
Di	58	60	50	25
Tr	20	10	-	-
Cal	2	-	12	15
Grt	-	-	4	5
Zs	10	5	-	-
Wo	-	-	5	5
Phl	10	5	-	-
Pl	-	10	5	-
Ser	-	10	-	-

Table 4.8: XRF Geochemistry and modal mineralogy of selected calc-silicate skarn samples from the mine area. Adjacent marble compositions are given (D = dolomite-normative; C = calcite-normative) to show variation of skarn chemistry related to source marble. All samples from Nygruvan. Samples 555/32, 454/03 & 454/31 are drill core samples from the stratigraphic footwall of the orebody; sample UZ20 is taken from the 500m level, stratigraphically above the ore horizon. Geochemical data in wt %; mineralogical data in estimated volume %. Original XRF data in Appendix E.

4.6 MINERALOGY OF CALC-SILICATE SKARNS

Metacarbonate - metavolcanic contacts are normally transitional and reflect the relative mobility of Si, Al, Fe, Mg, Ca and K away from the source lithology. Silica addition to marble produces diopside, wollastonite, tremolite etc., depending on the original Ca:Mg:Fe* ratio of the metacarbonate unit. Calc-silicate skarns developed adjacent to calcite-normative marbles are dominated by wollastonite and subordinate diopside (Fig. 4.27); dolomite-normative marbles produce wollastonite-free skarns dominated by diopside and tremolite.

In most skarn units, the mineralogy progressively changes with distance away from the carbonate unit towards the metavolcanic rock (schematically illustrated in Fig. 4.26) due to the relative mobility of silica compared to other elements such as aluminium. In many cases, the transition from marble to skarn is somewhat gradational over a distance of 10-40 cm, where the calc-silicate content of the marble gradually increases until carbonate phases become subordinate. The transition from skarn to metavolcanic tends to be somewhat sharper, usually marked by a distinct colour change from green calc-silicate material to mid-grey metavolcanic. However, 10-20 cm-thick bands of calc-silicate may occur within the metavolcanic material for up to 6 m from the main skarn horizon contact (see section 3.2.2 for a full description).

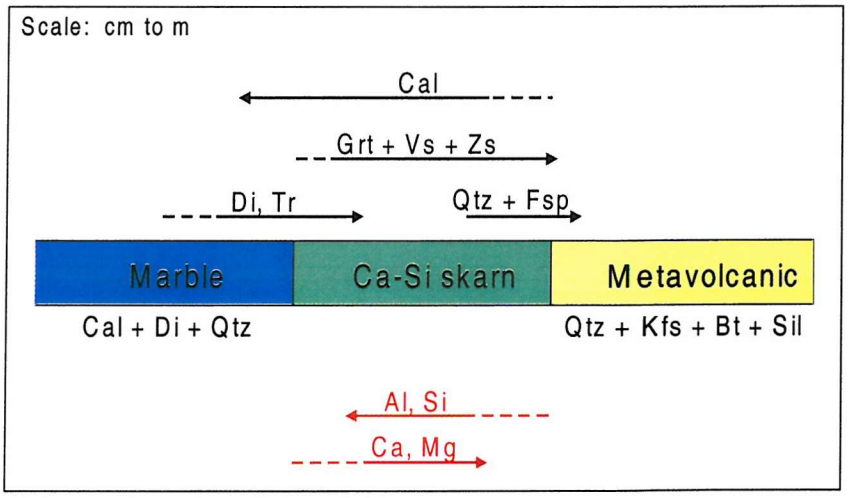

Figure 4.26: Schematic diagram to show the chemical and mineralogical variations through a calc-silicate skarn unit developed at the boundary between a carbonate unit and a volcanic unit during prograde metamorphism. Black arrows show the direction of increasing proportions of particular mineral phases; red arrows indicate the direction of movement of chemical components.

Low-Al skarns typically comprise massive, coarse-grained aggregates of simple calc-silicate minerals, usually diopside with minor tremolite. However, most skarn horizons contain some aluminium, usually accommodated in grossular and zoisite. Vesuvianite forms very large anhedral masses in highly Al-rich assemblages (Fig. 4.27C). Garnets developed in calc-silicate skarns in the mine area contain appreciable quantities of Fe and Mn, particularly in skarns developed close

to the ore zone. Garnets form the main repository for manganese, with minor amounts sometimes found in hedenbergitic diopside and tremolite-actinolite crystals. Typical mineral analyses of common minerals found in a range of calc-silicate skarns are given in Table 4.9.

With increasing proximity to adjacent metavolcanic units, the calc-silicate skarns tend to become more mineralogically variable, often showing intricate, mm-scale compositional layering between quartz/feldspar-rich horizons and calc-silicate/carbonate-rich horizons. The reaction and diffusion of components from different layers has created a complex multicoloured sequence of thin reaction skarns (Fig. 4.27E), many of which are entirely comprised of a single mineral phase such as garnet, wollastonite, calcite and quartz.

	Diopside		*Diopside*		*Tremolite*	
Sample No.	**UZ8** *(n = 2)*		**UZ45** *(n = 3)*		**UZ22** *(n=1)*	
	wt % oxide	S.D	wt % oxide	S.D	wt % oxide	S.D
SiO_2	49.79	0.17	49.49	0.17	51.85	0.00
TiO_2	-	-	0.02	0.03	0.18	0.00
Al_2O_3	-	-	-	-	2.66	0.00
FeO (total)	18.52	0.04	22.79	0.65	11.07	0.00
MnO	1.79	0.09	3.10	0.22	2.19	0.00
MgO	8.10	0.25	4.32	0.28	17.26	0.00
CaO	20.84	0.42	20.26	0.41	11.15	0.00
Na_2O	0.85	0.02	-	-	1.15	0.00
K_2O	0.02	0.03	-	-	0.09	0.00
H_2O	-	-	-	-	2.16	0.00
Total	99.88		99.97		99.75	
Si	1.93	0.01	1.99	0.00	7.49	0.00
Ti	-	-	-	-	0.02	0.00
Al	-	-	-	-	0.45	0.00
Fe^{2+}	0.20	0.01	0.01	0.01	1.34	0.00
Fe^{3+}	0.41	0.01	0.75	0.02	-	-
Mn	0.06	0.00	0.11	0.01	0.27	0.00
Mg	0.47	0.01	0.26	0.02	3.72	0.00
Ca	0.87	0.02	0.87	0.02	1.73	0.00
Na	0.06	0.00	-	-	0.32	0.00
K	-	-	-	-	0.02	0.00
OH	-	-	-	-	2.08	0.00
O	6.00	0.00	6.00	0.00	24.00	0.00

Table 4.9: Typical average SEM chemical analyses and stoichiometry for key mineral phases found in calc-silicate skarns from the mine area. Chemical data are wt% oxide; stoichiometry in ionic proportions. Original data in Appendix F.

	Grossular		*Zoisite*		*Wollastonite*		*Vesuvianite*	
Sample No.	**UZ8 (n = 3)**		**1557/14 (n = 1)**		**451/07 (n=2)**		**451/19 (n = 1)**	
	wt % oxide	S.D	wt % oxide	S.D	wt % oxide	S.D	wt % oxide	S.D
SiO_2	36.53	1.89	40.83	0.00	49.80	0.26	36.27	0.00
TiO_2	0.18	0.12	-	-	-	-	3.21	0.00
Al_2O_3	21.49	1.11	29.60	0.00	-	-	17.07	0.00
FeO (total)	11.44	8.68	3.78	0.00	0.21	0.06	2.84	0.00
MnO	8.02	3.76	0.33	0.00	1.22	0.10	-	-
MgO	-	-	-	-	-	-	1.67	0.00
CaO	20.95	9.01	23.91	0.00	48.76	0.23	37.69	0.00
Na_2O	1.17	0.43	-	-	-	-	-	-
K_2O	-	-	0.05	0.00	-	-	-	-
H_2O	-	-	1.50	0.00	-	-	-	-
Total	100.00		100.00		99.99		98.75	
Si	2.83	0.08	2.84	0.00	0.96	0.01	17.34	0.00
Ti	0.01	0.01	0.16	0.00	-	-	1.15	0.00
Al	1.96	0.06	2.27	0.00	-	-	9.62	0.00
Fe^{2+}	0.51	0.32	0.22	0.00	-	-	1.13	0.00
Fe^{3+}	0.24	0.24	-	-	-	-	-	-
Mn	0.53	0.26	0.02	0.00	0.02	0.00	-	-
Mg	-	-	-	-	-	-	1.20	0.00
Ca	1.73	0.70	1.78	0.00	1.01	0.00	19.31	0.00
Na	0.18	0.07	-	-	-	-	-	-
K	-	-	-	-	-	-	-	-
OH	-	-	0.70	0.00	-	-	-	-
O	8.00	0.00	13.00	0.00	3.00	0.00	3.00	0.00

Table 4.9 (cont): Typical and average SEM chemical analyses of key mineral phases found in calc-silicate skarns from the mine area. Chemical data are wt% oxide; stoichiometry in ionic proportions. S.D = standard deviation. Original data in Appendix F.

Figure 4.27: Mineralogical features of calc-silicate skarns.

A) Wollastonite-diopside skarn containing elongate, twinned laths of wollastonite (grey-yellow-white) and more equant grains of brightly-coloured diopside (blue-orange). Crystals are aligned to define the dominant S_1 foliation. Sample 454/30, Nygruvan. Cross polarised light.

B) Large, anhedral vesuvianite mass in wollastonite-bearing skarn. Vesuvianite has been overgrown by anhedral diopside (blue and pink), and is cross-cut by a thin calcite vein. Sample ZV3003, Hilda South. Cross polarised light.

C) Zoned vesuvianite crystals showing anomalous blue interference colours. Sample UZ22, 500m level, Nygruvan. Cross polarised light.

D) Zoisite crystals (probably replacing garnet or plagioclase) accompanied by sphene, quartz and diopside. Sample UZ23, 500m level, Nygruvan. Cross polarised light.

E) Hand specimen of finely banded calc-silicate skarn. Main constituents of individual reaction layers are labelled: Di = diopside; Cal = calcite; Qtz + Kfs = quartz + K-feldspar; Grt = garnet (grossular).

F) Hydrogrossular rims enveloping a mix of fine grained carbonate material and clinochlore/serpentine. Sample ZV3004, Dalby. Cross polarised light.

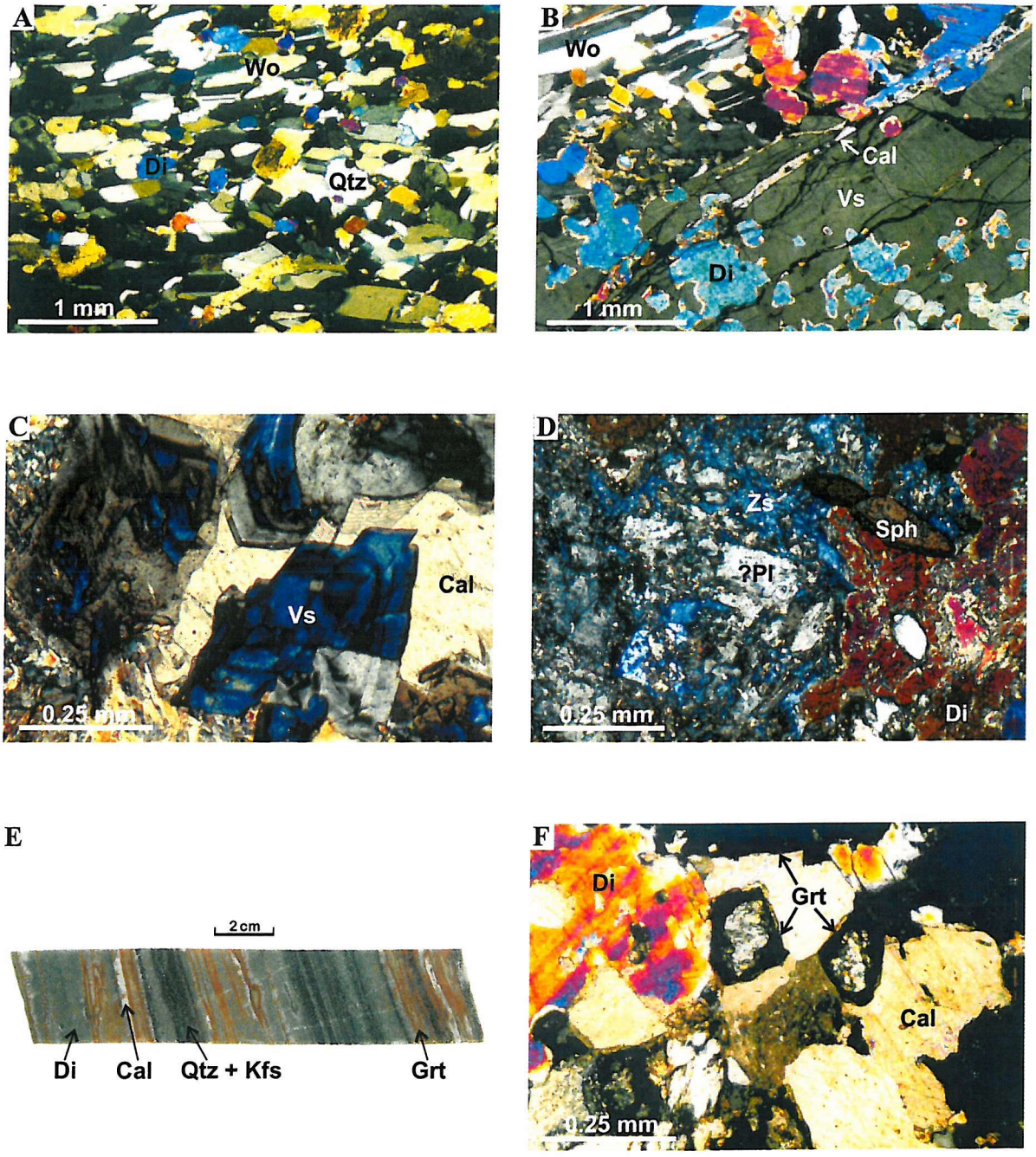

Figure 4.27: Mineralogical features of calc-silicate skarns

4.7 SUMMARY

4.7.1 Metavolcanic rocks

- Geochemical analyses show that the metavolcanic rocks of the Isåsen and Zinkgruvan formations are rhyolitic to rhyodacitic in composition. A few samples are deficient in both silica and alkali metals, suggesting that they are more basic in composition.
- Isåsen Formation volcanic rocks were intensely potassic altered as a result of replacement of Na by K (alkali metasomatism) in plagioclase prior to metamorphism. Intensely-altered samples contain up to 14 wt% K_2O, and comprise Qtz + Kfs (± Bt).
- Zinkgruvan Formation volcanics show variable pre-metamorphic potassic enrichment, containing an average of 5-7 wt% K_2O. Most samples comprise Qtz + Kfs + Pl + Bt (± Grt).
- LA-ICPMS and SEM analyses of chemical variations across garnets from garnetiferous horizons and magnetite skarns in Zinkgruvan Formation metavolcanic sequences shows that major element profiles are homogenised, but REE and trace element variations are preserved. Zonation characteristics, combined with textural evidence, suggests that garnets in these horizons crystallised at or shortly after peak metamorphism.

4.7.2 Metacarbonate rocks

Summary of metacarbonate geochemistry

- Marbles are composed of original carbonate material that has been affected by a number of alteration events.
- The metacarbonate rocks of the Zinkgruvan district can be divided into calcite-dominant and dolomite-dominant marbles based on their present (post-metamorphic) composition and mineralogy.
- District marbles contain low levels of Si, Al and K. The most probably source is admixture of approximately 10% volcanic ash.
- Marbles in the mine area have been subject to Fe-Mn enrichment, probably originally accommodated in the development of ankerite but broken down during prograde metamorphism.
- Some marbles from the mine area contain levels of silica and potassium which cannot be accounted for by simple mixing of carbonate sediment and volcanic ash. These components are thought to be the result of fluid influx.
- The geochemistry of the metacarbonate rocks display a continuum between 'pure' carbonate and 'pure' volcanic material as a result of admixture and metamorphic reaction.

Regional marbles

- Regional marbles sampled from Glanshammar underwent pre-metamorphic complete dolomitisation (probably a pre-metamorphic event), but are otherwise unaffected by any of the alteration processes observed in the district and mine area marble samples, save for minor silica addition.

District samples

- District samples comprise a mix of calcite-normative and dolomite-normative marbles.
- Metacarbonate rocks from the Zinkgruvan district show evidence for addition of around 10% volcanic ash.

Mine area marbles

- Mine area metacarbonate rocks are variably dolomitised, with complete dolomitisation of the footwall in the western parts of the mine. Marbles from the eastern part tend to be calcite-normative.
- Dolomitic marbles have been subject to Fe-Mn enrichment, probably accommodated in the development of Mn-bearing ankerite. Ankerite is not preserved in present-day assemblages due to high grade metamorphism, and dolomite is low in FeO and MnO.
- Marbles have undergone localised silicification and K-enrichment, features not observed in most district samples, and attributed to localised fluid events in the mine area which may be related to the mineralisation process.

4.7.3 Calc-silicate skarns

- Calc-silicate skarns formed by component exchange and reaction between adjacent carbonate and quartzofeldspathic units during prograde metamorphism.
- Skarns are commonly compositionally zoned parallel to the contact between adjacent lithologies.
- Zonation is related to the relative mobility and diffusion rates of different elements between the 'source rocks'.
- Highly variable geochemistry and mineralogy make fluid events more difficult to identify in these rocks compared to the marbles.

CHAPTER 5

METAMORPHISM

CHAPTER 5: METAMORPHISM

5.1 INTRODUCTION

Mineral assemblages in metamorphic rocks have long been used to gain an estimate of the pressure-temperature conditions experienced by rocks during metamorphism (Goldschmidt, 1911; Barrow, 1912; Eskola, 1915, 1920). The mineral phases produced at a given pressure and temperature are controlled primarily by bulk rock chemistry, but can also be influenced by the presence/absence and composition of any fluid present during metamorphism.

Rocks in the Bergslagen region have undergone high temperature, low pressure metamorphism (see Chapter 2), and this is directly evidenced in the Zinkgruvan district by the development of migmatites and high temperature gneisses. Previous research has ascertained that peak metamorphism reached upper amphibolite facies (Henriques, 1964; Hedström *et al.*, 1989), but the physiochemical conditions have never been quantified. An accurate picture of the peak conditions is essential in order to evaluate the nature of fluids present in the system prior to and during metamorphism.

Estimations of P-T conditions during peak metamorphism and subsequent retrogressive events have been made using mineral parageneses from different rock types from the district. This technique uses the presence and absence of key mineral phases and assemblages in conjunction with phase diagrams to constrain P-T conditions. Metapelitic assemblages from the Viksjön Formation provide good indication of peak P-T conditions because the peak phases are controlled mainly by bulk rock chemistry, regardless of the fluid composition during metamorphism. Calc-silicate and metacarbonate assemblages can also provide good P-T estimates but are strongly influenced by fluid chemistry. By using a combination of different rock types, a comprehensive picture of the physical and chemical conditions prevailing during prograde and retrograde metamorphism can be established.

More detailed quantification of metamorphic conditions can be attained by applying geothermobarometric techniques to specific mineral phases. The potential and validity of several such techniques are explored in section 5.6.

5.2 PROGRADE METAMORPHISM: METAPELITIC ASSEMBLAGES

5.2.1 The KFMASH system

The principle components of 90% of pelitic rocks are represented by the SiO_2-Al_2O_3-MgO-FeO-K_2O-H_2O (KFMASH) system, which can be subdivided into a number of simpler sub-systems (AFM, AKF, KFASH, KMASH etc.). Pelitic rocks may contain small amounts of other components (CaO, Na_2O, MnO) which cause minor complications in phase relationships, but do not significantly alter the occurrence of most index minerals. However, a significant quantity of CaO will not allow staurolite to form, and MnO has a strong influence over the stability fields of garnet and garnet + chlorite (section 5.6.3).

5.2.2 Peak assemblages at Zinkgruvan

Petrographic analysis of the Viksjön Formation migmatites and quartzofeldspathic gneisses exposed underground at Nygruvan revealed the peak metamorphic assemblage to be Qtz + Kfs + Bt + Sil (± Pl) (see Chapter 4 for petrographic detail). These rocks provide the best constrained data as they are apparently unaffected by pre-metamorphic metasomatism and post-peak alteration (Chapter 4).

The presence of sillimanite indicates temperatures of at least 600°C at moderate pressures (Fig. 5.1). The absence of muscovite, cordierite and kyanite from the peak assemblage further constrains P-T conditions. The absence of muscovite is particularly important as the muscovite-out isograd effectively subdivides the sillimanite stability field (Fig. 5.1), and has important implications for the onset of partial melting (section 5.2.3). Muscovite breaks down in the presence of quartz and is removed from the assemblage at approximately 650-700°C at moderate pressures (4-6 kbar) by the reaction:

$$\mathbf{Ms + Qtz \rightarrow Sil + Kfs + H_2O} \qquad [1]$$

This reaction produces K-feldspar and sillimanite, and is sometimes referred to as the second sillimanite isograd (the first being the phase transition to sillimanite from either kyanite or andalusite) (Evans & Guidotti, 1966).

Fig. 5.1 shows the petrogenetic grid devised for the KFMASH system by Spear & Cheney (1989). This grid is based on experimental data obtained from the less complex KMASH and KFASH systems, and takes into account the changes in the Mg-Fe partitioning in solid solution phases. Earlier grids (e.g., Brown, 1975; Kepezhinskas & Khlestov, 1977; Labotka, 1981) assumed fixed compositions for solid solution phases.

The P-T conditions represented by the muscovite- and cordierite-free assemblage Qtz + Kfs + Bt + Sil (+ Grt) are shown by the shaded area in Fig. 5.1. This field gives a peak P-T estimate of T = 600-800°C, P = 2-8 kbar. As the metasediments have undergone partial melting (section 5.2.3), a curve representing the minimum melting temperatures for wet (H_2O-saturated) granite further constrains peak temperatures to a ***minimum*** of 650°C at moderate pressures. However, the presence of myrmekite and perthites suggest that it may be in excess of 700°C (Smith, 1974), and melting may have occurred at higher temperatures still if water activity was low.

The petrogenetic grid shown in Fig. 5.1 is contoured with isopleths of Fe/(Fe+Mg) for garnets in assemblages containing biotite + garnet. The dependence of Fe + Mg partitioning on temperature and pressure allows garnets in such assemblages to be used as metamorphic indicators. However, in the case of garnet-bearing quartzofeldspathic gneisses of the Zinkgruvan Formation, the Fe/(Fe+Mg) ratios in garnets are inconsistent with crystallisation at high (>700°C) temperatures. Zinkgruvan garnets consistently yield Fe/(Fe+Mg) ratios of 0.84-0.96, where ratios of <0.8 would be expected of garnets crystallising at 700°C or above. This may be due to either a) re-equilibration of high-temperature garnets to lower temperatures and pressure during retrogression or b) formation at a later, lower grade stage in the evolution of the rock package, possibly related to an influx of fluid. The data and their implications are explored in detail in section 5.6.

The Zn-spinel gahnite ($ZnAl_2O_4$) occasionally occurs in sillimanite-bearing quartzofeldspathic gneisses and metaquartzite assemblages. Spinel is an indicator of high temperatures in all rock types (Frost, 1991), and gahnite is commonly associated with highly metamorphosed Zn-Pb deposits, e.g., Broken Hill, Australia (Spry, 1987); Mamandur, southern India (Chattopadhyay, 1999) and Aggeneys, South Africa. (Spry & Scott, 1986).

The lower pressure limit of peak metamorphism is constrained by the absence of cordierite, which appears at lower pressure or increasing temperatures by the breakdown of biotite and sillimanite through the following reaction:

$$\mathbf{Bt + Sil \rightarrow Grt + Crd + H_2O} \qquad [2]$$

This transition takes place at temperatures of around 750-800°C at moderate (~5 kbar) pressure. At higher temperatures still, low-Al assemblages may develop orthopyroxene as a product of the biotite dehydration reaction:

$$\mathbf{Bt \rightarrow Opx + Kfs + H_2O} \qquad [3]$$

In summary, the metapelitic assemblages of the Viksjön Formation in the mine area indicate peak metamorphic conditions of **700-750°C** and around **5 (± 2) kbar** pressure. Field C in Fig. 5.1 shows the P-T conditions represented by the sillimanite-bearing migmatites. Approximately 3 km further south, sillimanite-bearing gneisses (± Ms) occur without the association of melt, indicating that temperatures were not sufficiently high to trigger partial melting. These melt-absent gneisses are represented by Field B in Fig. 5.1.

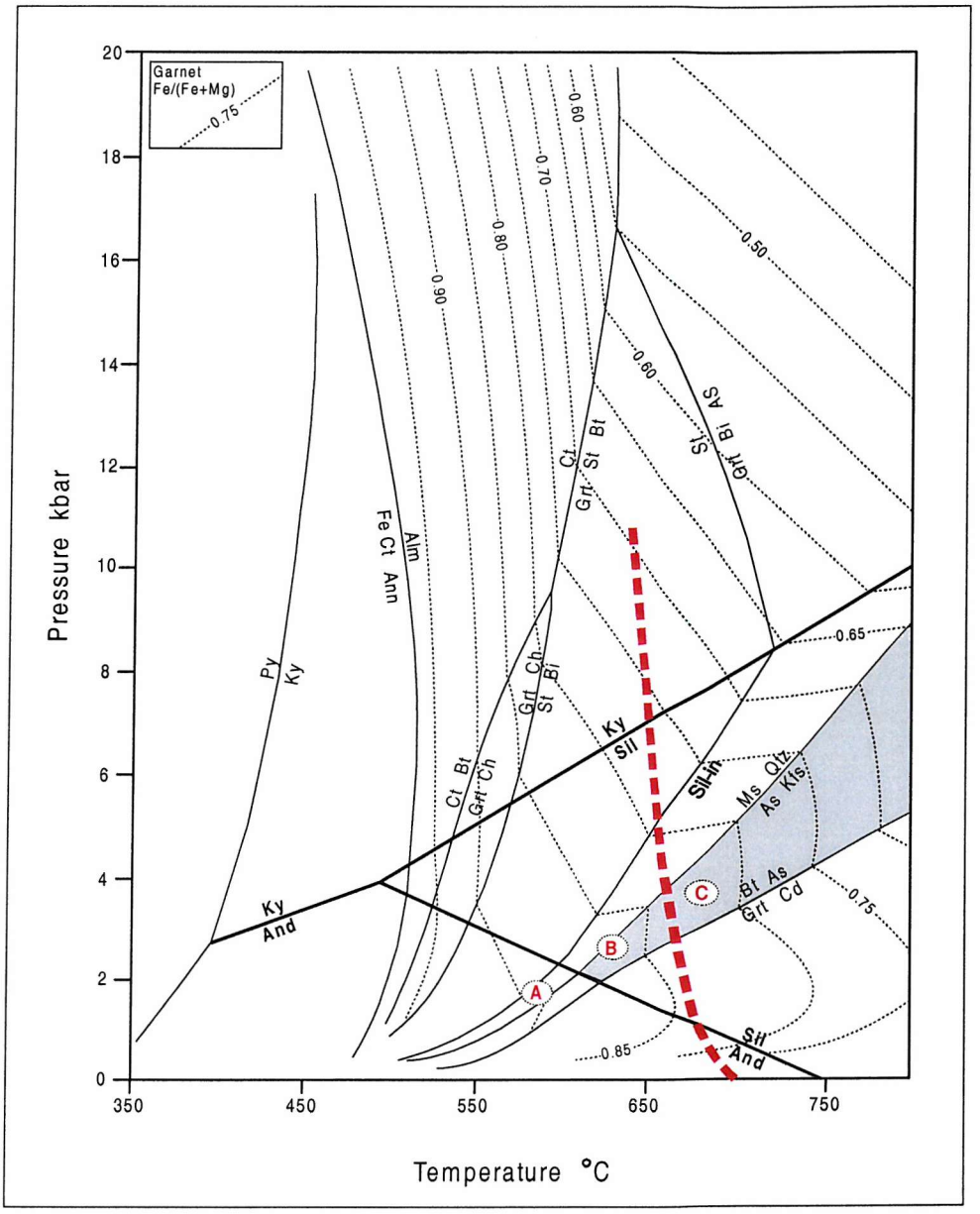

Figure 5.1: Petrogenetic grid for metasediments (KFMASH system) contoured with isopleths of Fe/(Fe+Mg) in rocks containing garnet + biotite. Dashed red line represents the onset of melting for wet granitic rocks. Dashed black lines represent isopleths for Fe/(Fe+Mg) ratios in garnets. Shaded area shows the P-T conditions represented by the peak assemblage Qtz + Kfs + Bt + Sil observed in the mine area. Field A corresponds to conditions experienced by rocks in the south of the district; Field B represents development of sillimanite gneisses without partial melting; Field C represents conditions in the mine area where migmatisation (partial melting) has occurred. See text and Fig. 5.4 for locations. Adapted from Spear & Cheney (1989). Mineral abbreviations in Appendix A.

5.2.3 Partial melting (migmatisation)

Elevated temperatures during metamorphism can lead to the onset of melting in some rocks. In water-saturated quartz and feldspar-bearing rocks, melting can initiate at temperatures of around 650-700°C (Bucher & Frey, 1994). Partial melting is shown by the development of migmatites and veined gneisses in the Viksjön Formation near the mine (Fig. 3.4). The onset of partial melting is mainly controlled by water activity (aH_2O) in the rock, which may be in part sourced from mica dehydration reactions. Water released through muscovite breakdown in pelites can react with quartz and feldspar and trigger partial melting by the reaction:

$$\mathbf{Qtz + Fsp + H_2O \rightarrow melt} \qquad [4]$$

Decreasing aH_2O in the system causes the normal muscovite dehydration reaction [1] to occur at lower temperatures (red lines in Fig. 5.2). Decreasing aH_2O has the opposite effect on the melting point of the rock (solidus curve), meaning that partial melting will take place at higher temperatures. The intersection of the solidus curve and the Ms-out isograd (black circle and grey line in Fig. 5.2) at a given aH_2O marks the highest possible stability for Ms + Qtz in that system. Below the intersection, muscovite decomposes by straightforward dehydration, producing K-feldspar and sillimanite as solid phases [1]. Above the intersection, muscovite disappears through partial melting [5] where the K-feldspar and H_2O components dissolve directly into the melt, leaving sillimanite as a solid phase:

$$\mathbf{Qtz + Ms \rightarrow Sil + melt} \qquad [5]$$

In a typical pelite system under H_2O-saturated conditions (aH_2O=1), muscovite breaks down at low pressure (< 4 kbar) to produce solid Kfs and Sil phases with H_2O by-product [1]. At around 4 kbar, the Ms-out isograd intersects the incipient melting curve (red dot, Fig. 5.3), so at pressures > 4 kbar muscovite dissolves by partial melting [5].

Partial melting in most pelites is ***vapour-absent***, that is any water released during dehydration reactions will dissolve directly into the melt without entering a vapour phase [5]. These partial melts are not saturated with respect to H_2O. This is evidenced by high-temperature mineral assemblages in granulite facies rocks which would have otherwise melted if a vapour phase was present (Spear, 1995). Any water present in pore spaces and fractures will assist melting, but as soon as melt is produced, H_2O will preferentially dissolve into it, reducing aH_2O and thus raising the melting temperature of the remaining rock.

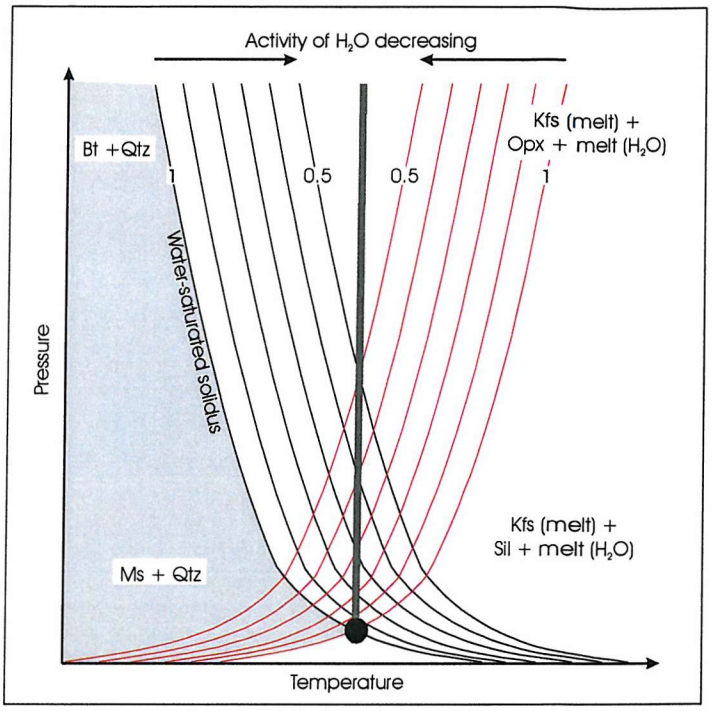

Figure 5.2: Schematic diagram to show the effects of water activity (aH_2O) on the solidus curve (black) and Ms-out isograd (red) during high-temperature metamorphism of pelites. The grey shaded field represents the Ms stability field in Qtz-bearing rocks. Modified after Bucher & Frey (1994). Mineral abbreviations in Appendix A.

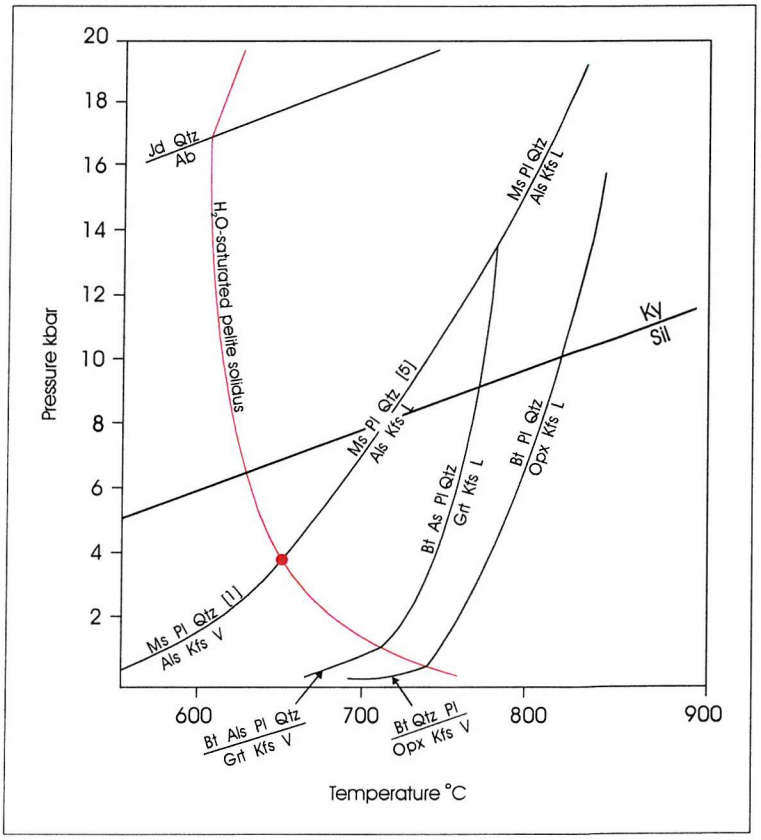

Figure 5.3: P-T diagram showing the transition from melt-absent Ms breakdown [1] to partial melting through Ms dehydration [5]. After Spear (1995). Mineral abbreviations in Appendix A.

5.2.4 Lower grade areas to the south

Preservation of sedimentary structures and peak metamorphic assemblages in the Viksjön Formation in the Höksjön area (Fig. 3.1) demonstrate lower grade metamorphism in comparison with the mine area.

Metasedimentary schists contain the peak assemblage Qtz + Bt + Pl + And + Ms. The presence of muscovite and andalusite suggest that this part of the basin experienced lower grade metamorphism, with temperatures of <650°C (Fig 5.1) and pressures of 2-3 kbar.

From south to north across the Zinkgruvan Basin, increasing grade in metapelites is shown by three distinct associations (figs 5.1 & 5.4):

(A) And + Ms + Bt assemblages.

(B) Sil + Bt (± Ms) (± St) associations **without** migmatisation.

(C) Sil + Bt + Kfs associations **with** migmatites.

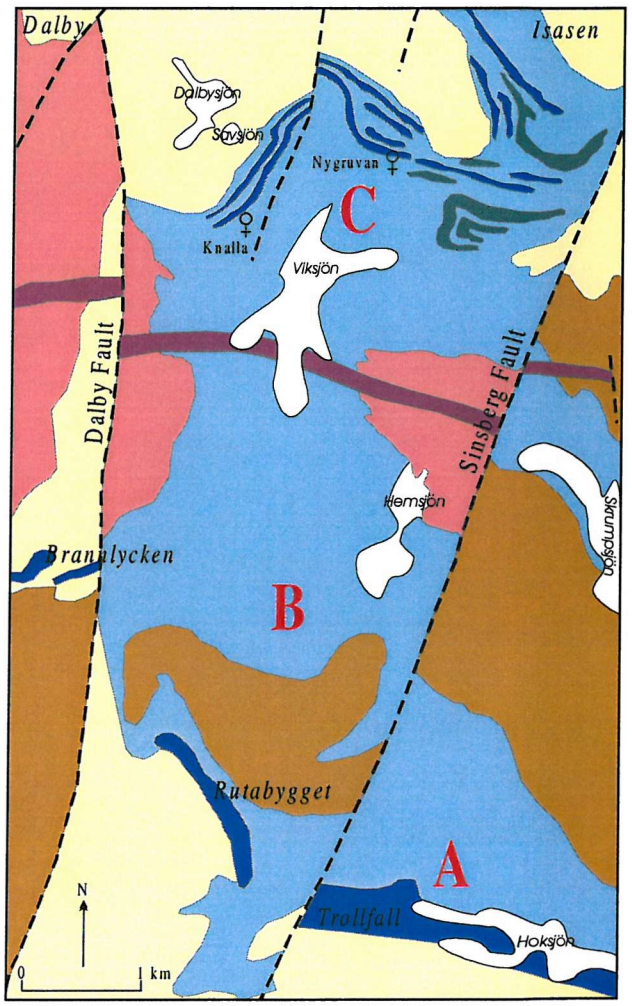

*Figure 5.4: Geological map to show distribution of metamorphic facies in the Zinkgruvan Basin. A = And + Bt + Ms assemblages; B = Sil + Bt (± Ms) associations **without** melt; C = Sil + Bt + Kfs associations **with** melt. For key see Fig. 3.1. Mineral abbreviations given in Appendix A.*

5.3 PROGRADE METAMORPHISM: METABASIC ASSEMBLAGES

Amphibolite bodies at Zinkgruvan contain the peak assemblage Hbl + An + Bt, typical of upper amphibolite facies metamorphism. The absence of actinolite and epidote, and the transition from albitic to more Ca-rich plagioclase indicates that peak temperatures exceeded those required by greenschist and epidote-amphibolite facies metamorphism.

Clinopyroxene formed from breakdown of hornblende is also not developed in these rocks, constraining the upper temperature limit of peak metamorphism to approximately 780°C (Fig. 5.5)

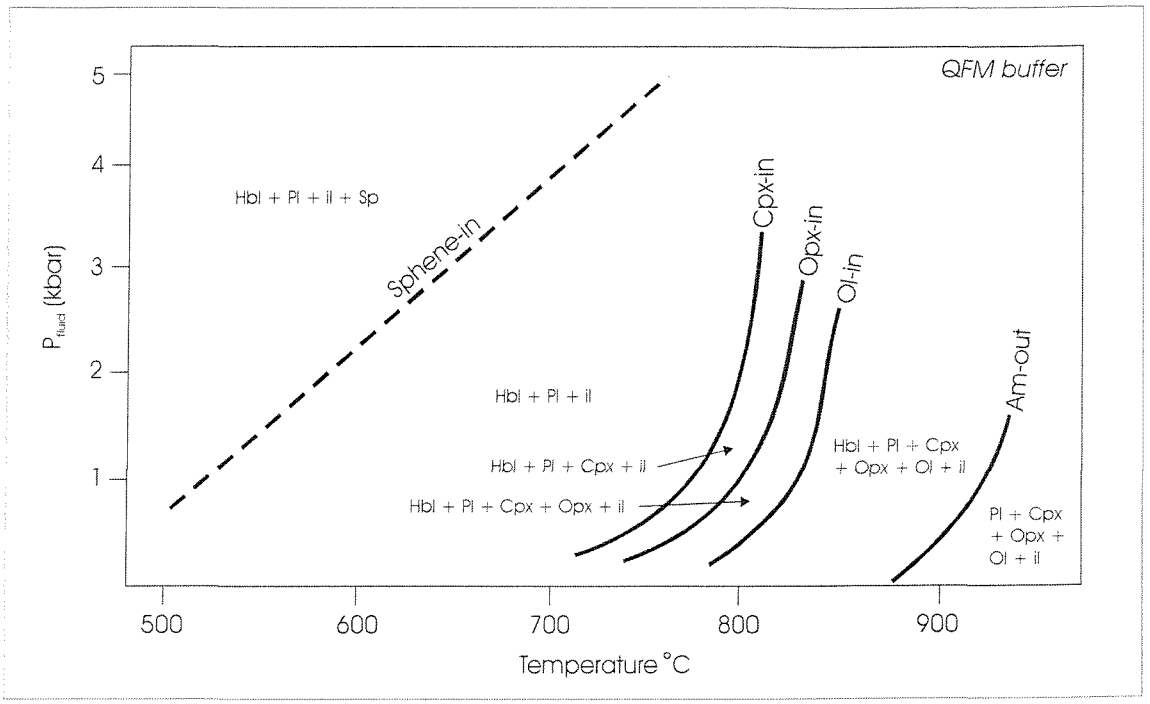

Figure 5.5: P-T relationships for metabasic rocks under fO_2 conditions defined by the QFM (quartz-fayalite-magnetite) buffer which is appropriate for the metamorphic conditions experienced at Zinkgruvan. Mineral abbreviations in Appendix A. Modified after Spear (1981). Mineral abbreviations in Appendix A.

5.4 PROGRADE METAMORPHISM: CALC-SILICATE ASSEMBLAGES

5.4.1 The CMS-HC and CAS-HC systems

The estimate of peak metamorphic P-T conditions from metapelitic and metabasic assemblages provides constraints within which the metamorphic regime can be further investigated using metacarbonate and calc-silicate assemblages, which are sensitive to fluid composition as well as changes in pressure and temperature.

The principal components of marbles and calc-silicate rocks are represented by the CaO-MgO-SiO_2-H_2O-CO_2 (CMS-HC) and CaO-Al_2O_3-SiO_2-H_2O-CO_2 (CAS-HC) systems respectively. In this section, temperature determinations are mostly based on mineral assemblages from metacarbonate rocks (CMS-HC system) whilst calc-silicate skarn assemblages help constrain fluid composition. All temperature estimates are based on a peak pressure of 5 kbar, as estimated in section 5.2.

Metamorphism of calcitic or dolomitic limestone produces assemblages containing quartz, calcite, dolomite, tremolite, diopside, forsterite and wollastonite, depending on bulk rock composition and metamorphic grade. A small amount of detrital quartz in an otherwise pure dolomite or limestone will produce a range of calc-silicate minerals during metamorphism. The phase changes due to increasing metamorphic grade involve decarbonation and dehydration reactions that occur as the carbonate phases progressively react with the silica-bearing phases such as quartz, tremolite and diopside to produce new assemblages. Fig. 5.6 shows the key components of the CMS-HC system.

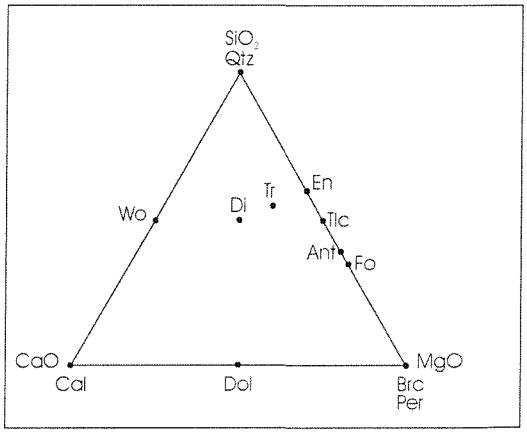

Figure 5.6: Composition triangle for the CMS-HC system, projected from H_2O and CO_2 to show the key mineral phases. See Appendix A for mineral abbreviations.

5.4.2 Calc-silicate minerals as P-T indicators

Metamorphism of siliceous limestones produces a characteristic sequence of minerals with increasing temperature (Eskola, 1922; Bowen, 1940; Tilley, 1948). In the Zinkgruvan area, the key minerals in this sequence are:

talc → tremolite → diopside → forsterite → wollastonite

Assemblages bearing tremolite, diopside, and forsterite are useful indicators of metamorphic conditions as each phase has a well-defined P-T field. Fig. 5.7 shows the relative stability of these minerals in siliceous dolomites in a sillimanite geotherm terrain, with sillimanite present and kyanite absent. The conditions shown on this diagram are likely to be a fair representation of the palaeogeotherm as deduced from the mineral assemblages of the metapelites and migmatites (section 5.2).

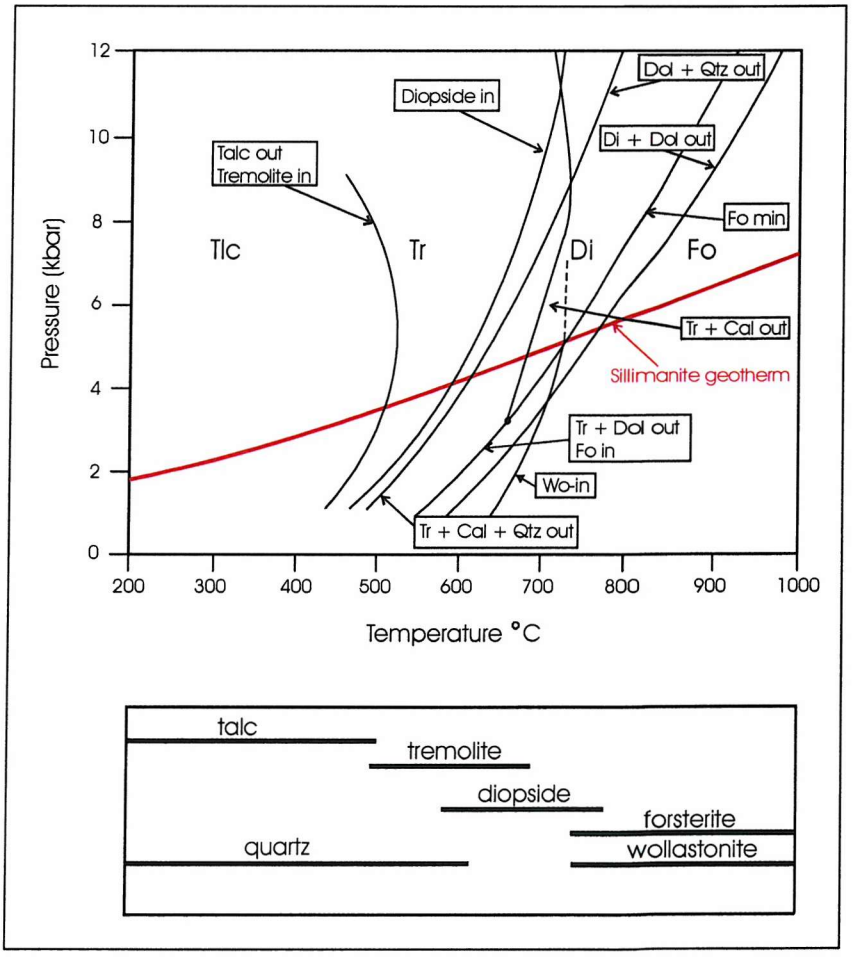

Figure 5.7: Generalised isograds and mineral zone boundaries in siliceous limestones and dolomites in a sillimanite geotherm terrain. Adapted from Bucher & Frey (1994). Wollastonite-in isograd after Greenwood (1967). Mineral abbreviations in Appendix A.

5.4.3 The importance of fluid composition

Calc-silicate mineral stability is strongly influenced by fluid composition during metamorphism. Most prograde reactions in carbonate rocks evolve H_2O and CO_2 as by-products, which directly influence the fluid chemistry. In metacarbonate systems, the fluid chemistry is usually transitional between pure H_2O and CO_2, and is expressed as the mole fraction of CO_2 (XCO_2). Most reactions that take place during prograde metamorphism of siliceous limestones and dolomites increase XCO_2 in the fluid (Fig. 5.8), so that increasingly higher temperatures are required to drive the reaction as more CO_2 is generated.

A closed system will involve a change in the composition of the fluid as more CO_2 or H_2O is released with increasing grade. In other words, the fluid will progressively change composition depending on the chemistry of the volatiles that are released or consumed by mineral breakdown. Open systems allow the gain or loss of fluids, so that the components generated by devolatilisation are diluted in an external fluid and do not strongly affect fluid chemistry. Influx of an aqueous (low XCO_2) fluid is common, and allows reactions to occur at lower temperatures. Alternatively, an open system can allow the escape of CO_2 generated by prograde reaction, thus lowering XCO_2 in the system. Substantial infiltration of fluid from an external source may be sufficient to drive metamorphism as mineral phases become unstable under progressively H_2O-rich conditions (Fig. 5.8). Note that the sequence of reactions occurring under increasingly aqueous conditions at constant temperature can be almost identical to those produced by heating at a fixed fluid composition.

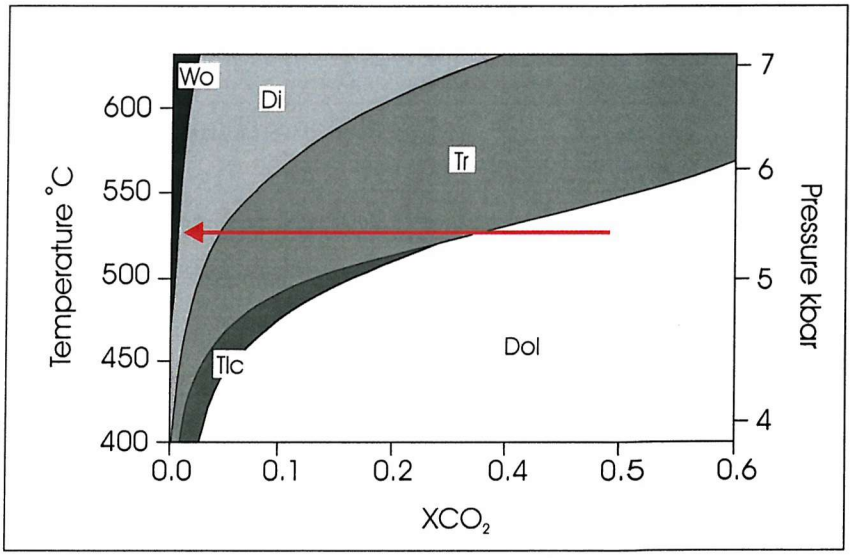

Figure 5.8: T-X diagram to show the effect of infiltration of an aqueous fluid at constant temperature in a siliceous limestone. The red line shows the change in fluid composition. The stable phase will change from Dol → Tr → Di → Wo with decreasing XCO_2. Modified after Bucher & Frey (1994).

5.4.4 Metamorphism of siliceous dolomites

Siliceous dolomitic limestones with a starting composition of Dol + Cal + Qtz will undergo a predictable sequence of reactions with increasing grade of metamorphism, as described below. The mineral assemblage produced at each stage of metamorphism is controlled by the Ca:Mg:Si ratio of the rock and fluid composition. Some dolomites may contain magnesite as an original mineral phase and will plot to the right of the Qtz-Dol tie line (figs 5.6 & 5.9), in which case talc-forming reactions occur at low grades. However, the majority of marbles at Zinkgruvan do not have a suitable composition to form these reactions, so they are considered only briefly. Temperatures quoted below are for metamorphism at ~5 ± 1 kbar and mixed-volatile fluid composition (~0.5 XCO_2), except where stated. Mineral stability fields at increasing temperatures of metamorphism are given in Fig. 5.9 and the relevant petrogenetic grid in Fig. 5.10.

Talc, the lowest-temperature calc-silicate index mineral, forms by reaction of quartz and dolomite under aqueous conditions in Mg-rich marbles [6]. It is stable up to approximately 500°C at low to moderate pressure (figs 5.7 & 5.10), beyond which it reacts to form tremolite [7], [8]:

(Tlc-in) $\mathbf{Dol + Qtz + H_2O \rightarrow Tlc + Cal + CO_2}$ [6]

$\mathbf{Dol + Tlc + Qtz \rightarrow Tr + CO_2}$ [7]

$\mathbf{Cal + Tlc \rightarrow Tr + Dol + CO_2 + H_2O}$ [8]

Tremolite is the first metamorphic mineral formed in normal siliceous dolomites (Cal + Dol + Qtz protolith). It is stable over a range of P-T conditions, forming through decomposition of dolomite in the presence of quartz at ~500-550°C [9] (Fig. 5.10). The first occurrence of tremolite provides a mappable isograd that roughly corresponds to the lower limit of amphibolite facies metamorphism.

(Tr-in) $\mathbf{Dol + Qtz + H_2O \rightarrow Cal + Tr + CO_2}$ [9]

With increasing temperature and high XCO_2 (i.e., water absent), reaction [9] will produce diopside instead of tremolite (Fig. 5.10, reaction [10]). Tremolite becomes unstable and reacts with quartz and calcite above 575°C to form diopside [11]. Above ~640-650°C, once all quartz has been consumed by reaction [11] (or if quartz was previously consumed in tremolite-forming reactions) diopside is generated by reaction [12].

(Di-in) $\mathbf{Tr + Cal + Qtz \rightarrow Di + H_2O + CO_2}$ [11]

$\mathbf{Tr + Cal \rightarrow Dol + Di + H_2O + CO_2}$ [12]

Forsterite is the highest-temperature index mineral formed in siliceous dolomites. The first appearance of forsterite (Fo-in isograd, Fig. 5.7) results from breakdown of diopside by reaction [13] at ~650-700°C. At pressures greater than 8 kbar (kyanite-type geotherm) this reaction

requires extreme temperatures (>800°C) unless an externally-derived aqueous fluid is introduced into the system.

(Fo-in) $\mathbf{Dol + Di \rightarrow Cal + Fo + CO_2}$ [13]

Forsterite forms at lower temperatures in Mg-rich marbles through the breakdown of talc [14] and tremolite [15] (Fig. 5.10).

$\mathbf{Dol + Tlc \rightarrow Tr + Fo + CO_2}$ [14]

$\mathbf{Dol + Tr \rightarrow Fo + Di + H_2O + CO_2}$ [15]

5.4.5 Metamorphism of siliceous limestones

Siliceous limestones with an initial composition of Cal + Qtz + Dol (Cal > Dol) undergo a similar sequence of prograde reactions to a siliceous dolomite at 0.5 XCO_2 and 5 kbar pressure (figs 5.9 & 5.10). However, the peak assemblages at each stage of metamorphism are different, as illustrated in Table 5.2. At temperatures in excess of 700°C, calcite-dominant assemblages produce wollastonite as a function of the breakdown of quartz and calcite:

$\mathbf{Cal + Qtz \rightarrow Wo + CO_2}$ [16]

Greenwood (1967) showed this reaction to be strongly affected by XCO_2. For $XCO_2 = 0.5$ the equivalent stable assemblage in siliceous dolomites is Cal + Dol + Fo (Fig. 5.9), but under aqueous conditions (XCO_2 close to 0.0) the wollastonite-in reaction can occur at much lower temperatures (figs 5.8 & 5.10).

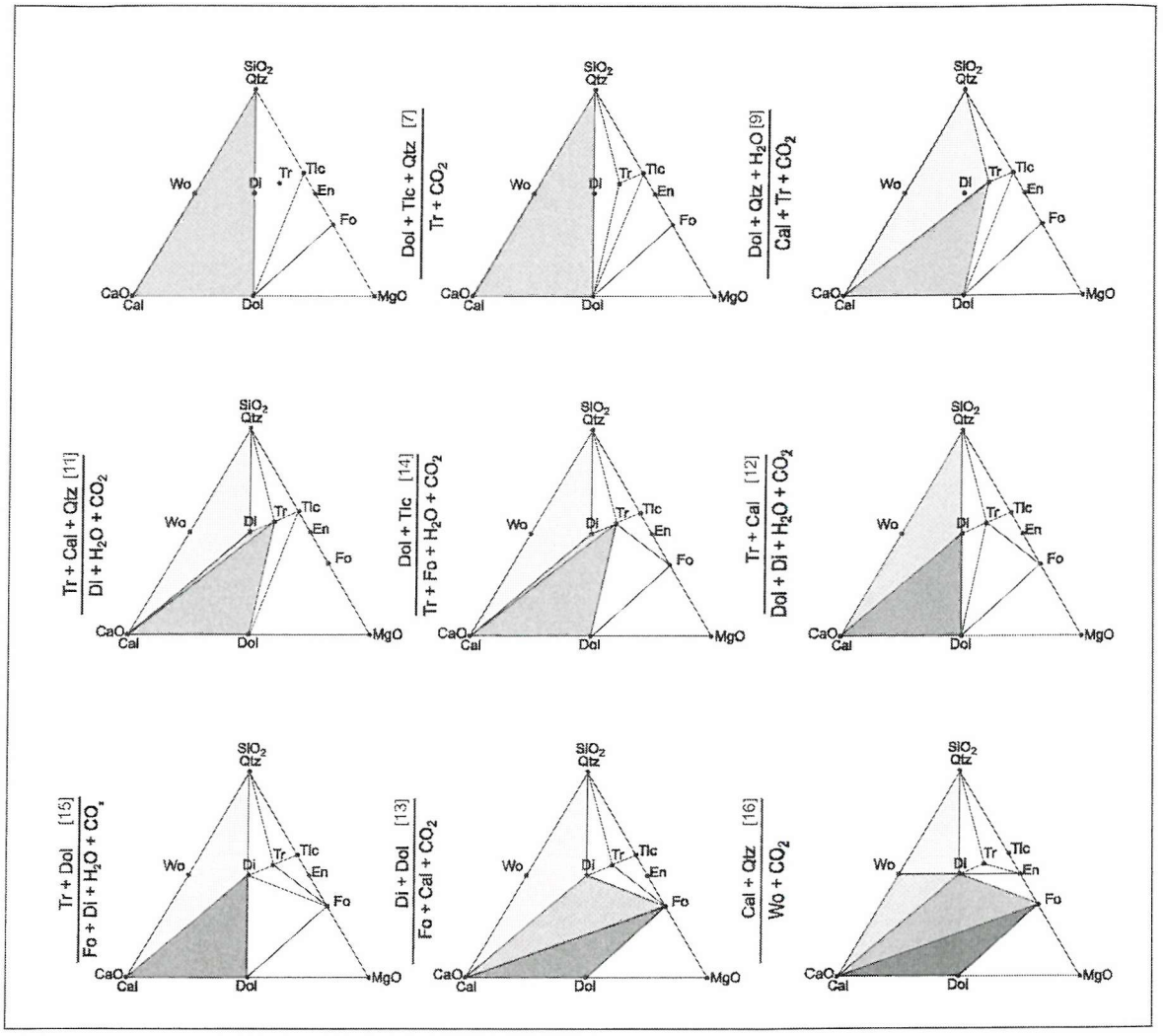

Figure 5.9: Series of CaO-MgO-SiO_2 ternary diagrams to show stable mineral assemblages at increasing temperatures of metamorphism. Shaded fields indicate stable mineral assemblages for siliceous dolomites and limestones. Relevant petrogenetic grid is given in Fig. 5.10. Modified after Spear (1995). Mineral abbreviations in Appendix A.

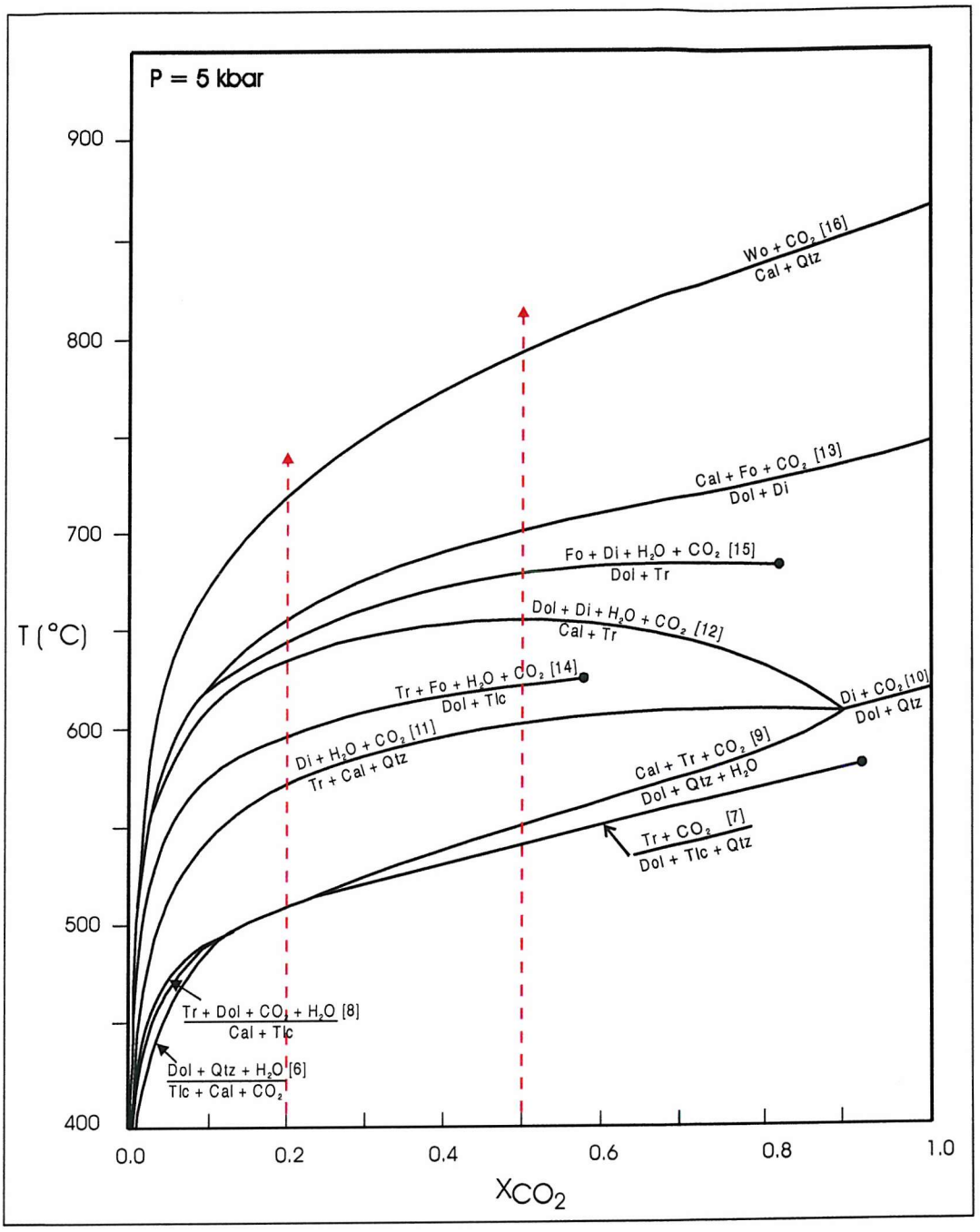

Figure 5.10: T-XCO_2 diagram for the CMS-HC system, showing key reactions for metamorphism at fixed pressure (P = 5 kbar). Calcite present in excess. Red lines show the path of isobaric metamorphism at 0.2 and 0.5 XCO_2. Refer to figure 5.9 for phase diagrams showing stable mineral assemblages after each reaction. Modified after Spear (1995). Mineral abbreviations in Appendix A.

5.4.6 Effects of bulk composition

Limestone and dolomite protoliths will obviously produce different mineral assemblages and reaction sequences during metamorphism, but the amount of silica in the system also causes significant mineralogical variations. At low metamorphic grade, silica content has a minor effect on the mineral assemblage produced, but becomes increasingly important with rising temperature. Calcitic and SiO_2-rich dolomites are able to form diopside at lower temperature than SiO_2-poor dolomites, which depend on the release of Ca and Si from tremolite breakdown for diopside formation. At high temperatures, SiO_2-rich dolomites contain sufficient silica to form both diopside and forsterite at >700°C, whereas SiO_2-poor varieties can only produce forsterite. A similar relationship is seen at high temperatures in calcitic limestones: SiO_2-poor varieties consume all their quartz in the formation of wollastonite, producing a peak assemblage of Cal + Wo + Di. Highly siliceous limestones may contain enough SiO_2 to sustain quartz at high grades, creating a peak assemblage of Qtz + Wo + Di. However, the quantity of silica required to produce this assemblage implies that the original protolith is actually a calc-arenite rather than a true limestone.

Fig. 5.11 And Table 5.1 show the variation in assemblages as a result of bulk composition. The four compositions marked represent SiO_2-poor and SiO_2-rich dolomites and limestones.

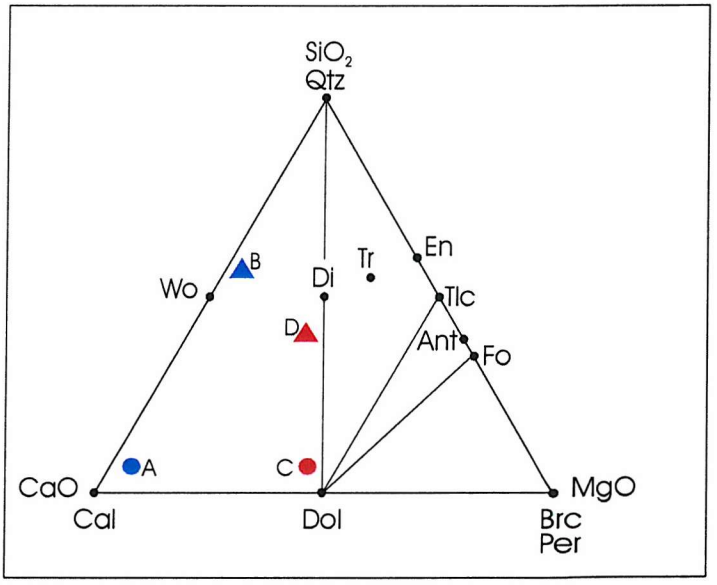

Figure 5.11: CaO-MgO-SiO_2 ternary diagram showing the position of 4 hypothetical metacarbonate rocks. A = SiO_2-poor limestone; B = SiO_2-rich limestone; C = SiO_2-poor dolomite; D = SiO_2-rich dolomite. All protoliths contain Cal + Dol + Qtz in varying quantities. The mineral assemblages formed in each rock type during prograde metamorphism are given in Table 5.2. Mineral abbreviations in Appendix A.

Reaction	Siliceous limestone		Siliceous dolomite		Approximate T (°C)	
	Comp A	Comp B	Comp C	Comp D	0.2 XCO_2	0.5 XCO_2
9	Cal + Qtz + Tr	Cal + Qtz + Tr	Cal + Dol + Tr	Cal + Dol + Tr	510	550
11	Cal + Qtz + Di	Cal + Qtz + Di	Cal + Dol + Tr	Cal + Dol + Tr	570	600
12	Cal + Qtz + Di	Cal + Qtz + Di	Cal + Dol + Di	Cal + Dol + Di	630	645
13	Cal + Qtz + Di	Cal + Qtz + Di	Cal + Dol + Fo	Cal + Di + Fo	650	690
16	Cal + Di + Wo	Qtz + Di + Wo	Cal + Dol + Fo	Cal + Di + Fo	715	780

Table 5.1: Comparison of mineral assemblages produced by progressive metamorphism of siliceous dolomites and limestones. Note that at higher grades, the SiO_2 content of the rock has an important effect on mineral stability and that all reactions occur at higher T with increasing XCO_2. Refer to Fig. 5.11 for positions of rock types on CaO-MgO-SiO_2 ternary diagram and Fig. 5.9 for relevant phase diagrams.

5.4.7 Peak assemblages in Zinkgruvan metacarbonate rocks

Peak P-T conditions in the mine area were estimated by plotting the chemistry of marble and calc-silicate marble samples (determined from XRF analyses, Appendix E) on ternary diagrams, onto which the mineral stability fields at increasing grades of metamorphism are superimposed (Fig. 5.12). Fluid composition and pressure are fixed at 0.2 XCO_2 (see section 5.4.9) and 5 kbar (section 5.2). The chemical composition of the rock determines which phases are present at different metamorphic grades. Comparison of mineral assemblages observed in thin section with predicted assemblages at specific stages of metamorphism (Table 5.2) allows an estimation of the peak P-T regime. Although the compositions of minerals in the samples studied contain minor of Fe* and Mn, these elements are not included on the ternary diagrams for simplicity. The effect of these additional components on mineral stability fields is difficult to assess, but by comparing temperature estimates from calc-silicate and carbonate assemblages to those gained from other lithologies, any significant differences in P-T estimates can be detected. The addition of FeO* + MnO to MgO shifts sample positions to the right by only 2-3%, which does not alter the predicted peak mineral assemblage for the majority of the samples.

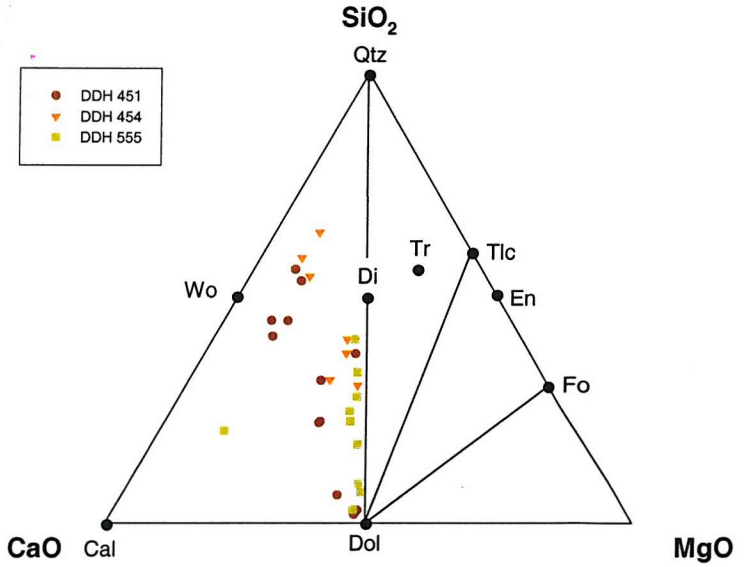

[9] Dol + Qtz + H_2O = Cal + Tr + CO_2

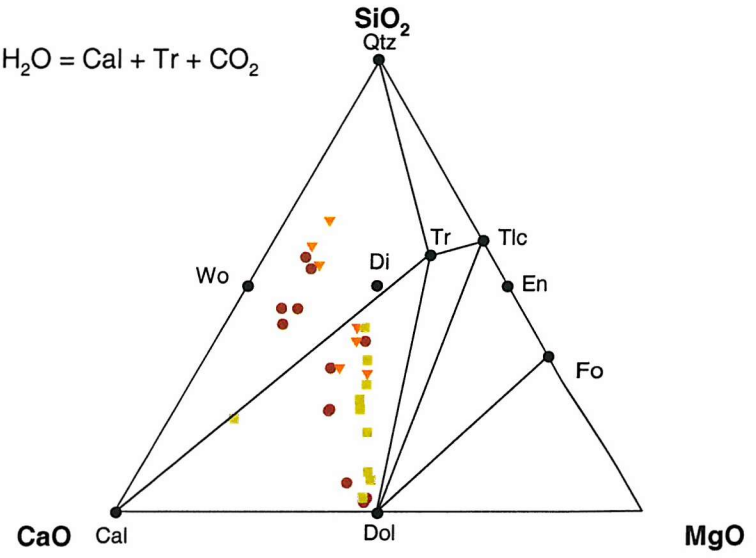

[11] Tr + Cal + Qtz = Di + H_2O + CO_2

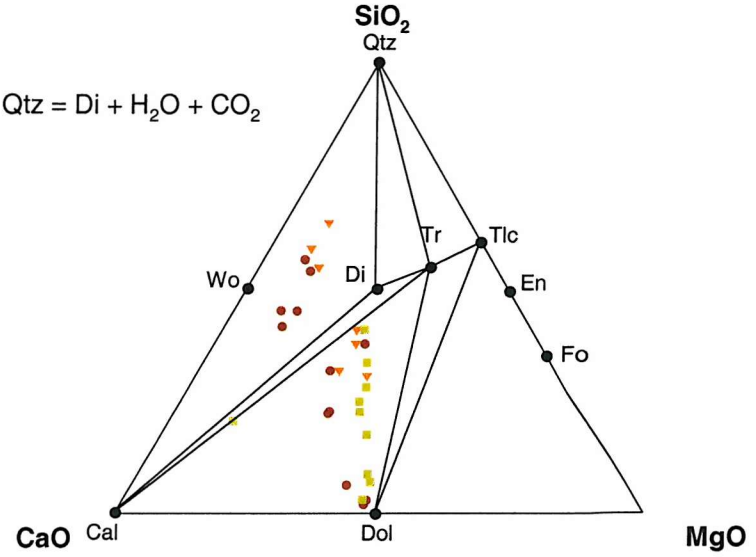

Figure 5.12 Series of CaO-MgO-SiO_2 ternary diagrams showing stable mineral assemblages during prograde metamorphism of Zinkgruvan Formation carbonate rocks at P=5 kbar and XCO_2 = 0.2. Relevant petrogenetic grid given in Fig. 5.10. Adapted from Spear (1995).

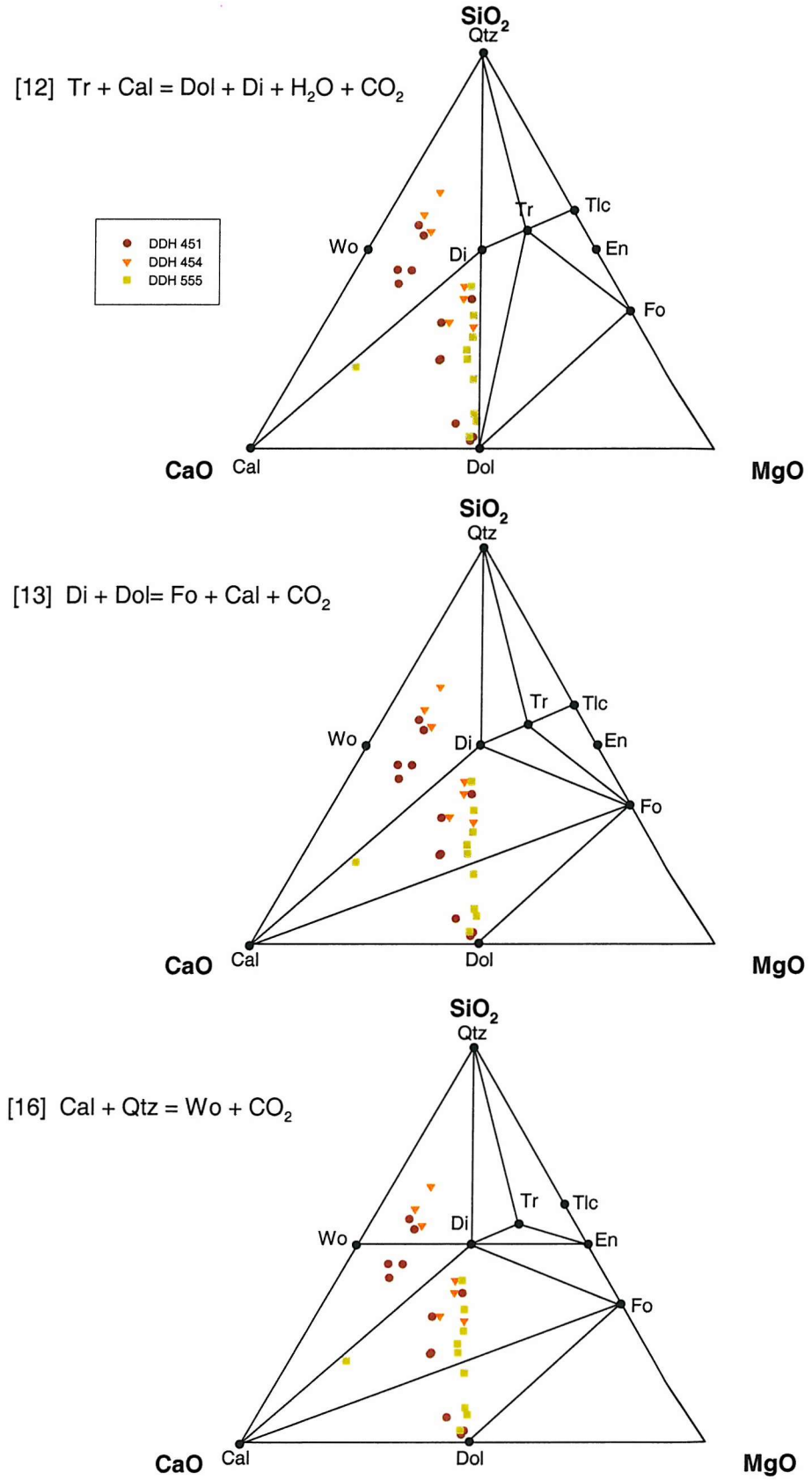

Figure 5.12 Series of CaO-MgO-SiO_2 ternary diagrams showing stable mineral assemblages during prograde metamorphism of Zinkgruvan Formation carbonate rocks at P=5 kbar and XCO_2 = 0.2. Relevant petrogenetic grid given in Fig. 5.10. Adapted from Spear (1995).

Sample	Observed	SiO_2:CaO:MgO	Before [9]	After [9]	After [11]	After [12]	After [13]	After [16]
451/15	Cal + Qtz + Di	45:47:8	Cal + Dol + Qtz	Cal + Qtz + Tr	Cal + Qtz + Di	Cal + Qtz + Di	Cal + Di + Qtz	Cal + Di + Wo
451/16	Cal + Qtz + Di	48:43:9	Cal + Dol + Qtz	Cal + Qtz + Tr	Cal + Qtz + Di	Cal + Qtz + Di	Cal + Di + Qtz	Cal + Di + Wo
451/17	Cal + Qtz + Di	48:46:6	Cal + Dol + Qtz	Cal + Qtz + Tr	Cal + Qtz + Di	Cal + Qtz + Di	Cal + Di + Qtz	Cal + Di + Wo
451/18	Cal + Qtz + Di	59:35:6	Cal + Dol + Qtz	Cal + Qtz + Tr	Cal + Qtz + Di	Cal + Qtz + Di	Cal + Di + Qtz	Cal + Qtz + Wo
451/19	Cal + Qtz + Di + Wo	57:36:7	Cal + Dol + Qtz	Cal + Qtz + Tr	Cal + Qtz + Di	Cal + Qtz + Di	Cal + Di + Qtz	Cal + Qtz + Wo
454/04	Cal + Di + Fo	35:39:26	Cal + Dol + Qtz	Cal + Dol + Tr	Cal + Dol + Tr	Cal + Dol + Di	Cal + Di + Fo	Cal + Di + Fo
454/24	Cal + Di	46:35:19	Cal + Dol + Qtz	Cal + Qtz + Tr	Cal + Qtz + Di	Cal + Qtz + Di	Cal + Qtz + Di	Cal + Di + Wo
454/26	Cal + Di + Fo	43:37:20	Cal + Dol + Qtz	Cal + Qtz + Tr	Cal + Tr + Di	Cal + Dol + Di	Cal + Di + Fo	Cal + Di + Fo
454/28	Cal + Qtz + Di	62:33:5	Cal + Dol + Qtz	Cal + Qtz + Tr	Cal + Qtz + Di	Cal + Qtz + Di	Cal + Qtz + Di	Cal + Qtz + Wo
454/29	Cal + Qtz + Di	58:34:8	Cal + Dol + Qtz	Cal + Qtz + Tr	Cal + Qtz + Di	Cal + Qtz + Di	Cal + Qtz + Di	Cal + Qtz + Wo
454/30	Qtz + Di + Wo	68:26:6	Cal + Dol + Qtz	Cal + Qtz + Tr	Cal + Qtz + Di	Cal + Qtz + Di	Cal + Qtz + Di	Cal + Qtz + Wo
454/40	Cal + Di + Fo	36:43:21	Cal + Dol + Qtz	Cal + Qtz + Tr	Cal + Tr + Di	Cal + Dol + Di	Cal + Di + Fo	Cal + Di + Fo
555/07	Cal + Di + Fo	36:45:19	Cal + Dol + Qtz	Cal + Qtz + Tr	Cal + Tr + Di	Cal + Dol + Di	Cal + Di + Fo	Cal + Di + Fo
555/10	Cal + Di + Fo	7:34:59	Cal + Dol + Qtz	Cal + Dol + Tr	Cal + Dol + Tr	Cal + Dol + Di	Cal + Dol + Fo	Cal + Dol + Fo
555/14	Cal + Fo	26:46:28	Cal + Dol + Qtz	Cal + Dol + Tr	Cal + Dol + Tr	Cal + Dol + Di	Cal + Di + Fo	Cal + Di + Fo
555/15	Cal + Dol + Fo	11:53:36	Cal + Dol + Qtz	Cal + Dol + Tr	Cal + Dol + Tr	Cal + Dol + Di	Cal + Dol + Fo	Cal + Dol + Fo
555/17	Cal + Dol + Fo	9:54:37	Cal + Dol + Qtz	Cal + Dol + Tr	Cal + Dol + Tr	Cal + Dol + Di	Cal + Dol + Fo	Cal + Dol + Fo
555/18	Cal + Di + Wo	46:33:21	Cal + Dol + Qtz	Cal + Qtz + Tr	Cal + Qtz + Di	Cal + Qtz + Di	Cal + Qtz + Di	Cal + Di + Wo
555/20	Cal + Dol + Fo	4:38:58	Cal + Dol + Qtz	Cal + Dol + Tr	Cal + Dol + Tr	Cal + Dol + Di	Cal + Dol + Fo	Cal + Dol + Fo
555/22	Cal + Dol + Fo	21:32:47	Cal + Dol + Qtz	Cal + Dol + Tr	Cal + Dol + Tr	Cal + Dol + Di	Cal + Di + Fo	Cal + Di + Fo
555/28	Cal + Fo	39:37:24	Cal + Dol + Qtz	Cal + Dol + Tr	Cal + Dol + Tr	Cal + Dol + Di	Cal + Di + Fo	Cal + Di + Fo
555/29	Cal + Di + Fo	23:68:9	Cal + Dol + Qtz	Cal + Qtz + Tr	Cal + Qtz + Di	Cal + Qtz + Di	Cal + Qtz + Di	Cal + Di + Wo
555/33	Cal + Di + Fo	29:27:44	Cal + Dol + Qtz	Cal + Dol + Tr	Cal + Dol + Tr	Cal + Dol + Di	Cal + Di + Fo	Cal + Di + Fo
555/35	Cal + Di + Fo	33:41:26	Cal + Dol + Qtz	Cal + Dol + Tr	Cal + Dol + Tr	Cal + Dol + Di	Cal + Di + Fo	Cal + Di + Fo

Table 5.2: Comparison of observed mineral assemblages with predicted mineral assemblages for metacarbonate rocks from the Zinkgruvan Formation. Shaded areas show where predicted assemblage matches observed assemblage. Figures in brackets [ ] refer to reaction numbers. Reactions involving talc are omitted as they are irrelevant for these rocks. Refer to Fig. 5.10 for relevant petrogenetic grid and Fig. 5.12 for ternary diagrams showing mineral stability fields.

Metamorphism at Zinkgruvan has produced six diagnostic peak assemblages in the marbles and calc-silicate marbles (Table 5.2), dependent on the bulk chemistry of the protolith (Chapter 4):

Calcitic protolith:	Cal + Qtz + Di
	Qtz + Di + Wo
	Cal + Qtz + Wo
Dolomitic protolith:	Cal + Di + Fo
	Cal + Dol + Fo
	Cal + Fo + Chu

Comparisons of observed mineral assemblages with predicted assemblages (Table 5.2) shows that the majority of samples experienced metamorphic conditions consistent with those required for reaction [13]. The widespread occurrence of forsterite in dolomite-normative samples indicates ***minimum*** peak temperatures of **650°C** at 0.2 XCO_2 and 5 kbar pressure. Tremolite is absent from the peak assemblages, showing that temperatures must have exceeded 630°C. The presence of wollastonite in calcitic/quartz-rich samples implies temperatures in excess of those represented by reaction [16]. This indicates temperatures of **>700°C** under the relevant physiochemical conditions, or the influx of an externally-derived aqueous fluid into the system. Assemblages containing Cal + Di + Qtz are not suitable P-T indicators as they are stable over a wide temperature range.

Other peak metamorphic phases

Other peak metamorphic minerals in the marbles and calc-silicate marbles include Al_2O_3 ± K_2O-bearing phases as a result of contamination of the carbonate rock prior to metamorphism (Chapter 4).

Clinochlore is a common phase in metamorphosed dolomites containing aluminium, and although chlorite group minerals are generally regarded as low temperature phases, clinochlore in dolomitic marbles is actually stable over a broad range of metamorphic grades, breaking down at high temperatures (>650°C) to form spinel:

$$\mathbf{Dol + Chl \rightarrow Cal + Fo + Spl + CO_2 + H_2O} \quad [17]$$

$$\mathbf{Cal + Chl \rightarrow Di + Fo + Spl + CO_2 + H_2O} \quad [18]$$

Pleonaste spinel is a common constituent of the dolomitic marbles at Zinkgruvan, and is commonly reported in marbles from inner zones of contact metamorphic aureoles (e.g., Rice, 1977). Clinochlore is also present, but rarely occurs in samples containing pleonaste, showing that in the majority of cases metamorphic grade exceeded the temperatures required by reaction [17].

In many samples, the clinochlore is clearly a retrogressive phase, forming intergrowths with serpentine pseudomorphing after forsterite.

Phlogopite is present in almost all marble and calc-silicate marbles, representing a degree of potassium contamination prior to or during metamorphism (Chapter 4). If the source of the contamination is detrital K-feldspar, this transforms to phlogopite at very low grade by the reaction:

$$\mathbf{Dol + Kfs + H_2O \rightarrow Phl + Cal + CO_2} \qquad [19]$$

Phlogopite is stable in marbles to very high temperatures (Fig. 5.13), and is often found in marbles in the high-T zone of contact aureoles.

The contamination of a relatively pure carbonate rock with components such as aluminium can affect the conditions under which key mineral-forming reactions take place. For example, the formation of phlogopite may consume silica that would otherwise be used in calc-silicate mineral-forming reactions, so that silica is depleted earlier than in a phlogopite-free rock. If the phlogopite is generated by metamorphism of original detrital K-feldspar, then the silica allocation is not a problem. However, if potassium is introduced into the system via a fluid without accompanying silica, then formation of phlogopite will remove silica from the calc-silicate 'budget'. The same principle applies to components such as Mg, which may be accommodated in clinochlore rather than forsterite and so on. Fig. 5.13 illustrates the phase relationships in a metacarbonate system with K and Al contaminants.

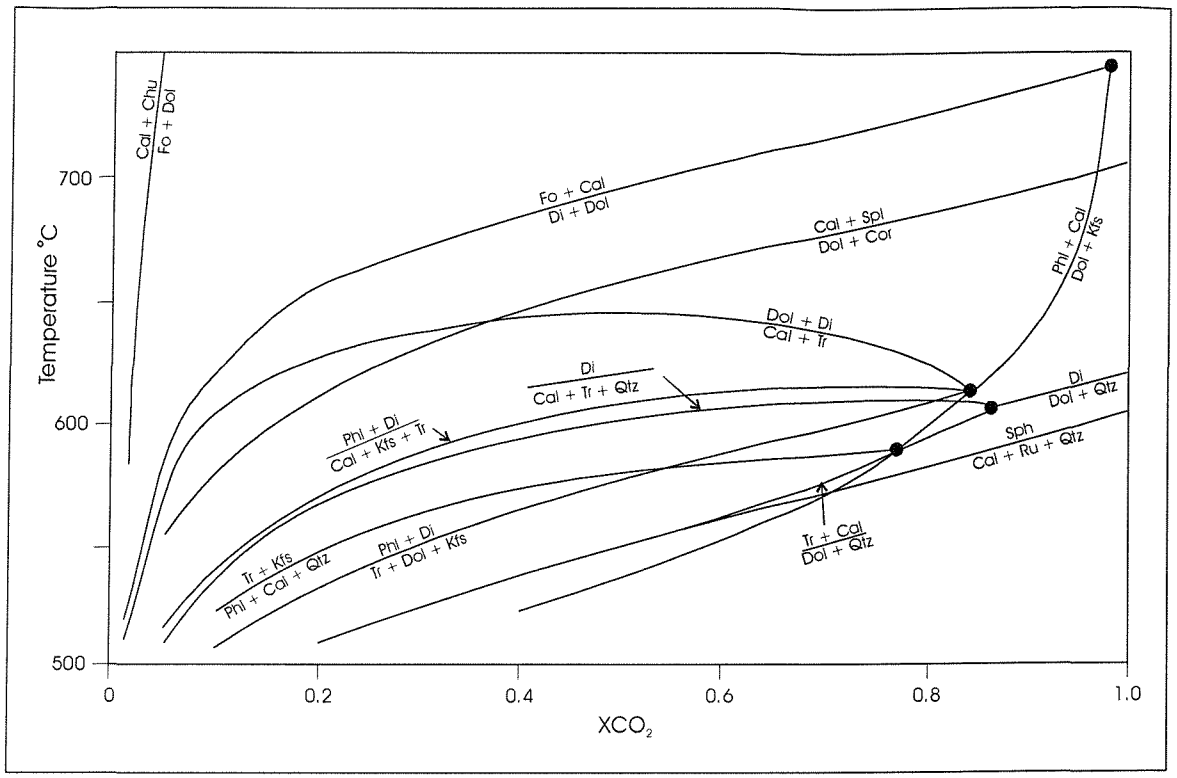

Figure 5.13: Isobaric T-XCO_2 diagram for marble assemblages in the system CaO-MgO-SiO_2-Al_2O_3-K_2O-CO_2-H_2O. P = 6 kbar. Adapted from Satish-Kumar & Niimi (1998).

The presence of phlogopite has important implications for the stability of the relatively rare mineral ***clinohumite***, which is observed in a few dolomitic marble samples from the mine area. Any fluorine present in the system (for example, that released by the breakdown of tremolite) will preferentially partition into clinohumite in metacarbonate rocks with the appropriate composition. However, the presence of phlogopite will alter the fluorine partitioning coefficient as phlogopite formation will consume fluorine. Clinohumite stability is partly dependent on the mole fraction of fluorine in the mineral, so with increasing X_F^{Chu}, clinohumite is able to exist at higher XCO_2 conditions (Fig. 5.14). Clinohumite stability was extensively investigated in Rice (1980), who showed that pressure, XCO_2 and X_F^{Chu} control the occurrence of this mineral in impure dolomitic limestones. Clinohumite can form in marbles by the following reactions, depending on the above variables and the bulk composition of the rock (Fig. 5.14):

$$\mathbf{Fo + Dol + H_2O \rightarrow Chu + Cal + CO_2} \quad [20]$$

$$\mathbf{Tr + Dol + H_2O \rightarrow Chu + Cal + CO_2} \quad [21]$$

Reaction [20] is the main clinohumite-forming mechanism in marbles, and occurs at increasing pressures with decreasing XCO_2 (Fig. 5.15).

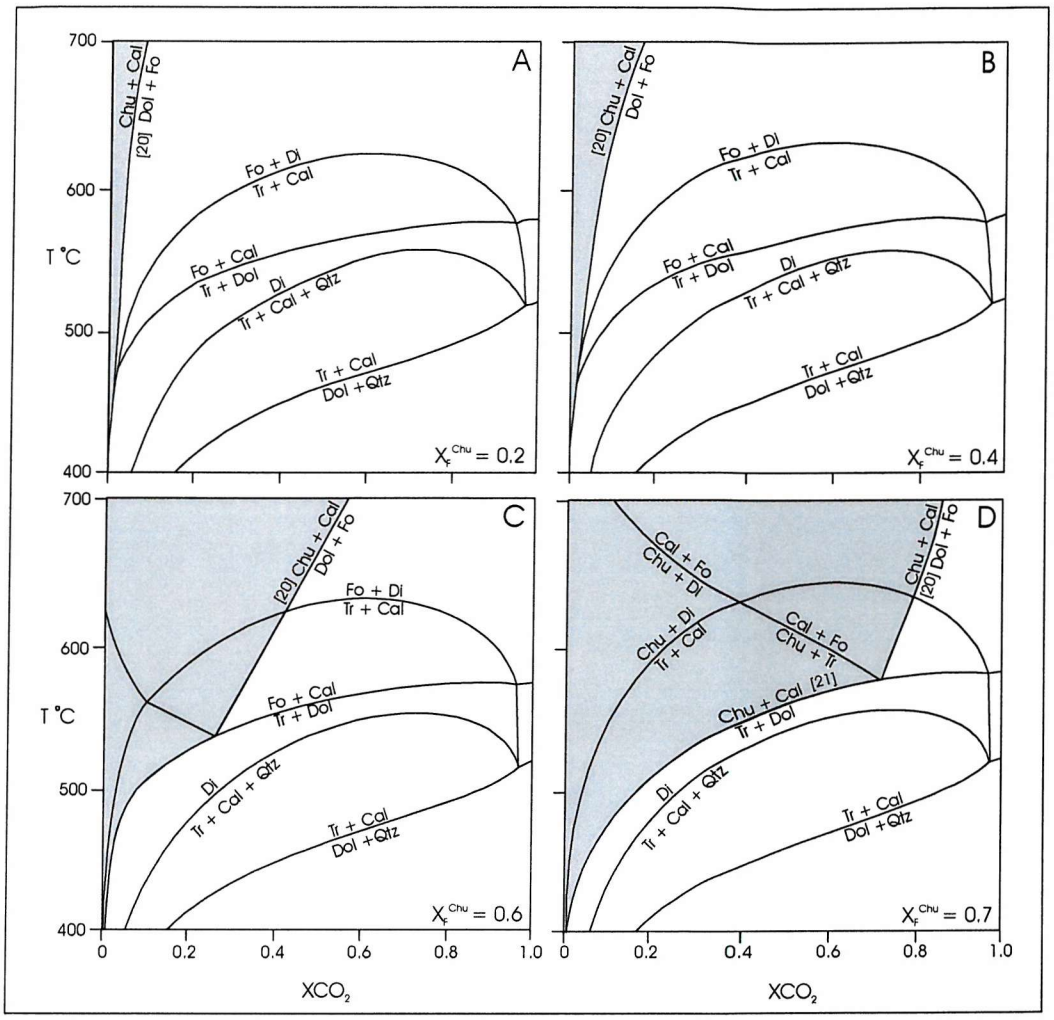

Figure 5.14: T-X diagrams to show the increasing stability of clinohumite in marbles with increasing mole fraction of fluorine in clinohumite relative to tremolite. A = 0.2 X_F^{Chu}; B = 0.4 X_F^{Chu}; C = 0.6 X_F^{Chu}; D = 0.7 X_F^{Chu}. P = 2 kbar. Shaded areas mark the stability field for Chu + Cal. After Rice (1980).

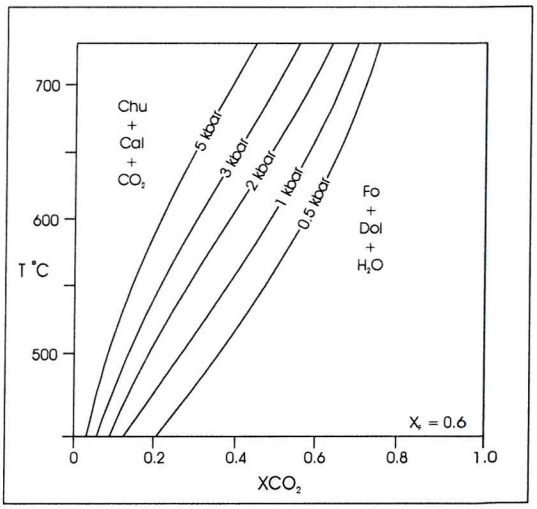

Figure 5.15: Experimental T-X diagram showing the effects of XCO_2 and pressure on the main clinohumite-forming reaction [20] at fixed X_F^{Chu}. After Rice (1980).

The occurrence of clinohumite in the Zinkgruvan marbles is consistent with the high temperature aqueous conditions indicated by the other peak phases, and its presence has important implications for fluid composition (see section 5.4.9). Its restricted occurrence may be due to only localised areas of favourable physiochemical conditions, or it could have been present in abundance, but is now replaced by the widespread serpentine which has pseudomorphed the majority of forsterite in the dolomitic marbles (section 5.6.1).

5.4.8 Peak assemblages in calc-silicate skarns

Calc-silicate skarns contain combinations of the following peak metamorphic phases, depending on bulk rock chemistry: Di + Cal + Qtz ± Grs ± Wo ± Ves ± An ± Tr.

At Zinkgruvan, banded calc-silicate skarns are believed to have developed through reaction between metacarbonate horizons and adjacent quartzofeldspathic lithologies during prograde metamorphism. Research on metamorphism of marly or calcareous sediments shows diopside to be the highest-temperature phase (Ferry, 1983a,b). Grossular and wollastonite are the high-temperature phases in calc-silicate skarns under aqueous conditions (Fig. 5.16A) (section 5.4.9), and grossular may be replaced by anorthite under more CO_2-rich conditions (Fig. 5.16A). Tremolite may be stable with diopside in some skarns (Ferry, 1983a,b) but also forms distinctly later (lower-T) overgrowths. Vesuvianite is stable across a range of temperatures and pressures, and is therefore not a useful P-T indicator.

The peak assemblages observed in calc-silicate skarns provide no additional data to constrain peak metamorphic conditions at Zinkgruvan. However, they are consistent with P-T determinations made from other lithologies, and are more useful as indicators of fluid composition (5.4.9).

5.4.9 Metamorphic fluid composition

Fluid composition can be deduced from the presence of specific mineral phases in the peak assemblages. The occurrence of wollastonite and grossular in calc-silicate marbles and skarns gives a clear indication that peak metamorphism was accompanied by an aqueous (low XCO_2) fluid. Wollastonite is unable to develop in closed system pure marbles, so an externally-derived H_2O-rich fluid is required for this phase to evolve. Fig. 5.16 shows the stability of wollastonite and grossular with reference to fluid composition.

Aqueous fluids are also necessary for the formation of clinohumite (Fig. 5.14). The presence of humite group minerals in marbles indicates fluorine in the metamorphic fluid, as hydroxyl end-member phases of the Humite group are rare (Deer *et al.*, 1992). Clinohumite forms under low P_{HF} conditions (as opposed to the similar mineral chondrodite, which requires high P_{HF} conditions). The original source of the fluorine is uncertain: the simplest explanation is a localised

sedimentary contaminant in the original limestone, with fluorine taken up by tremolite, phlogopite and clinohumite during metamorphism. However, the widespread pegmatite intrusions may have introduced fluorine into the marbles prior to or during metamorphism, or fluorine may have been associated with other boron-bearing fluids (e.g., hydrothermal fluids), which is manifested in some rocks as tourmaline.

5.4.10 Lower grade areas to the south

Marbles outcropping in the south of the basin around lake Höksjön show evidence of lower grade metamorphism, consistent with observations made in metapelitic assemblages from the same area (section 5.2.4). Marbles from this area contain the peak assemblage Qtz + Cal + Tr, indicative of temperatures below approximately 600°C (Figs 5.9 & 5.10). As there is no mineralogical or textural evidence to suggest that these are retrogressive assemblages, it is interpreted that this area has experienced significantly lower grades of metamorphism compared to the mine area.

A

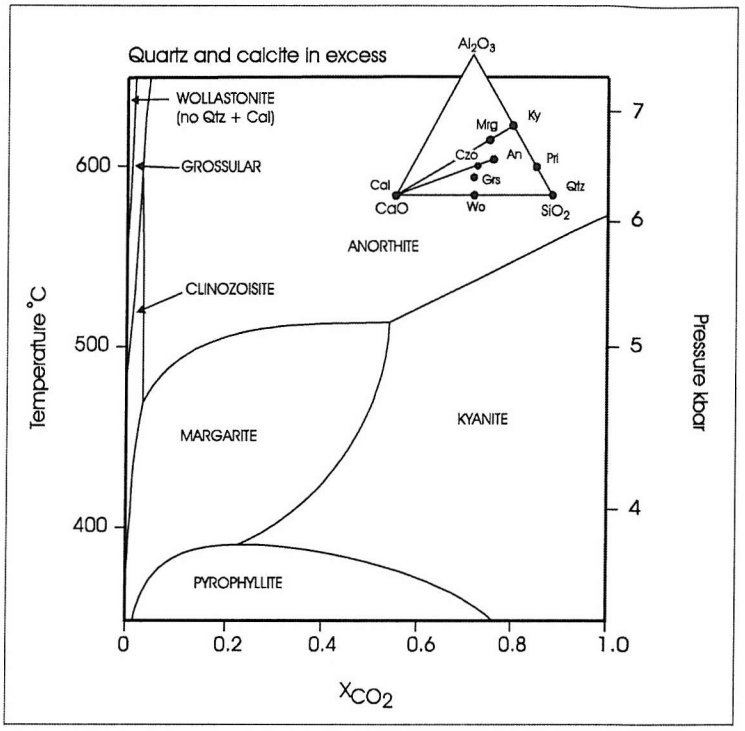

B

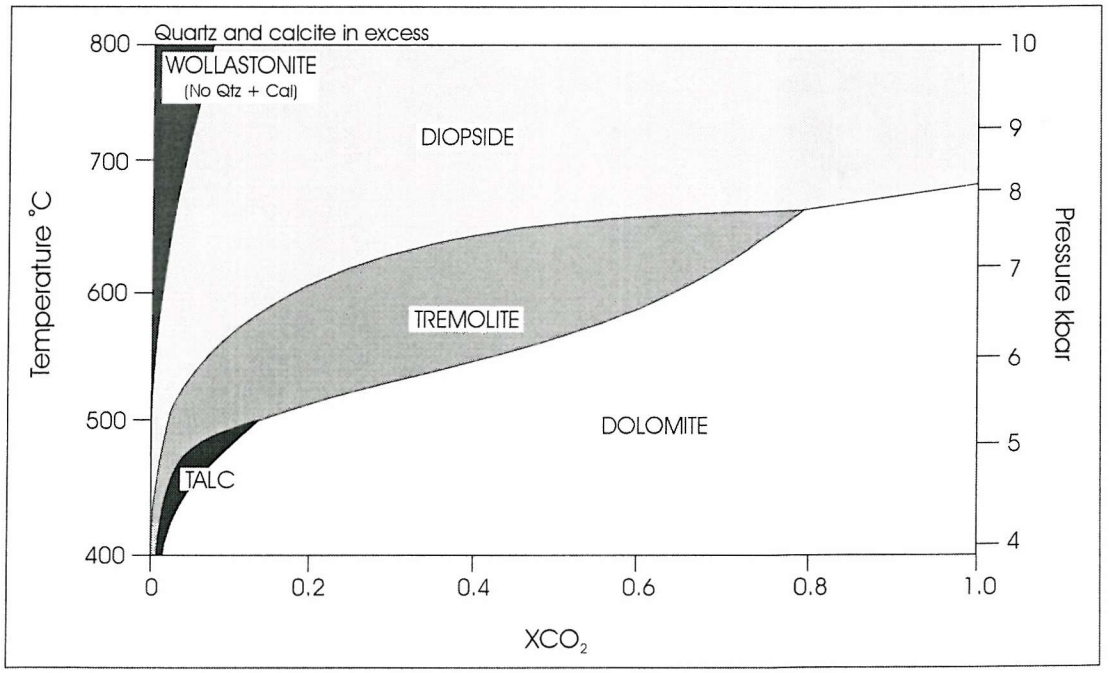

Figure 5.16: P-T-X relationships for A) the CAS-HC system and B) the CMS-HC system with excess quartz and calcite in kyanite terrains. Note that wollastonite can only exist under low XCO_2 (H_2O-rich) conditions. Although these diagrams relate to a higher pressure regime than is observed at Zinkgruvan, Winkler (1979) shows similar petrographic relationships at P=2 kbar. Adapted from Bucher & Frey (1994).

5.5 RETROGRADE METAMORPHISM

Lower temperature mineral phases in disequilibrium with the peak assemblage indicate retrograde metamorphism. The phases commonly pseudomorph or partially replace higher temperature minerals, for example, serpentine pseudomorphing forsterite, and zoisite after plagioclase or garnet. In other places, retrogressive phases (such as tremolite) form distinct overprints on the peak assemblage. These mineral associations not only act as monitors of P-T conditions, but can also provide constraints on fluid chemistry.

Pressure is assumed to be lower than that prevailing during peak metamorphism. In the lowest grade areas around lake Höksjön (Fig. 3.1), pressure is estimated to have been at a maximum of 3 kbar during peak conditions, so it is likely that pressures during retrogression were lower than this. Unlike the peak metamorphic assemblages, the products of retrogressive metamorphism at Zinkgruvan are not useful indicators of pressure.

Analysis of the mineral assemblages has revealed that there were at least two stages of retrogressive metamorphism, described below.

5.5.1 Retrogression at <550°C

Marbles and calc-silicate marbles

Serpentinisation

Forsterite partially or wholly pseudomorphed by serpentine is widely recognised. In many samples, the degree of serpentinisation is uneven across an individual thin section, causing complete alteration of some forsterite aggregates, but only partial alteration of others. Serpentine masses may be accompanied by fine grained clinochlore, and magnetite is nearly always developed as a by-product of the alteration, usually concentrated along the margins and fractures within the serpentine mass.

The transformation from pure forsterite to serpentine (antigorite) requires addition of silica, and must take place under aqueous conditions. However, if the forsterite contains a component of fayalite (Fe-olivine), serpentinisation can progress via a two-stage reaction which requires no addition of silica from an external source. The fayalite component undergoes oxidation [22], producing magnetite and releasing silica. That silica is then free to react with the forsterite component to produce serpentine [23].

$$\underset{\text{Fayalite}}{3Fe_2SiO_4} + O_2 \rightarrow \underset{\text{Magnetite}}{2Fe_3O_4} + 3SiO_{2aq} \qquad [22]$$

$$\underset{\text{Forsterite}}{3Mg_2SiO_4} + SiO_{2aq} + 2H_2O \rightarrow \underset{\text{Serpentine}}{2Mg_3Si_2O_5(OH)_4} \quad [23]$$

Forsterite in the Zinkgruvan marbles usually contains 4-7 wt% FeO (Chapter 4; Appendix F), equating to forsterite with the composition range $Fo_{90}Fa_{10}$ to $Fo_{95}Fa_5$, which is a typical composition for forsterite in marble. In this case, with a 9:1 ratio of forsterite to fayalite in the olivine, reactions [22] and [23] can only produce serpentine + magnetite if silica from an external source is involved in addition to the silica generated by oxidation of the fayalite component [24]:

$$\underset{\text{Olivine}}{3(9Mg_2SiO_4 + Fe_2SiO_4)} + 6\ \underset{\text{Qtz}}{SiO_2} + 18H_2O + 10O_2 \rightarrow \underset{\text{Serpentine}}{18Mg_3Si_2O_5(OH)_4} + \underset{\text{Magnetite}}{2Fe_3O_4} \quad [24]$$

For this reaction to proceed, the silica required to drive forsterite breakdown is three times greater than that which can be supplied through fayalite oxidation.

O'Hanley (1996) produced a T-XCO_2 grid showing generation of antigorite directly from breakdown of forsterite without silica addition (Fig. 5.17):

$$34\ Fo + 20\ Cal + 31\ H_2O + 20\ CO_2 \rightarrow Atg + 20\ Dol \quad [25]$$

Given the large ratio of Fo:Atg and associated necessary volume change required for this reaction to take place, this alteration mechanism seems less likely for the Zinkgruvan marbles. Thin section investigation shows that for most serpentine-bearing marbles, calcite is the dominant carbonate phase following dolomite consumption during prograde reactions; if reaction [25] had taken place, large quantities of dolomite would be present in the assemblage.

Serpentinisation occurs at temperatures below ~500°C at <5 kbar pressure (Fig. 5.17) (Chernosky *et al.*, 1988; Connolly & Trommsdorff, 1991; O'Hanley, 1996), although Fe-bearing olivines may remain stable to lower temperatures.

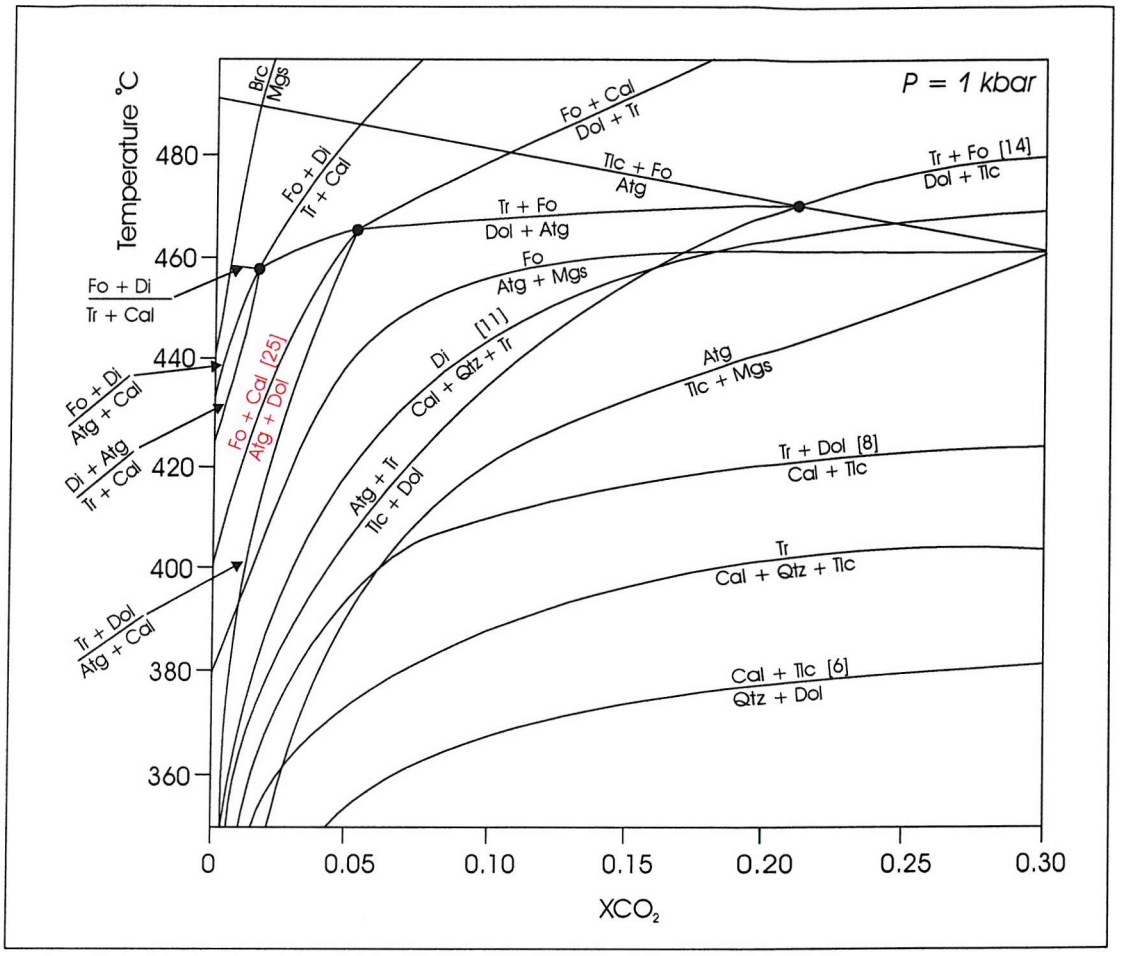

Figure 5.17: T-XCO_2 phase diagram for the system CaO-MgO-SiO_2-H_2O-CO_2 to show stability of serpentine minerals in calc-silicate rocks. P = 1 kbar. Modified after O'Hanley (1996). Note that the majority of antigorite-forming reactions here involve talc or tremolite with forsterite, which is not a stable assemblage at Zinkgruvan as marbles are not sufficiently Mg-rich to produce this paragenesis. Possible antigorite-forming reaction for the Zinkgruvan marbles highlighted in red. Reactions previously described in this chapter are numbered accordingly.

Clinochlore

Although it can be stable to high temperatures in marbles (see section 5.4.7), clinochlore occurs as an overprinting retrograde phase in several dolomitic marble samples. Retrograde clinochlore also occurs intergrown with serpentine pseudomorphing after forsterite. No prograde clinochlore is observed. Clinochlore as a retrograde product indicates temperatures <650°C (see section 5.4.7).

Tremolite

Tremolite is a common retrograde mineral in many of the marbles, forming euhedral rhombs overprinting the peak assemblage. Tremolite forms by the simple reversal of the prograde reactions [12] and [11] below 650°C, which requires the addition of H_2O and CO_2 (Fig. 5.10):

$$\mathbf{Dol + Di + H_2O + CO_2 \rightarrow Cal + Tr} \qquad [26]$$

$$\mathbf{Di + H_2O + CO_2 \rightarrow Cal + Tr + Qtz} \qquad [27]$$

Dolomite exsolution

The exsolution of small dolomite rhombs within formerly high-temperature Mg-bearing calcite is indicative of re-equilibration at lower temperatures and is observed in several marble samples from the mine area. This reaction can be used as a geothermometer, and is explored further in section 5.6.2.

Quartzofeldspathic gneisses and migmatites

Evidence for retrogression is less apparent in these rocks than in the metacarbonate and calc-silicate lithologies. Sillimanite and microcline crystals show no evidence for re-equilibration to lower P and T, although muscovite forms small, overprinting crystals aligned at a high angle to the dominant S_1 cleavage in some samples. Sericite development is widespread in plagioclase crystals and along grain boundaries, as in most of the rock types at Zinkgruvan.

In some quartzofeldspathic gneisses in the footwall to the orebody, large garnet aggregates overprint the dominant S_1 foliation. Examination of the garnet chemistry in these rocks suggests that some formed as post-peak growths – this is described further in section 5.6.3 and in Chapter 6.

5.5.2 Retrogression at ~200-300°C

The second stage of retrogression is estimated to have occurred at approximately 200-300°C. The main product of this event is widespread sericitisation of feldspar in all rock types. Serpentinised marbles show late-stage replacement of serpentine by iddingsite/Fe-oxide material, and calc-silicate skarns commonly exhibit hydrogrossular rims developed around zoisite, sericitised feldspar and calcite. All retrograde products from this stage of the metamorphic evolution are characteristic of interaction of the rock mass with a highly oxidising and possibly acidic aqueous fluid.

5.5.3 Volume changes

In theory, the majority of reactions described above involve a change in either the volume and/or mass of the rock. The conservation of mass or volume is an important consideration in the mechanics of a closed system. Pseudomorph processes demonstrate that transformations can occur without any apparent significant volume change, although an increase in mass is inevitable if volume is conserved. However, in an open system, such as at Zinkgruvan, volume changes can be easily accommodated by deformation or dissolution of carbonate material.

5.6 QUANTIFICATION OF P-T BY GEOTHERMOBAROMETRY

Geothermometric and barometric techniques using chemical compositions of key mineral phases have been applied to the Zinkgruvan assemblages to quantify T (-P) conditions. Many of the techniques hinge on the presence of several key minerals in order for the techniques to be valid, and in most cases, the results obtained from applying these methods yield data well below the estimated peak values. The reasons for this discrepancy will be considered.

5.6.1 Dolomite exsolution

Calcite crystallising at high temperatures has the capacity to accommodate significant proportions of Mg in its structure (up to 25%). High-Mg calcite becomes unstable as the assemblage cools and re-equilibrates to lower P-T conditions. The re-equilibration process involves exsolution of the $MgCO_3$ component (dolomite) from the calcite host (Fig. 5.19). The mole fraction of $MgCO_3$ in calcite co-existing with dolomite is therefore temperature-dependent and can provide a useful geothermometer (Graf & Goldsmith, 1955, 1958; Harker & Tuttle, 1955; Goldsmith & Newton, 1969; Bickle & Powell, 1977; Anovitz & Essene, 1987).

Several samples of metacarbonate rock from the Zinkgruvan Formation at the mine exhibit small blebs of exsolved dolomite within coarse grained calcite. If an accurate measurement of the volume of exsolved dolomite can be made, this can be converted to an estimate of the mole fraction of $XMgCO_3$ present in the rock prior to re-equilibration. However, this can be extremely difficult to do due to exsolution of dolomite along cleavage planes of calcite crystals.

SEM probe analysis of calcite in equilibrium with dolomite (with no observed exsolution) shows that the calcite contains very small quantities of the $XMgCO_3$ component, inconsistent with crystallisation at the high temperatures (>700°C) experienced during peak metamorphism (Table 5.4). Indeed, the values recorded suggest temperatures of 200-450°C. These low values of $XMgCO_3$ may be the result of sub-microscopic 'invisible' exsolution as described above, in which case the measured $XMgCO_3$ is lower than it should be for crystallisation at >700°C.

Sample	Atomic % Ca	Atomic % Mg	$XMgCO_3$ in calcite
ZR02	48.88	0.62	0.01
ZR06	48.61	1.39	0.02
ZR06	49.22	0.77	0.01
ZR06	48.41	1.59	0.03
1557/26	48.93	0.93	0.02

Table 5.4: SEM analyses and calculation of X_{MgCO_3} in calcite co-existing with dolomite from the Zinkgruvan Formation marbles. Samples ZR06 and 1557/26 are from the mine; sample ZR02 from Vinnern West (see Appendix B for location).

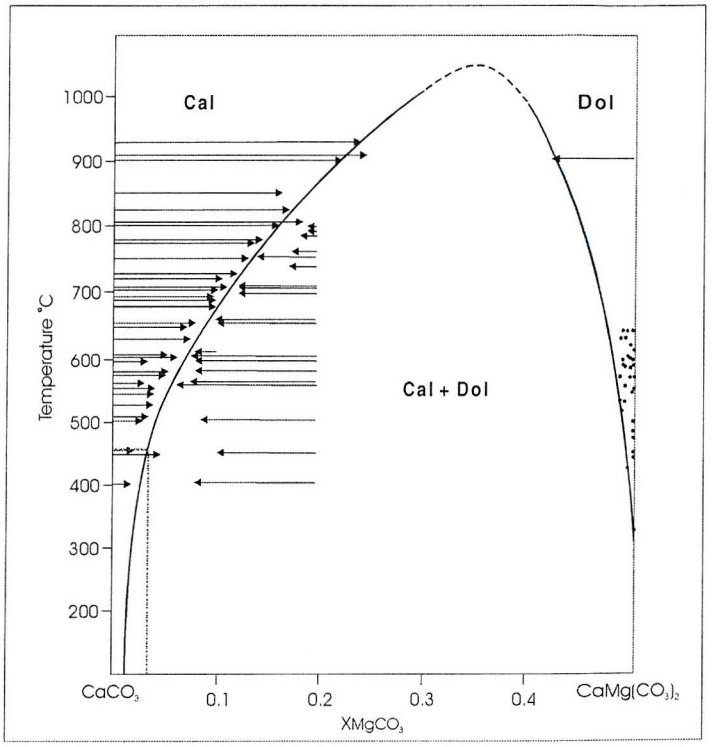

Figure 5.19: The calcite-dolomite solvus fitted to experimental data. Arrowheads show the final composition, and the direction of the arrow shows the direction of composition shift. Experimental pressures corrected to 2 kbar. The points near the dolomite limb represent natural dolomites coexisting with calcite. Red dashed line shows the temperatures represented by 0.03 X_{MgCO_3} in calcite. Modified after Anovitz & Essene (1987).

This indicates that either the calcite has formed as a retrograde product, or that the calcite has re-equilibrated at lower (post-peak) temperatures. Although some calcite will be formed during retrogression (e.g., through formation of tremolite from diopside, reactions [24] and [25]), the presence of exsolved dolomite within some crystals is indicative of re-equilibration at approximately 450-500°C (Fig. 5.19), if the highest value (0.03) for X_{MgCO_3} is used.

5.6.2 Fe/(Fe+Mg) ratios in garnets

Spear & Cheney (1989) showed that Fe/(Fe + Mg) ratios in garnets can be used as a P-T indicator for low-Al metapelites in the KFMASH system containing garnet + biotite (see section 5.2.2). At peak conditions of 700°C and 5 kbar, the Fe/(Fe + Mg) ratio of garnets in chemical equilibrium with the rest of the assemblage is expected to be around 0.75 (Fig. 5.1). Garnets formed or re-equilibrated at lower temperatures will have higher Fe/(Fe + Mg) ratios.

Garnets formed in some quartzofeldspathic gneisses (also KFMASH system) of the Zinkgruvan Formation contain Fe/(Fe + Mg) ratios which are inconsistent with crystallisation at the high temperatures of peak metamorphism. The crystallisation temperature indicated by Fe/(Fe+Mg) ratios in these garnets ranges from 535 to 600°C (Table 5.5), significantly lower than the peak estimate of approximately 750°C. There are several possible reasons for this discrepancy:

1) Garnets have re-equilibrated to lower pressures and temperatures during retrogressive metamorphism.
2) Garnet growth is post-peak metamorphism.
3) Significant whole-rock MnO has altered the stability field of garnet and lowered the temperature at which garnet first appears in the assemblage (Symme & Spear, 1992).

Textural evidence shows that whilst some garnets (in highly Fe-rich horizons) appear to overprint the S_1 fabric (see section 4.2.2), this is not the case for the garnets investigated here. These garnets show syn-metamorphic growth fabrics, and therefore the high measured Fe/(Fe + Mg) ratios are not due to post-peak nucleation. However, it is inevitable that they have been affected by retrograde metamorphism and have re-equilibrated at lower P and T, at least on their rims. SEM EDS element mapping and spot analyses along a traverse across individual crystals revealed no discernible chemical zonation, indicating either complete re-equilibration or homogenisation at high temperature, the latter of which is apparently inconsistent with the Fe/(Fe + Mg) given in Table 5.4.

Garnet stability is affected by the presence of MnO in the rock chemistry. Whole rock $X_{Mn} > 0.01$ (X_{Mn} = Mn/(Mn + Fe + Mg)) increases the garnet stability field, permitting garnet to develop over a wide range of Fe/Mg compositions, rather than restricting its growth to rocks with a high Fe/Mg ratio (Spear & Cheney, 1989; Symme & Spear, 1992). A small amount of MnO also allows the first appearance of garnet to occur at lower temperatures than in an equivalent Mn-free sample, and Spear & Cheney (1989) reported that the spessartine component in garnet can significantly alter its stability, particularly in chlorite-bearing assemblages. All samples used in this particular investigation contain > 0.5 whole rock X_{Mn}, so it must be assumed that Mn has had a significant impact on the stability of garnets in these rocks, and that the metamorphic temperatures calculated using the garnet Fe/(Fe + Mg) ratio are unreliable as an accurate indicator of peak

metamorphic or re-equilibration conditions, even though the temperatures appear to be consistent with the first major retrogressive event, identified through mineral assemblages (section 5.5.1).

Sample	*Garnet Fe (At %)*	*Garnet Mg (At %)*	*Garnet Fe/(Fe + Mg)*	*T @ 5 kbar*[§]	*Whole rock MnO (wt%)*	*Whole rock X_{Mn}*	*Garnet MnO (wt%)*	*Garnet X_{Mn}*
231/13*	0.21	0.02	**0.92**	540	0.23	0.06	12.8	0.45
	0.21	0.02	**0.92**	540			13.57	0.46
	0.22	0.02	**0.92**	540			12.78	0.44
	0.27	0.04	**0.86**	580			12.86	0.38
	0.30	0.03	**0.91**	545			11.74	0.34
	0.28	0.02	**0.93**	535			11.12	0.35
	0.28	0.05	**0.86**	580			10.13	0.32
	0.18	0.02	**0.92**	540			16.12	0.55
	0.21	0.02	**0.93**	535			13.07	0.46
	0.20	0.01	**0.94**	530			12.51	0.45
671/19*	0.38	0.07	**0.84**	600	0.39	0.05	9.67	0.25
	0.38	0.06	**0.86**	580			9.92	0.25
	0.38	0.07	**0.85**	590			9.8	0.25
	0.39	0.07	**0.85**	590			10.05	0.25
	0.38	0.06	**0.85**	590			9.91	0.25
	0.38	0.07	**0.85**	590			10.12	0.26
	0.40	0.06	**0.86**	580			8.7	0.22
	0.40	0.06	**0.86**	580			8.29	0.21
	0.40	0.06	**0.86**	580			8.46	0.22
671/21*	0.33	0.05	**0.86**	580	1.21	0.18	14.71	0.37
	0.33	0.07	**0.83**	610			13.83	0.35
	0.33	0.06	**0.84**	605			14.18	0.36
	0.33	0.05	**0.88**	565			15	0.38
	0.33	0.06	**0.85**	590			13.93	0.35
	0.33	0.06	**0.85**	590			14.14	0.36
	0.33	0.06	**0.85**	590			14.08	0.35
	0.33	0.06	**0.85**	590			14.61	0.36
1557/09	0.23	0.04	**0.87**	575	1.08	0.082	3.51	0.08
	0.23	0.04	**0.84**	600			2.67	0.07
	0.24	0.04	**0.84**	600			2.7	0.06
	0.24	0.04	**0.86**	580			3.43	0.08
	0.23	0.04	**0.84**	600			3.23	0.07
	0.21	0.05	**0.82**	625			4.06	0.09
	0.24	0.04	**0.87**	575			3.74	0.09
UZ23	0.14	0.01	**0.96**	525	No whole-rock data available		12.1	0.34
	0.15	0.01	**0.96**	525			12.02	0.31
	0.13	0.01	**0.96**	525			13.75	0.39

Table 5.5: Fe/(Fe+Mg) ratios in garnets from quartzofeldspathic gneisses of the Zinkgruvan Formation. [§]*Temperature estimates based on a peak pressure of 5 kbar (see section 5.2) from the grid devised by Spear & Cheney (Fig. 5.1).* X_{Mn} *= Mn/(Mn + Fe + Mg). Samples marked * are calculated using SEM-EDS data from Bengtsson (2000) (Appendix F). Remaining data collected on JEOL JSM SEM (Appendix F).*

5.7 SUMMARY

Peak metamorphic conditions at Zinkgruvan and the surrounding area have been constrained and quantified using key mineral associations. Stages of retrogressive metamorphism have been identified in a similar way. Mineral assemblages have also been used to define fluid composition during metamorphism. The main conclusions are summarised below.

5.7.1 Peak metamorphic conditions

- Peak metamorphic mineral assemblages have revealed a metamorphic gradient across the Zinkgruvan Basin, from upper amphibolite facies (sillimanite zone) in the mine area to lower amphibolite facies (andalusite zone) in the south of the basin, a distance of approximately 8 km.
- In the mine area, the peak metamorphic assemblages gave the following estimates of P-T:

Rock type	*Peak assemblage*	*Temperature (°C)*	*Pressure (kbar)*	*Notes*
Metapelites	Qtz + Kfs + Sil + Bt (No Ms,Ky,Cd,Grt)	>650°C	3-7 kbar	Myrmekites and perthites suggest >700°C
Amphibolites	Hbl + Pl + Bt (No Cpx)	<780°C	-	
Calcitic marbles	Cal + Di + Wo Cal + Qtz + Wo	>700°C	5 kbar (±2)	Wo indicates low XCO_2 fluid
Forsterite marbles	Cal + Dol + Fo Cal + Di + Fo	>650°C	5 kbar (±2)	

Table 5.6: Summary of peak metamorphic conditions estimated from key mineral assemblages in various rock types.

- Metapelitic assemblages from the lower grade area to the south contain the peak assemblage Qtz + And + Kfs + Bt, indicating peak P/T conditions of ~600°C and around 3 kbar pressure.
- Fluid chemistry during metamorphism is reflected in the presence of wollastonite and grossular in calc-silicate marbles and skarns. Both phases indicate the presence of an **aqueous fluid** (~0.2 XCO_2), and the occurrence of clinohumite suggests a component of fluorine was also present.
- This shows that the system was either capable of strongly buffering the fluid composition to a more H_2O-rich composition, or the chemistry was buffered by an externally-derived fluid. An open system is clearly indicated by the presence of wollastonite in many of the calcitic marbles.

- Aqueous fluid may have been sourced from the dehydration of adjacent quartzofeldspathic (metavolcanic/metasedimentary) units through the breakdown of hydrous minerals such as micas and amphiboles during prograde metamorphism.

5.7.2 Retrogressive metamorphism

- Petrographic investigation suggests that the rock package at Zinkgruvan has been subjected to at least two phases of retrogression:
- Re-equilibration of assemblages at around 550°C, evidenced by development of zoisite, serpentine and tremolite in metacarbonate and calc-silicate rocks.
- Further retrogression at temperatures of ~250-300°C, evidenced by widespread sericitisation, replacement of serpentine by iddingsite/saponite in some dolomitic marbles, and formation of hydrogrossular rims around higher temperature minerals in calc-silicate skarns. Mineralogical evidence shows that this stage of retrogression was also accompanied by a highly aqueous fluid.

5.7.3 Geothermobarometry

- Exsolution of dolomite from calcite indicates re-equilibration of calcite at temperatures <500°C.
- Fe/(Fe+Mg) ratios in some garnets from quartzofeldspathic gneisses are inconsistent with crystallisation at peak temperatures of ~700°C. This, along with textural evidence, suggests that some garnet growth is post-peak, around 550-650°C. The presence of whole-rock MnO alters the stability field of garnet and may mean this form of geothermometry is inaccurate for these rocks.

CHAPTER 6

ISOTOPE GEOCHEMISTRY OF METACARBONATE ROCKS

CHAPTER 6: ISOTOPE GEOCHEMISTRY OF METACARBONATE ROCKS

6.1 INTRODUCTION

This chapter deals with the isotope characteristics of metacarbonate rocks of the Zinkgruvan district. Strontium isotope analyses were carried out at the University of Southampton using a thermal ionisation mass spectrometer (TIMS) (see Appendix H for operating procedures). Strontium isotopic ratios allow determination of the origins of strontium in the samples concerned and in particular an evaluation of the contribution of radiogenic ^{87}Sr from continental sources.

Stable isotope (C, O) analyses were carried out at the University of Lucerne as part of undergraduate research projects funded by North Ltd, and the data have subsequently been made available to be assessed as part of this research. Additional carbonate isotopic data for Zinkgruvan are sourced from Hallberg *et al.* (1994) and other published sources. Analyses of the isotopic characteristics of the metacarbonate rocks complements the major element geochemistry work (Chapter 4) in identifying alteration and/or contamination events and revealing the nature of the fluids responsible for chemical alteration. However, it is recognised that the isotope systematics of these rocks may have been modified during metamorphism in addition to diagenetic and hydrothermal processes.

6.2 STRONTIUM ISOTOPE STUDIES

6.2.1 Background

Strontium has four naturally occurring isotopes: ^{84}Sr (0.56%), ^{86}Sr (9.86%), ^{87}Sr (7.0%) and ^{88}Sr (82.85%). With the exception of ^{87}Sr, all of the Sr isotopes display constant ratios with respect to each other. However, because ^{87}Sr is contributed to by the decay of ^{87}Rb (with a half life of 4.8×10^{10} years), the ratios of this isotope to the other Sr isotopes varies according to the initial composition of the rock, its age and the Rb/Sr ratio of the rock itself (Wickman, 1948). By convention, the $^{87}Sr/^{86}Sr$ ratio is used to describe relative values of ^{87}Sr between samples (Faure, 1986), and it can be used to characterise environments of deposition under which the minerals precipitated as well as the provenance and migration of water. The use of Sr ratios in the study of carbonate rocks is particularly useful because minerals such as calcite substitute small amounts of Sr for Ca. They preferentially take up strontium and exclude rubidium during precipitation, and thus preserve the Sr isotopic ratio of the parent solution.

Release of Sr by chemical weathering

The abundance of strontium in the hydrosphere is entirely controlled by the nature of the geology exposed at or near the surface, where it is removed from the rocks by chemical weathering. The isotopic composition of water that has interacted with a strontium-bearing rock is controlled by:

a) The age of the source rock
b) Rb and Sr concentrations in the source rock
c) Solubilities of the minerals involved in chemical weathering

Due to the generation of ^{87}Sr by radioactive decay of ^{87}Rb, older rocks are enriched in radiogenic ^{87}Sr compared to younger rocks, thus increasing the proportion of ^{87}Sr in weathering solutions. Therefore, weathering solutions derived from old continental material have higher $^{87}Sr/^{86}Sr$ ratios than solutions originating from the breakdown of young volcanic material.

Water from different sources will have different Sr isotopic ratios depending on the geology of the catchment area. The major Rb-bearing silicate minerals (e.g., K-feldspar, mica) are more resistant to weathering relative to the main Sr-bearing minerals (e.g., plagioclase and calcite). Strontium (a significant part of which is radiogenic) is therefore more readily released through chemical weathering than rubidium, resulting in enrichment in ^{87}Sr in local waters. Because of the resistance of Rb-rich minerals to weathering, radiogenic ^{87}Sr is also retained in those minerals so that the solution produced by chemical weathering of a rock generally has a lower $^{87}Sr/^{86}Sr$ ratio than the source rock, and the residual rock mass will have a higher Rb/Sr ratio than unweathered equivalents (Faure, 1986).

Strontium in the oceans

Strontium concentration in the oceans is approximately 8×10^3 µg/litre (8 ppm). The Sr isotopic ratio ($^{87}Sr/^{87}Sr$) is controlled by the input from three main sources:

a) Weathering of continental crust: generally contributes high $^{87}Sr/^{86}Sr$ (~ 0.740 for granitic basement) to the hydrosphere (see above for explanation). However, large expanses of basic igneous rocks produce much lower Sr isotopic ratios of around 0.704.
b) Strontium derived from young volcanic rocks of the oceanic crust which contain non-radiogenic Sr.
c) Strontium sourced from Phanerozoic marine carbonate rocks: the solutions produced by weathering of carbonates will inherit the original signature of the parent solution of the carbonate, unless it has been modified by post-depositional processes.

Faure (1986) estimated that these sources respectively contribute approximately 15, 25 and 60% of strontium to the modern oceans. Carbonates are the main source due to their high strontium content and susceptibility to weathering. Freshwater bodies (rivers, lakes etc) inherit

their Sr isotopic signature from the local geology, so the range for freshwater carbonates is broad, but limited by the values for basic igneous rocks and old granitic plutons (Veizer & Compston, 1974).

As strontium is transported via weathering solutions into the oceans, it undergoes mixing and homogenisation so that modern oceans have an average $^{87}Sr/^{86}Sr$ ratio of **0.70906 ± 0.00003**, which shows no spatial variation around the globe. The continuous contribution of continental strontium to the oceans should theoretically raise the oceanic $^{87}Sr/^{86}Sr$ ratio, but the low concentration of strontium in freshwater sources (average 8-100 ppb) compared to the high concentration in the oceans (8 ppm), coupled with the long residence time of strontium in seawater (5×10^6 years) means that constant isotopic ratios for the modern ocean are maintained. As well as receiving strontium from weathering processes, the ocean loses strontium through the precipitation of carbonate minerals and alteration of basaltic ocean crust. Spooner (1976) proposed that Sr isotopic exchange during hydrothermal alteration of MORB could lower the seawater $^{87}Sr/^{86}Sr$ ratio by 0.0011, effectively balancing the high $^{87}Sr/^{86}Sr$ input from continental run-off.

The modern day $^{87}Sr/^{86}Sr$ ratio of seawater is remarkably similar to the values preserved by late Proterozoic marine carbonates. Strontium isotopic variations of Precambrian oceans are hard to assess due to the comparative lack of unaltered marine carbonate samples, and the lack of index fossils to aid dating. However, carbonate samples from the late Archaean contain similar $^{87}Sr/^{86}Sr$ ratios to the mantle (Veizer & Compston, 1976), indicating either very active hydrothermal circulation or increased levels of basaltic volcanism (= low Rb/Sr ratios) at that time, and the lack of pre-existing carbonate rocks to contribute radiogenic ^{87}Sr to the cycle. Early Proterozoic rocks dated at 2.5 - 2.0 Ga display a significant increase in Sr ratio relative to mantle values (Fig. 6.1), probably due to the increase in radiogenic ^{87}Sr input from weathering of continental crust. Fig. 6.1 shows the variation of $^{87}Sr/^{86}Sr$ in Precambrian marine carbonate rocks. The average $^{87}Sr/^{86}Sr$ ratio of the oceans is known to have fluctuated during the Phanerozoic, and this is reflected in the isotopic changes in marine carbonates (Peterman *et al.*, 1970; Veizer & Compston, 1974; Brass, 1976; Burke *et al.*, 1982) (Fig. 6.2).

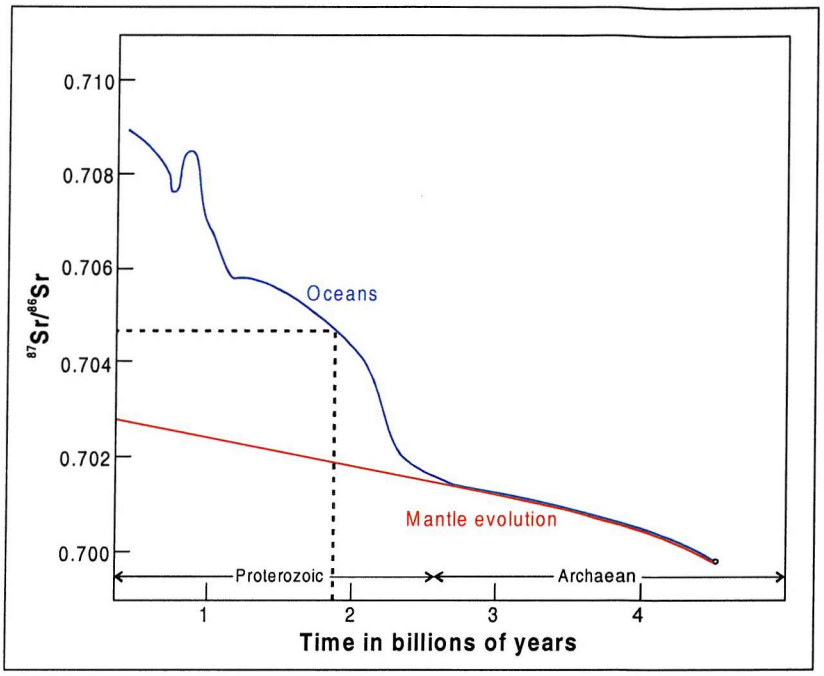

Figure 6.1: Variation of $^{87}Sr/^{86}Sr$ in Precambrian marine carbonate rocks. Data show that the Sr isotopic composition of the oceans was similar to that of the mantle during the Archaean, after which erosion of continental material caused the oceanic Sr isotopic ratio to increase due to input of radiogenic ^{87}Sr from decay of ^{87}Rb. Black dashed line shows expected original Sr composition of marine carbonate rocks of 1.87 Ga age. Modified after Faure (1986).

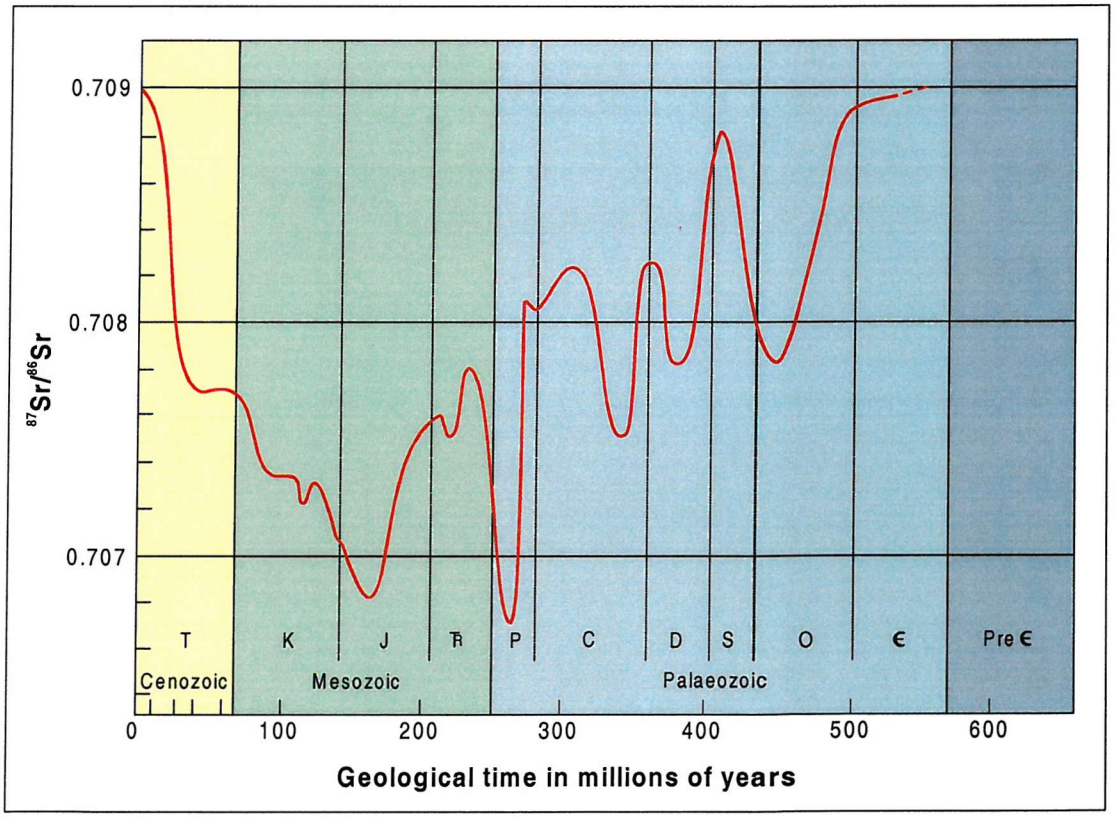

Figure 6.2: Changes in $^{87}Sr/^{86}Sr$ ratios in marine carbonate rocks during the Phanerozoic. Modified after Burke et al. (1982).

Variations in oceanic strontium ratios can be related to the changes in the geology exposed on the surface. Increases in ^{87}Sr are caused by an increase in the contribution of strontium from continental and marine carbonate sources, whilst declines are attributed to increasing contribution from young volcanic sources.

Faure *et al.* (1965) modelled the strontium isotopic composition of the ocean using the following equation:

$$\left(\frac{^{87}Sr}{^{86}Sr}\right)_{SW} = \left(\frac{^{87}Sr}{^{86}Sr}\right)_{V} v + \left(\frac{^{87}Sr}{^{86}Sr}\right)_{S} s + \left(\frac{^{87}Sr}{^{86}Sr}\right)_{M} m$$

Where:

$\left(\frac{^{87}Sr}{^{86}Sr}\right)_{SW}$ = *value of this ratio in seawater*

$\left(\frac{^{87}Sr}{^{86}Sr}\right)_{V, S, M}$ = *value of this ratio in Sr contributed to the oceans by volcanic (V), old sialic (S) and marine carbonate (M) rocks*

and the coefficients v, s, & m are decimal fractions representing the proportions of Sr in seawater contributed by volcanic, old sialic and marine carbonate material respectively

This model limits the $^{87}Sr/^{86}Sr$ ratio of seawater to 0.704 to 0.720. However, measured values indicate that strontium composition has only varied from 0.7065 to 0.7090 during the Phanerozoic (Faure, 1986). In a broad sense, the variations in oceanic $^{87}Sr/^{86}Sr$ can be related to global tectonic events, but model values do not take into account the effects of carbonate diagenesis, dolomitisation, glaciation and changes in ocean floor spreading rate, which can affect the Sr isotopic ratio preserved in marine carbonates.

Strontium in carbonate rocks

Carbonate rocks are a major sink for strontium. Calcite preferentially takes up strontium during precipitation and excludes rubidium, so the $^{87}Sr/^{86}Sr$ ratio of a particular carbonate sample will not change significantly with time. Precipitation of carbonates and other evaporite minerals does not cause fractionation of strontium isotopes, so these minerals preserve the isotopic ratio of their parent solutions, providing they have not been subject to post-depositional alteration processes. Two main processes are responsible for creating anomalous strontium isotope ratios in the early stages of carbonate formation:

1) *Change/anomalies in water composition*: Marine carbonates inherit their isotopic Sr ratio directly from seawater. Given that the $^{87}Sr/^{86}Sr$ concentration in the present day oceans is

homogenous and constant at 0.70906, most modern carbonates reflect this value. However, carbonates forming in a nearshore environment may be affected by river discharges and spatially restricted isotopic effects relating to local geology. Many nearshore carbonates will contain higher $^{87}Sr/^{86}Sr$ ratios due to the influence of continentally-derived waters flowing into marine basins. Freshwater carbonates are more isotopically variable, with their composition directly reflecting the local geology of the drainage area. Carbonates deposited in basins or lakes in areas where old granitic basement is exposed will have high $^{87}Sr/^{86}Sr$ values. In areas of active volcanism, $^{87}Sr/^{86}Sr$ ratios will be low due to the paucity of radiogenic ^{87}Sr in the system, except where ^{87}Sr is inherited from melting of pre-existing continental crust.

2) *Diagenesis/low grade metamorphism*: Diagenetic processes can change the Sr isotopic composition of a marine carbonate rock only if the isotopic composition of the pore fluid changes in the time period between carbonate sedimentation/precipitation and diagenesis itself. This process is a function of time; early diagenesis rarely causes isotopic change because the seawater in the pore spaces is unlikely to have changed in composition since carbonate formation. However, late diagenesis and lithification processes acting during deep burial may involve the introduction of fluids with different (usually continental) isotopic signatures, which can cause isotopic exchange. Minor isotopic re-equilibration between carbonate material and ^{87}Sr-rich clay minerals may occur, in which case the carbonate $^{87}Sr/^{86}Sr$ ratio may increase slightly (Peterman *et al.*, 1970; Biscaye & Dasch, 1971). Veizer & Compston (1974) concluded that most diagenetic processes result in no or only a slight positive change in $^{87}Sr/^{86}Sr$ ratios in metacarbonate rocks.

Beyond the early stages of carbonate formation, chemical processes such as hydrothermal alteration and metamorphism can cause significant changes in strontium composition, depending on the nature of the fluids involved.

6.2.2 Strontium isotopes at Zinkgruvan

Six carbonate samples from the mine area and surrounding district were submitted for Sr analysis using a thermal ionisation mass spectrometer (TIMS). Results from these analyses are shown in Table 6.1; laboratory procedure and operating conditions are outlined in Appendix H.

Sample	*Description*	*Location*	*$^{87}Sr/^{86}Sr$ (measured)*	*Rb ppm*	*Sr ppm*	*Rb/Sr (m)*	*$^{87}Sr/^{86}Sr$ (initial)*	*Rb/Sr (initial)*
451/16	Mine area calcitic	DDH 451, Nygruvan	0.783099 ± 10	73.70	78.10	0.94	0.710628	2.65
555/22	Mine area dolomitic	DDH 555, Nygruvan	0.704810 ± 10	0.00	64.50	0.00	-	-
ZR02	District dolomitic	Gardshyttan	0.706308 ± 8	0.00	103.70	0.00	-	-
ZR04	District calcitic	Trollfall	0.704818 ± 15	0.00	119.80	0.00	-	-
ZR11	District dolomitic	Brännlycken	0.710131 ± 7	4.20	77.10	0.05	0.706302	1.14
ZR22	District dolomitic	Rytabygget	0.712611 ± 7	4.50	82.70	0.05	0.708780	1.14

Table 6.1: $^{87}Sr/^{86}Sr$ ratios and Rb concentrations of selected metacarbonate samples from Zinkgruvan and surrounding district determined by TIMS. Sr and Rb data from whole-rock XRF. Initial $^{87}Sr/^{86}Sr$ ratios calculated using the equation described below (not calculated for samples containing no measured Rb). Laboratory procedure and operating conditions outlined in Appendix H.

Based on Fig. 6.1, marine carbonate rocks from the early Proterozoic (~1.9 Ga) would be expected to yield $^{87}Sr/^{86}Sr$ ratios of approximately 0.704 - 0.705.

The results outlined in Table 6.1 range from relatively primitive Sr ratios for samples ZR04 and ZR02, to highly radiogenic values for sample 451/16. All samples analysed above have been subject to moderate to high grade metamorphism (Chapter 5), variable contamination by volcanic ash (Chapter 4), and potassic enrichment (Chapter 4), and most have been affected by dolomitisation (Chapter 4) so their isotopic signature is likely to have been modified by at least one geological process.

In assessing these data the concentration of Rb in each of these samples must be taken into account as it will produce ^{87}Sr by radioactive decay. The initial $^{87}Sr/^{86}Sr$ ratio (at 1.9Ga, prior to Rb decay) can be calculated using the following equation:

$$\left(\frac{^{87}Sr}{^{86}Sr}\right)_m = \left(\frac{^{87}Sr}{^{86}Sr}\right)_i + \frac{^{87}Rb}{^{86}Sr}\left(e^{\lambda t} - 1\right)$$

where: m = measured value
i = initial value
$t = 1.9 \times 10^9$ years
$\lambda = {}^{87}Rb$ decay constant: 1.42×10^{-11}

This equation assumes that no additional Rb has been introduced into the rock since t = 0 (1.9 Ga).

The anomalously high $^{87}Sr/^{86}Sr$ value for sample 451/16 is caused by the presence of radiogenic ^{87}Sr, and is accompanied by a high Rb concentration (Rb/Sr = 0.94). Rb (and its daughter isotope ^{87}Sr) in this sample is sourced from the pre-metamorphic potassic alteration event (Chapter 4, section 4.2.1), which is clearly observed as K-feldspar in thin section. The variation in Rb and Sr levels in metacarbonate rocks as a result of alkali metasomatism is discussed in Chapter 4 (section 4.3.3). Contribution of Rb from K-rich fluids, and from volcanic ash contamination (see below) has resulted in very high $^{87}Sr/^{86}Sr$ values for sample 451/16. However, calculation of the initial $^{87}Sr/^{86}Sr$ ratio shows that the original carbonate sediment contained elevated ^{87}Sr levels, indicating incorporation of non-radiogenic ^{87}Sr or an alternative (non-volcanic) source of radiogenic ^{87}Sr, such as continentally-derived siliclastic material.

Samples 555/22 and ZR04 show the lowest Sr ratios, and are close to the predicted seawater isotopic composition of ~0.7047 for the early Proterozoic (Fig. 6.1). These samples are relatively pure with low SiO_2 and Al_2O_3 contents, indicating that they have not been significantly contaminated by volcanic ash (calculations indicate 0.77% and 1.15% volcanic ash contribution for ZR04 and 555/22 respectively). Furthermore, both samples contain <0.05 wt% K_2O, showing that they have not been subject to potassic alteration. The low Sr ratio is unexpected for sample 555/22 as the mine area is known to have undergone substantial alteration (Chapter 4), including dolomitisation and silicification, although major element geochemistry suggests that this sample has only been modified by dolomitisation. It is possible that the Sr isotopic composition of sample 555/22 has been affected by the isotopic signature of nearby metabasite units, which could lower the original value. However, drill core logging (Appendix C) shows the nearest metabasite to be situated several metres away, so it is unlikely that it would affect the carbonate values.

The 'clean' nature of both 555/22 and ZR04 indicates that their low Sr isotopic ratios are likely to represent the original ratio of the seawater at the time of carbonate precipitation. Given that 555/22 and ZR04 have similar Sr isotopic values, but one is dolomitised and the other is not, this implies that the Sr composition of the carbonate units was not significantly modified by the dolomitisation process. This in turn may indicate that the dolomitisation event was relatively early, with seawater being the main fluid involved.

Samples ZR11 and ZR22 show slightly elevated Sr isotopic ratios and Rb concentrations (Rb/Sr = 0.05) (Table 6.1). This suggests that they have been affected by ^{87}Rb- or ^{87}Sr-rich material. Both samples show evidence of volcanic ash contamination, as described in Chapter 4 (section 4.3.2) which may have been slightly affected by the potassic alteration event, resulting in an increase in their Sr isotopic ratio relative the original marine carbonate signature. However, calculations of initial $^{87}Sr/^{86}Sr$ ratios for both these samples show that they are slightly higher than predicted in Fig. 6.1 and shown by samples 555/22 and ZR04. This is probably due to the original carbonate containing additional non-radiogenic ^{87}Sr, contribution of radiogenic ^{87}Sr from a source

other than volcanic ash, or analytical error (although standard deviation for both samples is only ±7, so errors in isotopic analysis are unlikely).

6.2.3 Summary of Sr isotope data

- The Sr isotopic composition of metacarbonate rocks in the Zinkgruvan district vary widely from primitive values close that of early Proterozoic seawater (~0.7047), to more radiogenic values of > 0.7100.
- Extremely high Sr ratios are the result of Rb enrichment (and subsequent decay to ^{87}Sr) related to potassic alteration in marbles, resulting in present day Sr ratios in excess of 0.7800. However, back-calculation to remove ^{87}Sr contributed by decay of hydrothermal or volcanic ^{87}Rb shows that the samples were enriched in ^{87}Sr from an alternative source, probably detrital material or ^{87}Sr in hydrothermal fluid leached from older continental material (?basement).
- Contamination of carbonate sediment by volcanic ash has resulted in an increase in the Sr isotopic ratios. This may be due to the volcanic material itself, but is more likely to reflect weak K-Rb alteration of the volcanic component.
- Dolomitisation appears to have had no systematic effect on the Sr isotopic composition of the metacarbonate rocks. Dolomitised samples show a range of $^{87}Sr/^{86}Sr$ values from a primitive 0.7048 up to 0.7126, and an apparently unaltered calcitic sample (ZR04) and a dolomitised sample (555/22) show very similar values.
- This may indicate that the timing of dolomitisation was relatively soon after deposition, so that seawater was still the dominant isotopic influence and the Sr values were consequently not significantly altered.

Drawing conclusions from such a limited sample set is difficult, particularly on rocks of this age with a potentially complex geological history masked by high-grade metamorphism. It is clear from the conclusions above that Sr isotopes can give only limited information on the fluid history of the metacarbonate rocks. For more detailed information on the physiochemical conditions prevailing at the time of deposition or during fluid alteration events other geochemical indicators must be used, such as stable isotope studies. Stable isotopes allow more detailed interpretation of events affecting the carbonate rocks, since different geological materials have well-defined isotopic ranges, and the sources of fluid have more distinct isotopic signatures.

6.3 STABLE ISOTOPES

6.3.1 Oxygen

Oxygen naturally occurs as three isotopes: ^{16}O (99.763%), ^{17}O (0.0375%) and ^{18}O (0.1995%). Oxygen isotopic composition is measured as a ratio of $^{18}O/^{16}O$ and compared to a standard. The most commonly used standard is Standard Mean Ocean Water (SMOW), defined by Craig (1961), but in some cases PDB (Peedee Belemnite) may be used for carbonate minerals. The oxygen isotopic composition of a sample is expressed as $\delta^{18}O$, in parts per mil (‰) relative to SMOW.

$$\delta^{18}O = \left[\frac{(^{18}O/^{16}O)_{smpl} - (^{18}O/^{16}O)_{std}}{(^{18}O/^{16}O)_{std}}\right] \times 10^3$$

Most geological samples show enrichment in ^{18}O relative to the SMOW standard (expressed as a positive $\delta^{18}O$ value) because ^{18}O is preferentially concentrated into rock-forming minerals. Typical $\delta^{18}O$ ranges for different geological materials are shown in Fig. 6.3.

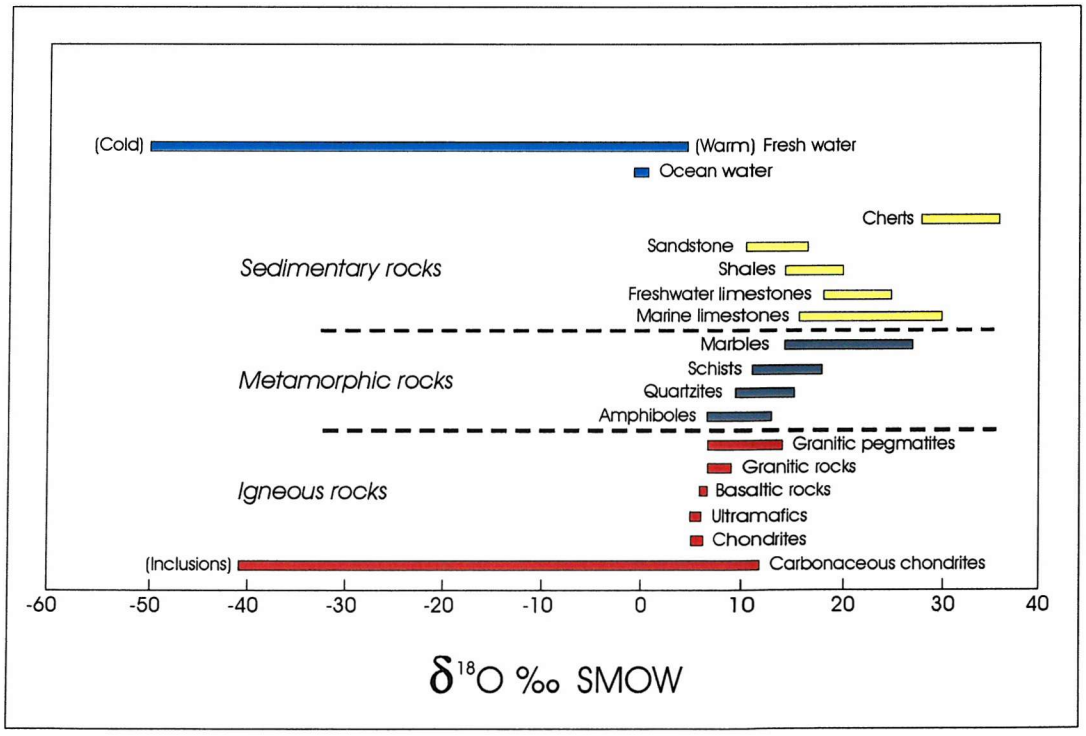

Figure 6.3: Typical $\delta^{18}O$ ranges for common rocks and minerals. After Mason & Moore (1982).

Isotopic distribution

The distribution of oxygen isotopes between minerals is a function of temperature and the isotopic fractionation factor (α) of the minerals involved. The fractionation factor defines the way in which a particular isotope will partition between different phases when the system is at equilibrium, and is defined as:

$$\alpha = R_A/R_B$$

where: R_A = The ratio of heavy:light isotope in phase A
R_B = The ratio of heavy:light isotope in phase B

This relationship is strongly dependent on temperature: where two mineral phases equilibrate with the same oxygen reservoir at a particular temperature, the differences in their $\delta^{18}O$ values relative to the same standard will be a function of temperature. In this situation, assuming that no subsequent alteration to the isotopic composition has occurred, the differences in $\delta^{18}O$ between the two mineral phases indicates that they have different isotopic fractionation factors at that given temperature relative to the oxygen reservoir concerned (e.g., hydrothermal fluid). It is known that lower temperature rocks show larger $\delta^{18}O$ variation than higher temperature rocks, due to a higher degree of re-equilibration at high temperatures.

Research has shown (Epstein & Taylor, 1967) that mineral phases dominated by Si – O – Si bonds have a greater tendency to become enriched in ^{18}O compared to minerals dominated by Si – O – Al or Si – O – Mg bonds. Therefore, quartz is far more enriched in heavy oxygen than olivine, and so acidic igneous rocks are more enriched in O^{18} than mafic rocks (Fig. 6.3). Magnetite and ilmenite have the lowest oxygen isotope fractionation. In sedimentary rocks, isotopic composition is inherited from the source rocks. However, metamorphic processes, hydrothermal activity or weathering can cause re-equilibration in all rock types so that the mineral phases change their isotopic signature towards that of the fluid present at the time of alteration.

Fluid sources

The isotopic composition of fluids varies with the source of the water (figs 6.4 & 6.5), and most fluids (particularly hydrothermal fluids) have a complex chemical history due to mixing with other fluids from different sources. The chemistry of juvenile water from the mantle is estimated from mafic and ultramafic rocks, which have a range of +6‰ to +7‰ $\delta^{18}O$ relative to SMOW (Fig. 6.3). Fresh (meteoric) water is particularly depleted in ^{18}O due to the seawater evaporation process, which preferentially concentrates ^{16}O into the evaporating phase. This means that meteoric water has a negative $\delta^{18}O$ value relative to SMOW, and the $\delta^{18}O$ value of water becomes increasingly negative towards high altitudes and latitudes. The temperature of natural waters also affects the $\delta^{18}O$ value, with warmer waters containing more ^{18}O (Fig. 6.3).

The isotopic composition of natural waters is often expressed in terms of $\delta^{18}O$ and hydrogen composition (δD). Fig. 6.4 shows the variation in hydrogen and oxygen isotopic composition for a range of natural waters, and the change in water composition as a result of water-rock interaction and mixing of water from two different sources.

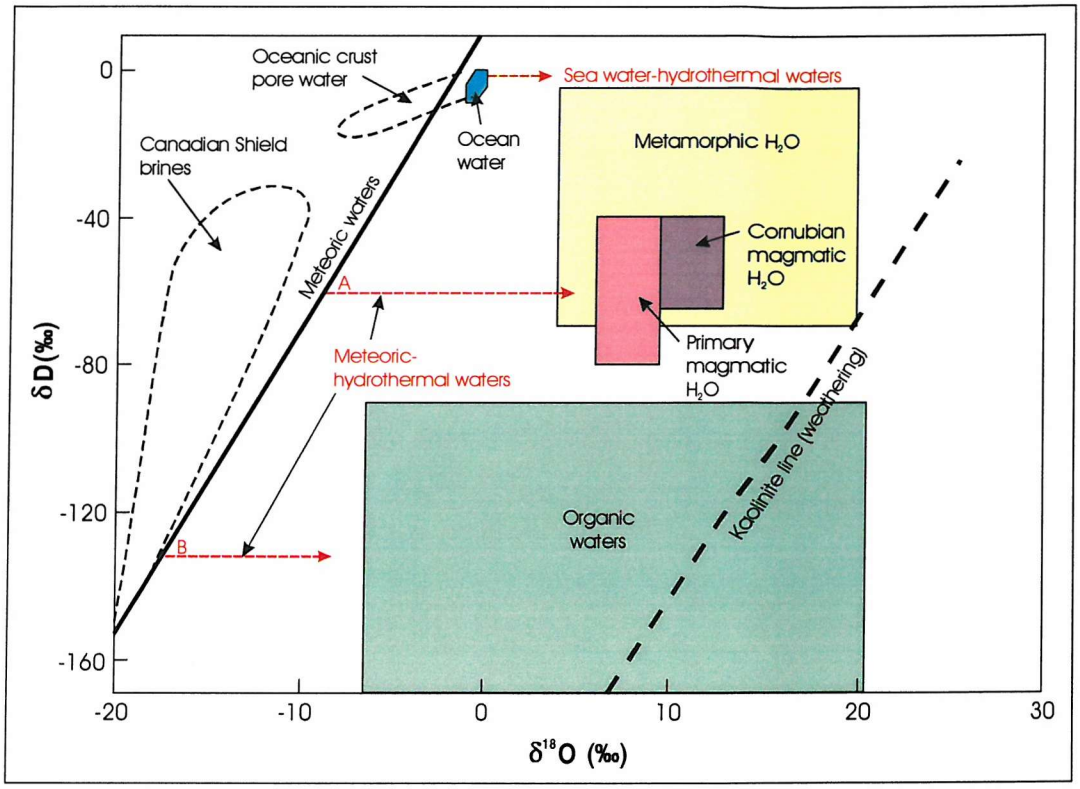

Figure 6.4: Isotopic compositions and fields for various natural waters. The kaolinite weathering line is provided for reference. ^{18}O-shift trends due to water-rock interaction, and exchange in hydrothermal systems are shown for seawater and meteoric waters of compositions A and B (red dashed arrows). Modified after Sheppard (1986).

Isotopic variation over time

The change in $\delta^{18}O$ in carbonate sediments over geological time has been extensively researched, and there is an apparent irregular trend towards increasing $\delta^{18}O$ in younger limestones (Baertschi, 1957; Clayton & Degens, 1959; Degens & Epstein, 1962; Keith & Weber, 1964; Dontsova *et al.*, 1972; Schidlowski *et al.*, 1975, etc.). The most significant increase is observed in freshwater and marine limestones of Jurassic age and younger. Keith & Weber (1964) reported average $\delta^{18}O$ values of -11.4‰ for Precambrian marine limestones, -9.7‰ in the Cambrian, and -1.2‰ for the Quaternary. Patterns in freshwater limestones are somewhat more irregular.

Whilst this trend may in part be due to the decrease in ocean temperature over time, it is generally accepted that post-depositional recrystallisation and equilibration with ^{18}O-depleted meteoric water (Clayton & Degens, 1959) is more likely to be responsible, with older rocks having undergone a greater degree of equilibration, or isotopic exchange with pore water at elevated

temperatures. Marine carbonate rocks provide a direct measure of the isotopic composition of the oceans, provided that they have not been chemically altered after deposition.

Dolomitisation is the most common alteration process affecting carbonate rocks. If dolomite is precipitated directly from seawater in equilibrium with co-existing calcite, isotope fractionation factors empirically dictate that the dolomite will contain $\delta^{18}O$ values approximately 5‰ to 7‰ higher than those measured in co-existing calcite (Bowen, 1988). In reality this is not observed, probably because the majority of dolomites are formed from alteration of calcite, so that the isotopic composition varies non-systematically as a reflection of the chemistry of the altering fluid. However, the degree of change in $\delta^{18}O$ in the carbonate depends on the timing of dolomitisation. Alteration to dolomite soon after deposition is unlikely to create much isotopic variation as the fluid held in the pore spaces of the carbonate sediment is likely still to be seawater, which will act as a buffer between the original carbonate and the infiltrating fluid. At the other end of the spectrum, dolomitisation occurring some time after deposition, and even after lithification will cause the carbonate to re-equilibrate with the dolomitising fluid.

Veizer & Hoefs (1976) suggested that this variation in dolomite formation can be related to the evolution of different depositional facies through geological time. Most Precambrian carbonates originated as lime mud in restricted hypersaline basins, often accompanied by blue-green algae. The impermeability of such sediments dictates that all chemical and mineralogical change must occur in the early stages of diagenesis, when seawater is the most common pore fluid and dolomite crystallisation is penecontemporaneous with calcite formation. The development of reef facies and other biochemical carbonates during the Phanerozoic resulted in highly permeable carbonate units favourable for continuous diagenetic solution and replacement of calcite by dolomite in the presence of hyposaline, low-^{18}O waters, creating isotopically lighter dolomite compared to the typical Precambrian carbonates.

6.3.2 Carbon

Carbon exists as two stable isotopes, ^{12}C (98.89%) and ^{13}C (1.11%), and a radiogenic isotope (^{14}C). Carbon isotopic composition is measured in terms of the $^{13}C/^{12}C$ ratio relative to the Peedee Belemnite (PDB) standard, and is expressed as parts per mil using delta notation (‰ $\delta^{13}C$).

$$\delta^{13}C = \left[\frac{(^{13}C/^{12}C)_{smpl} - (^{13}C/^{12}C)_{std}}{(^{13}C/^{12}C)_{std}} \right] \times 10^{3}$$

The distribution of carbon isotopes is controlled by biological synthesis and isotopic exchange reactions in carbon compounds. Temperature and fractionation factors play a similar role in carbon isotope distribution as they do for oxygen isotope distribution (see section 6.3.1).

^{12}C is preferentially taken up by organisms during photosynthesis because the lighter isotope tends to have faster reaction times during metabolic processes. Heavy carbon (^{13}C) is concentrated in non-organic carbon compounds such as carbonate minerals. Because materials such as coal and petroleum are sourced from organic matter, they inherit light carbon (^{12}C) from their source material. The range of $\delta^{13}C$ values found in natural carbon-bearing materials is shown in Fig. 6.5.

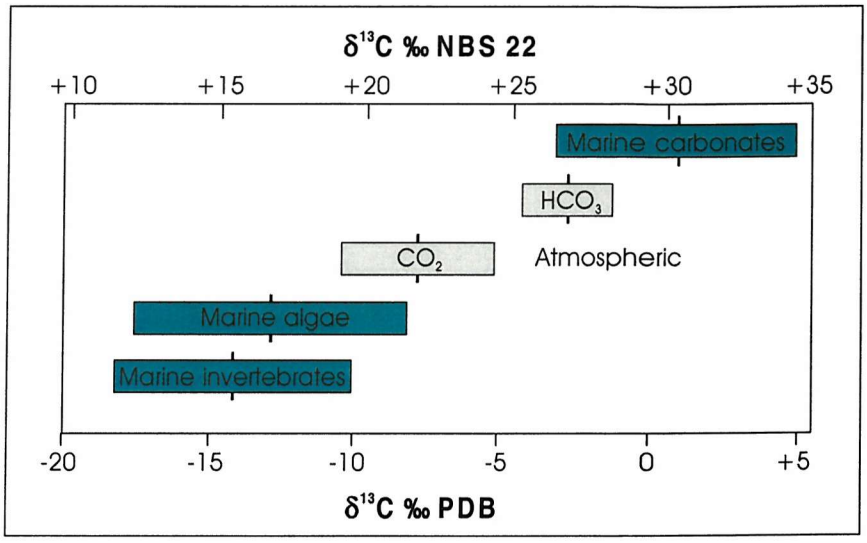

Figure 6.5: Carbon isotope variation in naturally-occurring carbon-bearing materials relative to the PDB (Peedee Belemnite) standard and the NBS 22 (petroleum) standard. Isotopic values relating to plant matter are omitted as they are not relevant to the Proterozoic, but they plot in the range -15 to -35 ‰relative to PDB. Modified after Mason & Moore, 1982.

Fig. 6.5 shows that most marine materials are enriched in ^{13}C relative to non-marine materials. This is because the heavier isotope is concentrated in the oceans through isotopic exchange between atmospheric CO_2 and marine bicarbonate, resulting in preferential partitioning of ^{12}C into the atmosphere:

$$H^{12}CO_3^{2-}{}_{(aq)} + {}^{13}CO_{2(g)} \rightarrow H^{13}CO_{3(aq)} + {}^{12}CO_{2(g)}$$

The isotopic composition of carbonate minerals precipitated from aqueous solution is controlled by the isotope chemistry of the water, temperature, and the fractionation of carbon isotopes between the precipitating mineral, the dissolved CO_2 and bicarbonate in the water (Faure, 1986). Research on fractionation factors for carbonate species in aqueous solutions by Emrich *et al.* (1970) shows that carbonate material precipitated in isotopic equilibrium with CO_2 is enriched in ^{13}C by approximately 10‰ at 20°C. The isotopic exchange between dissolved CO_2 in seawater and calcium carbonate is as follows:

$$H^{13}CO_3^{2-}{}_{(aq)} + Ca^{12}CO_3 \rightarrow H^{12}CO_3 + Ca^{13}CO_3$$

Local variations in the isotopic composition of the seawater affect $\delta^{13}C$ values in carbonate minerals. Freshwater carbonates contain higher proportions of ^{12}C than marine carbonates, and show greater variation in the range of $\delta^{13}C$ values. This is thought to be due to the contribution of isotopically light CO_2 derived from plant respiration in freshwater environments.

Analyses of various carbon-bearing materials ages show that $^{13}C/^{12}C$ ratios have not significantly changed over geological time (Craig, 1953; Baertschi, 1957; Degens & Epstein, 1962; Keith & Weber, 1964; Becker & Clayton, 1972; Veizer & Hoefs, 1976). Veizer & Hoefs (1976) reported that Cambrian carbonate rocks are enriched in ^{13}C by 3‰ compared to Cenozoic limestones. In contrast, Keith & Weber (1964) measured average $\delta^{13}C$ contents of -0.26‰ (± 3.09‰) for Precambrian limestones and -0.13‰ (± 2.61‰) for Cambrian and younger rocks.

6.3.3 The effects of metamorphism

Metamorphism can have a profound effect on the isotopic characteristics of a rock. The stable isotope composition of metamorphic rocks is controlled by the following factors:

1) The original isotopic composition of the pre-metamorphic protolith
2) Changes in isotopic composition through volatilisation processes
3) Isotopic exchange with metamorphic fluids
4) Temperature of isotopic exchange

Whilst all rocks have an isotopic signature representative of the environment in which they formed, the process of metamorphism usually alters that signature, even in 'closed' systems. The

most common process responsible for isotopic change is volatilisation, which involves dehydration, decarbonation and desulphidation as metamorphic grade increases.

Volatilisation

The liberation of volatile components (e.g., CO_2, H_2O, CH_4, etc) during prograde metamorphism has a profound effect on the isotopic composition of a rock, and the greater the degree of volatilisation, the larger the observed isotopic exchange.

The process of volatilisation can be modelled in two ways: batch volatilisation and Rayleigh volatilisation. Both processes involve preferential segregation of heavy isotopes (^{18}O and ^{13}C) into the volatile phase, leaving the residual rock relatively enriched in the light isotopes (Fig. 6.6).

1) Batch volatilisation

Batch volatilisation (Nabelek *et al.*, 1984), also termed 'closed system' (Brown *et al.*, 1985), 'one-step fluid escape' (Valley & O'Neil 1984) and 'single stage' (Bowman *et al.* 1985) involves continuous generation of volatile phases from the rock without their release from the system until volatilisation is complete. This means that the rock is in continual contact with the evolved volatile-rich fluid, and therefore undergoes re-equilibration. Because the rock has been depleted in heavy isotopes by the volatilisation process, isotopic equilibration with the evolved fluid will return the $\delta^{13}C$ and $\delta^{18}O$ values of the rock back towards their original values (i.e., the δ values will increase again). The extent of re-equilibration depends on the temperature, the degree of volatilisation and the time delay between volatile generation and fluid release. The greater these factors are, the greater the change in isotopic composition between the original protolith and the metamorphosed equivalent.

Batch volatilisation can be expressed as:

$$\delta f = \delta i - (1 - F)\ 1000 \ln \alpha$$

where: δi = Initial isotopic value of the rock

δf = Final isotopic vlaue of rock

F = Mole fraction of the element remaining in the rock after volatilisation

α = Fractionation factor (fluid-rock)

In reality, batch volatilisation involves the evolution of large quantities of fluid and a resulting huge volume (and pressure) increase, which cannot usually be sustained by the rock volume. Most systems are forced to release fluid due to overpressure.

2) *Rayleigh volatilisation*

This model is the opposite end-member to the batch volatilisation model described above. Rayleigh volatilisation (Rayleigh, 1896; Epstein, 1959) involves the continuous exchange and removal of small amounts of liquid as it is generated during prograde metamorphism. This process is also known as Rayleigh distillation, 'open system volatilisation' (Brown *et al.*, 1985) and, for carbonate systems, 'continuous decarbonation' (Bowman *et al.*, 1985).

Continual removal of volatile phases which preferentially partition heavy isotopes means that as metamorphism progresses, the volatiles are sourced from a rock that is increasingly enriched in light isotopes, so the fluid evolved at the end of the volatilisation process is isotopically lighter than that evolved at the start.

Fig. 6.6 compares the isotopic effects of the two volatilisation models. Note that the effects for the two models are similar for F = 1.0 down to F = 0.6 (the calc-silicate limit), after which Rayleigh volatilisation results in a dramatic decrease in ^{18}O in both the evolved CO_2 and the residual rock. The calc-silicate limit is applicable to most metamorphic systems, and is the point at which the release of CO_2 is limited by the formation of calc-silicate minerals that retain oxygen and subsequently prevent further volatile release. Therefore, for oxygen, and for F values of 0.6 to 1.0 it doesn't really matter which model is assumed. The curves below F = 0.6 in Fig. 6.6 are hypothetical, although the model may still be applied to carbon and hydrogen isotope systematics.

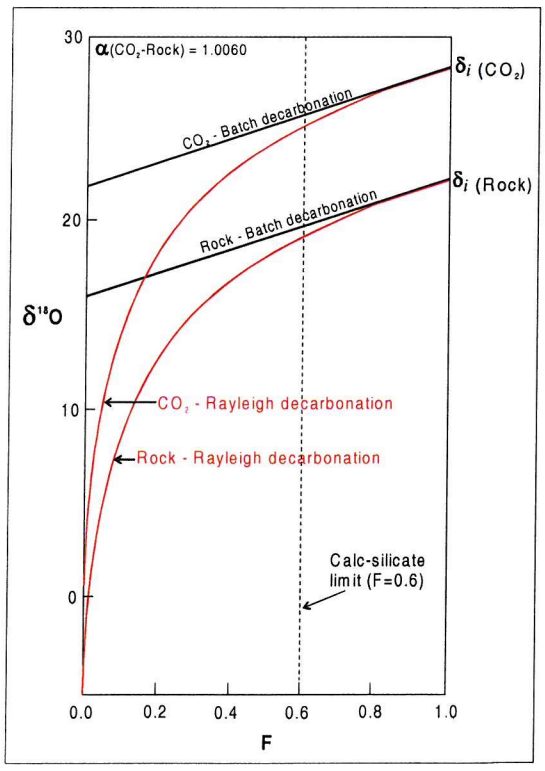

Figure 6.6: Diagram to show the progressive depletion of ^{18}O in a rock subject to batch volatilisation (black lines) and Rayleigh volatilisation (red curves). Calc-silicate limit (F=0.6) is shown as a dashed black line. F is the mole fraction of oxygen remaining in the rock, with 1.0 representing the original value of oxygen in the rock normalised to 100. Fractionation factor (CO_2-rock) = 1.0060. After Valley (1986).

Dehydration is the most common form of metamorphic volatilisation, and the extent of isotopic change can be correlated with the amounts of water released during this process. For oxygen isotopes, the effects of dehydration are quite small (<1‰). At low metamorphic temperatures (400-500°C), the released H_2O is isotopically lighter than the rock, causing ^{18}O enrichment in the rock. As metamorphism progresses above 500°C, the released water becomes heavier, and dehydration starts to cause ^{18}O depletion in the rock, effectively counteracting the earlier removal of ^{16}O. For hydrogen isotopes, the effects of dehydration are much greater, primarily because the mole fraction of hydrogen remaining in the rock (F) can decrease to zero.

The decarbonation process is the cause of a large loss of volatile components, particularly in marls and metacarbonate rocks. Research by Nabelek *et al.* (1984) revealed a strong correlation between the magnitude of ^{13}C depletion and the amount of decarbonation, showing that the decarbonation process is intermediate between the 'batch' and 'Rayleigh' models. In rocks containing an appreciable proportion of carbonate phases, decarbonation during metamorphism can cause significant decrease in the $\delta^{13}C$ value of the rock. However, the amount of CO_2 that can be lost through this process is limited by the amount of oxygen available for release. Most carbonate rocks contain at least a small proportion of silica, which reacts with carbonate phases during metamorphism to produce calc-silicate minerals (see Chapter 5). These reactions (e.g. the formation of diopside from breakdown of dolomite and quartz) not only release CO_2, but also lock the oxygen up in silicate phases so that it is no longer available for release as a volatile phase unless the metamorphic temperature increases to the point where the calc-silicate mineral itself becomes unstable and breaks down.

Diffusion

Isotopic change during metamorphism is greatly facilitated by the presence of a fluid. For most metamorphic systems, macro-scale fluid transport is achieved via channelised pathways, i.e, fracture networks. A small amount of isotopic equilibration occurs via volume diffusion, that is, the chemical transfer of materials through a crystal lattice. Equilibration can also occur by diffusion of chemical components through a static fluid infilling pore spaces, grain boundaries and micro-fractures in the rock mass.

The extent of isotopic change due to fluid flow is dependent on a number of factors (Valley, 1986):

1) The nature of phases in the system
2) Temperature, pressure and time
3) The rate and extent of deformation
4) Presence or absence of fluids
5) Isotopic gradient

Isotopic exchange via diffusion is most pronounced at elevated temperatures (i.e., >700°C), where diffusion is at its most efficient. Diffusion becomes less important at low metamorphic temperatures and in granulite facies rocks where aqueous fluids are largely absent. These relationships were demonstrated by Rye *et al.* (1976) for marbles interbedded with metapelites.

Whilst peak metamorphic temperatures may be preserved in the isotopic ratios of many metamorphic rocks, isotopic re-equilibration continues during the cooling stages of metamorphism, particularly if this stage is protracted and slow. In some cases, the gradual change in fluid composition over time is recorded in crystals displaying isotopic zonation. Metamorphic isotopic signatures may be overprinted by later-stage hydrothermal or weathering events.

6.4 STABLE ISOTOPE STUDIES AT ZINKGRUVAN

Stable isotope (carbon and oxygen) data for metacarbonate rocks of the Zinkgruvan mine and surrounding area were supplied by North Ltd and Anders Hallberg of the Swedish Geological Survey. Data supplied by the mine (analyses carried out as part of undergraduate Honours projects, see Appendix H) have not previously been evaluated in relation to whole rock chemistry, mineralogy and fluid history. Preparation and sampling information is given in Appendix H. Samples are divided into three sets: regional marbles, district marbles and mine area marbles, using the same criteria outlined at the beginning of Chapter 4. In addition, data from the Zinkgruvan basin are compared to other published Bergslagen stable isotope data in section 6.4.5.

6.4.1 Regional overview

Marine origins for various Bergslagen carbonate rocks have been proposed by Oen *et al.* (1986) and Boekschoten *et al.* (1988), based on field and petrographic evidence (e.g., the presence of stromatolites).

A preliminary study of stable isotope chemistry of ore-related carbonates from the Falun deposit by Billström *et al.* (1985) showed that carbonate samples near mineralisation display significant depletion in heavy isotopes $\delta^{18}O$ and $\delta^{13}C$ (Fig. 6.7A), probably through a combination of metamorphic decarbonation and interaction with hydrothermal fluid. In the same study, carbonate samples sourced several kilometres from sulphide mineralisation showed $\delta^{13}C$ values of around 0, and significantly elevated $\delta^{18}O$ values compared with ore-related carbonate samples.

De Groot & Sheppard (1988) provided a comprehensive overview of the stable isotope characteristics of different types of carbonate bodies in western Bergslagen. In their study they showed that most stratabound carbonate units contain $\delta^{13}C$ values close to zero (Fig. 6.7B), but their $\delta^{18}O$ values varied in association with mineralised horizons, with ^{18}O depletion occurring in units related to Fe oxide deposits. All stratabound carbonate $\delta^{13}C$ values fall within the range for early to mid-Proterozoic marine carbonates as defined by Veizer & Hoefs (1976), although no dolomite samples fall in the Proterozoic dolomite field of Veizer & Hoefs (1976). Carbonate formed as veins and as a result of skarn alteration display lower $\delta^{13}C$ but similar $\delta^{18}O$ values compared to stratabound carbonates.

Hallberg *et al.* (1994) carried out isotopic analyses of calcite from marbles and calc-silicate skarns from two drill holes at Zinkgruvan. These data show restricted $\delta^{18}O$ values of 17 (±2) ‰ relative to SMOW, and a large variation in $\delta^{13}C$ from -1 to -10‰ relative to PDB. These data are discussed with the other mine area samples in section 6.4.3.

An unpublished study by Gebeyehu (1991) focused on C-O isotope characteristics of metacarbonate rocks (marbles) at the Garpenberg deposit, eastern Bergslagen. Here, metacarbonate rocks were shown to be of marine origin, with modification of $\delta^{18}O$ values by

hydrothermal activity related to base metal mineralisation, and slight depletion in $\delta^{13}C$ in dolomitised metacarbonate samples relative to non-dolomitised samples. These data are compared to the Zinkgruvan data in sections 6.4.4 and 6.4.5.

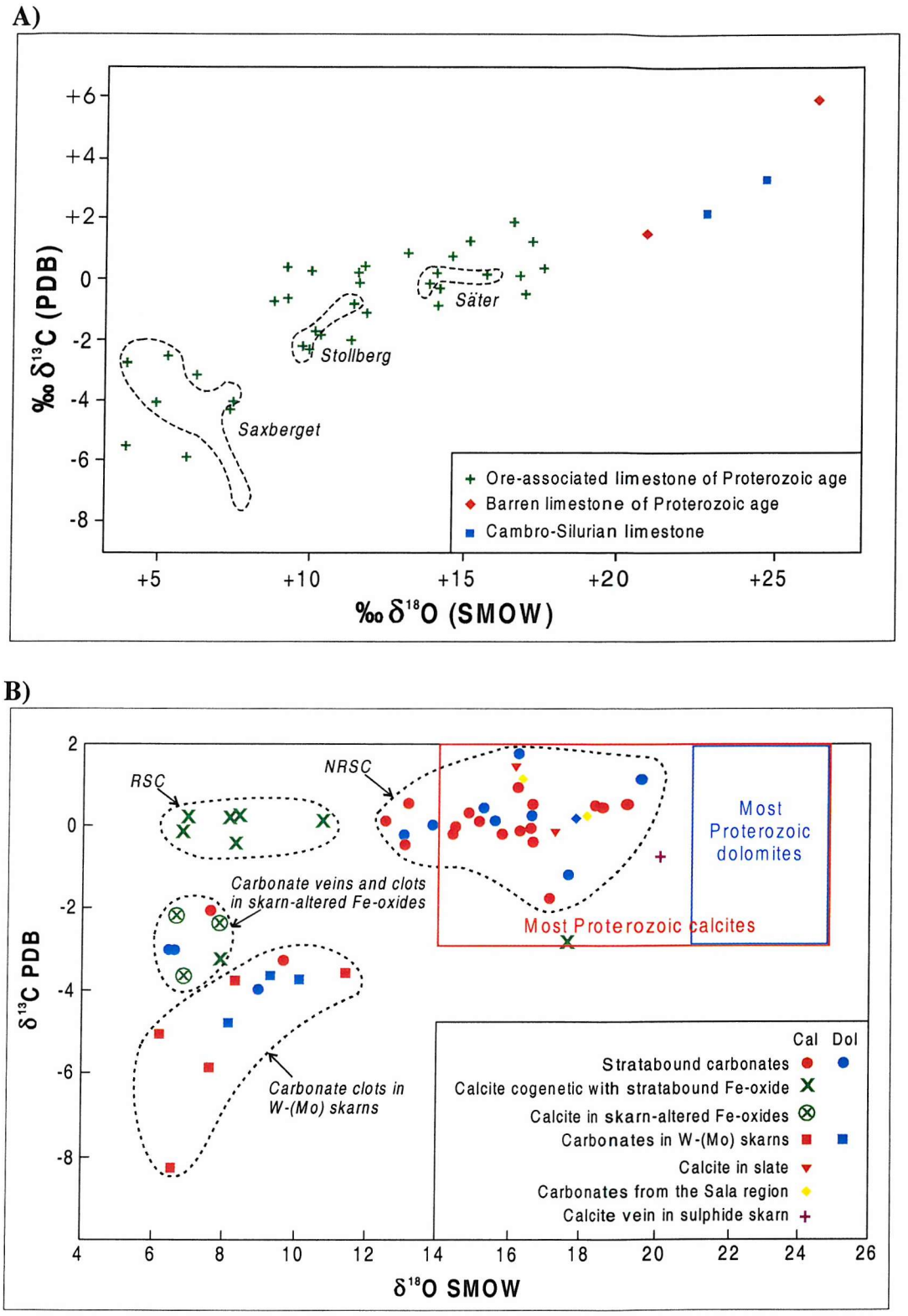

Figure 6.7: A) Stable isotope compositions of carbonate rocks published by Billström et al. (1985). Note that samples near mineralisation are apparently depleted in ^{13}C and ^{18}O relative to carbonate samples situated several kilometres from mineralisation. B) Stable isotope composition of carbonate samples from western Bergslagen. Red and blue boxes show the composition of typical Early to Middle Proterozoic calcites and dolomites, as defined by data from Veizer & Hoefs (1976). RSC = carbonates related to stratiform Fe-oxide mineralisation; NRSC = carbonates not related to stratiform Fe-oxide mineralisation. Two carbonate samples from Sala (central Bergslagen) are included for comparison. Modified after De Groot & Sheppard (1988).

6.4.2 Regional metacarbonate samples

Dolomitic marble samples from Glanshammar show little mineralogical or geochemical evidence for post-depositional chemical alteration aside from dolomitisation (Chapter 4). Analysis of their carbon and oxygen isotopic composition shows that they have $\delta^{13}C$ values of around zero (± 0.5‰) relative to PDB, and $\delta^{18}O$ values of between +17.79 and +19.81‰ relative to SMOW (Fig. 6.8A). These data strongly suggest a marine origin for these samples, although they display isotopically lighter $\delta^{18}O$ than the field of 'typical Proterozoic dolomites' as defined by Veizer & Hoefs (1976). However, as Billström *et al.* (1985), De Groot & Sheppard (1988), Schidlowski *et al.* (1975) and Hallberg *et al.* (1994) have shown, this is common in Bergslagen carbonates and is usually ascribed to pre-metamorphic alteration patterns. Given that these samples show no petrological or chemical evidence for alteration except dolomitisation, it must be assumed that either:

a) the carbonate had lower than average $\delta^{18}O$ at the time of deposition;
b) water with a significant meteoric (^{16}O-rich) component was involved in the dolomitisation process, although $\delta^{13}C$ values in these samples appear to have been unaffected by dolomitisation;
c) ^{18}O was lost through metamorphic decarbonation processes.

The Glanshammar samples fall towards the isotopically heavier end of the range when compared with the rest of the $\delta^{18}O$ data for the Zinkgruvan area, suggesting that they are amongst the least altered samples in the dataset. Despite some ^{18}O depletion, and bearing in mind dolomite's relative resistance to isotopic re-equilibration when compared with calcite, the Glanshammar samples can again be used as an 'unaltered' baseline against which to compare the stable isotope geochemistry of district and mine area samples.

A)

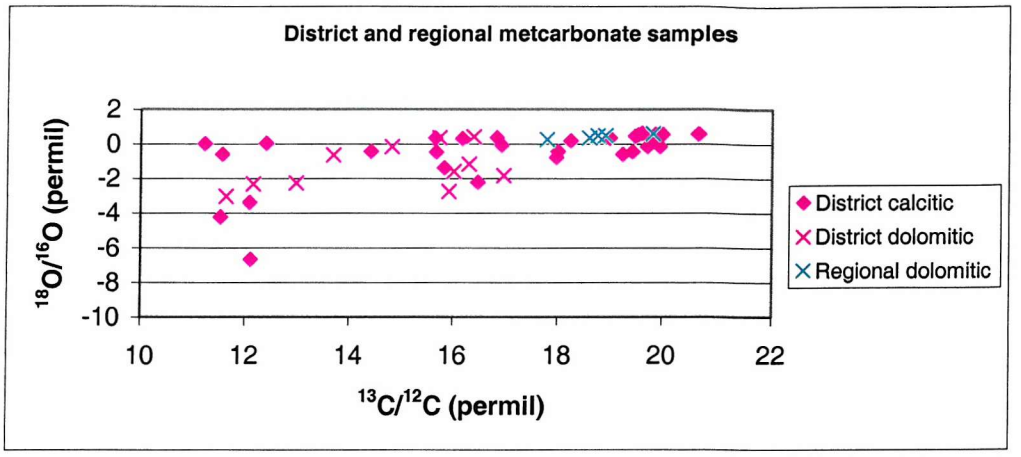

B)

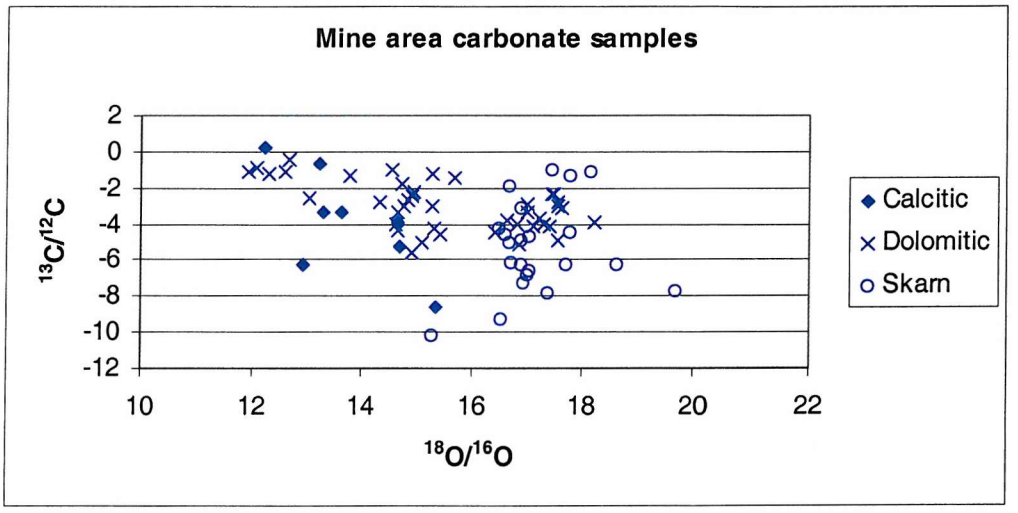

Figure 6.8: Plots to show variation in $\delta^{13}C$ (PDB) and $\delta^{18}O$ (SMOW) for A) regional (pale blue) and district (pink) carbonate samples and B) mine area (dark blue) carbonate samples.

6.4.3 District metacarbonate samples

From a tight cluster around $\delta^{13}C = 0$, district samples of carbonate rock show a broad decrease of $\delta^{13}C$ coupled with decreasing $\delta^{18}O$ (Fig. 6.8A), and display a slightly wider range of $\delta^{18}O$ data compared to carbonates from the mine area. Both district and mine area sample sets will be affected to some degree by decarbonation during metamorphism, but the opposing trends in Figs 6.8A & B indicate that the mine area marbles have been affected by different chemical processes to the district marbles.

The district carbonate sample set can be subdivided based on geographic location (Fig. 6.9). Ten samples were taken from the area to the north of Zinkgruvan, in close proximity to intensely

potassic-altered metavolcanic rocks. The remaining samples originate from areas to the south and southwest of Zinkgruvan (see sample location map, Appendix B).

a) Calcitic marbles

Calcite-dominant samples display relatively restricted $\delta^{13}C$ compositions, with the majority of samples falling in the range of -1.0 to +0.7‰ relative to PDB (red symbols, Figs 6.9 and 6.10), clearly indicative of a marine origin. A few samples define a trend of decreasing $\delta^{13}C$ with decreasing CO_2 (Fig. 6.10A); all samples falling along this trend are calc-silicate marbles containing appreciable quantities (up to ~40 vol%) of skarn minerals (diopside, garnet, etc.) and are all sampled from the area to the north of the mine. This trend reflects the loss of ^{13}C during open system decarbonation, and/or exchange with a metasomatic fluid depleted in ^{13}C. The calc-silicate minerals developed in these samples are not the natural mineral phases developed through isochemical metamorphism of silica-contaminated carbonate material, but represent chemical exchange with an aluminous source, such as nearby metavolcanic material, and/or fluid infiltration prior to or during metamorphism (see Chapter 4, section 4.3). These samples also show depletion in ^{18}O (Fig. 6.9) relative to most of the sample set, and may be considered intermediate in composition between 'true' marbles and 'true' calc-silicate skarns, falling on a line between the two.

The spread of data at $\delta^{13}C = \sim 0$ towards more ^{18}O-depleted (^{16}O-enriched) is mainly due to loss of heavy oxygen (^{18}O) through decarbonation. The least altered sample is that which shows the highest $\delta^{13}C$ and $\delta^{18}O$ values (marked in Fig. 6.9), as metamorphism and fluid interaction will cause both these parameters to decrease. The degree of ^{16}O enrichment is controlled by the duration of water-rock interaction, and the volume of fluid present. Longer interaction times and larger volumes of fluid will result in a greater magnitude of ^{16}O enrichment.

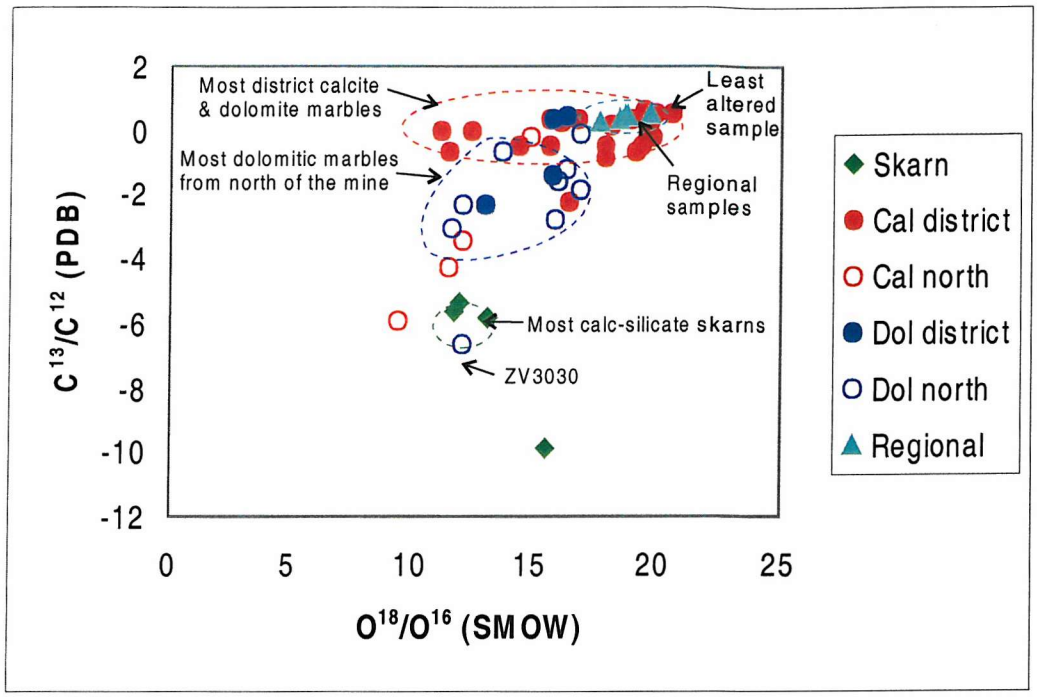

Figure 6.9: $\delta^{18}O$ vs $\delta^{13}C$ compositions for district marbles, subdivided on the basis of their geographic position as well as mineralogical composition. Samples from the north of Zinkgruvan (open symbols) show a more restricted range of $\delta^{18}O$ and greater depletion in ^{13}C than samples from the rest of the district. This may be linked to the potassic enrichment event that has affected the metavolcanic strata in the north of the area. Regional samples from Glanshammar (turquoise triangles) and district calc-silicate skarns (green diamonds) are plotted for comparison.

b) Dolomitic marbles

The dolomitic marble samples are generally depleted in ^{13}C compared to calcitic samples, with most samples exhibiting $\delta^{13}C$ in the range +0.3 to -3 ‰ (PDB) (Fig. 6.9). One sample (ZV3030) is excessively depleted in ^{13}C, but thin section analysis reveals it to be heavily calc-silicate altered.

Sampling of dolomitic marbles from around the Zinkgruvan Basin is limited, with only four samples located away from the northern area. However, two samples from Vinnern West showing $\delta^{13}C$ values of around +0.3‰ can be compared to a third, 'skarny' (calc-silicate mineral-rich) sample from the same location which displays a considerably lower $\delta^{13}C$ value of -2.30‰. This implies that the formation of calc-silicate minerals and resultant loss of CO_2 has had a significant impact on the $\delta^{13}C$ isotopic signature of the samples.

The remaining dolomitic samples from the north of Zinkgruvan are more depleted in ^{13}C, falling in the range -1 to -3‰ (PDB). The $\delta^{18}O$ data for these samples are more restricted than those measured for the district calcitic samples, falling in the range +11.5 to +17.0‰ (SMOW). Again, when compared to the least altered carbonate sample (Fig. 6.9), it is apparent that the dolomite samples have either lost ^{18}O through decarbonation or have interacted with an isotopically light (^{16}O-rich) fluid, causing the $\delta^{18}O$ value to decrease.

c) Calc-silicate skarns

The few calc-silicate skarn samples for which data are available show $\delta^{13}C$ values of around -6‰ $\delta^{13}C$ relative to PDB (Fig. 6.10A), with one strongly ^{13}C-depleted sample having a value of -9.8‰. $\delta^{18}O$ values for the same samples show a restricted range of +11.5 to +13.0 ‰ (SMOW) (Fig. 6.10B), although the highly ^{13}C-depleted sample is slightly enriched in ^{18}O (15.53‰).

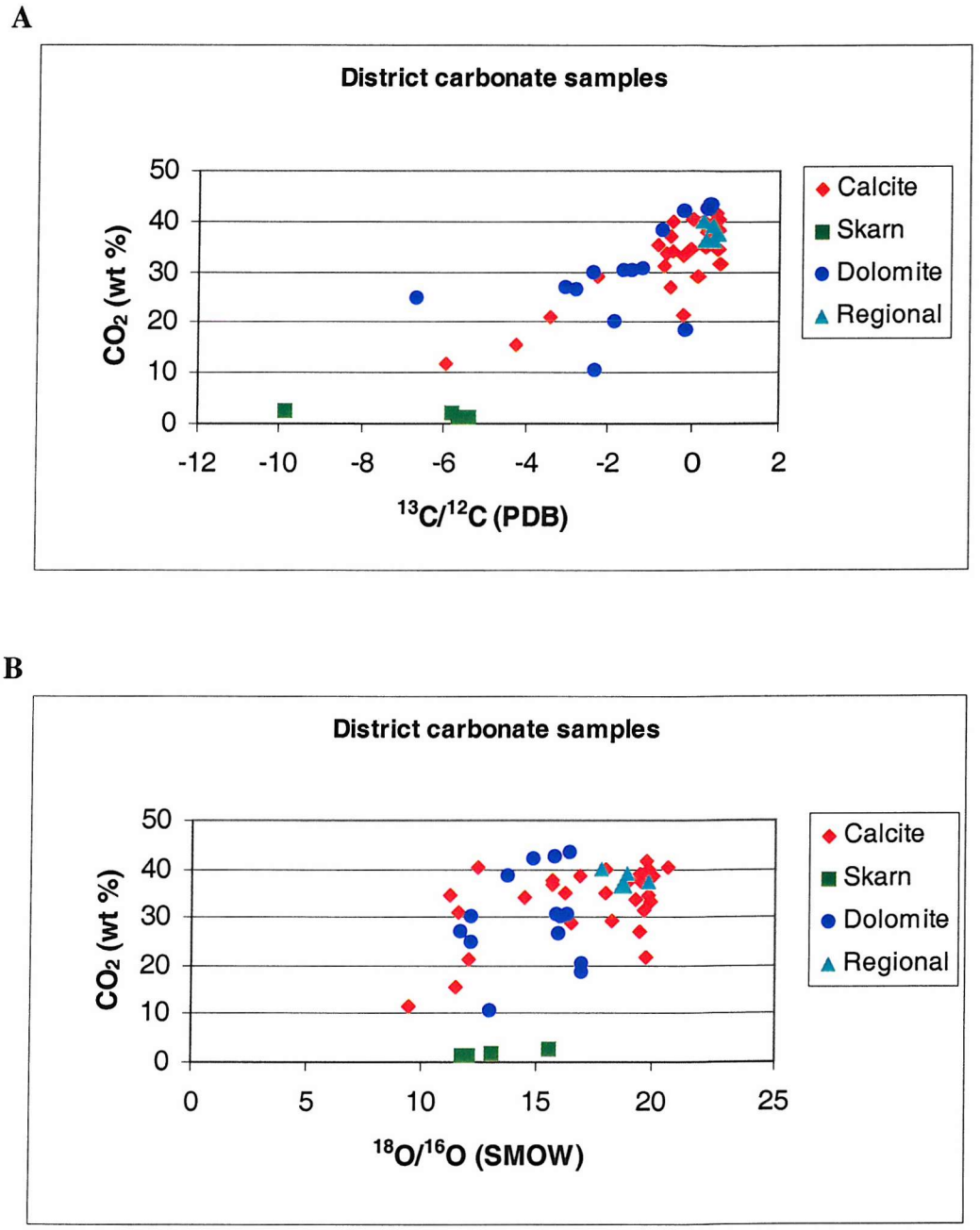

Figure 6.10: Stable isotope geochemistry of district marble samples related to whole-rock CO_2 content.

A) $\delta^{13}C$ vs CO_2: note the restricted $\delta^{13}C$ range for most calcite samples compared to the dolomite samples. Dolomite samples show a strong relationship between decreasing $\delta^{13}C$ and decreasing CO_2. Calc-silicate skarns are strongly depleted in ^{13}C.

B) $\delta^{18}O$ vs CO_2: Data show no correlation between $\delta^{18}O$ and CO_2 content, although dolomitic samples appear to contain a much narrower range of $\delta^{18}O$ than calcitic samples, and plot towards the heavier end of the range.

6.4.4 Mine area metacarbonate samples

Fig. 6.11 shows the stable isotopic composition of all carbonate samples from Zinkgruvan. These data are sourced from the mine, an unpublished study carried out by Hallberg *et al.* (1994), and published literature. Unpublished data for carbonates from the Garpenberg Zn-Pb deposit (Gebeyehu, 1991) are included for comparison (a detailed comparison of Zinkgruvan carbonates to other Bergslagen Zn-Pb deposits is given in section 6.4.5).

Fig. 6.11 illustrates the overall trend of increasing $\delta^{18}O$ with decreasing $\delta^{13}C$ for metacarbonate samples from the mine area (shown more clearly in Fig. 6.8B). This trend is the opposite to that observed in district samples (Fig. 6.8A). It is clear from Fig. 6.11 that the Zinkgruvan mine area metacarbonate rocks are apparently unusually depleted in ^{13}C and enriched in ^{18}O compared to the district and regional samples (figs 6.8 & 6.12) and the Garpenberg data.

The data for the mine area are sourced from sampling of four drill cores. DDH 231 and 671 are located in the western part of Nygruvan; DDH 898 and DDH 660 are from the Cecilia orebody. Analysis of the stable isotope data in terms of their source location shows that all the samples have a similar range of $\delta^{18}O$ values (+12 to +20‰), but $\delta^{13}C$ is highly variable, ranging from 0 to -10‰ (figs 6.11 & 6.12). However, no geographic trends can be discerned from these data, although analyses from Hallberg *et al.* (1994) fall towards the heavier end of the $\delta^{18}O$ range than the data supplied for the same drill hole by the mine.

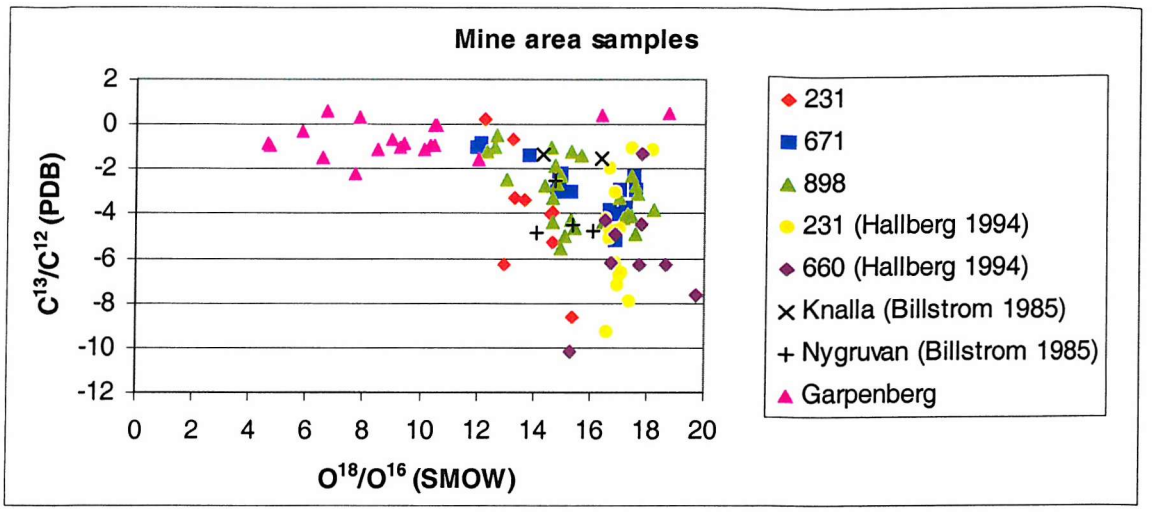

Figure 6.11: Stable isotope data for metacarbonate samples from the mine area. Data comprises that supplied by North Ltd, unpublished data from Hallberg et al. (1994), and published data from Billström (1985). Unpublished data for Garpenberg (another large Bergslagen Zn-Pb deposit) is included for comparison (Gebeyehu, 1991). Note that the Zinkgruvan carbonate data is far more depleted in ^{13}C and enriched in ^{18}O than the Garpenberg data.

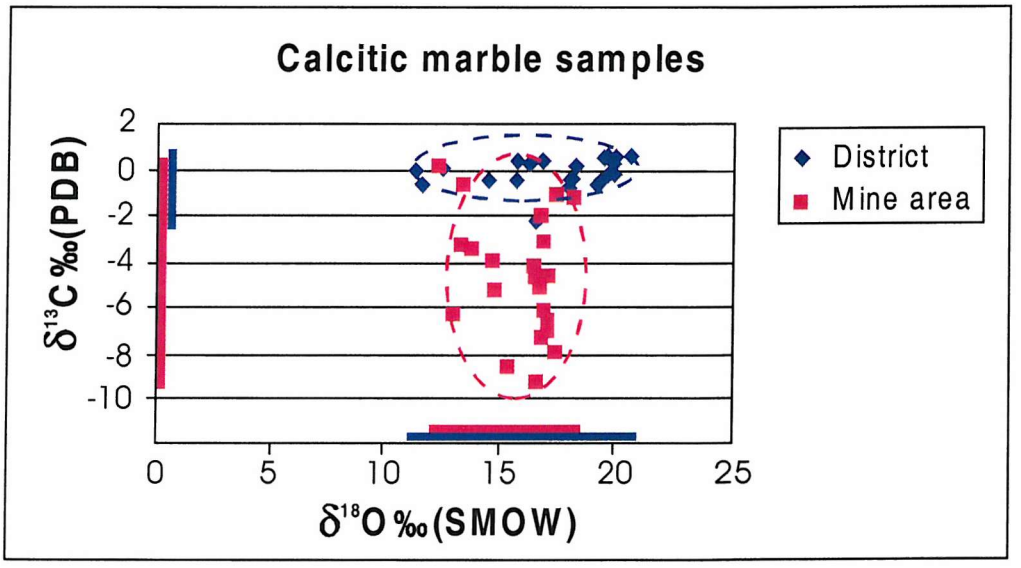

Figure 6.12: Comparison of $\delta^{18}O$ and $\delta^{13}C$ values of mine area (pink symbols) and district (blue symbols) metacarbonate rocks. Coloured bars represent the isotopic ranges for the datasets shown.(pink = mine area, blue = district). Note depletion in ^{13}C in mine area samples relative to district sample set, but similarity in $\delta^{18}O$ ranges.

Causes of ^{13}C depletion

Possible causes of ^{13}C depletion are decarbonation during metamorphism due to calc-silicate formation (Chapter 5), and interaction with a ^{12}C-rich fluid.

Equilibration with a ^{12}C-rich fluid could have a pronounced impact on the $\delta^{13}C$ isotopic composition of the mine area carbonate rocks. A fluid carrying a significant methane (CH_4) component derived from graphite could produce a shift towards isotopically lighter $\delta^{13}C$ values. Fig. 6.13 shows the predicted $\delta^{13}C$ compositions of CH_4 and CO_2 gases generated from graphite

with a $\delta^{13}C$ value of -15‰. Minor amounts of graphite have been reported from metavolcanic and metasedimentary rocks in the Zinkgruvan area (Billström, 1985), so it is possible that CO_2 or CH_4 derived from the graphite may have contributed towards decreased $\delta^{13}C$ values in nearby carbonate rocks. However, graphite was not observed in samples taken for this study.

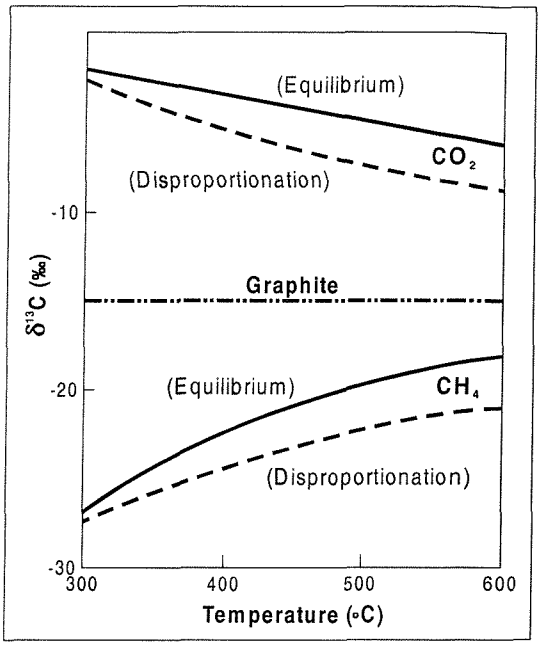

Figure 6.13: Predicted $\delta^{13}C$ values for CO_2 and CH_4 generated from graphite with a $\delta^{13}C$ composition of -15‰. The equilibrium curved (solid lines) are for equilibrium among CO_2, CH_4 and graphite; the disproportionation curves (dashed lines) represent equilibrium only between CO_2 and CH_4. Modified after Ohmoto & Goldhaber (1997).

Decarbonation processes preferentially partition the heavy isotope into the volatile phase, but in pure marbles this process alone could not produce excessive ^{13}C depletion. Many of the district carbonates and those from the Garpenberg deposit have also undergone upper amphibolite grade metamorphism, but do not show $\delta^{13}C$ values below -3‰.

However, careful investigation of the $\delta^{13}C$ isotopic variations in relation to the amount of silica (i.e., the skarn component) in the mine samples clearly shows that the $\delta^{13}C$ values decrease with increasing silica content (Fig. 6.14B). Marble samples with a low silica content (e.g., most district marbles and all regional samples) show values of around zero. As shown in Fig. 6.9 for district marble samples, the $\delta^{13}C$ value clearly decreases with increasing calc-silicate (skarn) content, with pure calc-silicate rocks having values as low as -10‰.

Formation of calc-silicate minerals during prograde metamorphism (described in Chapter 5) due to reaction between carbonate and silicate minerals generates CO_2 as a by-product. Partitioning of the heavy carbon isotope (^{13}C) into the volatile phase results in a decrease in the $\delta^{13}C$ value of the remaining rock. Therefore, the higher the degree of calc-silicate formation (as a

function of temperature and % silica in the parent rock), the greater the amount of CO_2 evolved during metamorphism, and the greater the depletion in ^{13}C.

The differences in $\delta^{13}C$ values between the Zinkgruvan data and the Garpenberg data can be attributed to the amount of silica in the samples. Garpenberg marble samples are shown to be relatively pure, containing 51.08% (± 5%) CaO, and containing >30 wt% CO_2 (Fig. 6.14). Therefore, the relative lack of silica in these samples means that only limited calc-silicate formation (and therefore limited ^{13}C depletion) occurred during metamorphism, despite similar peak metamorphic temperatures compared to those experienced at Zinkgruvan.

A greater degree of ^{13}C depletion in samples from the north of the mine (Fig. 6.9) can probably be linked to potassic alteration in that area, which may have also introduced additional silica into the carbonate rocks.

A

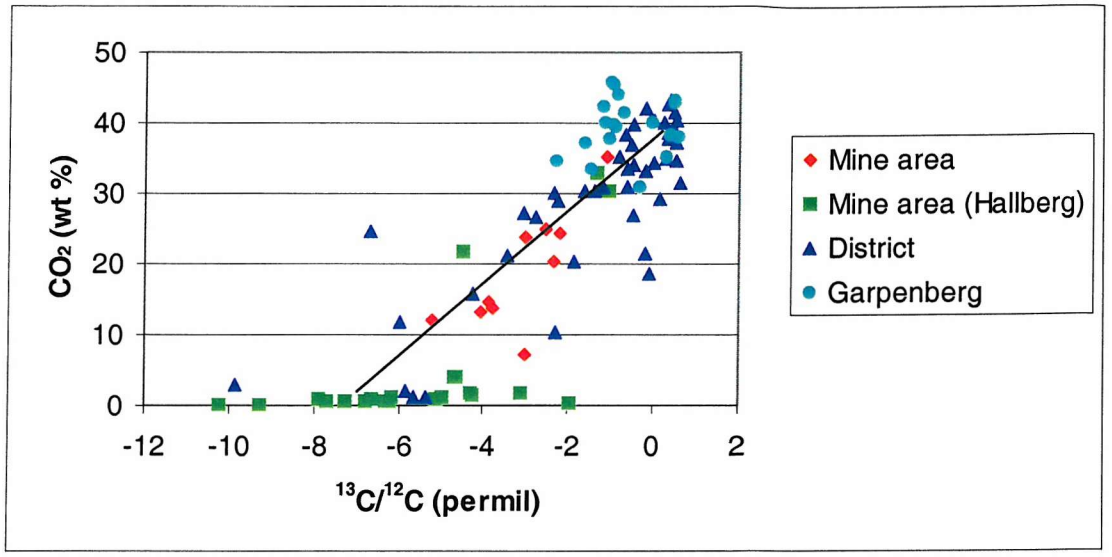

B

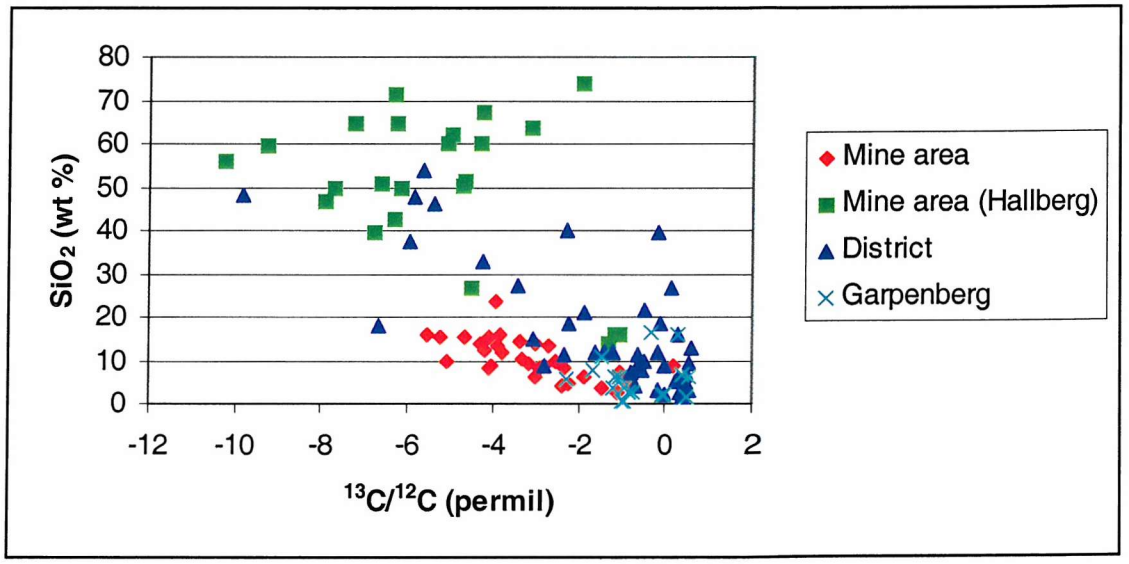

Figure 6.14:
A) $\delta^{13}C$ depletion related to % CO_2, and B) % SiO_2, i.e., amount of calc-silicate formation in metacarbonate samples. Garpenberg samples are relatively pure marbles and do not show excursion to low $\delta^{13}C$ values. Zinkgruvan mine area and district samples show significant ^{13}C depletion with increasing calc-silicate content (= decreasing % CO_2). Data sourced from Hallberg et al. (1994) (green squares) are particularly depleted in ^{13}C because the majority of calcite crystals analysed were sourced from pure calc-silicate skarns rather than from marbles. Line in Fig. 6.14A shows the trend of the data, representing the degree of ^{13}C fractionation due to calc-silicate formation.

In the sample set provided by Hallberg *et al.* (1994), only 4 of the calcite samples analysed came from true marbles containing >50% calcite. The remaining 17 calcite samples were sourced from calc-silicate skarns containing <10% calcite, which is why this sample set displays such depleted $\delta^{13}C$ values. However, the CO_2-poor samples which plot along the baseline in Fig. 6.14A show a range of $\delta^{13}C$ values from -2 to -10‰. Examination of whole-rock geochemistry does not

reveal any systematic chemical changes with the degree of ^{13}C depletion aside from a general increase in the concentrations of all major elements except calcium. In other words, Ca-rich calc-silicate skarns tend to be less depleted in ^{13}C than Ca-poor, Al-rich skarns. The simplest explanation for the variation in skarn geochemistry is the proximity of volcanic material, as described in Chapter 4 (section 4.6), particularly if the volcanic rocks contain graphite as reported by Billström (1985). This concept is summarised in Fig. 6.15.

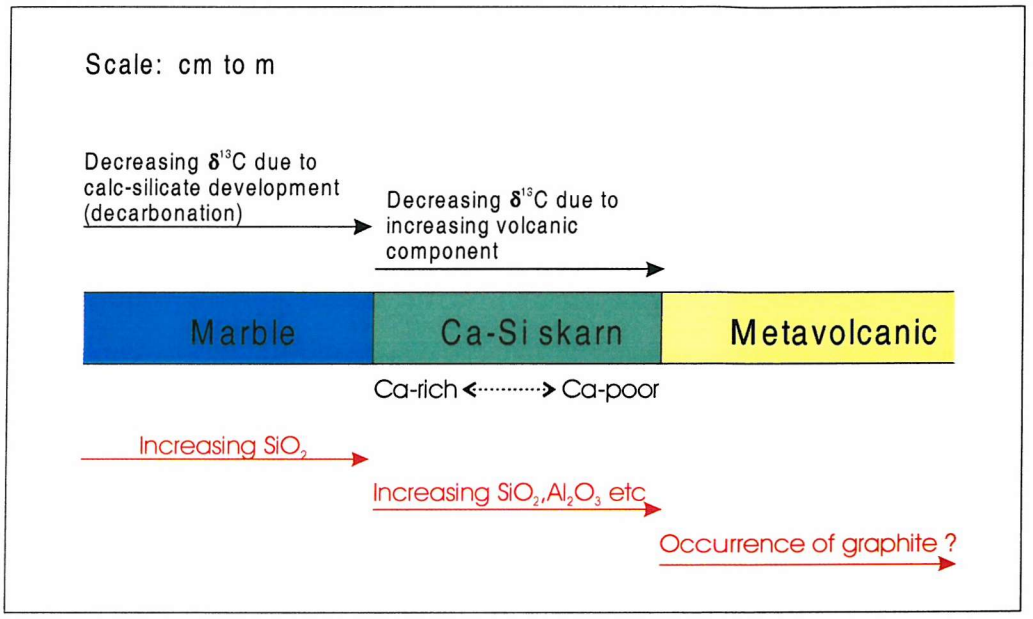

Figure 6.15: Summary diagram to show variation in metacarbonate chemistry and C isotope characteristics with proximity to volcanic material.

^{18}O depletion

The mine samples show little change in their $\delta^{18}O$ composition relative to district and regional samples, irrespective of their silica content. This implies that the expected loss of ^{18}O during metamorphic decarbonation may have been buffered by the aqueous fluids present during metamorphism. If this is so, these fluids must have been rich in ^{18}O relative to ^{16}O, which would be expected if the source of the fluids is dominantly through the metamorphic breakdown of hydrous minerals (because the heavy isotope will be preferentially partitioned into the volatile phase).

6.4.5 Zinkgruvan in a Bergslagen Province context

Zinkgruvan appears to have stable isotope characteristics that are unique amongst the Bergslagen base metal sulphide deposits. Relative to data from carbonates at the base metal deposits of Garpenberg, Saxberget, Stollberg and Gruvåsen (see Fig. 1.1 for location), carbonate rocks at Zinkgruvan are enriched in $\delta^{18}O$ and depleted in $\delta^{13}C$ (Fig. 6.16). Aside from the five samples from Saxberget which also show moderate depletion in $\delta^{13}C$, carbonate rocks from other major base metal deposits contain $\delta^{13}C$ values of between +0.56 and -2.28‰ relative to PDB (Fig. 6.16). Although some Zinkgruvan samples fall into this range, the majority fall below -2‰, with the most depleted sample at -10‰.

In addition, Zinkgruvan data form a distinct grouping when compared to all other carbonate stable isotope data from around the Bergslagen Province (Fig 6.17). Although Zinkgruvan samples fall within the same range of $\delta^{18}O$ and $\delta^{13}C$ values shown by the other Bergslagen samples as a whole, they fall towards the O^{18}-rich end of the spectrum, and are more depleted in ^{13}C than most of the other Bergslagen samples.

As the data in previous sections of this chapter have shown, the stable isotope characteristics of a carbonate rock (particularly $\delta^{13}C$) are strongly affected by decarbonation during metamorphism, and the greater the level of silica contamination in the original carbonate, the greater the degree of decarbonation and therefore ^{13}C loss. Whilst the data in figs 6.16 & 6.17 ***appear*** to identify the Zinkgruvan carbonates as isotopically distinct in the Bergslagen Province, sampling bias may contribute to the apparent anomaly. Zinkgruvan samples cover a range of metacarbonate rock types, from pure marble containing <10% non-carbonate minerals, to pure calc-silicate skarns containing <5% calcite. The Garpenberg sample set (Gebeyehu, 1991) comprises only very pure marbles and dolomites, and does not include calc-silicate skarns which would yield more depleted $\delta^{13}C$ values than the marbles.

However, as the degree of ^{13}C depletion appears to be strongly related to SiO_2 content, Zinkgruvan marbles may be anomalous in terms of their silica contamination relative to most other metacarbonate rocks in Bergslagen. Zinkgruvan is relatively close to the supposed volcanic centre at Godegård (Allen *et al.*, 1996) and may therefore have been more prone to volcanic ash contamination than areas distal to volcanic activity. Silica enrichment via fluid infiltration may have also provided the extra silica required for calc-silicate formation, although it seems unlikely that this type of alteration should be exclusive to Zinkgruvan.

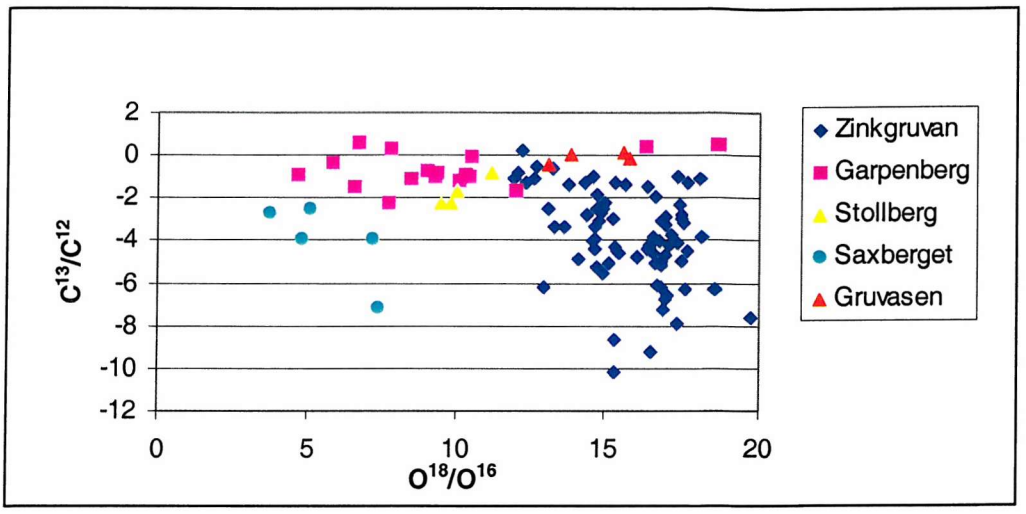

Figure 6.16: Comparison of Zinkgruvan carbonate stable isotope data to that from other Bergslagen base metal sulphide deposits. Garpenberg data from Gebeyehu (1991); Stollberg and Saxberget data from Billström et al. (1985); Gruvåsen data from de Groot & Sheppard (1988). Zinkgruvan data from Hallberg et al. (1994), Billström et al. (1985) and North Ltd. See Fig. 1.1 for location of base metal deposits.

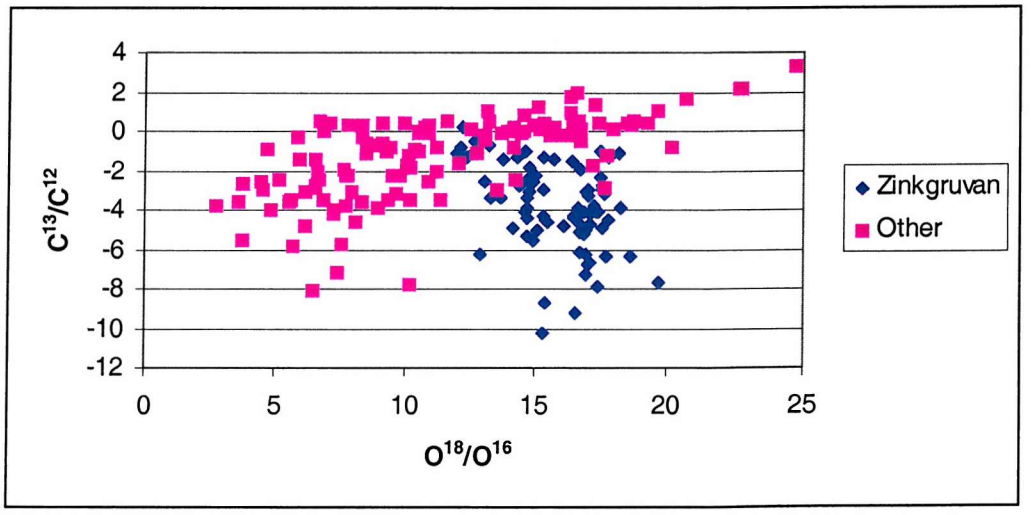

Figure 6.17: Comparison of Zinkgruvan carbonate stable isotope data to all other Bergslagen carbonate stable isotope data. Data sources: Hallberg et al (1994), Billström (1985), Billström et al (1985),de Groot & Sheppard (1988), Schidlowski et al. (1975) and Gebeyehu (1991).

Excursion of the majority of the Bergslagen data towards lower $\delta^{18}O$ compositions suggests interaction with hydrothermal fluids, probably combined with some loss of ^{18}O through decarbonation. That Zinkgruvan metacarbonates do not show the same ^{18}O depletion despite having reached upper amphibolite grade metamorphism suggests:

a) Zinkgruvan metacarbonates preserve (or are moderately close to) the original $\delta^{18}O$ value of the carbonate, meaning that other Bergslagen carbonates have been preferentially depleted in ^{18}O and/or enriched in ^{16}O.

Or

b) Zinkgruvan carbonates were also depleted in ^{18}O in line with the rest of Bergslagen, but were subsequently affected by a source of heavy oxygen which raised the $\delta^{18}O$ values back towards their original composition.

Increasing the $\delta^{18}O$ value of a sample is difficult as oceanic, meteoric and hydrothermal waters are all isotopically light (see Fig. 6.5), so any interaction between these fluids and a carbonate will result in a decrease in $\delta^{18}O$. Even primary magmatic fluid, although isotopically heavier than fresh or meteoric water, usually has lower $\delta^{18}O$ values than the Zinkgruvan carbonates. It therefore seems more likely that the overall heavier $\delta^{18}O$ signature in the Zinkgruvan carbonates is an original feature, rather than a result of alteration (^{18}O-enrichment).

The temperature of the fluid present at the time of alteration/dolomitisation, and the water-rock ratio can have significant effects on isotopic equilibration. Higher temperature fluids acting in a system with a high fluid/rock ratio can preferentially partition more heavy oxygen (^{18}O) into the rock relative to a similar system where lower temperature fluids are interacting with the rock at low fluid/rock ratios (e.g., Hitzman *et al.*, 1998). The spread of data for Bergslagen carbonates shown in Fig. 6.17 could represent a regional variation in the temperature of the dolomitising fluid, or a change in the fluid/rock ratio. The cluster of Zinkgruvan towards the heavier end of the $\delta^{18}O$ range suggests these rocks equilibrated with a dolomitising fluid of a higher temperature or at a higher fluid/rock ratio relative to most other areas of the province.

6.5 SUMMARY

6.5.1 Strontium isotopes

- The Sr isotopic compositions of metacarbonate rocks in the Zinkgruvan district vary widely from primitive values close that of early Proterozoic seawater (~0.7047), to more radiogenic values of > 0.7100.
- Extremely high $^{87}Sr/^{86}Sr$ ratios are the result of Rb enrichment related to potassic alteration in marbles, resulting in Sr ratios in excess of 0.7800.
- Contamination of carbonate sediment by volcanic ash has resulted in an increase in the Sr isotopic ratios. This may be due to the presence of the volcanic material itself, but is more likely to reflect weak K-Rb alteration of the volcanic component.
- Dolomitisation appears to have had no systematic effect on the Sr isotopic composition of the metacarbonate rocks. Dolomitised samples show a range of $^{87}Sr/^{86}Sr$ values from a primitive 0.7048 up to 0.7126, and an apparently unaltered calcitic sample (ZR04) and a dolomitised sample (555/22) show very similar values.

- This may indicate that the timing of dolomitisation was relatively soon after deposition, so that seawater was still the dominant isotopic influence and the Sr values were consequently not significantly altered.

6.5.2 Stable (C, O) isotopes

- Regional marble samples from the Glanshammar district display $\delta^{13}C$ and $\delta^{18}O$ characteristics typical of marine carbonates, with $\delta^{13}C = 0$ (± 0.5‰), and $\delta^{18}O = 18.77$ (± 0.73‰).
- Metacarbonate samples from the Zinkgruvan district show a range of $\delta^{13}C$ and $\delta^{18}O$ values. Most calcitic samples show a marine signature, but dolomite samples are slightly depleted in $\delta^{13}C$ (down to -3‰). In general, samples from the K-altered area to the north of the mine are more depleted in $\delta^{13}C$ than other district samples. Calc-silicate skarns are heavily depleted in $\delta^{13}C$, mainly due to loss of ^{13}C during metamorphic decarbonation, but CO_2 or CH_4 derived from graphite may also contribute to the negative shift.
- In the mine area, all samples fall in the range of +12 to +20‰ for $\delta^{18}O$, which is similar to the range shown by district samples. However, $\delta^{13}C$ values range from 0 to -10‰.
- Careful investigation of mine sample geochemistry has revealed that the most ^{13}C-depleted samples are calc-silicate skarns rather than true marbles.
- All samples show a clear relationship between decreasing CO_2 and/or silica content and increasing ^{13}C depletion. This can be accounted for by the loss of ^{13}C into volatile phases during prograde metamorphism (decarbonation). The higher the silica content in the carbonate rock before or during metamorphism, the greater the amount of calc-silicate formation and thus greater ^{13}C depletion.
- The geochemistry of skarn samples shows that Ca-rich calc-silicate skarns are less depleted in ^{13}C than Ca-poor, Al-rich skarns. This can be related to the proximity of the sample to a metavolcanic unit, which may contribute isotopically light carbon derived from graphite.
- Apparent differences in the isotope characteristics of Zinkgruvan metacarbonate rocks with limestones and dolomites from other Bergslagen base metal deposits is largely due to the degree of silica contamination in the carbonate sediment. Whilst Zinkgruvan may be more Si-enriched than many other deposits in the province, the apparent differences may simply be due to sampling bias.
- $\delta^{18}O$ values for Zinkgruvan carbonates are ^{16}O-enriched compared to the average value of +24‰ reported for Proterozoic calcite by Veizer & Hoefs (1976). This negative shift may be partly due to interaction with hydrothermal fluids in a sub-seafloor setting (Billström, 1985) combined with loss of ^{18}O during decarbonation.
- Although all samples fall within the $\delta^{18}O$ range for metamorphic waters, the shift of district and mine samples to more ^{18}O depleted values suggests interaction with hydrothermal fluids.

Regional samples appear to be fixed at around +20‰ relative to SMOW. Some ^{18}O depletion may be due to decarbonation effects, but fluid/rock ratios and fluid temperature during dolomitisation may have contributed to the range of $\delta^{18}O$ values observed.

CHAPTER 7

ORE PETROLOGY AND MINERALISATION PROCESSES

CHAPTER 7: ORE PETROLOGY & MINERALISATION PROCESSES

7.1 INTRODUCTION

The massive sulphides of the ore zone and associated disseminated mineralisation occurring at Zinkgruvan are examined in this chapter to assist with definition of ore-forming fluid chemistry and to evaluate the impact of metamorphism on the sulphide assemblages. Ore petrology does not form a major part of this study because the host rocks provide clearer and more detailed evidence for the fluid evolution of the mine area.

Textural relationships between sulphide, silicate and carbonate minerals allows first order evaluation of the timing relationships between mineralisation events and metamorphism. Mineralisation pre-dates metamorphism, with peak temperatures in excess of 700°C (Chapter 5), causing recrystallisation of the original textures and some chemical remobilisation. Even so, the sulphide assemblages, their chemistry and relative abundance provide insight into the mineralising process, its timing in the geological development of the district as a whole, and physiochemical conditions prevailing at the time of deposition. This chapter serves to highlight the key features of the mineralisation and make basic interpretations of the ore-forming environment so that the data from the previous chapters can be incorporated into a more holistic model. Genetic models and discussion of the key features of Zinkgruvan are addressed in Chapter 8.

Although sampling was difficult due to the friable nature of the ore and lack of sample material after assaying, the following parts of the Zinkgruvan orebodies were sampled for petrographic and geochemical study:

- Massive sulphide ore from the Nygruvan orebody are from drill holes 640, 648 and 649 from 800 m level Nygruvan.
- Burkland copper mineralisation from DDH 1557.
- Pyrrhotite mineralisation lying stratigraphically above the Zn-Pb mineralisation from the 650 m level in the Nygruvan part of the mine.

Zn-Pb-Ag mineralisation at Knalla was not sampled during this study. A detailed account of the individual orebodies is beyond the scope of this study (see Hedström *et al.* (1989) and Henriques (1964) for more detailed descriptions).

Petrological observations were made using standard reflected light microscopy on 30μm polished thin sections, and individual mineral analyses were carried out using a scanning electron microscope (JEOL JSM 6400 with EDS attachment) as described at the beginning of Chapter 4 and in Appendix F.

7.2 SULPHIDE ASSEMBLAGES

7.2.1 Distribution of mineralisation

Economic sulphide mineralisation is contained within two ore layers, the Main Ore and the Parallel Ore. Orebody descriptions, ore grades and metal zonation are presented in Chapter 3 (section 3.3). Mineralisation shows lateral and vertical variation in composition and grade, with mm-scale layering comprising alternate bands of sulphide and gangue material. To the west, in the Burkland area, the main Zn-Pb mineralisation is partly underlain by a zone of Cu-rich mineralisation, interpreted by Hedström *et al.* (1989) as a stockwork feeder zone.

Sulphide mineralisation is also widely disseminated through the enclosing rock package, mainly in the footwall to the orebody. The Isåsen Formation volcanics contain very little metalliferous mineralisation aside from occasional magnetite. The Zinkgruvan Formation has variable sulphide and oxide content, from discrete layers of relatively dense sphalerite impregnation accompanied by galena, pyrrhotite and minor chalcopyrite in metavolcanic rocks, to concentrations of magnetite produced through serpentinisation of forsterite-bearing marbles. In the Burkland area, marble units host disseminated Cu (+ Ni + Co) mineralisation. A distinct horizon of apparently stratiform pyrrhotite mineralisation occurs stratigraphically above the main Zn-Pb mineralisation near the contact of the Zinkgruvan Formation with the overlying Viksjön metasedimentary rocks. Metalliferous minerals in the Viksjön Formation are generally limited to magnetite and occasional pyrite, probably of detrital origin.

7.2.2 Sulphide assemblages in the Nygruvan orebody

Sulphide assemblages in the orebodies and enclosing rocks are relatively simple, comprising variable quantities of sphalerite, galena, pyrrhotite and chalcopyrite. Sphalerite is almost always dominant in the Nygruvan sulphide assemblages. Pyrite is rare throughout the Zinkgruvan district, and commonly appears to have a late or secondary origin.

Massive sphalerite forms distinct yellow to deep red bands (Fig. 7.1A) interlayered with quartzofeldspathic and calc-silicate rich material. The gangue layers usually contain heavy concentrations of disseminated sphalerite and galena with accessory pyrrhotite. Sphalerite forms irregular, angular crystals of varying sizes, apparently interstitial to the surrounding silicate phases (Fig. 7.1B). Henriques (1964) observed "*The outlines of the [sphalerite] grains are determined from the adjoining minerals*". In many places, sphalerite has migrated along silicate grain boundaries, and penetrates along the cleavage planes of mica and calcite. Chalcopyrite inclusions are common (Fig. 7.1C), with their distribution often controlled by the crystallographic structure of the host sphalerite. Pyrrhotite inclusions also occur, but are not so strongly crystallographically

controlled, forming randomly oriented rounded blebs of 8 to >75μm in diameter. Small anhedral crystals of pyrrhotite commonly occur around the margins of sphalerite masses.

Galena occurs alongside sphalerite, also forming irregular, angular masses but is usually devoid of inclusions. Galena is more easily mobilised than sphalerite, and commonly forms fracture infills cross-cutting the main fabric of the rock, and haloes of disseminations around larger sulphide masses (Fig. 7.1D). Henriques (1964) reported intergrowths of sphalerite and galena that suggest galena has replaced sphalerite in many places.

Original ore textures have been largely obliterated by high temperature recrystallisation during metamorphism, and now mostly form massive, anhedral aggregates. Complex intergrowths of different sulphide phases are relatively rare, and the colloform sphalerite textures observed in many unmetamorphosed Zn-Pb deposits are absent. In some places sulphide phases (mainly sphalerite) completely enclose isolated grains of quartz and other silicate minerals (Fig. 7.1A), but in most places the sulphide grain boundaries are defined by silicate minerals.

7.2.3 Sulphide assemblages in the Burkland orebody

The Burkland orebody is very similar to the Nygruvan orebody to the SE except that it locally contains elevated Cu-Co-Ni and near the western margins some pyrrhotite-rich sections. The Zn orebody was not examined during this study. In the stratigraphic footwall to the Zn-Pb mineralisation lies a body of Cu mineralisation disseminated in dolomitised, forsterite-bearing marbles (Fig. 7.2A). Hedström *et al.* (1989) reported sulphide-bearing silicate veins forming a Cu-rich stockwork, but this mineralisation style was not observed in this study. The disseminated chalcopyrite-rich mineralisation also contains appreciable quantities of sphalerite, galena and pyrrhotite, particularly on the margins of the main Cu mineralisation and where the host rock is more enriched in calc-silicate minerals (Fig. 7.2B). Magnetite is also common, forming distinctly larger and more angular crystals compared to the magnetite evolved through serpentinisation of forsterite.

In the Burkland FW Cu orebody, chalcopyrite forms large irregular masses (up to > 400μm across) with occasional pyrrhotite inclusions. Sphalerite occurs along fracture and cleavage planes within the chalcopyrite mass but does not usually extend into surrounding silicate material. Remobilisation has caused chalcopyrite to penetrate along silicate grain boundaries and into dolomite and mica cleavage planes. In many samples, thin rims of chalcopyrite are developed around silicate grains (e.g., forsterite/serpentine) away from the larger chalcopyrite masses. In addition to large, irregular masses of chalcopyrite, most samples show sub-microscopic blebs of chalcopyrite disseminated throughout the carbonate/calc-silicate assemblage, particularly within carbonate crystals.

Galena infills extensive networks of hairline fractures within silicate material (Fig. 7.2E) and forms intergrowths with chalcopyrite and sphalerite in the less Cu-rich ores (Fig. 7.2B). In a few samples (e.g., 1557/32), galena forms large, subhedral masses with a fringe of galena veins extending out into surrounding carbonate minerals.

In highly chalcopyrite-rich areas of the orebody, pyrrhotite is relatively scarce, forming small (~10-15μm) inclusions within chalcopyrite. On the margins of the orebody, where sphalerite and galena are more common, pyrrhotite occurs in larger proportions, usually forming rounded inclusions and intergrowths in the sphalerite masses. The distribution of sulphide mineral phases in the Burkland orebody can be related to metal solubilities in hydrothermal fluids, and is discussed in section 7.4.2. Small quantities of Ni and Co-bearing sulphide minerals (Fig. 7.2C) occur in the Burkland FW Cu orebody. Ni-bearing sulphide (?niccolite) forms small (< 25μm), rounded, pink-coloured inclusions in galena (Fig. 7.2D) and occasional larger crystals of pentlandite are found (sample 1557/26). SEM analyses of sulphide mineralisation in sample 1557/15 revealed the presence of a Cu-Sb-Zn sulphide mineral intergrown with chalcopyrite (Table 7.1B), and sub-microscopic inclusions of platinum-rich material in magnetite have been identified in sample 1557/17. Freibergite, Ag-rich tetrahedrite (Ag, Cu, Fe, As, Sb sulphide) was tentatively identified in very small amounts in the Knalla part of the mine by Henriques (1964).

7.2.4 Pyrrhotite mineralisation

A distinct band of pyrrhotite mineralisation (known as the 'pyrrhotite horizon') occurs approximately 100 m stratigraphically above the major Zn-Pb mineralisation, and can be traced in outcrop for some distance across the mine area (Fig. 3.4). Pyrrhotite mineralisation is hosted in a quartzofeldspathic rock located at the edge of the transition zone between the Zinkgruvan Formation and the overlying migmatites of the Viksjön Formation. Thin section analysis shows pyrrhotite partially replacing perthitic feldspars, and forming interstitial masses (Fig. 7.2F). The potential origins of this mineralisation are discussed in section 7.4.3.

7.2.5 Disseminated mineralisation

Disseminated sphalerite is common throughout the Zinkgruvan Formation, occurring in most of the major rock types except the amphibolite bodies, which contain only minor sphalerite at their margins. This suggests that the amphibolite bodies were intruded after the mineralisation. Concentrations of disseminated sphalerite are most distinct in the metavolcanic rocks, where sphalerite occurs in zones of discrete layers, often accompanied by a slight increase in biotite and/or garnet content. These sphalerite-rich layers often show a sharp cut-off at the base with a gradual decrease in sphalerite concentration towards the top, and are often repeated several times in a 50 cm core section.

Elsewhere, however, sphalerite is evenly distributed, forming a background content of about 5 vol% in most metavolcanic rocks. Sphalerite forms discrete angular grains as well as inclusions in Fe-rich minerals such as garnet and biotite.

In metacarbonate rocks, sphalerite is scarce, except in the mineralised marbles below the Burkland orebody, and layered concentrations are not observed. Magnetite, a by-product of alteration of forsterite to serpentine (see section 5.5.1), is usually the dominant metalliferous phase in Zinkgruvan Formation marbles away from the Burkland FW Cu mineralisation.

Calc-silicate skarns have a highly variable sulphide content, depending on their proximity to mineralised metavolcanic units (see Chapter 4), and their position relative to the main orebody itself. Most skarns contain a few volume % of sphalerite, galena and pyrrhotite, especially those near the main mineralisation horizons. In all cases, sphalerite is concentrated in garnet-rich layers within banded skarns. Pyrrhotite and galena are usually associated with sphalerite concentrations, but do not show the same strong link to garnet concentrations.

Figure 7.1: Sulphide assemblages and textural features of the Nygruvan orebody

A) Massive sphalerite ore with 'rafts' of silicate crystals (quartz, tremolite & garnet). Sample 648/08, plane polarised transmitted light.

B) 'Interstitial' galena and sphalerite. Sample 640/03, PPL reflected light.

C) Typical Nygruvan sulphide assemblage: Sph (+ Cpy inclusions) + Gal + Cpy. Sample 454/02, plane polarised reflected light.

D) Typical Nygruvan sulphide assemblage: Sph + Gal + Po. Note the difference in polishing relief between Po and Gal. Sulphide mass is surrounded by a halo of fine disseminations of galena. Sample 649/10, plane polarised transmitted light.

E) Cpy masses (opaque) developed along the fabric and around margins of fibrolite. Sample 454/02, sillimanite gneiss. Plane polarised transmitted light.

F) Same field of view as E), but in reflected light. Sample 454/02, plane plarised reflected light.

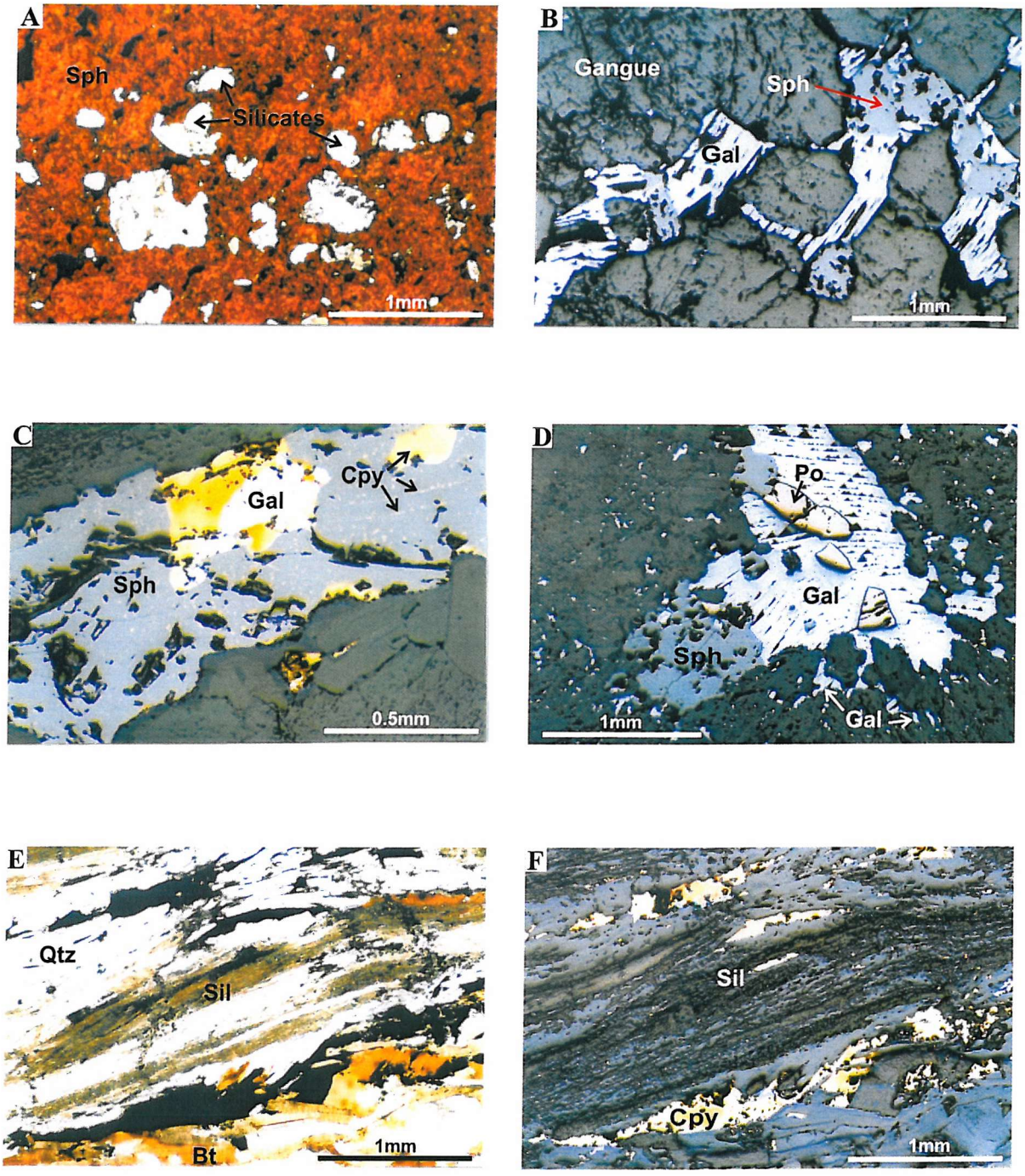

Figure 7.1: Sulphide assemblages and textural features from the Nygruvan orebody

Figure 7.2: Sulphide assemblages and textural features of the Burkland orebody and the pyrrhotite horizon

A) Coarse-grained Cpy cross-cut by veins of Sph which appear to post-date most of the silicate veins. Sample 1557/24, plane polarised reflected light.

B) Sph-rich Burkland mineralisation:Sph + Gal + Po. Sample 1557/24, plane polarised reflected light.

C) Ni-Co sulphide mineral surrounded by Cpy and Gal. Blue specks in the silicate mass are tarnish. Sample 1557/32, plane polarised reflected light.

D) Intergrowth of niccolite (Ni) and Gal. Pale pink Ni is outlined by black dotted line for clarity. Sample 1557/32, plane polarised reflected light.

E) Fine network of Gal veins infilling fractures. Sample 1557/24, plane polarised reflected light.

F) Pyrrhotite developed between silicate crystals in the pyrrhotite horizon, Nygruvan. Sample UZ5, plane polarised reflected light.

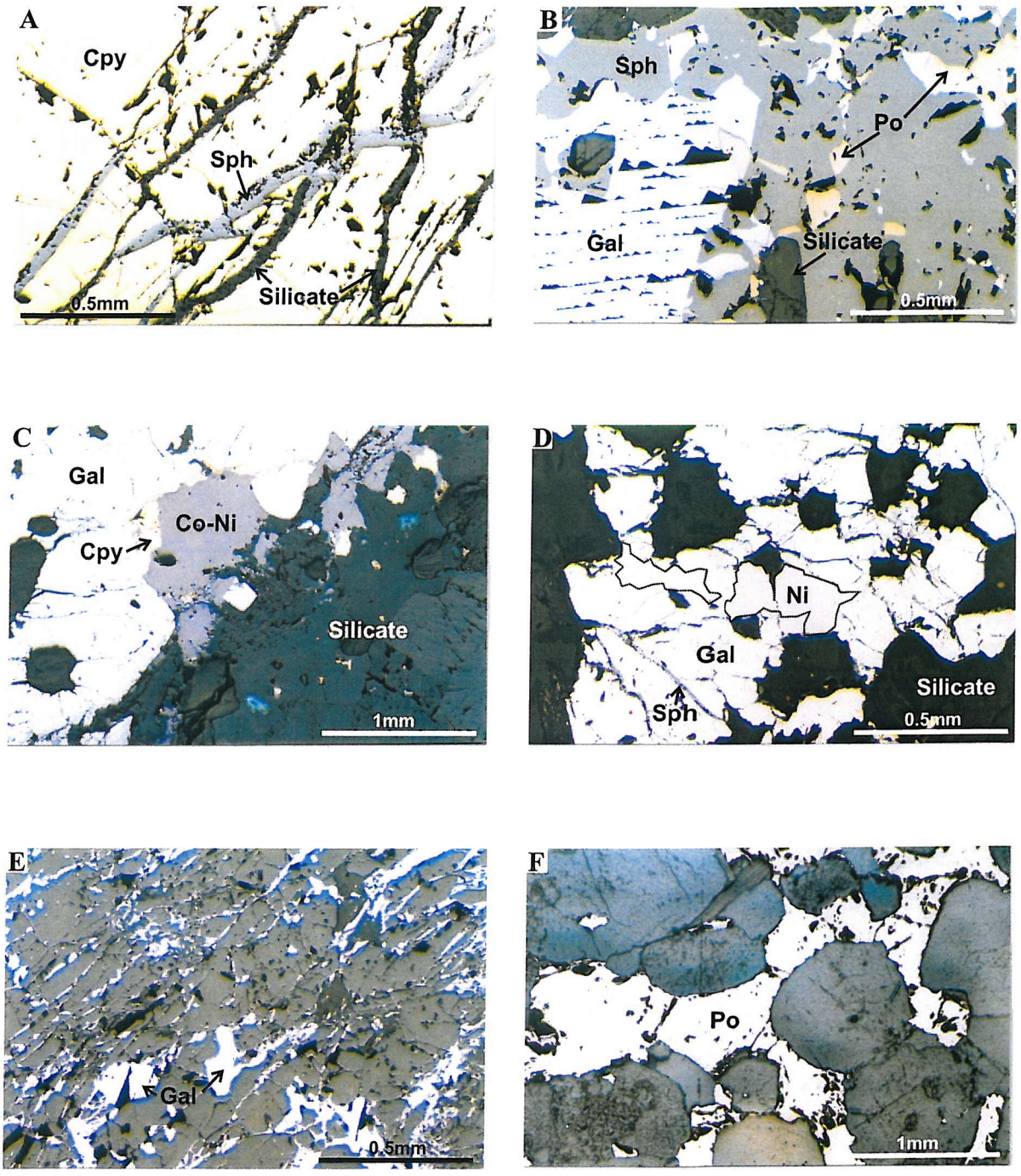

Figure 7.2: Sulphide assemblages and textural features from the Burkland orebody and pyrrhotite horizon.

7.3 SULPHIDE MINERAL CHEMISTRY

Sulphides in the Nygruvan and Burkland orebodies have been investigated using SEM techniques described at the beginning of Chapter 4. Chemical change due to metamorphism, unusual mineral compositions and inclusions which may help define the chemical properties of the mineralising fluid were studied. Selected SEM analyses of sulphide minerals are presented in Table 7.1. Original data and SEM methods are provided in Appendix F.

7.3.1 Sphalerite

Sphalerite contains appreciable amounts of lattice-bound Fe, varying with the host rock type. Disseminated sphalerite in metavolcanic rocks of the Zinkgruvan Formation contain the lowest Fe content at approximately 4 atomic % Fe. Sphalerite accompanying the FW copper mineralisation at Burkland contains 5-7 at% Fe, whilst sphalerite occurring in magnetite-rich Fe skarns in DDH 451 has a Fe content of around 10 atomic % (Table 7.1). Henriques (1964) reported Fe contents of between 2.0 and 7.1 at% for Nygruvan ores, and identified a spatial zonation in Fe content from 2-5 at% Fe in the upper levels of the mine, to a maximum of 5-7.5 at% Fe between 250m and 400m levels, decreasing back to 2-5 at% below 400m level. The amount of Fe in sphalerite varies as a function of temperature, pressure and sulphur activity, and has been discussed with reference to the sphalerite geobarometer in Chapter 5 (section 5.6.1).

7.3.2 Galena

Galena (PbS) was more difficult to analyse in this study due to its smaller grain size. However, the limited number of analyses that exist from Nygruvan samples show it to be relatively clean, with little or no impurities. Henriques (1964) reports up to 0.25% Bi and up to 0.196 wt% Ag in galena from Knalla (see section 7.3.5). These ores have not been investigated here.

7.3.3 Pyrrhotite

Pyrrhotite (FeS) is the dominant Fe sulphide in the Zinkgruvan orebodies. SEM analyses (Table 7.1A & B) show it to be relatively pure, with minor concentrations of Zn and Cu appearing in some analyses, but this is probably the result of sub-microscopic inclusions of sphalerite and chalcopyrite.

7.3.4 Chalcopyrite

Chalcopyrite ($CuFeS_2$) in the Burkland FW Cu orebody has quite a variable chemistry, with fluctuations in Fe and Cu content of several per cent, evidenced by the large standard deviation values in Table 7.1B. However, much of this variation may again be due to the SEM sampling small pyrrhotite inclusions within the chalcopyrite mass.

7.3.5 Native silver

Native silver occurs as fracture-fill in strongly deformed areas of the mine, particularly in the Knalla part of the mine, and is assumed to have been remobilised from argentiferous galena in the main Zn-Pb(-Ag) ore. It rarely occurs at Nygruvan, and its distribution is restricted to Pb-rich ore in the western parts of the deposit (see Fig. 3.9B).

Henriques reports Ag contents between 0.059 and 0.196 wt% in galena from Knalla; these ores have not been analysed as part of this study, and no silver was observed in the Nygruvan ores.

Sample No.	**451/03**		**555/07**		**451/13**		**555/06**		**555/07**		**555/07**	
Orebody	**Nygruvan**		**Nygruvan**		**Nygruvan**		**Nygruvan**		**Nygruvan**		**Nygruvan**	
Mineral	**Sphalerite**		**Sphalerite**		**Pyrrhotite**		**Pyrrhotite**		**Pyrrhotite**		**Chalcopyrite**	
Lithology	**Fe skarn**		**Marble**		**Fe skarn**		**Marble**		**Marble**		**Marble**	
n	**2**		**1**		**2**		**4**		**3**		**1**	
	Wt %	*S.D*	*Wt %*	*S.D*	*Wt %*	*S.D*	*Wt %*	*S.D*	*Wt %*	*S.D*	*Wt %*	*S.D*
ZnO	44.09	0.27	48.74	-	-	-	0.11	0.13	0.11	0.19	-	-
FeO (tot)	9.67	0.10	7.88	-	50.32	0.61	55.83	0.71	55.92	0.63	36.37	-
MnO	-	-	-	-	-	-	0.13	0.12	0.18	0.11	-	-
CuO	-	-	-	-	-	-	0.09	0.13	0.01	0.01	20.35	-
PbO	-	-	-	-	-	-	-	-	-	-	-	-
SO_3	46.24	0.37	41.94	-	49.68	0.61	43.44	0.46	43.23	0.24	42.86	-
Total	99.99		98.56		100.00		100.03		100.04		99.58	

Table 7.1A: SEM analyses for sulphide minerals in the vicinity of the Nygruvan orebody. Data are wt% oxide; S.D = standard deviation, n = number of analyses.

Sample No.	**1557/14**		**1557/14**		**1557/30**		**1557/14**		**1557/26**		**1557/15**	
Orebody	**Burkland**		**Burkland**		**Burkland**		**Burkland**		**Burkland**		**Burkland**	
Mineral	**Sphalerite**		**Chalcopyrite**		**Chalcopyrite**		**Pyrrhotite**		**Pentlandite**		**Cu-Sb-Zn sulphide**	
Lithology	**Marble**		**Marble**		**Marble**		**Marble**		**Marble**		**Ca-Si skarn**	
n	**3**		**2**		**7**		**1**		**1**		**4**	
	Wt %	*S.D*	*Wt %*	*S.D*	*Wt %*	*S.D*	*Wt %*	*S.D*	*Wt %*	*S.D*	*Wt %*	*S.D*
ZnO	48.50	0.69	0.02	0.03	-	-	-	-	-	-	4.44	0.28
FeO (tot)	5.38	0.04	25.12	0.28	23.52	2.72	50.93	-	24.33	-	0.81	0.19
CuO	-	-	27.65	0.19	29.75	4.03	-	-	0.03	-	25.72	0.74
PbO	-	-	-	-	-	-	-	-	-	-	-	-
NiO	-	-	-	-	-	-	-	-	26.92	-	-	-
Sb_2O_5	-	-	-	-	-	-	-	-	-	-	13.77	0.37
SO_3	46.08	0.03	47.21	0.05	46.72	1.35	49.06	-	48.57	-	55.27	0.50
Total	99.96		100.00		100.00		99.99		99.93		100.00	

Table 7.1B: SEM analyses for sulphide minerals from the Burkland orebody. Data are wt % oxide; S.D = standard deviation, n = no. of analyses.

7.4 TIMING OF MINERALISATION

The inclusion of sulphide minerals into peak metamorphic silicate phases is a clear indication that sulphide mineralisation occurred prior to metamorphism. Sub-microscopic inclusions of galena are observed in K-feldspar in migmatites and quartzofeldspathic gneisses, and the occurrence of the Zn-spinel gahnite and the Pb-bearing feldspar amazonite in peak assemblages clearly indicate the presence of Zn and Pb prior to or at the time of peak metamorphism. Larger inclusions of sphalerite occur in garnets, and streaks of chalcopyrite are developed along the fabric in fibrolite masses (Fig. 7.1E & F).

Textural evidence (section 7.2) from the sulphide ores is also consistent with metamorphism to high temperatures, with little of the original textures preserved. Later stage remobilisation of the sulphide mineralisation is evident in the migration of sphalerite and particularly galena into and along fractures which cross-cut peak assemblages and the dominant S_1 fabric, and the development of stope-scale masses of remobilised galena. Concentrations of coarse-grained pyrrhotite and galena are commonly observed at the margins of pegmatite bodies and quartz veins, indicating remobilisation by siliceous fluids during the late stages of metamorphism.

That primary sulphide mineralisation occurred prior to metamorphism is relatively easy to conclude. The timing in terms of the pre-metamorphic evolution of the rock package is impossible to resolve directly from sulphide mineral textures, but is discussed further in Chapter 8.

7.5 DISCUSSION & INTERPRETATION

The sulphide mineralogy at Zinkgruvan is relatively simple. Co-existing iron and zinc sulphides are common mineral assemblages in hydrothermal ore deposits (Barnes, 1997), but the paucity of pyrite and almost total dominance of pyrrhotite is unusual in such a large base metal sulphide deposit.

7.5.1 Effects of metamorphism

Metamorphic processes and their effect on the sulphide assemblages must be considered before making interpretations of ore formation conditions based on present-day assemblages and mineral compositions. The effects of metamorphism on sulphides is dependent on the metamorphic grade and the nature of the sulphide phase. At low metamorphic grades, more refractory phases such as sphalerite and pyrite will retain their original structure and composition while softer sulphides such as galena, pyrrhotite and chalcopyrite readily undergo recrystallisation. With increasing grade, pyrite begins to lose sulphur and above ~720°C (at low P) converts to pyrrhotite (Fig. 7.3). At high metamorphic grades, sphalerite becomes texturally and compositionally homogenised and equilibrates with adjacent Fe sulphides (Craig & Vaughan, 1981).

The dominance of pyrrhotite as the main Fe sulphide phase may be due to two reasons. Firstly, the mineralising system could have been low in sulphur (i.e., Fe:S = >1), causing deposition of sulphur-poor pyrrhotite rather than pyrite (see Fig. 7.3). Alternatively, pyrite was an original Fe-sulphide phase and converted to pyrrhotite during prograde metamorphism. If the sulphur released by this reaction was removed from the system (resulting in a decrease in aS_2), or taken up in the formation of another sulphide phase then the reaction could not have been reversed during metamorphic cooling, and pyrrhotite would remain dominant. Hedström *et al.* (1989) attributed the distribution of pyrrhotite and pyrite to primary depositional processes. A similar Zn-Pb deposit at Garpenberg, 300 km NE of Zinkgruvan contains pyrite as the dominant Fe-sulphide phase, but has only experienced peak metamorphic temperatures of around 550°C, not high enough to allow the transformation from pyrite to pyrrhotite.

No colloform, banded textures commonly found in low-temperature Zn-Pb deposits were observed in sphalerite at Zinkgruvan, although some large scale colour banding (described in section 7.2.2), created by broad changes in the FeS component, is present. The FeS content of sphalerite coexisting with Fe-sulphides such as pyrite and pyrrhotite is a function of confining pressure and sulphur activity (aS_2). As such, sphalerite may be used (in a general sense) as a barometer. At elevated temperatures (e.g., during metamorphism), solid state diffusion is more rapid, and sphalerite equilibrates with adjacent Fe-sulphides. However, re-equilibration during post-metamorphic cooling can result in false estimates of pressure.

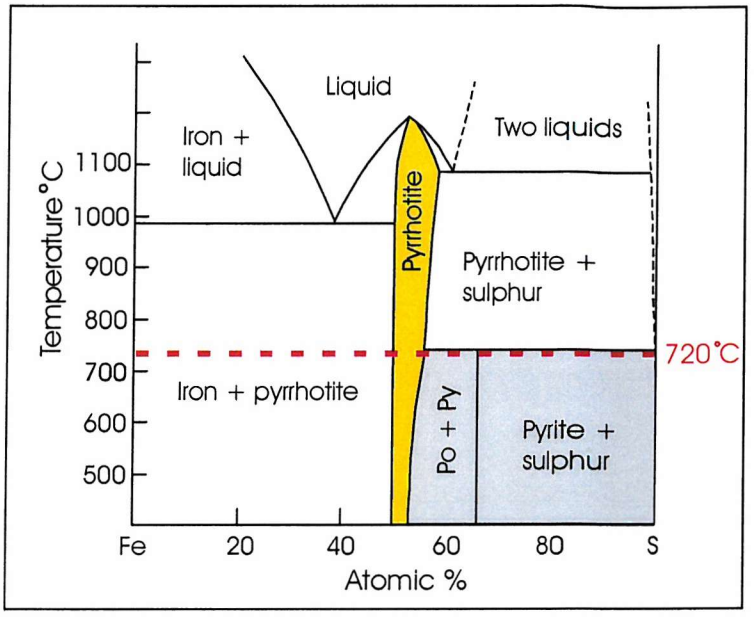

Figure 7.3: Phase relationships in the Fe-S system at low pressure. Red dashed line represents peak metamorphic conditions estimated from silicate/carbonate mineral assemblages. The upper thermal stability of pyrite increases by ~14°C per kbar of confining pressure. Pyrite stability field shaded grey; pyrrhotite-only stability field shaded yellow. Pyrite converts to pyrrhotite with loss of sulphur above 720°C. Modified after Vaughan & Craig (1978).

7.5.2 Ore fluid chemistry

Hedström *et al.* (1989) proposed that the ore-forming fluids were sourced from heated chloric seawater leaching the volcanic basement, resulting in a dense, chloride-rich, neutral to slightly acidic solution at temperatures around 225-250°C. A seawater origin for the mineralising fluids is consistent with theories proposed by Freitsch (1982a, b), Lagerblad & Gorbatschev (1985) and Vivallo (1985), amongst others. Fluid inclusion data cannot be used for defining the composition of the ore-forming fluids due to destruction or resetting by high-temperature metamorphism (Chomiak & Lindblom, 1995).

Zn and Pb are most efficiently transported as chloride complexes (Vaughan, 1976; Ruaya & Seward, 1986; Barrett & Anderson, 1988; Seward & Barnes, 1997). Bisulphide complexes of Zn and Pb are also possible, but are less soluble, and are therefore unlikely to be responsible for forming large Zn-Pb deposits. Modern hydrothermal solutions from active submarine vents such as the Salton Sea are chloride-rich, and the chloride ion (Cl^-) is often quoted as the most abundant transport ligand in hydrothermal solutions (e.g., Seward & Barnes, 1997; Scott, 1997). The solubility of Zn and Pb as chloride species is favoured by increasing salinity, temperature and acidity (decreasing pH), and decreasing sulphur activity (aH_2S). Therefore, the most efficient Zn-Pb carrying fluid will be a hot, acidic brine with low aH_2S. Acidity is easily produced by seawater-rock interactions during hydrothermal circulation, in particular the removal of Mg from

seawater (with an original pH of ~8) to form minerals such as chlorite. Most hydrothermal fluids sampled from modern submarine hydrothermal vents are acidic (average pH = ~3-6) as a result of seawater-rock interactions, and acidity may also be increased by subsurface precipitation of metal sulphides.

Fe-Mn enrichment observed in the footwall to the Zinkgruvan orebodies indicates that these components must have also been carried in the ore solutions. This infers that the solutions were slightly reducing with $aH_2S > aSO_4^{2-}$, as Fe and Mn transport is favoured by low pH and low fO_2 (Spry & Wonder, 1989). The presence of very low but anomalous quantities of gold (mostly <0.1 g/t Au; S. Sädböm, pers. comm) indicates the presence of minor H_2S in the fluid. Low aH_2S fluids are supported by the absence of pyrite and presence of pyrrhotite, ***if it assumed that pyrrhotite is a primary phase and not a metamorphic product.*** Transport of Zn and Pb as chloride complexes in acidic, reduced solutions is controlled by the following reactions (Large *et al.*, 1996; Seward & Barnes, 1997):

$$ZnCl_4^{2-} + H_2S \leftrightarrow ZnS + 2H^+ + 4Cl^-$$

$$PbCl^{3-} + H_2S \leftrightarrow PbS + 2H^+ + 3Cl^-$$

The temperature required for a mineralising brine can be estimated based on the likely concentrations of Zn and Pb carried in acidic, weakly reduced fluids. Large *et al.* (1996) speculated on the likely temperature of brines responsible for forming Broken Hill-type deposits, using a maximum range of concentration of 1-1000 ppm Zn, where fluids containing <1 ppm Zn are unlikely to form economic deposits, and fluids containing >1000 ppm are geologically unlikely based on source rock metal considerations. This range is reasonable and consistent with previous estimates (e.g., Seward & Barnes, 1997) of metal concentrations in hydrothermal fluids responsible for generating massive sulphide deposits (Fig. 7.4A). Fig. 7.4B shows the likely fluid temperatures for hypersaline, acidic, reduced brines containing variable dissolved metal content.

The salinity of the fluids responsible for generating Zn-Pb mineralisation at Zinkgruvan are difficult to estimate given the lack of reliable pre-metamorphic fluid inclusion data. A preliminary study of fluid inclusions in the Zinkgruvan district by Chomiak & Lindblom (1995) showed metamorphic (secondary) fluid inclusions to be weakly saline, containing carbonate daughter mineral phases rather than halite, which would be expected in hypersaline inclusions. Low salinity metamorphic fluid inclusions are inevitable following flushing of the system with aqueous-carbonic metamorphic fluids derived from dehydration reactions (Chapter 5). It is possible that primary inclusions could contribute some saline fluid to these secondary inclusions, but the likelihood of primary inclusions being preserved after peak temperatures of >700°C is remote. However, ore-forming fluids from most other large Zn-Pb deposits are known to be highly saline, so it is reasonable to infer high salinities for ore-forming fluids at Zinkgruvan.

Hypersaline brines may have been produced by dissolution of evaporite beds, which have been identified in many other Broken Hill-type deposits (see Chapter 8), and tentatively proposed by Hedström *et al.* (1989) to explain some of the more exotic lithologies at Zinkgruvan. Regardless of its source, high salinity is required to transport the concentrations of Zn-Pb required to form a deposit as large as Zinkgruvan.

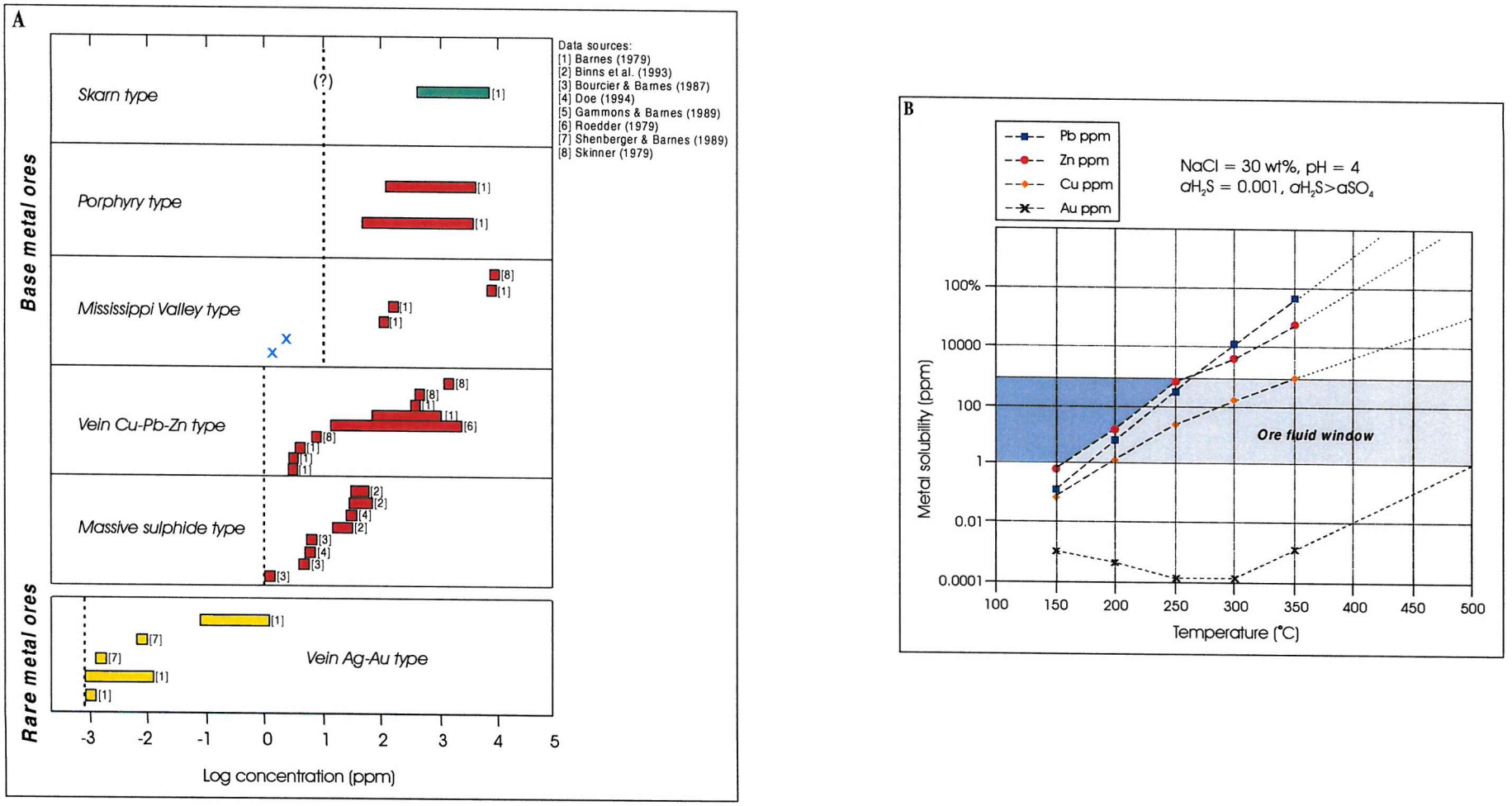

Figure 7.4: ***A****) Concentrations of base and rare metals in ore fluids from five different types of ore deposits, based on fluid inclusion observations, measured geothermal data and thermodynamic calculations of saturation conditions. Data represent the dominant ore solution concentrations for Cu, Pb and Zn in the base metal deposits (red), and Ag, Au and Hg in rare metal deposits (yellow). Blue crosses represent non-ore forming concentrations; dashed lines represent the minimum concentration values for each type of deposit. Modified after Seward & Barnes (1997).* ***B****) Temperature-solubility diagram for Pb, Zn, Cu and Au in hypersaline, acidic, reduced brines. The ore fluid window (1 – 1000ppm Zn) is shaded pale grey; sulphide deposition occurs to the left (lower temperature) of the saturation lines, metal transport occurs to the right (higher temperature) of the saturation lines. Zn-Pb deposition conditions shaded purple. After Large et al. (1996).*

Fig. 7.4B shows that Zn and Pb will precipitate from hydrothermal solution at < 250-150°C (to the left of the solubility line); at higher temperatures (i.e., to the right of the solubility curve), metals will remain in solution. The quantity of Cu dissolved in the same fluid at 250°C is much lower than Zn or Pb, so for the same level of metal concentration, Cu requires higher temperatures than Pb and Zn to stay in solution, and will therefore precipitate from a cooling solution earlier than Pb and Zn. This difference in solubilities (discussed further below) is consistent with chalcopyrite (and accompanying silica) precipitation in a feeder zone below the main Zn-Pb ore as mineralising fluids ascended towards the seafloor and began to decrease in temperature. Zonation of Cu, Zn, Pb and Fe sulphides in the Burkland Zn orebody and underlying Cu mineralisation is consistent with solubility trends (i.e., Cpy will precipitate first at higher temperatures, therefore at greater depth and closer to the fluid source). Subsurface precipitation of chalcopyrite may also have been triggered or assisted by adiabatic boiling as pressure decreased towards the surface, but there is no textural evidence for this preserved at Zinkgruvan. Hedström *et al.* (1989) proposed that boiling was inhibited by water depth in the basin, although the presence of stromatolite structures and the volcanic textural evidence presented by Allen *et al.* (1996) contradicts this.

Sulphide precipitation is triggered by chemical changes in the hydrothermal environment. For the fluids described above, precipitation will initiate as a result of temperature decrease, pressure decrease, pH increase, dilution of the solution, fluid mixing and oxidation. Hedström *et al.* (1989) suggested a drop in temperature for the primary triggering mechanism for sulphide deposition, which is generally true for chloride-complexed metal species in solution. However, the host rock package at Zinkgruvan is representative of oxidised basin conditions, so expulsion of reduced ore solutions into this environment will also cause oxidation of the fluid and subsequent destabilisation of metal complexes held in solution. It is most likely, therefore, that precipitation resulted from a combination of fluid oxidation and the temperature decrease, pressure decrease and pH change resulting from dilution of ore fluids by seawater. Sulphur availability, discussed in section 7.5.3 below, is also a critical factor in metal sulphide precipitation.

The zonation observed in many exhalative base metal deposits is a function of metal solubilities. A thorough investigation of the metal zonation patterns at Zinkgruvan is well beyond the scope of this study, but Hedström *et al.* (1989) describe an increase in Zn/Pb ratios away from the Cu-rich 'feeder zone' (see Fig. 3.9), which is consistent with Cu, Zn and Pb solubilities. These authors ascribe the stratiform pyrrhotite mineralisation at the base of the Viksjön Formation to late-stage, lower temperature (<170°C, based on pyrrhotite solubility in weakly acidic, reduced saline fluids) precipitation from the same fluid that precipitated sphalerite and galena. However, sulphur isotope studies (e.g., Billström, 1991) reveal slightly depleted $\delta^{34}S$ values for the pyrrhotite horizon compared to sphalerite and galena in the ore zones, which may indicate a different origin for these

sulphides or a significant change in the chemistry of the mineralising fluid. This is discussed further in section 7.5.3.

The effect of hot, acidic brines interacting with the carbonate rocks of the Zinkgruvan Formation can only be speculated on as any original textures have been destroyed and recrystallised during metamorphism. However, it is likely that there was at least some replacement of carbonate by sulphide due to the corrosive nature of the fluid acting on a highly reactive carbonate rock. Such interaction results in an increase in the pH of the solution, causing metal sulphide precipitation by the following reactions:

$$CaCO_3 + 2H^+ \leftrightarrow Ca^{2+} + H_2CO_3$$

$$ZnCl_n^{2-} + H_2S \leftrightarrow ZnS + 2H^+ + nCl^-$$

Carbonate dissolution may have contributed to the Cu-rich disseminated mineralisation observed in the Burkland marble-hosted orebody, and/or may have increased the porosity of the carbonate rock, allowing further infiltration of mineralising fluids. Interaction of acidic brines with carbonates was probably also important in the Fe-Mn enrichment process, discussed in Chapter 8.

7.5.3 Sulphur sources

Sulphur isotope studies can reveal the sources of ore components and physiochemical conditions prevailing at the time of ore deposition. Billström (1985, 1991) revealed the Zinkgruvan ores to contain $\delta^{34}S$ values between -6 to +17, with the majority of samples falling in the range between -3 to +5‰ (Fig. 7.5). Sphalerite is generally isotopically heavier than galena (average +2.5‰ and +0.5‰ respectively), consistent with cogenetic $\delta^{34}S$ isotopic fractionation and equilibration of these two minerals from a common fluid (Fig. 7.6). However, Billström (1991) reports that the magnitude of ^{34}S fractionation is variable throughout the mine, indicating fluctuation between isotopic equilibrium and non-equilibrium conditions. $\delta^{34}S$ of co-existing Fe-sulphide ranges from -5 to +7‰.

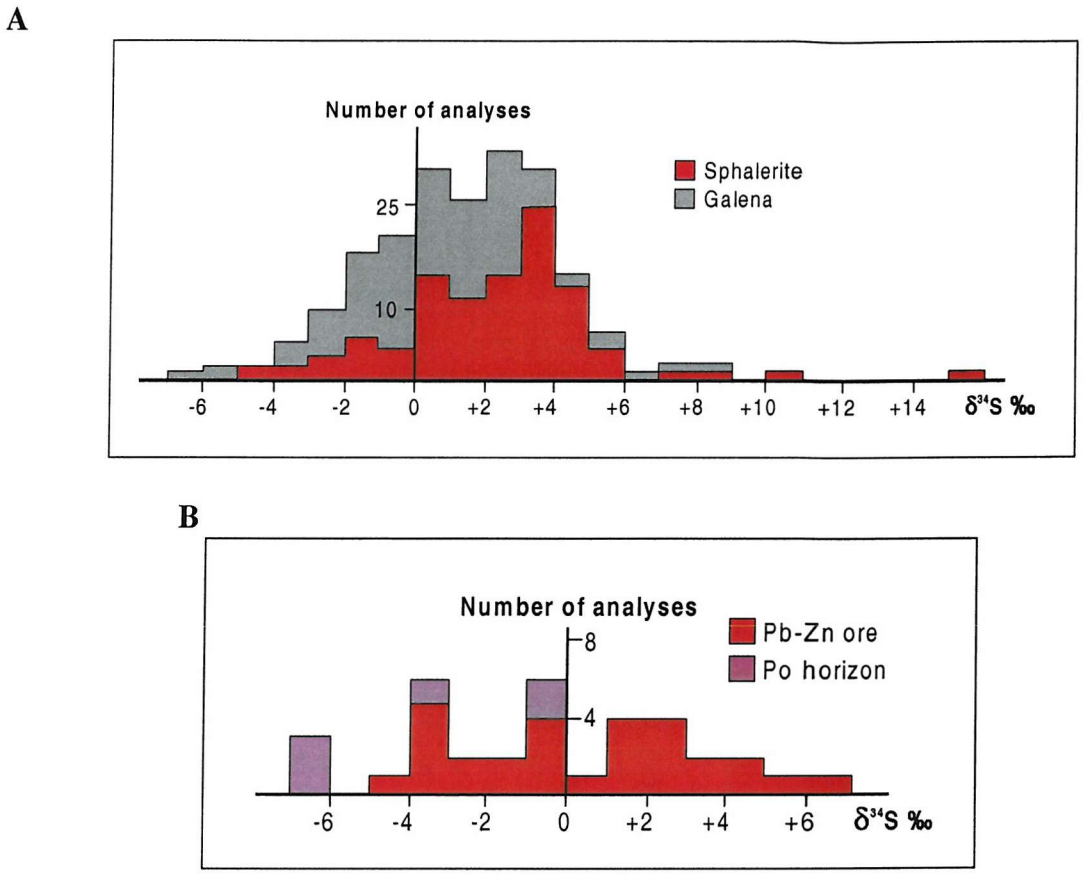

Figure 7.5: Histograms showing $\delta^{34}S$ distribution for Zn-Pb ore (A) and the pyrrhotite horizon (B) at Zinkgruvan. After Billström (1985, 1991).

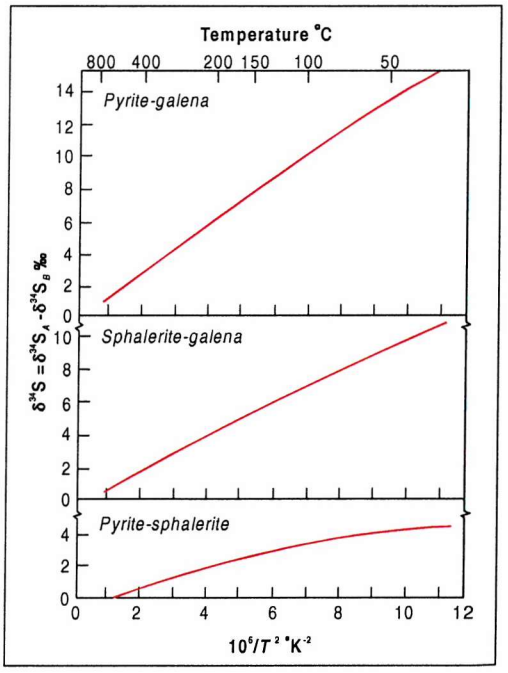

Figure 7.6: Fractionation of sulphur isotopes among cogenetic mineral pairs as a function of temperature, based on calculated values of isotope equilibrium by Sakai (1968). After Faure (1986).

Billstrom (1985, 1991) considered that the narrow range of $\delta^{34}S$ values for galena and sphalerite indicate a hydrothermal origin, with sulphur derived from leaching of the volcanogenic basement, and subsequent addition of bacteriogenic sulphur at the deposition site. This is consistent with later Pb isotope studies by Billström (1990) and Sundblad (1994) that identify the metavolcanic suite (the Isåsen Formation) as the source of ore lead (see Chapter 2). The Fe sulphides in the Zn-Pb ore and the pyrrhotite horizon have more negative $\delta^{34}S$ values and are not in isotopic equilibrium with coexisting sphalerite and galena. Billström (1985, 1991) suggested a primary sedimentary origin for the Fe sulphide minerals (including the pyrrhotite mineralisation stratigraphically above the Zn-Pb horizon), with precipitation occurring in a system closed to H_2S and SO_4 and sulphur derived from bacterial reduction of seawater sulphate. However, Billström did not consider the effects of metamorphism on the sulphide assemblages or the possibility of the pyrrhotite mineralisation being a metamorphic product of an originally pyrite-dominant orebody. The loss of sulphur during high temperature prograde metamorphic transformation of pyrite to pyrrhotite (see section 7.4.1) could result in isotopically lighter $\delta^{34}S$ pyrrhotite due to the preferential partition of ^{32}S into pyrrhotite, and subsequent loss of ^{34}S into the volatile phase. Re-equilibration with the metamorphic fluid (of unknown $\delta^{34}S$ composition) could also produce Fe sulphides with anomalous, negatively-skewed, non-equilibrium $\delta^{34}S$ values relative to sphalerite and galena, whose isotopic composition would have remained unaffected by metamorphism. On this basis, a common hydrothermal origin for both the Zn-Pb and Fe sulphide ores cannot be discounted, although reduction of seawater sulphate probably also contributed to the sulphur source. In addition, it would be unusual for a base metal deposit of the size of Zinkgruvan to have formed via hydrothermal processes without producing some Fe sulphide.

7.6 SUMMARY

- Zn-Pb mineralisation at Zingruvan is stratiform and tabular, underlain by an irregular, sub-stratiform zone of marble-hosted disseminated chalcopyrite and silicate-sulphide mineralisation, which may represent the feeder zone for the ore-forming fluids.
- Major mineralisation is hosted in the Zinkgruvan Formation, with no significant mineralisation in the underlying Isåsen Formation. The overlying Viksjön Formation is essentially barren with the exception of a stratiform pyrrhotite-rich layer near the boundary with the Zinkgruvan Formation. Disseminated sphalerite is present in the Zinkgruvan Formation, particularly in the metavolcanic rocks.
- Sulphide assemblages in the Nygruvan orebody are simple, comprising sphalerite and galena with subordinate pyrrhotite and chalcopyrite. Pyrite is rare.
- The Burkland FW Cu orebody comprises disseminated chalcopyrite with lesser sphalerite, galena and pyrrhotite. Minor Co-,Ni-, Sb- and As-bearing sulphides also occur.
- Original sulphide textures have been destroyed and compositions have been altered by high grade metamorphism.
- Mineralisation was likely generated by hot (~250°C), acidic, weakly reducing ($aH_2S > aSO_4$) brines expelling at or near the seafloor. Seawater was probably the main source of fluid; sulphur was mainly derived via leaching of the volcanic basement, with some additional sulphur generated from bacteriogenic reduction of sulphate at the vent site.
- Sulphide zonation in the Burkland FW Cu orebody, and in the Zinkgruvan orebodies is consistent with the relative solubilities of the constituent metals in hydrothermal solution. Low solubility Cu sulphides precipitated first (at higher temperature) in the 'feeder zone', followed by Pb and Zn further away.
- Mineralisation occurred prior to the peak of metamorphism because the sulphide ores, the Zn-spinel gahnite and Pb-bearing amazonite feldspar form part of the metamorphic assemblage.

CHAPTER 8

DISCUSSION

CHAPTER 8: DISCUSSION

8.1 INTRODUCTION

This chapter examines and evaluates the data presented in previous sections with respect to genetic ore models, in the context of the Bergslagen Province, and in terms of Broken Hill-type (BHT) deposits worldwide. The key geological features of the deposit are discussed, and their significance in terms of ore genesis is assessed.

Zn-Pb mineralisation at Zinkgruvan exhibits characteristics commonly found in both sedimentary-exhalative (SEDEX) and volcanogenic massive sulphide (VMS) style mineralisation. As such, it has been previously classified as a BHT deposit (Beeson, 1990; Parr & Plimer, 1993; Walters, 1996), a mineralisation style intermediate between SEDEX and VMS type deposits. These deposit classifications are described below.

8.2 CLASSIFICATION OF Zn-Pb DEPOSITS

The classification of stratabound and stratiform Zn-Pb deposits is complex. Stanton (1972) grouped all stratabound base metal mineralisation together, with sediment-hosted deposits forming one end-member, and volcanic-associated deposits the other. However, many other researchers preferred a twofold subdivision (e.g., Barnes (1975), Solomon (1976), Gustafson & Williams (1981), Franklin *et al.* (1981), Sangster (1983), Eckstrand (1984) etc.), based on host lithology, tectonic setting, ore position relative to fluid source, and mineralisation characteristics. Ore deposits associated with sedimentary facies and processes form the SEDEX group; deposits associated with or related to volcanogenic processes are known as VMS deposits. Both categories contain subdivisions and numerous variations, but are based on a common model involving subaqueous expulsion of metalliferous fluids into a depositional basin.

A brief description of these two broad genetic groups is outlined below, along with a discussion of Broken Hill-type deposits. These are often grouped with SEDEX-style mineralisation but in fact show characteristics of both SEDEX and VMS mineralisation.

8.2.1 Sedimentary-exhalative (SEDEX) deposits

SEDEX-style (also known as stratiform sediment-hosted) mineralisation is traditionally thought of as Zn-Pb(-Cu) mineralisation hosted in black shales, believed to have formed through pressure-induced expulsion of basin (connate) fluids via fault structures during basin subsidence. However, this category has been expanded to encompass ores formed in localised basins on the seafloor as a result of protracted hydrothermal activity during continental rifting, with ore hosted in a variety of sedimentary facies. SEDEX-style deposits account for more than 50% of the world's reserves of Zn and Pb (Goodfellow *et al.*, 1993), and also contain economically important quantities of Ag

and Cu. The average size of SEDEX deposits is an order of magnitude larger than most volcanogenic massive sulphide deposits. SEDEX deposits range from early Proterozoic (~1900 Ma) to the Carboniferous (320 Ma) in age, with minor deposits in the Jurassic. Most are associated with post-rift reactivation of extensional structures rather than the initial stages of continental breakup (Goodfellow *et al.*, 1993). Host rocks are typically basinal sediments deposited in rift-bounded troughs or half-grabens.

SEDEX mineralisation occurs as lens-like, tabular bodies a few metres to tens of metres thick and >1 km in diameter, comprising finely laminated pyrite-rich sulphide material intercalated with clastic and chemical sediment layers which may show soft sediment deformation indicative of synsedimentary mineralisation. Mineralised feeder zones below the Zn-Pb ore are absent from many SEDEX deposits, indicating a position distal to the hydrothermal vent site, or lack of preservation. More proximal deposits may contain a Cu-rich stockwork feeder zone with associated silicification and replacement textures. Sulphide mineralogy tends to be simple, comprising pyrite and/or pyrrhotite, sphalerite, galena and minor chalcopyrite. An increase in Zn/Pb ratio away from the vent complex (where identified) is a distinguishing feature of SEDEX mineralisation. Dolomitisation of footwall carbonate rocks and weak Mn alteration haloes are common features, and barite-rich horizons may be developed laterally to sulphide mineralisation.

Subdivision of the SEDEX class has been proposed on many occasions, and the result is a confused and often misinterpreted variety of informal sub-categories. A major component of the SEDEX class is the Irish-type Zn-Pb deposits. These are exclusively carbonate-hosted, with Zn-Pb mineralisation sourced from metalliferous basinal brines ascending and expelling through faults in restricted marine basins. Fossil hydrothermal chimneys found at Silvermines and Tynagh indicate expulsion of ore fluids onto the basin floor, but many Irish deposits also show replacement textures typical of epigenetic mineralisation (Hitzman & Large, 1986).

Mississippi Valley-type (MVT) mineralisation describes epigenetic, fracture-controlled Zn-Pb(-Ba-F) deposits hosted in reef or platform carbonate rocks developed in orogenic foreland settings. These deposits are usually associated with collisional tectonic events, which drive the expulsion of connate brines out of existing basins and into carbonate (or occasionally sandstone) ore 'reservoirs'. The metal content of MVT deposits is highly variable, and may contain important amounts of copper, fluorite and/or barite.

The source, transport and deposition mechanism of sulphide minerals in SEDEX deposits is varied and complex, with fluid chemistry largely controlled by the sedimentary fill in the source basin. Metals may be transported as bisulphuide, chloride and organometallic complexes, with sulphur either carried as H_2S or sulphate in the same solution, or provided from an external source at the deposition site. Ore fluids are typically reduced, and produce pyrite-rich orebodies, commonly displaying distinct metal zonation from Cu → Pb →Zn → Ba, Fe, Mn. Modern analogues of

SEDEX-type mineralisation are the Atlantis II complex in the Red Sea, Middle Valley on the Juan de Fuca Ridge, and the Salton Sea, California (Goodfellow *et al.*, 1993). An idealised section through a SEDEX deposit is provided in Fig. 8.1.

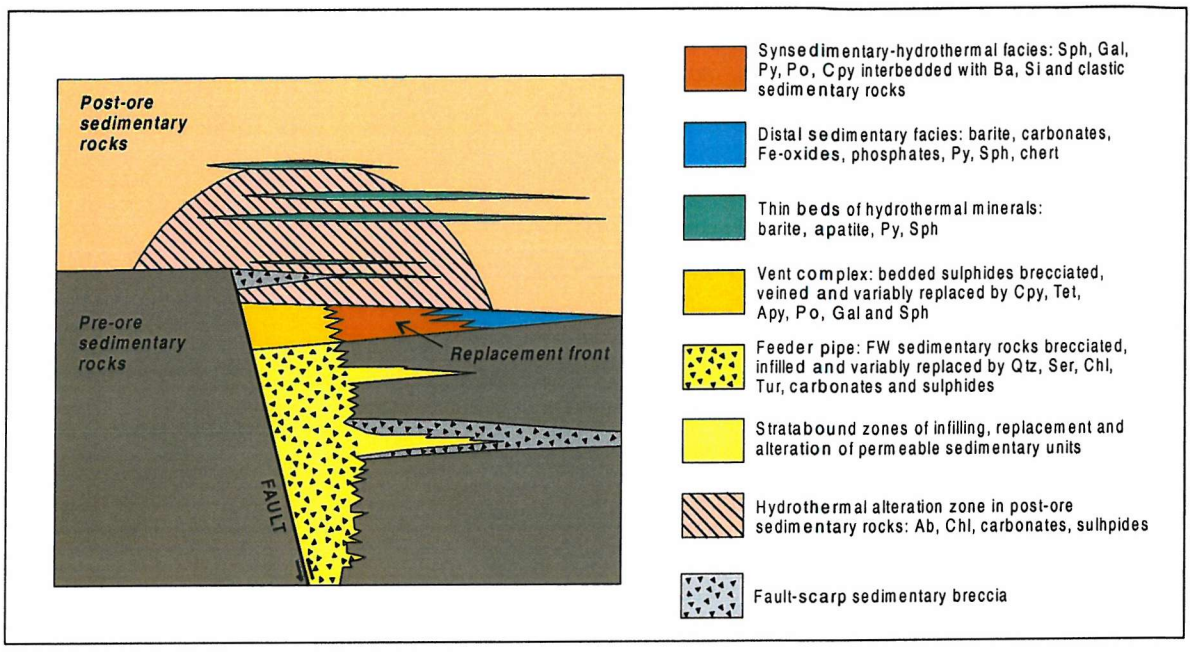

Figure 8.1: Idealised section through a typical SEDEX deposit, showing all the key features. Modified after Goodfellow et al. (1993).

Giant stratabound Zn-Pb deposits, mainly of Proterozoic age, are usually classed as SEDEX style mineralisation. However, a number of deposits such as Broken Hill (Australia), Gamsberg and Aggeneys (South Africa), Balmat (Canada), Zinkgruvan (Sweden), and several smaller deposits in the McArthur River and Mount Isa provinces (Australia) display characteristics of both SEDEX and VMS style mineralisation, and are therefore considered by some (e.g., Beeson, 1990; Parr & Plimer, 1993; Walters, 1996) to belong to a distinct group of stratiform, sediment-hosted Zn-Pb deposits known as Broken Hill-type. This group is described separately in section 8.3.

8.2.2 Volcanogenic massive sulphide (VMS) deposits

VMS deposits are generated by hydrothermal circulation through a volcanic pile and expulsion of mineralised brines onto the seafloor. Mineralisation is usually located at the boundary between two volcanic units or at the interface between volcanic and sedimentary rocks, and is often associated with the products of explosive volcanism.

VMS deposits show a range of genetic types related to different stages of volcanic arc evolution. Cyprus-type deposits are developed in oceanic and back-arc settings, commonly associated with ophiolite suites (e.g., Troodos Complex, Cyprus). Mineralisation is Cu and pyrite-rich, and may

contain minor Au. Besshi-type Cu-Zn deposits generated during the early stages of island arc formation are associated with calc-alkaline volcanism and thick greywacke sequences. The late stages in island arc evolution give rise to Kuroko-type mineralisation (Fig. 8.2), developed within felsic volcanic sequences and comprising varied sulphides of Zn + Cu + Pb ± Au ± Ag.

VMS deposits are more commonly divided according to ore composition, into a Cu-Zn group and a Zn-Pb-Cu group. The Cu-Zn mineralisation tends to form semi-concordant massive Fe sulphide-rich orebodies hosted in mafic volcanic sequences and underlain by a network of stringer veins. The Zn-Pb-Cu deposits comprise tabular, concordant and pyrite-rich orebodies hosted in felsic volcanic sequences (often with a significant sedimentary component) with a less distinct stringer zone than the Cu-Zn types (Franklin, 1993).

Mineralisation is generated from leaching of the volcanic pile and/or oceanic crust by circulating hydrothermal fluids, sourced from seawater and/or magmatic fluids. Hot (>200°C), mineralised fluids are expelled onto the seafloor at vent sites, where chimneys may develop to create black and white smokers. Modern submarine analogues are observed along the Mid Atlantic Ridge, East Pacific Rise, Guayamas Basin and the Juan de Fuca Ridge. VMS deposits are commonly lens- or bowl-shaped, usually underlain by a discordant, funnel-shaped zone of stockwork copper mineralisation. Zonation of metals around and above the vent site is pronounced, particularly in Kuroko-type deposits (Fig. 8.2), usually with a brecciated zone developed immediately above the stockwork. Chloritic and sericitic footwall alteration affects a funnel-shaped area of country rock surrounding the stockwork mineralisation, and a broader zone of more diffuse stratabound footwall hydrothermal alteration is common (Gemmell & Herrmann, 2001).

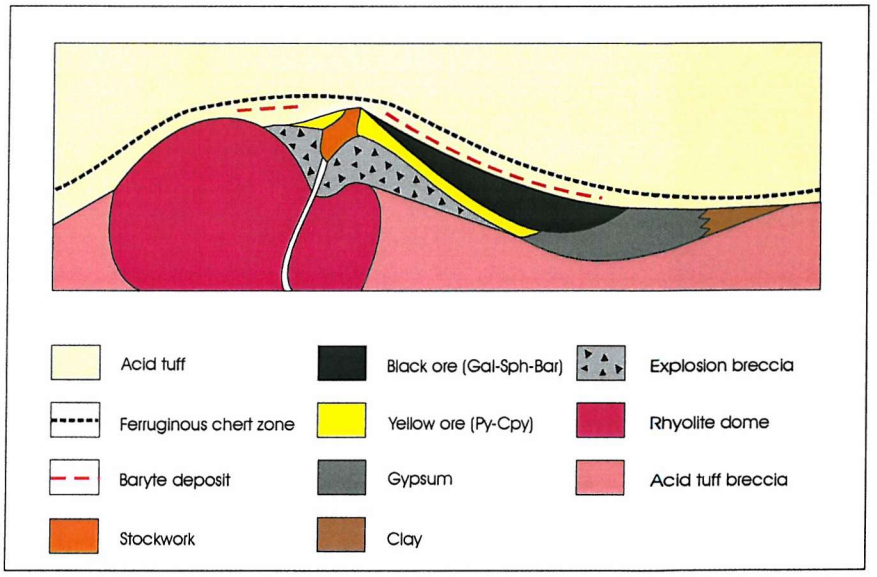

Fig. 8.2: Cross section through a Kuroko-type VMS deposit to show structure and zonation of sulphide minerals and ore types. Modified after Sato (1977).

Barrie & Hannington (1999) proposed a subdivision of the VMS group into five sub-categories, based on the host rock composition (Table 8.1). Gibson *et al.* (1999) highlighted the differences in VMS mineralisation caused by the type of volcanic product in the footwall to the orebody. Sequences dominated by impermeable lava flows host focused hydrothermal exhalation at or immediately below the seafloor, underlain by stringer mineralisation and a vertically extensive but laterally restricted zone of hydrothermal alteration. Focused venting results in the build-up of lens-shaped sulphide mounds and lenticular orebodies. Conversely, volcaniclastic-dominated sequences are more likely to host subsurface sulphide mineralisation precipitated in pore spaces due to the trapping of unfocused hydrothermal discharge by entrained seawater. Replacement of volcaniclastic layers creates tabular and sheet-like stratiform orebodies, surrounded by broad, diffuse zones of hydrothermal alteration. The nature of the host rock is ultimately linked to the position of the vent site relative to the volcanic centre: volcaniclastic-hosted deposits occur in shallow water (<500 m), proximal to volcanism, whereas lava flow-hosted mineralisation occurs in deeper water (>1000 m) in more distal areas. Water depth is important in regulating adiabatic boiling of ore-forming solutions (which in turn affects sulphide precipitation mechanisms), and also has implications for the formation of vent structures, such as black smokers which are only found in water depths of >1000 m (Hannington *et al.*, 1995).

Host rock composition	***Definition***	***Ave. size (Mt)***	***Ave. Cu wt%***	***Ave. Pb wt%***	***Ave. Zn wt%***	***Ave. Au g/t***	***Ave. Ag g/t***
Mafic	>75% M <1% F <10% S	2.80	2.04	0.10	1.82	2.56	20.00
Bimodal-mafic	>50% M >3% F	5.10	1.88	0.75	4.22	1.52	36.50
Mafic-siliclastic	~50% M ~50% S	11.00	1.74	1.83	2.43	0.84	19.80
Bimodal-felsic	>50% F <15% S	5.20	1.44	1.64	5.63	2.06	92.80
Bimodal-siliclastic	~50% F+M ~50% S	23.70	1.10	1.84	4.16	1.13	84.40

Table 8.1 Classification of VMS deposits by host rock composition. M = mafic volcanic rocks; F = felsic volcanic rocks; S = siliclastic rocks. Modified after Barrie & Hannington (1999).

8.3 BROKEN HILL-TYPE (BHT) MINERALISATION

Broken Hill-type deposits exhibit a number of distinctive features that set them apart from most SEDEX and VMS Zn-Pb deposits. The most distinctive features of BHT deposits are:

- Stratigraphic position and host rock sequence
- Tectonic setting
- Age
- Distribution of mineralisation and associated subordinate metalliferous deposits
- Occurrence of chemical sediments
- Metamorphic grade

The majority of BHT deposits are early to mid Proterozoic (1.9-1.6 Ga), hosted in supracrustal sequences developed in intracratonic rift-type tectonic settings (Barnes, 1980; Plimer, 1984, 1986; Rickard, 1987; Parr & Rickard, 1987; Beeson, 1990). Other large SEDEX Zn-Pb deposits such as those at Mount Isa and McArthur River (Australia) also formed around this time, and possibly represent unmetamorphosed equivalents of BHT deposits (Sangster, 1990; Goodfellow *et al.*, 1993). The sizes and metal grades of some of the major orebodies considered to be BHT are shown in Table 8.2.

Deposit	*District*	*Age (Ga)*	*Size (Mt)*	*Zn (wt%)*	*Pb (wt%)*	*Cu (wt%)*	*Ag (g/t)*	*Host rock*
Broken Hill	Broken Hill, Australia	1.67-1.69	280	8.5	10	0.14	148	CS
Zinkgruvan	Bergslagen, Sweden	1.87-1.89	40	10	5.5	?	100	CS
Garpenberg	Bergslagen, Sweden	1.87-1.89	0.22	5.0	4.0	0.4	130	CS
Falun	Bergslagen, Sweden	1.87-1.89	35+	5.0	2.0	0.7	35	?IF
Sala	Bergslagen, Sweden	1.87-1.89	5	2.0	4.2	0.7	350	CS
Gamsberg	Namaqualand, South Africa	~1600 Ma	150	7.1	0.5	0.02	6	IF
Aggeneys	Namaqualand South Africa	~1600 Ma	38	3.0	6.0	?	82	IF
Pegmont	Mount Isa, Australia	~1600 Ma	11	3.7	8.4	-	11	IF
Cannington	Mount Isa, Australia	~1600 Ma	44	4.4	11.6	-	538	CS
Balmat	Grenville, Canada	1400-1100 Ma	25	9.0	1.0	-	-	CS

Table 8.2: Sizes and grades of the major BHT deposits. Data from Beeson (1990), Parr & Plimer (1993), Williams (1998) and Walters & Bailey (1998). CS = calc-silicate hosted ore; IF = iron formation hosted ore.

8.3.1 Stratigraphy of the host sequence

BHT mineralisation occurs in the transition zone between underlying felsic volcanic rocks and overlying sedimentary facies rocks (Fig. 8.3). The transition zone usually comprises a mixture of volcanics, clastic sediments and chemical sediments (commonly carbonates), interpreted to represent the waning stage of volcanism and onset of the main basin subsidence phase. Most deposits have been affected by high-temperature, low pressure metamorphism (section 8.3.2).

The volcanic sequence typically comprises felsic volcanic rocks displaying pronounced alkali metasomatism varying from Na-rich (albite-rich) volcanics in the lower parts of the sequence, to K-rich (orthoclase/microcline-rich) volcanics in the upper part. Volcanism is commonly reported to be bimodal, but basic volcanics are subordinate. A trend from lava flow-dominant sequences in the lower part of the volcanic pile, to more volcaniclastic-dominated sequences in the upper part is common.

The transition zone is typically dominated by marine carbonate rocks, metamorphosed into a range of impure marbles and calc-silicate skarns. Metamorphosed chemical sediments such as banded iron formations, metacherts, garnet-rich quartzites, tourmalinites and manganiferous horizons are characteristic of this interval in the stratigraphy. Metaevaporite horizons (identified on geochemical evidence) are observed in some deposits (e.g., Balmat and Broken Hill), and many carbonates preserve shallow water textures and structures. A key feature of this unit, which hosts the Zn-Pb ore, is the formation of the component lithologies in an oxidising environment.

The overlying metasedimentary rocks are typically metapelites and greywackes, representative of the progression into the flysch facies of basin development. These rocks are not genetically related to Zn-Pb mineralisation, but their rapid deposition probably contributed to the preservation of the underlying sulphide deposits.

Typical alteration characteristics of BHT deposits include the alkali metasomatism in the underlying metavolcanic sequence, and a Mn-rich halo below and laterally adjacent to the ore zone. Alkali metasomatism in Bergslagen has been attributed to sub-seafloor hydrothermal alteration of the volcanics via circulating seawater (Arvanitidis & Rickard, 1981; Freitsch, 1982a; Oen *et al.*, 1982; Lagerblad & Gorbatschev, 1985; Oen & Hellingwerf, 1988; Hellingwerf, 1997; see chapters 2 and 4). Oxygen isotope research in the Broken Hill district shows that circulating oceanic water may have been the dominant fluid involved in mineralisation (Cartwright, 1999), although pronounced, region-wide alkali metasomatism is not observed here, probably due to tightly confined hydrothermal conduits. However, similar potassic alteration styles in the McArthur River province, Australia, have been attributed to various episodes of meteoric, evaporite-derived and connate fluid circulation (Cooke *et al.*, 1998; Davidson, 1998).

Mn alteration is suggested to be a product of hydrothermal exhalation, depositing Mn-rich carbonate material around the vent site and altering footwall rocks (Stumpfl, 1979; Large & McGoldrick, 1998; Large *et al.*, 2000) (see section 8.5.3).

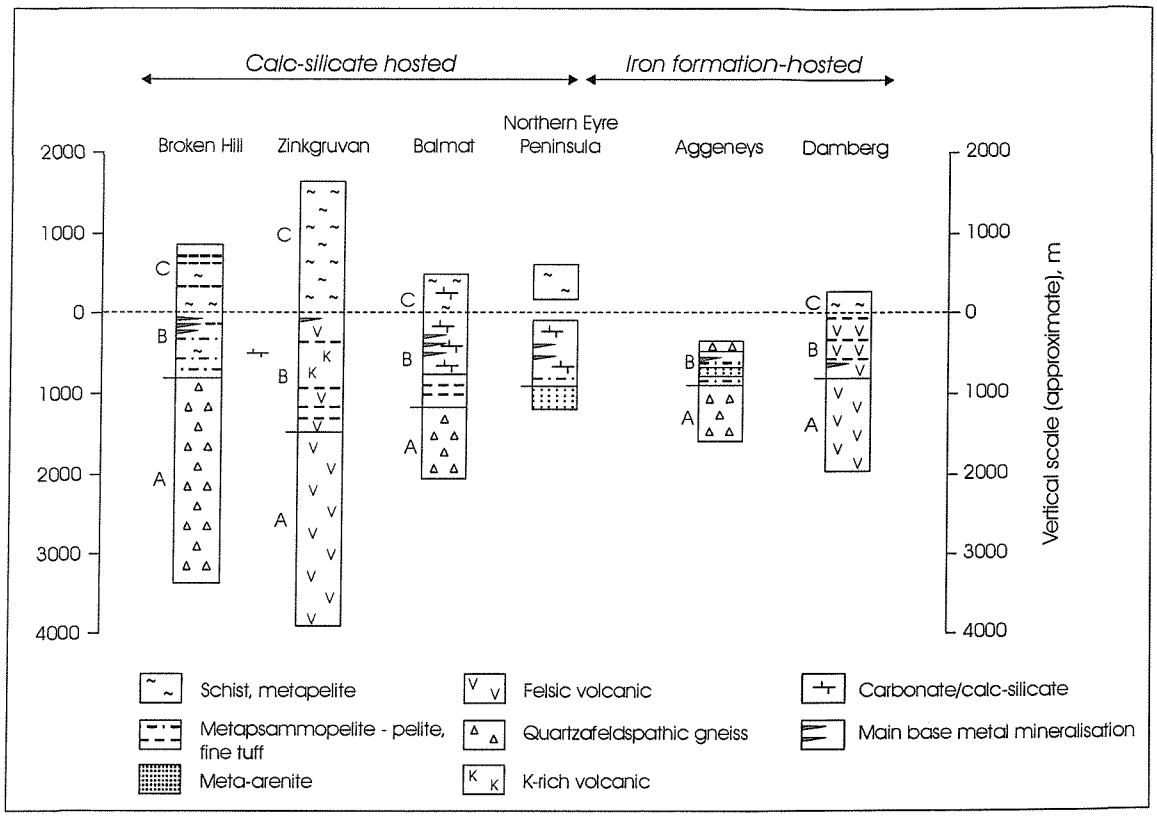

Figure 8.3: Comparison of stratigraphic sequences hosting BHT mineralisation: Broken Hill (Australia), Zinkgruvan (Sweden), Balmat (Canada), Northern Eyre Peninsula (Australia), Aggeneys and Damberg (South Africa). Note that base metal mineralisation occurs at approximately the same stratigraphic interval (Unit B) in all deposits. Quartzofeldspathic gneisses occurring stratigraphically below mineralisation are likely metamorphosed felsic volcanics. Modified after Beeson (1990).

8.3.2 Tectonic setting

A key feature of BHT deposits is their association with the transition from a dominantly igneous regime to a dominantly sedimentary regime. Reconstructions of the palaeoenvironment in areas hosting BHT-style mineralisation have concluded intracratonic rift or back-arc basin terranes (e.g., Dunnet, 1979; Oen *et al.*, 1982; Willis *et al.*, 1983; Plimer, 1984; Moore *et al.*, 1990; Allen *et al.*, 1996), with mineralisation occurring at the beginning of the sag phase during waning volcanic activity. Increase in crustal heat flow during rifting due to crustal thinning and subsequent adiabatic decompression, in addition to the heat generated from the cooling volcanic pile and subvolcanic intrusions, played a key part in the initiation and fuelling of hydrothermal circulation.

8.3.3 Mn-rich lithologies

Fe-Mn alteration commonly forms a halo around large SEDEX-type stratabound Zn-Pb deposits (e.g., McArthur River deposits, Australia), and Mn haloes are reported from Palaeozoic and Mesozoic deposits of central Europe; Broken Hill, Australia, and Gamsberg, South Africa (Stumpfl, 1979). A strong association between Zn-rich BHT-style mineralisation and dolomitic carbonates is documented by Beeson (1990) for the Balmat deposit in the NW Adirondacks, and in the Grenville Province, Quebec. Mn alteration in BHT deposits tends to be more intense than for SEDEX mineralisation; Large *et al.* (1996) reported averages of 0.2 to 1.5 wt% MnO for SEDEX Mn haloes compared to 1-10 wt% MnO for BHT deposits. Mn alteration haloes are rarely reported from VMS-style mineralisation, but Mn haloes developing around present day hydrothermal vent sites have been observed in the Red Sea, Mid Atlantic Ridge, East African Rift Valley and the Galapagos Spreading Ridge (Stumpfl, 1979).

In most metamorphosed deposits, the principal Mn-carrying mineral is garnet, with lesser amounts present in pyroxene, stilpnomelane and amphibole. In some cases (e.g., Gamsberg), sphalerite may be manganiferous. In BHT deposits, Mn is present in banded iron formations, garnet sandstones, quartzites and calc-silicate rocks; most of these have been classed as chemical sediments or exhalites by Lottermoser (1988), Slack *et al.* (1989), Beeson (1990), Parr (1992), Parr & Plimer (1993), etc.

Fe-Mn alteration in the McArthur River deposits shows distinct zonation (e.g., Lady Loretta deposit), with siderite and pistomesite (siderite containing 30-50 mol% $MgCO_3$) developed closest to mineralisation, surrounded by a zone of ankerite/Fe-dolomite alteration grading out to dolomite (Carr, 1984; Large & McGoldrick, 1998). At the HYC deposit, Mn alteration is distinct (up to 12 wt% MnO) but slightly displaced from the ankerite/Fe-dolomite halo, suggesting that Mn and Fe enrichment may have occurred via different alteration mechanisms.

Large *et al.* (2000) attributed the Mn halo at HYC to the release of cool Mn-bearing brines into the McArthur Basin where they precipitated Mn-carbonates in areas where oxidised and reduced basin fluids underwent mixing. The presence of Mn-rich horizons is an indicator of the redox and pH conditions both in the hydrothermal fluid and in the depositional basin at the time of mineralisation. Fe and Mn transport is favoured by acidic, low fO_2 fluids. Precipitation (as Mn carbonate or oxide) is triggered by oxidation, increasing pH and/or decreasing temperature, and will occur if reduced Mn/Fe-bearing hydrothermal fluids mix with oxidised basin waters. The strong association of BHT mineralisation with oxidised host rock facies is favourable for Mn deposition. Weaker Mn haloes in SEDEX style Zn-Pb deposits may be explained by the dominance of anoxic facies (traditionally black shales), although it is recognised that SEDEX mineralisation also occurs in oxidised host rocks. The lateral extent of Mn alteration haloes is partially controlled by the density (and therefore temperature and salinity) of the fluid or brine, and

the difference in redox between brine and basin waters. Low density, hot fluids may form a plume which rises and spreads laterally before precipitating Mn, resulting in a wide halo. Large Mn haloes will also be produced if oxidation of the Mn-fluid is sluggish, allowing more time for dispersal. Conversely, high density brines will either deposit their load close to the vent site or form a bottom flow (depending on temperature) which will spread out slowly from the vent sites and produce a more constricted alteration zone.

8.3.4 Metamorphism

BHT deposits occur in highly deformed terrains where high temperature, low pressure metamorphism (upper amphibolite to granulite facies) has obscured or destroyed most of the original textures in both the host rocks and the ore horizons. Intense deformation in the Broken Hill and Gamsberg districts has made reconstruction of stratigraphy and original ore distribution problematic. A major effect of the metamorphism is partial or total remobilisation of mineralisation in most BHT deposits, resulting in local thickening and coarsening of the orebody (Lawrence, 1973; Parr & Plimer, 1993). Retrograde metamorphism may also cause ore remobilisation (e.g., Both, 1975).

8.3.5 Mineralisation

Zn-Pb mineralisation typically forms tabular to lenticular bodies associated with either calc-silicate rocks or iron formations (Beeson, 1990) (Fig. 8.3). Calc-silicate hosted deposits (e.g., Zinkgruvan, Broken Hill, Balmat) tend to be Zn-rich and Fe-poor, whilst BIF-hosted mineralisation is Pb and Fe-rich. As such, sulphide assemblages vary widely from Fe and S-poor ores such as those at Broken Hill, to pyrite-rich ores at Gamsberg and Falun. Zn/Pb ratios are highly variable within and between deposits. Copper mineralisation is present at some but not all BHT deposits, chiefly occurring stratigraphically below the Zn-Pb ore or in laterally equivalent locations. Some of these occurrences may represent feeder zones for Zn-Pb-bearing ore fluids (e.g., Hedström *et al.*, 1989), but there is no firm evidence for this. Sulphur isotopes tend to cluster around 0‰, with the exception of Broken Hill which displays values of between -3.8‰ and +6.7‰, and the South African deposits which range from +8.9‰ to +29.2‰ (Parr & Plimer, 1993).

BHT deposits are characterised by episodic, extremely active, short-lived hydrothermal events (Parr & Plimer, 1993). Stacking of multiple lenses of high-grade ore material at Broken Hill and the intense but localized hydrothermal alteration is evidence of high heat flow and a tightly focused mineralising fluid pathway. Broken Hill is by far the largest deposit in the BHT group in terms of metal grade and tonnage, being an order of magnitude larger than Zinkgruvan (Table 8.3). This may be due to differences in the chemistry of mineralising fluids, metal source and/or

tectonic regime compared to most other BHT deposits. As such, Broken Hill may represent an end-member of the BHT style.

8.3.6 Genetic models

The genesis of BHT mineralisation is a controversial topic. Debate over epigenetic versus syngenetic interpretations has been in progress for some time (e.g., Wright *et al.*, 1987; Barnes & Willis, 1989; Haydon & McConachy, 1989), although most authors now recognise a syngenetic origin for mineralisation (Parr & Plimer, 1993; Large *et al.*, 1996; Bodon, 1998; Cartwright, 1998).

Parr & Plimer (1993) suggested two potential models for the formation of BHT deposits, based on the extent of continental rifting (Fig. 8.4). They suggested that mineralisation at Broken Hill occurred in a deep rift environment, generated by hydrothermal activity initiated and driven by intrusion of granitic sills into wet sediments and the heat from crustal thinning. Fluids derived from the magmatic bodies (and possibly some mantle-derived fluids (Plimer, 1985, 1988) mixed with seawater and leached the sedimentary succession (including evaporite horizons), resulting in rapid expulsion of metal-bearing fluids onto the seafloor, tightly focused along an as-yet unidentified fault in a half-graben setting, followed by rapid burial by turbiditic sediments (Fig. 8.4A). Intrusion of basaltic material into wet sediment may have also contributed to the hydrothermal regime (Plimer, 1988). The lack of widespread hydrothermal alteration in this setting is a function of the extremely focused nature of the mineralisation and the rapidity of brine exhalation and sulphide precipitation, although the high grade metamorphic overprint may have obscured hydrothermal patterns.

In the second model of Parr & Plimer (1993), mineralisation characterised by widespread regional alteration and a wide variety of ore deposits is attributed to a failed, shallow rift setting such as that proposed for the Bergslagen Province (Oen *et al.*, 1982), where hydrothermal vent systems were more widespread and longer-lived (Fig. 8.4B). These differences in tectonic setting may account for the huge difference in deposit size between the Broken Hill orebody and other BHT deposits. Parr & Plimer (1993) argued that although Broken Hill represents the type example for BHT deposits, it is in fact an unusual end-member of a range of deposit styles.

An alternative model for the Broken Hill deposit was proposed by Wright *et al.* (1987) and Haydon & McConchay (1989), whose reinterpretation of quartzofeldspathic gneisses as psammites rather than metavolcanic rocks led to the suggestion of an 'inhalative' (Clemmey, 1985) genesis, similar to the traditional SEDEX model. In this model, ore formation is suggested to have occurred via compactive expulsion of connate fluids into a subsurface sand body, and comparisons are drawn with the Laisvall Zn-Pb deposit in the Skellefte Field, Sweden. The unusual lithologies,

interpreted as chemical sediments by supporters of the BHT classification, are attributed to low temperature fluid-rock and fluid-fluid interaction.

Gibson *et al.* (1999) classed the Zinkgruvan and Garpenberg deposits as volcaniclastic-hosted VMS-style mineralisation (see section 8.2.2), with subsurface precipitation of sulphides in a marine environment.

A

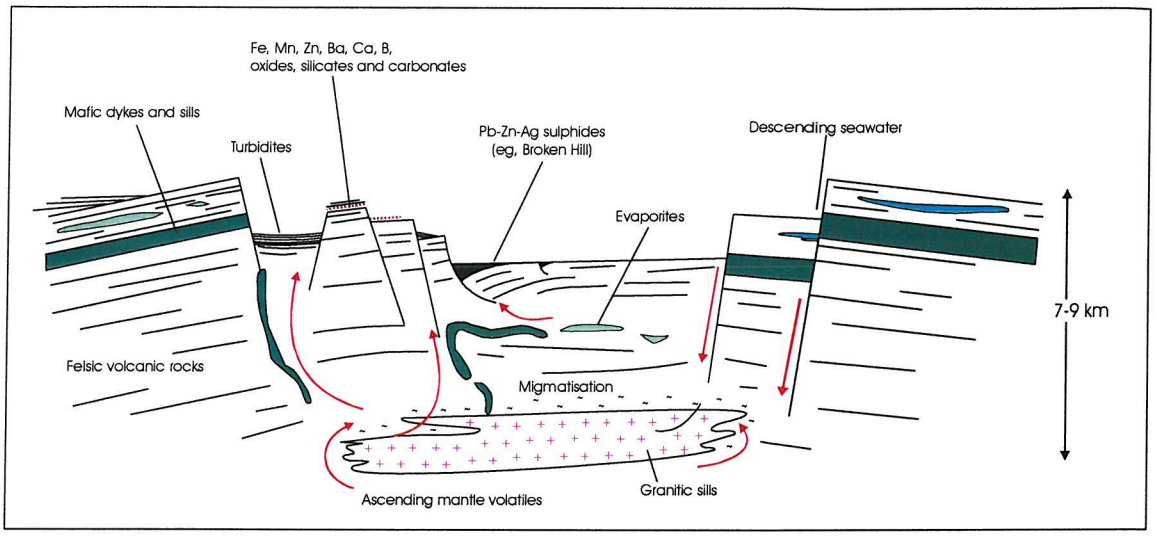

B

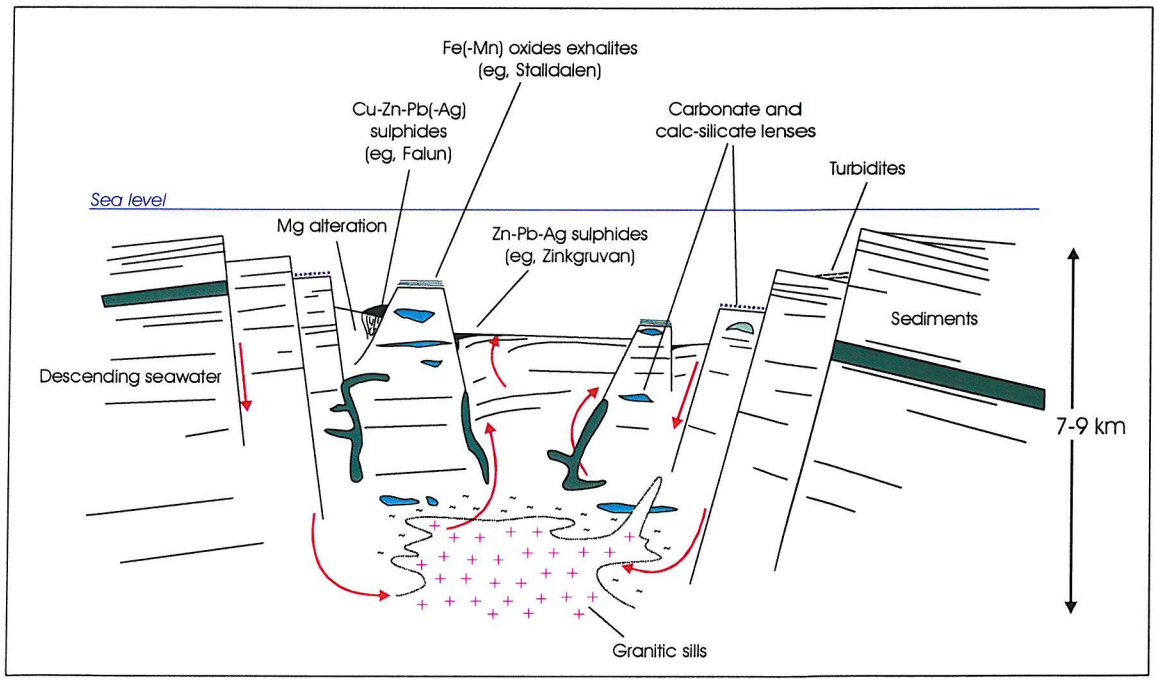

Figure 8.4: Models for BHT style mineralisation in A) palaeoenvironments dominated by deep rifting and some tapping of mantle fluids; B) palaeoenvironments dominated by shallow, probably failed, rifting characterised by hydrothermal alteration and a wide variety of mineral deposits. After Parr & Plimer (1993).

Large & Davidson (1991) used oxygen fugacities (fO_2) of basin waters and mineralising fluids to explain the range of large Proterozoic Zn-Pb mineralisation styles. In this model, metal zonation is related to variations in fO_2 controlled by basin topography and the distance from the hydrothermal vent site. A similar model was proposed for the Bergslagen Province Fe-Mn mineralisation by Freitsch (1982b) and Zakrzewski (1982) (see Chapter 2). The common association of BHT Zn-Pb mineralisation with Fe-silicate and Fe-oxide facies is a likely result of the expulsion of hot, reduced brines into an oxidised marine basin (Parr & Plimer, 1993; Cooke *et al.*, 1999).

Brine chemistry in SEDEX deposits is thought to be controlled by the depositional basin fill (Badham, 1981; Large, 1983; Lydon, 1983; Sawkins, 1984). Brine composition in BHT and other SEDEX-style orebodies has recently been investigated by Large (1999) and Cooke *et al.* (1999, 2000). Cooke *et al.* (1999, 2000) compared the brine chemistry of a number of giant Australian Proterozoic Zn-Pb deposits, and proposed that different mineralisation styles related to fundamental differences in their fluid composition. The McArthur River deposits are Ba, Au and Sn-poor, indicating oxidised ore fluids incapable of carrying significant amounts of these elements expelling into a reduced basin. These deposits are commonly surrounded by a Fe-Mn alteration halo (section 8.3.3). Conversely, the Selwyn-type deposits of Cooke *et al.* (1999, 2000) were generated from reduced, acidic brines sourced from connate fluids in shales venting into reduced depositional environments, and are characterised by widespread barite and distinct sulphide vent complexes.

BHT deposits are the product of acidic, reduced brines flowing into oxidised basins (Cooke *et al.*, 1999). This is indicated by small, but significant quantities of Au occurring in many BHT deposits (e.g., an average 0.13g/t Au at Broken Hill). High H_2S in solution promotes Au bisulphide transport, but inhibits Zn-Pb transport, so fluids at Broken Hill must have been rich enough in H_2S to carry small quantities of Au, but sufficiently H_2S-poor and acidic to allow transport of high concentrations of Zn and Pb. Low H_2S is also indicated by the paucity of Fe sulphides at Broken Hill (Large *et al.*, 1996).

8.3.7 Summary of the key features of BHT deposits

The key features of Broken Hill-type mineralisation are as follows:

- Mineralisation is hosted in the transition zone between underlying metavolcanic rocks and overlying metasediments.
- The host sequence is commonly early to mid Proterozoic in age.
- Regional tectonic setting is usually interpreted as an intracontinental rift setting, with the stratigraphic sequence reflecting the transition from syn-rift volcanism to more stable basin sedimentation during the thermal sag and basin subsidence phases.

- The sequence is typically metamorphosed to upper amphibolite or granulite facies, often accompanied by intense and complex deformation.
- Zn-Pb mineralisation is stratiform, with lens-shaped or tabular orebodies hosted in a mixed sequence of carbonates, chemical sediments of unusual composition (often interpreted as exhalites or meta-evaporites), clastic material and volcanic rocks.
- Metal zonation is the reverse of traditional SEDEX deposits (Zn → Pb), showing (Cu) → Pb → Zn → Mn, Fe.
- Sulphur isotope ($\delta^{34}S$) data are tightly clustered, usually around 0‰, with the majority of sulphur sourced from hydrothermal fluids.
- Mineralising fluids are interpreted to be reduced and weakly acidic, with precipitation of metals in an oxidised depositional environment, indicated by the oxidised basin fill lithologies.
- Mineralisation is often surrounded by a Mn (-Fe) rich alteration halo that is more intense than SEDEX halos.
- The metavolcanic sequence in the footwall of the orebody usually shows evidence of alkali metasomatism, with the lower parts of the sequence Na-enriched and the upper parts K-enriched.

The presence of these key features in major BHT deposits is summarised and compared with other stratiform Zn-Pb deposits in Table 8.3.

	Broken Hill Australia	*Zinkgruvan Sweden*	*Balmat Canada*	*Gamsberg S. Africa*	*HYC Australia*	*Lady Loretta Australia*	*Sullivan Canada*	*Navan Ireland*	*Noranda Canada*	*Kuroko Japan*
Age	1.67-1.69 Ga	1.87-1.89 Ga	~1.4 Ga	~1.6 Ga	~1.68 Ga	~1.65 Ga	~1.4 Ga	350 Ma	Archaean	Miocene
Intracratonic rift setting	✓	✓	✓	✓	✓	?	✓	✓	?	×
Associated volcanism	✓	✓	✓	✓	Minor Volcanics Only	×	×	Minor basic volcanism	✓	✓
Bimodal volcanism	Basic component is minor	? Dominantly felsic*	✓	✓	×	×	×	×	✓	Basics present but minor
Volcanic → sedimentary host sequence	✓	✓	✓	✓	×	×	×	×	×	✓
Chemical sediments	✓	✓ ?	✓	✓	Carbonates only	Carbonates only	✓	Carbonates + silica ironstones	×	? chert
High metamorphic grade	✓	✓	✓	✓	×	×	×	×	?	×
Na-K metasomatism	✓	✓	?	×	✓	×	×	×	Sericitic alteration only	×
Mn alteration halo	✓	✓	✓	✓	✓	✓	?	✓	×	×
Oxidised host facies	✓	✓	✓	✓	×	×	✓	?	×	?
Laterally extensive mineralisation	✓	✓	×	✓	?	×	×	✓	×	×
Presence of Cu-rich feeder zone	×	✓	?	?	?	×	×	×	✓	✓

*Table 8.3: Summary of the key diagnostic geological features of some major BHT (red), SEDEX (green) and VMS (blue) style Zn-Pb deposits. * Volcanism in Bergslagen is reportedly bimodal, but the volume of basic rocks at Zinkgruvan is small.*

8.4 ZINKGRUVAN IN A BERGSLAGEN PROVINCE CONTEXT

Bergslagen hosts a wide variety of ore deposits (see Chapter 2), most of which are associated with the regional transition from volcanic to sedimentary regimes. Large-scale ore-forming processes associated with basin subsidence in response to crustal extension in a continental rift or back-arc setting are indicated.

The Zinkgruvan deposit is the largest Zn-Pb-bearing deposit in Bergslagen, and although it has many features in common with other base metal deposits in the province, it is anomalous in terms of its size, intensity of potassic alteration, lack of Mg enrichment, and paucity of Fe sulphides.

Base metal mineralisation in Bergslagen varies in character from the Fe-rich Cu-Zn-Pb Falun deposit in the north of the province, to the Fe-poor Zn-Pb(-Ag) Zinkgruvan deposit. Allen *et al.* (1996) proposed that these two deposits represent end-member products of a common hydrothermal process, and divided them into 'stratiform ash-siltstone (SAS) hosted' Zn-Pb-Ag deposits as at Zinkgruvan, and 'stratabound volcanic-associated limestone skarn (SVALS) hosted' Zn-Pb-Ag-Cu-Au deposits as at Falun and Garpenberg) based on the host rock characteristics and orebody morphology (see Chapter 2 for a more detailed description).

In the context of the Bergslagen base metal orebodies, Zinkgruvan appears to represent the more sediment-dominated (SEDEX-like) end of the spectrum despite close association with felsic volcanics, whilst deposits such as Falun have more in common with VMS mineralisation. It appears that many of the variations in mineralisation in Bergslagen are due to facies changes in the host sequence, and the effect that this has on alteration mechanisms and fluid-rock interaction. However, common characteristics of Bergslagen base metal deposits are:

- Association with K-rich host rocks (Zinkgruvan is exceptionally K-enriched)
- Association with Mn-enriched horizons
- Distinct zones of Mg-enrichment (absent at Zinkgruvan)
- Location of mineralisation at the transition from volcanic to sedimentary facies.
- Mineralisation is often associated with Fe ores.

8.5 ZINKGRUVAN AS AN EXAMPLE OF BHT MINERALISATION?

Zinkgruvan has been classified as a Broken Hill-type deposit by Beeson (1990), Parr & Plimer (1993), Walters (1996) and Allen *et al.* (1996). This section summarises and evaluates the genetic implications of the major geological and geochemical features of the Zinkgruvan deposit in relation to the BHT model, in both a regional (Bergslagen) and a global context.

In the literature, comparisons of BHT mineralisation styles vary from deposit scale (i.e., Broken Hill vs Zinkgruvan) to regional scale where numerous deposits from one area are considered as a whole (i.e., Broken Hill Province vs Bergslagen Province). The Bergslagen Province has been compared to the Broken Hill terrane by many authors (Beeson, 1990; Parr & Plimer, 1993; Walters, 1996; Allen *et al.*, 1996), with different deposit types in Bergslagen reflecting the variety of BHT style mineralisation, ranging from volcanic-dominant (VMS-like) to more sediment-dominant (closer to traditional SEDEX-style) regimes. In retrospect, it is apparent (section 8.3.5) that the Broken Hill deposit may not be a suitable representative example of BHT style mineralisation, given its relative size and lithological peculiarities. It is more likely an extreme end-member. Zinkgruvan may also present the same problems in that it represents one of a range of mineralisation styles which fall under the BHT classification. Therefore, it may be more appropriate to consider the whole of the Bergslagen Province as an example of BHT style mineralisation, rather than one individual deposit.

8.5.1 Stratigraphy and tectonic setting

The main Zn-Pb mineralisation at Zinkgruvan occurs towards the top of the transition zone separating the underlying dominantly metavolcanic sequence from the overlying metasedimentary sequence. The volcanic sequence is composed of rhyolitic-dacitic rocks with local minor basic intercalations, which may be younger in age. The metasedimentary sequence (Viksjön Formation) is dominated by pelitic metasediments. The transition zone (Zinkgruvan Formation) comprises a mixture of acidic volcanics, sediments and carbonate units, which, following metamorphism, now exist as a spectrum of marbles and calc-silicate skarns. The oxidised nature of these host rocks is consistent with BHT characteristics.

The carbonate sediments may have a mixed origin: the presence of stromatolitic structures in other parts of the region and stable isotope studies suggest a marine origin. It has been suggested that carbonate rocks and skarns may be exhalative in origin (e.g, Hallberg *et al.*, 1994; Parr & Plimer, 1993), although this interpretation is not supported by this study. 'Exotic' skarn lithologies in similar geological terranes (e.g., Broken Hill, Australia) are commonly interpreted as exhalites and/or evaporites on the basis of geochemical evidence (e.g., Lottermoser, 1988, 1989, 1991; Slack *et al.*, 1989; Parr, 1992). Exhalite lithologies are considered to be common by-products of hydrothermal activity in VMS-style deposits.

Exhalite and meta-evaporite lithologies have been the subject of speculation in many publications on BHT deposits, and exhalative chemical sediments are a common feature associated with hydrothermal activity. In the Zinkgruvan area, unusual lithologies such as garnet sandstones and tourmalinites have been interpreted as exhalites, but it is suspected from the present research that many lithologies perceived as 'unusual' or 'exotic' are in fact the product of metamorphic reactions between adjacent layers of differing chemistry. Evaporites may have been deposited, as reported from Broken Hill (e.g., Cook & Ashley, 1992), but their identification in such high grade metamorphic terrane is unreliable. Great difficulties lie in distinguishing chemical precipitates resulting from seawater evaporation from those produced by hydrothermal exhalation in terranes where the rocks have been exposed to metamorphic temperatures in excess of 700°C. Both mechanisms involve an increase in the concentration of salts in seawater, and the products will have similar major element geochemistry. Trace element and isotope geochemistry may help to distinguish such beds (as demonstrated by Slack *et al.* (1989) at Broken Hill), but the benefits of identifying them are minimal in terms of ore genesis models, unless they contribute a significant amount of saline brine to the mineralising system.

The occurrence of base metal mineralisation within this interval of the stratigraphic sequence is common throughout Bergslagen, and is characteristic of BHT mineralisation. The transition zone represents the waning stage of volcanism and the onset of basin subsidence. Heat from the volcanic pile and crustal attenuation was probably responsible for the initiation of hydrothermal circulation within the volcanic pile and subsequent mineralisation. Oen *et al.* (1982) interpreted the Bergslagen Province as a failed rift environment, whereas Allen *et al.* (1996) proposed a continental back-arc setting. Both models involve stretching and attenuation of the crust, resulting in high heat flow and volcanism.

8.5.2 K-enrichment and alkali metasomatism in volcanic rocks

K-enriched rocks associated with base metal mineralisation are well documented from the Broken Hill deposit, Australia. Here, a broad-scale change from Na-dominant rocks in the lower part of the volcanic sequence underlying mineralisation to K-rich rocks in the upper parts is strikingly similar to alkali metasomatism patterns observed in volcanic sequences in Bergslagen, the Mount Isa region (Australia), and many other BHT terranes. Na-rich volcanics occurring below VMS-style mineralisation are common, but associated K-rich volcanics are rare. Potassic alteration is commonly found associated with Cu porphyry deposits, where alkaline, highly saline fluids are released during the late-stage consolidation of the igneous mass, resulting in localised K-enrichment. However, this style of alteration occurs at very high temperatures (> 600°C, Pollard, 1983), so is unlikely to be responsible for the intense potassic alteration observed in BHT deposits. Low temperature (< 300°C) formation of K-feldspar has been reviewed by Skauli (1993) in

relation to a zone of intense potassic alteration below the Bleikvassli Zn-Pb-Cu SEDEX orebody in northern Norway, where microcline gneiss underlying base metal mineralisation contains up to 11.6 wt% K_2O. Skauli (1993) concluded that this alteration was caused by pre-metamorphic alkali metasomatism of pelitic sediments.

The Bergslagen regional K-Na metasomatism is interpreted as a consequence of circulation of heated seawater through the volcanic pile (Arvanitidis & Rickard, 1981; Freitsch, 1982a, b; Lagerblad & Gorbatschev, 1985), driven by heat from the cooling rocks and regionally high heat flow generated by crustal attenuation and plutonism (Chapter 2). Freitsch (1982a) proposed that the differences in alkali enrichment could be produced by changes in the texture and permeability of the original volcanic precursor. K-enriched rocks represent more permeable protoliths (e.g., tuffs and pyroclastic layers) which were more susceptible to hydration and hydrothermal alteration than underlying rocks; less permeable rocks (e.g., porphyritic lavas) were Na-altered. This theory was based on the chemical changes observed during the hydration and devitrification of seafloor basalts where potassium removed from seawater is accommodated in the development of K-rich smectite. Similar mechanisms in Bergslagen, involving the formation of K-rich clays during sub-seafloor hydrothermal alteration of felsic volcanic rocks and subsequent high temperature metamorphism, could account for the microcline-rich rocks observed in the upper parts of the metavolcanic sequence. De Groot & Baker (1992) provide a detailed description of chemical and mineralogical transformations involved in the regional K-Na metasomatic process.

Mineralisation at Zinkgruvan is associated with exceptionally high, localised enrichment to 12-14 wt% K_2O in the Isåsen Formation metavolcanics, distinct from the lower intensity regional K-Na metasomatism which produced altered volcanic rocks containing ~6 wt% K_2O (Freitsch, 1982a). The intense K-enrichment indicates hydrothermal activity focused in the Zinkgruvan vicinity, probably due a combination of higher heat flow, more intense leaching of K from stratigraphically lower parts of the sequence, differences in hydrothermal fluid composition (e.g., lower pH, different fluid source). Hellingwerf (1988) ascribed differences in regional and local potassic alteration to differences in temperature, with localised enrichment produced by hotter fluids. The chemical and mineralogical mechanisms behind intense K-enrichment are poorly understood due to metamorphic overprint. However, the event is an indicator of intense hydrothermal activity, and its close spatial link to Zn-Pb mineralisation and increasing intensity towards the stockwork Cu feeder zone at Zinkgruvan (Hedström *et al.*, 1989) clearly indicates a genetic link to the ore-forming process. Intense K-alteration is therefore a potential tool in the exploration for large base metal deposits in BHT terranes.

8.5.3 Fe-Mn enrichment

At Zinkgruvan, Fe-Mn alteration is observed in dolomite-dominant marbles, particularly in the stratigraphic footwall to the orebody, but zonation is evident. Fe-Mn enrichment here is distinct though relatively weak, with Mn contained within grossular, diopside, tremolite, forsterite (knebelite) and vesuvianite in calc-silicate skarns and impure marbles, and in garnet in quartzofeldspathic gneisses. Calcite and dolomite are generally Mn-free following metamorphism but may be slightly ferroan. Similar trends are apparent at Broken Hill, Australia.

Original Fe-Mn enrichment patterns may have been partially homogenised, dispersed or obscured by high metamorphic temperatures and structural complexities, although Stumpfl (1979) maintained that Mn halos could survive granulite facies metamorphism. There is a clear link between Fe-Mn enrichment and mineralisation at Zinkgruvan.

The Fe-Mn enrichment is most evident in dolomitised marbles, where Fe and Mn substituted for Mg in dolomite. Calcite marbles are unable to accommodate significant Fe-Mn and do not clearly reflect this enrichment. This pattern clearly shows that localised Fe-Mn enrichment in the mine area occurred after or during dolomitisation, which is known to be a regional event (Chapter 4). Dolomitised samples show no hydrothermal signature compared to calcitic marbles, so it is likely that dolomitisation occurred in a near-surface sub-seafloor environment via circulation of seawater. This seawater may then have descended further into the crust to contribute to the large-scale hydrothermal circulation. The fluids carrying Fe and Mn are likely to have circulated through the hydrothermal convection system and will have been Mg-poor (and therefore unable to cause dolomitisation) due to formation of chlorite and other clay minerals during sub-seafloor alteration processes. Even high temperature hydrothermal fluids issuing from modern vent complexes contain very low or undetectable levels of Mg (Franklin, 1986; Hajash & Chandler, 1981) due to this Mg-removal mechanism. Many base metal deposits in Bergslagen are spatially associated with Mg-rich alteration zones which are clearly genetically related to the mineralisation process. Similar Mg alteration observed in many VMS deposits is thought to form by entrainment or down-pull of cold seawater in the immediate vent area, causing localised, intense Mg-alteration, usually in the form of chloritisation (e.g., Mottl, 1983). However, Mg-enrichment is not observed at Zinkgruvan.

It is unclear whether Mn was expelled through hydrothermal venting and accumulated as carbonate matter (Mn-bearing ankerite or rhodochrosite), as suggested by Large *et al.* (2000) for HYC, or whether alteration occurred in a sub-seafloor environment. Interaction of an acidic Fe-Mn-bearing brine with reactive, dolomite-rich, semi-lithified carbonate material could produce ankerite but is unlikely to cause the wide alteration halo associated with many BHT deposits, where dispersal of Mn in a hydrothermal plume is a more realistic mechanism.

8.5.4 Mineralisation

Zn-Pb mineralisation at Zinkgruvan is pre-metamorphic, contained within two large tabular, sheetlike orebodies (the Main and Parallel ores), with a number of subsidiary lens-shaped orebodies (e.g., Savsjön, Cecilia, 8 and 10 Lens). Zn-Pb mineralisation is underlain in the western part of the mine area by a semi-concordant Cu orebody comprising stringer vein networks and disseminated chalcopyrite hosted in dolomitised marble. The sulphide assemblages are consistent with the BHT concept of precipitation from a hot, slightly acidic, reduced brine expelling into an oxidised depositional basin.

The close association of the Cu-rich orebody stratigraphically below the main Zn-Pb mineralisation is suggestive of a VMS-style submarine hydrothermal vent system, with the main Zn-Pb ores deposited proximal to the vent site, as recognised by Hedström *et al.*, (1989). Metal zonation in the orebodies is consistent with a single, focused source of mineralising fluids; the presence of the Knalla Fault close to the proposed feeder zone suggests that its pre-metamorphic equivalent could have played a key role in focusing hydrothermal fluids.

The lateral extent of the Zinkgruvan Main and Parallel ores is a particular feature of the Zinkgruvan deposit. Metamorphism and deformation may have caused tectonic redistribution of the ore, stretching it into more discrete, thinner layers, but the preservation of cyclic sulphide deposition (Billström, 1985) contradicted this; any original small-scale sulphide zonation or distribution patterns are likely to have been homogenised by major remobilisation. Mechanisms for forming laterally extensive orebodies such as Zinkgruvan include dispersal of brine away from the vent site, either via a buoyant plume or by a dense along-bottom flow, or subsurface replacement of a particular stratigraphic horizon. Hedström *et al.* (1989) and Allen *et al.* (1996) envisaged dense saline brines, emitted from a number of different vents at different times, pooling in topographic depressions on the seafloor. This model explains the presence of individual subsidiary ore lenses in the western area of the mine, but does not necessarily account for the lateral extent of the main Zn-Pb mineralisation, which could have been created by near-surface replacement of chemically reactive layers (as inferred by Allen *et al.* (1996) for Bergslagen's Garpenberg and Stollberg deposits). The unfortunate lack of textural evidence means that no unequivocal sulphide deposition mechanism can be inferred.

8.5.5 Summary

The nature and mechanisms of ore formation at Zinkgruvan are difficult to resolve due to the lack of original textural information, structural disruption, intense hydrothermal alteration in the footwall, and high metamorphic grade. However, it is clear that Zinkgruvan is a hydrothermal ore but is neither a true SEDEX nor VMS-type deposit, containing features that are characteristic of both mineralisation styles. As such, it may be classified as a Broken Hill-type deposit.

CHAPTER 9

CONCLUSIONS AND FUTURE WORK

CHAPTER 9: CONCLUSIONS & FUTURE WORK

9.1 GEOLOGICAL HISTORY OF THE ZINKGRUVAN Zn-Pb(-Ag) DEPOSIT

9.1.1 Tectonic setting

The history of the rock sequence hosting the Zinkgruvan Zn-Pb(-Ag) mineralisation began in the early Proterozoic (~1.9Ga), with the development of a large depositional basin that now forms the Bergslagen Province in response to extensional tectonics, either as a result of intracratonic rifting or the development of a continental back-arc basin (Oen *et al.*, 1982; Allen *et al.*, 1996). The Zinkgruvan Basin formed within this larger structure, probably as a third-order basin. Extensive felsic volcanism originating from a number of volcanic centres across Bergslagen gave rise to a rapidly-deposited (~15 myr) 8 km-thick sequence of acidic lavas, pyroclastic rocks and volcaniclastic material erupted from shallow water to subaerial vents (Allen *et al.*, 1996). Granitoid intrusion and injection of dolerite dykes accompanied volcanism.

The nearest recognised volcanic centre to Zinkgruvan was located at Godegård, ~10 km to the SE. It generated several kilometres of interbedded dacites, rhyolites, pyroclastic rocks, tuffs, their reworked equivalents and small volumes of basalt and dolerite (Isåsen Formation), deposited in shallow to moderately deep marine environments within the Zinkgruvan Basin. As the volcanic system matured, the bulk composition of the volcanics evolved from dacitic to a more rhyolitic composition. Subsidence of the regional Bergslagen basin equalled the volcanic output, and has been estimated at 1 km per million years (Allen *et al.*, 1996).

The heat generated by the volcanism and synvolcanic granitoid intrusions, combined with that contributed by thermal doming and crustal attenuation, initiated large-scale hydrothermal circulation in the volcanic pile. The fluids caused regional sub-seafloor alkali alteration (see section 9.2.1), with the fluids becoming progressively more acidic and saline through fluid-rock reactions. Leaching of metals from the wall rocks variably enriched the hydrothermal fluids in Si, Fe, Mn, Ca, K, Na, Rb, Zn, Pb and Ba, and depleted them in Mg (Fig. 9.1A).

9.1.2 Onset of sedimentation (waning volcanism) phase

As volcanism began to wane at ~1.86 Ga and basin subsidence increased, clastic and chemical sedimentation began to dominate over volcanism in the Zinkgruvan Basin. Localised calm, shallow marine environments enabled stromatolites to become established, and large thicknesses of carbonate mud were deposited on the seafloor, interbedded with tuff layers and admixed with ash and reworked volcanic detritus to form the Zinkgruvan Formation and lateral equivalents. Some areas of the Zinkgruvan Basin may have been subaerially exposed, as evidenced by volcanic

textures, or were sufficiently shallow to permit the precipitation of evaporite minerals, although there is no firm evidence to prove this.

Immediately below the seafloor, circulating seawater caused patchy regional diagenetic dolomitisation of partially lithified carbonate sediment. This zone of dolomitisation probably represented the uppermost part of the underlying large-scale hydrothermal system initiated soon after the onset of volcanism.

Deeper below the seafloor, circulating hydrothermal fluids caused regional alkali metasomatism of the volcanic sequence, with Na-enrichment/K-depletion occurring in the lower, hotter parts of the convection system, and K-enrichment/Na-depletion affecting the upper parts. Metasomatism took place through alteration of feldspars, with albite stable in the lower, hotter parts of the system, and plagioclase altering to sericite or K-feldspar in the upper parts depending on the acidity of the hydrothermal fluid and K and Si activity (see Fig. 4.3).

In the Zinkgruvan area, hydrothermal activity was locally intensified, perhaps due to higher heat flow and/or focusing of hydrothermal fluids. Potassic enrichment here was extreme, resulting in volcanic rocks containing up to 14 wt% K_2O in the Isåsen Formation. As the basin continued to subside and fill with the mixed lithologies of the Zinkgruvan Formation, potassic enrichment waned slightly in intensity and became more patchy, but continued to affect the volcanic rocks, including the volcanic component of the carbonate rocks. Fluid-rock interaction is likely to have caused the salinity of the hydrothermal fluid to increase and the pH to decrease (i.e., become more acidic).

Mineralised fluids rich in Zn, Fe and Mn created widespread disseminated sphalerite mineralisation and preferential Fe-Mn enrichment of dolomitised carbonate rocks. It is unclear whether Fe-Mn enrichment occurred solely through surface hydrothermal exhalation with subsequent enrichment of dolomitised carbonates on the seafloor, or whether sub-seafloor alteration also occurred via penetration of acidic mineralising fluids through semi-lithified carbonate sediment.

Surface hydrothermal venting may have also produced fluids rich in Si, Ca, B, Ba and Mn, which, on mixing with cold seawater, precipitated a range of unusual chemical sediments ('exhalites') such as barite-rich horizons, tourmalinites, chert and so on (see Fig. 9.1B).

9.1.3 Mineralisation phase

As volcanism began to peter out, hydrothermal activity reached its peak with expulsion of hot (~250°C), acidic (pH ~ 4), reduced ($aH_2S > aSO_4$) mineralised brines (section 7.5.2) at or immediately below the seafloor. Fluids were probably focused along a pre-existing structure (e.g., the Knalla Fault or its pre-metamorphic precursor), and expelled in a series of pulses. Below the surface, the combination of temperature and pressure decrease, and mixing of

reduced hydrothermal brines with oxidised seawater caused precipitation of low-solubility Cu as chalcopyrite in a laterally restricted network of silica-rich veins, whilst Zn and Pb remained in solution. Interaction of the acidic hydrothermal fluids with subsurface dolomites resulted in disseminated chalcopyrite mineralisation, with sphalerite and galena occurring on the margins of the orebody.

Above the Cu-rich mineralisation, precipitation of the main Zn-Pb mineralisation occurred on mixing of the mineralising brines with cold, oxidised seawater. The subsequent temperature decrease, pH change and oxidation of the brine caused sulphide precipitation, with sulphur sourced partly from the fluid itself, and partly from bacteriogenic reduction of seawater sulphate at the deposition site. Pulsed hydrothermal exhalation created finely laminated ores, interlayered with thin horizons of carbonate and siliclastic material. Ore generation occurred in two main phases, corresponding to the Main Ore and the Parallel Ore. It is unclear whether the main Zn-Pb mineralisation occurred via surface exhalation or by replacement of an unconsolidated, chemically reactive sediment layer (e.g., carbonate) just below the surface. The seawater contained within such a sediment layer could have triggered Zn-Pb sulphide deposition in the same way as described above for a true exhalative mechanism, with mineralisation stratigraphically confined by a cap of volcanic ash or reworked volcanic sediment. The extension of mineralisation eastwards from the feeder zone suggests that a half-graben situation, with a topographic high to the west, could have influenced the distribution of mineralisation towards the east (see Fig. 9.1C). However, a similar geometry could be produced by later faulting or lack of sulphide preservation to the west.

9.1.4 Sedimentation phase

With the tectonic regime becoming stable, and heat flow in the Zinkgruvan Basin decreasing, hydrothermal activity and volcanism ceased. Basin sedimentation became dominated by argillaceous facies with interbedded psammitic layers (the Viksjön Formation), possibly representing turbidite deposits (Fig. 9.1D).

9.1.5 Metamorphism

The onset of regional metamorphism occurred around 1.85 Ga. In the Zinkgruvan region, north-south compression resulted in an E-W trending synclinal structure, with the steep northern limb (hosting the mineralisation) overturned. Subsequent E-W compression created subsidiary folding on the northern limb of the main fold. The volcanosedimentary sequence underwent high grade regional metamorphism, ranging from upper amphibolite facies (sillimanite zone) in the mine area, decreasing to lower amphibolite facies (andalusite zone) further to the south. The volcanic rocks were transformed into a series of quartzofeldspathic gneisses, with the intensely K-

altered Isåsen Formation rocks consisting entirely of quartz and microcline. The less K-altered Zinkgruvan Formation volcanic rocks became quartz-microcline-biotite(-sillimanite) gneisses. Carbonate units in the Zinkgruvan Formation were metamorphosed into a series of impure calcitic and dolomitic marbles, with the proportion of calc-silicate minerals reflecting the amount of original admixed volcanic ash. Interaction between adjacent carbonate and quartzofeldspathic units produced a range of calc-silicate lithologies, often displaying intricate reaction banding. In the mine area, the metasediments of the Viksjön Formation underwent partial melting due to their higher water content, forming migmatites and high grade gneisses with rafts of calc-silicate-rich and mafic material. Further south, the metasediments were transformed into andalusite-muscovite-bearing schists and gneisses.

Metamorphism peaked at 720 ± 50°C and 5 ± 1 kbar in the mine area, and at ~600°C, 3 kbar further south at Höksjön. Fluids present at the time of metamorphism were dominantly aqueous (low CO_2), with the system open to external fluids and volatile loss. Formation of calc-silicate minerals in carbonate rocks and adjacent lithologies resulted in a loss of CO_2 and depletion of ^{13}C from those rocks. $\delta^{18}O$ remained relatively constant due to re-equilibration with the aqueous metamorphic fluid.

The majority of original textures in both the ore layers and the host rocks were destroyed during metamorphic recrystallisation and re-equilibration. The thermal peak of metamorphism outlasted the deformational phase, so most rocks have a strong granoblastic overprint. Metamorphism caused some remobilisation of mineralisation, with more ductile sulphides such as galena being remobilised into fractures and along cleavage planes of peak metamorphic minerals. Any pyrite present was transformed to pyrrhotite where peak temperatures exceeded 720°C, with resultant loss of sulphur and alteration of the $\delta^{34}S$ values of the Fe-sulphides.

Peak metamorphism was followed by two phases of retrograde metamorphism. The first event, at ~550°C, was accompanied by aqueous fluids and caused serpentinisation of forsterite, overprinting tremolite growth and zoisite formation after grossular. A second event at ~250°C caused replacement of serpentine by iddingsite/saponite and widespread sericitisation.

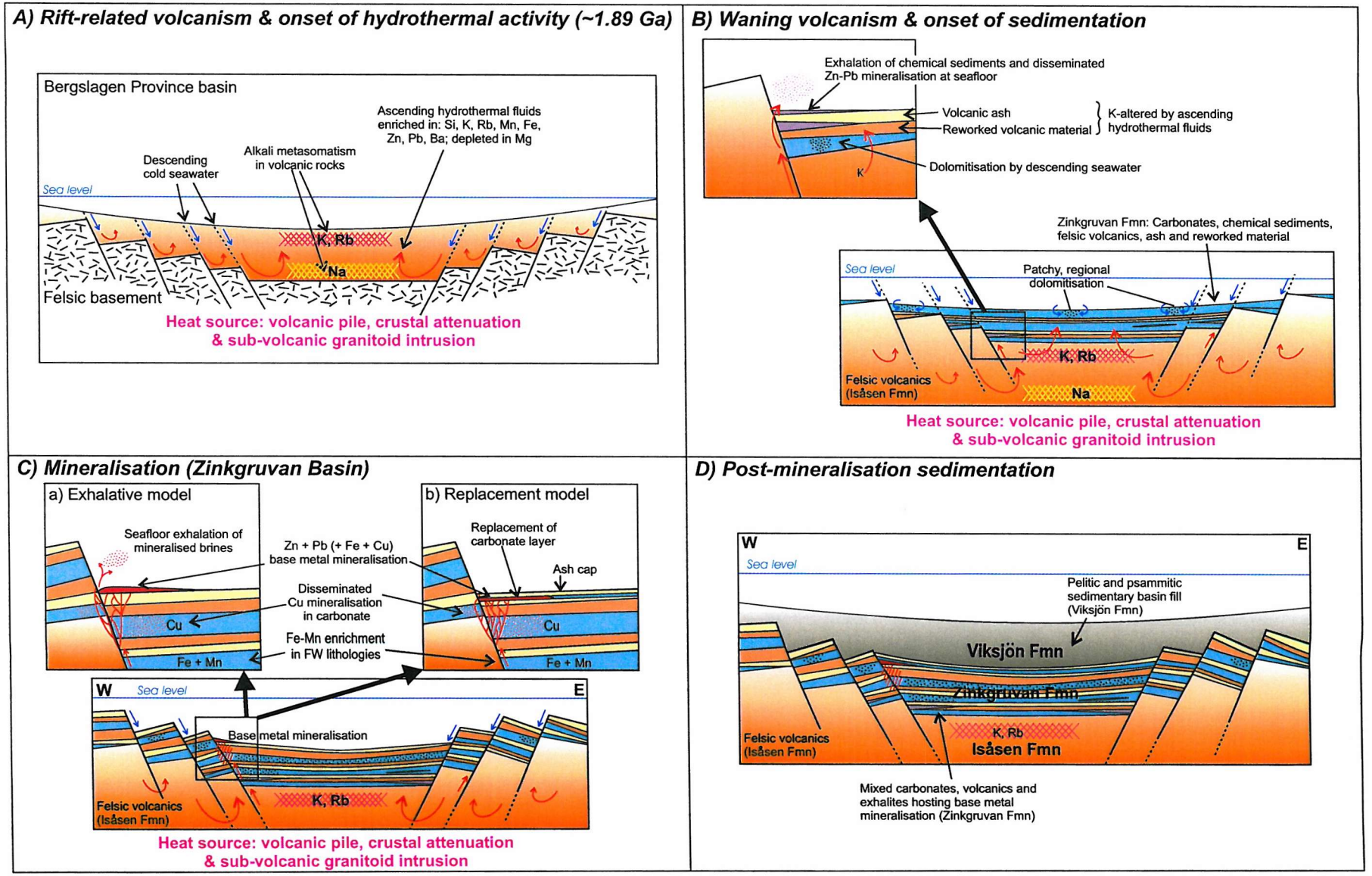

Figure 9.1: Schematic model of the stages in the development of the Zinkgruvan Zn-Pb(-Ag) ore deposit. See text for details.

9.2 IMPLICATIONS FOR EXPLORATION

The search for new ore reserves is an ongoing process at most working mines, and Zinkgruvan is no exception. Exploration programmes at Zinkgruvan are focused not only on extending the working life of the current operation, but also on the discovery of new Zn-Pb deposits in the surrounding district.

The key geological factors in the formation of the Zinkgruvan Zn-Pb deposit are:

- Situation of mineralisation near the top of the transition zone between metavolcanic strata (below) and metasedimentary strata (above), representative of an increasingly stable period in basin evolution when there was enough heat to drive hydrothermal circulation, but sufficient stability to allow deposition and preservation of large quantities of sulphide minerals;
- Sufficiently permeable and fractured volcanic rocks to allow hydrothermal circulation and leaching of metals from these rocks;
- Presence of a structural weakness to concentrate ore-bearing fluids and focus hydrothermal discharge.

Potential vectors to mineralisation in this terrane are:

- Presence of intense potassic alteration (>10 wt% K_2O) in metavolcanic rocks, distinguishable from regional potassic alteration (~5-6 wt% K_2O). Intense potassic alteration may also be evident in associated or overlying carbonate rocks;
- Presence of Fe-Mn enrichment in footwall rocks. This is most easily identified in dolomite-dominant marbles and calc-silicate skarns;
- Presence of unusual 'chemical sediments', which indicate hydrothermal activity. However, these can be difficult to identify, and do not necessarily signify ore-forming conditions.

9.3 SUMMARY AND FUTURE WORK

9.3.1 Summary

The key contributions of this research to the understanding of the geological evolution of the Zinkgruvan Zn-Pb(-Ag) deposit are:

- Detailed petrographic description of the lithologies present in the host rocks, particularly the metavolcanic and metacarbonate rocks;
- Defining the relationships between bulk rock chemistry, mineralogy and metamorphic grade in metavolcanic and metacarbonate rocks;
- Identification of chemical and mineralogical characteristics resulting from fluid and alteration events, and the significance of those fluid events in relation to mineralisation;

- Quantification of P-T conditions and fluid chemistry during peak and retrograde stages of metamorphism, both at the mine and in lower-grade areas further south in the Zinkgruvan Basin.

9.3.2 Future work

- Further characterisation of the nature of fluids involved in the geological evolution of the Zinkgruvan deposit (in particular, mineralisation and metamorphism) can be carried out using analyses of hydrogen isotopes (δD) in conjunction with oxygen isotope ($\delta^{18}O$) data. This will provide a more accurate assessment of fluid sources, and could potentially highlight fluid pathways if a suitable sampling programme is implemented.
- The structural evolution of the mine area is still poorly understood. Reconstruction of orebody geometry could greatly aid the understanding of the ore-forming processes, particularly in the western areas of the deposit, where the relationship of several subsidiary (but economically important) ore lenses to the main Zn-Pb mineralisation remains unresolved. Displacement of mineralised horizons by brittle faulting, and the remobilisation of sulphide ore on a range of scales (including the relationship between economic mineralisation and large-scale fold structures) has not yet been addressed. Understanding the effects of deformation and metamorphism on the ore is important for predicting the location of future reserves, and is a key factor in effective exploration programmes.
- Further study of the copper orebody at Burkland is required to understand ore fluid migration and the early stages of base metal mineralisation at Zinkgruvan. This area of the mine is still relatively unknown, and the extension of Cu-rich mineralisation at depth is still under investigation. The relationship between Cu mineralisation, intensity of hydrothermal alteration, and the Knalla Fault structure is an important component in the evolution of mineralisation at Zinkgruvan.

REFERENCES

REFERENCES

Allen, J.M. & Fawcett, J.J. (1982) Zoisite-anorthite-calcite stability in H2O-CO2 fluids and 5000 bars: an experimental and SEM study. *Journal of Petrology* **23**: 215-239.

Allen, R.L., Lundström, I., Ripa, M., Simenov, A. & Christofferson, H. (1996) Facies analysis of a 1.9Ga, continental margin, back-arc, felsic caldera province with diverse Zn-Pb-Ag (Cu-Au) sulphide and Fe oxide deposits, Bergslagen region, Sweden. *Economic Geology* **91**: 979-1008.

Anovitz, L.M. & Essene, E.J. (1987) Phase equilibria in the system $CaCO_3$-$MgCO_3$-$FeCO_3$. *Journal of Petrology* **28**: 389-414.

Arvanitidis, N. & Rickard, D. (1981) REE geochemistry of an early Proterozoic volcanic ore district, Dammberg, central Sweden. *Geol. Inst., Stockholm University, Ore Research Group Annual Report*: 105-135.

Atherton, M.P. & Edmonds, W.M. (1966) An electron microprobe study of some zoned garnets from metamorphic rocks. *Earth and Planetary Science Letters* **1**: 185-193.

Åberg, G. (1978) Precambrian geochronology of south-eastern Sweden. *Geologiska Foereningen i Stockholm Foerhandlingar* **100**: 125-154

Åberg, G. & Persson, L. (1984) Radiometric dating of Precambrian rocks in Smaaland, southeastern Sweden. *Geologiska Foereningen i Stockholm Foerhandlingar* **106**: 319-325.

Badham, J.P.N. (1981) Shale-hosted Pb-Zn deposits; products of exhalation of formation waters? *Transactions of the Institution of Mining and Metallurgy Section B* **90**: 70-76.

Baertschi, P. (1957) Messung und Deutung reltiver Haufigskeitvariationen von ^{18}O und ^{13}C in Karbonatgesteinen und Mineralen. *Schwiez. Mineral. Petrog. Mitt.* **37**: 73-152.

Baker, J.H (1985) The petrology and geochemistry of 1.8-1.9Ga granitic magmatism and related sub-seafloor hydrothermal alteration and ore-forming processes, W. Bergslagen, Sweden. *GUA Papers in Geology* **1 (21)**: 204pp.

Baker, J.H. & Hellingwef, R.H. (1988) The geochemistry of tungsten-molybdenum-bearing granites and skarns from western Bergslagen, central Sweden. *Proceedings of the 7th IAGOD Symposium:* 327-338.

Barnes, A.D. (1999) Origins of geochemical variations in the rocks of the Zinkgruvan Zn-Pb-(Ag) ore deposit, Bergslagen district, Sweden. Unpublished BSc Honours thesis, James Cook University.

Barnes, H.L. (1975) Zoning of ore deposits: types and causes. *Transactions of the Royal Society of Edinburgh* **69**: 295-311.

Barnes, H.L. (1979) Solubilities of ore minerals. In: Barnes, H.L. (ed) Geochemistry of hydrothermal ore deposits, 2nd Edition. Jon Wiley & Sons, p404-460.

Barnes, R.G (1980) Mineralisation in the Broken Hill Block and their relationship to stratigraphy. In: Stephens, B.P.J. (ed) A Guide to the Stratigraphy and Mineralisation in the Broken Hill Block, New South Wales. *New South Wales Geological Survey Records* **20**: 33-70.

Barnes, H.L. (ed) (1997) Geochemistry of Hydrothermal Ore Deposits. John Wiley & Sons, 972pp.

Barnes, R.G. & Willis, I.L. (1989) The stratigraphic setting of Pb-Zn-Ag mineralisation at Broken Hill. *Economic Geology* **82**: 826-856.

Barrett, T.J. & Anderson, G.M. (1988) The solubility of sphalerite and galena in 1-5 m NaCl solutions to 300°C. *Geochemica et Cosmochemica Acta* **52**: 813-820.

Barrie, C.T. & Hannington, M.D. (1999) Classification of volcanic-associated massive sulfide deposits based on host-rock composition. In: Barrie, C.T. (ed) Volcanic-Associated Massive Sulphide Deposits: Processes and Examples in Modern and Ancient Settings. *Reviews in Economic Geology* **8**: 1-11.

Barrow, G. (1912) On the geology of lower Dee-side and the southern Highland Border. *Proceedings of the Geologists' Association* **23**: 274-290.

Barton, P.B. & Toulmin, P. (1966) Phase relations involving sphalerite in the Fe-Zn-S system. *Economic Geology* **61**: 815-849.

Barton, P.B. (Jnr) & Skinner, B.J. (1979) Sulfide mineral stabilities. In: Barnes, H.L. (ed) Geochemistry of Hydrothermal Ore Deposits, 2nd edition. J. Wiley & Sons New York, p278-403.

Bea, F., Pereira, M.D. & Stroh, A. (1994) Mineral/leucosome trace-element partitioning in a peraluminous migmatite (a laser ablation ICP-MS study). *Chemical Geology* **117**: 291-312.

Bea, F., Montero, P., Garuti, G. & Zacharini, F. (1997) Pressure-dependence of rare earth element distribution in amphibolite and granulite grade garnets: A LA-ICP-MS study. *Geostandards Newsletter* **21**: 253-270.

Becker, R.H. & Clayton, R.N. (1972) Carbon isotopic evidence for the origin of a banded iron formation in Western Australia. *Geochemica et Cosmochemica Acta* **36**: 577-595.

Beeson, R. (1990) Broken Hill-type lead-zinc deposits - an overview of their occurrence and geological setting. *Transactions of the Institution of Mining and Metallogeny* **99**: B163-175.

Bengtsson, V. (2000) Lithogeochemical characteristics of a profile across the Nygruvan orebody, Zinkgruvan, south-central Sweden. Unpublished report, University of Gothenberg.

Bickle, M.J. & Powell, R. (1977) Calcite-dolomite geothermometry for iron-bearing carbonates: the Glockner area of the Tauern Window, Austria. *Contributions to Mineralogy and Petrology* **59**: 281-292.

Billström, K. (1985) Isotopic studies of two early Proterozoic sulphide ores in the Bergslagen district, south-central Sweden. *Meddelanden från Stockholms Universitets Geologiska Institution*, No **263**.

Billström K. (1990) A lead isotope study of two sulphide deposits and adjacent igneous rocks in south-central Sweden. *Mineralium Deposita* **25**: 152-159.

Billström, K. (1991) Sulphur isotope compositions in the Åmmeberg Zn-Pb ore deposit, south-central Sweden: genetic implications. *Geologische Rundschau* **80**: 717-727.

Billström, K., Åberg, G. & Nord, A.G. (1985) Stable isotope data of Bergslagen carbonates and their potential use for sulphide ore prospecting. *Geologiska Föreningens i Stockholm Förhandlingar* **107**: 169-173.

Binns, R.A., Scott, S.D., Bodonov, Y.A., Lisitzin, A.P., Gordeev, V.V., Gurvich, E.G., Finlayson, E.J., Boyd, T., Dotter, L.E., Wheller, G.E. & Muravyev, K.G. (1993) Hydrothermal Fe and Si oxyhydroxide deposits from South Pacific interplate volcanoes and East Pacific Rise axial and off-axial regions. *Economic Geology* **88**: 2122-2153.

Biscaye, P.E. & Dasch, J.E. (1971) The rubidium, strontium, strontium-isotope system in deep-sea sediments: Argentine Basin. *Journal of Geophysical Research* **76**: 5087-5096.

Bodon, S.B. (1998) Paragenetic relationships and their importance for ore genesis at the Cannington Ag-Pb-Zn deposits, Mount Isa Inlier, Queensland, Australia. *Economic Geology* **93**: 1463-1488.

Boekschoten, G.J., Van der Raad, A.C., Kenter, J.A.M. & Reymer, J.J.G. (1988) Note on a mid-Proterozoic stromatolite limestone, south of Grythyttan, Bergslagen, Sweden. *Geologie en Mijnbouw* **67**: 467-469.

Both, R.A. (1975) Remobilisation of mineralisation during retrograde metamorphism, Broken Hill, New South Wales, Australia. In: Verwoerd, W.J. (ed), Mineralisation in metamorphic terranes, p481-489.

Bourcier, W.L. & Barnes, H.L. (1987) Ore solution chemistry VII: Stabilities of chloride and bisulfide complexes of zinc to 350°C. *Economic Geology* **82**: 1839-1863.

Bowen, N.L. (1940) Progressive metamorphism of siliceous limestone and dolomite. *Journal of Geology* **48**: 225-274.

Bowen, R. (1988) Isotopes in the Earth Sciences. Elsevier Applied Science, 647 pages.

Bowman, J.R., Covert, J.J., Clark, A.H. & Maatthieson, G.A. (1985) The Cantung E Zone scheelite orebody, Tungsten, NW Territories: O, H and C isotope studies. *Economic Geology* **80**: 1872-1985.

Brass, G.W. (1976) The variation of marine $^{87}Sr/^{86}Sr$ ratio during Phanerozoic time: Interpretation using a flux model. *Geochemica et Cosmochemica Acta* **40**: 721-730.

Brown, E.H. (1975) A petrogenetic grid for reactions producing biotite and other Al-Fe-Mg silicates in the greenschist facies. *Journal of Petrology* **16**: 258-271.

Brown, P.E., Bowman, J.R. & Kelly, W.C. (1985) Petrologic and stable isotope constraints on the source and evolution of skarn-forming fluids at Pine Creek, California. *Economic Geology* **80**: 72-95.

Bryndzia, L.T., Scott, S.D. & Spry, P.G. (1988) Sphalerite and hexagonal pyrrhotite geobarometer: experimental calibration and application to the metamorphosed sulphide ores of Broken Hill, Australia. *Economic Geology* **83**: 1193-1204.

Bucher, K. & Frey, M. (1994) Petrogenesis of metamorphic rocks, 6th Edition: Complete revision of Winkler's textbook. Springer, 318pp.

Burke, W.H., Denison, E.A., Hetherington, R.B., Helson, H.F. & Otto, J.B. (1982) Variation of seawater $^{87}Sr/^{86}Sr$ throughout Phanerozoic time. *Geology* **10**: 516-519.

Carr, G.R. (1984) Primary geochemical and mineralogical dispersion in the vicinity of the Lady Loretta Zn-Pb-Ag deposit, Northwest Queensland. *Journal of Geochemical Exploration* **22**: 217-238.

Cartwright, I. (1998) Regional scale fluid flow and origins of Pb-Zn-Ag mineralisation at Broken Hill, Australia: constraints from oxygen isotope geochemistry. *Water-Rock Interaction* **9**: 529-532.

Cartwright, I. (1999) Regional isotope zonation at Broken Hill, New South Wales, Australia: Large-scale fluid flow and implications for Pb-Zn-Ag mineralisation. *Economic Geology* **94**: 357-374.

Chattopadhyay, P.K. (1999) Zn-spinel in the metamorphosed Zn-Pb-Cu sulphide deposit at Mamandur, southern India. *Mineralogical Magazine* **63**: 743-755.

Chernosky, J.V. (Jnr), Berman, R.G. & Bryndzia, L.T. (1988) Chapter 9: Stability, phase relationships and thermodynamic properties of chlorite and serpentine group minerals. In: Bailey, S.W. (ed) Hydrous phyllosilicates (exclusive of micas). *Mineralogical Society of America Reviews in Mineralogy* **19**: 725 pages.

Chomiak, B. & Lindblom, S. (1995) Structural analysis of fluid inclusion trails in quartz phenocrysts from the Zinkgruvan Basin, south-central Sweden, and implications for metamorphic fluid evolution. Informal Summary of Results, Stockholm University. Unpublished report.

Clayton, R.N. & Degens, E.T. (1959) Use of C isotope analyses for differentiating fresh-water and marine sediments. American Association of Petroleum Geologists Bulletin 43: 890-897.

Clemmey, H. (1985) Sedimentary ore deposits. In: Brenchley, P.J. & Williams, B.P.J. (eds) Sedimentology: Recent developments and applied aspects. Geological Society of London Special Publication 18: 229-247.

Connolly, J.A.D. & Trommsdorff, V. (1991) Petrogentic grids for metacarbonate rocks: pressure-temperature phase-diagram projection for mixed volatile systems. *Contributions to mineralogy and Petrology* **108**: 93-105.

Cook, N.D.J. & Ashley, P.M. (1992) Meta-evaporite sequence, exhalative chemical sediments and assocaited rocks in the Proterozoic Willyama Supergroup, South Australia: implications for metallogenesis. *Precambrian Research* **56**: 211-226.

Cooke, D.R., Bull, S.W., Donovan, S. & Rogers, J.R. (1998) K-metasomatism and base metal depletion in volcanic rocks from the McArthur Basin, Northern Territory – implications for base metal mineralisation. *Economic Geology* **93**: 1237-1263.

Cooke, D.R., Large, R.R., Bull, S.W. & McGoldrick, P.J. (1999) Brine Chemistry and the spectrum of sediment-hosted Pb-Zn deposits. In: Stanley, C.J. *et al* (eds) Mineral deposits: Processes to Processing. *Proceedings of the fifth biennial SGA meeting and the tenth quadrennial IAGOD symposium.*

Cooke, D.R., Large, R.R., Bull, S.W. & McGoldrick, P.J. (2000) The importance of oxidised brines for the formation of Australian Proterozoic stratiform sediment-hosted Pb-Zn (sedex) deposits. *Economic Geology* **95**: 1-18.

Cox, K.G., Bell, J.D. & Pankhurst, R.J. (1979) The interpretation of igneous rocks. Unwin Hyman, 450 pages.

Craig, H. (1953) The geochemistry of the stable isotopes of carbon. *Geochemica et Cosmochemica Acta* **3**: 53-92.

Craig, H. (1961) Standard for reporting concentrations of deuterium and oxygen-18 in natural waters. *Science* **133**: 1833.

Craig, J.R. & Vaughan, D.J. (1981) Ore microscopy and ore petrography. John Wiley & Sons, 406pp.

Cygan, R.T. & Lasaga, A.C. (1985) Self-diffusion of magnesium in garnet at 750 to 900°C. *American Journal of Science* **285**: 328-350.

Davidson, G.J. (1998) Alkali alteration styles and mechanisms, and their implications for a 'brine factory' source of base metals in the rift-related McArthur Group, Australia. *Australian Journal of Earth Science* **45**: 33-49.

De Groot, P.A. & Sheppard, S.M.F. (1988) Carbonate rocks from Bergslagen, central Sweden: Isotopic (C,O,H) evidence for marine deposition and alteration by hydrothermal processes. *Geologie en Mijnbouw* **67**: 177-188.

Deer, W.A., Howie, R.A. & Zussman, J. (1992) An introduction to the rock-forming minerals, 2nd Edition. Prentice Hall, 696 pages.

Degens, E.T. & Epstein, S. (1962) Relationships between O^{18}/O^{16} ratios in coexisting carbonates, cherts and diatomites. *American Association of Petroleum Geologists Bulletin* **46**: 534-542.

Dickson, J.A.D. (1966) Carbonate identification and genesis as revealed by staining. *Journal of Sedimentary Petrology* **36**: 491-505.

Doe, B.R. (1994) Zinc, copper and lead in mid-ocean ridge basalts and the source rock control on Zn/Pb in ocean-ridge hydrothermal deposits. *Geochemica et Cosmochemica Acta* **58**: 2215-2223.

Dontsova, E.I., Migdisov, A.A. & Ronov, A.B. (1972). On the causes of variation of oxygen isotope composition in the carbonate strata of the sedimentary column. *Geochem. Int.* **9**: 885-891.

Dunnet, D. (1979) Some aspects of the Panantarctic cratonic margin in Australia. *Philosophical Transactions of the Royal Society London, Series A* **280**: 641-654.

Eckstrand, O.R. (ed) (1984) Canadian Mineral Deposit Types: A Geological Synopsis. *Geological Survey of Canada Economic Report* **36**. Ottawa, Canada.

Emrich, K. Ehhalt, D.H. & Vogel, J.C. (1970) Carbon isotope fractionation during the precipitation of calcium carbonate. *Earth and Planetary Science Letters* **8**: 363-371.

Epstein, S. (1959) The variation of the $^{18}O/^{16}O$ ratio in nature and some geologic implications. In: Ableson, P.H. (ed) Researches in Geochemistry. J. Wiley & Sons New York, p217-240

Epstein, S. & Taylor, H.P. (Jnr) (1967) Variation in O^{18}/O^{16} in minerals and rocks. In: Abelson, P.H. (ed) Researches in Geochemistry Volume 2. J. Wiley & Sons New York, 663 pages.

Eskola, P. (1915) On the relations between the chemical and mineralogical composition in the metamorphic rocks of the Orijarvi region. *Bulletin de la Commission Geologique de Finlande* **44**.

Eskola, P. (1920) The mineral facies of rocks. *Norges Geologisk Tiddskrift* **6**: 143-194.

Eskola, P. (1922) On contact phenomena between gneiss and limestone in western Massachusetts. *Journal of Geology* **30**: 265-294.

Evans, B.W. & Guidotti, C.V. (1966) The sillimanite-potash feldspar isograd in western Maine, U.S.A. *Contributions to Mineralogy and Petrology* **12**: 25-62.

Faure, G. (1986) Principles of Isotope Geology (2nd Edition). John Wiley & Sons New York, 589 pages.

Faure, G., Hurley, P.M. & Powell, J.L. (1965) The isotopic composition of strontium in surface water from the North Atlantic Ocean. *Geochemica et Cosmochemica Acta* **29**: 209-220.

Ferry, J.M. (1983a) Regional metamorphism of the Vassalboro Formation, south-central Maine, USA: a case study of the role of fluid in metamorphic petrogenesis. *Journal of the Geological Society of London* **140**: 551-576.

Ferry, J.M. (1983b) Mineral reactions and element migration during metamorphism of calcareous sediments from the Vassalboro Formation, south-central Maine. *American Mineralogist* **68**: 334-354.

Fischer, H. (2000) Geochemical study of marbles coming from the Zinkgruvan region, Bergslagen, south central Sweden. Unpublished diploma work, Universite de Lausanne.

Franklin, J.M. (1986) Volcanic-associated massive sulphide deposits: an update. In: Andrew, C.J., Crowe, R.W.A., Finlay, S., Pennell, W.M. & Pyne, J.F. Geology and Genesis of Mineral Deposits in Ireland. Irish Association for Economic Geologists, p49-69.

Franklin, J.M. (1993) Volcanic-associated massive sulphide deposits. In: Kirkham, R.V., Sinclair, W.D., Thorpe, R.I. & Duke, J.M. (eds): Mineral Deposit Modelling. *Geological Society of Canada Special Paper* **40**: 315-334.

Franklin, J.M., Lydon, J.W. & Sangster, D.F. (1981) Volcanic-associated massive sulphide deposits. *Economic Geology 75th Anniversary Volume*: 485-627.

Freitsch, R. (1982a) Alkali metasomatism in the ore-bearing metavolcanics of central Sweden. *Sveriges Geologiska Undersökning, Serie C*, No. **791**.

Freitsch, R. (1982b) A model for the formation of the iron, manganese and sulphide ores of central Sweden. *Geologische Runschau* **71**: 206-212.

Frost, B.R. (1991) Stability of oxide minerals in metamorphic rocks. In: Lindsley, D.H. (ed) Oxide minerals: petrologic and magnetic significance. *Mineralogical Society of America Reviews in Mineralogy* **25**: 469-487.

Gaal, G. & Gorbatschev, R. (1987) An outline of the Precambrian evolution of the Baltic shield. *Precambrian Research* **35**: 15-52.

Gammons, C.H. & Barnes, H.L. (1989) The solubility of Ag_2S in near-neutral aqueous solutions at 25 to 300°C. *Geochemica et Cosmochemica Acta* **53**: 279-290.

Gebeyehu, M. (1991) Geochemistry and C-O isotope studies of limestone and dolomite in the Garpenberg district, south central Sweden. Unpublished manuscript, Stockholm University.

Geijer, P. & Magnusson, N.H. (1944) De mallansvenska järnmalmernas geologi. *Sveriges Geologiska Undersökning Serie C*: **35**.

Gemmell, J.B. & Herrmann, W. (2001) A special issue devoted to alteration associated with volcanic-hosted massive sulphide deposits, and its exploration significance. *Economic Geology* **96**: 909-912.

Gibson, H.L., Morton, R.L & Hudak, G.J. (1999) Submarine volcanic processes, deposits and environments suitable for the location of volcanic-associated massive sulphide deposits. In: Barrie, C.T. (ed) Volcanic-Associated Massive Sulphide Deposits: Processes and Examples in Modern and Ancient Settings. *Reviews in Economic Geology* **8**: 13-51.

Goldschmidt, V.M (1911) Die kontaktmetamorphose im kristianiagebiet. *Vidensk. Skrifter. I. Mat.-Naturv. K*, **11**.

Goldsmith, J.R. & Newton, R.C. (1969) P-T-X relationships in the system $CaCO_3$-$MgCO_3$ at high temperatures and pressures. *American Journal of Science* **267A**: 160-190.

Goodfellow, W.D., Lydon, J.W. & Turner, R.J.W. (1993) Geology and genesis of stratiform sediment-hosted (SEDEX) Zn-Ag-Pb sulphide deposits. In: Kirkham, R.V., Sinclair, W.D., Thorpe, R.I. & Duke, J.M. (eds): Mineral Deposit Modelling. *Geological Society of Canada Special Paper* **40**: 201-252.

Graf, D.L. & Goldsmith, J.C. (1955) Dolomite-magnesian calcite relations at elevated temperatures and CO_2 pressures. *Geochemica et Cosmochemica Acta* **7**: 109-128.

Graf, D.L. & Goldsmith, J.C. (1958) The solid solubility of $MgCO_3$ in $CaCO_3$: a revision. *Geochemica et Cosmochemica Acta* **13**: 218-219.

Grant, J.A. (1986) The isocon diagram – a simple solution to Gresens' equation for metasomatic alteration. Economic Geology **81**: 1976-1982.

Greenwood, H.J. (1967) Mineral equilibria in the system MgO-SiO_2-H_2O-CO_2. In: Abelson, P.H. (ed) Researches in Geochemistry, Volume 2. J. Wiley & Sons, New York, p542-567.

Gresens, R.L. (1967) Composition-volume relationships of metasomatism. Chemical Geology **2**: 47-65.

Grip, E. (1978) Sweden. In: Bowie, S.H.U., Kvalheim, A. & Haslam, H.W. (eds) Mineral deposits of Europe, Volume 1: Northwest Europe. Institute of Mining and Metallurgy, London. 362pp.

Gustafson, L.B. & Williams, N. (1981) Sediment-hosted stratiform deposits of copper, lead and zinc. *Economic Geology 75th Anniversary Volume*: 139-178.

Hajash, A. & Chandler, G.W. (1981) An experimental investigation of high-temperature interactions between seawater and rhyolite, andesite, basalt and peridotite. *Contributions to Mineralogy and Petrology* **78**: 240-254.

Hallberg, A. (1989) Metal sources in the early Proterozoic Svecofennian terrain of central Sweden: Pb isotope evidence. *Mineralium Deposita* **24**: 250-257.

Hallberg, A., Martinsson, O. & Hellingwerf, R. (1994) Exhalites, evaporites and other exotic components related to deposition of massive sulphide ore in southern Bergslagen. North Ltd unpublished report, 27 pages.

Hannington, M.D., Jonasson, I.R., Herzig, P.M. & Petersen, S. (1995) Physical and chemical processes of seafloor mineralisation at mid-ocean ridges. In: Humphris, S.E., Zierenberg, R.A., Mullineaux, L.S> & Thomson, R.E. (eds) Seafloor Hydrothermal Systems: Physical, Chemical, Biological and Geological Interactions. *AGU Geophysical Monograph* **91**: 115-157.

Harker, R.I. & Tuttle, O.F. (1955) Studies in the system CaO-MgO-CO_2, part 2: limits of solid solution along the binary join $CaCO_3$-$MgCO_3$. *American Journal of Science* **253**: 274-282.

Haydon, R.C. & McConachy, G.W. (1989) The stratigraphic setting of Pb-Zn-Ag mineralisation at Broken Hill – a reply. *Economic Geology* **84**: 191-194.

Hedström, P., Simenov, A. & Malmström, L. (1989) The Zinkgruvan ore deposit, south-central Sweden: a Proterozoic, proximal Zn-Pb-Ag deposit in distal volcanic facies. *Economic Geology* **84**: 1235-1261.

Hellingwerf, R.H. (1988) Regional and local potassic alterations in western Bergslagen, Sweden, and their relation to sulphide mineralisation. *Proceedings of the 7th Quadrennial IAGOD Symposium*: 471-477.

Hellingwerf, R.H. (1995) Regional and local hydrothermal alterations in the footwall rocks below the Main Ore Zone at Zinkgruvan. NUTEK/PIM II Year 3 Report (unpublished), sub-project 92-534.

Hellingwerf, R.H. (1997) Regional and local hydrothermal alteration of Proterozoic metavolcanic footwall rocks of the Zinkgruvan Zn-Pb-Ag ore deposit, Central Sweden. *Neues Jarbuch Miner. Mh.* **11**: 491-518.

Hellingwerf, R.H., Gatedal, K., Gallagher, V. & Baker, J.H. (1994) Tourmaline in the central Swedish ore district. *Mineralium Deposita* **29**: 189-205.

Henriques, A. (1964) Geology and ores of the Åmmeberg District (Zinkgruvan), Sweden (PhD thesis). *Arkiv för mineralgi och geologi* **V4 (1)**: 246 pages.

Hickmott, D. & Spear, F.S. (1992) Major- and trace-element zoning in garnets from calcareous pelites in the NW Shelbourne Falls Quadrangle, Massachusetts: garnet growth histories in retrograded rocks. *Journal of Petrology* **33**: 965-1005.

Hickmott, D.D., Shimizu, N., Spear, F.S. & Selverstone, J. (1987) Trace element zoning in a metamorphic garnet. *Geology* **15**: 573-576.

Hitzman, M.W. & Large, D. (1986) A review and classification of the Irish carbonate-hosted base metal deposits. In: Andrew, C.J, Crowe, R.W.A., Finlay, S., Pennell, W.M. & Pyne, J.F. (eds) Geology and Genesis of Mineral Deposits in Ireland. Irish Assocation for Economic Geology, p217-238.

Hitzman, M.W., Allan, J.R. & Beaty, D.W. (1998) Regional dolomitization of the Waulsortian limestone in southeastern Ireland: Evidence of large-scale fluid flow driven by the Hercynian Orogeny. Geology **26**: 547-550.

Hjelmqvist, S. (1937) Beskrivning till kartbladet Smedjebacken. *Sveriges Geologiska Undersökning* **Aa181**.

Hollister, L.S. (1966) Garnet zoning: an interpretation based on the Rayleigh fractionation model. *Science* **154**: 1647-1651.

Hoschek, G. (1980) Phase relations of a simplified marly rock system with application to the Western Hohe Tauern (Austria). *Contributions to Mineralogy and Petrology* **73**: 53-68.

Högbom, A.G. (1910) Precambrian Geology of Sweden. *Bulletin of the Geological Institute Uppsala* **10**: 1-80.

Hummel, D. (1875) Om Sveriges lagrade urberg. *Sveriges Geologiske Undersökning, Serie C*: **15**.

Hutchison, M.N. & Scott, S.D. (1981) Sphalerite geobarometry in the Cu-Fe-Zn-S system. *Economic Geology* **76**: 143-153.

Jaffe, H.W. (1951) The role of yttrium and other minor elements in the garnet group. *American Mineralogist* **36**: 133-155.

Johansson, Å. & Rickard, D. (1985) Some new lead isotope determinations from the Proterozoic sulfide ores of central Sweden. *Mineralium Deposita* **20**: 1-7.

Johanssen, H.E. (1906) Till frågan om de mallansvenka järnmalmernas bildningsätt. *Geologiska Föreningens i Stockholm Förhandlingar* **28**: 516-538.

Johanssen, H.E. (1907) Till frågan om de mallansvenka järnmalmernas bildningsätt. *Geologiska Föreningens i Stockholm Förhandlingar* **29**: 143-186, 285-300.

Johansson, H.E. (1910) The Ammeberg zinc ore field. *Geologiska Foereningen i Stockholm Foerhandlingar* **32(4)**: 1051-1078.

Karlsson, L. (1980) The metavolcanics in Saxberget: their relation to high grade metamorphism and intrusions. *ORG 80*, Stockholm University, 22-44.

Keith, M.L. & Weber, J.N. (1964) Carbon and oxygen isotopic composition of selected limestones and fossils. *Geochemica et Cosmochemica Acta* **28**: 1787-1816.

Kepezhinskas, K.B. & Khlestov, V.V. (1977) The petrogenetic grid and subfacies for middle-temperature metapelites. *Journal of Petrology* **18**: 114-143.

Kretz, R. (1983) Symbols for rock-forming minerals. *American Mineralogist* **68**: 227-229.

Kinnaird, J.A. (1985) Hydrothermal alteration and mineralisation of the alkaline orogenic ring complexes of Nigeria. *Journal of African Earth Sciences* **3**: 229-252.

Kumpulainen, R. (1994) Sedimentary successions of the Närkesberg and Zinkgruvan areas, southern Bergslagen. Evaluation of the regional and local ore-forming environment of the Åmmeberg type deposits, NUTEK-PIM II Project, Report B (unpublished).

Kumpulainen, R.A., Mansfield, J. & Sunblad, K. (1996) Stratigraphy, age and Sm-Nd isotope systematics of the country rocks to Pb-Zn deposits, Åmmeberg, Sweden. *Economic Geology* **91**: 1009-1021.

Labotka, T.C. (1981) Petrology of an andalusite-type regional metamorphic terrane, Paramint Mountains, California. *Journal of Petrology* **22**: 261-296.

Lager, I. (1986) The Dannemora Iron ore deposit. *Sveriges Geologiska Undersökning Series Ca* **61**: 26-30.

Lagerblad, B. & Gorbatschev, R. (1985) Hydrothermal alteration as a control of regional geochemistry and ore formation in the central Baltic Shield. *Geologische Rundschau* **74**: 33-49.

Lanzirotti, A. (1995) Yttrium zoning in metamorphic garnets. *Geochemica et Cosmochemica Acta* **59**: 4105-4110.

Large, D.E. (1983) Sediment-hosted massive sulphide lead-zinc deposits: an empirical model. In: Sangster, D.F. (ed) Short Course in Sediment-hosted Stratiform Lead-Zinc Deposits, p1-29. Mineralogical Association of Canada.

Large, R.R. (1999) Evidence for pulsed brine exhalation in the formation of giant Proterozoic stratiform sediment hosted Zn-Pb-Ag deposits of Northern Australia. In: Stanley *et al.* (eds) Mineral Deposits: Processes to Processing, p3-6.

Large, R.R. & Davidson, G.J. (1991) Controls of brine chemistry on the spectrum of Proterozoic sediment-hosted base metal deposits. In: Specialist Group in Economic Geology Ore Fluids Conference, Canberra, Australia – Abstracts. Bureau of Mineral Resources, Geology and Geophysics, Record No. 1990/95: 50-51.

Large, R.R. & McGoldrick, P.J. (1998) Lithogeochemical haloes and geochemical vectors to stratiform sediment hosted Zn-Pb-Ag deposits, 1. Lady Loretta Deposit, Queensland. *Journal of Geochemical Exploration* **63**: 37-56.

Large, R., Bodon, S., Davidson, G. & Cooke, D. (1996) The chemistry of Broken Hill-type ore formation - one of the keys to understanding the difference between SEDEX and BHT deposits. In: Pongratz, J. & Davidson, G.J. (eds) New Developments in Broken Hill-type Deposits. *CODES Special Publication No. 1*: 105-111.

Large, R.R., Bull, S.W. & McGoldrick, P.J. (2000) Lithogeochemical halos and geochemical vectors to sediment hosted Zn-Pb-Ag deopsits Part 2. HYC deposit, McArthur River, Northern Territory. *Journal of Geochemical Exploration* **68**: 105-126.

Lawrence, L.J. (1973) Polymetamorphism of the sulphide ores at Broken Hill. *Mineralium Deposita* **8**: 211-236.

Lindroth, G.T. (1925) Om den kemiska sammansättningen hos Ämmebergs zinkmalmfälts röda kalileptiter. *Geologiska Föreningens i Stockholm Förhandligar* **47**: 498-503.

Lindsley, D.H. (1991) Experimental studies of oxide minerals. In: Lindsley, D.H. (ed) 'Oxide minerals: Petrologic and magnetic significance'. *Mineralogical Society of America Reviews in Mineralogy* **25**.

Lottermoser, B.G. (1988) Rare earth element composition of garnets from the Broken Hill Pb-Zn-Ag orebodies, Australia. *Neues Jarbuch fuer Mineralogie* **9**: 423-431.

Lottermoser, B.G. (1989) Rare earth element study of exhalites within the Willyama Supergroup, Broken Hill Block, Australia. *Mineralium Deposita* **24**: 92-99.

Lottermoser, B.G. (1991) Trace element composition of exhalites associated with the Borken Hill sulphide deposit, Australia. *Economic Geology* **86**: 860 - 877.

Lundqvist, T. (1979) The Precambrian of Sweden. *Sveriges Geologiska Undersökning, Serie C* **278**: 87pp.

Lundstam, B. (1998) Exploration relevant geochemical and mineralogical variations surrounding the Knalla Mine at Zinkgruvan, Bergslagen, south-central Sweden. Unpublished report, University of Gothenberg, 33 pages.

Lundström, I. (1983) Beskrivning till berggrundskartan Lindesberg SV. *Sveriges Geologiska Undersökning* Af **126**: 140pp.

Lundström, I. (1987) Lateral variations in the supracrustal geology within the Swedish part of the southern Svecokarelian volcanic belt. *Precambrian Research* **35**: 353-365.

Lundström, I. (1988) Regional inter-relationships in the Proterozoic geology of Bergslagen and southwestern central Sweden. *Geologie en Mijnbouw* **67**: 157-164.

Lundström, I., Allen, R.L., Persson, P. & Ripa, M. (1998) Stratigraphies and depositional ages of Svecofennian Palaeoproterozoic metavolcanic rocks in E. Svealand and Bergslagen, south central Sweden. *Geologiska Föreningens i Stockholm Förhandlingar* **120**: 315-320.

Lusk, J., Scott, S.D. & Ford, C.E. (1993) Phase relations in the Fe-Zn-S system to 5 kbars and temperatures between 325 degrees and 150 degrees C. *Economic Geology* **88**: 1880-1903.

Lydon, J.W. (1983) Chemical parameters controlling the origin and deposition of sediment-hosted stratiform lead-zinc deposits. In: Sangster, D.F. (ed) Short Course in Sediment-hosted Stratiform Lead-Zinc Deposits, p175-250. Mineralogical Association of Canada.

MacLean, W.H. (1990) Mass change calculations in altered rock series. Mineralium Deposita **25**: 44-49.

MacLean, W.H. & Kranidiotis, P. (1987) Immobile elements as monitors of mass transfer in hydrothermal alteration: Phelps Dodge massive sulphide deposit, Matagami, Quebec. Economic Geology **82**: 951-962.

Magnusson, N.H. (1925) Persbergs malmtrakt. Beskrivning över mineralfyndigheter 2. *Kungl. Kommerskollegium*, Stockholm.

Magnusson, N.H. (1936) Berggrunden inom Kantorps malmtrakt. Sveriges Geologiske Undersökning, Series C, No. 401. (English summary).

Magnusson, N.H. (1940) Herrängsfältet och dess järnmalmer. *Sveriges Geologiska Undersökning Serie C* **431**.

Magnusson, N.H. (1950) Zinc and lead deposits of central Sweden. *Proceedings of the 18th International Geological Congress*, Great Britain, 1948. Section F, Part 7: 371-379.

Magnusson, N.H. (1970) The origin of iron ores in central Sweden and the history of their alterations. *Sveriges Geologiska Undersökning* **C643**: 1-127.

Mason, B. & Moore, C.B. (1982) Principles of Geochemistry, 4th Edition. J. Wiley & Sons, 344 pages.

Moore, J.M., Watkeys, M.K. & Reid, D.L. (1990) The regional setting of the Aggeneys/Gamsberg base metal deposits, Namaqualand, South Africa. In: Spry, P.G. & Bryndzia, L.T. (eds) Regional Metamorphism of Ore Deposits. Springer-Verlag, p77-95.

Mottl, M.J. (1983) Metabasalts, axial hot springs, and the structure of hydrothermal systems at mid-ocean ridges. *Geological Society of America Bulletin* **94**: 161-180.

Nabelek, P.I, Labotka, T.C., O'Neil, J.R. & Papike, J.J. (1984) Contrasting fluid/rock interaction between the Notch Peak granitic intrusion and argillites and limestones in western Utah: evidence from stable isotopes and phase assemblages. *Contributions to Mineralogy and Petrology* **86**: 25-34.

Nesbitt, R.W., Hirata, T., Butler, I.B. & Milton, J.A. (1997) UV Laser Ablation ICPMS; Some Applications in the Earth Sciences, *Geostandards Newsletter* **20**: 231-243.

O'Hanley, D.S. (1996) Serpentinites: records of tectonic and petrological history. *Oxford Monographs on Geology and Geophysics* **34**. Oxford University Press, Inc., 277 pages.

Oen, I.S. (1987) Rift-related igneous activity and metallogenesis in SW Bergslagen, Sweden. *Precambrian Research* **35**: 367-382.

Oen, I.S. & Hellingwerf, R.H. (1988) Textural evidence for seafloor, soft rock hydrothermal metamorphism in a garnet-scapolite-bearing metatuffite-exhalite-skarn-sphalerite ore sequence, Nora, Bergslagen, Sweden. *Geologie en Mijnbouw* **67**: 333-348.

Oen, I.S., Helmers, H., Verschure, R.H. & Wiklander, U. (1982) Ore deposition in a Proterozoic incipient rift zone environment: a tentative model for the Filipstad-Grythyttan-Hjulsö region, Bergslagen, Sweden. *Geologische Rundschau* **71**: 182-194.

Oen, I.S., De Maesschalck, A.A. & Lustenhower, W.J. (1986) Mid-Proterozoic exhalative-sedimentary Mn skarns containing possible microbial fossils, Grythyttan, Bergslagen, Sweden. *Economic Geology* **81**: 1533-1543.

Ohlsson, L.G. (1979) Tungsten occurrences in central Sweden. *Economic Geology* **74**: 1012-1034.

Ohmoto, H. & Goldhaber, M.B. (1997) Chapter 11: Sulfur and Carbon Isotopes. In: Barnes, H.L. (ed) Geochemistry of Hydrothermal Ore Deposits, 3rd Edition. J. Wiley & SonsNew York, 972pp.

Parr, J.M. (1992) Rare-earth element distribution in exhalites associated with Broken Hill-type mineralisation at the Pinnacles deposit, New South Wales, Australia. *Chemical Geology* **100**: 73-91.

Parr, J.M. & Rickard, D. (1987) Early Proterozoic subaerial volcanism and its relationship to Broken Hill-type mineralisation in central Sweden. In: Pharoah, T.C. & Rickard, D. (eds) Geochemistry and mineralisation of Proterozoic volcanic suites. *Geological Society of London Special Publication* **33**: 81-93.

Parr, J.M. & Plimer, I.R. (1993) Models for Broken Hill-type lead-zinc-silver deposits. In: Kirkham, R.V., Sinclair, W.D., Thorpe, R.I., & Duke, J.M. (eds) Mineral Deposit Models. *Geological Society of Canada Special Paper* **40**: 253-288.

Patchett, P.J., Gorbatschev, R. & Todt, W. (1987) Origin of continental crust of 1.9-1.7Ga age: Nd isotopes in the Svecofennian orogenic terrains of Sweden. *Precambrian Research* **35**: 145-160.

Pearce, N.J.G., Perkins, W.T., Westgate, J.A., Gorton, M.P., Jackosn, S.E., Neal, C.R. & Chenery, S.P. (1997) A compilation of new and published major and trace element data for NIST SRM 610 and SRM 612 partially certified glass reference materials. *Geostandards Newsletter* **21**: 115-144.

Peterman, Z.E., Hedge, C.E. & Tourtelot, H.A. (1970) Isotopic composition of strontium in seawater throghout Phanerozoic time. *Geochemica et Cosmoschemica Acta* **34**: 105-120.

Plimer, I.R. (1979) Sulphide rock zonation and hydrothermal alteration at Broken Hill, Australia. *Transactions of the Institute of Mining and Metallogeny* **88**: B161-176.

Plimer, I.R. (1984) The mineralogical history of the Broken Hill Lode, New South Wales. *Australian Journal of Earth Sciences* **31**: 379-402.

Plimer, I.R. (1985) Broken Hill Pb-Zn-Ag deposit - a product of mantle metasomatism. *Mineralium Deposita* **20**: 147-153.

Plimer, I.R. (1986) Sediment-hosted exhalative Pb-Zn deposits – products of contrasting ensialic rifting. *Transactions of the Geological Society of South Africa* **89**: 57-73.

Plimer, I.R. (1988) Broken Hill, Australia and Bergslagen, Sweden – why God and Mammon bless the Antipodes! *Geologie en Mijnbouw* **67**: 265-278.

Pollard, P.J. (1983) Magmatic and postmagmatic processes in the formation of rocks associated with rare element deposits. *Transactions of the Institute of Mining and Metallogeny* **92**: B1-9.

Pyle, J.M. & Spear, F.S. (1999) Yttrium zoning in garnet: Coupling of major and accessory phases during metamorphic reactions. *Geological Materials Research* **1 (6)**: 1-49.

Rayleigh, J.W.S. (1896). Theoretical considerations respecting the separation of gases by diffusion and similar processes. *Philos. Mag.* **42**: 493.

Rice, J.M. (1977) Contact metamorphism of impure dolomitic limestone in the Boulder Aureole, Montana. *Contributions to Mineralogy and Petrology* **59**: 237-259.

Rice, J.M. (1980) Phase equilibria involving humite minerals in impure dolomitic limestones. Part I: Calculated stability of clinohumite. *Contributions to Mineralogy and Petrology* **71**: 219-235.

Rickard, D.T. (1978) The Svecokarelian anomalous ore lead line. *Geologiska Foereningen i Stockholm Foerhandlingar* **100**: 19-29.

Rickard, D. (1987) Proterozoic mineralisation styles. In: Pharoah, T.C., Beckinsale, R.D. & Rickard, D. (eds) Geochemistry and mineralisation of Proterozoic volcanic suites. *Geological Society of London Special Publication* **33**: 23-35.

Rickard, D. (1988) Regional metamorphism in the Bergslagen Province, south central Sweden. *Geologie en Mijnbouw* **67**: 139-155.

Roedder, E. (1979) Fluid inclusions assamples of ore fluids. In: Barnes, H.L. (ed) Geochemistry of Hydrothermal Ore Deposits, 2nd Edition. John Wiley & Sons, p684-737.

Rona, P.A., Klinkhammer, G., Nelson, T.A., Trefry, J.H. & Elderfield, H. (1986) Black smokers, massive sulphides and vent biota at the Mid-Atlantic Ridge. *Nature* **321**: 33-37.

Ruaya, J.R. & Seward, T.M. (1986) The stability of chlorozinc (II) complexes in hydrothermal solutions up to 350°C. *Geochemica et Cosmochemica Acta* **50**: 651-661.

Rye, R.O., Schuilling, R.D., Rye, D.M. & Jansen, J.B.H. (1976) Carbon, hydrogen, and oxygen isotope studies of the regional metamorphic complex at Naxos, Greece. *Geochemica et Cosmochemica Acta* **40**: 1031-1049.

Sakai, H. (1968) Isotopic properties of sulphur compounds in hydrothermal processes. *Geochemical Journal* **2**: 29-49.

Sangster, D.F. (ed) (1983) Short Course in Sediment-hosted Stratiform Lead-Zinc Deposits. Mineralogical Association of Canada.

Sangster, D.F. (1990) Mississippi Valley-type and SEDEX lead-zinc deposits: a comparitive examination. *Transactions of the Institute of Mining and Metallogeny* **99**: B21-B42.

Satish-Kumar, M. & Niimi, N. (1998) Fluorine-rich clinohumite from Ambasamudram marbles, southern India: mineralogical and preliminary FTIR spectroscopic characterisation. *Mineralogical Magazine* **62**: 509-519.

Sato, T. (1977) Kuroko deposits: their geology, geochemistry and origin. In: Gass, I.G. (ed) Volcanic Processes in Ore Genesis. *Geological Society Special Publication* **7**: 153-161.

Sawkins, F.J., 1984. Ore genesis by episodic dewatering of sedimentary basins: application to giant Proterozoic lead-zinc deposits. *Geology* **12**: 451-454.

Schenberger, D.M. & Barnes, H.L. (1989) Solubility of gold in sulfide solutions from 150 to 350°C. *Economic Geology* **53**: 269-278.

Schidlowski, M., Eichmann, R. & Junge, Ch. E. (1975) Precambrian sedimentary carbonates: carbon and oxygen isotope geochemistry and implications for the terrestrial oxygen budget. *Precambrian Research* **2**: 1-69.

Schwandt, C.S., Papike, J.J. & Shearer, C.K. & Brearly, A.J. (1993) A SIMS investigation of REE chemistry of a garnet in garnetite associated with the Broken Hll Pb-Zn-Ag orebodies, Australia. *Canadian Mineralogist* **31**: 371-379.

Scott, S.D. (1976) Application of the sphalerite geobarometer to regionally metamorphosed terrains. *American Mineralogist* **61**: 661-670.

Scott, S.D (1997) Submarine hydrothermal systems and deposits. In: Barnes, H.L. (ed) Geochemistry of Hydrothermal Ore Deposits. John Wiley & Sons, p797-875.

Scott, S.D. & Barnes, H.L. (1971) Sphalerite geothermometry and geobarometry. *Economic Geology* **66**: 653-669.

Seward, T.M. & Barnes, H.L. (1997) Metal transport by hydrothermal fluids. In: Barnes H.L. (ed) Geochemistry of Hydrothermal Ore Deposits. John Wiley & Sons, p435-486.

Sheppard, S.M.F. (1986) Characterization and isotopic variations in natural waters. In: Valley, J.W., Taylor, H.P. (Jnr) & O'Neil, J.R. (eds) Stable isotopes in high temperature geological processes. *Mineralogical Society of America Reviews in Mineralogy* **16**: 165-183.

Skauli, H. (1993) A metamorphosed, potassic alteration zone associated with the Bleikvassli Zn-Pb-Cu orebody, Northern Norway. *Lithos* **31**: 1-15.

Skinner, B.J. (1979) The many origins of hydrothermal mineral deposits. In: Barnes, H.L. (ed) Geochemistry of Hydrothermal Ore Deposts, 2nd Edition. John Wiley & Sons, p1-21.

Slack, J.F., Palmer, M.R. & Stevens, B.P.J. (1989) Boron isotope evidence for the involvement of non-marine evaporites in the origin of the Broken Hill ore deposits. *Nature* **342**: 913-916.

Smith, J.V. (1974) Feldspar Minerals, Volume 1: Crystal structure and physical properties. Springer-Verlag, 622pp.

Solomon, M. (1976) 'Volcanic' massive sulphide deposits and their host rocks – a review and an explanation. In: Wolf, K.H. (Ed) Handbook of Stratabound and Stratiform Ore Deposits Volume 6: 21-54. Elsevier, Amsterdam.

Spear, F.S. (1981) An experimental study of hornblende stability and compositional variation in amphibolite. *American Journal of Science* **281**: 697-734.

Spear, F.S. (1995) Metamorphic phase equilibria and pressure-temperature-time paths. Mineralogical Society of America Monograph, 799 pages.

Spear, F.S. & Cheney, J.T. (1989) A petrogeneitc grid for pelitic schists in the system SiO_2-Al_2O_3-FeO-MgO-K_2O-H_2O. *Contributions to Minerology and Petrology* **101**: 149-164.

Spear, F.S. & Kohn, M.J. (1996) Trace element zoning in garnet as a monitor of crustal melting. *Geology* **24**: 1099-1102.

Spooner, E.T.C. (1976) The strontium isotopic composition of seawater, and seawater-oceanic crust interaction. *Earth and Planetary Science Letters* **31**: 167-174.

Spry, P.G. (1987) The chemistry and origin of zincian spinel associated with the Aggeneys Cu-Pb-Zn-Ag deposits, Namaqualand, South Africa. *Mineralium Deposita* **22**: 262-268.

Spry, P.G. & Scott, S.D. (1986) The stability of zincian spinels in sulfide systems and their potential as exploration guides for metamorphosed massive sulphide deposits. *Economic Geology* **81**: 1446-1463.

Spry, P.G. & Wonder, J.D. (1989) Manganese-rich garnet rocks associated with the Broken Hill lead-zinc-silver deposit, New South Wales, Australia. *Canadian Mineralogist* **27**: 275-292.

Stanton, R.L. (1972) Ore Petrology. McGraw-Hill, New York.

Stålhös, G. (1969) Beskrivning till Stockholmtraktens berggrund. *Sveriges Geologiska Undersökning, Serie Af* **110**: 190 pages.

Stålhös, G. (1972) Beskrivning till berggrundskartbladen Uppsala SV och SO. *Sveriges Geologiska Undersökning*: Af 105-106.

Stumpfl, E.F. (1979) Manganese haloes surrounding metamorphic stratabound base metal deposits. *Mineralium Deposita* **14**: 207-217.

Sundblad, K. (1994) A genetic reinterpretation of the Falun and Åmmeberg ore types, Bergslagen, Sweden. *Mineralium Deposita* **29**: 170-170.

Sundblad, K., Ahl, M. & Schöberg, H. (1993) Age and geochemistry of granites associated with Mo-mineralisations in western Bergslagen, Sweden. *Precambrian Research* **64**: 319-335.

Sundius, N. (1923) Grythyttefältets geologi. (English summary). *Sveriges Geologische Undersökning, Serie C* **312**.

Symmes, G.H. & Ferry, J.M. (1992) The effect of whole-rock MnO content on the stability of garnet in pelitic schists during metamorphism. *Journal of Metamorphic Geology* **10**: 221-237.

Tilley, C.E. (1948) Earlier stages in the metamorphism of siliceous dolomites. *Mineralogical Magazine* **28**: 272-276.

Tilley, C.E. (1951) A note on the progressive metamorphism of siliceous limestones and dolomites. *Geological Magazine* **88**: 175-178.

Tucker, M.E. (1988) Techniques in Sedimentology. Blackwells, Oxford. 394pp.

Valley, J.W. (1986) Stable isotope geochemistry of metamorphic rocks. In: Valley, J.W., Taylor, H.P. (Jnr) & O'Neil, J.R. (eds) Stable isotopes in high temperature geological processes. *Mineralogical Society of America Reviews in Mineralogy* **16**: 445-489.

Valley, J.W. & O'Neil, J.R. (1984) Fluid heterogeneity during granulaite facies metamorphism in the Adirondacks: stable isotope evidence. *Contributions to Mineralogy and Petrology* **85**: 158-173.

Van der Velden, W., Baker, J., Maesschalk, S. & Van Meerten, T. (1982) Bimodal early Proterozoic volcanism in the Grythytte field and associated volcano-plutonic complexes, Bergslagen, central Swede. *Geologische Rundschau* **71**: 171-181.

Vaughan, D.J. (1976) Sedimentary geochemistry and mineralogy of the sulfides of lead, zinc, copper and iron and their occurrence in sedimentary ore deposits. In: Wolf, K.H. (ed) Handbook of stratabound and stratiform ore deposits; I. Principles and general studies; Vol. 2, Geochemical studies. Elsevier, p317-363.

Vaughan, D.J. & Craig, J.R. (1978) Mineral chemistry of metal sulfides. Cambridge University Press, 493pp.

Vaughan, D.J. & Craig, J.R. (1997) Sulfide ore mineral stabilities, morphologies and ore intergrowth textures. In: Barnes, H.L. (ed) Geochemistry of Hydrothermal Ore Deposits, 3rd Edition. John Wiley & Sons, 972 pages.

Veizer, J. (1990) Trace elements and isotopes in sedimentary carbonates. In: Reeder, R.J. (ed) Carbonates: Mineralogy and Chemistry. *Mineralogical Society of America Reviews in Mineralogy* **11**: 265-299.

Veizer, J. & Compston, W. (1974) $^{87}Sr/^{86}Sr$ composition of seawater during the Phanerozoic. *Geochemica et Cosmochemica Acta* **38**: 1461-1484.

Veizer, J. & Compston, W. (1976) $^{87}Sr/^{86}Sr$ in Precambrian carbonates as an index of crustal evolution. *Geochemica et Cosmochemica Acta* **40**: 905-94.

Veizer, J. & Hoefs, J. (1976) The nature of O^{18}/O^{16} and C^{13}/C^{12} secular trends in sedimentary carbonate rocks. *Geochemica et Cosmochemica Acta* **40**: 1387-1395.

Vivallo, W. (1984) The metamorphism of supracrustal rocks at Garpenberg, south-central Sweden. *Geologiska Foereningen i Stockholm Foerhandlingar* **106**: 257-267.

Vivallo, W. (1985) The geology and genesis of the Proterozoic massive sulphide deposit at Garpenberg, central Sweden. *Economic Geology* **80**: 17-32.

Vivallo, W. & Rickard, D. (1984) Early Proterozoic ensialic spreading-subsidence; evidence from the Garpenberg Enclave, central Sweden. *Precambrian Research* **26**: 203-221.

Vivallo, W. & Rickard, D. (1990) Genesis of an early Proterozoic zinc deposit in high grade metamorphic terrane, Saxberget, central Sweden. *Economic Geology* **85**: 714-736.

Walters, S.J. (1996) An overview of Broken Hill-type deposits. In: Pongratz, J. & Davidson, G.J. (eds) New Developments in Broken Hill-type Deposits. *CODES Special Publication No. 1*: 1-10.

Walters, S. & Bailey, A. (1998) Geology and mineralisation of the Cannington Ag-Pb-Zn deposit: an example of Broken Hill-type mineralisation in the Eastern Succession, Mount Isa inlier, Australia. *Economic Geology* **93**: 1307-1329.

Welin, E. (1987) The depositional evolution of the Svecofennian supracrustal sequence in Finland and Sweden. *Precambrian Research* **35**: 95-113.

Welin, E. & Stålhös, G. (1987) Maximum age of the synmetamorphic Svecokarelian fold phases in south central Sweden. *Geologiska Foereningen i Stockholm Foerhandlingar* **108**: 31-34.

Wickman, F.W. (1948) Isotope ratios – A clue to the age of certain marine sediments. *Journal of Geology* **56**: 61-66.

Will, T.M., Powell, R., Holland, T. & Guiraud, M. (1990) Calculated greenschist facies mineral equilibria in the system CaO-FeO-MgO-Al_2O_3-SiO_2-CO_2-H_2O. *Contributions to Mineralogy and Petrology* **104**: 353-368.

Williams, P.J. (1998) Metalliferous economic geology of the Mt Isa Eastern Succession, Queensland. *Australian Journal of Earth Sciences* **45**: 329-341.

Willis, I.L., Brown, R.E, Stroud, W.J. & Stevens, B.P.J. (1983) The early Proterozoic Willyama Supergroup: Stratigraphic subdivision and interpretation of high to low grade metamorphic rocks in the Broken Hill Block, New South Wales. *Journal of the Geological Society of Australia* **30**: 195-224.

Winkler, H.G.F. (1979) Petrogenesis of metamorphic rocks. Springer-Verlag, 348 pages.

Wintsch, R.P. (1985) The possible effects of deformation on chemical processes in metamorphic fault zones. In: Thompson, A.B. & Rubie, D.C. (eds) Metamorphic Reactions – Kinetics, Textures, and Deformation. Springer-Verlag, p251-268.

Woodsworth, G.J. (1977) Homogenization of zoned garnet from pelitic schists. *Canadian Mineralogist* **15**: 230-242.

Wright, J.V., Haydon, R.C. & McConachy, G.W. (1987) Sedimentary model for the giant Broken Hill Pb-Zn deposit, Australia. *Geology* **15**: 598-502.

Yang, P., Rivers, T. & Jackson, S. (1999) Crystal-chemical and thermal controls on trace-element partitioning between co-existing garnet and biotite in metamorphic rocks from western Labrador. *Canadian Mineralogist* **37**: 443-468.

Yardley, B.W.D. (1977) An empirical study of diffusion in garnet. *American Mineralogist* **62**: 793-800.

Zakrzewski, M.A. (1982) Geochemical facies model of ore formation in the Grythyttan-Hällefors area, Bergslagen, central Sweden. *Geologische Rundschau* **71**: 195-205.

APPENDICES

APPENDIX A

MINERAL ABBREVIATIONS

(after Kretz, 1983)

Ab	Albite
Act	Actinolite
Adr	Andradite
Alm	Almandine
Aln	Allanite
Als	Alumino-silicate
Am	Amphibole
An	Anorthite
And	Andalusite
Ank	Ankerite
Ap	Apatite
Apy	Arsenopyrite
Atg	Antigorite
Ath	Anthophyllite
Aug	Augite
Ax	Axinite
Bn	Bornite
Brc	Brucite
Brt	Barite
Bst	Bustamite
Bt	Biotite
Cal	Calcite
Cc	Chalcocite
Ccn	Cancrinite
Cpy	Chalcopyrite
Chl	Chlorite
Chn	Chondrodite
Chu	Clinohumite
Cld	Chloritoid
Crn	Corundum
Cum	Cummingtonite
Czs	Clinozoisite
Di	Diopside
Dol	Dolomite
En	Enstatite
Ep	Epidote
Fac	Ferroactinolite
Fo	Forsterite
Ged	Gedrite
Gh	Gehlenite
Gal	Galena
Grs	Grossular
Grt	Garnet
Gru	Grunerite
Hbl	Hornblende
Hc	Hercynite
Hd	Hedenbergite
Hu	Humite
Ilm	Ilmenite
Kfs	K-feldspar
Ky	Kyanite
Mgt	Magnetite
Mgs	Magnesite
Mnz	Monazite
Mrg	Margarite
Ms	Muscovite
Mtc	Monticellite
Ol	Olivine
Opx	Orthopyroxene
Or	Orthoclase
Per	Periclase
Phl	Phlogopite
Pl	Plagioclase
Po	Pyrrhotite
Prp	Pyrope
Py	Pyrite
Qtz	Quartz
Scp	Scapolite
Ser	Sericite
Sil	Sillimanite
Sph	Sphalerite
Spl	Spinel
Spn	Sphene
Sps	Spessartine
Serp	Serpentine
St	Staurolite
Stb	Stilbite
Tlc	Talc
Tr	Tremolite
Tur	Tourmaline
Ves	Vesuvianite
Wo	Wollastonite
Zs	Zoisite
Zrn	Zircon

APPENDIX B

SAMPLE LOCATIONS

Map B1 shows the locations of district metacarbonate samples taken for this study. The map is reproduced from the Swedish Geological Survey 1:50 000 scale geological map, sheet Af 165 (9F Finspång).

The locations of other samples taken for this research are detailed in Appendix C (drill core samples) and in Table B1 (UZ samples from underground exposures).

Sample	*Location*	*Description*
UZ 1	650 level, P1 to Burkland section	Foliated, biotite-rich migmatite
UZ 2	working from western end of drive to	Granodiorite from migmatite melt
UZ 3	eastern end (i.e., up structural section)	Mafic inclusion from granodiorite melt
UZ 4	"	Migmatite with a more felsic composition
UZ 5	"	Pyrrhotite horizon within migmatite
UZ 6	"	Very dark biotite-rich rock with large fsp blasts
UZ 7	"	Mafic dyke
UZ 8	"	Banded calc-silicate containing garnets
UZ 9	"	Marble containing biotite bands
UZ 10	"	Diopside vein
UZ 11	"	Metaquartzite
UZ 12	"	Garnet-bearing pegmatite
UZ 13	"	"Quartzitic leptite" with calc-silicate bands
UZ 14	"	Fine grained banded "leptite"
UZ 15	500 level, P1 through to ore body.	Medium grained migmatitic gneiss
UZ 16	"	Granodiorite from migmatite melt
UZ 17	"	Gneiss
UZ 18	"	Felsic dyke within calc-silicates
UZ 19	"	Western margin of dyke with calc-silicates
UZ 20	"	Calc-silicate material (banded)
UZ 21	"	Massive quartzitic rock with Po along fractures
UZ 22	"	Garnet-rich layer within calc-silicate bands
UZ 23	"	Siliceous, banded leptite
UZ 24	"	Folded banded leptite material
UZ 25	"	Garnet-bearing quartzite
UZ 26	"	Margin of granitic dyke
UZ 27	"	Centre of granitic dyke
UZ 28	"	Edge of calc-silicate unit

Table B1: Locations and description of underground samples (UZ series) taken for this study.

Map B1: Locations of regional metacarbonate (ZR series) samples

(Map reproduced from the SGU 1:50 000 Finspång geological map)

Sample	*Location*	*Description*
UZ 30	450 level, P1 through to main drive	Migmatitic leptite with areas of melt
UZ 31	"	Green diopside skarn
UZ 32	"	Schistose leptite
UZ 33	"	Biotite rich leptitic rock, crystalline in places
UZ 34	"	Pyrrhotite horizon within leptitic unit
UZ 35	"	Skarn banded leptite/banded calc-silicate
UZ 36	"	Bt/fsp rock with anastomosing texture
UZ 37	350 level, Burkland drive	White "leptite" with darker ?bt porphyroblasts
UZ 38	800 level (950), stope 260	Banded calc-silicate within ore zone
UZ 39	"	Banded calc-silicate within ore zone
UZ 40	"	Granitic pegmatite in ore zone
UZ 41	"	Calc-silicate material in ore zone
UZ 42	"	Main ore zone - Zn/Pb ore
UZ 43	"	NO SAMPLE!
UZ 44	"	Garnet veining within Ca-Si in ore zone
UZ 45	"	Pyrrhotite-rich calc-silicate material
UZ 46	"	Main ore zone - Zn/Pb ore
UZ 47	800 level exploration drive into HW	Coarse grained dolomitic marble
UZ 48	"	Dark siliceous material forming fracture infill
UZ 49	"	Epidote infilling cracks in marble
UZ 50	"	Dark, fine gr. siliceous boudin within marble
UZ 51	"	Dark, fine gr. siliceous boudin within marble
UZ 52	"	Ca-Si rim around dark siliceous boudin
UZ 53	"	More calcitic marble with brown laminae
UZ 54	"	Biotite rich layers within 'leopard' marble
UZ 55	"	Finely laminated white and brown marble
UZ 56	"	Dark, fine gr. bands parallel to marble foliation
UZ 57	"	Calc-silicate rim around dyke
UZ 58	"	Marble adjacent to dyke intrusion
UZ 59	"	Epidote developed in marble near shear
UZ 60	"	Green mineral developed alongside dykes
UZ 61	"	Sample of dark, fine grained dyke material
UZ 62	"	Massive marble with blotchy calc-silicate
UZ 63	"	Banded, calc-silicate rich "leptite"
UZ 64	"	Darker, more biotite-rich "leptite" (schist)
UZ 65	"	Biotite-rich, fine grained foliated marble
UZ 66	"	Calc-silicate from boundary with "leptite"
UZ 67	"	Dark, fine grained dyke material with garnets
UZ 68	"	Mafic, biotite-rich inclusion within marble
UZ 69	"	Purple amphoedolite within qtz vein in marble
UZ 70	"	Grey siliceous alteration material - ?dyke??
UZ 71	"	Biotite-rich schist with white fsp pblasts
UZ 72	"	Granodiorite from migmatite melt
UZ 73	"	Thin calc-silicate vein within marble
UZ 74	"	Dark, slightly banded calc-silicate material
UZ 75	"	Amphoedolite within quartz vein in marble

Table B1 (cont.): Locations and description of underground samples (UZ series) taken for this study.

APPENDIX C

DRILL CORE LOGS

Detailed drill core logging was carried out on selected cores whilst on fieldwork at Zinkgruvan. Drill cores are graphically represented here, according to the key below. Positions of samples taken for this study are marked in red; older sample positions are marked in purple.

	Metavolcanic rock	ZnS	Disseminated sphalerite
	K-altered metavolcanic rock	PbS	Disseminated galena
	Metacarbonate rock	Cu Cpy	Disseminated chalcopyrite
	Metaquartzite	FeS Po	Disseminated pyrrhotite
	Calc-silicate skarn	W	Wollastonite
	Fe-rich skarn	G	Garnet
	Amphibolite	Sil	Sillimanite
	Pegmatite	QV	Quartz vein
	Granodiorite	~ ~ ~	Gneissic texture
	Massive Zn-Pb mineralisation	1557/09	Sample number (this study)
= = =	Calc-silicate layers	454/16	Sample number (mine sample)
= = =	Quartzitic layers		

DDH 451 DRILL CORE LOG AND SAMPLE POSITIONS
250m level, Nygruvan

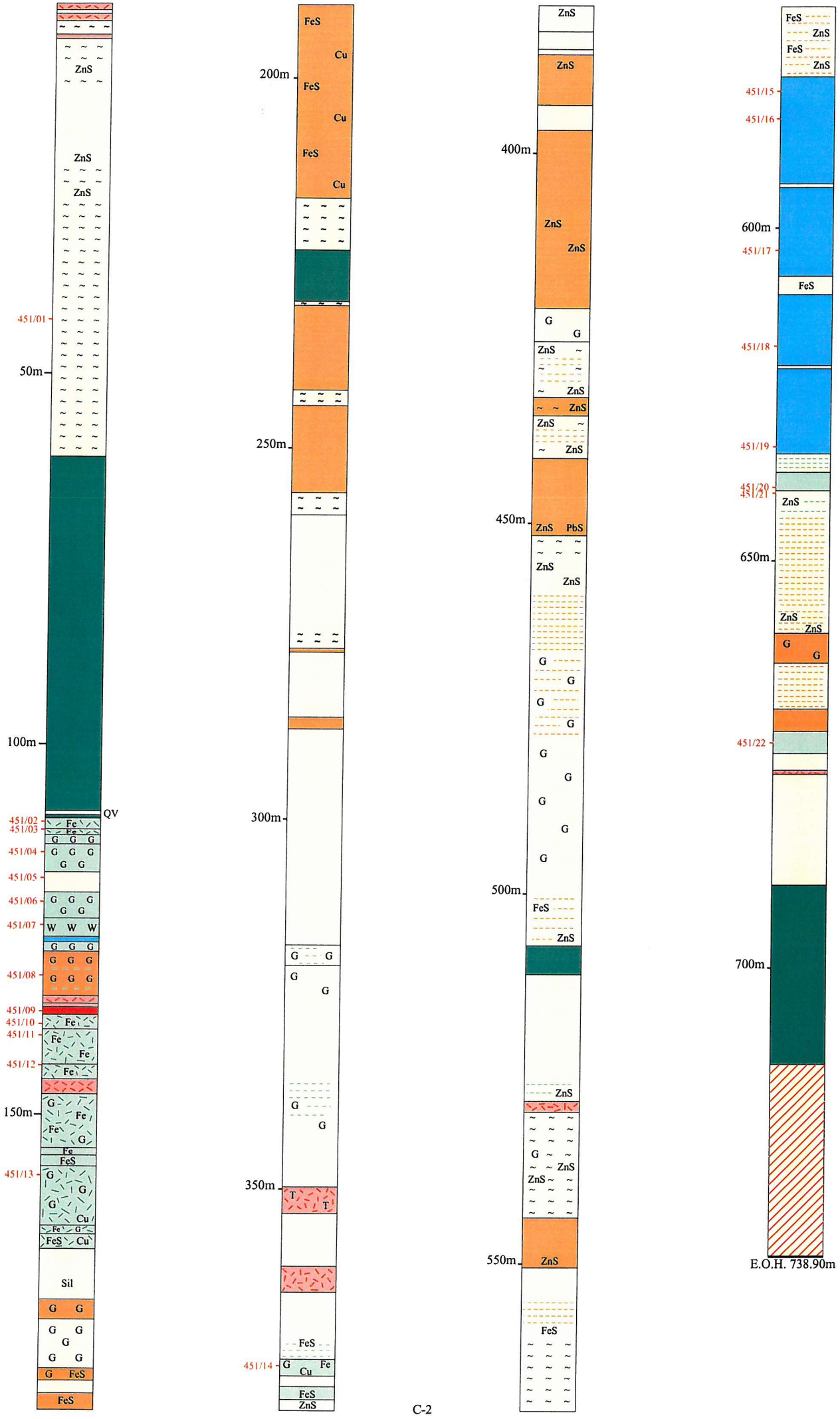

DDH 454 DRILL CORE LOG AND SAMPLE POSITIONS
250m level, Nygruvan

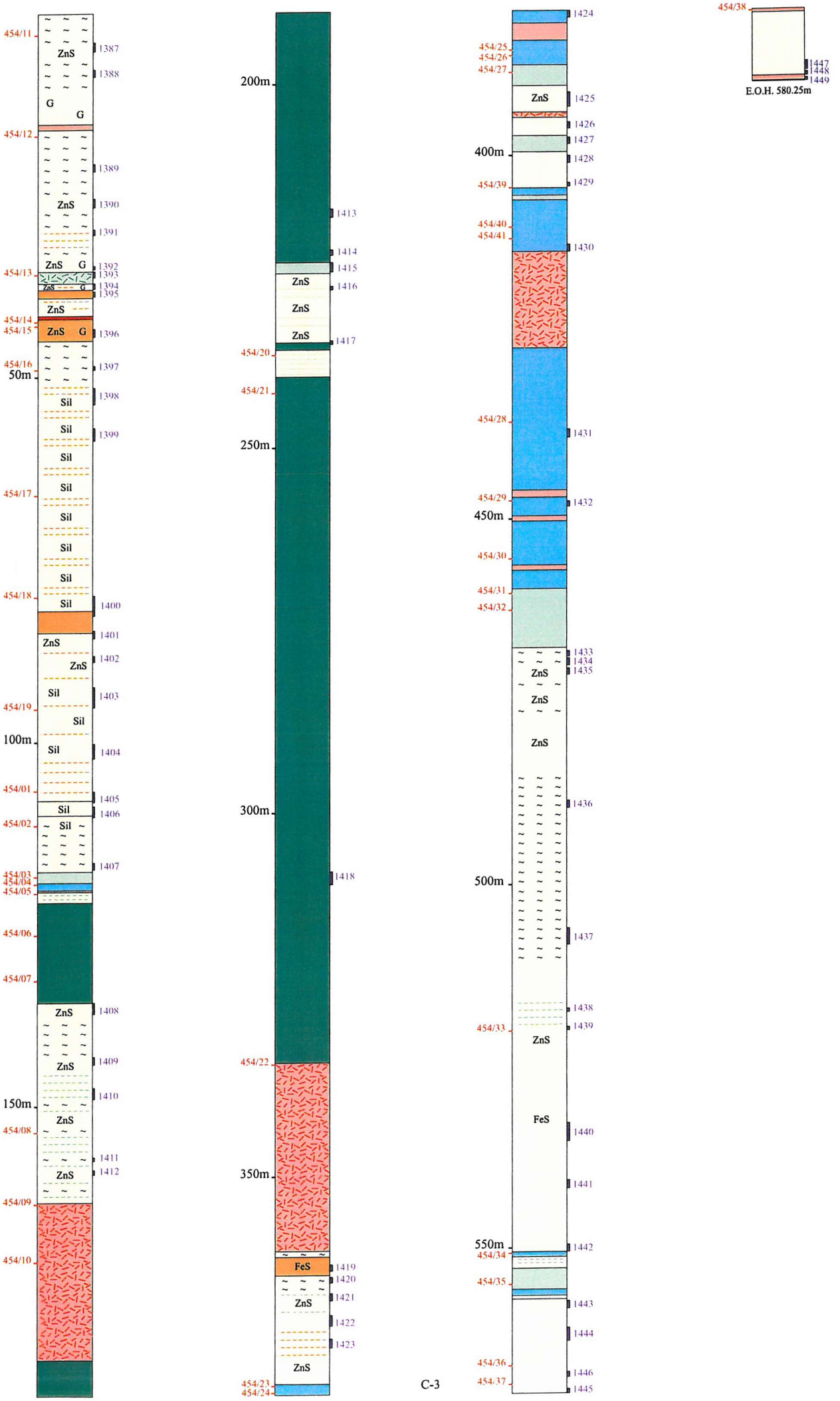

DDH 555 DRILL CORE LOG AND SAMPLE POSITIONS
250m level, Nygruvan

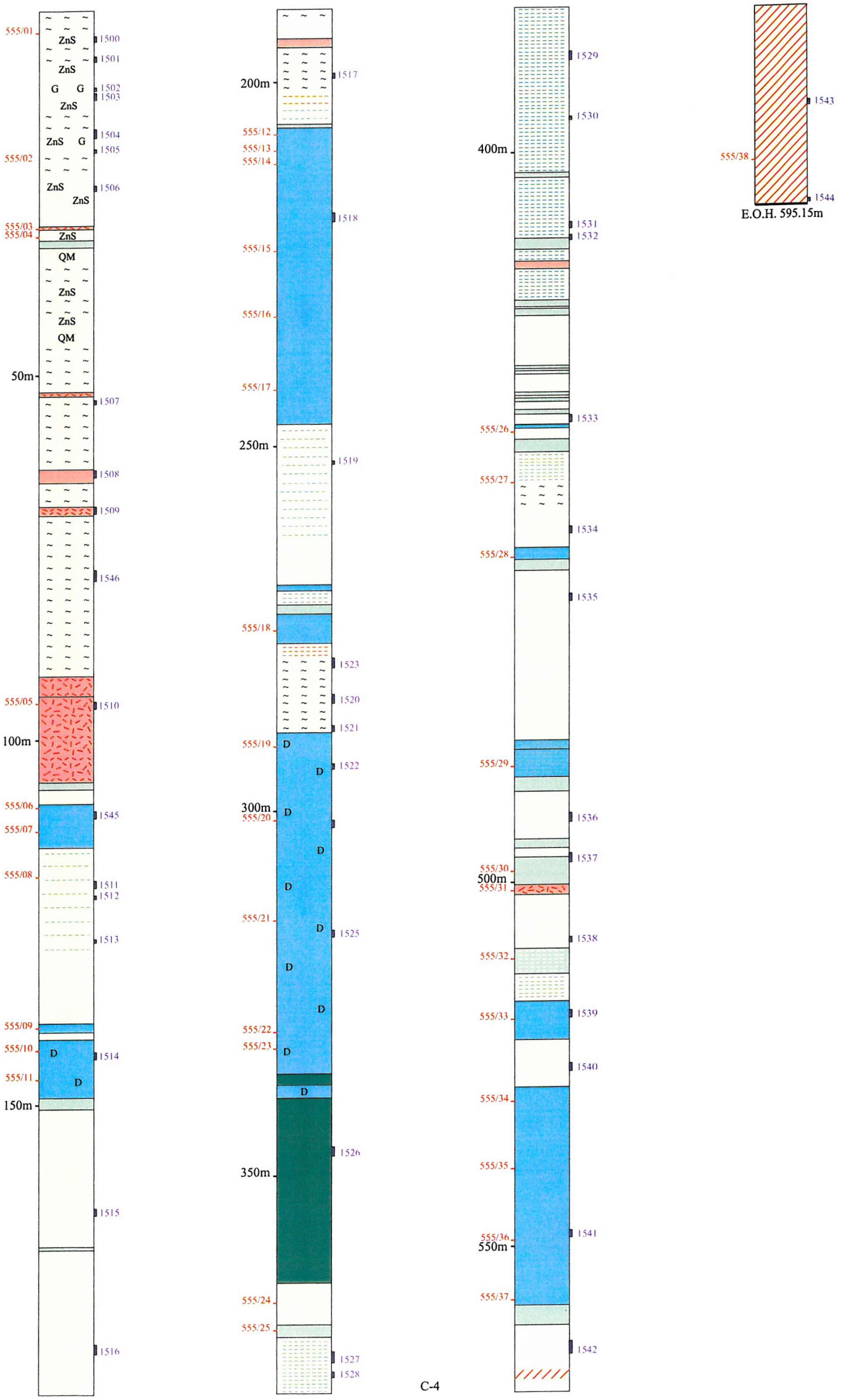

DDH 670 DRILL CORE LOG AND SAMPLE POSITIONS
800m level, Nygruvan orebody

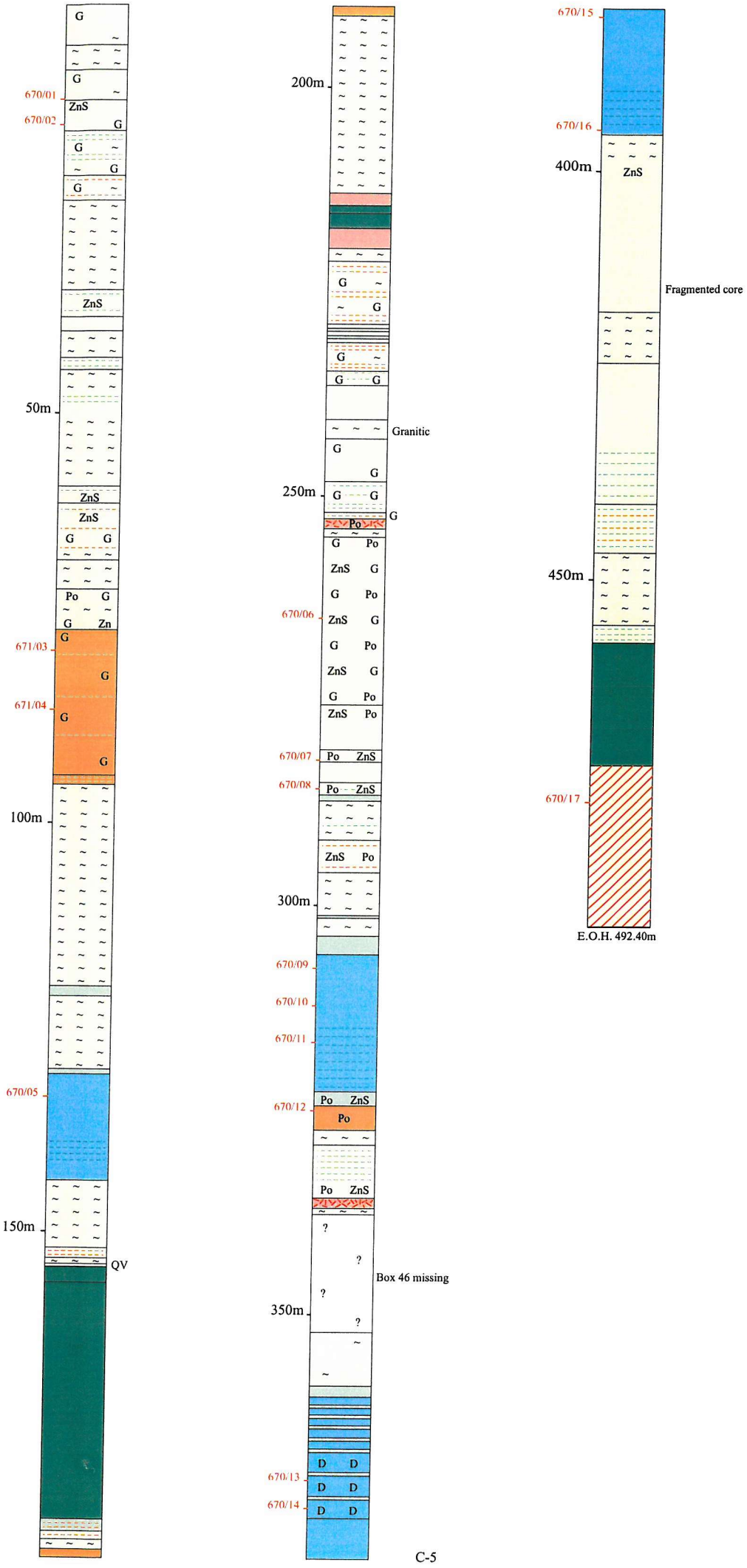

DDH 671 DRILL CORE LOG AND SAMPLE POSITIONS
800m level, Nygruvan orebody

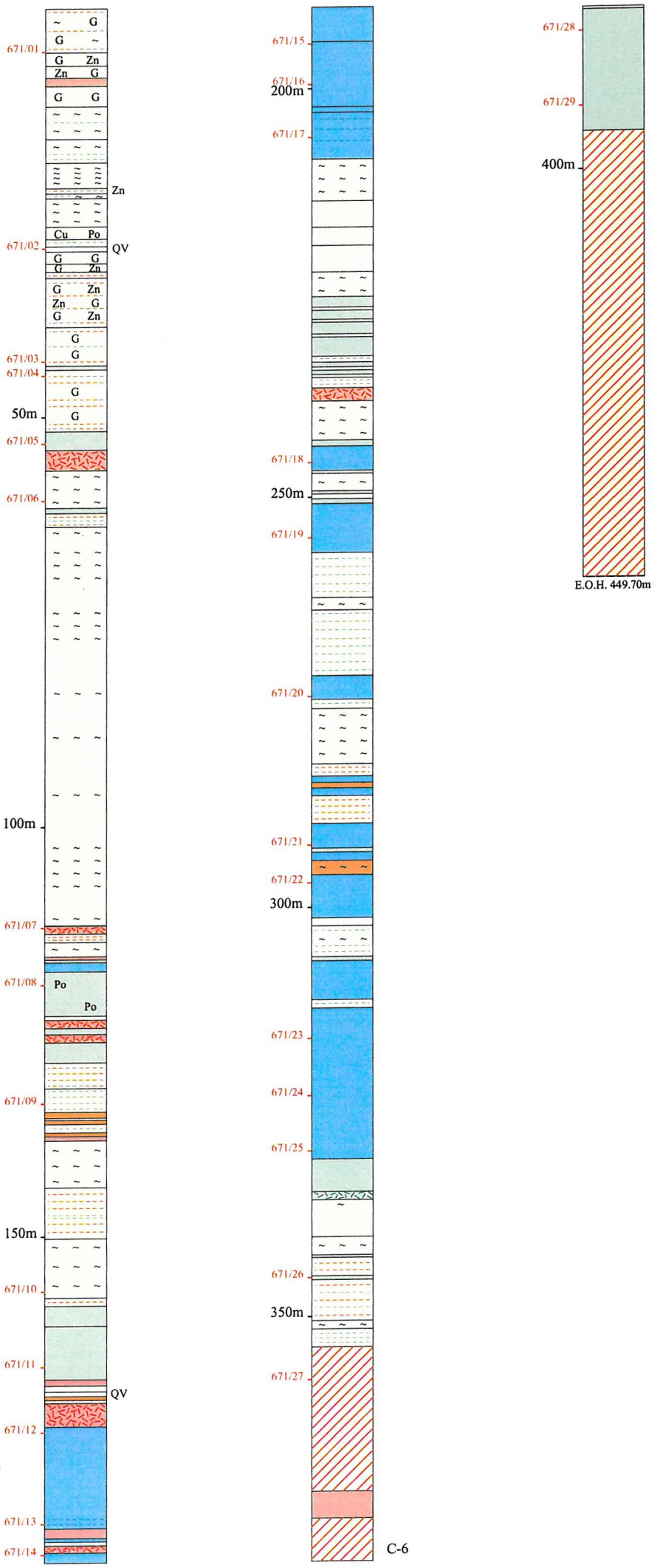

DDH 1557 DRILL CORE LOG AND SAMPLE POSITIONS
800m level, Burkland East (Cu orebody)

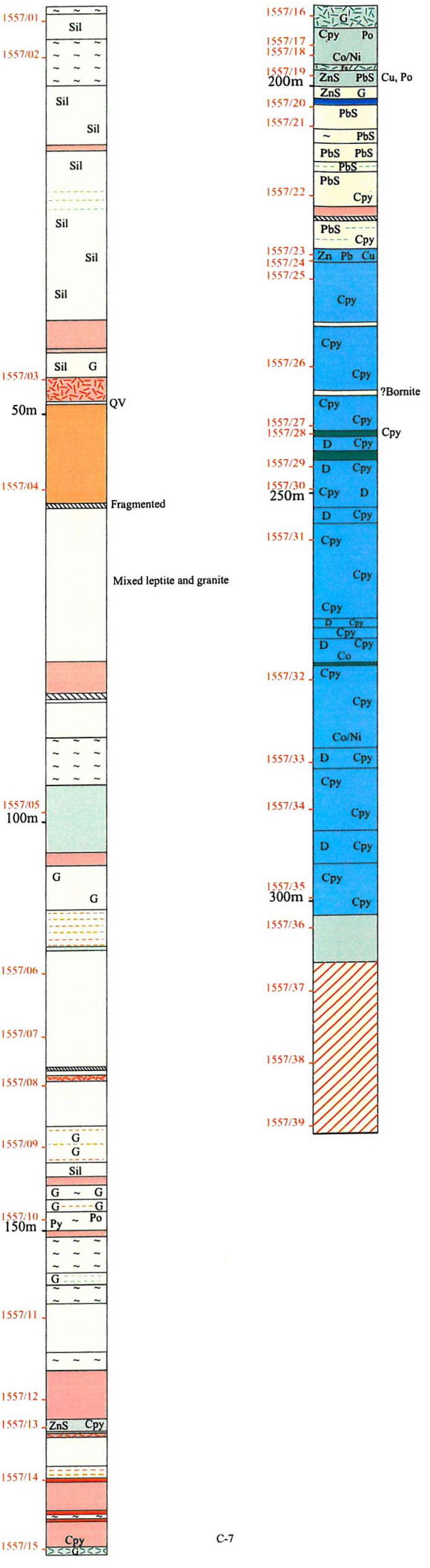

APPENDIX D

PETROGRAPHIC DESCRIPTION

Thin section work was carried out using a transmitted polarised light petrological microscope with standard 30μm thin sections and polished thin sections. Most thin sections were prepared at the School of Ocean & Earth Science (SOES), but some were contributed by the mine and from other studies. Carbonate samples prepared at SOES were stained to distinguish between calcite, ferroan calcite, dolomite and ferroan dolomite (Table D1).
It is unfeasable to include a complete set of all thin section descriptions (>400) made during the course of this research. Instead, a summary of the estimated modal percentages of constituent minerals for each sample examined is provided (Table D2).

Carbonate staining

Carbonate-bearing samples (marbles and calc-silicate skarns) were partially (half slide) etched and stained prior to covering using the method described by Dickson (1966).
Etching was carried out using 1.5% hydrochloric acid solution, in which the thin section was partially immersed for 10 seconds at room temperature. Following this, a combined stain of Alizarin Red S and potassium ferrocyanide was applied. The stain was freshly prepared for each batch of thin sections through the following method:

1) 0.2g Alizarin Red S dissolved in 100ml of 1.5% HCl solution.
2) 2g potassium ferrocyanide dissolved in 100ml of 1.5% HCl solution.
3) Mix two solutions together at a ratio of 3 parts Alizarin Red S solution to 2 parts potassium ferrocyanide solution.

Thin sections were partially immersed in the mixed stain solution for 30 seconds, then washed in distilled water and dried before being covered.

Carbonate staining using the combined stain produces the following results:

Mineral	*Etching effect*	*Stain colour with Alizarin Red S*	*Stain colour with potassium ferrocyanide*	*Combined result*
Calcite (non-ferroan)	Considerable (relief reduced)	Pink to red-brown	None	Pink to red-brown
Calcite (ferroan)	Considerable (relief reduced)	Pink to red-brown	Pale to deep blue depending on Fe content	Mauve to blue
Dolomite (non-ferroan)	Negligible (relief maintained)	None	None	Colourless
Dolomite (ferroan)	Negligible (relief maintained)	None	Very pale blue	Very pale blue (turquoise-green in thin section)

Table D1: Effects of different staining processes on carbonate minerals. After Tucker (1988).

Appendix D

Table D2: Summary of thin section analyses

Sample	Qtz	Kfs	Pl	Bt	Sil	And	St	Act	Ms	Ser	Cht	Grt	Cal	Dol	Di	Wo	Fo	Serp	Sap	Phl	Chl	Zs	Tr	Tlc	Spn	Spl	Opq	?
UZ1	55		25	20																							<1	
UZ2	50	5	40	5								<1																
UZ3	30		19	30				15		5																	1	
UZ4	33	25	20	15						5		1															1	
UZ5	*	*	*	*																					*		*	
UZ6	25	10	20	25	15				5																			
UZ7	10		25	19				45																			1	
UZ8	*											*	*		*							*			*		*	
UZ9										*			*		*					*	*							
UZ10	*	*	*	*								*			*								*					
UZ11	50	32		10						5	1	2															<1	
UZ12	33	30		10	25							1															1	
UZ13	60		5	15								20																
UZ14	74	5										10	1										5				5	
UZ15	25	15	15	30	15																							
UZ16	30	40	10	10																							10	
UZ17	20	34		25	15		5																				1	
UZ18	20		40	5				35																				
UZ19	*		*	*				*hbl		*												* Ep						
UZ20	*	*							*	*			*		*	*												
UZ21	50	15		15					15																		5	
UZ22		*	*							*			*									*	*					
UZ23	54		5	10						10		15											1				5	
UZ24	55	10		20								10															5	
UZ25	*	*		*	*	*				*		*															*	
UZ26	60	20		5	10	<<1			5																			
UZ27	50	20		15	10				5																			
UZ28	45	15	10	15						10																	5	
UZ30	*	*	*	*																							*	
UZ31				*									*		*							*	*				*	

** Denotes mineral present but quantities not estimated*

Appendix D

Table D2: Summary of thin section analyses

Sample	Qtz	Kfs	Pl	Bt	Sil	And	St	Act	Ms	Ser	Cht	Grt	Cal	Dol	Di	Wo	Fo	Serp	Sap	Phl	Chl	Zs	Tr	Tlc	Spn	Spl	Opq	?
UZ32	25	40	25	9																							1	
UZ33	*		*	*								*															*	
UZ34	*		*	*	*																						*	
UZ35	*		*	*	*					*																	*	
UZ36	40	30	5	15								10																
UZ37	65	33		2																								
UZ38	*	*	*	*	*							*	*		*							*	*			*		
UZ39	25	10										15	10		25							10			5			
UZ40	50	40		5							5																	
UZ41	*					*						*	*		*	*									*			
UZ42	*		*	*								*											*				*	
UZ44	*		*	*						*		*	*														*	
UZ45				*								*										*	*				*	
UZ46	*		*									*	*		*												*	
UZ47													5	80			10			3						2		
UZ52													40	35				15		10			<1					
UZ53													<1	80			12			8						<1		
UZ54													50	20			9	25		5							1	
UZ58													15	65			10	9			<1					1	<1	
UZ59													25	20			18	25		10	2							
451/01	60	15			10				10			5																
451/03				*				*				*	*										*		*		*	
451/04	40											3	2		2								30					
451/05	60	5										4	1		30													
451/06	10	10	5										2		60								12		1			
451/07	15	20										3	2		45	15												
451/08	25	8										5	2		43							10	5		2			
451/10				*								*			*Cum										*		*	
451/11				*				*					*		*												*	
451/12																												
451/13																												
451/14	25			10											40							5	5				15	

** Denotes mineral present but quantities not estimated*

Appendix D

Table D2: Summary of thin section analyses

Sample	Qtz	Kfs	Pl	Bt	Sil	And	St	Act	Ms	Ser	Cht	Grt	Cal	Dol	Di	Wo	Fo	Serp	Sap	Phl	Chl	Zs	Tr	Tlc	Spn	Spl	Opq	?
451/15	10	15											40	5	25												5	
451/16	15	15											40	5	25													
451/17	25		5										35		35													
451/18																												
451/19	10	5										5	25		15	20												
451/20	15	10													30					10		5	25				5	
451/21																												
451/22																												
555/01																												
555/02	55	25		10								7															3	
555/03																												
555/04																												
555/05	50	25		18	2				5																			
555/06													30	5				40		15							10	
555/07													45	5			5		15	20							10	
555/08																												
555/09													30		20			30		10							10	
555/10													5	60				25									10	
555/11													20	20	15			20		20							5	
555/12													10	60				20		5							5	
555/13													20	40				30		10								
555/14													50	5				25		18							2	
555/15													10	60				20		5							5	
555/16													5	60				20		5							10	
555/17													5	55				25		10							5	
555/18	10												25		20	10				25			10					
555/19													5	60				22		1						3	9	
555/20													3	73				15		2						<1	7	
555/21														75				15		5						<1	5	
555/22													40	25				30		<1							5	
555/23													5	85				5									5	
555/24	15	5													25							10	45					

** Denotes mineral present but quantities not estimated*

Appendix D

Table D2: Summary of thin section analyses

Sample	Qtz	Kfs	Pl	Bt	Sil	And	St	Act	Ms	Ser	Cht	Grt	Cal	Dol	Di	Wo	Fo	Serp	Sap	Phl	Chl	Zs	Tr	Tlc	Spn	Spl	Opq	?
555/25																												
555/26													25	10				40		15							10	
555/27																												
555/28													5	35				40		15							5	
555/29													45	10	15			2		15							1	12
555/30												*	*		*					*		*						
555/31	*	*	*										*										*		*		*	
555/32	*												*		*					*		*					*	
555/33														35				30									5	
555/34																												
555/35													35	10				30		20							5	
555/36	73	10																				15		2				
454/01	15			30	35				15																		5	
454/02	5												40					25	10	15							5	
454/02	40			25	30																						5	
454/03	*		*												*					*		*						
454/04	5												30		5			30	10	15							5	
454/05	40		5							10		30	5		10												<1	
454/06	*		*	*											*								*					
454/07	*		*	*																			*					
454/08	50		15									5			10							5			5		10	
454/09	40	50		3					7																			
454/10	75		5	10								5															5	
454/11	40	30		20	8							2																
454/12	*	*	*	*	*							*																
454/13				*								*			*							*					*	
454/14	55			15								30															<1	
454/16	45			20	35																							
454/17	60		3	15	2							15															5	
454/18	50			25	5							10										<1					10	
454/19	50			25	20																						5	
454/23	15	10																		20			50				5	

* *Denotes mineral present but quantities not estimated*

Appendix D

Table D2: Summary of thin section analyses

Sample	Qtz	Kfs	Pl	Bt	Sil	And	St	Act	Ms	Ser	Cht	Grt	Cal	Dol	Di	Wo	Fo	Serp	Sap	Phl	Chl	Zs	Tr	Tlc	Spn	Spl	Opq	?
454/24													40		30					30								
454/25													10	40	5			5		15			20				5	
454/26													*	*			*	*	*	*			*					
454/27	15	13													40								30		2			
454/28																												
454/29	25	20											25		30													
454/30	*	*										*			*	*									*			
454/31	30	10										3	10		35	10									2			
454/32	39														60												1	
454/34														50	25					25								
454/35													40					30		20							10	
454/36	40	50		8																					2			
454/37	20	25										25	15		15													
454/38	40	50		5																			5					
454/39													35		15					20			25				5	
454/40													40		15			25		10							10	
454/41													40		20			25		10							5	
ZR01	50									5										15			30					
ZR02													50		1			20			24						5	
ZR03	90												7										3					
ZR04	8												85		7													
ZR05	10	5											70		8						3							4
ZR06														55				20		15						5	5	
ZR08													35	10				35		10							10	
ZR09	25												45		15								15					
ZR10	<1													80	10					10								
ZR11													40					35		7.5	7.5						10	
ZR12													63							15			20				2	
ZR13													60		<1			25		10							5	
ZR17	10	2											10	45	33													
ZR19													30	20				20		5	10					5	10	
ZR20	10	15										20	35		15												5	

** Denotes mineral present but quantities not estimated*

Appendix D

Table D2: Summary of thin section analyses

Sample	Qtz	Kfs	Pl	Bt	Sil	And	St	Act	Ms	Ser	Cht	Grt	Cal	Dol	Di	Wo	Fo	Serp	Sap	Phl	Chl	Zs	Tr	Tlc	Spn	Spl	Opq	?
ZR21													70					20								10		
ZR22													30	20				30		15							5	
1557/01	25	20		50	5																							
1557/02	*	*	*	*					*			*																
1557/03	*	*	*							*																		
1557/04			25					60			5											5					5	
1557/06	35	20		30	15																						<1	
1557/07	25	35		25	15																							
1557/08	40		43	15	2																							
1557/09	30		15	25								30																
1557/10	40		15	30								5															10	
1557/11	40		15									25											15				5	
1557/12	35	38	15	10																							2	
1557/13	15														35								20				25	5
1557/14	*	*	*										*		*							*	*				*	
1557/15				*								*	*		*						*		*					
1557/16	40														60													
1557/17	15											2.5	5		50								2.5			25		
1557/18													*	*			*		*	*							*	
1557/19												*	*		*					*			*				*	
1557/20	50			7																5							38	
1557/21	30	30		25																10							5	
1557/22	*	*		*																							*	
1557/23															60					5						10	25	
1557/24												25			10					35			10				20	
1557/25				40										50													10	
1557/26													15	55				20								1	10	
1557/27													10	60				15		<1						5	10	
1557/28	30			35										15	20													
1557/29													20	50				18		5							7	
1557/30													10	60				8		7							15	
1557/31													45	15				20		5							15	

* *Denotes mineral present but quantities not estimated*

Appendix D

Table D2: Summary of thin section analyses

Sample	Qtz	Kfs	Pl	Bt	Sil	And	St	Act	Ms	Ser	Cht	Grt	Cal	Dol	Di	Wo	Fo	Serp	Sap	Phl	Chl	Zs	Tr	Tlc	Spn	Spl	Opq	?
1557/32													30	20				25		5							20	
1557/33													10	55				20		5							10	
1557/34													25	30				25		5							15	
1557/35														75				10		5							10	
1557/36													5	15	50					30								
1557/36	50	30		15											5													
1557/37	45	40		2																			5		3		5	
1557/38	*	*		*																			*		*		*	
1557/39	*	*		*												*							*		*			
670/01	45			5				15				10													25			
670/02	40	5										20			20							5			15			
670/03	*			*								*											*					
670/04				40								50													5		5	
670/05													50				30			10						<1	10	
670/06	*			*						*		*															*	
670/07	30	30		15				5																	15		5	
670/08	30	10													40								15					5
670/09	50	<1	5												45								<1					
670/10													30		40					25							5	
670/11	5	5											15		55	10				10								
670/12	2												2		83	4				5			2					
670/13			5										20	25	45	5						<1			<1			
670/14	5	5											30	25	20					15								
670/15	30												20		15	35												
672/01	50											15			10								10			5		10
672/02	35	25		20	15				5																			
672/03	25	5		10								30													25		5	
672/04	*	*		*	*				*																	*		
672/05	25	15		25	20					12																	3	
672/06	*	*		*						*											*							
672/07	40			5				45*				10															<1	
672/08	50											10			35								5				<1	

** Denotes mineral present but quantities not estimated*

Appendix D

Table D2: Summary of thin section analyses

Sample	Qtz	Kfs	Pl	Bt	Sil	And	St	Act	Ms	Ser	Cht	Grt	Cal	Dol	Di	Wo	Fo	Serp	Sap	Phl	Chl	Zs	Tr	Tlc	Spn	Spl	Opq	?
672/09	25	40						20				9															5	
672/10	69			10								15			1												5	
672/11	*		*	*								*															*	
672/12	30			25								40															5	
672/13	*	*		*								*															*	
672/14	45	15		20								20															<1	
672/15	25			25							5	45																
640/01	*	*		*								*			*							*	*					
640/02	*	*										*			*												*	
640/03															*								*				*	
640/04	*																					*					*	
640/05	*																					*					*	
640/06	*	*										*											*		*		*	
640/07		*		*								*	*		*							*					*	
640/08	*	*										*			*												*	
648/01	*	*										*	*		*							*	*				*	
648/02	*	*		*								*				*												
648/03	15	5										10	50		15	5												
648/04	9	20											55		15							1						
648/05	*	*										*			*								*					
648/06	*												*	*							*						*	
648/07												*	*		*								*					
648/08	*																						*				*	
648/09	25	20	30	25																								
648/10	15	8										5			60							8			2			2
649/01	50	5	5									8			5							5	22					
649/02	*	*										*	*		*							*	*		*			
649/03	45			25				10				20															2	
649/04	10	50										10			10	20												
649/05	*	*											*		*							*			*			
649/06	*	*										*			*	*												Ves
649/07	*	*													*							*			*		*	

* *Denotes mineral present but quantities not estimated*

Appendix D

Table D2: Summary of thin section analyses

Sample	Qtz	Kfs	Pl	Bt	Sil	And	St	Act	Ms	Ser	Cht	Grt	Cal	Dol	Di	Wo	Fo	Serp	Sap	Phl	Chl	Zs	Tr	Tlc	Spn	Spl	Opq	?
649/08	15	65	20					<1																				
649/09	10											15			40								30				5	
649/10													60	5			5	5	10	1							14	
649/12	65			30						5																	<1	
649/13	*											*	*														*	
231/2.40	40		15	10	5				2	8																	20	
231/22.0	35		10									5	<1		25							15					10	
231/41.60	45	15	10	15																							15	
231/57.60	*	*										*	*		*	*												
231/58.4	15											20	30		15	20												
231/90.90	*		*									*			*	*									*			
231/92.50	15	10	9									1	45		20													
231/102.0	40		8	25						15		10															2	
231/111.50	65	<1	10	20	5																							
231/140.75	75			10	15																							
231/150.85	50		15	25	10																							
231/157.70	65		15	12	8																							
231/166.60	45	2	5									30											10				8	
231/171.40	65	2	2	10						5		10	1														5	
231/176.55	60	15	5							5		5	1									4					5	
231/183.20	*	*										*	*		*	*												
231/185.10	70	15						5				5															5	
231/194.20	*	*	*										*		*							*						
231/200.40	75	10		10								5															<1	
231/204.35	*	*										*	*		*	*						*					*	
231/205.10	*	*										*	*		*	*											*	
231/232.10	40	20	14	25								5															1	
231/254.20	45	20		20	10																						<1	
231-1	40		25	20																					<1		15	
231-3	*	*	*	*																								Tour
231-6A	*	*										*	*		*	*						*			*			
231-7		15										10	20		25	30												

* *Denotes mineral present but quantities not estimated*

Appendix D

Table D2: Summary of thin section analyses

Sample	Qtz	Kfs	Pl	Bt	Sil	And	St	Act	Ms	Ser	Cht	Grt	Cal	Dol	Di	Wo	Fo	Serp	Sap	Phl	Chl	Zs	Tr	Tlc	Spn	Spl	Opq	?
231-8	*	*		*									*		*					*			*					Ves
231-10	35		15	15	20					15																		
231-11	55		5	30	10																							
231-13	45		5	15								15	1		4								15					
231-15	30	25									10	18											17				9	1
231-16	*	*	*									*	*		*							*			*			
231-17	39									10		10	5									15	5		15			1
231-18	35		5	2						5		15										5	15		8		10	
1270/478.2													35	5	5		10	20		10	5						10	Chu
1270/566.8													40	4			3	22		15						7	1	8 Chu
898-1	45	40		5							3																7	
898-3	40	25		10		20			5																			
898-4	45	25		15					5																			10
898-7	40	35		20		<1																					5	
898-8	65			20						15																		
898-9		*	*										*		*							*			*		*	
898-10															75								10					15 Ba
898-11											5		1		75					<1		5	9					5
898-14													1		77					2	5	5	10					
898-15										2					58						5	10	25					
898-16	40	15		25						15																		5
898-17	*	*		*					*	*					*								*		*			
898-18	15			15						20					35								15					
898-20	10	5													50								35					
898-22	45		5	38									2										10					
898-23			*										*		*					*			*					
898-24	60		10	20																			10					
898-26	68	10		20	2																							
898-27A			1							14					40						10		15					20
898-27B	50			20							<1				15								15					
898-29	85			15					<1			<1															<1	
898-30A	*											*	*		*	*						*						

** Denotes mineral present but quantities not estimated*

Appendix D

Table D2: Summary of thin section analyses

Sample	Qtz	Kfs	Pl	Bt	Sil	And	St	Act	Ms	Ser	Cht	Grt	Cal	Dol	Di	Wo	Fo	Serp	Sap	Phl	Chl	Zs	Tr	Tlc	Spn	Spl	Opq	?
898-30B	59		10									15	1		10							5						
898-31	79			10								8													1		2	
898-32	44	30	10	15																							1	
898-33	<1	5													95													
898-34	5	5	1										<1	60								1	25					3
898-35	*			*						*											*		*				*	
671-19	60			15						10		10															5	
671-20	35	43	15	2					2																			
671-21	33			20						10		25													6		6	
671-22	<1												1		84								15					
671-23	30	35		20	15																							
671-25													2		85								3				10	
671-27	25	35		20	15					5																		
671-29	15	25													25								35					
671-30	25	30		15											10								20					
671-31	25	40		20	15																							
671-32													*		*					*		*	*		*			
671-34										*			*		*					*		*			*			
671-36	40	40		15	5																							
671-37	*		*	*						*					*								*					
671-38															85								15					
671-40	35	40		10						8			2								1	1	3					
ZV0867	20	25		25					30?																			
ZV1063	*								*												*	*	*				*	
ZV1086	15		10	20		30			10	15																		
ZV1093													*	*	*					*								
ZV1093	5												45		30					20								
ZV1094													*		*								*					
ZV1095	20	25		30					<1																			22 alt
ZV1099	*	*										*			*	*							*				*	
ZV1698													50	20				20		5							<1	5
ZV1699	20											25	20		20							?15						

** Denotes mineral present but quantities not estimated*

Appendix D

Table D2: Summary of thin section analyses

Sample	Qtz	Kfs	Pl	Bt	Sil	And	St	Act	Ms	Ser	Cht	Grt	Cal	Dol	Di	Wo	Fo	Serp	Sap	Phl	Chl	Zs	Tr	Tlc	Spn	Spl	Opq	?
ZV1700													50	7				35		5						2	1	
ZV1701	5	5										1	74		15													
ZV1702	*	*		*																		*						
ZV1703	*	*											*		*						*	*	*					
ZV1703	6	6											80		8													
ZV1704													35	25			20			15							5	
ZV1885	*		*										*		*													
ZV1886										5			5		80							2	5		3			
ZV1887	15	40	10					35																				
ZV1888													30	40			20									5	5	
ZV1889													40	45			3	12										
ZV1890													40	20				35									5	
ZV1891		7	10									8	45		15	15												
ZV1893													15	65			15			5								
ZV1894													55	15			2	28										
ZV1894													5		90			5										
ZV1896										*					*					*	*	*	*				
ZV1917	57	5	5	10								10													5		8	
ZV3433													45	5			2	28		15							5	
ZV4918	35	20	30	15																								
ZV4919	35		15	15					25																			10 ?Vs
ZV4920	45		30	10					10		5																	
ZV4921	65			25					5																		5	
ZV4922	60			15					20																		5	
ZV4923	60	20		15							5																	
ZV4924	50	32		10							8																	
ZV4925	40	25	15								20																	
ZV4947													60	5				35			<1							
ZV3002		*										*	*		*								*		*		*	*
ZV3003	10	1													40	20											10	V10
ZV3004	6											8	35		30	8						11						2
ZV3005	10	15	10							5			40		20													

** Denotes mineral present but quantities not estimated*

Appendix D

Table D2: Summary of thin section analyses

Sample	Qtz	Kfs	Pl	Bt	Sil	And	St	Act	Ms	Ser	Cht	Grt	Cal	Dol	Di	Wo	Fo	Serp	Sap	Phl	Chl	Zs	Tr	Tlc	Spn	Spl	Opq	?
ZV3006													55	5			5	25		5						1	4	
ZV3007													70							5			25				<1	
ZV3008													77							8			15					
ZV3009	30												40		15								15					
ZV3010	25												35		25								15					
ZV3011	8												84		5								3					
ZV3012	15												60			10							15					
ZV3013	15												60			10							15					
ZV3015													40	40				12			8							<1 Chu
ZV3017			*											*	*			*					*					
ZV3018													59		12		1	20		8								
ZV3019													*	*	*			*										
ZV3020													49					40		10								1
ZV3021													75		20			5										
ZV3022			2										70		23								5					
ZV3023													45				25			30							<1	
ZV3024													45	8			30	10		5	2						<1	
ZV3027													54								15							12 Chu + 18?
ZV3029													55	5			28			2						3	2	5Chu
ZV3031	10	5										30	10		20	15						5	5					
ZV3032												18	67		15													
ZV3033													55		25						20							
ZV3034													85		10						3	2						
ZV3035												2	85	8														5
ZV3036													80		5								3					12
ZV3037	15												74										10				1	
ZV3038													20		68						2							10
ZV3040													40	4				30		15	10						1	
ZV3043													70	10	8					10			2					
ZV3044													60	8				17		10	3		2					
ZV3045													75	7	18													
HF44													70	5						10	5							10

** Denotes mineral present but quantities not estimated*

Appendix D

Table D2: Summary of thin section analyses

Sample	Qtz	Kfs	Pl	Bt	Sil	And	St	Act	Ms	Ser	Cht	Grt	Cal	Dol	Di	Wo	Fo	Serp	Sap	Phl	Chl	Zs	Tr	Tlc	Spn	Spl	Opq	?
HF45													80							5	5			10				
ZV5464	35	10		25	30																							
ZV5473	25							15				30											25				5	
ZV5473	25		30	35								5															5	
501	*								*												*						*	
Z2	25		20	20					35																			
Z3	30		20	25					25																			
Z4	*			*		*			*																			
Z6	30		10	20	5	10			24																			1 Tour
630.1.1			20					55 hbl		15																	10	
630.4.1			15					65 hbl		12	5																3	
509.1.3	20	30		15	25				10																			
628.1.1	*		*	*					*																			
991	10	89																										1
559.1	24		15	25	15	1			10																			
4222.5	10	1										5	50	5	29													

** Denotes mineral present but quantities not estimated*

APPENDIX E

X-RAY FLUORESCENCE SPECTROMETRY

Sample preparation

Solid rock samples (core samples and lump samples from surface) were initially crushed using a jaw crusher, then ground using a TEMA gyratory mill with a tungsten carbide barrel. A Philips PW1400 automatic sequential wavelength-dispersive X-ray fluoresence spectrometer was used to determine major and trace element concentrations in fused beads and pressed powder pellets respectively.

Major element analysis

Analysis for major elements was carried out on fused beads. For carbonate rocks, 100% lithium metaborate flux was used, and for non-carbonate rocks, a mixed flux of 80% lithium metaborate 20% lithium tetraborate was used.

Sample were dried overnight at 110°C and weighed. Samples were then ignited at ~960°C overnight to decompose carbonate, organic and sulphide matter. However, it is possible that some water may have been lost from minerals such as clays, amphiboles etc. The loss on ignition was calculated by re-weighing samples after ignition.

Ignited samples were mixed with the appropriate flux at a 10:1 flux:sample ratio for carbonates, and a 5:1 ratio for non-carbonates. Fusing was carried out at 1200°C in platinum crucibles to form a homogenous bead for analysis.

In the preparation of some of the carbonate samples, gas (presumed to be CO_2 from the breakdown of dolomite) was released during the beading process, indicating that ignition prior to fusing was not complete. In these samples, therefore, the calculated LOI (Table E3) is lower than expected.

Trace element analysis

Trace element analysis was carried out on pressed pellets of approximately 10g of non-ignited powder mixed with a binder of water-based 8% polyvinyl alcohol (PVA). The pelleting procedure used a 40mm diameter die and a pressure of 12 tons per square inch.

Errors

Quantitative XRF analysis is subject to a number of systematic and random errors (Table E1). Sources of error stem from contamination of samples during preparation and sample inhomogeneity. The precision (reproducibility) of XRF analysis is controlled by the concentration of elements, and the ease with which they become excited during the XRF procedure. For

elements present in concentrations well above their detection limit (>10 times DL), precision is generally less than 1%. The accuracy of the XRF (its ability to produce the 'true' value) can be assessed by analysing certified standard reference materials alongside unknown samples.

	Source	***Random***	***Systematic***
1.	Sampling	a	a
	Sample preparation (particle size)	0 – 1 %	0 – 5
	Sample inhomogeneity	-	0 – 50
2.	Excitation source	0.05 – 0.2	0.05 – 0.5
	Spectrometer	0.05 – 0.1	0.05 – 0.1
3.	Counting statistics	Time dependent	-
	Deadtime losses	-	0 – 25
4.	Primary absorption	-	0 – 50
	Secondary absorption	-	0 – 25
	Enhancement	-	0 - 15

Table E1: Estimation of errors inherent in XRF analysis. Some are not under the analyst's control (a).

Detection limits

While detection limits over most of the atomic number range spectrum lie in the low ppm range, the sensitivity of the XRF falls off towards the long wavelength limit, mainly due to low fluorescence yields, and the increasing influence of absorption of X-rays by the sample. As a result, poor detection limits are generally found for the lower atomic numbers i.e. below Na on the periodic table (Table E2).

Element	*Possible interferences*	*L.L.D. ppm*
As		6
Ba	Ce, high As	10
Cl	W	50
Cr	V	4
Cu	Cu from X-ray tube	3
I		4
Ni		1.5
Nb	Y	1.5
Pb	Bi	1.5
Rb	High U	1.5
S		50
Sr		1.5
Th	High Pb	2
U	High Rb	3
V		4
Zn		1.5
Zr	Sr	1.5

Table E2: Detection limits of selected elements for the PW1400 XRF (Rh anode x-ray tube).

Calculation of non-sulphide FeO (FeO*)

The proportion of total Fe contained within non-sulphide phases for a given sample was calculated using the equation below, which assumes that all Fe sulphide is FeS (including the proportion found in sphalerite and chalcopyrite), and then corrects for the sulphur contained in chalcopyrite, sphalerite and galena.

$$FeO^* = 0.0001286 \times [6993Fe_2O_3 - 1.745(S - 0.5Cu - 0.489Zn - 0.155Pb)]$$

Appendix E Table E3

Metacarbonate rocks: Mine and near-mine samples

Sample	Location	DDH	SiO2	TiO2	Al2O3	Fe2O3	FeO*	MnO	MgO	CaO	Na2O	K2O	P2O5	CO2	SUM
ZV5480	Burkland Cu	1557	3.47	0.01	0.39	5.97	3.53	0.50	20.91	31.17	0.01	0.00	0.00	37.59	100.02
ZV5485	Burkland Cu	1557	18.88	0.25	5.54	17.47	13.64	1.16	8.55	16.80	0.05	1.99	0.38	28.93	100.00
ZV5486	Burkland Cu	1557	8.26	0.05	2.23	10.18	8.17	0.94	16.17	30.31	0.02	0.74	0.03	31.07	100.00
ZV5487	Burkland Cu	1557	10.89	0.08	2.80	7.52	6.24	0.67	17.26	29.30	0.04	1.28	0.00	30.16	100.00
ZV5488	Burkland Cu	1557	4.75	0.02	0.75	6.01	4.13	0.60	18.58	32.01	0.02	0.13	0.03	37.10	100.00
ZV5490	Burkland Cu	1557	6.63	0.02	0.88	6.21	5.50	0.61	18.20	31.00	0.02	0.31	0.05	36.07	100.00
ZV5491	Burkland Cu	1557	12.74	0.00	0.45	10.51	6.36	0.67	24.09	41.31	0.01	0.14	0.00	10.10	100.02
ZV5492	Burkland Cu	1557	8.74	0.00	0.26	6.57	4.74	0.56	20.88	29.56	0.01	0.07	0.00	33.35	100.00
ZV5493	Burkland Cu	1557	6.63	0.03	0.84	7.18	5.07	0.48	19.13	30.53	0.01	0.44	0.00	34.75	100.02
ZV5495	Burkland Cu	1557	11.04	0.02	0.67	9.37	6.62	0.54	24.67	33.94	0.01	0.24	0.07	19.45	100.02
ZV5496	Burkland Cu	1557	5.69	0.00	0.29	6.54	4.27	0.57	21.55	29.70	0.01	0.06	0.00	35.61	100.02
ZV1709	Burkland Po		13.42	0.05	2.19	37.48	20.86	1.41	6.41	26.05	0.03	0.96	0.17	11.83	100.00
ZV1710	Burkland po		15.40	0.07	2.40	34.24	3.91	1.38	6.89	10.61	0.04	1.35	0.14	27.50	100.00
ZV1713	Burkland po		8.15	0.05	1.26	11.59	9.90	1.67	14.37	32.29	0.01	0.52	0.00	30.11	100.02
ZV1719	Burkland po		6.17	0.04	0.83	36.77	7.84	0.69	7.89	19.56	0.01	0.50	1.08	26.48	100.02
ZV1720	Burkland po		22.64	0.05	0.69	34.97	6.16	2.76	3.69	9.21	0.04	0.29	0.12	25.54	100.00
ZR21	Bu ventilation shaft		12.42	0.09	4.02	5.25	4.84	0.54	20.11	32.67	0.22	0.02	0.02	24.04	99.40
ZV3106	Nygruvan	231	11.63	0.04	1.13	0.71	0.62	0.16	3.88	47.69	0.36	0.33	0.01	27.72	93.66
ZV3306	Nygruvan	231	46.30	0.20	8.43	3.49	3.11	0.72	2.98	25.50	0.26	2.39	0.05	1.23	91.55
ZV3308	Nygruvan	231	51.30	0.74	11.30	4.73	4.04	0.80	8.17	15.10	0.69	3.51	0.17	2.19	98.70
ZV3316	Nygruvan	231	56.40	0.26	11.00	4.43	3.96	0.43	2.26	15.10	0.29	4.62	0.05	5.16	100.00
Z92005	Nygruvan	231	55.20	0.45	10.10	6.70	6.28	0.84	3.00	17.70	0.20	2.30	0.15	3.36	100.00
Z92007	Nygruvan	231	57.90	0.43	11.70	5.00	4.75	0.45	2.40	17.80	0.30	2.90	0.12	1.00	100.00
Z92008	Nygruvan	231	24.80	0.10	3.70	3.10	3.05	0.86	2.80	38.80	0.10	1.10	0.05	24.59	100.00
Z92010	Nygruvan	231	46.30	0.54	15.60	3.90	3.75	0.15	2.40	19.30	1.10	3.80	0.10	6.81	100.00
Z92011	Nygruvan	231	33.30	0.15	6.00	2.80	2.76	0.29	2.70	35.00	0.10	1.70	0.05	17.91	100.00
Z92012	Nygruvan	231	45.10	0.44	7.30	4.60	4.38	0.30	3.10	30.80	0.30	0.90	0.15	7.01	100.00
Z92013	Nygruvan	231	47.50	0.41	9.80	3.80	3.66	0.19	2.10	29.00	0.40	1.80	0.12	4.88	100.00
Z92014	Nygruvan	231	13.80	0.02	1.50	0.40	0.59	0.13	1.20	47.70	0.10	0.40	0.02	34.73	100.00
Z92019	Nygruvan	231	53.00	0.24	10.50	3.60	3.49	0.96	2.10	21.80	0.30	2.10	0.06	5.34	100.00

Sample numbers shaded grey indicate analyses carried out at University of Southampton

Appendix E Table E3

Metacarbonate rocks: Mine and near-mine samples

Sample	Location	DDH	SiO2	TiO2	Al2O3	Fe2O3	FeO*	MnO	MgO	CaO	Na2O	K2O	P2O5	CO2	SUM
Z92024	Nygruvan	231	16.10	0.07	2.70	1.50	1.59	0.30	0.80	44.10	0.01	1.50	0.04	32.90	100.02
Z92025	Nygruvan	231	51.50	0.37	12.10	3.60	3.49	0.49	1.50	18.20	0.20	6.20	0.10	5.74	100.00
Z92028	Nygruvan	231	50.10	0.28	9.60	4.50	4.30	0.62	1.90	23.40	0.10	4.30	0.09	5.11	100.00
Z92031	Nygruvan	231	59.90	0.18	8.70	6.70	5.73	1.85	1.60	14.20	0.10	4.60	0.09	2.08	100.00
Z92033	Nygruvan	231	59.60	0.23	8.80	5.30	4.23	1.26	1.50	15.60	0.10	4.20	0.10	3.31	100.00
Z92040	Nygruvan	231	46.50	0.09	3.80	2.80	1.72	2.80	2.90	19.10	0.10	1.00	0.11	20.80	100.00
Z92041	Nygruvan	231	39.50	0.15	4.60	2.99	1.21	2.99	3.00	14.80	0.00	1.00	0.14	30.83	100.00
ZV3109	Nygruvan	671	5.81	0.02	0.42	6.75	5.97	0.57	16.14	33.99	0.01	0.02	0.01	29.70	93.44
ZV3112	Nygruvan	671	5.18	0.05	0.58	1.37	1.26	0.15	21.82	32.79	0.02	0.39	0.01	34.98	97.34
ZV3113	Nygruvan	671	14.82	0.11	1.98	2.68	2.44	0.13	19.71	29.41	0.02	1.50	0.03	20.24	90.63
ZV3115	Nygruvan	671	22.58	0.05	1.64	5.73	5.13	0.48	14.77	30.20	0.01	0.98	0.05	13.56	90.04
ZV3116	Nygruvan	671	24.90	0.05	1.20	4.10	3.65	0.43	16.97	29.69	0.01	0.85	0.04	14.00	92.23
ZV3117	Nugruvan	671	24.32	0.13	3.62	4.63	4.19	0.42	17.25	27.00	0.02	2.16	0.06	12.72	92.32
ZV3118	Nygruvan	671	19.48	0.11	2.36	5.51	4.87	0.54	18.95	28.09	0.02	1.29	0.03	17.08	93.46
ZV3119	Nygruvan	671	8.42	0.03	0.33	5.74	5.14	0.52	17.35	33.09	0.01	0.37	0.01	27.72	93.59
ZV3121	Nygruvan	671	13.34	0.03	0.47	5.12	4.59	0.62	18.65	31.83	0.01	0.40	0.01	23.83	94.30
ZV3122	Nygruvan	671	22.68	0.08	3.39	8.51	5.61	0.65	17.40	25.30	0.02	1.40	0.03	12.54	92.00
ZV3120	Nygruvan	671	17.67	0.05	1.74	4.69	4.20	0.46	16.91	29.10	0.01	0.74	0.11	28.55	100.02
ZV3322	Nygruvan	671	51.80	0.03	2.81	7.67	6.91	0.88	12.70	20.20	0.10	0.34	0.01	2.68	99.22
ZV3325	Nygruvan	671	53.20	0.02	0.80	6.98	6.25	0.54	14.80	19.70	0.04	0.22	0.02	2.58	98.90
ZV3332	Nygruvan	671	52.50	0.12	4.98	6.22	5.56	0.45	11.90	19.00	0.11	0.94	0.04	1.84	98.10
ZV3334	Nygruvan	671	42.80	0.16	8.81	5.34	4.83	0.30	14.20	16.30	0.08	4.23	0.04	1.24	93.50
ZV3338	Nygruvan	671	53.20	0.03	1.23	7.58	6.86	0.61	14.30	20.50	0.04	0.14	0.02	1.65	99.30
ZV3130	Cecilia	898	13.50	0.06	2.04	4.48	3.92	0.44	18.72	30.52	0.02	0.62	0.04	24.34	94.79
ZV3131	Cecilia	898	12.62	0.06	2.31	6.03	5.41	0.50	17.11	30.97	0.01	0.29	0.02	22.36	92.28
ZV3133	Cecilia	898	15.87	0.03	1.00	5.21	3.88	0.52	16.59	30.52	0.01	0.09	0.03	20.86	90.72
ZV3136	Cecilia	898	16.66	0.12	2.90	3.53	3.20	0.36	7.12	37.54	0.03	1.10	0.04	17.67	87.07
ZV3137	Cecilia	898	19.63	0.10	2.53	4.01	3.45	0.32	17.79	28.64	0.02	1.18	0.04	17.30	91.56
ZV3138	Cecilia	898	8.79	0.02	-0.02	2.32	2.12	0.26	19.25	33.23	-0.01	0.10	0.01	26.58	90.54
ZV3139	Cecilia	898	9.18	0.01	0.23	1.14	1.05	0.11	20.58	34.06	-0.01	0.02	0.01	26.80	92.13

Sample numbers shaded grey indicate analyses carried out at University of Southampton

Appendix E Table E3

Metacarbonate rocks: Mine and near-mine samples

Sample	Location	DDH	SiO2	TiO2	Al2O3	Fe2O3	FeO*	MnO	MgO	CaO	Na2O	K2O	P2O5	CO2	SUM
ZV3140	Cecilia	898	17.10	0.11	1.61	2.00	1.83	0.11	22.02	30.49	0.02	0.91	0.03	20.31	94.72
ZV3141	Cecilia	898	24.80	0.11	3.61	2.79	2.47	0.11	16.66	27.43	0.02	2.61	0.03	12.79	90.96
ZV3144	Cecilia	899	23.23	0.11	3.05	2.31	2.06	0.09	19.69	27.76	0.02	1.95	0.04	14.30	92.54
ZV3145	Cecilia	898	16.12	0.11	1.42	2.12	1.93	0.09	22.50	30.03	0.03	1.21	0.02	20.90	94.55
ZV3147	Cecilia	898	22.85	0.06	2.19	1.70	1.51	0.09	20.89	28.31	0.02	1.57	0.02	14.81	92.51
ZV3149	Cecilia	898	30.80	0.12	6.65	9.89	5.25	0.88	12.02	19.45	0.03	2.42	0.05	17.71	100.00
ZV3150	Cecilia	898	18.80	0.07	2.78	3.11	2.67	0.35	15.59	26.02	0.01	0.77	0.07	32.46	100.02
ZV3349	Cecilia	898	40.70	0.01	5.19	21.30	8.98	0.44	4.29	15.00	0.08	0.88	0.02	11.24	99.15
ZV3350	Cecilia	898	52.60	0.06	0.86	4.90	4.39	0.38	17.80	18.20	0.05	0.02	0.03	3.30	98.20
ZV3351	Cecilia	898	50.80	0.09	2.89	6.14	5.49	0.47	15.90	18.90	0.08	0.28	0.06	2.80	98.40
ZV3354	Cecilia	898	51.90	0.02	0.91	4.03	3.61	0.36	17.20	20.70	0.04	0.04	0.04	2.51	97.75
ZV3355	Cecilia	898	53.30	0.08	2.59	4.82	4.36	0.34	15.70	19.00	0.06	0.41	0.03	3.02	99.35
ZV3358	Cecilia	898	51.70	0.15	7.10	3.15	2.86	0.09	14.70	16.50	0.10	3.08	0.03	2.75	99.35
ZV3360	Cecilia	898	56.80	0.14	4.96	2.57	2.34	0.08	13.90	15.80	0.17	3.67	0.03	1.83	99.95
ZV3363	Cecilia	898	53.00	0.09	3.06	2.52	2.25	0.11	17.30	19.50	0.04	0.57	0.03	3.13	99.35
ZV3373	Cecilia	898	51.20	0.10	3.71	8.09	7.08	1.15	10.70	19.20	0.26	1.31	0.02	3.56	99.30
ZV3374	Cecilia	898	59.70	0.19	4.46	6.99	6.27	0.85	8.79	15.90	0.30	0.91	0.08	1.78	99.95
ZV3491	Nygruvan	555	1.46	0.02	0.13	2.12	1.89	0.30	23.32	31.80	0.01	0.07	0.01	40.80	100.03
ZV3492	Nygruvan	555	24.11	0.13	3.12	3.19	2.86	0.24	15.07	28.11	0.02	2.27	0.02	23.72	100.00
ZV3493	Nygruvan	555	11.49	0.04	0.49	4.39	3.94	0.68	19.46	32.35	0.01	0.38	0.04	30.69	100.02
555/07	Nygruvan	555	22.35	0.19	5.24	7.57	5.30	0.55	12.06	28.28	0.31	3.42	0.07	16.39	96.43
555/10	Nygruvan	555	4.52	0.02	0.50	9.61	6.72	0.73	20.22	35.42	0.30	0.04	0.04	28.72	100.12
555/14	Nygruvan	555	17.35	0.04	4.36	1.99	1.39	0.23	15.49	34.21	0.33	2.20	0.02	22.76	98.98
555/15	Nygruvan	555	6.82	0.02	0.80	2.49	1.74	0.32	23.01	34.00	0.11	0.04	0.01	28.62	96.24
555/17	Nygruvan	555	5.47	0.02	0.53	2.46	1.72	0.35	23.96	34.61	0.10	0.15	0.01	29.24	96.89
555/18	Nygruvan	555	34.52	0.11	3.66	3.05	2.13	0.28	15.49	25.08	0.35	1.91	0.07	13.06	97.57
555/20	Nygruvan	555	2.26	0.02	0.47	2.78	1.95	0.40	24.88	36.94	0.03	0.01	0.01	30.38	98.19
555/21	Nygruvan	555	1.57	0.02	0.58	2.39	1.67	0.33	25.08	38.13	0.10	0.03	0.01	31.07	99.32
555/22	Nygruvan	555	14.52	0.02	0.16	3.86	2.70	0.39	21.99	33.07	0.08	0.02	0.02	23.31	97.43
555/28	Nygruvan	555	28.79	0.05	1.68	4.15	2.90	0.39	18.18	28.00	1.19	0.85	0.03	15.99	99.31

Sample numbers shaded grey indicate analyses carried out at University of Southampton

Appendix E Table E3

Metacarbonate rocks: Mine and near-mine samples

Sample	Location	DDH	SiO2	TiO2	Al2O3	Fe2O3	FeO*	MnO	MgO	CaO	Na2O	K2O	P2O5	CO2	SUM
555/29	Nygruvan	555	15.11	0.09	2.63	2.55	1.78	0.25	6.13	45.98	0.31	0.91	0.06	23.66	97.69
555/33	Nygruvan	555	23.42	0.10	2.82	5.97	4.17	0.86	21.68	35.69	0.38	1.28	0.07	6.36	98.63
555/34	Nygruvan	555	33.38	0.06	1.73	3.49	2.44	0.49	17.32	27.60	0.43	0.33	0.03	14.13	98.99
555/35	Nygruvan	555	22.35	0.12	3.22	4.05	2.83	0.58	18.19	28.00	0.49	1.91	0.05	19.78	98.72
ZV 3005	Isåsen	O/C	27.18	0.09	3.80	2.99	2.65	0.19	5.12	37.66	0.10	1.21	0.06	21.14	99.53
ZV 3006	Isåsen	O/C	4.23	0.02	0.41	3.61	3.23	0.46	18.42	30.96	0.00	0.08	0.03	38.37	96.59
ZR05	Isasen	O/C	25.42	0.06	2.40	2.74	2.43	0.23	3.02	42.69	0.46	0.40	0.04	20.65	98.12
ZR06	Isasen quarry	O/C	6.91	0.05	2.64	1.65	1.63	0.25	24.49	32.44	0.06	0.42	0.02	28.42	97.35
ZR17	Jakobsgruvan		41.23	0.15	6.42	2.82	2.21	0.36	7.25	28.76	1.92	0.75	0.06	11.03	100.75
ZR18	Jakobsgruvan		43.76	0.13	5.33	11.08	8.18	0.56	7.86	23.55	0.62	0.45	0.06	5.28	98.68
ZR19	E. Broangen		14.32	0.08	3.11	10.04	9.10	0.52	17.93	29.77	0.05	0.02	0.05	22.43	98.33
ZR20	Aspelund		21.23	0.10	4.42	1.76	1.55	0.88	0.42	49.73	0.72	0.09	0.04	20.71	100.10
ZV 3023	Finnafallet	1350	18.32	0.07	3.23	11.48	4.76	2.05	12.29	26.04	0.05	2.01	0.06	18.69	94.30
ZV 3024	Finnafallet	1350	20.87	0.02	0.51	4.48	4.01	0.53	20.27	27.58	0.00	0.13	0.05	20.35	94.79
ZV 3025	Finnafallet	1350	11.58	0.03	0.62	2.77	2.41	0.44	20.55	31.69	0.00	0.00	0.06	30.15	97.88
ZV 3026	Finnafallet	1350	11.90	0.02	0.56	2.77	2.48	0.41	21.65	30.64	0.00	0.09	0.03	30.73	98.79
ZV 3027	Finnafallet	1350	8.82	0.09	1.79	5.21	-5.26	1.10	13.63	33.89	0.00	0.00	0.01	26.49	91.04
ZV 3028	Långgölen	1353	14.70	0.03	0.88	4.94	4.34	0.58	18.95	31.04	0.00	0.35	0.01	27.07	98.56
ZV 3029	Långgölen	1353	11.44	0.06	1.75	3.32	2.93	0.63	20.40	32.33	0.00	0.00	0.02	30.02	99.98
ZV3454	Långgölen	1353	52.76	0.04	1.48	7.65	6.89	0.59	14.24	23.89	0.09	0.06	0.02	-0.82	100.00
ZV3455	Långgölen	1353	20.41	0.03	1.20	5.57	4.98	0.70	19.15	29.57	0.00	0.34	0.02	23.02	100.00
ZV3456	Långgölen	1353	11.04	0.05	1.54	3.69	3.31	0.64	20.42	30.19	0.00	0.28	0.02	32.13	100.00
ZV4988	Dalbysjön	952	40.30	0.24	5.15	4.33	3.81	0.42	15.10	21.30	0.02	1.66	0.07	2.26	90.85
ZV4989	Dalbysjön	952	37.10	0.15	6.78	12.70	11.17	1.31	8.98	18.00	0.04	4.03	0.07	0.54	89.70
ZV4991	Dalbysjön	952	41.10	0.15	6.01	22.70	18.41	1.38	7.59	17.00	0.11	0.52	0.12	3.33	100.01
ZV4993	Dalbysjön	952	39.20	0.22	7.47	12.40	7.48	0.89	7.43	15.50	0.01	3.00	0.30	12.10	98.52
ZV4994	Dalbysjön	952	14.40	0.10	2.46	18.70	15.27	1.94	11.20	26.90	0.01	1.05	0.35	2.81	79.92
ZV4997	Dalbysjön	952	50.00	0.26	6.77	8.05	4.94	1.03	9.11	18.40	0.14	1.56	0.14	4.14	99.60
ZV3433	Dalbysjön	1272	13.57	0.06	2.52	9.53	7.94	1.00	14.73	28.43	0.01	1.13	0.00	29.03	100.00
ZV3434	Dalbysjön	1272	2.66	0.00	0.25	6.47	6.36	0.74	17.79	30.76	0.00	0.01	0.00	41.33	100.00

Sample numbers shaded grey indicate analyses carried out at University of Southampton

Appendix E Table E3

Metacarbonate rocks: Mine and near-mine samples

Sample	Location	DDH	SiO2	TiO2	Al2O3	Fe2O3	FeO*	MnO	MgO	CaO	Na2O	K2O	P2O5	CO2	SUM
ZV3435	Dalbysjön	1272	10.90	0.03	0.57	6.69	5.03	0.77	17.05	29.77	0.00	0.02	0.25	33.96	100.00
ZV3436	Dalbysjön	1272	15.58	0.06	2.09	8.50	7.27	1.06	15.31	28.23	0.01	1.25	0.18	27.75	100.00
451/15	Nygruvan	451	32.06	0.09	3.78	2.64	1.84	0.33	5.76	34.14	0.79	2.58	0.05	16.02	98.24
451/16	Nygruvan	451	33.34	0.12	4.46	2.34	1.64	0.20	6.12	29.68	0.42	2.71	0.05	16.81	96.25
451/17	Nygruvan	451	34.69	0.14	5.40	2.77	1.94	0.25	4.71	33.04	0.91	2.56	0.05	14.19	98.72
451/18	Nygruvan	451	43.73	0.23	7.88	2.73	1.91	0.16	4.18	25.88	0.79	3.45	0.07	8.79	97.89
451/19	Nygruvan	451	42.97	0.11	4.59	3.21	2.24	0.32	5.57	26.86	0.52	3.00	0.05	9.38	96.59
ZV3481	Tostebacka	452	44.13	0.76	12.62	11.37	9.91	0.49	5.92	19.11	0.75	0.27	0.08	4.49	100.00
ZV3483	Tostebacka	452	19.41	0.10	4.15	5.78	5.16	0.94	15.24	28.34	0.02	1.79	0.03	24.19	100.00
ZV3494	Tostebacka	453	21.87	0.09	4.31	2.00	1.79	0.19	2.76	37.55	0.19	2.37	0.05	28.62	100.00
ZV3495	Tostebacka	453	26.60	0.10	3.70	2.19	1.97	0.15	1.63	38.64	0.23	2.18	0.06	24.53	100.00
ZV3496	Tostebacka	453	28.27	0.09	3.94	2.96	2.65	0.29	3.75	37.00	0.17	1.22	0.06	22.25	100.00
ZV3485	Tostebacka	454	27.03	0.12	4.18	4.74	3.87	0.49	15.17	26.39	0.05	2.42	0.05	19.38	100.00
ZV3486	Tostebacka	454	54.35	0.06	3.16	6.20	5.54	0.72	15.02	22.46	0.02	0.78	0.07	-2.84	100.00
ZV3487	Tostebacka	454	23.58	0.08	3.24	5.27	4.46	0.73	16.66	27.68	0.26	1.74	0.03	20.73	100.00
ZV3488	Tostebacka	454	31.93	0.13	5.32	2.76	2.56	0.18	3.19	32.29	0.26	3.09	0.07	20.79	100.00
454/04	Nygruvan	454	23.96	0.08	2.29	8.48	5.93	0.47	17.39	26.69	0.24	1.02	0.05	17.29	97.95
454/24	Nygruvan	454	33.30	0.11	4.38	4.10	2.86	0.48	14.14	25.34	0.25	2.34	0.07	12.83	97.34
454/26	Nygruvan	454	30.77	0.06	2.68	5.18	3.62	0.84	14.86	26.61	0.65	1.55	0.05	12.93	96.18
454/28	Nygruvan	454	44.88	0.20	8.97	2.86	2.00	0.16	4.02	23.61	0.85	4.64	0.06	7.86	98.10
454/29	Nygruvan	454	42.49	0.21	7.22	3.52	2.46	0.16	6.02	24.47	0.63	4.11	0.07	9.27	98.18
454/40	Nygruvan	454	24.67	0.04	1.40	6.76	4.72	0.74	14.08	29.73	0.24	0.75	0.03	15.57	94.00

Sample numbers shaded grey indicate analyses carried out at University of Southampton

Appendix E Table E4
Metacarbonate rocks: District samples

Sample	Location	SiO2	TiO2	Al2O3	Fe2O3	FeO*	MnO	MgO	CaO	Na2O	K2O	P2O5	CO2	SUM
ZV1601	Höksjön	4.93	0.00	0.30	0.29	0.22	0.03	0.84	49.54	0.00	0.00	0.00	44.07	100.00
ZV1604	Höksjön	2.10	0.00	0.31	0.28	0.25	0.02	0.92	54.52	0.00	0.02	0.00	41.83	100.00
ZV1606	Höksjön	28.72	0.07	3.00	1.27	1.00	0.05	7.73	31.85	0.00	0.82	0.06	26.43	100.00
ZV1608	Höksjön	1.57	0.00	0.23	0.19	0.18	0.03	2.39	54.82	0.00	0.00	0.00	40.77	100.00
ZV1611	Höksjön	2.61	0.00	0.33	0.22	0.20	0.04	5.26	48.39	0.00	0.08	0.00	43.07	100.00
ZV1612	Höksjön	5.06	0.05	1.13	0.64	0.56	0.03	4.80	46.87	0.00	0.34	0.00	41.08	100.00
Zv1613	Höksjön	10.86	0.01	0.45	1.12	1.02	0.09	15.64	33.41	0.00	0.00	0.00	38.42	100.00
ZV1614	Höksjön	3.51	0.00	0.38	0.25	0.22	0.03	2.83	52.89	0.00	0.00	0.00	40.11	100.00
Zv1616	Höksjön	3.94	0.00	0.36	0.19	0.18	0.02	1.02	51.55	0.00	0.05	0.00	42.87	100.00
ZV1619	Höksjön	1.87	0.00	0.22	0.13	0.12	0.02	0.76	55.72	0.00	0.00	0.00	41.28	100.00
ZV1620	Höksjön	3.46	0.00	0.39	0.58	0.51	0.04	2.06	51.48	0.00	0.07	0.00	41.92	100.00
ZV 3009	Höksjön	26.78	0.01	0.32	0.24	0.14	0.03	2.42	39.45	0.00	0.00	0.01	29.03	98.31
ZV 3000	Högalund	32.85	0.10	3.61	4.12	3.38	0.50	2.17	38.98	0.12	1.07	0.07	15.70	99.29
ZV 3001	Åsberget	48.03	0.22	7.16	1.20	0.93	0.41	0.31	39.02	0.00	0.01	0.18	2.72	99.25
ZV 3002	Ervingsberg	53.59	0.09	6.20	8.07	7.05	0.42	2.31	22.24	0.56	4.14	0.16	1.22	99.01
ZV 3003		45.91	0.26	11.35	8.63	7.84	0.39	3.05	26.34	0.09	1.04	0.10	1.28	98.43
ZV 3004		37.52	0.09	4.34	3.18	2.85	0.35	6.97	35.16	0.09	0.14	0.04	11.61	99.48
ZV 3007	Godegård	11.66	0.03	0.70	0.33	-0.39	0.03	5.82	45.86	0.00	0.22	0.03	33.10	97.78
ZV 3008		3.20	0.02	0.45	0.17	0.11	0.04	2.68	51.97	0.00	0.08	0.02	40.18	98.80
ZV 3010	Näset	39.48	0.02	0.49	0.51	0.44	0.02	4.15	32.97	0.00	0.00	0.02	21.55	99.21
ZV 3011		5.33	0.01	0.37	0.23	0.19	0.01	1.10	52.14	0.00	0.06	0.01	40.00	99.26
ZR04	Trollfall	5.72	0.00	0.11	0.28		0.00	0.87	64.49	0.13	0.04	0.01	29.08	100.72
ZV 3012	Trollfall	6.84	0.03	0.96	0.33	0.22	0.02	1.18	52.03	0.00	0.04	0.02	37.11	98.56
ZV 3013		5.12	0.02	0.38	0.28	0.23	0.02	1.57	52.41	0.00	0.10	0.02	38.89	98.81
ZV 3014		4.12	0.02	0.36	0.18	0.13	0.01	1.05	51.74	0.00	0.03	0.02	41.57	99.09
ZV 3015		2.51	0.03	0.81	0.89	0.78	0.14	19.09	31.52	0.00	0.00	0.01	42.44	97.45
ZV 3016		1.37	0.02	0.44	0.48	0.42	0.09	17.63	33.97	0.00	0.00	0.01	43.26	97.26
ZV 3017		40.14	0.01	0.33	0.39	0.34	0.05	16.34	30.32	0.00	0.00	0.01	10.41	97.99
ZV 3018		7.35	0.02	0.53	0.27	0.19	0.07	7.15	46.21	0.00	0.07	0.02	35.17	96.85
ZV 3019		9.80	0.05	1.64	0.74	0.63	0.05	2.57	48.20	0.15	0.11	0.03	33.92	97.27

Sample numbers shaded grey indicate analyses carried out at University of Southampton

Appendix E Table E4
Metacarbonate rocks: District samples

Sample	Location	SiO2	TiO2	Al2O3	Fe2O3	FeO*	MnO	MgO	CaO	Na2O	K2O	P2O5	CO2	SUM
ZV 3020		11.63	0.03	0.62	0.56	0.40	0.05	13.91	37.27	0.00	0.16	0.01	30.32	94.56
ZV 3021		4.56	0.02	0.48	0.17	0.12	0.02	2.58	52.04	0.00	0.04	0.02	38.39	98.32
ZV 3022		9.47	0.01	0.40	0.23	0.12	0.03	4.17	48.58	0.00	0.02	0.01	34.53	97.45
ZV 3030	Nyhyttan	17.83	0.02	0.57	1.84	1.59	0.30	16.95	31.44	0.00	0.06	0.01	24.67	93.69
ZV 3031		47.49	0.23	8.77	2.92	2.63	0.40	3.91	33.30	0.00	0.05	0.06	1.96	99.09
ZV 3032		5.85	0.02	1.12	0.21	0.15	0.01	1.42	52.04	0.00	0.00	0.02	37.64	98.33
ZV 3033	Västervik	11.47	0.06	2.01	1.20	1.06	0.07	6.59	44.81	0.00	0.00	0.03	30.94	97.16
ZV 3034	Västervik	8.70	0.03	0.95	0.74	0.65	0.05	3.97	48.64	0.00	0.00	0.03	34.37	97.47
ZV 3035	Västervik	5.19	0.02	0.40	0.37	0.31	0.04	1.63	53.18	0.00	0.00	0.01	38.61	99.45
ZV 3036		4.92	0.01	0.60	0.81	0.70	0.06	4.36	49.28	0.00	0.00	0.02	37.71	97.77
ZV 3037		15.68	0.01	0.26	0.54	-1.51	0.17	0.71	46.05	0.00	0.01	0.01	34.97	98.41
ZV 3038		18.30	0.02	0.62	0.69	0.57	0.11	7.15	43.87	0.00	0.05	0.02	28.98	99.81
ZV 3039		7.53	0.04	1.33	2.02	1.79	0.11	1.73	48.93	0.00	0.32	0.02	36.91	98.94
ZV 3040		8.62	0.04	1.50	0.62	0.53	0.09	9.13	41.74	0.00	0.51	0.01	33.47	95.73
ZV 3041		21.36	0.04	1.28	0.62	0.54	0.12	10.57	38.44	0.04	0.24	0.03	26.79	99.55
ZV 3042		12.83	0.03	0.67	0.37	0.26	0.03	7.80	44.40	0.00	0.19	0.02	31.57	97.91
ZV 3043		1.91	0.02	0.48	0.33	0.20	0.34	2.10	52.59	0.00	0.08	0.02	40.42	98.28
ZV 3044		2.93	0.03	0.74	0.40	0.32	0.09	18.04	33.45	0.00	0.15	0.02	41.89	97.74
ZV 3045		2.97	0.01	0.21	0.15	0.11	0.10	1.53	53.08	0.00	0.00	0.01	39.78	97.84
ZR02	Gardshyttan	12.28	0.07	2.19	0.76	0.72	0.05	16.37	41.19	0.11	0.01	0.18	25.81	99.01
ZR08	Bredsjon	13.60	0.02	0.40	4.70	4.44	0.68	19.83	32.84	0.11	0.23	0.04	25.51	97.95
ZR09	Tybble	20.96	0.00	0.13	0.47	0.44	0.13	2.19	49.62	0.22	0.02	0.01	25.40	99.16
ZR10	Meltorp	4.70	0.02	0.49	0.40	0.40	0.13	4.67	60.70	0.59	0.16	0.02	29.03	100.92
ZR11	Brannlycken	18.21	0.04	1.39	1.28	1.17	0.15	19.23	35.52	0.22	0.16	0.02	23.83	100.08
ZR12	Brannlycken	8.53	0.03	0.83	0.56	0.53	0.18	5.84	56.80	0.23	0.02	0.01	27.51	100.52
ZR13	Brannlycken	16.60	0.04	1.60	1.27	1.18	0.13	18.71	34.45	0.08	0.19	0.02	23.85	96.95
ZR22	Rytabygget	15.87	0.10	2.78	1.27	1.17	0.07	17.10	36.95	0.30	0.13	0.18	24.39	99.15

Sample numbers shaded grey indicate analyses carried out at University of Southampton

Appendix E Table E5
Regional metacarbonate samples

Sample	Location	SiO2	TiO2	Al2O3	Fe2O3	FeO*	MnO	MgO	CaO	Na2O	K2O	P2O5	CO2	SUM
ZV3046	Glanshammar	5.15	0.01	0.02	0.82	0.71	0.12	23.71	32.43	0.01	0.02	0.01	37.78	100.07
ZV3047	Glanshammar	3.63	0.01	0.25	0.79	0.70	0.23	25.22	31.01	0.02	0.07	0.01	38.78	100.01
ZV3048	Glanshammar	2.37	-0.01	0.02	0.60	0.50	0.10	24.45	32.32	0.01	0.02	0.01	40.18	100.07
ZV3049	Glanshammar	5.42	0.02	0.42	0.88	0.75	0.10	23.60	31.71	0.02	0.07	0.01	37.77	100.01
ZV3050	Glanshammar	2.80	0.01	0.23	0.50	0.44	0.06	23.89	32.05	0.01	0.05	0.01	40.42	100.03
ZV6369	Glanshammar	5.14	0.01	0.77	1.50	1.05	0.14	1.10	48.93	0.14	0.35	0.00	41.91	100.00
ZV6367	Glanshammar	0.44	0.00	0.15	0.84	0.59	0.12	20.53	33.87	0.00	0.00	0.00	44.06	100.00
ZV6366	Glanshammar	2.26	0.00	0.33	0.96	0.67	0.21	18.44	34.04	0.05	0.00	0.00	43.71	100.00
ZV6365	Glanshammar	3.27	0.01	1.09	0.49	0.35	0.04	21.81	31.40	0.04	0.27	0.00	41.57	100.00
ZV6364	Glanshammar	8.53	0.07	2.64	1.57	1.10	0.24	18.45	30.04	0.02	0.93	0.00	37.52	100.00
ZV6363	Glanshammar	1.47	0.00	0.40	0.55	0.38	0.05	23.00	32.72	0.00	0.00	0.00	41.81	100.00
ZV6362	Glanshammar	6.91	0.00	0.43	0.60	0.42	0.07	23.18	31.87	0.05	0.09	0.00	36.81	100.00
ZV6361	Glanshammar	18.91	0.00	0.36	0.86	0.60	0.07	23.51	29.75	0.00	0.00	0.00	26.53	100.00
ZV6360	Glanshammar	23.57	0.00	0.27	0.68	0.48	0.05	18.84	29.75	0.00	0.00	0.00	26.84	100.00
ZV6359	Glanshammar	6.43	0.01	0.98	0.73	0.51	0.10	19.22	34.52	0.00	0.05	0.00	37.97	100.00
ZV6358	Glanshammar	32.13	0.12	12.76	0.99	0.69	0.04	19.72	16.95	0.17	3.26	0.04	13.82	100.00
ZV6357	Glanshammar	23.82	0.13	9.63	1.39	0.97	0.06	15.08	23.95	0.93	3.22	0.03	21.76	100.00
ZV6356	Glanshammar	4.34	0.00	0.35	0.51	0.35	0.06	18.88	35.37	0.00	0.00	0.00	40.50	100.00
ZV6355	Glanshammar	15.28	0.11	4.28	0.81	0.56	0.06	18.93	28.20	0.08	1.09	0.00	31.17	100.00
ZV6354	Glanshammar	20.32	0.00	0.17	0.45	0.31	0.06	21.44	30.02	0.00	0.00	0.00	27.55	100.00
ZV6353	Glanshammar	17.41	0.00	0.35	0.66	0.46	0.11	22.21	31.60	0.00	0.00	0.00	27.67	100.00
ZV6352	Glanshammar	5.51	0.00	0.40	2.15	1.50	0.46	20.75	31.98	0.00	0.02	0.00	38.73	100.00
ZV6351	Glanshammar	1.24	0.00	0.46	6.70	4.68	0.65	1.29	49.81	0.01	0.07	0.00	39.77	100.00
ZV6348	Glanshammar	49.06	0.23	6.51	18.22	12.74	2.21	2.45	2.86	0.02	3.48	0.18	14.78	100.00
ZV6346	Glanshammar	32.38	0.08	5.30	3.87	2.70	0.32	1.36	21.58	0.89	2.43	0.03	31.77	100.00
ZV6339	Glanshammar	6.35	-0.01	0.28	0.63	0.44	0.10	27.56	33.26	0.00	0.00	0.00	31.84	100.00
ZV6338	Glanshammar	0.91	0.00	0.26	0.23	0.16	0.08	0.86	58.75	0.00	0.00	0.00	38.91	100.00
ZV6337	Glanshammar	8.31	0.01	0.79	1.93	1.35	0.55	24.44	34.06	0.02	0.00	0.01	29.89	100.00
ZV6336	Glanshammar	0.67	0.00	0.21	0.12	0.08	0.07	2.83	57.87	0.00	0.00	0.00	38.24	100.00
ZV6335	Glanshammar	5.62	0.01	1.50	0.68	0.48	0.08	1.37	51.61	0.09	0.48	0.00	38.57	100.00

Appendix E Table E5
Regional metacarbonate samples

Sample	Location	SiO2	TiO2	Al2O3	Fe2O3	FeO*	MnO	MgO	CaO	Na2O	K2O	P2O5	CO2	SUM
ZV6334	Glanshammar	13.66	0.05	3.51	0.78	0.54	0.08	3.57	44.50	0.19	1.24	0.00	32.43	100.00
ZV6332	Glanshammar	1.69	0.00	0.49	0.66	0.46	0.16	0.80	56.21	0.03	0.02	0.00	39.94	100.00
ZV6331	Glanshammar	0.75	0.00	0.24	0.55	0.39	0.18	1.10	57.94	0.00	0.00	0.00	39.24	100.00
ZV6330	Glanshammar	7.50	0.02	1.66	1.66	1.16	0.14	1.96	47.58	0.07	0.72	0.00	38.70	100.00
ZV6329	Glanshammar	3.17	0.02	1.20	2.59	1.81	0.25	3.78	51.41	0.00	0.00	0.00	37.59	100.00
ZV6328	Glanshammar	8.75	0.01	1.13	0.75	0.53	0.21	0.49	47.23	0.08	0.79	0.00	40.57	100.00
ZV6326	Glanshammar	3.10	-0.01	0.57	0.59	0.41	0.18	2.67	53.69	0.03	0.05	0.00	39.13	100.00
ZV6325	Glanshammar	1.46	0.00	0.25	0.47	0.33	0.17	0.87	58.32	0.00	0.00	0.00	38.46	100.00
ZV6324	Glanshammar	2.40	0.00	0.43	0.77	0.54	0.33	1.43	55.05	0.00	0.00	0.00	39.60	100.00
ZV6323	Glanshammar	1.15	0.00	0.30	0.29	0.20	0.14	0.65	57.65	0.03	0.00	0.00	39.79	100.00
ZV6322	Glanshammar	1.24	0.00	0.48	0.37	0.26	0.15	1.70	57.65	0.00	0.00	0.00	38.41	100.00
ZV6321	Glanshammar	23.12	0.00	0.98	3.99	2.79	0.43	10.65	33.19	0.04	0.00	0.00	27.60	100.00
ZV6319	Glanshammar	1.68	0.00	0.22	0.18	0.13	0.05	0.77	56.13	0.00	0.00	0.00	40.96	100.00
ZV6318	Glanshammar	53.53	0.04	2.84	5.75	4.02	0.46	21.39	18.08	0.18	0.15	0.07		102.48

Appendix E Table E6
Metavolcanic samples

SAMPLE	HOLE	POSITION	SiO2	Al2O3	Na2O	K2O	CaO	MgO	FeO*	FeO (tot)	MnO	TiO2	P2O5	SUM
ZV10001	231	Zinkgruvan HW	54.9	10.9	1.08	3.46	1.01	2.5	1.14	17.54	0.05	0.26	0.058	100.11
ZV10002	231	Zinkgruvan HW	55.7	12.1	0.76	3.51	1.19	1.97	0.25	16.19	0.11	0.35	0.079	99.39
ZV10003	231	Zinkgruvan HW	65.9	4.2	0.15	0.35	0.89	3.6	9.99	18.23	0.57	0.31	0.099	98.22
ZV10004	231	Zinkgruvan HW	65.7	8	0.23	1.77	1.11	3.3	14.39	16.22	0.37	0.39	0.145	98.38
ZV10005	231	Zinkgruvan HW	57.3	5.3	0.15	0.49	11.44	4.18	6.24	13.55	2.68	0.27	0.14	98.87
ZV10006	231	Zinkgruvan HW	60.4	12.1	0.6	4.05	1.34	2.01	0.13	12.89	0.11	0.35	0.071	99.83
ZV10007	231	Zinkgruvan HW	70.8	11	0.48	2.91	2.17	2.51	0.32	6.97	0.09	0.31	0.121	100.48
ZV10008	231	Zinkgruvan HW	61.3	14.3	1	3.7	1.84	3.33	3.65	8.62	0.1	0.34	0.073	97.03
ZV10009	231	Zinkgruvan HW	59.6	10.9	0.3	3.86	12.12	4.53	3.36	6.44	0.45	0.31	0.094	100.03
ZV10010	231	Zinkgruvan HW	69.8	12.9	1.14	3.94	2.29	2.99	1.24	5.69	0.16	0.4	0.072	101.41
ZV10011	231	Zinkgruvan HW	71.3	11.5	1.47	3.86	2.04	2.47	1.5	5.4	0.36	0.42	0.076	100.74
ZV10014	231	Zinkgruvan HW	72.1	12.1	0.89	5.41	2.46	1.86	3.33	3.74	0.07	0.35	0.056	99.36
ZV10025	231	Zinkgruvan HW	70.1	10.9	0.48	5.94	4.3	1.68	4.5	5.26	1.08	0.27	0.07	100.52
ZV10026	231	Zinkgruvan HW	71.5	10.7	0.33	4.67	3.55	2.27	5.14	5.47	1.12	0.3	0.101	100.31
ZV10027	231	Zinkgruvan HW	81.3	8.9	0.5	6.13	0.58	0.43	0.65	0.7	0.07	0.17	0.044	98.88
ZV10028	231	Zinkgruvan HW	67	13.4	0.44	6.82	2.57	2.78	3.74	3.87	0.21	0.35	0.059	97.76
ZV10029	231	Zinkgruvan HW	62.3	10.4	0.12	6.92	13.82	1.03	3.85	4.13	0.87	0.28	0.073	100.13
ZV10030	231	Zinkgruvan HW	67.3	12.6	0.46	8.01	2.06	1.24	2.21	3.91	0.23	0.4	0.097	97.21
ZV10031	231	Zinkgruvan HW	66.9	11.9	0.34	8.09	3.72	1.39	2.25	2.99	0.46	0.3	0.071	96.59
ZV10032	231	Zinkgruvan HW	65.1	14.5	0.84	7.5	1.08	1.82	3.26	3.35	0.09	0.33	0.022	94.7
ZV10058	231	Zinkgruvan orezone	65.9	11.6	0.49	4.9	8.02	2.63	4.97	5.24	0.6	0.32	0.056	100.16
ZV10059	231	Zinkgruvan orezone	61.8	17.6	1.1	8.21	3	2.26	6.24	6.25	0.24	0.45	0.038	101.09
ZV10060	231	Zinkgruvan orezone	56.6	13	0.63	5.06	3.12	2.75	8.31	10.9	1.03	0.66	0.176	96.47
ZV10061	231	Zinkgruvan orezone	54.2	7.6	0.9	4.04	4.06	0.76	0.87	6.47	0.97	0.25	0.1	87.38
ZV10062	231	Zinkgruvan orezone	50.1	8.5	1.2	3.85	4.54	0.75	0.99	7.5	0.79	0.25	0.099	86.28
ZV10063	231	Zinkgruvan orezone	55.8	8.5	0.99	3.23	3.77	1.17	0.16	5.03	0.38	0.25	0.095	87.39
ZV10064	231	Zinkgruvan orezone	69.5	12.2	0.32	4.23	4.07	2.17	3.99	4.85	0.33	0.27	0.042	98.85
ZV10065	231	Zinkgruvan orezone	72.8	12.5	0.34	4.86	3.02	1.77	3.61	4.04	0.22	0.27	0.028	100.25
ZV10066	231	Zinkgruvan orezone	69.3	12.5	0.32	4.21	4.06	2.15	3.97	4.84	0.32	0.27	0.041	98.87
ZV10067	231	Zinkgruvan orezone	76.7	10.8	0.32	2.62	2.89	2.02	4.18	4.63	0.2	0.27	0.018	100.68

Appendix E Table E6
Metavolcanic samples

SAMPLE	HOLE	POSITION	SiO2	Al2O3	Na2O	K2O	CaO	MgO	FeO*	FeO (tot)	MnO	TiO2	P2O5	SUM
ZV10068	231	Zinkgruvan FW	66.3	11.1	0.48	4.23	6.3	3.19	4.31	5.24	0.78	0.42	0.129	99.09
ZV10069	231	Zinkgruvan FW	65	14.4	0.78	5.58	2.05	3.76	5.25	6.01	0.21	0.67	0.16	98.96
ZV10070	231	Zinkgruvan FW	69.5	14	1.22	5.92	1.53	2.72	3.54	3.52	0.14	0.27	0.018	98.87
ZV10071	231	Zinkgruvan FW	75.1	12	0.6	5.35	1.45	2.88	2.82	2.94	0.11	0.28	0.034	100.84
ZV10072	231	Zinkgruvan FW	74.6	13.1	0.5	5.3	0.77	3.8	2.69	2.75	0.06	0.28	0.052	101.28
ZV10073	231	Zinkgruvan FW	71.5	13.3	0.74	6.87	0.39	3.02	2.67	2.72	0.07	0.17	0.016	98.85
ZV10074	231	Zinkgruvan FW	69.5	13.9	0.45	7.23	0.43	3.72	4.18	4.52	0.06	0.74	0.115	100.82
ZV10075	231	Zinkgruvan FW	70.9	13.2	0.47	7.05	1.36	3.5	2.93	3	0.28	0.42	0.079	100.48
ZV10081	452	Zinkgruvan FW	67.8	14.8	0.53	6.71	0.89	4.08	4.59	4.64	0.04	0.66	0.197	100.38
ZV10082	452	Zinkgruvan FW	47.7	15.9	1.7	2.25	10.92	6.94	12.24	12.45	0.23	0.88	0.071	99.16
ZV10083	452	Zinkgruvan FW	46.6	15.9	1.92	1.53	11.23	8.15	12.5	12.62	0.22	0.9	0.063	99.21
ZV10084	452	Zinkgruvan FW	49.6	12.4	1.04	0.32	19.13	5.61	10.79	11.13	0.39	0.83	0.071	100.7
ZV10088	452	Zinkgruvan FW	64	13.3	1.02	7.26	0.81	2.33	4.42	4.75	0.07	0.31	0.075	94.27
ZV10090	452	Zinkgruvan FM	74.6	14.5	1.85	0.34	7.73	1.45	1.58	1.59	0.06	0.42	0.06	102.61
ZV10091	452	Zinkgruvan FW	68	12.9	0.42	6.24	0.42	2.75	9.39	9.17	0.11	0.28	0.018	100.34
ZV10094	453	Zinkgruvan FW	69.7	11.3	0.8	3.4	1.39	3.22	4.42	4.74	0.24	0.22	0.042	95.32
ZV10095	453	Zinkgruvan FW	68.3	12.1	0.47	4.06	0.61	2.75	6.56	6.82	0.23	0.34	0.024	95.88
ZV10096	453	Zinkgruvan FW	71.2	13.2	0.67	5.23	1.43	2.08	3.11	3.12	0.07	0.33	0.021	97.38
ZV10099	453	Zinkgruvan FW	69.9	12.7	0.3	5.37	0.21	3.13	3.42	3.41	0.02	0.24	0.01	95.3
ZV10101	453	Zinkgruvan FW	62.5	10.7	0.38	5.78	0.76	2.59	2.06	3.74	0.05	0.19	0.019	89.3
ZV10102	453	Zinkgruvan FW	69.1	11.8	0.37	4.95	0.26	2.86	1.94	3.35	0.02	0.24	0.01	93.6
ZV10103	453	Zinkgruvan FW	66.8	10	0.23	3.15	1.74	3.52	8.28	10.53	0.2	0.19	0.014	97.38
ZV10104	453	Zinkgruvan FW	68.6	12	0.22	3.98	1.44	2.51	4.89	4.92	0.07	0.29	0.013	94.06
ZV10106	453	Zinkgruvan FW	63.1	12.6	0.82	6.15	2.93	3.46	3.62	3.88	0.13	0.47	0.125	93.89
ZV10107	453	Zinkgruvan FW	66.6	12.2	1	4.07	3.11	3.75	5.31	5.45	0.16	0.36	0.084	96.97
ZV10109	454	Zinkgruvan FW	68.7	14.1	0.47	6.65	0.98	3.75	4.8	4.82	0.02	0.64	0.173	100.34
ZV10113	454	Zinkgruvan FW	82.3	9.9	0.37	3.43	0.19	1.95	2.19	2.21	0.03	0.19	0.019	100.69
ZV10114	454	Zinkgruvan FW	56.9	19.1	0.66	9.64	0.32	2.69	3.15	4.85	0.08	0.37	0.036	96.29
ZV10116	454	Zinkgruvan FW	69	12.3	0.83	6.97	5.54	1.97	3.3	3.53	0.2	0.27	0.105	101.06
ZV10118	454	Zinkgruvan FW	68.6	14.3	1.18	9.93	0.16	3.19	2.22	2.52	0.02	0.32	0.022	100.4

Appendix E Table E6
Metavolcanic samples

SAMPLE	HOLE	POSITION	SiO2	Al2O3	Na2O	K2O	CaO	MgO	FeO*	FeO (tot)	MnO	TiO2	P2O5	SUM
ZV10119	454	Zinkgruvan FW	75.1	12.8	1.17	6.28	1.85	2.21	1.68	1.68	0.05	0.2	0.034	101.39
ZV10139	456	Zinkgruvan FM	75.6	9.3	0.48	6.75	0.68	0.68	0.35	4.58	0.02	0.24	0.06	100.33
ZV10140	456	Zinkgruvan FW	66.5	15	0.72	12.05	1.06	0.77	0.48	1.57	0.02	0.37	0.074	98.65
ZV10141	456	Zinkgruvan FM	71.1	14.5	0.59	11.8	0.66	0.53	0.71	1.44	0.02	0.36	0.064	101.42
ZV10144	456	Zinkgruvan FM	76	12	0.35	9.37	0.91	0.8	0.73	0.76	0.02	0.3	0.07	100.61
ZV10146	457	Zinkgruvan FW	71	12.2	0.67	6.15	1.94	2.38	1.78	3.48	0.05	0.46	0.172	99.73
ZV10147	457	Zinkgruvan FW	72.3	10.7	0.94	5.62	0.75	2.45	2.63	3.03	0.02	0.42	0.131	96.68
ZV10148	457	Zinkgruvan FW	62.4	11.5	0.42	6.99	7.81	4.29	4.41	4.6	0.26	0.29	0.086	99.05
ZV10153	457	Zinkgruvan FW	71.4	11.6	0.36	9.05	0.38	0.72	1.45	2.52	0.05	0.29	0.061	97.3
ZV10154	457	Zinkgruvan FW	63.1	13.3	0.58	10.6	4.48	1.77	2.71	3.28	0.24	0.32	0.463	99.23
ZV10155	457	Zinkgruvan FM	45.7	14.9	0.49	9.71	0.77	5.23	12.06	14.5	0.44	0.55	0.181	94.98
ZV10170	458	Zinkgruvan HW	65.5	16.5	2.29	3.88	1.3	2.06	5.2	5.3	0.05	0.57	0.069	97.58
ZV10171	458	Zinkgruvan HW	55.7	14.7	1.79	3.29	1.48	3.01	6.62	14.6	0.04	0.49	0.086	98.78
ZV10172	458	Zinkgruvan HW	61.3	14.6	2.06	3.09	1.49	2.84	4.18	10.31	0.06	0.51	0.115	99.16
ZV10174	458	Zinkgruvan HW	72	2.2	0.13	0.14	4.71	4.09	4.9	12.46	0.05	0.06	0.165	99.43
ZV10175	458	Zinkgruvan HW	56.7	15.3	2.02	3.3	4.21	2.76	8.31	8.48	0.1	1.55	0.782	95.29
ZV10176	458	Zinkgruvan HW	62.2	11.8	0.89	2.5	1.94	5.01	8.19	13.2	0.18	0.34	0.306	100.65
ZV10179	458	Zinkgruvan HW	66.5	15.1	2.8	1.91	3.23	2.23	4.67	4.72	0.08	0.65	0.142	97.42
ZV10180	458	Zinkgruvan HW	53.5	19.8	1.25	3.95	0.88	3.09	7.82	7.83	0.07	0.81	0.06	91.26
ZV10181	458	Zinkgruvan FW	66.2	9.8	0.31	6.99	6.84	2.92	2.61	4.6	0.28	0.24	0.088	99.47
ZV10182	458	Zinkgruvan FW	68.5	8.8	0.28	5.6	7.78	3.57	3.68	4.52	0.27	0.23	0.065	100.27
ZV10183	458	Zinkgruvan FW	57	17.8	0.36	12.5	1.4	5.47	3.49	4.46	0.08	0.84	0.181	100.6
ZV10184	458	Zinkgruvan FW	59.8	14.7	0.58	10.6	3.97	2.61	2.4	3.79	0.21	0.33	0.245	98.53
ZV10191	506	Zinkgruvan HW	84	7.8	0.59	5.02	0.38	1.05	0.77	1.93	0.02	0.21	0.057	101.62
ZV10192	506	Zinkgruvan HW	77.9	6.8	0.34	1.73	4.63	3.23	2.71	4.39	0.22	0.25	0.072	100.48
ZV10193	506	Zinkgruvan HW	76	8.3	0.48	5.03	0.54	1.45	1.28	6.02	0.05	0.36	0.129	100.56
ZV10194	506	Zinkgruvan HW	73.2	7.3	0.28	1.91	4.78	3.36	3.78	5.16	0.37	0.22	0.123	98.07
ZV10195	506	Zinkgruvan HW	78.7	10.3	0.95	5.67	1.05	1.51	2.27	2.52	0.04	0.31	0.1	101.33
ZV10196	506	Zinkgruvan FW	74.1	10.8	0.47	6.8	0.9	2.9	2.64	3.4	0.04	0.89	0.184	100.89
ZV10198	511	Zinkgruvan FW	67.9	10.4	0.68	7.21	2.74	2.08	1.44	3.05	0.16	0.26	0.105	96.31

Appendix E Table E6
Metavolcanic samples

SAMPLE	HOLE	POSITION	SiO2	Al2O3	Na2O	K2O	CaO	MgO	FeO*	FeO (tot)	MnO	TiO2	P2O5	SUM
ZV10199	511	Zinkgruvan FW	65.3	11.6	0.75	7.18	2.43	3.81	3.22	4.19	0.17	0.35	0.168	97.24
ZV10200	511	Zinkgruvan FW	60.8	13.9	1.34	8.05	1.37	2.84	3.7	4.38	0.1	0.47	0.137	94.38
ZV10203	511	Zinkgruvan FW	44.2	17.4	0.4	4.1	11.32	7.8	10.39	10.43	0.55	1.01	0.203	97.54
ZV10204	511	Zinkgruvan FW	18.6	5.1	0.14	2.67	30.39	10.65	9.07	9.64	0.86	0.22	0.134	79.63
ZV10205	511	Zinkgruvan FW	50.2	10.2	0.42	6	11.51	7.97	8.84	9.54	0.89	0.3	0.243	98.5
ZV10206	511	Zinkgruvan FW	26.1	8.3	0.14	4.46	19.22	9.42	12.88	13.95	0.75	0.25	3.2	89.41
ZV10228	517	Zinkgruvan HW	63	12	1.58	2.34	1.82	2.65	7.03	9.77	0.12	0.42	0.142	95.09
ZV10229	517	Zinkgruvan HW	60.8	10.4	0.27	2.38	2.82	4.36	6.29	12.28	0.14	0.35	0.151	96.64
ZV10230	517	Zinkgruvan HW	54.5	12.8	1.79	2.55	1.76	3.21	2.08	17.21	0.06	0.5	0.256	101.43
ZV10231	517	Zinkgruvan HW	58	9.42	0.09	2.14	1.53	5.31	20.03	21.11	0.12	0.56	0.218	99.02
ZV10232	517	Zinkgruvan HW	67.2	3.67	0.21	0.35	5.41	4.72	5.25	15.53	0.13	0.13	0.286	102.25
ZV10233	517	Zinkgruvan HW	60.2	9.15	1.14	2.29	1.85	3.13	0.24	17.11	0.05	0.28	0.239	102.99
ZV10234	517	Zinkgruvan HW	56.9	18.2	1.36	5.37	1.36	2.42	5.75	6.38	0.06	0.64	0.08	93.07
ZV10235	517	Zinkgruvan HW	63.5	15.1	1.74	4.95	1.47	1.92	4.28	4.45	0.1	0.5	0.066	93.87
ZV10237	517	Zinkgruvan HW	59.5	17.7	1.74	3.9	1.41	2.61	6.66	6.89	0.11	0.77	0.056	94.8
ZV10241	555	Zinkgruvan FW	75.4	10.3	0.43	6.36	1.76	1.21	0.51	1.54	0.14	0.32	0.176	98.45
ZV10242	555	Zinkgruvan FW	68.3	11.2	0.75	4.25	1.9	3.55	3.95	5.78	1.13	0.43	0.135	99
ZV10243	555	Zinkgruvan FW	68.2	12.1	0.93	5.87	0.82	2.09	3.52	5.34	0.39	0.37	0.145	97.82
ZV10259	556	Zinkgruvan FW	70.5	13.9	0.48	7.32	2.18	1.55	3.39	3.56	0.19	0.29	0.063	100.25
ZV10260	556	Zinkgruvan FM	71	10.8	0.38	8.91	6.58	0.09	0.34	0.37	0.12	0.34	0.16	98.78
ZV10265	559	Zinkgruvan FM	13	3.41	0.06	1.19	36.8	12.8	8.27	9.06	1.14	0.1	0.129	78.59
ZV10266	559	Zinkgruvan FM	9.93	2.23	0.02	0.83	37.8	13.3	6.86	8.3	1.18	0.05	0.117	74.74
ZV10267	559	Zinkgruvan FM	13.1	1.49	0.04	1.2	34.5	14.2	7.74	9.58	1	0.06	0.139	76.6
ZV10268	559	Zinkgruvan FM	12	1.09	0.03	0.67	36.2	14.3	7.9	12.18	0.94	0.08	0.111	81.03
ZV10269	559	Zinkgruvan FM	17.4	3.99	0.04	3.22	31	10.6	8.91	11.44	0.87	0.34	0.163	81.06
ZV10274	560	Zinkgruvan FM	69.7	13.6	0.77	11.7	1.14	0.78	0.44	1.25	0.03	0.33	0.1	99.87
ZV10275	560	Zinkgruvan FM	68.4	12.9	0.49	11.4	1.5	0.88	0.28	2.22	0.03	0.36	0.099	99.81
ZV10279	560	Zinkgruvan FM	67.5	10.5	0.29	8.56	4.71	1.95	5.55	5.38	0.12	0.28	0.082	99.39
ZV10282	570	Zinkgruvan FM	72.1	12.4	0.43	9.24	1.24	0.56	0.43	2.89	0.06	0.16	0.027	100.25
ZV10285	570	Zinkgruvan HW	64.5	14.8	1.58	4.99	1.26	2.69	4.16	6.05	0.07	0.51	0.086	97.43

Appendix E Table E6
Metavolcanic samples

SAMPLE	HOLE	POSITION	SiO2	Al2O3	Na2O	K2O	CaO	MgO	FeO*	FeO (tot)	MnO	TiO2	P2O5	SUM
ZV10286	570	Zinkgruvan HW	57.9	20.1	1.54	4.5	0.84	3.05	7.25	7.41	0.07	0.76	0.082	96.33
ZV10292	574	Zinkgruvan HW	75.8	12.4	0.58	3.31	1.44	3.27	3.55	3.55	0.06	0.22	0.012	100.66
ZV10293	575	Zinkgruvan orezone	74.2	11	0.26	4.58	2.01	2.1	4.69	5.03	0.24	0.24	0.027	100.04
ZV10294	575	Zinkgruvan orezone	73.4	13.4	0.32	6.11	1.15	1.76	3.83	3.91	0.1	0.28	0.024	100.49
ZV10295	579	Zinkgruvan FW	68.8	12.2	0.63	5.51	2.13	4.21	3.15	3.23	0.14	0.34	0.058	97.39
ZV10298	579	Zinkgruvan FW	66.3	14.5	0.46	7.41	0.95	2.42	2.71	2.79	0.06	0.29	0.053	95.29
ZV10300	579	Zinkgruvan FW	62.3	10.9	0.31	7.88	9.85	0.26	1.24	1.25	0.14	0.54	0.136	93.57
ZV10303	579	Zinkgruvan FW	66.3	14	0.48	7.14	0.78	3.81	4.9	4.9	0.04	0.65	0.195	98.31
ZV10306	580	Zinkgruvan FW	67.6	12.9	0.51	8.03	2.03	3.09	3.19	3.79	0.37	0.41	0.127	99.61
ZV10308	580	Zinkgruvan orezone	65.9	12.7	0.45	7.57	1.55	2.4	5.36	6.84	0.53	0.38	0.161	99.49
ZV10314	581	Zinkgruvan HW	52.7	19.2	1.32	4.48	0.75	2.9	7.44	7.44	0.07	0.78	0.06	89.71
ZV10315	581	Zinkgruvan HW	58.6	17.7	1.86	4.51	1.19	2.76	7	7.01	0.06	0.84	0.071	94.61
ZV10316	581	Zinkgruvan HW	61.3	10.1	0.78	2.1	1.29	4.66	15.92	17.67	0.24	0.45	0.259	99.66
ZV10317	581	Zinkgruvan HW	72.1	11.9	0.91	6.87	0.95	1.47	2.23	2.7	0.09	0.2	0.022	97.44
ZV10322	581	Zinkgruvan HW	69.3	13.5	1.33	5.48	0.82	1.66	2.75	2.76	0.07	0.19	0.011	95.13
ZV10324	581	Zinkgruvan HW	65.5	13.7	1.1	7.19	1.56	3.37	3.87	4.05	0.13	0.33	0.042	97.11
ZV10325	581	Zinkgruvan HW	67.7	15	0.98	7.92	2.01	1.93	2.29	2.72	0.14	0.37	0.064	99.06
ZV10327	581	Zinkgruvan HW	70.6	12.6	0.75	6.96	2.28	2.11	4.09	4.34	0.16	0.36	0.083	100.42
ZV10330	581	Zinkgruvan HW	69.6	10.6	0.42	7.48	3.08	1.04	1.43	2.15	0.2	0.18	0.036	95.26
ZV10332	581	Zinkgruvan HW	65.6	15.4	0.69	6.63	0.59	2.41	4.69	4.71	0.07	0.33	0.02	96.53
ZV10334	581	Zinkgruvan orezone	62.8	14.6	0.45	10.37	0.28	2.86	4.14	4.09	0.07	0.3	0.03	95.92
ZV10335	581	Zinkgruvan orezone	32.5	6.7	2.9	2.6	1.72	1.73	5.24	5.19	0.2	0.14	0.056	67.83
ZV10336	581	Zinkgruvan orezone	65.1	11.8	0.51	7.26	2.1	3.22	3.06	4.31	0.16	0.29	0.044	96.8
ZV10337	581	Zinkgruvan orezone	28.5	7.4	1.15	2.93	6.08	1.64	2.08	5.39	0.34	0.17	0.082	65.95
ZV10338	581	Zinkgruvan orezone	62.3	13.6	0.52	6.39	5.49	3.63	4.54	5.99	0.29	0.36	0.118	99.6
ZV10339	581	Zinkgruvan orezone	68.4	11	0.43	5.17	4.35	2.95	3.33	3.54	0.2	0.26	0.091	96.59
ZV10340	581	Zinkgruvan FW	71.1	12.6	0.94	7.51	0.76	2.32	2.18	2.38	0.04	0.25	0.054	98.07
ZV10341	581	Zinkgruvan FW	66.1	13.3	0.56	8.41	1.27	2.82	2.37	4.28	0.37	0.4	0.131	99.17
ZV10342	581	Zinkgruvan FW	65.2	12.2	0.39	8.1	4.9	2.9	2.85	4.04	0.55	0.28	0.102	99.58
ZV10343	581	Zinkgruvan FW	64.9	13.4	0.51	7.5	0.77	3.1	6.86	8	0.42	0.32	0.067	99.73

Appendix E Table E6
Metavolcanic samples

SAMPLE	HOLE	POSITION	SIO2	Al2O3	Na2O	K2O	CaO	MgO	FeO*	FeO (tot)	MnO	TiO2	P2O5	SUM
ZV10344	581	Zinkgruvan FM	56.4	7	0.28	1.6	4.25	4.68	6.38	17.97	0.43	0.17	0.214	98.51
ZV10345	581	Zinkgruvan FM	64.6	9.7	0.43	5.92	7.6	3.9	3.32	4.72	0.4	0.26	0.115	98.91
ZV10346	581	Zinkgruvan FW	67.7	10.4	0.61	7.39	1.79	1.34	0.03	2.21	0.1	0.3	0.103	94.74
ZV10347	581	Zinkgruvan FW	74.1	11.2	0.48	8.29	0.66	0.61	0.28	1.13	0.02	0.26	0.067	97.71
ZV10348	581	Zinkgruvan FW	72.8	10.9	0.5	7.78	0.81	0.65	0.04	1.25	0.03	0.28	0.098	96.47
ZV10349	581	Zinkgruvan FW	65.1	15.2	0.57	9.66	0.34	2.3	6.32	6.86	0.05	0.41	0.062	100.84
ZV10350	581	Zinkgruvan FW	62.4	7.3	0.25	1.05	1.39	5.92	16.91	18.89	0.2	0.21	0.233	98.89
ZV10351	581	Zinkgruvan FW	65.9	11.1	0.25	5.67	1.1	3.06	8.04	10.77	0.21	0.25	0.071	99.7
ZV10353	581	Zinkgruvan FW	67.2	12.2	0.3	7.89	1.21	2.22	5.4	6.49	0.14	0.22	0.044	98.5
ZV10354	581	Zinkgruvan FW	74.3	10.2	0.33	5.48	1.79	1.72	2.57	3.3	0.12	0.17	0.023	97.83
ZV10355	581	Zinkgruvan FW	60.9	18.5	0.58	11.19	0.16	2.59	3.51	3.69	0.05	0.29	0.026	98.1
ZV10359	581	Zinkgruvan FW	51.5	18.1	0.49	9.29	4.57	6.4	5.15	7.6	0.24	0.49	0.083	99.97
ZV10370	587	Zinkgruvan FW	67.4	12	0.86	8.02	1.65	2.03	2.58	5.92	0.34	0.37	0.112	100.59
ZV10371	587	Zinkgruvan FW	74.8	11.9	0.99	7.4	0.16	1.97	2.64	2.72	0.03	0.23	0.023	100.29
ZV10372	639	Zinkgruvan FW	64.1	13	0.64	5.58	2.44	4.29	2.98	4.46	0.31	0.42	0.127	96.88
ZV10373	639	Zinkgruvan FW	62.3	15	0.55	6.06	2.68	3.57	2.78	2.87	0.31	0.38	0.122	94.13
ZV10374	639	Zinkgruvan FW	64.8	12.7	0.57	6.09	2.03	3.62	3.45	4.96	1.26	0.42	0.127	98.22
ZV10375	639	Zinkgruvan FW	62.6	12	0.49	4.47	2.06	3.99	3.11	6.5	1.98	0.46	0.14	97.23
ZV10376	639	Zinkgruvan FW	63.9	10.9	0.54	3.48	2.19	4.24	3.94	8.14	1.26	0.37	0.136	98.01
ZV10377	639	Zinkgruvan FW	62.9	13.1	0.51	5.94	2.09	3.82	3.83	5.17	1.4	0.38	0.106	96.97
ZV10378	639	Zinkgruvan FW	69.4	12.7	0.36	7.88	0.78	2.38	3.21	3.26	0.03	0.22	0.016	97.05
ZV10380	650	Zinkgruvan HW	61.4	14.3	1.92	3.67	1.21	2.77	0.53	9.81	0.05	0.42	0.084	99.82
ZV10381	650	Zinkgruvan HW	63.2	12.1	2.05	1.86	1.79	2.87	0.03	10.52	0.07	0.41	0.135	99.76
ZV10391	677	Zinkgruvan FW	70.4	12.7	0.32	9.36	1.47	2.96	1.53	1.96	0.06	0.37	0.094	99.91
ZV10392	677	Zinkgruvan FW	64.7	10.9	0.38	6.67	7.7	5.14	3.05	4.03	0.21	0.27	0.092	100.65
ZV10393	677	Zinkgruvan FW	70.5	11.1	0.29	9.31	4.42	2.02	1.07	2	0.14	0.15	0.064	100.45
ZV10394	677	Zinkgruvan FW	69.3	12.2	0.34	7.83	0.48	3.02	5.78	6.02	0.24	0.4	0.027	100.02
ZV10397	677	Zinkgruvan orezone	34	2.89	1.11	0.15	20.5	4.71	7.65	9.95	1	0.1	0.114	80.52
ZV10398	690	Zinkgruvan HW	71.3	12.2	0.96	4.74	2.72	1.59	1.84	2.17	0.09	0.28	0.095	96.37
ZV10399	690	Zinkgruvan HW	73.8	11.4	0.9	5.06	2.92	1.32	2.2	2.68	0.37	0.26	0.053	99.04

Appendix E Table E6
Metavolcanic samples

SAMPLE	HOLE	POSITION	SiO2	Al2O3	Na2O	K2O	CaO	MgO	FeO*	FeO (tot)	MnO	TiO2	P2O5	SUM
ZV10412	690	Zinkgruvan orezone	70.8	11.9	1.74	3.68	2.51	2.01	3.37	3.52	0.11	0.31	0.059	96.71
ZV10413	690	Zinkgruvan orezone	61.9	10.6	1.18	3.8	2.22	2.03	3.29	7.47	0.43	0.25	0.124	94.53
ZV10414	690	Zinkgruvan orezone	66.9	10.6	0.69	3.07	5.15	2.8	2.51	4.33	0.76	0.26	0.121	96.27
ZV10415	690	Zinkgruvan orezone	67.4	11.8	0.37	7.19	2.21	1.35	1.57	1.76	0.09	0.21	0.06	92.55
ZV10417	8502	Zinkgruvan orezone	68.6	12.8	0.31	6.94	3.9	1.53	5.67	5.66	0.15	0.34	0.092	100.33
ZV10418	8502	Zinkgruvan FW	73.7	12.3	0.4	8.83	0.34	0.72	2.24	2.23	0.02	0.21	0.025	98.8
ZV10419	8502	Zinkgruvan orezone	64.6	13.5	0.52	8.9	0.84	1.31	4.82	4.99	0.09	0.54	0.158	95.86
ZV10420	8502	Zinkgruvan orezone	49.6	11.4	0.93	4.46	5.49	2.3	7.36	10.34	0.26	0.4	0.284	90.92
ZV10425	8502	Zinkgruvan FM	72.8	13.4	0.64	9.46	0.35	0.66	2.36	2.35	0.04	0.29	0.033	100.04
ZV10427	8502	Zinkgruvan HW	64.1	10.7	0.21	5.19	11.25	4.4	3.28	3.27	0.67	0.27	0.062	100.16
ZV10428	8502	Zinkgruvan HW	63.7	16.7	0.73	8.89	2.42	1.63	3.61	3.64	0.11	0.34	0.027	98.21
ZV10430	8506	Zinkgruvan FM	70.7	11.8	0.5	4.82	3.37	2.61	3.1	4.39	0.2	0.38	0.146	99.92
ZV10431	8506	Zinkgruvan FM	70.2	13.6	0.71	6.89	1.9	2.51	3.42	3.66	0.15	0.39	0.084	100.25
ZV10432	8506	Zinkgruvan FM	67.8	10.8	0.59	5.91	3.61	1.75	5.02	6.76	0.31	0.22	0.293	99.31
ZV10434	8509	Zinkgruvan FM	61.2	16.7	0.1	3.51	1.56	5.97	5.36	8.36	0.15	0.71	0.106	99.71
ZV10435	8509	Zinkgruvan FM	57.7	15.5	0.87	4.4	0.94	3.17	6.17	6.44	0.07	0.64	0.089	90
ZV10436	8509	Zinkgruvan FM	57.8	16.7	0.44	3.8	0.48	3.82	6.37	9.2	0.05	0.49	0.082	94.19
ZV10437	8509	Zinkgruvan FM	56.7	18.4	0.93	6.12	0.5	3	4	5.55	0.04	0.48	0.078	92.55
ZV10438	8509	Zinkgruvan FM	59.4	18.1	0.5	5.63	0.45	3.21	4.22	6.88	0.04	0.52	0.09	96.08
ZV10445	8510	Zinkgruvan FM	53.3	18.8	1.21	5.63	1.55	4.13	5.23	5.7	0.2	0.65	0.068	91.47
ZV10554	248	Zinkgruvan FM	73.7	11.2	0.4	8.74	1.75	0.91	1.67	1.67	0.07	0.33	0.08	98.85
ZV10581	889	Zinkgruvan FM	58.6	9.28	0.68	6.14	12.5	6.69	4.45	4.45	0.38	0.26	0.1	99.08
ZV10582	889	Zinkgruvan FM	42.5	17	0.23	9.24	7.97	7.65	6.55	6.55	0.19	1.07	0.19	92.59
ZV10583	889	Zinkgruvan FM	55.6	9.66	0.27	7.67	11.6	7.12	5.14	5.14	0.4	0.43	0.12	98.01
ZV10595	942	Zinkgruvan FM	63.1	16.7	0.68	12.5	0.78	1.71	2.6	2.6	0.05	0.91	0.2	99.23
ZV10596	942	Zinkgruvan FM	73.9	12.3	0.63	9.89	0.63	0.49	0.82	0.82	0.05	0.3	0.06	99.07
ZV10597	942	Zinkgruvan FM	64.2	9.95	0.49	7.31	5.03	4.67	3.68	3.68	0.19	0.21	0.05	95.78
ZV10598	942	Zinkgruvan FM	58.3	11.8	0.54	7.99	10	4.9	4.49	4.49	0.37	0.23	0.05	98.67
ZV10599	942	Zinkgruvan FM	69	15.5	0.44	12	0.6	0.58	0.96	0.96	0.03	0.43	0.1	99.64
ZV10600	942	Zinkgruvan FM	65.2	13.9	0.33	11.2	5.16	1.54	1.34	1.34	0.13	0.38	0.09	99.27

Appendix E Table E6
Metavolcanic samples

SAMPLE	HOLE	POSITION	SiO2	Al2O3	Na2O	K2O	CaO	MgO	FeO*	FeO (tot)	MnO	TiO2	P2O5	SUM
ZV10601	942	Zinkgruvan FM	62.5	15	0.36	7.02	8.47	1.53	2.48	2.48	0.14	0.45	0.18	98.13
ZV10602	942	Zinkgruvan FM	65.8	14.6	0.45	11.8	0.56	0.69	3.03	3.03	0.03	0.43	0.1	97.49
ZV10603	942	Zinkgruvan FM	81.8	9.03	0.39	7.3	0.29	0.22	0.56	0.56	0.02	0.25	0.07	99.93
ZV10604	942	Zinkgruvan FM	69.4	15.5	0.47	12.4	0.78	0.41	0.46	0.46	0.02	0.49	0.1	100.03
ZV10605	942	Zinkgruvan FM	67.2	9.94	0.4	7.92	6.84	3.41	2.86	2.86	0.23	0.29	0.07	99.16
ZV10606	942	Zinkgruvan FM	77.3	10.9	0.41	9.18	0.61	0.23	0.33	0.33	0.02	0.34	0.1	99.42
ZV10626	994	Zinkgruvan FM	72.8	12.7	0.56	9.87	0.78	0.36	0.74	0.74	0.02	0.37	0.09	98.29
ZV10627	994	Zinkgruvan FM	62	11.6	0.45	7.9	4.49	2.01	7.16	7.16	0.12	0.34	0.1	96.17
ZV10628	994	Zinkgruvan FM	61.9	15.9	0.56	12.8	1.61	1.33	3.24	3.24	0.05	0.48	0.14	98.01
ZV10629	994	Zinkgruvan FM	54.9	16	0.41	11.5	2.77	2	6.08	6.08	0.08	0.54	0.22	94.5
ZV10630	994	Zinkgruvan FM	60.8	14	0.41	11	3.39	1.79	3.54	3.54	0.11	0.38	0.14	95.56
ZV10631	994	Zinkgruvan FM	68.7	7.99	0.43	6.48	5.43	2.99	4.05	4.05	0.2	0.22	0.09	96.58
ZV1113		Zinkgruvan FM	62.57	11.41	0.68	6.64	0.86	5.08	2.24	2.66	0.06	0.3	0.08	90.62
ZV1117		Zinkgruvan FM	66.84	13.36	1.37	6.99	1.33	0.82	1	1	0.03	0.2	0.05	91.99
ZV1118		Zinkgruvan FM	64.73	11.03	0.28	6.18	0.07	2.71	2.87	2.87	0.05	0.24	0.04	88.19
ZV1120		Zinkgruvan FM	69.17	11.48	0.38	8.75	0.14	0.35	0.85	0.86	0.01	0.18	0.03	91.36
ZV1121		Zinkgruvan FM	68.15	11.39	0.3	5.17	0.09	2.7	2.97	2.97	0.02	0.19	0.04	91.02
ZV1122		Zinkgruvan FM	68.88	12.02	0.37	6.34	0.03	1.72	2.97	2.97	0.04	0.19	0.06	92.62
ZV1123		Zinkgruvan FM	67.53	11.61	1.04	3.18	1.92	3.4	2.71	2.71	0.03	0.23	0.03	91.68
ZV1127		Zinkgruvan FM	65.28	12.06	0.84	4.52	0.31	2.23	2.4	2.4	0.02	0.22	0.03	87.91
ZV1129		Zinkgruvan FM	68	12.08	0.16	4.8	0.02	3.93	2.62	2.62	0.02	0.22	-0.01	91.84
ZV1130		Zinkgruvan FM	61.48	11.86	0.62	6.16	0.16	2.02	5.58	5.57	0.1	0.23	0.08	88.28
ZV1133		Zinkgruvan FM	63.33	13.1	0.55	6.51	0.63	1.18	2.73	2.73	0.11	0.23	0.08	88.44
ZV1136		Zinkgruvan FM	62.84	13.19	0.46	3.94	2.12	2.71	4.46	4.49	0.2	0.31	0.08	90.39
ZV1159		Zinkgruvan FM	66.08	14.07	0.54	10.82	0.06	0.28	1.22	1.23	0.03	0.17	0.05	93.35
ZV1161		Zinkgruvan FM	65.07	13.31	0.45	7.13	1.42	1.05	1.4	1.4	0.09	0.18	0.04	90.14
ZV1164		Zinkgruvan FM	65.08	13.68	1.94	1.8	4.34	0.29	1.83	2.42	0.08	0.22	0.08	90.19
ZV1167		Zinkgruvan FM	66.82	12.34	1.48	5.53	0.66	0.24	3.49	3.52	0.08	0.22	0.09	91.01
ZV1172		Zinkgruvan FM	62.08	13.32	0.34	6.78	0.02	3.15	2.92	2.92	0.02	0.35	0.07	89.06
ZV1173		Zinkgruvan FM	51.49	15.92	0.5	11.34	0.33	6.08	4.05	4.03	0.13	0.58	0.19	90.62

Appendix E Table E6
Metavolcanic samples

SAMPLE	HOLE	POSITION	SiO2	Al2O3	Na2O	K2O	CaO	MgO	FeO*	FeO (tot)	MnO	TiO2	P2O5	SUM
ZV1174		Zinkgruvan FM	66.18	12.44	0.28	6.35	0.03	3.02	2.78	2.76	0.03	0.31	0.07	91.49
ZV1177		Zinkgruvan FM	58.69	11.49	0.36	6.23	4.2	7.36	3.64	4.01	0.19	0.27	0.09	93.13
ZV1178		Zinkgruvan FM	63.18	13.35	0.19	4.69	0.12	1.86	5.04	5.04	0.06	0.3	0.07	88.86
ZV1179		Zinkgruvan FM	72.42	11.04	0.21	8.51	0.06	-0.15	0.31	0.31	0	0.2	0.03	92.62
ZV1180		Zinkgruvan FM	64.47	12.91	0.49	5.57	0.76	1.54	5.46	5.47	0.07	0.39	0.1	91.77
ZV1181		Zinkgruvan FM	58	15.07	0.33	6.72	0.14	1.9	6.65	6.65	0.08	0.32	0.07	89.28
ZV1182		Zinkgruvan FM	69.03	11.67	0.27	9.04	0.51	0.51	1.8	1.8	0.04	0.22	0.04	93.13
ZV1183		Zinkgruvan FM	68.63	10.56	0.3	4.37	1.64	1.9	2.52	2.52	0.04	0.22	0.03	90.21
ZV1184		Zinkgruvan FM	63.39	13	0.29	7.03	0.05	2.21	3.9	3.91	0.05	0.37	0.1	90.41
ZV1188		Zinkgruvan FM	68.59	11.41	0.23	8.89	0.79	0.57	1.07	1.08	0.04	0.23	0.06	91.89
ZV1189		Zinkgruvan FM	60.55	11.68	0.34	3.37	1.6	2.55	4.45	7.14	0.21	0.31	0.14	89.66
ZV1190		Zinkgruvan FM	69.36	11.5	2.01	3.7	1.63	1.76	3.49	3.51	0.05	0.22	0.05	93.8
ZV1191		Zinkgruvan FM	66.25	11.35	0.23	8.63	0.61	0.87	1.82	1.84	0.04	0.28	0.04	90.15
ZV1194		Zinkgruvan FM	64.98	12.2	0.42	4.9	0.06	2.8	3.15	3.15	0.02	0.19	0.06	88.78
ZV1195		Zinkgruvan FM	63.44	11.18	0.32	5.46	0.06	1.94	4.76	4.76	0.04	0.23	0.04	87.47
ZV1196		Zinkgruvan FM	68.73	11.91	0.44	5.15	0.17	2.8	1.93	1.93	0.01	0.31	0.05	91.49
ZV1198		Zinkgruvan FM	66.72	12.51	0.31	6.15	0.09	3.08	2.04	2.04	0.02	0.22	0.03	91.17
ZV1204		Zinkgruvan FM	64.69	12	0.28	6.33	0.1	2.6	2.87	2.87	0.03	0.24	0.04	89.17
ZV1207		Zinkgruvan FM	63.19	11.94	0.44	4.92	0.28	1.62	4.39	4.39	0.04	0.23	0.05	87.09
ZV1208		Zinkgruvan FM	68.83	11.05	0.28	5.47	0.03	1.13	4.44	4.44	0.03	0.29	0.07	91.62
ZV1209		Zinkgruvan FM	60.02	11.44	0.39	4.16	0.13	4.34	5.84	5.84	0.05	0.44	0.09	86.89
ZV1210		Zinkgruvan FM	63.6	12.34	0.86	3.82	1.14	2.68	5.11	5.11	0.04	0.37	0.08	90.03
ZV1211		Zinkgruvan FM	62.81	10.9	1.18	3.15	1.35	1.78	5.7	5.74	0.04	0.42	0.05	87.43
ZV1212		Zinkgruvan FM	65.01	14.72	0.27	2.28	0.07	7.27	0.71	0.71	0.02	0.18	0.02	90.54
ZV1213		Zinkgruvan FM	71.44	9.25	0.27	2.1	0.53	2.42	4.3	4.33	0.03	0.18	0.04	90.6
ZV1214		Zinkgruvan FM	65.12	12.62	0.27	3.89	0.02	2.84	4.78	4.78	0.02	0.28	0.07	89.92
ZV1215		Zinkgruvan FM	66.31	12.09	0.32	5.9	0.01	2.3	3.15	3.15	0.01	0.19	0.06	90.34
ZV1216		Zinkgruvan FM	68.16	11.34	0.12	1.43	0.03	7.95	1.62	1.62	0.01	0.4	0.07	91.13
ZV1217		Zinkgruvan FM	66.98	10.95	0.3	6.07	0.01	1.81	3.11	3.11	0.01	0.2	0.04	89.49
ZV1218		Zinkgruvan FM	69.88	12.66	0.5	2.23	0.06	5.63	0.63	0.63	0.01	0.29	0.04	91.93

Appendix E Table E6
Metavolcanic samples

SAMPLE	HOLE	POSITION	SiO2	Al2O3	Na2O	K2O	CaO	MgO	FeO*	FeO (tot)	MnO	TiO2	P2O5	SUM
ZV1223		Zinkgruvan FM	68.2	11.74	0.63	5.74	0.33	1.15	3.83	3.83	0.03	0.23	0.06	91.93
ZV1225		Zinkgruvan FM	68.73	11.89	1	4.45	0.13	3.25	2.58	2.58	0.03	0.25	0.08	92.39
ZV1226		Zinkgruvan FM	63.64	11.53	0.65	5.27	0.06	3.17	5.35	5.35	0.02	0.54	0.08	90.31
ZV1227		Zinkgruvan FM	66.18	10.91	0.38	3.53	0.27	3.42	4.72	4.72	0.02	0.34	0.07	89.83
ZV1228		Zinkgruvan FM	68.91	10.01	0.19	3.41	0.17	1.76	5.18	5.2	0.03	0.2	0.05	89.93
ZV1229		Zinkgruvan FM	71.01	11.36	0.49	2.81	0.08	4.17	1.85	1.85	0.02	0.19	0.05	92.03
ZV1230		Zinkgruvan FM	71.74	10.93	3.46	1.25	0.1	3.32	0.78	0.78	0.01	0.25	-0.01	91.84
ZV1237		Zinkgruvan FM	59.83	13.74	1.36	6.76	0.57	6.13	1.44	1.44	0.02	0.4	0.06	90.31
ZV1238		Zinkgruvan FM	63.06	13.43	0.65	5.87	0.11	3.9	2.75	2.75	0.02	0.29	0.07	90.15
ZV1241		Zinkgruvan FM	60.74	12.86	0.26	5.92	0.03	2.15	6.25	6.25	0.05	0.29	0.08	88.63
ZV1242		Zinkgruvan FM	61.24	13.6	0.3	6.15	0.33	1.61	6.3	6.3	0.06	0.3	0.04	89.92
ZV1253		Zinkgruvan FM	65.94	11.92	0.11	4.49	0.68	2.54	3.01	3.01	0.08	0.21	0.04	89.02
ZV1259		Zinkgruvan FM	63.36	11.01	0.51	4	0.05	4.74	3.44	3.86	0.01	0.44	0.08	88.25
ZV1263		Zinkgruvan FM	77.41	7.25	0.61	2.46	0.1	0.86	5.44	5.44	0.01	0.86	0.12	95.12
ZV1265		Zinkgruvan FM	63.53	13.05	0.37	5.63	0.07	2.35	5.39	5.39	0.06	0.31	0.04	90.79
ZV1274		Zinkgruvan FM	59.74	15.95	0.32	2.83	0.04	9.3	1	1	0.01	0.44	0.07	89.71
ZV1279		Zinkgruvan FM	67.74	11.42	1.62	4.37	0.32	1.18	4.62	4.62	0.02	0.3	0.08	91.67
ZV1280		Zinkgruvan FM	65.02	10.81	0.71	3.12	1.43	1.81	5.16	5.53	0.05	0.27	0.09	89.22
ZV1288		Zinkgruvan FM	67.61	12.28	0.3	2.41	0.13	6.28	1.09	1.09	0.01	0.22	0.05	90.38
ZV1289		Zinkgruvan FM	61.03	12.48	0.72	4.37	0.67	3.08	5.59	5.62	0.03	0.39	0.08	88.49
ZV1290		Zinkgruvan FM	73.52	10.97	0.49	2.52	0.06	4.16	0.55	0.55	0.01	0.19	-0.01	92.46
ZV1296		Zinkgruvan FM	67.79	11.84	2.05	3.46	0.31	2.18	2.61	2.61	0.02	0.2	0.03	90.49
ZV1297		Zinkgruvan FM	70.68	11.23	0.74	6.03	0.08	1.29	1.92	1.92	0.01	0.15	-0.01	92.11
ZV1298		Zinkgruvan FM	60.15	11.62	0.44	6.19	0.02	2.98	8.17	8.26	0.02	0.43	0.07	90.22
ZV1303		Zinkgruvan FM	69.93	11.38	2.21	2.17	0.12	4.29	1.12	1.12	0.01	0.21	-0.01	91.43
ZV1304		Zinkgruvan FM	57.05	11.58	0.17	4.54	0.07	4.21	8.36	8.36	0.04	0.53	0.09	86.64
ZV1305		Zinkgruvan FM	58.1	10.48	0.16	2.51	0.03	3.76	8.44	8.68	0.04	0.28	0.06	84.21
ZV1306		Zinkgruvan FM	65.71	9.83	0.68	2.75	0.27	4.22	3.14	3.14	0.03	0.21	0.04	86.88
ZV1307		Zinkgruvan FM	63.49	12.8	0.57	4.33	0.14	2.82	4.21	4.3	0.02	0.27	0.07	88.84
ZV1312		Zinkgruvan FM	68.9	11.4	2.83	2.3	0.2	3.86	0.94	0.94	0.01	0.17	0.04	90.65

Appendix E Table E6
Metavolcanic samples

SAMPLE	HOLE	POSITION	SiO2	Al2O3	Na2O	K2O	CaO	MgO	FeO*	FeO (tot)	MnO	TiO2	P2O5	SUM
ZV1315		Zinkgruvan FM	69.75	11.42	5.58	0.82	0.12	1.79	1.05	1.05	0.01	0.21	0.02	90.77
ZV1323		Zinkgruvan FM	64.61	12.02	3.11	1.3	3.19	2.3	4.68	4.68	0.05	0.73	0.26	92.25
ZV1327		Zinkgruvan FM	67.54	11.41	2.75	1.22	2.5	1.66	3.85	3.85	0.06	0.43	0.19	91.6
ZV1328		Zinkgruvan FM	69.35	9.9	1.58	3.13	0.27	2.17	3.99	3.99	0.01	0.62	0.1	91.12
ZV1334		Zinkgruvan FM	66.64	11.77	0.21	1.83	0.03	5.86	1.34	1.34	0.01	0.2	-0.01	87.87
ZV1335		Zinkgruvan FM	58.09	8.7	0.2	1.69	0.23	7.82	9.35	9.37	0.02	0.17	0.05	86.36
ZV1348		Zinkgruvan FM	63.18	11.53	0.95	1.34	0.15	5.68	3.82	3.82	0.03	0.2	0.03	86.9
ZV1349		Zinkgruvan FM	67.91	11.52	0.31	2.31	0.04	4.78	1.7	1.7	0.01	0.19	0.05	88.83
ZV1351		Zinkgruvan FM	64.71	11.81	0.67	3.68	0.11	4.4	3.41	3.41	0.02	0.37	0.05	89.22
ZV1352		Zinkgruvan FM	65.07	10.99	0.88	6.13	0.07	2.23	4.51	4.51	0.02	0.47	0.07	90.45
ZV1379		Zinkgruvan FM	64.72	11.43	1.01	5.13	0.07	2.23	4.24	4.24	0.02	0.35	0.08	89.28
ZV1380		Zinkgruvan FM	67.38	10.06	0.46	3.99	0.05	2.95	4.32	4.32	0.01	0.36	0.05	89.63
ZV1408		Zinkgruvan FM	53.37	17.92	7.36	-0.24	4.08	3.33	4.31	4.31	0.03	0.43	0.05	90.63
ZV1417		Zinkgruvan FM	69.87	10.08	1.71	2.55	0.35	1.88	2.39	2.39	0.02	0.38	0.08	89.32
ZV1423		Zinkgruvan FM	61.13	13.81	3.09	4.35	1.87	1.42	3.7	3.7	0.04	0.54	0.22	90.17
ZV1428		Zinkgruvan FM	64.24	7.92	0.08	0.92	0.34	10.11	4.28	4.28	0.02	0.5	0.09	88.5
ZV1430		Zinkgruvan FM	65.55	10.83	2.32	3.39	0.45	3.71	4.21	4.21	0.03	0.36	0.07	90.91
ZV1435		Zinkgruvan FM	68.36	9.57	1.54	2.45	0.46	2.75	3.57	3.65	0.03	0.72	0.1	89.66
ZV1441		Zinkgruvan FM	70.76	9.83	3.41	1.45	0.9	0.73	3.49	3.5	0.02	0.55	0.12	91.27
ZV1453		Zinkgruvan FM	70.43	8.49	0.09	1.23	0.08	4.7	2.75	2.75	0.02	0.41	0.05	88.25
ZV1460		Zinkgruvan FM	61.56	9.87	0.12	2.27	0.03	4.09	5.95	5.95	0.02	0.47	0.07	84.45
ZV1463		Zinkgruvan FM	67.55	9.1	0.29	2.84	0.06	3.01	4.87	4.87	0.02	0.31	0.03	88.09
ZV1465		Zinkgruvan FM	65.86	12.05	4.29	1.11	0.22	4.86	1.81	1.81	0.02	0.32	0.04	90.58
ZV1475		Zinkgruvan FM	65.67	11.56	3.32	2.95	0.94	1.57	3.88	3.88	0.05	0.7	0.13	90.77
ZV1486		Zinkgruvan FM	69.64	11.18	4.11	1.01	1.13	1.26	3.36	3.36	0.04	0.6	0.18	92.51
ZV1492		Zinkgruvan FM	67.06	10.79	4.31	2.06	0.14	2.19	2.94	2.94	0.02	0.33	0.06	89.91
ZV1496		Zinkgruvan FM	69.63	10.88	5.69	0.88	0.33	2.93	1.44	1.44	0.01	0.29	0.04	92.12
ZV1498		Zinkgruvan FM	63.66	15.18	5.19	4.31	0.53	1.4	2.29	2.29	0.02	0.31	0.1	92.99
ZV1669		Zinkgruvan FM	61.88	16.89	0.83	8.97	0.68	3.71	5.38	5.47	0.23	0.69	0.227	99.66
ZV1670		Zinkgruvan FM	81.78	8.83	0.05	3.39	1.92	2.57	1.92	3.01	0.59	0.09	0.095	103.02

Appendix E Table E6
Metavolcanic samples

SAMPLE	HOLE	POSITION	SiO2	Al2O3	Na2O	K2O	CaO	MgO	FeO*	FeO (tot)	MnO	TiO2	P2O5	SUM
ZV1671		Zinkgruvan FM	71.4	12.92	0.61	5.39	0.21	1.81	5.46	5.56	0.21	0.25	0.05	98.48
ZV1672		Zinkgruvan FM	70.27	14.15	0.96	5.25	1.14	1.36	3.09	3.07	0.11	0.28	0.073	96.68
ZV1673		Zinkgruvan FM	73.93	14.7	0.34	5.36	0.26	1.92	3.24	3.25	0.08	0.28	0.068	100.21
ZV1674		Zinkgruvan FM	73.54	14.11	0.2	5.48	1.04	2.07	2.72	2.94	0.22	0.26	0.095	100.19
ZV1675		Zinkgruvan FM	67.82	11.05	0.2	5.53	1.28	1.85	1.8	5.08	0.37	0.22	0.109	95.54
ZV1676		Zinkgruvan FM	69.48	11.62	0.35	4.96	1.37	2.16	2.69	5.83	0.45	0.24	0.112	98.24
ZV1677		Zinkgruvan FM	83.88	6.47	0.11	0.48	5.19	2.09	2.09	2.35	0.63	0.15	0.039	101.61
ZV1681		Zinkgruvan FM	68.81	15.85	0.62	8.98	0.84	2.64	3.1	3.52	0.11	0.24	0.086	101.92
ZV1682		Zinkgruvan FM	68.94	15.07	0.55	10.7	0.61	2.24	3.95	3.99	0.1	0.52	0.232	102.98
ZV1691		Zinkgruvan FM	72.86	15.33	0.75	4.53	0.27	4.29	2.28	2.29	0.03	0.24	0.072	100.69
ZV1695		Zinkgruvan FM	73.02	13.73	0.28	4.07	2.14	6.68	2.35	2.42	0.07	0.39	0.109	102.94
ZV1697		Zinkgruvan FM	54.58	19.32	0.6	11.38	0.1	3.92	5.22	5.16	0.15	0.42	0.133	95.82
ZV3301	231	Zinkgruvan FM	60.8	11.9	1.43	2.82	1.98	1.99	0.47	14.12	0.05	0.31	0.031	101.54
ZV3302	231	Zinkgruvan FM	66.9	10	0.65	2.19	2.13	2.1	1.71	9.8	1.3	0.33	0.035	99.11
ZV3303	231	Zinkgruvan FM	62.7	14.7	0.46	7.02	3.63	1.9	0.45	6.06	0.13	0.7	0.079	99.98
ZV3304	231	Zinkgruvan FM	68.5	12.8	0.52	3.86	2.56	1.9	0.35	6.32	0.07	0.36	0.052	99.66
ZV3305	231	Zinkgruvan FM	68.5	11.9	0.6	3.65	5.31	2.23	1.71	4.46	0.37	0.44	0.035	98.8
ZV3306	231	Zinkgruvan FW	46.3	8.43	0.26	2.39	31.37	2.98	3.11	3.14	0.72	0.2	0.022	95.83
ZV3307	231	Zinkgruvan FW	31.2	4.42	0.05	0.98	44.9	2.17	2.01	2	0.76	0.18	0.013	86.68
ZV3309	231	Zinkgruvan FM	74.9	13.6	0.5	4.03	0.7	2.35	2.54	2.55	0.11	0.21	0.009	98.97
ZV3310	231	Zinkgruvan FM	74.1	14.1	0.56	2.72	0.91	2.77	3.14	3.17	0.12	0.16	0.009	98.64
ZV3311	231	Zinkgruvan FM	77.8	11.4	0.36	2.93	1.6	2.39	2.72	2.77	0.12	0.22	0.009	99.63
ZV3312	231	Zinkgruvan FM	74.8	11.7	0.72	2.49	3.26	2.02	2.54	2.57	0.11	0.19	0.009	97.89
ZV3320	671	Zinkgruvan FM	69	15	0.52	7.11	0.38	2.95	2.98	3.01	0.06	0.3	0.013	98.36
ZV3321	671	Zinkgruvan FM	68.1	11.1	0.72	3.7	1.85	2.49	4.97	7.01	1.21	0.31	0.057	98.12
ZV3322	671	Zinkgruvan FW	51.8	2.81	0.1	0.34	24.85	12.7	6.91	6.9	0.88	0.03	-0.004	100.42
ZV3323	671	Zinkgruvan FM	79.9	9.8	0.18	4.3	0.23	2.1	2.1	2.19	0.01	0.22	0.009	99.01
ZV3324	671	Zinkgruvan FM	75.8	11.4	0.17	5.98	0.17	2.68	2.49	2.51	0.01	0.22	0.009	98.96
ZV3326	671	Zinkgruvan FM	67.2	12.1	0.41	6.1	5.36	5.45	2.28	2.28	0.09	0.21	0.017	99.21
ZV3327	671	Zinkgruvan FM	69.2	12.9	0.38	5.61	2.94	3.94	2.79	2.79	0.01	0.45	0.022	98.23

Appendix E Table E6
Metavolcanic samples

SAMPLE	HOLE	POSITION	SiO2	Al2O3	Na2O	K2O	CaO	MgO	FeO*	FeO (tot)	MnO	TiO2	P2O5	SUM
ZV3328	671	Zinkgruvan FM	59.4	13.5	0.41	6.25	8.59	7.42	3.26	3.26	0.04	0.43	0.035	99.32
ZV3336	671	Zinkgruvan FM	70.6	13.6	0.49	5.97	1.54	3.28	2.69	2.69	0.04	0.72	0.052	98.97
ZV3340	671	Zinkgruvan FM	64.6	14.6	0.37	11.3	2.4	1.45	3	3	0.09	0.48	0.048	98.33
ZV3341	898	Zinkgruvan FM	71.6	14	0.88	10.8	0.43	0.35	0.93	1.1	0.01	0.39	0.026	99.66
ZV3342	898	Zinkgruvan FM	59.8	18.1	0.54	10.3	2.66	3.95	2.8	2.8	0.05	0.29	0.017	98.49
ZV3343	898	Zinkgruvan FM	74.8	13.3	0.45	5.63	0.52	2.28	1.56	1.56	-0.01	0.18	0.009	98.71
ZV3344	898	Zinkgruvan FM	72.1	13.2	0.53	6.36	0.28	2.91	2.09	2.09	-0.01	0.3	0.013	97.76
ZV3345	898	Zinkgruvan FM	57.5	15.2	0.36	9.49	4.32	4.57	4.85	4.98	0.08	1.36	0.096	98.02
ZV3346	898	Zinkgruvan FM	70.4	14.3	0.68	8.92	1.81	1.95	1.4	1.44	0.02	0.21	0.017	99.77
ZV3347	898	Zinkgruvan FM	63.6	12.7	0.59	8.48	6.53	4.15	2.05	2.24	0.12	0.39	0.057	98.95
ZV3348	898	Zinkgruvan FM	69	11.5	0.44	4.61	2.82	4.57	4.22	4.22	0.1	0.44	0.031	97.71
ZV3349	898	Zinkgruvan FW	40.7	5.19	0.08	0.88	18.45	4.29	8.95	19.16	0.44	0.01	0.009	93.83
ZV3350	898	Zinkgruvan FW	52.6	0.86	0.05	0.02	22.39	17.8	4.39	4.41	0.38	0.06	0.013	98.59
ZV3351	898	Zinkgruvan FW	50.8	2.89	0.08	0.28	23.25	15.9	5.49	5.52	0.47	0.09	0.026	99.32
ZV3352	898	Zinkgruvan FM	67.4	14.2	0.76	7.97	1.44	2.92	2.52	2.52	0.04	0.4	0.039	97.67
ZV3353	898	Zinkgruvan FM	75	12	0.59	5.72	0.36	2.51	2.29	2.29	-0.01	0.37	0.013	98.84
ZV3356	898	Zinkgruvan FW	54.1	17.5	0.47	10.1	6.3	6.79	2.01	2.04	0.02	0.75	0.105	98.19
ZV3357	898	Zinkgruvan FM	53.6	10.9	0.18	5.9	15.99	11.1	2.03	2.03	0.06	0.25	0.022	100.02
ZV3362	898	Zinkgruvan FM	73.6	9.08	0.18	4.5	3.51	5.21	3.08	3.1	-0.01	0.48	0.035	99.69
ZV3364	898	Zinkgruvan FM	68	10.5	0.16	4.83	6.2	5.53	2.65	2.65	0.02	0.25	0.022	98.16
ZV3365	898	Zinkgruvan FM	65.9	15.6	0.3	10.7	0.48	3	2.53	2.55	-0.01	0.36	0.017	98.92
ZV3366	898	Zinkgruvan FM	74.2	11.6	0.15	6.9	0.53	2.51	2.69	2.71	-0.01	0.3	0.013	98.91
ZV3371	898	Zinkgruvan FM	69.5	11.9	0.24	6.67	6.58	1.3	2.44	2.56	0.38	0.33	0.035	99.62
ZV3372	898	Zinkgruvan FM	68.5	12.6	0.44	8.13	2.56	2.29	1.85	4.33	0.11	0.26	0.017	100.37
ZV3457	1353	Zinkgruvan FM	74.38	12.1	0.17	3.32	0.27	6.38	2.36	2.4	0.02	0.31	0.029	99.4
ZV3459	1353	Zinkgruvan FM	75.04	11.63	0.2	3.67	0.17	3.42	4.54	4.6	0.04	0.21	0.017	99.03
ZV3460	1353	Zinkgruvan FM	75.35	11.43	0.7	3.61	0.5	5.25	2.58	2.6	0.03	0.34	0.022	99.84
ZV3461	1353	Zinkgruvan FM	63.41	15.62	2.3	2.64	2.41	14.05	1.69	1.7	0.01	0.37	0.05	102.58
ZV3462	1353	Zinkgruvan FM	73.74	11.98	2.51	2.02	2.17	6.08	1.62	1.63	0.01	0.32	0.039	100.5
ZV3463	1353	Zinkgruvan FM	83.8	7.92	0.3	2.65	0.05	3.14	1.19	1.35	0.01	0.26	0.05	99.6

Appendix E Table E6
Metavolcanic samples

SAMPLE	HOLE	POSITION	SiO2	Al2O3	Na2O	K2O	CaO	MgO	FeO*	FeO (tot)	MnO	TiO2	P2O5	SUM
ZV3465	1354	Zinkgruvan FM	70.12	11.15	0.45	2.88	0.96	5.74	7.3	7.32	0.06	0.17	0.01	98.86
ZV3468	1354	Zinkgruvan FM	76.16	11.87	0.61	3.05	0.45	4	2.71	2.77	0.02	0.2	0.013	99.17
ZV3469	1354	Zinkgruvan FM	75.53	12.26	0.57	3.91	0.55	4.12	1.98	1.99	0.02	0.19	0.017	99.16
ZV3470	1354	Zinkgruvan FM	69.62	12.5	0.67	5.97	0.2	2.8	5.6	6.22	0.02	0.46	0.044	98.79
ZV3471	1354	Zinkgruvan FM	75.38	11.94	0.86	6.56	0.06	1.75	2.5	2.51	0.02	0.13	0.011	99.24
ZV3472	1354	Zinkgruvan FM	74.06	12.01	0.92	6.29	0.29	2.36	2.69	2.7	0.02	0.12	0.015	98.79
ZV3473	1354	Zinkgruvan FM	74.76	11.43	0.65	4.72	0.11	3.67	3.22	3.22	0.03	0.19	0.013	98.79
ZV3476	1354	Zinkgruvan FM	74.49	11.45	0.49	7.17	0.08	1.57	3.75	3.78	0.01	0.22	0.02	99.29
ZV3479	1354	Zinkgruvan FM	74.09	12.15	0.54	6.69	0.09	2.64	2.84	2.87	0.03	0.15	0.012	99.26
ZV3480	1354	Zinkgruvan FM	74.76	12.02	0.7	6.01	0.05	2.99	2.94	2.94	0.03	0.14	0.007	99.65
ZV4946	1350	Zinkgruvan FM	61.7	12.3	0.42	6.93	5.15	5.23	5.64	5.65	0.19	0.53	0.11	99.12
ZV4947	1350	Zinkgruvan FW	14	0.62	0.06	0.17	29.1	19.9	2.56	2.56	0.83	0.04	-0.01	99.36
ZV4948	1350	Zinkgruvan FM	49.9	13.8	0.75	6.78	0.67	1.88	0.42	18.14	0.04	0.5	0.08	105.87
ZV4949	1350	Zinkgruvan FM	60.5	8.48	0.72	2.55	2.08	4.08	17.77	18.6	0.24	0.35	0.15	98.14
ZV4950	1350	Zinkgruvan FM	55.1	9.14	0.11	2.99	1.28	3.77	23.8	24.18	0.49	0.49	0.11	97.83
ZV4988	952	Zinkgruvan FW	40.3	5.15	0.02	1.66	21.3	15.1	3.94	4.03	0.42	0.24	0.07	97.48
ZV4989	952	Zinkgruvan FW	37.1	6.78	0.04	4.03	18	8.98	11.56	11.81	1.31	0.15	0.07	98.78
ZV4990	952	Zinkgruvan FM	49.6	9.96	0.21	7.14	11.3	5.88	9.03	9.28	0.95	0.45	0.19	99.3
ZV4990B	952	Zinkgruvan FM	49.7	9.96	0.21	7.11	11.2	5.91	9.3	9.3	0.95	0.46	0.19	
ZV4991	952	Zinkgruvan FW	41.1	6.01	0.11	0.52	17	7.59	19.1	21.11	1.38	0.15	0.12	96.04
ZV4992	952	Zinkgruvan FM	59.6	13.7	0.03	7.74	3.18	4.93	4.76	5.07	0.18	0.45	0.11	96.3
ZV4993	952	Zinkgruvan FW	39.2	7.47	-0.01	3	15.5	7.43	7.85	11.53	0.89	0.22	0.3	89.21
ZV4994	952	Zinkgruvan FW	14.4	2.46	-0.01	1.05	26.9	11.2	15.84	17.39	1.94	0.1	0.35	96.82
ZV4995	952	Zinkgruvan FM	75.7	9.71	0.32	3.82	1.76	2.34	3.05	3.64	0.24	0.19	0.03	99.38
ZV4996	952	Zinkgruvan FM	68.7	12.1	0.04	4.91	4.44	3.13	3.22	3.77	0.44	0.31	0.07	99.04
ZV4997	952	Zinkgruvan FW	50	6.77	0.14	1.56	18.4	9.11	5.18	7.49	1.03	0.26	0.14	96.4
ZV5001		Zinkgruvan FM	74	12.3	0.44	4.92	0.78	2.64	2.38	2.4	0.08	0.23	0.04	98.96
ZV5002		Zinkgruvan FM	72.2	10.2	0.37	5.11	4.67	1.4	4.83	4.89	0.27	0.25	0.07	99.95
ZV5002B		Zinkgruvan FM	72.2	10.2	0.37	5.09	4.66	1.39	4.94	4.94	0.28	0.25	0.07	
ZV5003		Zinkgruvan FM	67	11.4	0.76	4.63	5.39	3.3	4.43	4.43	0.42	0.33	0.05	98.65

Appendix E Table E6
Metavolcanic samples

SAMPLE	HOLE	POSITION	SiO2	Al2O3	Na2O	K2O	CaO	MgO	FeO*	FeO (tot)	MnO	TiO2	P2O5	SUM
ZV5003B		Zinkgruvan FM												
ZV5004		Zinkgruvan FM	68.9	10.6	0.37	6.6	4.65	2.07	3.7	3.89	0.43	0.32	0.06	98.56
ZV5005		Zinkgruvan FM	61	8.84	0.36	3.9	11.1	5.26	5.94	5.9	1.31	0.27	0.08	98.36
ZV5005B		Zinkgruvan FM	59.68	8.71	0.36	3.86	13.51	4.87	5.66	5.66	1.2	0.25	0.03	
ZV5006		Zinkgruvan FM	64.7	14.2	1.4	8.02	1.21	1.31	0.99	4.6	0.07	0.37	0.07	100.36
ZV5007		Zinkgruvan FM	46.5	15.3	0.55	3.8	10.1	6.5	11.78	12	0.44	0.83	0.06	98.31
ZV5008		Zinkgruvan FM	73.9	11.7	0.89	5.21	1.47	1.37	3.88	4.18	0.26	0.26	0.04	100.22
ZV5010		Zinkgruvan FM	65.9	10.9	-0.01	6.81	4.54	1.42	4.4	4.58	0.94	0.25	0.05	96.42
ZV5011		Zinkgruvan FM	67.6	9.57	0.26	5.34	2.96	1.29	1.27	4.32	0.49	0.21	0.04	94.27
ZV5012		Zinkgruvan FM	77.5	10.3	-0.01	4.72	1.36	1.39	1.9	2.18	0.22	0.27	0.07	99.14
ZV5013		Zinkgruvan FM	70.4	13.5	0.58	6.04	0.21	2.51	3.46	3.45	0.12	0.41	0.07	98.75
ZV5014		Zinkgruvan FM	77.1	12.5	0.55	1.73	3.09	1.69	1.84	1.84	0.3	0.21	0.02	99.94
ZV5014B		Zinkgruvan FM	77	12.4	0.54	1.74	3.09	1.69	1.84	1.84	0.29	0.21	0.02	
ZV5015		Zinkgruvan FM	74.1	10.4	0.17	8.33	1.54	0.65	1.37	2.21	0.56	0.25	0.06	99.26
ZV5016		Zinkgruvan FM	70.7	11.8	0.69	6.9	1.12	1.58	3.92	4.3	0.15	0.31	0.03	98.87
ZV5017		Zinkgruvan FM	65.1	12.9	-0.01	8.66	2.21	1.43	3.79	5.5	0.41	0.35	0.1	99.1
ZV5018		Zinkgruvan FM	70.8	13.5	0.89	6.59	0.83	1.56	3.23	3.23	0.17	0.47	0.13	99.41
ZV5022		Zinkgruvan FM	78.3	10.9	0.69	6.94	0.91	0.31	1.39	1.43	0.09	0.15	0.03	100.43
ZV5023		Zinkgruvan FM	68.6	12.4	0.66	2.83	5.67	1.59	4.64	4.91	0.42	0.56	0.12	99.05
ZV5024		Zinkgruvan FM	69.2	13.4	1.99	3.39	3.59	1.75	3.48	3.49	0.15	0.39	0.14	99.01
ZV5025		Zinkgruvan FM	70	10.5	0.16	2.96	1.13	2.09	7.63	9.39	1.06	0.26	0.08	100.86
ZV5033		Zinkgruvan FM	73.5	9.84	-0.01	5.06	0.16	2.53	2.61	3.89	0.11	0.24	0.07	98.11
ZV5034		Zinkgruvan FM	74	12.3	0.17	6.72	0.08	2.47	2.89	2.87	0.1	0.15	0.03	100.01
ZV5035		Zinkgruvan FM	68.5	13.7	0.22	6.85	0.95	2.98	4.08	4.08	0.08	0.58	0.15	99
ZV5036		Zinkgruvan FM	82.6	5.36	0.2	2.47	0.28	0.57	4.57	5.86	0.53	0.18	0.05	99.95
ZV5037		Zinkgruvan FM	68.2	12.3	-0.01	6.25	0.78	1.52	7.57	7.88	0.64	0.3	0.06	99.02
ZV5038		Zinkgruvan FM	77.4	10.8	0.09	4.41	0.1	2.34	2.84	2.83	0.04	0.22	0.03	99.21
ZV5038B		Zinkgruvan FM	77.4	10.8	0.09	4.43	0.09	2.34	2.83	2.83	0.04	0.22	0.03	
ZV5039		Zinkgruvan FM	74.8	11.7	0.04	5.31	1.19	1.71	2.74	2.7	0.38	0.45	0.13	99.48
ZV5040		Zinkgruvan FM	68.8	11.1	-0.01	2.69	5.99	2.52	3.05	4.26	1.08	0.29	0.12	100.05

Appendix E Table E6
Metavolcanic samples

SAMPLE	HOLE	POSITION	SiO2	Al2O3	Na2O	K2O	CaO	MgO	FeO*	FeO (tot)	MnO	TiO2	P2O5	SUM
ZV5041		Zinkgruvan FM	70.1	14	0.27	7.24	0.63	2.19	3.09	3.05	0.15	0.32	0.05	99.21
ZV5042		Zinkgruvan FM	66	14	-0.01	6.9	2.27	1.74	2.74	3.84	0.28	0.4	0.11	98.03
ZV5043		Zinkgruvan FM	71.5	12.5	-0.01	8.77	0.53	2.37	1.13	1.83	0.06	0.34	0.09	99.39
ZV5044		Zinkgruvan FM	64.2	11.7	0.25	9.1	6.57	2.68	2.98	3.01	0.2	0.38	0.06	98.93
ZV5045		Zinkgruvan FM	68.8	14.3	0.32	12.4	0.16	0.52	2.32	2.36	0.04	0.41	0.07	99.71
ZV5046		Zinkgruvan FM	66.8	14.8	0.35	13	0.07	0.75	2.2	2.24	0.05	0.43	0.07	98.98
ZV5047		Zinkgruvan FM	68.8	14.1	0.38	12.6	0.11	0.45	2.01	2.01	0.02	0.43	0.06	99.3
ZV5048		Zinkgruvan FM	67.6	14.4	0.41	12	0.58	1.07	2.68	2.72	0.06	0.44	0.11	99.76
ZV5049		Zinkgruvan FM	69.7	13.5	0.55	11.8	0.31	0.44	2.24	2.24	0.02	0.4	0.06	99.31
ZV5050		Zinkgruvan FM	67.7	9.54	-0.01	4.99	5.43	4.43	2.49	3.84	0.26	0.25	0.09	98.99
ZV5050B		Zinkgruvan FM	67.6	9.51	-0.01	4.97	5.48	4.46	3.88	3.88	0.26	0.25	0.09	
ZV5051		Zinkgruvan FW	51.1	7.11	0.16	3.32	19.7	8.4	5.46	5.49	0.42	0.17	0.06	99.45
ZV5052		Zinkgruvan FM	85.7	6.54	0.23	4.47	0.15	0.83	1.59	1.58	0.12	0.11	0.03	100.13
ZV5053		Zinkgruvan FM	71.5	10.6	0.28	7.06	1.44	2.47	4.16	4.23	0.13	0.27	0.07	98.6
ZV5054		Zinkgruvan FM	68.9	8.5	-0.01	4.38	5.98	1.82	2.71	4.94	0.54	0.25	0.1	98.44
ZV5055		Zinkgruvan FM	79.9	9.33	0.21	4.48	0.85	1.76	2.61	2.69	0.06	0.26	0.04	100.18
ZV5056		Zinkgruvan FM	71	12.3	-0.01	4.55	2.81	1.95	2.57	3.04	0.34	0.38	0.09	98.57
ZV5061		Zinkgruvan FM	48.9	14.4	0.2	10.4	4.08	1.39	0.58	5.96	0.9	0.35	0.07	90.56
ZV5062		Zinkgruvan FM	71.9	12.1	-0.01	7.13	0.97	1.85	3.57	3.64	0.24	0.47	0.1	99.57
ZV5062B		Zinkgruvan FM	71.7	12.1	-0.01	7	0.98	1.87	3.63	3.63	0.24	0.47	0.1	
ZV5063		Zinkgruvan FM	57.3	18.6	0.55	10.9	0.41	3.56	4.39	4.41	0.12	0.69	0.16	98.06
ZV5064		Zinkgruvan FM	53.7	11.8	0.94	5.54	0.84	1.85	0.68	18.23	0.09	0.38	0.07	106.92
ZV5066		Zinkgruvan FM	59.9	6.21	0.08	3.91	1.43	1.13	5.57	5.35	1.62	0.18	0.07	85.67
ZV5067		Zinkgruvan FM	68.1	9.77	1.73	5.89	1.8	1.55	3.24	4.42	0.52	0.26	0.05	96.14
ZV5068		Zinkgruvan FM	66.9	14	0.4	7.45	0.63	3.58	4.51	4.62	0.03	0.63	0.18	99.53
ZV5069		Zinkgruvan FM	73.6	12.8	0.26	5.51	2.71	1.42	1.52	1.5	0.2	0.24	0.04	99.36
ZV5070		Zinkgruvan FM	70.9	12.6	0.27	6.16	1.14	2.72	3.72	3.72	0.08	0.51	0.16	98.87
ZV5071		Zinkgruvan FM	68.6	13.3	0.49	7.21	0.75	2.22	4.6	4.57	0.25	0.4	0.11	98.92
ZV5072		Zinkgruvan FM	66.9	14	0.64	10.1	0.1	2.17	3.53	3.49	0.13	0.21	0.04	98.6
ZV5073		Zinkgruvan FM	70.2	11.3	-0.01	4.24	5.55	2.5	3.7	4.19	0.46	0.31	0.08	99.77

Appendix E Table E6
Metavolcanic samples

SAMPLE	HOLE	POSITION	SiO2	Al2O3	Na2O	K2O	CaO	MgO	FeO*	FeO (tot)	MnO	TiO2	P2O5	SUM
ZV5074		Zinkgruvan FM	75.9	8.85	-0.01	3.52	0.32	0.83	3.94	7.68	0.86	0.36	0.09	101.86
ZV5074B		Zinkgruvan FM	76.2	8.88	-0.01	3.54	0.31	0.83	7.72	7.72	0.85	0.36	0.09	
ZV5075		Zinkgruvan FM	63	16.2	0.43	11.8	1.92	3.84	1.88	1.92	0.06	0.2	0.03	100.11
ZV5076		Zinkgruvan FM	73.9	11.7	0.61	8.24	0.07	1.41	2.98	3	0.03	0.22	0.02	99.78
ZV5078	452	Zinkgruvan FW	72.8	13.6	0.44	9.03	1.65	0.91	1.7	1.7	0.04	0.25	0.065	100.5
ZV5078B	452	Zinkgruvan FW			0.38		2.1		1.76	1.76				
ZV5079	452	Zinkgruvan FW	65.6	13.8	0.41	8.31	0.74	2.56	5.02	5.21	0.1	0.53	0.138	97.65
ZV5080	452	Zinkgruvan FW	67	11.9	0.46	3.22	8.59	3.38	3.66	4.11	0.33	0.41	0.162	100.25
ZV5081	452	Zinkgruvan FW	51.9	14.6	1.52	1.18	15.5	4.32	8.82	9.13	0.27	0.81	0.087	99.47
ZV5082	452	Zinkgruvan FW	70.6	12.6	0.64	6.79	4.87	1.51	3.19	3.38	0.15	0.34	0.088	101.08
ZV5083	452	Zinkgruvan FW	68.8	13.3	0.69	5.75	3.13	2.68	4.3	4.48	0.11	0.54	0.14	99.73
ZV5084	452	Zinkgruvan FW	67.3	13.1	1.41	5.88	2.95	2.45	3.7	3.92	0.09	0.48	0.12	97.82
ZV5085	452	Zinkgruvan FW	70.6	11.9	0.57	7.29	1.07	1.87	3.46	4.13	0.07	0.33	0.107	98.26
ZV5086	452	Zinkgruvan FW	71.2	11.8	0.55	6.7	1.96	1.48	3.01	3.55	0.07	0.35	0.076	98.03
ZV5087	452	Zinkgruvan FW	69.9	13.8	1.78	7.95	1.17	1.3	1.56	1.59	0.03	0.34	0.038	97.93
ZV5088	452	Zinkgruvan FW	69.5	13.3	0.69	8.82	1.92	1.2	2.55	2.62	0.08	0.53	0.126	98.84
ZV5089	452	Zinkgruvan FW	60.7	13.7	0.5	5.56	2.27	3.17	5.77	6.07	0.11	0.42	0.104	93.02
ZV5090	452	Zinkgruvan FW	67.4	14.5	0.53	6.19	0.43	3.66	4.56	4.56	0.05	0.58	0.139	98.04
ZV5090B	452	Zinkgruvan FW			0.46		-0.7		4.14	4.14				
ZV5091	452	Zinkgruvan FW	70.8	11.7	0.85	4.48	1.68	3.5	6.67	6.7	0.15	0.17	0.043	100.1
ZV5092	452	Zinkgruvan FW	74.9	11.8	0.67	5.43	3.09	1.44	2.38	2.59	0.12	0.15	0.087	100.46
ZV5093	452	Zinkgruvan FW	67.7	13.7	1.24	7.17	2.88	2.84	3.59	3.59	0.1	0.57	0.175	99.98
ZV5094	452	Zinkgruvan FW	68.2	13.7	0.88	8.38	0.92	3.03	3.36	3.35	0.05	0.58	0.159	99.25
ZV5095	452	Zinkgruvan FW	75.1	12.4	0.64	4.01	0.8	3.56	3.75	3.75	0.04	0.16	0.025	100.49
ZV5096	452	Zinkgruvan FW	68.8	13	0.44	4.06	3.08	4.47	5.7	5.69	0.11	0.3	0.039	100.03
ZV5097	452	Zinkgruvan FW	69.7	12.8	0.91	6.61	1.24	4.54	4.48	4.48	0.07	0.52	0.086	100.98
ZV5098	452	Zinkgruvan FW	67.2	14.6	0.83	5.19	0.72	4.03	3.99	4.02	0.1	0.4	0.048	97.2
ZV5099	452	Zinkgruvan FW	72.5	12.3	1.35	5.64	0.84	2.85	2.75	2.73	0.08	0.44	0.055	98.8
ZV5100	452	Zinkgruvan FW	63.4	13.1	0.58	5.11	3.27	3.35	5.55	6.97	0.38	0.37	0.138	98.23
ZV5101	452	Zinkgruvan FW	55	15.1	0.58	7.44	2.38	3.81	6.36	9.43	0.42	0.47	0.139	97.32

Appendix E Table E6
Metavolcanic samples

SAMPLE	HOLE	POSITION	SiO2	Al2O3	Na2O	K2O	CaO	MgO	FeO*	FeO (tot)	MnO	TiO2	P2O5	SUM
ZV5102	452	Zinkgruvan FW	71	13.7	0.59	4.91	1.43	3.05	3.98	4.73	0.16	0.25	0.067	100.45
ZV5102B	452	Zinkgruvan FW			0.51		2.1		4.15	4.15				
ZV5103	452	Zinkgruvan FW	77.9	9.1	1.49	1.08	2.58	1.62	1.81	2.53	0.21	0.25	0.084	97.63
ZV5104	452	Zinkgruvan FW	75.6	12.3	1.02	4.31	1.85	2.75	2.93	2.97	0.12	0.24	0.024	101.23
ZV5105	452	Zinkgruvan FW	65.1	16.3	1.07	7.5	1.24	3.96	4.08	4.39	0.17	0.3	0.09	100.52
ZV5106	452	Zinkgruvan FW	70.7	11.5	0.64	3.03	3.04	2.93	3.32	5.24	0.29	0.34	0.091	99.31
ZV5107	452	Zinkgruvan FW	71.5	14.7	0.38	7.08	0.29	3.65	2.76	2.85	0.05	0.31	0.023	100.91
ZV5108	452	Zinkgruvan FW	54.5	4.2	0.03	1.14	19.93	10.6	7.88	7.84	0.95	0.11	0.046	99.37
ZV5109	452	Zinkgruvan FW	60.9	5	0.35	2.43	16.77	10.03	4.02	3.98	0.44	0.09	0.052	100.05
ZV5110	452	Zinkgruvan FW	57.1	18.7	1.05	10.44	2.6	6.17	2.65	3.16	0.07	0.35	0.095	100.09
ZV5111	452	Zinkgruvan FW	66.4	13.4	0.83	7.92	2.95	4.39	2.11	3.29	0.11	0.34	0.103	100.52
ZV5112	452	Zinkgruvan FW	68.9	13.2	1.05	8.23	0.62	4.77	2.65	3.23	0.06	0.33	0.05	101.08
ZV5113	452	Zinkgruvan FW	57.5	18.6	1.25	10.87	1.12	6.83	3.63	3.63	0.09	0.48	0.027	100.43
ZV5114	452	Zinkgruvan FW	84	5.7	1.58	0.38	1.59	0.54	0.46	3.52	0.03	0.17	0.07	99.87
ZV5114B	452	Zinkgruvan FW			1.21		1.4		3.18	3.18				
ZV5115	452	Zinkgruvan FW	64.7	16.4	1.26	8.65	0.38	4.82	2.74	2.74	0.02	0.46	0.028	99.47
ZV5116	452	Zinkgruvan FW	71.6	14.1	3.5	0.73	5.21	3.11	1.54	1.54	0.02	0.3	0.101	100.23
ZV5117	452	Zinkgruvan FW	71.6	12.9	1.78	5.34	1.68	3.28	3.06	3.09	0.06	0.29	0.036	100.11
ZV5118	452	Zinkgruvan FW	70.7	18.6	1.33	0.37	9.49	0.3	0.39	0.4	0.01	0.34	0.043	101.59
ZV5119	452	Zinkgruvan FW	74.1	12.4	0.43	4.61	0.81	2.91	4.64	4.81	0.04	0.34	0.031	100.56
ZV5120	452	Zinkgruvan FW	70.2	13	0.49	4.88	2.03	3.33	4.79	4.9	0.11	0.38	0.036	99.42
ZV5121	452	Zinkgruvan FW	66.9	13.9	0.51	7.52	0.24	2.93	7.83	7.91	0.16	0.39	0.039	100.62
ZV5122	452	Zinkgruvan FW	68.3	12.5	0.73	5.2	1.19	2.22	7.25	8.14	0.26	0.28	0.106	99.66
ZV5123	452	Zinkgruvan FW	69.8	12	0.64	5.72	0.97	2.48	6.55	8.15	0.29	0.36	0.084	101.21
ZV5124	452	Zinkgruvan FW	67.6	12.7	1.42	3.14	1.91	3.16	8.68	9.19	0.3	0.42	0.072	100.16
ZV5125	452	Zinkgruvan FW	68.9	7.3	0.12	2.02	0.35	3.45	10.75	14.46	0.82	0.25	0.06	99.42
ZV5126	452	Zinkgruvan FW	61.4	9.2	0.09	2.97	0.69	4.37	18.69	19.03	0.73	0.18	0.039	98.86
ZV5126B	452	Zinkgruvan FW			0.05		1.96		18.52	18.52				
ZV5127	452	Zinkgruvan FW	76.2	12.3	0.6	4.38	0.39	2.55	3.93	3.93	0.06	0.22	0.013	100.65
ZV5128	452	Zinkgruvan FW	77	10.9	0.6	5.06	0.8	2.75	3.16	3.17	0.04	0.19	0.013	100.55

Appendix E Table E6
Metavolcanic samples

SAMPLE	HOLE	POSITION	SiO2	Al2O3	Na2O	K2O	CaO	MgO	FeO*	FeO (tot)	MnO	TiO2	P2O5	SUM
ZV5129	452	Zinkgruvan FW	76	12.6	0.78	6.42	0.17	2.26	2.2	2.21	0.02	0.23	0.011	100.71
ZV5130	452	Zinkgruvan FW	77.4	12.4	0.68	5.34	0.2	2.2	2.28	2.28	0.02	0.23	0.011	100.76
ZV5131	452	Zinkgruvan FW	73.2	12.7	0.4	4.59	0.76	3.06	5.19	5.29	0.06	0.35	0.03	100.51
ZV5132	452	Zinkgruvan FW	74.1	12.3	0.51	4.6	2.3	1.94	4.3	4.44	0.07	0.35	0.033	100.71
ZV5133	452	Zinkgruvan FW	66	12.1	0.44	4.73	1.19	2.65	9.27	9.57	0.29	0.34	0.053	98.12
ZV5134	452	Zinkgruvan FW	72.2	11.7	0.32	2.59	4.11	3.73	3.9	4.84	0.22	0.32	0.105	100.79
ZV5135	452	Zinkgruvan FW	75.3	11.3	0.51	4.34	1.52	2.22	4.56	4.88	0.15	0.27	0.041	100.75
ZV5136	452	Zinkgruvan FW	75.5	12.5	0.35	5.13	0.15	3.22	3.44	3.44	0.02	0.23	0.018	100.56
ZV5137	452	Zinkgruvan FW	75.1	12.2	0.55	7.61	0.24	1.68	2.43	2.46	0.02	0.18	0.014	100.06
ZV5138	453	Zinkgruvan FW	74.1	13.1	0.48	8.96	0.91	0.62	1.21	1.23	0.04	0.22	0.053	99.73
ZV5138B	453	Zinkgruvan FW			0.36		0.98		1.08	1.08				
ZV5139	453	Zinkgruvan FW	68.4	14.1	0.9	8.25	1.84	1.88	2.7	2.75	0.1	0.69	0.137	99.11
ZV5141	453	Zinkgruvan FW	65	12.2	1.61	4.27	3.39	3.42	7.14	7.2	0.25	0.41	0.136	97.95
ZV5142	453	Zinkgruvan FW	68.4	11.9	0.3	6.39	2.05	2.46	6.8	6.97	0.1	0.23	0.045	98.93
ZV5143	453	Zinkgruvan FW	72.4	11.3	0.3	6.49	2.4	1.56	3.73	3.86	0.07	0.16	0.033	98.66
ZV5144	453	Zinkgruvan FW	67.3	12.7	0.64	3.98	4.57	2.29	2.79	4	0.67	0.4	0.188	98.31
ZV5145	453	Zinkgruvan FW	68	13.4	0.93	4.69	1.61	2.94	3.52	3.74	0.15	0.29	0.063	96.14
ZV5146	453	Zinkgruvan FW	73.5	12.6	1.96	3.03	1.9	2.65	2.44	2.46	0.03	0.36	0.038	98.58
ZV5147	453	Zinkgruvan FW	67.6	13.5	0.74	4.82	0.88	3	3.83	3.79	0.12	0.26	0.054	94.79
ZV5148	453	Zinkgruvan FW	73.7	6.9	0.37	0.33	6.52	1.97	3.55	5.66	0.95	0.21	0.111	98.48
ZV5149	453	Zinkgruvan FW	71.3	11.2	1.09	2.92	2.02	2.62	5.6	6.03	0.31	0.22	0.042	98.25
ZV5150	453	Zinkgruvan FW	66.9	11.8	0.6	3.96	1.06	2.47	6.23	9.05	0.35	0.42	0.066	98.72
ZV5150B	453	Zinkgruvan FW			0.69		1.54		8.77	8.77				
ZV5151	453	Zinkgruvan FW	71.4	12.1	0.5	4.3	1.17	2.56	6.93	7.39	0.35	0.42	0.172	100.69
ZV5152	453	Zinkgruvan FW	66.8	14	0.91	7.79	0.56	2.17	3.11	3.12	0.03	0.32	0.027	95.75
ZV5153	453	Zinkgruvan FW	70.5	10.9	0.53	4.68	0.83	2.67	6.84	6.94	0.24	0.3	0.031	97.69
ZV5154	453	Zinkgruvan FW	68.8	8.3	0.67	2.81	0.81	1.2	3.67	7.78	0.22	0.22	0.077	95.15
ZV5155	453	Zinkgruvan FW	76	11.5	0.46	5.54	0.55	3.09	2.98	3.01	0.02	0.31	0.03	100.55
ZV5156	453	Zinkgruvan FW	76.3	10.8	0.5	5.22	1.02	3.06	3.05	3.21	0.05	0.32	0.032	100.59
ZV5157	453	Zinkgruvan FW	74.4	11.7	0.36	5.11	0.28	2.65	3.73	3.82	0.03	0.25	0.015	98.7

Appendix E Table E6
Metavolcanic samples

SAMPLE	HOLE	POSITION	SiO2	Al2O3	Na2O	K2O	CaO	MgO	FeO*	FeO (tot)	MnO	TiO2	P2O5	SUM
ZV5158	453	Zinkgruvan FW	71.7	11.9	0.39	4.4	1.84	3.18	3.19	3.21	0.07	0.35	0.026	97.07
ZV5159	453	Zinkgruvan FW	76.8	11.4	0.34	4.11	0.55	2.72	3.91	3.92	0.02	0.22	0.01	100.09
ZV5160	453	Zinkgruvan FW	71.6	12	0.39	5.27	0.45	3.04	3.85	3.87	0.04	0.25	0.01	96.93
ZV5161	453	Zinkgruvan FW	74.3	11.7	0.32	4.66	0.25	2.93	4.7	4.73	0.07	0.26	0.01	99.24
ZV5162	453	Zinkgruvan FW	67	10	0.26	4.1	1.94	3.46	2.92	5.97	0.08	0.22	0.01	94.41
ZV5162B	453	Zinkgruvan FW			0.2		1.96		6.21	6.21				
ZV5163	453	Zinkgruvan FW	67.8	9.7	0.18	3.66	0.57	3.53	12.47	12.69	0.31	0.22	0.009	98.76
ZV5165	453	Zinkgruvan FW	75.9	10.5	2.92	2.29	0.38	2.37	4.48	4.61	0.04	0.16	0.018	99.29
ZV5166	453	Zinkgruvan FW	67.1	13.5	1.8	5.32	0.84	3.49	6.57	6.64	0.11	0.65	0.117	99.65
ZV5167	453	Zinkgruvan FW	75.4	9.5	3	1.44	0.48	2.89	6.91	7.07	0.07	0.35	0.064	100.44
ZV5168	453	Zinkgruvan FW	75.5	10.9	5.14	0.77	0.81	2.1	4.28	4.33	0.05	0.54	0.099	100.27
ZV5169	454	Zinkgruvan FW	69.6	13.5	0.67	7.23	0.6	3.6	3.55	3.94	0.03	0.4	0.088	99.87
ZV5170	454	Zinkgruvan FW	62.5	11	0.4	4.15	7.17	5.83	3.78	4.01	0.3	0.36	0.104	96.21
ZV5171	454	Zinkgruvan FW	55.8	7.5	0.91	3.58	0.82	2.17	15.57	18.55	0.95	0.28	0.155	94.44
ZV5172	454	Zinkgruvan FW	73.5	11.2	0.55	4.94	4.19	2.29	1.75	2.56	0.29	0.26	0.083	100.55
ZV5173	454	Zinkgruvan FW	66.3	12.9	0.6	7.14	1.41	2.54	4.71	6.03	0.3	0.41	0.124	99.07
ZV5174	454	Zinkgruvan FW	75.9	4.5	0.53	2.23	0.84	1.26	10.22	11.14	0.77	0.19	0.068	98.49
ZV5174B	454	Zinkgruvan FW			0.12		1.26		10.66	10.66				
ZV5175	454	Zinkgruvan FW	67.9	5.6	0.73	1.22	1.06	1.7	14.62	16.29	1.22	0.19	0.072	97.63
ZV5176	454	Zinkgruvan FW	82.6	7.4	0.35	1.15	2.52	1.42	1.41	2.14	0.04	0.14	0.024	98.88
ZV5177	454	Zinkgruvan FW	77.8	9.1	0.31	4.13	0.43	2.1	1.94	3.16	0.04	0.19	0.02	98.81
ZV5178	454	Zinkgruvan FW	79	7.5	0.29	2.73	0.87	1.36	1.62	2.82	0.04	0.13	0.021	96.96
ZV5179	454	Zinkgruvan FW	83.6	6.9	0.31	1.92	1.9	1.26	1	1.72	0.03	0.13	0.021	98.86
ZV5180	454	Zinkgruvan FW	71.9	13.1	0.34	4.97	0.35	3.04	2.36	2.95	0.03	0.28	0.022	97.45
ZV5181	454	Zinkgruvan FW	65	16.9	0.41	6.94	0.14	3.69	3.1	3.21	0.02	0.34	0.021	96.79
ZV5182	454	Zinkgruvan FW	59.4	18.5	0.51	9.6	0.16	3.19	2.73	3.72	0.03	0.33	0.025	96.89
ZV5183	454	Zinkgruvan FW	74.7	11.8	0.71	7.17	0.61	3.22	2.49	2.62	0.02	0.21	0.022	101.17
ZV5184	454	Zinkgruvan FW	72.5	11.8	1.18	5.19	1.67	2.73	3.85	4.35	0.07	0.37	0.108	100.74
ZV5185	454	Zinkgruvan FW	65.1	12.1	0.59	3.61	6.45	3.41	3.83	4.82	0.42	0.36	0.2	98.48
ZV5186	454	Zinkgruvan FW	72.6	13.3	0.61	6.99	1.28	2.59	2.98	2.99	0.07	0.53	0.083	101.05

Appendix E Table E6
Metavolcanic samples

SAMPLE	HOLE	POSITION	SiO2	Al2O3	Na2O	K2O	CaO	MgO	FeO*	FeO (tot)	MnO	TiO2	P2O5	SUM
ZV5186B	454	Zinkgruvan FW			0.39		1.12		3.01	3.01				
ZV5187	454	Zinkgruvan FW	65.7	12.7	0.59	6.78	6.81	3	3.44	4.2	0.42	0.3	0.124	101.08
ZV5188	454	Zinkgruvan FW	65	15	0.62	5.52	3.99	4.86	3.92	4.32	0.23	0.47	0.144	100.83
ZV5189	454	Zinkgruvan FW	70.2	13.3	0.86	7.64	1.45	2.67	3.68	3.92	0.08	0.35	0.089	100.9
ZV5190	454	Zinkgruvan FW	72.9	12	0.64	2.89	3.43	2.4	2.86	3.9	0.14	0.26	0.104	99.7
ZV5191	454	Zinkgruvan FW	74.6	11.8	0.55	9.3	1.27	0.96	0.29	1.34	0.03	0.23	0.093	100.99
ZV5192	454	Zinkgruvan FW	73.5	10.6	0.63	1.86	3.9	3.04	1.71	3.52	0.14	0.3	0.124	99.15
ZV5193	454	Zinkgruvan FW	71.4	11.3	0.72	7.45	1.92	2.88	0.46	2.58	0.07	0.25	0.064	99.66
ZV5194	454	Zinkgruvan FW	68.6	12.9	0.7	7.32	1.94	3.91	1.71	2.72	0.07	0.27	0.081	99.31
ZV5195	454	Zinkgruvan FW	72.8	9.8	0.77	7.24	0.69	0.95	0.28	1.9	0.02	0.24	0.066	97.15
ZV5196	454	Zinkgruvan FW	67.4	15	1.02	10.32	0.14	2.78	1.53	1.88	0.02	0.32	0.019	99.07
ZV5197	454	Zinkgruvan FW	62.3	17.2	0.82	13.65	0.24	3.76	2.18	2.18	0.03	0.41	0.025	100.62
ZV5198	454	Zinkgruvan FW	69	11.5	0.64	8.97	0.99	1.39	0.61	2.92	0.03	0.26	0.057	98.12
ZV5198B	454	Zinkgruvan FW			0.34		1.12		2.91	2.91				
ZV5199	454	Zinkgruvan FW	60.4	14.6	0.78	7.81	1.41	5.41	4.63	5.3	0.04	0.85	0.275	97.38
ZV5200	454	Zinkgruvan FW	69.2	14.3	0.79	7.68	0.34	3.57	3.31	3.65	0.02	0.36	0.07	100.17
ZV5201	454	Zinkgruvan FW	71.7	11.1	0.88	6.41	0.9	2.69	2.62	3.73	0.02	0.3	0.07	99.03
ZV5202	454	Zinkgruvan FW	73.1	12.6	0.57	5.62	1.2	3.92	3.22	3.25	0.05	0.28	0.019	100.63
ZV5203	454	Zinkgruvan FW	70.6	13.1	0.55	5.96	0.62	4.39	3.21	3.27	0.01	0.44	0.039	99.02
ZV5204	454	Zinkgruvan FW	64.3	15	1.34	9.51	0.22	5.25	3.17	3.7	0.02	0.32	0.019	99.92
ZV5205	454	Zinkgruvan FW	67.4	15	0.57	12.64	0.44	0.83	0.37	2.38	0.01	0.67	0.148	100.99
ZV5206	454	Zinkgruvan FW	70.7	13.8	2.14	6.09	1.15	3.38	2.57	2.58	0.02	0.25	0.018	100.13
ZV5207	454	Zinkgruvan FW	75.3	11.8	0.7	9	1.04	1.1	1.62	1.66	0.03	0.38	0.074	101.13
ZV5208	454	Zinkgruvan FW	71.9	13.7	0.66	10.78	1.08	0.95	1.4	1.44	0.03	0.37	0.069	101.02
ZV5209	454	Zinkgruvan FW	74.2	11.4	0.64	8.19	2.16	0.94	2.53	2.62	0.06	0.26	0.044	100.56
ZV5210	454	Zinkgruvan FW	77.1	11.6	0.81	8.44	0.34	0.65	2.04	2.06	0.02	0.27	0.042	101.35
ZV5210B	454	Zinkgruvan FW			0.57		-0.7		2.26	2.26				
ZV5211	455	Zinkgruvan FM	82.6	8.6	0.5	6.29	0.72	0.79	0.76	0.94	0.02	0.23	0.051	100.88
ZV5212	455	Zinkgruvan FM	74.9	13.1	0.65	10.3	0.47	0.67	0.59	0.64	0.02	0.36	0.075	101.21
ZV5213	455	Zinkgruvan FM	69	15.6	0.61	12.95	0.71	0.63	0.54	0.6	0.02	0.43	0.077	100.65

Appendix E Table E6
Metavolcanic samples

SAMPLE	HOLE	POSITION	SiO2	Al2O3	Na2O	K2O	CaO	MgO	FeO*	FeO (tot)	MnO	TiO2	P2O5	SUM
ZV5214	455	Zinkgruvan FM	69.8	14.5	1.41	10.44	0.31	0.61	0.71	0.86	0.01	0.39	0.071	98.46
ZV5215	455	Zinkgruvan FM	70.9	14.4	0.66	11.16	0.58	0.81	1.22	1.85	0.02	0.44	0.081	101.19
ZV5216	455	Zinkgruvan FM	50	18.2	0.57	9.14	1.66	6.34	8.68	9.97	0.07	1.51	0.246	98.3
ZV5217	455	Zinkgruvan FM	63.6	15.5	0.6	11.14	1.35	1.55	3.48	3.66	0.04	0.53	0.161	98.22
ZV5218	455	Zinkgruvan FM	68.2	15	0.53	11.7	0.75	1.2	2.07	2.19	0.02	0.48	0.113	100.24
ZV5220	456	Zinkgruvan FW	64.5	12.1	0.54	9.14	6.69	3.76	2.87	2.99	0.2	0.34	0.097	100.64
ZV5221	456	Zinkgruvan FW	75.1	9.6	0.33	7.3	1.5	1.26	1.12	1.92	0.05	0.3	0.099	98.65
ZV5224	456	Zinkgruvan FM	61.2	14.1	0.45	10.11	0.24	4.49	4.88	7.56	0.07	0.53	0.078	100.09
ZV5225	456	Zinkgruvan FM	67.4	13.7	0.62	11.07	1.53	0.81	0.58	3.66	0.04	0.31	0.06	100.62
ZV5226	456	Zinkgruvan FM	67.8	12.6	0.47	10.08	2.63	1.46	0.82	3.66	0.08	0.27	0.062	100.42
ZV5227	582	Zinkgruvan FM	66	14.9	0.63	12.5	1.41	1.96	2.21	2.3	0.05	0.62	0.17	100.6
ZV5228	582	Zinkgruvan FM	67.1	13.6	0.7	11.5	2.94	1.71	2.45	2.52	0.09	0.52	0.158	100.89
ZV5229	582	Zinkgruvan FM	64.2	14.7	0.86	12.6	3.38	1.63	1.94	2.03	0.07	0.53	0.148	100.21
ZV5231	8506	Zinkgruvan FM	73.1	12.2	0.61	6.46	1.04	2.23	2.75	3.04	0.06	0.23	0.057	99.33
ZV5235	8506	Zinkgruvan FM	72.4	12.4	1.54	4.58	1.14	1.97	4.46	4.54	0.08	0.24	0.024	98.96
ZV5236	8506	Zinkgruvan FM	71.3	12.7	0.85	7.92	2.57	0.53	1.35	1.43	0.11	0.22	0.028	97.7
ZV5237	8506	Zinkgruvan FM	71.5	12.8	0.43	10.2	1.95	0.05	0.39	0.4	0.04	0.2	0.048	97.63
ZV5238	457	Zinkgruvan FM	60.9	13	0.57	8.23	4.84	3.56	3.94	5.32	0.16	0.35	0.108	97.98
ZV5238B	457	Zinkgruvan FM			0.4		5.32		4.57	4.57				
ZV5247	457	Zinkgruvan FW	69.5	13.6	1.44	8.28	0.43	3.69	3.44	3.47	0.05	0.48	0.068	101.04
ZV5248	457	Zinkgruvan FM	70	3.1	0.18	0.69	1.34	2.79	4.01	15.17	0.04	0.1	0.047	98.62
ZV5249	457	Zinkgruvan FM	41.1	17.7	0.43	6.59	1.85	7.57	19.86	22.23	0.12	0.22	0.036	98.96
ZV5253	458	Zinkgruvan HW	65.5	15	2.11	2.63	2.09	3.06	8.04	8.3	0.11	0.53	0.184	99.65
ZV5254	458	Zinkgruvan HW	59	18.7	1.8	4.57	1.08	3.07	7.04	7.14	0.07	0.78	0.081	96.34
ZV5255	458	Zinkgruvan HW	56.6	18.4	1.26	4.64	0.66	3.5	7.6	8.98	0.06	0.82	0.07	95.63
ZV5256	458	Zinkgruvan HW	60.1	17.7	1.69	4.47	1.1	3.11	6.85	8.19	0.07	0.72	0.08	97.86
ZV5257	458	Zinkgruvan HW	63.4	16.7	2.1	4.19	1.65	2.45	5.79	6.05	0.06	0.7	0.074	97.51
ZV5258	458	Zinkgruvan HW	44.8	12.6	0.26	2.48	1.65	6.8	23.44	26.87	0.31	0.59	0.119	98.04
ZV5259	458	Zinkgruvan HW	61.8	15.9	2.33	4.72	2.86	2.2	6.07	6.16	0.04	1.06	0.538	97.65
ZV5260	458	Zinkgruvan HW	62.8	16.2	2.56	5.56	2.1	2.74	5.05	5.59	0.08	0.63	0.257	98.77

Appendix E Table E6
Metavolcanic samples

SAMPLE	HOLE	POSITION	SiO2	Al2O3	Na2O	K2O	CaO	MgO	FeO*	FeO (tot)	MnO	TiO2	P2O5	SUM
ZV5261	458	Zinkgruvan HW	56.7	19.2	1.35	4.6	0.68	3.39	8.54	8.56	0.1	0.94	0.069	95.6
ZV5262	458	Zinkgruvan HW	64.6	16.7	2.46	2.04	2.56	2.66	7.5	7.51	0.13	0.75	0.096	99.53
ZV5262B	458	Zinkgruvan HW			1.35		2.38		6.21	6.21				
ZV5263	458	Zinkgruvan HW	55.3	19.7	1.45	4.63	0.92	3.1	7.81	7.82	0.06	0.8	0.066	93.86
ZV5264	458	Zinkgruvan HW	63.7	10.5	0.93	1.27	3.46	3.35	12.52	14.45	0.58	0.45	0.13	99.7
ZV5265	458	Zinkgruvan HW	52.2	11.8	1.01	2.69	3.43	4.37	3.78	17.41	0.08	0.41	0.105	99.7
ZV5266	458	Zinkgruvan HW	72.3	13.8	1.13	4.73	1.39	2.46	2.63	2.66	0.09	0.24	0.028	98.86
ZV5267	458	Zinkgruvan HW	66.1	11.9	0.75	5.09	4.46	2.87	3.87	6.6	0.42	0.38	0.103	100.1
ZV5268	458	Zinkgruvan FW	65.7	14	2.08	0.34	0.34	4.36	7.46	4.42	0.02	0.34	0.021	96.98
ZV5269	458	Zinkgruvan FW	54.9	17.8	1.02	11.47	0.38	5.41	4.35	4.41	0.04	0.75	0.161	96.39
ZV5270	458	Zinkgruvan FW	64.3	14.4	0.56	10.47	1.53	2.77	1.91	2.79	0.07	0.53	0.141	98.1
ZV5271	458	Zinkgruvan FW	22.1	6.5	0.12	4	26.12	10.34	9.77	10.06	0.95	0.27	0.078	80.96
ZV5272	506	Zinkgruvan HW	59	18.8	1.64	4.58	0.99	2.85	6.93	6.94	0.06	0.71	0.07	95.65
ZV5273	506	Zinkgruvan HW	60.3	18	1.56	4.63	1.03	2.7	6.44	6.58	0.05	0.66	0.065	95.68
ZV5274	506	Zinkgruvan HW	83.1	8.6	0.46	6.31	0.33	0.84	0.64	1	0.02	0.09	0.024	101
ZV5274B	506	Zinkgruvan HW			0.31		-0.7		0.94	0.94				
ZV5276	506	Zinkgruvan HW	68.7	12.4	0.94	8	0.77	1.85	1.66	5.43	0.07	0.36	0.081	100.58
ZV5278	506	Zinkgruvan HW	77.9	9	0.71	5.31	1.21	1.4	1.34	2.27	0.04	0.21	0.085	99.29
ZV5279	506	Zinkgruvan HW	80	6.2	0.62	2.9	1.23	1.04	0.29	2.45	0.07	0.1	0.034	97.19
ZV5281	506	Zinkgruvan FW	69.7	14.7	0.27	5.63	0.28	4.07	2.32	2.66	0.02	0.33	0.032	97.85
ZV5282	506	Zinkgruvan FW	71.3	13.5	0.26	6.66	0.96	3.86	2.88	3	0.03	0.32	0.037	100.02
ZV5283	506	Zinkgruvan FW	70.9	13.2	0.43	8.6	0.32	2.8	3.09	3.17	0	0.27	0.017	99.75
ZV5284	555	Zinkgruvan FW	64.4	10.9	0.57	4.05	4.73	5.49	3.34	4.34	0.45	0.34	0.165	96.82
ZV5286	555	Zinkgruvan FW	68.8	13.5	0.8	6.91	1.5	2.81	2.79	3.9	0.25	0.38	0.091	99.76
ZV5286B	555	Zinkgruvan FW			0.44		1.82		3.34	3.34				
ZV5287	555	Zinkgruvan FW	67.2	13.4	0.51	7.39	1.17	2.14	3.42	4.93	0.33	0.47	0.133	98.68
ZV5288	555	Zinkgruvan FW	76.4	10.9	0.73	7.06	0.8	2.29	2.38	2.46	0.02	0.2	0.02	100.91
ZV5289	555	Zinkgruvan FW	72.1	14.2	0.99	8.15	1.48	1.01	2.58	2.71	0.02	0.43	0.132	101.29
ZV5290	555	Zinkgruvan FW	73.6	13.3	0.75	5.95	0.28	3.42	3.43	3.44	0.02	0.25	0.024	101.04
ZV5291	555	Zinkgruvan FW	12.7	0.6	0.55	0.13	35.29	18.95	6.83	7.08	0.66	0.04	0.015	76.13

Appendix E Table E6
Metavolcanic samples

SAMPLE	HOLE	POSITION	SiO2	Al2O3	Na2O	K2O	CaO	MgO	FeO*	FeO (tot)	MnO	TiO2	P2O5	SUM
ZV5292	555	Zinkgruvan FW	61.4	16.3	0.96	10.99	0.95	3.68	2.14	2.2	0.03	0.2	0.03	96.78
ZV5296	555	Zinkgruvan FW	70.5	12.8	0.55	5.35	1.35	3.83	4	4.05	0.02	0.42	0.049	98.95
ZV5297	555	Zinkgruvan FW	62.5	13	0.46	5.69	2.57	5.36	5.69	5.73	0.03	0.55	0.111	96.04
ZV5298	555	Zinkgruvan FW	70.9	14.4	0.64	7.45	0.49	3.77	2.3	2.3	0.02	0.26	0.041	100.27
ZV5298B	555	Zinkgruvan FW			0.43		-0.7		2.06	2.06				
ZV5300	555	Zinkgruvan FW	74.7	11.8	0.72	6.79	0.87	3.16	2.11	2.14	0.02	0.4	0.102	100.72
ZV5301	555	Zinkgruvan FW	75.7	13	0.46	6.23	0.63	2.79	1.59	1.6	0.02	0.1	0.01	100.54
ZV5303	555	Zinkgruvan FW	69.8	12.8	0.83	7.57	1.6	3.1	1.71	1.75	0.02	0.29	0.055	97.84
ZV5305	555	Zinkgruvan FW	69.9	13.7	0.74	8.41	0.57	2.48	1.38	1.39	0.01	0.16	0.017	97.37
ZV5306	555	Zinkgruvan FW	60.5	13.5	0.59	7.47	2.66	6.21	5.72	5.83	0.05	1.37	0.213	98.45
ZV5307	555	Zinkgruvan FW	71	14.5	0.99	9.3	0.22	2.61	2.08	2.08	0.01	0.22	0.014	100.95
ZV5308	555	Zinkgruvan FW	74.7	12.8	0.56	5.65	0.16	3.9	2.83	2.83	0.01	0.29	0.015	100.91
ZV5309	555	Zinkgruvan FW	71.3	13.5	0.59	6.01	0.67	4.23	2.67	2.67	0.02	0.32	0.057	99.36
ZV5311	555	Zinkgruvan FW	60.9	16	0.83	10.09	1.41	6.37	3.82	3.82	0.04	1.09	0.181	100.74
ZV5312	555	Zinkgruvan FW	68.8	13	0.78	5.55	1.86	4.91	3.61	3.62	0.06	0.47	0.074	99.13
ZV5313	555	Zinkgruvan FW	65.6	13.1	0.67	7.16	2.2	5.04	4.77	4.78	0.07	0.76	0.157	99.55
ZV5316	556	Zinkgruvan FW	73.2	12.7	0.72	9.66	0.2	0.29	0.32	1.01	0.01	0.29	0.076	99.07
ZV5317	556	Zinkgruvan FW	71.9	12.3	0.53	8.59	0.23	1.2	2.11	2.94	0.02	0.36	0.098	99.27
ZV5324	556	Zinkgruvan FW	67.3	13.5	0.4	6.92	2.28	4.05	5.01	5.05	0.29	0.46	0.098	100.52
ZV5326	556	Zinkgruvan FW	66.8	14.5	0.45	7.47	0.84	3.29	6.09	6.22	0.28	0.48	0.094	100.52
ZV5327	556	Zinkgruvan FW	68.5	14.2	0.3	5.87	1.52	2.69	4.94	5.09	0.12	0.66	0.122	99.15
ZV5335	570	Zinkgruvan HW	69.6	14.4	0.49	7.59	0.35	2.38	3.72	3.85	0.08	0.27	0.02	99.11
ZV5338	570	Zinkgruvan HW	80.9	10.6	1.15	6.83	0.36	0.39	0.43	1.06	0.02	0.18	0.025	101.81
ZV5339	570	Zinkgruvan HW	69.4	12	0.42	4.22	3.91	3.28	4.28	5.53	1.06	0.44	0.117	100.98
ZV5340	570	Zinkgruvan HW	66.1	13.9	0.82	4.81	5.02	2.92	2.74	4.57	0.26	0.43	0.111	99.85
ZV5341	570	Zinkgruvan HW	66.9	11.6	0.55	2.64	2.15	3.65	10.25	11.59	0.5	0.44	0.127	100.75
ZV5342	570	Zinkgruvan HW	59.9	12.4	1.33	3.6	1.83	3.64	9.96	12.15	0.09	0.5	0.139	96.58
ZV5343	570	Zinkgruvan HW	63	18.2	1.84	4.51	0.92	2.57	5.87	6.03	0.05	0.61	0.114	97.95
ZV5345	574	Zinkgruvan HW	66	13.1	0.58	7.41	2.8	2.7	5.05	6.69	0.2	0.36	0.089	100.68
ZV5346	574	Zinkgruvan HW	67.2	10.4	0.17	4.37	1.13	3.73	11.33	11.49	0.63	0.22	0.061	99.52

Appendix E Table E6
Metavolcanic samples

SAMPLE	HOLE	POSITION	SiO2	Al2O3	Na2O	K2O	CaO	MgO	FeO*	FeO (tot)	MnO	TiO2	P2O5	SUM
ZV5346B	574	Zinkgruvan HW			0.12		1.96		10.22	10.22				
ZV5347	574	Zinkgruvan HW	73.5	11.2	0.32	8.32	1.99	1.03	2.02	2.84	0.36	0.26	0.093	100.41
ZV5348	574	Zinkgruvan HW	72	13.6	0.75	5.01	0.69	2.6	3.02	3.02	0.09	0.19	0.013	97.98
ZV5349	574	Zinkgruvan HW	71.4	10.7	0.57	4.05	3.86	1.92	4.96	6.27	0.93	0.35	0.11	100.88
ZV5350	574	Zinkgruvan HW	73.8	12.9	0.46	3.94	1.81	2.57	3.17	3.21	0.09	0.21	0.018	99.04
ZV5351	574	Zinkgruvan HW	68.4	12.3	0.45	5.71	3.98	2.31	4.77	5.91	0.52	0.39	0.108	100.66
ZV5352	574	Zinkgruvan HW	72.8	13	0.68	8.6	0.81	1.26	3.24	3.3	0.11	0.28	0.022	100.9
ZV5353	574	Zinkgruvan HW	73.7	13	0.42	4.84	1.47	2.47	2.7	2.73	0.14	0.2	0.017	99.02
ZV5354	574	Zinkgruvan HW	73.6	11.7	0.37	6.11	2.6	1.6	2.73	3.39	0.31	0.21	0.038	100.26
ZV5355	574	Zinkgruvan HW	70	10.2	0.26	6.66	2.11	1.03	5.43	7.55	0.63	0.2	0.069	99.7
ZV5357	579	Zinkgruvan FW	68.7	9.8	0.2	4.27	3.11	2.76	4.12	6.18	0.42	0.33	0.163	97.69
ZV5358	579	Zinkgruvan FW	71.2	12.2	0.34	7.05	2.37	1.57	1.48	1.55	0.1	0.24	0.054	96.73
ZV5358B	579	Zinkgruvan FW			0.26		1.96		1.41	1.41				
ZV5359	579	Zinkgruvan FW	70	11.9	0.39	4.92	1.07	3.39	2.93	3.71	0.11	0.31	0.073	96.8
ZV5360	579	Zinkgruvan FW	68.9	14	0.41	7.92	0.6	3.13	3.51	3.53	0.06	0.52	0.131	99.22
ZV5361	579	Zinkgruvan FW	65.9	13.4	0.38	5.85	1.23	4.17	3.97	3.97	0.07	0.47	0.065	95.56
ZV5362	579	Zinkgruvan FW	65.2	12.5	0.47	8.7	0.96	2.02	3.15	3.4	0.07	0.3	0.067	93.99
ZV5363	579	Zinkgruvan FW	66.3	12.7	0.41	7.58	2.03	2.5	5.94	5.96	0.12	0.39	0.108	98.13
ZV5379	559	Zinkgruvan FW	71.2	10.7	0.22	9.26	2.49	2.61	2.47	2.97	0.23	0.08	0.026	100.18
ZV5381	559	Zinkgruvan FW	55.3	20.6	0.32	12.8	0.72	2.66	2.8	2.82	0.1	1.27	0.331	97.02
ZV5382	559	Zinkgruvan FW	71.3	13.6	0.83	11.4	0.49	2.04	1.02	1.09	0.03	0.15	0.02	100.99
ZV5382B	559	Zinkgruvan FW			0.82		0.98		1	1				
ZV5389	580	Zinkgruvan HW	60.5	9.1	0.31	4.49	9.97	5.56	6.08	7.1	1.23	0.23	0.085	99.31
ZV5390	580	Zinkgruvan orezone	67.5	13.2	0.76	8.43	0.67	2.3	1.96	2.99	0.08	0.34	0.104	98.03
ZV5391	580	Zinkgruvan orezone	64.1	13.1	0.45	7.37	1.11	2.52	6.36	8.28	0.44	0.37	0.097	99.14
ZV5392	580	Zinkgruvan orezone	64.9	13.4	0.39	10.38	2.95	1.64	1.37	1.74	0.09	0.31	0.074	96.67
ZV5393	580	Zinkgruvan FW	75.1	10.6	0.28	7.91	2.35	1.57	1.22	1.71	0.1	0.17	0.038	100.1
ZV5394	580	Zinkgruvan FW	77.1	11.3	1.71	3.49	1.52	3.47	2.8	2.86	0.04	0.21	0.021	101.76
ZV5394B	580	Zinkgruvan FW			1.35		1.26		2.33	2.33				
ZV5395	580	Zinkgruvan FW	66.2	13.7	1.07	2.84	4.3	5.31	3.13	3.39	0.07	0.25	0.189	97.46

Appendix E Table E6
Metavolcanic samples

SAMPLE	HOLE	POSITION	SiO2	Al2O3	Na2O	K2O	CaO	MgO	FeO*	FeO (tot)	MnO	TiO2	P2O5	SUM
ZV5396	580	Zinkgruvan FW	64.9	14.2	0.9	7.11	2.14	6.58	3.83	3.87	0.03	0.49	0.06	100.3
ZV5397	580	Zinkgruvan FW	71.6	12.7	1.28	7.84	0.92	2.15	2.35	2.36	0.02	0.47	0.058	99.4
ZV5399	580	Zinkgruvan FW	64	15	0.92	9.79	0.73	3.88	4.99	5	0.02	0.36	0.024	99.74
ZV5401	677	Zinkgruvan FW	80	9.3	0.34	4.8	0.34	3.25	1.75	2.09	0.01	0.4	0.077	100.78
ZV5402	677	Zinkgruvan FW	74.4	12.1	0.21	6.25	0.09	3	2.97	3.07	0.01	0.39	0.025	99.59
ZV5403	677	Zinkgruvan FW	63.6	13.3	0.4	7.05	4.44	6.46	3.22	3.79	0.02	0.5	0.115	99.93
ZV5404	677	Zinkgruvan FW	64.1	10.6	0.41	5.43	7.57	7.27	3.62	3.74	0.04	0.53	0.182	99.93
ZV5405	677	Zinkgruvan FW	62.9	15.6	0.48	10.3	1.68	4.8	2.56	2.72	0.02	0.37	0.052	98.99
ZV5410	677	Zinkgruvan FW	65.2	13.6	0.26	8.06	2.85	5.29	3.68	3.79	0.02	0.52	0.137	99.79
ZV5411	677	Zinkgruvan FW	74.4	12.6	0.21	6.84	0.14	3.18	2.73	2.82	0.01	0.25	0.02	100.53
ZV5412	677	Zinkgruvan FW	60.8	16.8	0.42	12.3	0.49	4.98	2.53	2.59	0.02	0.33	0.03	98.78
ZV5413	677	Zinkgruvan FW	83.3	8.17	0.24	5.98	0.79	1.07	0.5	0.67	0.02	0.16	0.034	100.51
ZV5414	677	Zinkgruvan FW	64.6	14.5	0.42	9.8	0.42	4.64	2.73	2.81	0.03	0.34	0.02	97.61
ZV5415	677	Zinkgruvan orezone	31.2	4.52	0.5	0.74	7.48	2.59	3.95	11.16	0.57	0.09	0.098	75.55
ZV5416	677	Zinkgruvan FW	77.3	9.06	0.51	6.16	0.8	1.25	1.11	2.95	0.08	0.2	0.101	99.71
ZV5417	677	Zinkgruvan FW	62.3	10.8	0.37	5.46	1.29	2.84	8.86	12	0.77	0.34	0.177	98.28
ZV5418	677	Zinkgruvan orezone	66.6	11.6	0.39	5.65	2.27	2.9	4.09	6.91	0.76	0.38	0.155	99.34
ZV5418B	677	Zinkgruvan orezone			0.19		2.24		6.82	6.82				
ZV5419	677	Zinkgruvan FW	75.1	8.53	0.61	6.22	1.02	1.08	0.14	3.14	0.06	0.21	0.089	98.76
ZV5420	677	Zinkgruvan HW	72.8	13.5	0.86	6.11	0.87	2.19	2.71	2.76	0.08	0.17	0.025	99.41
ZV5421	677	Zinkgruvan HW	68.2	12.8	0.45	4.94	3.7	3.19	4.67	5.43	0.35	0.68	0.208	100.36
ZV5422	677	Zinkgruvan HW	72.4	10.9	0.3	4.71	3.61	2.39	3.44	4.56	0.44	0.3	0.094	100.31
ZV5423	677	Zinkgruvan HW	76.5	12.7	0.5	4.11	1.9	2.35	2.28	2.33	0.08	0.17	0.019	100.71
ZV5424	8502	Zinkgruvan FW	69.3	13.9	0.75	6.32	1.74	2.99	3.37	3.37	0.05	0.55	0.136	99.11
ZV5425	8502	Zinkgruvan FW	62.9	10.3	0.12	7.9	16.93	0.28	1.4	1.4	0.25	0.43	0.155	100.69
ZV5426	8502	Zinkgruvan FW	70.2	14	0.53	7.34	2.14	1.96	3.4	3.42	0.1	0.36	0.094	100.17
ZV5427	8502	Zinkgruvan FW	64.3	13.3	0.49	5.02	3.76	2.71	5.24	5.27	0.2	0.52	0.133	95.78
ZV5428	8502	Zinkgruvan FW	71.5	13.3	0.37	8.95	0.64	1.2	3.43	3.44	0.06	0.23	0.026	99.73
ZV5429	8502	Zinkgruvan FW	76	11.4	0.28	8.7	0.38	0.51	1.51	1.53	0.02	0.23	0.036	99.1
ZV5430	8502	Zinkgruvan orezone	38	11.2	0.55	4.29	2.01	3.6	14.45	14.67	0.41	0.37	0.384	81.34

Appendix E Table E6
Metavolcanic samples

SAMPLE	HOLE	POSITION	SiO2	Al2O3	Na2O	K2O	CaO	MgO	FeO*	FeO (tot)	MnO	TiO2	P2O5	SUM
ZV5431	8502	Zinkgruvan FW	58.7	12.8	0.45	6.59	3.49	2.63	11.4	11.81	0.28	0.43	0.143	98.2
ZV5432	8502	Zinkgruvan orezone	37.7	8.5	0.16	3.03	3.56	2.13	10.33	14.82	0.55	0.24	0.107	80.07
ZV5433	8502	Zinkgruvan FM	70.3	12.6	0.39	9.69	0.59	0.9	3.14	2.39	0.06	0.27	0.035	97.28
ZV5435	8502	Zinkgruvan HW	68.8	13.2	0.62	5.58	0.23	2.94	6.21	6.21	0.14	0.26	0.02	98.02
ZV5436	8502	Zinkgruvan HW	65.8	16	0.81	9.15	0.3	1.36	2.66	2.65	0.06	0.33	0.02	96.49
ZV5437	8509	Zinkgruvan FM	73.6	12.8	0.28	6.66	0.57	1.44	2.73	2.77	0.08	0.19	0.026	98.47
ZV5438	8509	Zinkgruvan FM	70.4	9.9	0.04	0.08	11.62	0.7	6.77	6.84	0.19	0.31	0.059	100.23
ZV5447	8510	Zinkgruvan FM	73.1	11.1	0.2	5.19	2.66	2.05	3.76	4.68	0.76	0.27	0.085	100.63
ZV5449	8510	Zinkgruvan FM	77.5	11.2	0.57	6.92	0.31	0.83	2.42	2.52	0.06	0.19	0.024	100.19
ZV5450	8510	Zinkgruvan FM	70.8	14.7	0.62	10.7	0.29	0.61	1.88	1.99	0.04	0.23	0.029	100.07
ZV5451	8510	Zinkgruvan FM	76.4	11.4	0.5	6.8	0.4	0.64	1.85	2.46	0.04	0.25	0.041	99.31
ZV5459	8510	Zinkgruvan FM	73.2	12.4	1.14	4.38	2.24	1.92	3.4	3.67	0.13	0.26	0.021	99.5
ZV5460	8510	Zinkgruvan FM	67.5	14.5	0.33	4.96	3.42	3.13	4.06	4.76	0.28	0.44	0.08	99.75
ZV5461	8510	Zinkgruvan FM	71.7	13.1	0.37	5.92	0.89	2.58	3.34	3.74	0.08	0.26	0.019	98.85
ZV5462	8510	Zinkgruvan FM	68.2	13.1	0.21	6.94	1.8	3.33	3.18	3.61	0.11	0.37	0.122	97.99
ZV5463	8510	Zinkgruvan FM	70.2	11.5	0.55	4.31	2.95	3.76	3.77	4.18	0.17	0.44	0.099	98.35
ZV1892		Zinkgruvan FM	63.64	16.61	0.39	14.46	0.16	1.22	3.24	3.24	0.03	0.46	0.096	100.3
ZV1895		Zinkgruvan FM	66.65	12.19	0.48	6.28	1.39	3.34	3.46	3.45	0.05	0.53	0.076	94.43
ZV1901	DBH1462	Zinkgruvan FM	67.43	14.7	1.36	10.07	0.29	3.69	2.47	2.47	0.02	0.22	0.021	100.26

APPENDIX F

SCANNING ELECTRON MICROSCOPY

Operating conditions

Individual mineral analyses were obtained using the JEOL JSM 6400 Scanning Electron Microscope (SEM) at the School of Ocean and Earth Science, University of Southampton. Analyses were carried out on standard 30μm-thick polished thin sections coated with carbon. Count times were set at 100 seconds per analysis for maximum accuracy.

Calculation of stoichiometry from SEM data

Stoichiometric calculation of ionic proportions for individual mineral analyses have been carried out according to the standard methods outlined in Spear (1995) and Deer *et al.* (1992). For the majority of non-hydrous minerals, Fe_2O_3 (Fe^{3+}) has been estimated from FeO (Fe^{2+}) data using the cation balancing method described in Spear (1995); stoichiometric calculation of Fe^{3+} in hydrous minerals is not possible using this method. Hydrous minerals have been stoichiometrically calculated using the method outlined in Deer *et al.* (1992). As no measurement of H_2O can be made using SEM EDS analysis, H_2O has been estimated at approximately 5 wt% for phlogopite, 3 wt% for biotite, ~2 wt% for tremolite and 12 wt% for serpentine.

Repeat analyses were carried out for many samples. The data presented are mean average values, quoted with a standard deviation (S.D) and number of analyses (*n*). Average chemical analyses are quoted as weight % oxide.

Mineral analyses are arranged in the following order, with UZ series samples listed first, followed by drill hole samples and regional (ZR series) samples in numerical order. Sulphide analyses are summarised in Table 7.1, Chapter 7.

1. Olivines
2. Garnets
3. Vesuvianite
4. Epidotes
5. Wollastonite
6. Pyroxenes
7. Amphiboles
8. Micas (muscovite, biotite, phlogopite)
9. Clays (serpentine, saponite/iddingsite)
10. Feldspars (K-feldspar, Ba-feldspar, albite)
11. Spinels

Appendix F: SEM analyses

Sample No.	***555/06***		***555/07***		***1557/26***		***ZR02***		***ZR06***	
Location	Nygruvan		Nygruvan		Burkland		Gardshytten		Isåsen	
Mineral	Forsterite		Knebelite		Forsterite		Forsterite		Forsterite	
Lithology	Marble		Marble		Marble		Marble		Marble	
No. of samples (*n*)	1		6		1		1		4	
	Wt %	*S.D*	*Wt %*	*S.D*	*Wt %*	*S.D*	*Wt %*	*S.D*	*Wt %*	*S.D*
SiO_2	39.27	-	35.63	2.53	41.71	-	44.17	-	47.51	1.93
TiO_2	0.01	-	0.07	0.08	-	-	-	-	-	-
Al_2O_3	-	-	0.04	0.09	-	-	-	-	3.60	1.95
FeO (tot)	14.92	-	16.52	1.24	13.48	-	5.06	-	4.90	1.63
MnO	1.38	-	29.99	2.51	1.79	-	0.26	-	-	-
MgO	44.38	-	10.63	0.67	42.99	-	50.51	-	43.98	1.52
CaO	0.02	-	5.45	0.47	-	-	-	-	-	-
NaO	-	-	0.00	0.00	-	-	-	-	-	-
K_2O	0.04	-	0.13	0.08	-	-	-	-	-	-
SO_3	-	-	0.14	0.24	-	-	-	-	-	-
ZnO	-	-	0.00	0.00	-	-	-	-	-	-
PbO	-	-	1.25	0.34	-	-	-	-	-	-
Total	100.04		99.87		99.98		100.00		99.99	
	At. prop.	*S.D*	*At. prop.*	*S.D*	*At. prop.*	*S.D*	*At. prop.*	*S.D*	*At. prop.*	*S.D*
Si	0.99	-	1.10	0.07	1.06	-	1.07	-	1.17	0.05
Ti	-	-	-	-	-	-	-	-	-	-
Al	-	-	-	-	-	-	-	-	0.10	0.06
Fe^{3+}	-	-	-	-	-	-	-	-	-	-
Fe^{2+}	0.31	-	0.43	0.03	0.29	-	0.10	-	0.10	0.03
Mn	0.03	-	0.78	0.07	0.04	-	0.01	-	-	-
Mg	1.67	-	0.49	0.03	1.62	-	1.82	-	1.62	0.05
Ca	-	-	0.18	0.02	-	-	-	-	-	-
Na	-	-	-	-	-	-	-	-	-	-
K	-	-	-	-	-	-	-	-	-	-
O	6.00	-	6.00	0.00	6.00	-	6.00	-	6.00	0.00

Appendix F: SEM analyses

Sample No.	***UZ8***		***UZ23***		***UZ33***		***UZ42***		***UZ44***		***UZ45***		***UZ46***	
Location	Nygruvan 650m level		Nygruvan 500m level		Nygruvan 450m level		Nygruvan 950m level		Nygruvan 950m level		Nygruvan 950m level		Nygruvan 950m level	
Mineral	Garnet		Garnet		Garnet		Garnet		Garnet		Garnet		Garnet	
Lithology	Calc-silicate		Metavolcanic		Metavolcanic		Amphibolite		Metavolcanic		Calc-silicate		Quartzite	
No. of samples (*n*)	4		3		1		1		2		3		1	
	Wt %	*S.D*	*Wt %*	*S.D*	*Wt %*	*S.D*	*Wt %*	*S.D*	*Wt %*	*S.D*	*Wt %*	*S.D*	*Wt %*	*S.D*
SiO_2	36.20	1.69	37.06	0.08	36.26	-	37.09	-	47.74	6.07	36.79	0.02	39.96	-
TiO_2	0.17	0.10	0.03	0.06	-	-	0.08	-	-	-	0.06	0.01	0.57	-
Al_2O_3	21.42	0.92	19.26	0.35	18.74	-	18.87	-	20.26	0.25	18.61	0.09	19.82	-
FeO (tot)	12.74	7.55	23.08	2.00	36.10	-	23.26	-	10.86	7.01	21.63	0.69	3.68	-
MnO	9.02	3.68	12.62	0.98	4.00	-	12.28	-	2.46	1.51	15.14	0.57	3.55	-
MgO	0.02	0.04	1.04	0.41	1.31	-	0.55	-	0.00	0.00	0.24	0.12	0.00	-
CaO	19.15	8.19	6.85	1.30	3.57	-	7.83	-	18.35	0.13	7.48	0.20	32.39	-
NaO	1.07	0.40	-	-	-	-	-	-	-	-	-	-	-	-
K_2O	0.01	0.02	-	-	-	-	-	-	-	-	-	-	-	-
ZnO	0.21	0.18	-	-	-	-	-	-	0.32	0.45	-	-	-	-
Total	100.00		99.94		99.97		99.97		99.99		99.95		99.96	
	At. prop.	*S.D*	*At. prop.*	*S.D*	*At. prop.*	*S.D*	*At. prop.*	*S.D*	*At. prop.*	*S.D*	*At. prop.*	*S.D*	*At. prop.*	*S.D*
Si	2.82	0.07	3.00	0.00	2.97	-	3.01	-	3.72	0.44	3.00	0.00	3.06	-
Ti	0.01	0.01	-	-	-	-	0.01	-	-	-	-	-	0.03	-
Al	1.97	0.05	1.84	0.03	1.81	-	1.81	-	1.86	0.04	1.79	0.01	1.79	-
Fe^{3+}	0.32	0.21	1.42	0.11	2.22	-	1.43	-	-	-	1.28	0.04	0.21	-
Fe^{2+}	0.52	0.27	0.15	0.03	0.25	-	0.16	-	0.71	0.46	0.20	0.00	0.03	-
Mn	0.60	0.25	0.87	0.07	0.28	-	0.85	-	0.16	0.10	1.05	0.04	0.23	-
Mg	0.00	0.00	0.13	0.05	0.16	-	0.07	-	0.00	0.00	0.03	0.02	0.00	-
Ca	1.59	0.64	0.60	0.11	0.31	-	0.68	-	1.53	0.00	0.65	0.02	2.66	-
Na	0.16	0.06	-	-	-	-	-	-	-	-	-	-	-	-
K	0.00	0.00	-	-	-	-	-	-	-	-	-	-	-	-
Zn	0.01	0.01	-	-	-	-	-	-	0.02	0.03	-	-	-	-
O	12.00	0.00	12.00	0.00	12.00	-	12.00	-	12.00	0.00	12.00	0.00	12.00	-

Appendix F: SEM analyses

Sample No.	***451/03***		***451/13***		***670/04***		***672/03***		***1557/09***		***1557/15***		***ZR05***	
Location	Nygruvan		Nygruvan		Cecilia		Cecilia		Burkland		Burkland		Isåsen	
Mineral	Garnet		Garnet		Garnet		Garnet		Garnet		Garnet		Garnet	
Lithology	Fe skarn		Fe skarn		Metavolcanic		Metavolcanic		Metavolcanic		Calc-silicate		Marble	
No. of samples (*n*)	1		15		4		1		8		4		1	
	Wt %	*S.D*	*Wt %*	*S.D*	*Wt %*	*S.D*	*Wt %*	*S.D*	*Wt %*	*S.D*	*Wt %*	*S.D*	*Wt %*	*S.D*
SiO_2	36.73	-	36.55	0.76	37.75	1.50	26.61	-	37.55	1.22	41.25	2.58	39.53	-
TiO_2	-	-	0.02	0.03	-	-	-	-	-	-	-	-	-	-
Al_2O_3	20.06	-	18.24	0.39	19.59	0.78	14.98	-	18.39	0.91	15.51	4.17	18.13	-
FeO (tot)	15.11	-	24.53	3.79	29.93	1.45	37.14	-	38.05	1.23	20.04	5.22	3.50	-
MnO	17.97	-	13.06	2.88	6.46	0.37	15.00	-	3.00	0.75	4.97	4.53	0.21	-
MgO	0.35	-	0.64	0.27	0.51	0.17	0.00	-	1.98	0.86	3.51	3.01	1.94	-
CaO	9.75	-	6.93	3.88	5.75	0.71	6.23	-	1.07	0.20	13.90	3.09	36.68	-
NaO	-	-	-	-	-	-	0.00	-	-	-	-	-	-	-
K_2O	-	-	-	-	-	-	0.00	-	-	-	0.80	0.93	-	-
ZnO	-	-	-	-	-	-		-	-	-	-	-	-	-
Total	99.97		99.97		99.98		99.96		100.04		99.99		99.99	-
	At. prop.	*S.D*	*At. prop.*	*S.D*	*At. prop.*	*S.D*	*At. prop.*	*S.D*	*At. prop.*	*S.D*	*At. prop.*	*S.D*	*At. prop.*	*S.D*
Si	2.96	-	2.98	0.07	3.07	0.11	2.25	-	3.03	0.08	3.25	0.18	2.98	-
Ti	-	-	-	-	-	-	-	-	-	-	-	-	-	-
Al	1.91	-	1.75	0.05	1.88	0.07	1.49	-	1.86	0.09	1.44	0.40	1.61	-
Fe^{3+}	0.85	-	1.40	0.36	1.49	0.05	0.61	-	1.54	0.07	1.17	0.21	-	-
Fe^{2+}	0.17	-	0.28	0.17	0.55	0.88	2.01	-	1.12	1.34	0.15	0.12	0.22	-
Mn	1.23	-	0.90	0.20	0.45	0.03	1.07	-	0.21	0.05	0.33	0.30	0.01	-
Mg	0.04	-	0.08	0.03	0.06	0.02	0.00	-	0.24	0.10	0.41	0.35	0.22	-
Ca	0.84	-	0.60	0.33	0.50	0.06	0.56	-	0.09	0.02	1.17	0.27	2.96	-
Na	-	-	-	-	-	-	-	-	-	-	-	-	-	-
K	-	-	-	-	-	-	-	-	-	-	0.08	0.09	-	-
Zn	-	-	-	-	-	-	-	-	-	-	-	-	-	-
O	12.00	-	12.00	0.00	12.00	0.00	12.00	-	12.00	0.00	12.00	0.00	12.00	-

Appendix F: SEM analyses

Sample No.	***451/19***		***1557/14***		***1557/15***		***451/07***		***451/19***		***555/07***	
Location	Nygruvan		Burkland		Burkland		Nygruvan		Nygruvan		Nygruvan	
Mineral	Vesuvianite		Zoisite		Zoisite		Wollastonite		Wollastonite		Wollastonite	
Lithology	Calc-silicate		Calc-silicate		Calc-silicate		Calc-silicate		Ca-Si marble		Marble	
No. of samples (*n*)	1		1		2		2		1		1	
	Wt %	*S.D*	*Wt %*	*S.D*	*Wt %*	*S.D*	*Wt %*	*S.D*	*Wt %*	*S.D*	*Wt %*	*S.D*
SiO_2	36.27	-	40.84	-	42.06	0.45	49.80	0.26	48.16	-	47.86	-
TiO_2	3.21	-	-	-	-	-	-	-	0.06	-	0.25	-
Al_2O_3	17.07	-	29.60	-	23.04	0.25	-	-	-	-	-	-
FeO (tot)	2.84	-	3.77	-	6.42	8.77	0.21	0.06	-	-	0.25	-
MnO	-	-	0.33	-	6.51	8.91	1.22	0.10	0.23	-	0.31	-
MgO	1.68	-	-	-	0.30	0.00	0.00	0.00	0.00	-	0.10	-
CaO	37.69	-	23.91	-	20.95	0.22	48.76	0.23	51.20	-	49.66	-
NaO	-	-	-	-	-	-	-	-	-	-	0.00	-
K_2O	-	-	0.05	-	-	-	0.01	0.01	0.02	-	0.19	-
SO_3	0.30	-	-	-	-	-	-	-	-	-	0.40	-
ZnO	0.07	-	-	-	-	-	-	-	-	-	0.64	-
PbO	0.87	-	-	-	-	-	-	-	0.11	-	-	-
H_2O	-	-	1.50	-	1.50	0.00	-	-	0.23	-	-	-
Total	100.00		100.00		100.78		100.00		100.01		99.99	
	At. prop	*S.D*	*At. prop*	*S.D*	*At. prop*	*S.D*	*At. prop*	*S.D*	*At. prop.*	*S.D*	*At. prop*	*S.D*
Si	17.34	-	2.84	-	3.12	0.20	0.96	0.01	0.93	-	0.93	-
Ti	1.15	-	-	-	-	-	-	-	-	-	-	-
Al	9.62	-	0.16	-	0.01	0.02	-	-	-	-	-	-
Fe^{3+}	-	-	2.27	-	-	-	-	-	-	-	-	-
Fe^{2+}	1.13	-		-	2.00	0.15	-	-	-	-	-	-
Mn	0.00	-	0.22	-	0.38	0.52	0.02	0.00	-	-	0.01	-
Mg	1.20	-	0.02	-	0.42	0.58	-	-	-	-	-	-
Ca	19.31	-	0.00	-	0.03	0.00	1.01	0.00	1.06	-	1.03	-
Na	-	-	1.78	-	1.67	0.11	-	-	-	-	-	-
K	-	-	-	-	-	-	-	-	-	-	-	-
S	0.11	-	-	-	-	-	-	-	-	-	0.01	-
Zn	0.02	-	-	-	-	-	-	-	-	-	0.01	-
Pb	0.11	-	-	-	-	-	-	-	-	-	-	-
OH	-	-	0.70	-	0.43	0.40	-	-	-	-	-	-
O	3.00	-	13.00	-	13.00	0.00	3.00	0.00	3.00	-	3.00	-

Appendix F: SEM analyses

Sample No.	***UZ8***		***451/03***		***451/13***		***451/19***		***555/11***		***898/9***	
Location	Nygruvan		Nygruvan		Nygruvan		Nygruvan		Nygruvan		Cecilia	
Mineral	Diopside		Diopside		Diopside		Diopside		Diopside		Diopside	
Lithology	Calc-silicate		Fe skarn		Fe skarn		Marble		Marble		Calc-silicate	
No. of samples (*n*)	2		2		5		3		3		6	
	Wt %	*S.D*	*Wt %*	*S.D*	*Wt %*	*S.D*	*Wt %*	*S.D*	*Wt %*	*S.D*	*Wt %*	*S.D*
SiO_2	49.79	0.17	50.49	0.30	50.23	0.32	52.48	0.36	55.50	3.23	39.94	0.40
TiO_2	-	-	-	-	-	-	0.06	0.11	0.09	0.08	-	-
Al_2O_3	-	-	0.56	0.09	-	-	-	-	-	-	-	-
FeO (tot)	18.52	0.04	15.26	0.57	21.51	0.63	8.38	0.51	3.99	0.46	30.75	0.91
MnO	1.79	0.09	2.36	0.02	2.65	0.16	0.82	0.19	0.49	0.09	1.32	0.08
MgO	8.10	0.25	9.29	0.06	5.57	0.37	13.19	0.12	17.44	2.72	4.15	0.32
CaO	20.84	0.42	22.04	0.33	20.03	0.16	24.76	0.29	22.49	6.36	23.89	0.51
NaO	0.85	0.02	-	-	-	-	-	-	-	-	-	-
K_2O	0.02	0.03	-	-	-	-	-	-	-	-	-	-
SO_3	-	-	-	-	-	-	-	-	-	-	-	-
CuO							0.10	0.12	-	-	-	-
ZnO	0.09	0.12	-	-	-	-	0.08	0.12	-	-	-	-
PbO	-	-	-	-	-	-	0.12	0.21	-	-	-	-
H_2O	-	-	-	-	-	-	-	-	-	-	-	-
Total	100.00		100.00		99.99		100.00		100.00		100.05	
	At. prop	*S.D*	*At. prop*	*S.D*	*At. prop*	*S.D*	*At. prop*	*S.D*	*At. prop*	*S.D*	*At. prop*	*S.D*
Si	1.93	0.01	1.95	0.01	2.00	0.01	1.97	0.01	2.03	0.10	1.62	0.02
Ti	-	-	-	-	-	-	-	-	-	-	-	-
Al	-	-	0.03	0.00	-	-	0.00	0.00	-	-	-	-
Fe^{3+}	0.41	0.01	0.43	0.01	0.43	0.02	0.21	0.02	-	-	0.29	0.03
Fe^{2+}	0.20	0.01	0.07	0.01	0.28	0.38	0.06	0.04	0.12	0.01	0.76	0.03
Mn	0.06	0.00	0.08	0.00	0.09	0.01	0.03	0.01	0.02	0.00	0.05	0.00
Mg	0.47	0.01	0.54	0.00	0.33	0.02	0.74	0.01	0.95	0.14	0.25	0.02
Ca	0.87	0.02	0.91	0.01	0.86	0.01	1.00	0.01	0.88	0.25	1.04	0.02
Na	0.06	0.00	-	-	-	-	-	-	-	-	-	-
K	-	-	-	-	-	-	-	-	-	-	-	-
O	6.00	0.00	6.00	0.00	6.00	0.00	6.00	0.00	6.00	0.00	6.00	0.00

Appendix F: SEM analyses

Sample No.	***898/10***		***1557/14***		***1557/15***		***1557/19***		***ZR05***		***UZ22***		***UZ42***	
Location	Cecilia		Burkland		Burkland		Burkland		Isåsen		Nygruvan		Nygruvan	
Mineral	Diopside		Diopside		Diopside		Diopside		Diopside		Tremolite		Actinolite	
Lithology	Calc-silicate		Calc-silicate		Calc-silicate		Calc-silicate		Marble		Calc-silicate		Amphibolite	
No. of samples (*n*)	5		1		1		1		1		1		1	
	Wt %	*S.D*	*Wt %*	*S.D*	*Wt %*	*S.D*	*Wt %*	*S.D*	*Wt %*	*S.D*	*Wt %*	*S.D*	*Wt %*	*S.D*
SiO_2	50.68	2.34	56.28	-	51.45	-	50.85	-	53.12	-	51.85	-	48.68	-
TiO_2	0.00	0.00	-	-	-	-	-	-	-	-	0.18	-	-	-
Al_2O_3	0.00	0.00	-	-	-	-	-	-	-	-	2.66	-	1.84	-
FeO (tot)	6.41	2.89	16.05	-	18.21	-	19.75	-	11.23	-	11.08	-	27.84	-
MnO	0.74	0.35	0.00	-	1.66	-	1.91	-	1.26	-	2.19	-	1.70	-
MgO	13.68	2.34	15.07	-	7.56	-	6.38	-	11.19	-	17.26	-	6.82	-
CaO	28.49	6.06	12.34	-	21.11	-	21.10	-	23.20	-	11.15	-	11.13	-
NaO	0.00	0.00	-	-	-	-	-	-	-	-	1.15	-	0.00	-
K_2O	0.00	0.00	0.25	-	-	-	-	-	-	-	0.09	-	0.32	-
SO_3	-	-	-	-	-	-	-	-	-	-	-	-	-	-
ZnO	-	-	-	-	-	-	-	-	-	-	0.39	-	-	-
PbO	-	-	-	-	-	-	-	-	-	-	-	-	-	-
H_2O	-	-	-	-	-	-	-	-	-	-	2.16	-	2.20	-
Total	99.99		100.00		99.99		99.99		99.99		100.15		100.52	
	At. prop.	*S.D*	*At. prop.*	*S.D*	*At. prop.*	*S.D*	*At. prop.*	*S.D*	*At. prop.*	*S.D*	*At. prop.*	*S.D*	*At. prop.*	*S.D*
Si	1.88	0.08	2.13	-	2.02	-	2.01	-	2.02	-	7.49	-	7.54	-
Ti	-	-	-	-	-	-	-	-	-	-	0.45	-	0.34	-
Al	-	-	-	-	-	-	-	-	-	-	-	-	-	-
Fe^{3+}	-	-	-	-	-	-	-	-	-	-	0.02	-	-	-
Fe^{2+}	0.20	0.09	0.51	-	0.60	-	0.65	-	0.36	-	1.34	-	3.61	-
Mn	0.02	0.01	0.00	-	0.06	-	0.06	-	0.04	-	0.27	-	0.22	-
Mg	0.76	0.13	0.85	-	0.44	-	0.38	-	0.63	-	3.72	-	1.57	-
Ca	1.14	0.24	0.50	-	0.89	-	0.89	-	0.95	-	1.73	-	1.85	-
Na	-	-	-	-	-	-	-	-	-	-	0.32	-	-	-
K	-	-	0.01	-	-	-	-	-	-	-	0.02	-	0.06	-
OH	-	-	-	-	-	-	-	-	-	-	2.08	-	2.27	-
O	6.00	0.00	6.00	-	6.00	-	6.00	-	6.00	-	24.00	-	24.00	-

Appendix F: SEM analyses

Sample No.	***UZ44***		***451/03***		***451/13***		***555/06***		***555/11***		***1557/15***	
Location	Nygruvan		Nygruvan		Nygruvan		Nygruvan		Nygruvan		Burkland	
Mineral	Actinolite		Trem-Actinolite		Trem-Actinolite		Actinolite		Trem-Actinolite		Actinolite	
Lithology	Metavolcanic		Fe skarn		Grt horizon		Marble		Calc-silicate		Calc-silicate	
No. of samples (*n*)	2		1		1		1		2		1	
	Wt %	*S.D*	*Wt %*	*S.D*	*Wt %*	*S.D*	*Wt %*	*S.D*	*Wt %*	*S.D*	*Wt %*	*S.D*
SiO_2	50.90	0.41	49.66	-	50.86	-	32.21	-	58.18	0.52	47.59	-
TiO_2	0.02	0.02	-	-	-	-	-	-	0.08	0.12	-	-
Al_2O_3	1.31	0.28	-	-	-	-	1.88	-	-	-	7.33	-
FeO (tot)	25.77	0.42	19.70	-	19.90	-	26.09	-	3.33	1.54	18.50	-
MnO	1.39	0.10	2.71	-	2.64	-	2.14	-	0.43	0.03	0.44	-
MgO	7.38	0.26	5.46	-	6.17	-	17.45	-	21.98	0.33	18.91	-
CaO	11.15	0.04	20.47	-	18.41	-	15.36	-	13.99	0.61	5.18	-
NaO	-	-	-	-	-	-	-	-	-	-	-	-
K_2O	0.14	0.00	-	-	-	-	0.07	-	-	-	0.02	-
SO_3	-	-	-	-	-	-	0.16	-	-	-	-	-
CuO			-	-	-	-	0.04	-	-	-	-	-
ZnO	0.10	0.14	-	-	-	-	0.00	-	-	-	-	-
PbO			-	-	-	-	2.67	-	-	-	-	-
H_2O	2.20	0.00	2.00	-	2.00	-	2.20	-	2.00	0.00	2.00	-
Total	100.35		100.00		99.99		100.27		100.00		99.98	
	At. prop.	*S.D*	*At. prop.*	*S.D*	*At. prop.*	*S.D*	*At. prop.*	*S.D*	*At. prop.*	*S.D*	*At. prop.*	*S.D*
Si	7.77	0.06			7.81	-	5.43	-	8.02	0.02	6.95	-
Ti	-	-			-	-	-	-	0.01	0.01	1.05	-
Al	0.24	0.05			-	-	0.37	-	-	-	0.21	-
Fe^{3+}	-	-			-	-	-	-	-	-	0.00	-
Fe^{2+}	3.29	0.05			2.56	-	3.68	-	0.38	0.18	2.26	-
Mn	0.18	0.01			0.34	-	0.31	-	0.05	0.00	0.05	-
Mg	1.68	0.06			1.41	-	4.39	-	4.52	0.04	4.12	-
Ca	1.82	0.01			3.03	-	2.78	-	2.07	0.08	0.81	-
Na	-	-			-	-	0.00	-	-	-	0.00	-
K	0.03	0.00			-	-	0.01	-	-	-	0.00	-
OH	2.24	0.00			2.05	-	2.47	-	1.84	0.01	1.95	-
O	24.00	0.00			24.00	-	24.00	-	24.00	0.00	24.00	-

Appendix F: SEM analyses

Sample No.	***UZ75***		***451/03***		***451/13***		***454/13***		***670/04***		***672/03***		***555/07***	
Location	800m level		Nygruvan		Nygruvan		Nygruvan		Cecilia		Cecilia		Nygruvan	
Mineral	Muscovite		Biotite		Biotite		Biotite		Biotite		Biotite		Phlogopite	
Lithology	Marble		Fe skarn		Fe skarn		Fe skarn		Metavolcanic		Metavolcanic		Marble	
No. of samples (*n*)	1		1		5		1				1		1	
	Wt %	*S.D*	*Wt %*	*S.D*	Wt %	*S.D*	*Wt %*	*S.D*	*Wt %*	*S.D*	*Wt %*	*S.D*	*Wt %*	*S.D*
SiO_2	44.59	-	35.02	-	34.28	1.11	33.63	-	35.27	0.61	27.42	-	38.72	-
TiO_2	-	-	-	-	1.71	1.10	1.56	-	0.67	0.08	2.32	-	0.60	-
Al_2O_3	38.88	-	14.82	-	12.97	0.80	12.43	-	12.57	0.34	12.29	-	14.56	-
FeO (tot)	0.32	-	28.24	-	34.82	2.07	36.94	-	34.83	0.30	39.41	-	7.43	-
MnO	0.03	-	0.77	-	0.79	0.47	0.38	-	0.30	0.08	-	-	0.15	-
MgO	0.11	-	12.17	-	5.37	0.96	4.15	-	5.32	0.26	6.02	-	22.24	-
CaO	0.46	-	0.27	-	-	-	0.28	-	0.09	0.05	-	-	0.23	-
NaO	0.96	-	0.00	-	-	-	-	-	-	-	-	-	-	-
K_2O	9.56	-	6.54	-	7.45	1.29	8.42	-	8.38	0.45	10.38	-	10.80	-
SO_3	-	-	-	-	-	-	-	-	-	-	-	-	-	-
CuO	-	-	-	-	-	-	-	-	-	-	-	-	-	-
ZnO	0.16	-	-	-	-	-	-	-	-	-	-	-	-	-
PbO	-	-	-	-	-	-	-	-	-	-	-	-	0.26	-
H_2O	5.00	-	3.00	-	3.00	0.00	3.00	-	3.00	0.00	3.00	-	-	-
Total	100.07		100.84		100.38	0.00	100.78		100.44		100.84		5.00	-
	At. prop.	*S.D*	*At. prop.*	*S.D*	*At. prop.*	*S.D*	*At. prop.*	*S.D*	*At. prop*	*S.D*	*At. prop*	*S.D*	99.99	
Si	5.86	-			5.61	0.15	5.58	-	5.78	0.06	4.75	-	*At. prop*	*S.D*
Ti	-	-			0.21	0.13	0.19	-	0.08	0.01	0.30	-	5.54	-
Al	6.02	-			2.49	0.15	2.43	-	2.42	0.06	2.51	-	0.07	-
Fe^{3+}	-	-			-	-	-	-	-	-	-	-	2.46	-
Fe^{2+}	0.04	-			4.77	0.34	5.13	-	4.77	0.07	5.71	-	-	-
Mn	-	-			0.11	0.07	0.05	-	0.04	0.01	-	-	0.89	-
Mg	0.02	-			1.31	0.22	1.03	-	1.30	0.07	1.55	-	0.02	-
Ca	0.06	-			0.00	0.00	0.05	-	0.02	0.01	-	-	4.75	-
Na	0.24	-			0.00	0.00	-	-	-	-	-	-	0.04	-
K	1.60	-			1.56	0.28	1.78	-	1.75	0.08	2.29	-	-	-
OH	4.38	-			3.28	0.04	3.32	-	3.28	0.03	44.57	-	0.99	-
O	24.00	-			24.00	0.00	24.00	-	24.00	0.00	24.00	-	2.39	-
													24.00	-

Appendix F: SEM analyses

Sample No.	***555/11***		***ZR06***		***451/03***		***ZR02***		***ZR06***		***ZR22***		
Location	Nygruvan		Isåsen		Nygruvan		Gardshytten		Isåsen		Rytabygget		
Mineral	Phlogopite		Phlogopite		Chlorite		Clinochlore		Clinochlore		Clinochlore		
Lithology	Marble		Marble		Fe skarn		Marble		Marble		Marble		
No. of samples (*n*)	2		4		2		3		1		2		
	Wt %	*S.D*	*Wt %*	*S.D*	Wt %	*S.D*	*Wt %*	*S.D*	*Wt %*	*S.D*	*Wt %*	*S.D*	
SiO_2	40.09	0.15	38.07	0.18	28.83	0.01	31.41	0.45	34.49	-	34.50	3.76	
TiO_2	0.46	0.08	0.93	0.05	-	-	-	-	-	-	-	-	
Al_2O_3	13.50	0.44	14.91	0.21	15.60	0.48	22.61	0.27	20.21	-	17.35	5.01	
FeO (tot)	7.46	0.45	4.44	0.16	29.87	0.25	1.38	0.31	1.51	-	3.09	0.45	
MnO	0.16	0.02	-	-	0.89	0.01	0.00	0.00	0.034	-	-	-	
MgO	22.31	0.65	21.95	0.10	12.22	1.40	31.45	0.20	30.65	-	32.04	0.78	
CaO	0.33	0.08	-	-	0.29	0.12	0.12	0.05	0.097	-	-	-	
NaO	0.00	0.00	-	-	-	-	-	-	-	-	-	-	
K_2O	10.65	0.12	14.69	0.09	1.29	0.55	0.02	0.03	-	-	-	-	
SO_3	-	-	-	-	-	-	-	-	-	-	-	-	
CuO	-	-	-	-	-	-	-	-	-	-	-	-	
ZnO	-	-	-	-	-	-	-	-	-	-	-	-	
PbO	-	-	-	-	-	-	-	-	-	-	-	-	
H_2O	5.00	0.00	5.00	0.00	8.00	4.24	13.00	0.00	13.00	-	13.00	0.00	
Total	99.98		99.99		96.98		99.99		99.99		99.98		
	At. prop	*S.D*	*At. prop*	*S.D*	*At. prop*	*S.D*	*At. prop*	*S.D*	*At. prop*	*S.D*	*At. prop*	*S.D*	
Si	5.72	0.01	5.49	0.02	6.64	0.58	5.82	0.07	6.36	-	6.42	0.69	
Ti	0.05	0.01	0.10	0.01	-	-	-	-	-	-	-	-	
Al	2.27	0.06	2.53	0.03	4.22	0.24	4.93	0.07	4.40	-	3.80	1.10	
Fe^{3+}	-	-	-	-	-	-	-	-	-	-	-	-	
Fe^{2+}	0.89	0.06	0.54	0.02	5.75	0.45	0.21	0.05	0.23	-	0.48	0.07	
Mn	0.02	0.00	0.00	0.00	0.17	0.01	-	-	0.01	-	-	-	
Mg	4.75	0.13	4.72	0.02	4.21	0.84	8.69	0.05	8.43	-	8.89	0.21	
Ca	0.05	0.01	-	-	0.07	0.02	0.02	0.01	0.02	-	-	-	
Na	-	-	-	-	-	-	-	-	-	-	-	-	
K	1.94	0.03	2.70	0.02	0.37	0.13	-	-	-	-	-	-	
OH	4.76	0.01	4.81	0.00	12.00	5.45	16.07	0.03	16.00	-	16.14	0.02	
O	24.00	0.00	24.00	0.00	30.00	8.49	36.00	0.00	36.00	-	36.00	0.00	

Appendix F: SEM analyses

Sample No.	***555/06***		***555/07***		***555/11***		***ZR02***		***ZR06***		***555/06***		***555/11***	
Location	Nygruvan		Nygruvan		Nygruvan		Gardshytten		Isåsen		Nygruvan		Nygruvan	
Mineral	Serpentine		Serpentine		Serpentine		Serpentine		Serpentine		Saponite/Iddingsite		Saponite/Iddingsite	
Lithology	Marble		Marble		Marble		Marble		Marble		Marble		Marble	
No. of samples (*n*)	13		4		2		3				7		1	
	Wt %	*S.D*	*Wt %*	*S.D*	Wt %	S.D	*Wt %*	*S.D*	*Wt %*	*S.D*	*Wt %*	*S.D*	*Wt %*	*S.D*
SiO_2	39.78	3.79	45.71	2.77	42.03	0.57	44.07	1.36	33.04	-	41.04	2.66	49.02	-
TiO_2	0.06	0.08	0.02	0.02	0.04	0.05	-	-	0.01	-	0.02	0.03	0.10	-
Al_2O_3	0.89	1.70	-	-	0.15	0.09	-	-	9.23	-	1.22	2.10	0.69	-
FeO (tot)	9.75	8.11	17.54	4.84	30.18	0.42	4.12	1.69	13.27	-	28.32	9.09	30.40	-
MnO	0.59	0.49	4.08	2.04	2.77	0.21	0.08	0.07	0.27	-	1.98	0.76	2.73	-
MgO	35.56	7.01	18.96	6.60	11.05	0.04	39.54	2.88	31.21	-	25.73	7.48	14.86	-
CaO	0.13	0.11	1.64	0.87	1.50	0.02	0.11	0.03	0.00	-	0.31	0.25	2.08	-
NaO	0.00	0.00	-	-	-	-	-	-	0.00	-	-	-	0.00	-
K_2O	0.02	0.05	0.06	0.04	0.28	0.01	0.06	0.10	0.95	-	0.02	0.04	0.12	-
SO_3	0.17	0.27	-	-	-	-	-	-	-	-	-	-	-	-
CuO	0.08	0.10	-	-	-	-	-	-	-	-	0.17	0.17	-	-
ZnO	0.22	0.25	-	-	-	-	-	-	-	-	0.07	0.10	-	-
PbO	0.77	1.18	-	-	-	-	-	-	-	-	0.08	0.10	-	-
H_2O	12.00	0.00	12.00	0.00	12.00	0.00	12.00	0.00	12.00	-	1.12	1.68	-	-
Total	100.02		100.00		100.00		99.99		99.99		100.07		100.00	
	At. prop	*S.D*	*At. prop*	*S.D*	*At. prop*	*S.D*	*At. prop*	*S.D*	*At. prop*	*S.D*	*At. prop*	*S.D*	*At. prop*	*S.D*
Si	1.94	0.12	2.29	0.10	2.22	0.02	2.08	0.07	1.64	-				
Ti	-	-	-	-	0.01	0.01	-	-	0.81	-				
Al	0.08	0.16	-	-	-	-	-	-		-				
Fe^{3+}	-	-	-	-	-	-	-	-	0.00	-				
Fe^{2+}	0.41	0.37	0.74	0.22	1.33	0.02	0.16	0.07	0.55	-				
Mn	0.03	0.02	0.17	0.09	0.12	0.01	-	-	0.01	-				
Mg	2.58	0.44	1.41	0.45	0.87	0.00	2.78	0.20	2.31	-				
Ca	0.01	0.01	0.09	0.05	0.09	0.00	0.01	0.00	0.00	-				
Na	-	-	-	-	-	-	-	-	0.00	-				
K	-	-	-	-	0.02	0.00	0.00	0.01	0.06	-				
OH	3.93	0.18	4.01	0.12	4.23	0.02	3.78	0.01	3.98	-				
O	9.00	0.00	9.00	0.00	9.00	0.00	9.00	0.00	9.00	-				

Appendix F: SEM analyses

Sample No.	***UZ22***		***451/07***		***451/19***		***672/03***		***898/9***		***898/9***		***UZ75***	
Location	Nygruvan		Nygruvan		Nygruvan		Cecilia		Cecilia		Cecilia		800m level	
Mineral	K-feldspar		K-feldspar		K-feldspar		K-feldspar		K-feldspar		Ba-feldspar		Albite	
Lithology	Calc-silicate		Calc-silicate		Ca-Si marble		Metavolcanic		Calc-silicate		Calc-silicate		Marble	
No. of samples (*n*)	2		1		1		1		1		4		1	
	Wt %	*S.D*	*Wt %*	*S.D*	Wt %	*S.D*	*Wt %*	*S.D*	*Wt %*	*S.D*	*Wt %*	*S.D*	*Wt %*	*S.D*
SiO_2	63.67	0.10	63.72	-	62.74	-	55.96	-	60.13	-	28.33	6.97	63.68	-
TiO_2	0.22	0.05	0.06	-	-	-	-	-	-	-	-	-	-	-
Al_2O_3	19.41	0.09	18.51	-	18.08	-	25.65	-	16.66	-	19.06	0.47	22.24	-
FeO (tot)	0.06	0.09	0.07	-	-	-	2.75	-	-	-	-	-	0.15	-
MnO	-	-	0.00	-	-	-	-	-	-	-	-	-	-	-
MgO	-	-	0.00	-	-	-	-	-	-	-	-	-	-	-
CaO	0.39	0.04	0.59	-	0.25	-	1.26	-	-	-	-	-	1.88	-
NaO	1.27	0.04	0.00	-	-	-	3.79	-	-	-	-	-	12.07	-
K_2O	14.93	0.11	17.05	-	17.40	-	7.10	-	21.59	-	3.27	3.17	-	-
SO_3	-	-	-	-	0.05	-	-	-	-	-	-	-	-	-
CuO	-	-	-	-	0.21	-	-	-	-	-	-	-	-	-
ZnO	0.06	0.07	-	-	-	-	-	-	-	-	-	-	-	-
PbO	-	-	-	-	1.28	-	-	-	-	-	-	-	-	-
BaO	-	-	-	-	-	-	-	-	1.62	-	49.35	9.72	-	-
H_2O	-	-	-	-	-	-	3.48	-	-	-	-	-	-	-
Total	100.01		100.00		100.00		99.99		100.01		100.00		100.02	-
	At. prop	*S.D*	*At. prop*	*S.D*	*At. prop*	*S.D*	*At. prop*	*S.D*	*At. prop*	*S.D*	*Wt %*	*S.D*	*At. prop*	*S.D*
Si	2.93	0.00	2.95	-	2.93	-	2.63	-	2.79	-	1.89	0.28	2.76	-
Ti	0.01	0.00	-	-	-	-	-	-	-	-	-	-	-	-
Al	1.05	0.00	1.01	-	1.00	-	1.42	-	0.91	-	1.52	0.16	1.14	-
Fe^{3+}	-	-	-	-	-	-	-	-	-	-	-	-		-
Fe^{2+}	-	-	-	-	-	-	0.11	-	-	-	-	-	0.01	-
Mn	-	-	-	-	-	-	-	-	-	-	-	-	-	-
Mg	-	-	-	-	-	-	-	-	-	-	-	-	-	-
Ca	0.02	0.00	0.03	-	0.01	-	0.06	-	-	-	-	-	0.09	-
Na	0.11	0.00	-	-	-	-	0.35	-	-	-	-	-	1.01	-
K	0.88	0.01	1.01	-	1.04	-	0.43	-	1.28	-	0.26	0.23	-	-
Ba	-	-	-	-	-	-	-	-	0.03	-	1.32	0.35	8.00	-
OH	-	-	-	-	-	-	-	-	-	-	-	-	-	-
O	8.00	0.00	8.00	-	8.00	-	8.00	-	8.00	-	8.00	0.00	13.00	-

Appendix F: SEM analyses

Sample No.	*UZ25*		*555/06*		*ZR06*		*1557/26*		*1557/26*		*672/03*	
Location	Nygruvan		Nygruvan		Isasen		Burkland		Burkland		Cecilia	
Mineral	Gahnite		Pleonaste		Pleonaste		Pleonaste		Pleonaste		Gahnite	
Lithology	Garnet quartzite		Marble		Marble		Marble		Marble		Gneiss	
No. of samples (*n*)	2		2		3		1		1		2	
	Wt %	*S.D*	*Wt %*	*S.D*	Wt %	*S.D*	*Wt %*	*S.D*	*Wt %*	*S.D*	*Wt %*	*S.D*
SiO_2	-	-	-	-	-	-	-	-	-	-	-	-
TiO_2	-	-	0.25	0.05	-	-	-	-	-	-	-	-
Al_2O_3	56.10	0.13	65.02	0.14	63.38	0.89	36.59	-	65.60	-	33.09	0.73
FeO (tot)	15.90	0.25	16.27	0.53	16.17	0.88	49.19	-	13.64	-	7.60	1.24
MnO	-	-	0.67	0.13	-	-	-	-	0.79	-	-	-
MgO	1.66	0.23	17.35	0.33	20.43	0.36	14.19	-	19.93	-	-	-
CaO	-	-	0.02	0.03	-	-	-	-	-	-	-	-
NaO	-	-	-	-	-	-	-	-	-	-	-	-
K_2O	-	-	0.05	0.08	-	-	-	-	-	-	-	-
SO_3	-	-	-	-	-	-	-	-	-	-	-	-
CuO	-	-	-	-	-	-	-	-	-	-	-	-
ZnO	26.32	0.11	-	-	-	-	-	-	-	-	59.26	1.97
PbO	-	-	-	-	-	-	-	-	-	-	-	-
BaO	-	-	-	-	-	-	-	-	-	-	-	-
H_2O	-	-	-	-	-	-	-	-	-	-	-	-
Total	99.99		100.06		100.00		99.97		99.96		99.95	-
	At. prop	*S.D*	*At. prop*	*S.D*	*At. prop*	*S.D*	*At. prop*	*S.D*	*At. prop*	*S.D*	*Wt %*	*S.D*
Si	-	-	-	-	-	-	-	-	-		-	-
Ti	-	-	-	-	-	-	-	-	-		-	-
Al	1.96	0.01	1.96	0.01	1.89	0.02	1.23	-	1.95		1.33	0.00
Fe^{3+}	0.35	0.01	0.32	0.02	0.23	0.01	0.40	-	0.23		-	-
Fe^{2+}	0.04	0.01	0.03	0.01	0.11	0.02	0.77	-	0.05		0.45	0.15
Mn	0.00	0.00	0.01	0.00	-	-	-	-	-		-	-
Mg	0.07	0.01	0.66	0.01	0.77	0.01	0.60	-	0.75		-	-
Ca	-	-	-	-	-	-	-	-	-		-	-
Na	-	-	-	-	-	-	-	-	-		-	-
K	-	-	-	-	-	-	-	-	-		-	-
Ba	-	-	-	-	-	-	-	-	-		-	-
OH	-	-	-	-	-	-	-	-	-		-	-
Zn	0.58	0.00	-	-	-	-	-	-	-	-	1.43	0.00
O	4.00	0.00	4.00	0.00	4.00	0.00	4.00		4.00		4.00	0.00

Appendix F: SEM analyses

APPENDIX G

LASER ABLATION INDUCTIVELY-COUPLED PLASMA MASS SPECTROMETRY

Laser ablation data were acquired using a VG Elemental PQ2+ ICP-MS coupled to a Spectron Laser Systems Nd-YAG UV (266nm) laser using a mixed He/Ar carrier gas.
Transects across individual mineral grains were made using a 30μm spot with an acquisition time of 30 seconds per site. Calibration of the trace element data acquired was done using a NIST 610 glass standard (e.g. Pearce *et al.* 1997). Matrix differences between mineral grains and the NIST glass were corrected using Ca as an internal standard (as detailed in Nesbitt *et al.* 1997).

Each analysis was performed as follows:
Gas blank (5 x 30 seconds, laser off)
10 x NIST standard (10 shots of 30 seconds each, averaged)
Sample unknowns (1 shot of 30 seconds per spot)
10 x NIST standard repeat (10 shots of 30 seconds each, averaged)

Following blank correction, internal correction and calibration, concentration values in ppm were determined and normalised to yttrium to remove non-sample induced variations caused by the ablation process (see tables G1 to G3). Reproducibility within the homogeneous NIST glass standards is typically better than 5%.

Appendix G Table G1
LA-ICPMS data, sample 454/13

Sample 454/13 Garnet 1

	Shot 1	Shot 2	Shot 3	Shot 4	Shot 5	Shot 6	Shot 7	Shot 8	Shot 9	Shot 10	Shot 11	Shot 12	Shot 13	Shot 14	Shot 15	Shot 16	Shot 17
La	0.454	0.289	0.018	0.006	0.009	0.064	0.039	0.003	0.017	0.058	0.001	0.003	0.026	0.017	-0.046	0.652	0.075
Ce	0.247	0.188	0.105	0.026	-0.002	0.044	0.082	0.045	0.033	0.046	0.007	0.018	0.026	0.050	0.041	0.700	0.204
Pr	0.592	0.614	0.350	0.119	0.129	0.148	0.137	0.036	0.027	0.119	0.052	0.219	0.319	0.049	0.199	1.999	0.607
Nd	2.247	3.899	1.436	0.491	0.478	0.721	0.721	0.692	0.922	0.944	0.689	0.588	0.660	0.889	1.735	4.233	2.750
Sm	32.394	43.526	30.476	9.603	8.465	11.075	8.413	9.781	8.681	9.835	11.310	11.562	10.235	9.207	30.076	71.764	34.806
Eu	47.654	112.161	77.893	22.176	21.335	31.005	31.915	20.688	20.822	23.251	23.590	25.436	22.385	24.235	93.671	203.851	63.600
Gd	151.181	185.147	125.753	61.648	65.759	87.717	89.781	68.056	60.653	66.572	72.009	76.212	72.800	72.058	163.114	250.128	150.932
Tb	226.636	242.550	177.419	126.148	129.849	147.823	158.859	129.793	120.372	129.196	127.973	134.597	145.627	140.743	217.666	320.530	229.658
Dy	278.006	273.659	236.405	211.525	206.102	212.249	233.518	203.539	212.752	218.030	213.271	223.450	222.808	221.680	259.592	316.494	286.254
Ho	220.280	193.247	201.754	236.180	227.942	201.788	228.042	231.224	243.311	258.751	238.186	239.955	238.159	221.374	210.227	217.701	229.254
Er	158.193	137.048	163.667	217.901	210.052	175.307	201.761	215.984	229.937	245.737	233.486	229.626	213.091	191.317	151.618	142.486	168.528
Tm	107.385	86.637	125.340	160.987	160.257	132.693	143.809	168.332	184.279	189.202	178.341	173.012	164.882	148.092	117.553	92.462	127.778
Yb	87.946	68.872	108.894	134.478	133.836	110.835	122.134	143.410	154.074	165.623	161.359	154.686	141.280	123.694	101.023	81.576	107.334
Lu	61.405	51.458	79.201	109.021	106.646	82.742	90.396	120.838	122.907	135.250	130.994	125.353	106.744	91.344	72.803	59.911	73.739

Sample 454/13 Garnet 2

	Shot 1	Shot 2	Shot 3	Shot 4	Shot 5	Shot 6	Shot 7	Shot 8	Shot 9	Shot 10
La	0.125	0.061	0.202	0.723	0.120	0.077	0.177	0.474	0.011	0.027
Ce	0.079	0.026	0.199	0.680	0.158	0.094	0.138	0.239	0.068	0.106
Pr	0.504	0.157	0.287	0.874	0.206	0.172	0.350	0.487	0.092	0.479
Nd	2.159	0.567	0.887	2.012	0.789	1.248	1.044	1.136	1.451	1.815
Sm	24.870	5.462	8.015	12.120	9.782	11.779	19.428	18.342	14.942	19.194
Eu	52.217	10.956	19.318	29.013	22.916	20.366	26.815	26.837	22.329	27.826
Gd	145.543	53.739	69.228	91.040	73.288	71.956	97.397	83.589	92.322	101.819
Tb	215.999	118.722	139.846	163.260	138.293	136.038	160.318	158.044	162.116	164.758
Dy	258.531	213.652	212.936	233.782	217.534	208.302	225.221	227.517	237.621	234.492
Ho	196.384	232.450	208.045	210.459	206.032	212.438	221.144	226.347	235.890	219.981
Er	150.017	212.249	176.357	170.696	180.794	190.659	199.253	203.436	212.207	190.999
Tm	104.757	155.663	132.375	127.997	137.240	148.300	155.435	148.173	174.214	143.405
Yb	86.211	121.243	104.645	101.740	109.042	127.998	135.662	139.936	151.060	126.887
Lu	59.403	95.304	78.263	80.209	84.021	99.209	109.651	105.715	131.635	101.063

Appendix G Table G1
LA-ICPMS data, sample 454/13

Sample 454/13 Garnet 3

	Shot 1	Shot 2	Shot 3	Shot 4	Shot 5	Shot 6	Shot 7	Shot 8	Shot 9	Shot 10	Shot 11	Shot 12	Shot 13	Shot 14	Shot 15
La	0.011	0.057	0.076	0.000	1.930	0.316	0.028	0.077	0.563	0.234	0.193	0.795	0.274	0.045	0.293
Ce	0.076	0.192	0.127	0.164	1.456	0.767	0.229	0.113	0.460	0.416	0.211	0.565	0.494	0.426	0.796
Pr	0.273	0.458	0.209	0.321	1.139	1.104	0.315	0.243	0.727	0.587	0.230	1.030	1.616	0.601	2.056
Nd	0.497	1.046	1.176	1.577	2.138	2.592	1.367	1.050	1.401	1.875	1.523	3.091	5.093	4.948	9.296
Sm	8.450	16.008	10.963	21.988	16.381	17.190	11.874	15.736	19.381	19.121	22.741	40.403	54.591	48.663	80.921
Eu	17.639	45.324	32.158	65.723	50.094	54.354	39.706	38.213	50.763	54.384	70.728	87.187	123.729	117.500	180.012
Gd	70.961	130.127	105.851	132.727	127.369	119.387	109.152	107.609	131.890	139.702	138.968	189.261	186.702	215.604	255.376
Tb	137.452	205.328	190.903	212.528	202.576	211.541	195.031	178.841	206.257	194.493	211.085	259.284	270.770	272.697	320.116
Dy	217.083	272.616	264.107	275.146	270.443	263.575	277.276	260.891	277.273	266.127	274.889	311.357	308.518	317.991	344.571
Ho	222.196	210.128	224.492	222.537	234.064	221.654	247.828	243.584	245.616	246.550	240.116	261.888	233.470	265.054	261.938
Er	189.669	164.333	172.402	166.541	191.128	169.167	193.752	200.045	213.971	209.183	197.039	223.052	197.664	209.873	195.597
Tm	140.103	114.301	119.146	123.902	131.778	122.737	133.286	147.446	156.371	173.195	156.909	171.582	151.073	153.494	171.461
Yb	113.217	90.336	90.688	102.912	106.352	97.946	104.288	117.446	130.211	144.545	147.987	148.127	131.246	132.466	170.456
Lu	88.129	71.147	64.366	72.591	78.615	73.161	74.849	85.411	100.568	117.791	102.429	125.405	101.736	104.741	142.802

Appendix G Table G2
LA-ICPMS data, sample 454/14

Sample 454/14 Garnet 1

	Shot 1	Shot 2	Shot 3	Shot 4	Shot 5	Shot 6	Shot 7	Shot 8	Shot 9	Shot 10	Shot 11
La	1.349	1.573	2.570	1.543	0.997	4.639	3.369	1.544	1.390	2.647	3.080
Ce	0.854	0.710	2.250	1.819	1.067	3.024	2.233	1.101	1.265	1.952	2.366
Pr	1.318	1.942	1.574	2.638	1.340	2.357	2.351	1.874	1.652	1.842	1.501
Nd	3.741	2.956	4.227	3.378	2.154	4.101	5.010	1.525	2.878	4.525	6.156
Sm	28.229	48.395	34.018	31.109	29.017	37.656	32.216	29.787	48.741	56.626	51.114
Eu	6.375	7.803	9.350	5.246	5.177	7.545	6.732	5.914	7.377	10.283	7.413
Gd	53.600	79.113	76.609	95.035	89.043	117.489	102.969	95.099	104.678	114.591	97.974
Tb	67.174	100.375	99.409	162.286	135.188	192.651	159.596	164.667	140.926	149.339	143.848
Dy	67.065	103.281	96.065	240.263	179.841	268.759	198.955	193.364	138.898	142.312	176.254
Ho	60.847	83.726	81.207	256.342	162.810	283.246	196.509	201.440	101.509	107.285	173.931
Er	51.383	60.009	62.236	250.057	146.519	277.474	192.181	203.075	82.278	89.150	160.125
Tm	53.085	52.839	58.644	234.746	131.510	268.362	191.096	171.302	84.051	72.961	166.823
Yb	45.657	54.236	44.116	212.194	137.167	258.022	193.575	166.222	73.292	63.910	173.959
Lu	39.912	42.433	32.716	174.573	113.438	216.501	158.304	144.428	52.646	46.316	146.504

Sample 454/14 Garnet 2

	Shot 1	Shot 2	Shot 3	Shot 4	Shot 5	Shot 6	Shot 7	Shot 8	Shot 9	Shot 10
La	1.398619	3.35555	4.35743	3.526082	4.114429	3.190851	3.773392	1.639796	1.513901	1.692012
Ce	0.768838	2.16168	2.997062	2.494983	3.15559	1.84012	3.073499	1.65426	1.218232	1.441243
Pr	0.91541	2.959247	3.56532	3.585881	3.204164	1.767946	4.063848	2.808411	1.540933	2.098261
Nd	1.816056	4.121825	7.644337	7.236186	6.54967	4.061298	9.286852	4.871458	4.15368	6.009698
Sm	24.06398	26.7387	49.87607	67.4239	62.40862	47.78562	53.52407	50.77162	48.54167	65.66154
Eu	7.401275	6.944219	13.91533	19.75484	15.22025	8.891031	8.448268	7.157362	8.297247	13.85913
Gd	58.13029	79.06638	88.33248	104.9654	119.5351	101.5769	135.8128	120.8037	134.2403	129.1006
Tb	87.07054	113.4334	133.8021	150.1749	146.483	150.4462	190.1387	164.2023	207.1944	189.0526
Dy	110.2405	134.3061	118.6297	122.4041	151.79	171.905	230.4865	230.467	294.4148	210.7116
Ho	98.5296	109.0824	103.4078	97.51467	112.2729	155.5183	212.8904	216.5652	294.4821	202.9001
Er	96.08766	93.31853	71.0902	77.08912	96.34691	147.8051	203.5623	209.6873	284.7617	182.8049
Tm	106.1644	89.71464	67.77567	72.57362	92.00047	146.5202	219.1439	212.981	274.7119	198.112
Yb	106.3207	90.11237	61.7757	64.50835	76.51862	158.1058	199.7789	228.6081	256.7514	191.9488
Lu	91.28245	72.95604	50.24759	46.04656	71.48094	124.6898	171.8682	186.9468	239.6988	161.5238

Appendix G Table G3
LA-ICPMS data, sample 1557/09

Sample 1557/09 Garnet 1

	Shot 1	Shot 2	Shot 3	Shot 4	Shot 5	Shot 6	Shot 7	Shot 8	Shot 9	Shot 10	Shot 11
La	-0.021	0.034	0.112	0.249	0.108	7.008	1.034	0.520	0.346	0.061	0.226
Ce	0.001	0.046	0.134	0.238	0.045	5.312	0.855	0.566	0.466	0.075	0.255
Pr	0.111	0.066	0.073	0.386	0.153	3.496	0.386	0.590	0.464	0.145	0.357
Nd	0.229	0.143	0.240	0.489	0.075	3.184	0.745	0.537	0.635	0.313	0.845
Sm	2.278	3.990	2.558	3.420	5.283	5.013	4.367	5.562	4.863	5.552	11.334
Eu	0.765	1.132	2.136	4.050	2.997	3.252	3.436	4.887	3.635	6.792	1.857
Gd	14.595	12.700	12.040	8.595	15.442	23.000	20.394	15.987	14.494	13.303	38.786
Tb	33.750	31.830	21.675	14.236	28.339	33.589	43.308	25.344	21.894	13.505	62.790
Dy	55.505	55.480	29.449	17.014	29.384	43.766	48.591	23.729	22.203	10.418	82.852
Ho	64.289	69.616	31.475	14.604	25.806	38.399	42.192	17.981	13.953	6.406	84.100
Er	76.417	76.805	33.153	13.556	19.949	30.256	35.668	13.520	9.812	6.104	90.607
Tm	82.064	83.058	42.715	14.337	14.652	24.878	25.212	10.394	7.234	7.320	103.148
Yb	90.996	92.415	52.248	16.001	15.829	19.999	20.606	9.812	8.593	7.783	117.440
Lu	85.320	78.283	45.908	15.152	11.342	14.683	12.932	5.727	6.549	9.506	101.255

Sample 1557/09 Garnet 2

	Shot 1	Shot 2	Shot 3	Shot 4	Shot 5	Shot 6	Shot 7	Shot 8	Shot 9	Shot 10	Shot 11	Shot 12	Shot 13
La	0.022	0.060	0.027	0.133	6.336	0.441	0.315	0.724	0.311	0.350	0.363	0.269	0.099
Ce	0.008	0.076	0.076	0.189	7.811	0.881	0.455	1.417	0.450	0.500	0.384	0.294	0.083
Pr	0.086	0.223	0.111	0.225	9.348	0.704	0.529	1.451	0.422	0.590	0.370	0.174	0.169
Nd	-0.068	0.302	0.245	0.348	10.553	0.929	0.443	1.935	0.724	0.805	0.378	0.270	0.345
Sm	0.620	2.967	1.212	1.482	16.546	3.807	1.417	5.519	6.058	4.593	4.572	3.291	2.698
Eu	1.236	2.288	1.889	1.036	4.026	1.443	1.108	2.017	2.407	2.503	3.619	1.307	1.499
Gd	3.226	20.236	16.375	19.885	33.114	16.856	9.772	28.326	27.759	22.641	22.533	21.435	17.344
Tb	13.609	43.561	43.653	39.869	48.766	31.226	21.917	47.116	52.930	28.857	30.996	21.094	16.748
Dy	28.740	57.198	64.049	64.092	68.065	41.447	33.675	62.086	68.400	32.127	35.334	28.581	17.493
Ho	47.261	55.387	62.876	65.429	69.823	49.268	38.496	59.736	63.303	25.293	25.684	25.879	13.538
Er	69.177	47.917	53.688	68.547	79.752	58.871	44.729	58.398	51.518	19.955	21.566	25.166	14.071
Tm	84.452	35.162	43.078	66.275	84.204	66.189	47.156	51.930	44.310	18.319	20.810	31.046	13.392
Yb	110.396	32.980	40.644	69.459	95.961	75.866	50.562	51.210	39.834	17.661	21.223	34.332	17.185
Lu	117.052	27.620	28.538	52.282	78.347	58.101	44.040	40.869	31.453	13.946	19.027	28.047	14.469

Appendix G Table G3
LA-ICPMS data, sample 1557/09

Sample 1557/09 Garnet 3

	Shot 1	Shot 2	Shot 3	Shot 4	Shot 5	Shot 6	Shot 7	Shot 8	Shot 9	Shot 10	Shot 11	Shot 12	Shot 13	Shot 14	Shot 15
La	0.039	0.124	0.003	0.541	0.305	0.043	0.070	0.292	0.184	0.416	0.131	0.078	0.239	1.186	0.025
Ce	0.024	0.050	0.042	0.754	1.047	0.141	0.108	0.510	0.288	0.451	0.111	0.041	0.299	1.460	0.018
Pr	0.070	0.131	0.067	1.042	2.301	0.108	0.219	0.625	0.187	0.405	0.053	0.080	0.388	1.323	0.083
Nd	0.059	0.115	0.165	1.453	4.536	0.480	0.242	1.070	0.307	0.338	0.099	0.118	0.487	1.090	0.162
Sm	0.949	1.257	1.392	3.444	24.784	2.629	1.614	4.130	1.064	0.749	1.035	1.407	2.593	1.736	1.893
Eu	0.388	0.957	0.496	1.376	6.826	1.024	1.096	1.024	0.331	0.502	0.615	1.458	1.355	1.898	1.205
Gd	6.428	11.304	13.277	21.428	114.008	26.809	28.496	23.971	15.900	12.435	18.167	13.956	15.677	5.582	13.067
Tb	10.672	19.002	30.576	51.258	231.206	72.338	79.594	76.818	49.024	36.059	46.234	34.889	27.456	3.009	14.888
Dy	9.516	20.146	38.501	81.835	290.255	134.033	158.351	131.849	98.364	80.969	85.046	58.012	31.348	4.670	14.215
Ho	5.729	10.534	29.933	80.033	253.310	153.383	178.766	152.046	122.173	105.521	91.078	68.629	24.200	5.504	8.526
Er	4.347	4.896	19.027	64.862	196.438	146.547	179.237	158.031	132.530	112.673	82.908	65.141	18.451	5.927	7.354
Tm	4.474	3.105	16.182	62.736	156.626	140.753	166.873	153.857	133.100	112.932	83.190	72.424	19.104	8.383	7.537
Yb	4.452	2.684	14.190	67.441	125.281	130.390	155.365	149.974	131.644	118.879	80.761	87.542	23.460	9.006	7.979
Lu	2.695	2.370	13.481	66.238	97.356	97.821	119.624	111.005	99.097	93.243	64.916	91.934	21.879	10.229	7.056

Sample 1557/09 Garnet 4

	Shot 1	Shot 2	Shot 3	Shot 4	Shot 5	Shot 6	Shot 7	Shot 8	Shot 9	Shot 10	Shot 11	Shot 12	Shot 13
La	0.019	0.023	0.227	0.260	0.031	0.148	0.162	0.015	616.126	3.432	0.773	0.197	0.202
Ce	0.017	0.020	0.186	0.215	0.014	0.177	0.154	0.070	430.793	4.130	0.754	0.349	0.077
Pr	0.027	0.094	0.177	0.095	0.018	0.269	0.125	0.084	350.688	1.710	0.442	0.238	0.159
Nd	0.064	0.210	0.343	0.383	0.197	0.133	0.253	0.124	220.279	0.973	0.352	0.413	0.176
Sm	1.671	1.900	2.643	2.829	1.929	2.272	3.544	2.265	88.962	3.208	4.009	1.971	2.293
Eu	0.522	1.065	1.898	1.179	1.722	1.314	1.360	1.391	11.978	2.979	4.075	1.655	1.034
Gd	14.707	16.494	17.069	18.010	19.303	18.377	21.399	20.739	68.602	24.703	26.505	17.702	18.134
Tb	23.573	14.515	24.811	28.618	24.568	23.512	27.353	30.065	62.401	38.471	28.438	16.998	28.359
Dy	40.625	16.742	28.151	38.506	32.575	34.386	36.809	38.489	66.123	55.972	30.105	19.942	57.922
Ho	52.702	13.753	24.052	37.698	32.498	34.592	37.500	43.186	58.811	56.117	25.326	15.777	89.219
Er	64.656	11.702	20.890	33.521	28.488	30.771	33.551	39.130	54.248	48.209	19.958	17.225	115.239
Tm	76.311	13.576	15.603	31.441	27.434	29.444	32.251	34.572	48.500	36.563	15.823	18.721	151.711
Yb	91.528	17.260	14.397	30.167	24.244	28.188	32.180	34.639	50.558	28.279	14.961	21.057	191.397
Lu	88.160	18.142	12.121	25.033	22.244	23.327	26.341	27.815	43.073	20.512	11.636	22.444	189.158

Appendix G Table G3
LA-ICPMS data, sample 1557/09

Sample 1557/09 Garnet 5

	Shot 1	Shot 2	Shot 3	Shot 4	Shot 5	Shot 6	Shot 7	Shot 8	Shot 9	Shot 10	Shot 11	Shot 12	Shot 13	Shot 14	Shot 15	Shot 16	Shot 17	Shot 18	Shot 19	Shot 20
La	0.107	0.060	0.497	0.206	0.182	0.047	0.021	0.086	0.087	1.597	0.252	0.114	0.075	0.352	0.876	0.082	0.057	0.027	0.072	0.041
Ce	0.025	0.003	0.321	0.114	0.205	0.074	0.031	0.089	0.085	1.428	0.306	0.101	0.055	0.471	0.676	0.092	0.031	0.033	0.082	0.016
Pr	0.135	0.036	0.571	0.315	0.163	0.075	0.035	0.182	0.360	1.117	0.170	0.106	0.145	0.569	0.596	0.087	-0.009	-0.009	0.154	0.049
Nd	0.153	0.190	0.712	0.447	0.188	0.268	0.259	0.408	0.205	1.104	0.453	0.323	0.307	0.701	0.573	0.266	0.174	0.188	0.194	0.268
Sm	1.342	1.521	4.330	4.566	2.908	3.423	3.151	1.385	3.051	3.294	3.465	3.644	3.966	4.924	2.743	3.137	2.529	3.201	1.657	1.464
Eu	1.086	2.436	2.958	5.182	3.651	3.449	2.296	1.407	2.643	1.877	1.867	2.358	4.168	3.744	4.799	4.241	4.494	3.465	1.386	1.846
Gd	12.036	11.433	15.487	17.583	21.903	28.667	21.447	17.701	21.694	22.977	20.306	19.413	21.851	22.041	20.762	25.421	19.284	18.044	18.619	17.397
Tb	6.296	3.950	10.192	13.387	19.848	24.373	16.949	20.952	18.583	17.444	14.199	17.044	15.608	17.859	16.743	22.034	14.164	10.481	15.711	9.163
Dy	8.613	3.846	7.729	9.637	17.265	22.710	19.246	30.387	20.762	21.410	14.277	16.108	14.449	17.456	23.590	24.571	17.509	15.065	22.214	14.617
Ho	8.891	3.327	6.178	5.594	10.410	16.300	15.085	30.914	15.637	15.999	11.752	11.367	9.145	11.517	23.999	20.148	16.501	14.580	26.000	16.134
Er	8.057	2.412	4.690	3.950	5.400	9.366	11.434	31.161	13.232	13.438	8.121	8.476	7.163	9.652	28.961	16.946	17.351	14.832	24.651	18.302
Tm	9.412	3.001	6.191	4.103	4.407	6.824	9.558	31.417	12.602	12.023	7.859	6.843	6.964	8.383	33.335	14.915	18.563	15.652	28.269	20.249
Yb	10.113	2.943	5.125	3.333	3.790	5.223	7.211	28.828	10.747	11.894	7.750	6.220	5.345	7.177	43.872	15.421	21.773	17.062	29.945	23.921
Lu	9.917	3.047	5.708	4.885	3.531	4.387	5.250	22.968	8.251	9.704	5.522	5.058	5.151	6.598	40.131	9.824	17.391	16.283	23.725	17.703

Sample 1557/09 Garnet 6

	Shot 1	Shot 2	Shot 3	Shot 4	Shot 5	Shot 6	Shot 7	Shot 8	Shot 9	Shot 10	Shot 11	Shot 12	Shot 13	Shot 14	Shot 15	Shot 16	Shot 17	Shot 18
La	0.012	0.195	0.441	0.208	2.073	0.203	0.078	0.008	0.017	7.423	1.778	0.482	0.078	0.075	0.037	0.033	0.030	0.000
Ce	0.010	0.255	0.681	0.317	2.952	0.338	0.109	0.044	0.025	6.068	1.914	0.386	0.112	0.108	0.036	0.012	0.019	0.025
Pr	0.066	0.244	0.864	0.170	3.118	0.339	0.125	0.086	0.038	4.800	1.265	0.408	0.069	0.177	0.129	-0.026	0.024	0.078
Nd	0.181	0.464	1.144	0.361	3.536	0.374	0.259	0.079	0.478	4.108	1.476	0.379	0.278	0.239	0.185	0.246	0.179	0.167
Sm	1.350	2.672	4.473	3.180	9.435	2.393	3.094	2.543	4.588	6.725	4.674	3.408	2.436	2.550	2.000	2.229	2.400	1.707
Eu	1.867	3.217	4.546	3.041	2.493	1.339	2.379	2.710	4.065	2.467	2.829	3.304	2.839	3.517	3.072	2.761	2.146	3.113
Gd	16.404	20.829	30.393	24.256	28.777	19.869	23.358	24.104	20.249	21.604	24.936	22.093	30.170	23.244	21.832	19.674	20.083	20.639
Tb	5.359	11.110	22.533	25.791	24.316	13.677	16.941	19.276	12.001	18.385	23.128	18.469	25.672	16.838	15.204	11.068	9.057	8.230
Dy	5.113	11.737	25.545	31.566	28.636	18.520	23.606	25.320	13.820	25.807	30.920	19.482	29.392	18.942	17.743	12.522	8.638	7.490
Ho	4.675	7.924	21.448	32.040	29.547	16.786	23.338	25.090	11.892	27.179	32.228	17.410	21.953	18.145	16.044	10.629	6.843	6.423
Er	3.511	7.728	21.948	34.258	33.643	17.794	23.414	22.986	10.289	30.076	33.918	15.099	18.019	14.580	16.473	8.461	4.713	5.011
Tm	4.353	8.164	25.218	34.444	41.880	19.123	22.934	26.990	10.800	34.298	37.105	14.702	13.442	16.133	16.407	7.701	3.677	5.412
Yb	3.272	7.201	27.489	43.026	49.868	19.486	22.603	29.575	9.314	41.403	39.789	12.049	11.037	15.751	17.431	7.951	2.964	9.025
Lu	3.126	6.213	24.050	33.936	45.550	14.212	17.371	24.787	8.430	37.263	28.877	8.775	6.930	13.302	13.515	6.478	2.695	10.322

APPENDIX H

ISOTOPE GEOCHEMISTRY

H.1 Stable (C, O) isotopes

Stable isotope analyses were carried out at the University of Lucerne. Samples were prepared for analysis by crushing and grinding samples to a fine powder and reacting with 100% H_3PO_4 under vacuum for 30 minutes (calcitic samples) and 20 hours (dolomitic samples). Evolved CO_2 was collected in liquid nitrogen traps and released into mixed ethanol and carbonic snow traps at -180°C. The collected CO_2 was then analysed in a Finnigans MAT 251 spectrometer. Stable isotope data from Fischer (2000) and Lindo (unpublished) are presented in tables H1.1 and H1.2.

H.2 Strontium isotopes

Carbonate samples were analysed for strontium using a seven-collector VG Sector 54 thermal ionisation mass spectrometer at the University of Southampton (School of Ocean & Earth Science). Because the samples analysed were carbonate rocks, pre-treatment with hydrochloric acid was required before dissolution in hydrofluoric acid. Methodology is outlined in sections H.2.1 – H.2.7.

$^{87}Sr/^{86}Sr$ isotope ratios were determined as an average of >100 ratios by measuring ion intensities in multidynamic collection mode. Isotope ratios were normalised to $^{86}Sr/^{88}Sr = 0.1194$. Measured values for the standards NBS SRM-987 and JMC321 were $^{87}Sr/^{86}Sr = 0.710252 \pm 15$ (2 s.d., n = 169) and $^{143}Nd/^{144}Nd = 0.511125 \pm 11$ (2 s.d., n = 45) respectively during the run period. External error on Sr was ±0.000013 (2 s.d.).

Sample	*Location*	*Lithology*	*δ18O*	*δ13C*
ZV3000	Högalund	Calcitic marble	11.527	-4.257
ZV3001	Åsberget	Calc-silicate skarn	15.533	-9.847
ZV3002	Ervingsberg	Calc-silicate skarn	11.797	-5.644
ZV3003	Hilda south	Calc-silicate skarn	12.002	-5.379
ZV3004	Dalby north	Calcitic marble	9.477	-5.958
ZV3005	Isåsen	Calcitic marble	12.083	-3.426
ZV3006	Isåsen	Dolomitic marble	13.689	-0.682
ZV3007	Godegård	Calcitic marble	19.949	-0.191
ZV3008	Höksjön	Calcitic marble	20.682	0.533
ZV3009	Höksjön	Calcitic marble	18.241	0.142
ZV3010	Höksjön	Calcitic marble	19.709	-0.189
ZV3011	Höksjön	Calcitic marble	19.858	0.235
ZV3012	Trollfall	Calcitic marble	19.532	0.509
ZV3013	Arsjon	Calcitic marble	19.474	0.432
ZV3014	Arsjon	Calcitic marble	19.707	0.493
ZV3015	Silverviken	Dolomitic marble	15.728	0.339
ZV3016	Silverviken	Dolomitic marble	16.386	0.391
ZV3017	Vinnern West	Dolomitic marble	12.973	-2.306
ZV3018	Vinnern East	Calcitic marble	17.970	-0.815
ZV3019	Vinnern East	Calcitic marble	14.417	-0.465
ZV3020	Dalmark	Dolomitic marble	15.825	-1.413
ZV3021	Sinsberg	Calcitic marble	20.003	0.519
ZV3022	Sinsberg	Calcitic marble	19.856	0.531
ZV3023	Finnafallet	Dolomitic marble	16.925	-0.111
ZV3024	Finnafallet	Dolomitic marble	16.968	-1.876
ZV3025	Finnafallet	Dolomitic marble	16.010	-1.631
ZV3026	Finnafallet	Dolomitic marble	16.302	-1.194
ZV3027	Finnafallet	Dolomitic marble	15.915	-2.789
ZV3028	Langgolen	Dolomitic marble	11.635	-3.061
ZV3029	Langgolen	Dolomitic marble	12.152	-2.359
ZV3030	Nyhytten	Dolomitic marble	12.112	-6.7
ZV3031	Nyhytten	Calc-silicate skarn	13.101	-5.829
ZV3032	Silverviken	Calcitic marble	18.989	0.309
ZV3033	Enemossen West	Calcitic marble	11.560	-0.634
ZV3034	Enemossen West	Calcitic marble	11.220	-0.021
ZV3035	Enemossen West	Calcitic marble	16.831	0.344
ZV3036	Enemossen West	Calcitic marble	15.650	0.316
ZV3037	Tybble	Calcitic marble	16.171	0.276
ZV3038	Mossgolen	Calcitic marble	16.471	-2.26
ZV3039	Mossgolen	Calcitic marble	15.666	-0.511
ZV3040	Mossgolen	Calcitic marble	19.236	-0.627
ZV3041	Bredsjon	Calcitic marble	19.423	-0.484
ZV3042	Lovdalen	Calcitic marble	19.603	0.602
ZV3043	Meltorp	Calcitic marble	12.394	0.008
ZV3044	Meltorp	Dolomitic marble	14.820	-0.18
ZV3045	Rytabygget	Calcitic marble	18.004	-0.472

Table H1.1: Stable isotope data from Fischer (2000).

Sample	*DDH*	*Depth down hole (m)*	$\delta^{18}O$	$\delta^{13}C$
ZV3101	231	10.00	14.697	-5.295
ZV3102	231	45.00	15.348	-8.696
ZV3103	231	58.30	13.304	-3.364
ZV3104A	231	74.1-74.5	14.659	-3.92
ZV3105	231	85.2	13.648	-3.417
ZV3106A	231	93.8-94.2	12.225	0.18
ZV3107	231	199.45	13.234	-0.672
ZV3108	231	213.8	12.92	-6.27
ZV3109A	671	116.3-117.0	14.951	-2.211
ZV3110	671	125.00	14.782	-3.075
ZV3111A	671	181.35-181.9	12.079	-0.859
ZV3112A	671	189.9-190.4	11.945	-1.095
ZV3113A	671	198.75-199.45	14.9	-2.527
ZV3114	671	208.50	13.775	-1.388
ZV3115A	671	244.7-245.35	16.844	-4.083
ZV3116A	671	255-255.45	16.626	-3.858
ZV3117A	671	273.15-273.65	16.852	-5.218
ZV3118A	671	284.15-284.6	17.237	-3.767
ZV3119A	671	291.85-292.35	17.577	-2.997
ZV3120A	671	300.8-301.35	17.017	-2.929
ZV3121A	671	318.8-319.3	17.475	-2.355
ZV3122A	671	333.7-334.1	15.269	-3.015
ZV3123	898	261.15	17.553	-4.957
ZV3124	898	278.6	16.423	-4.449
ZV3125	898	291.8	15.294	-1.283
ZV3126A	898	298.2-298.6	12.605	-1.1
ZV3127	898	299.25	12.317	-1.29
ZV3128	898	307.45	12.661	-0.512
ZV3129A	898	310.9-311.4	15.687	-1.448
ZV3130A	898	317.5-317.9	17.462	-2.376
ZV3131A	898	331-331.85	17.318	-4.077
ZV3132	898	332.8	17.415	-4.131
ZV3133A	898	336.65-337.4	17.006	-3.323
ZV3134A	898	342.7	17.561	-2.812
ZV3135A	898	349.25-349.7	17.649	-3.183
ZV3136A	898	356.8-357.4	18.236	-3.887
ZV3137A	898	369.3-369.8	17.119	-4.209
ZV3138A	898	392.1-392.7	14.558	-1.069
ZV3139A	898	411.7-412.4	14.727	-1.852
ZV3140A	898	430.15-430.75	15.098	-5.058
ZV3141A	898	440.4-440.8	15.446	-4.658
ZV3142A	898	446.5-446.8	14.916	-5.568
ZV3143	898	453.7	14.673	-4.429
ZV3144A	898	453.7-454.2	15.305	-4.325
ZV3145A	898	459.1-459.6	14.347	-2.79
ZV3146A	898	468.5-468.9	13.058	-2.54
ZV3147A	898	479-479.9	14.827	-2.711
ZV3148A	898	516.1-516.4	14.928	-2.376
ZV3149A	898	557.3-558	14.67	-3.364
ZV3150	671/898	342.7-343.3	14.607	-4.06

Table H1.2: Stable isotope data from Lindo (2000).

H.2.1 Carbonate pre-treatment method

1) Weigh 200mg or more dry rock powder onto clean aluminium foil and transfer to a Savillex PTFE digestion vessel.
2) Add 5ml of 6M ARISTAR HCl to powdered sample. Add small amounts of additional acid until effervescing ceases. Transfer contents of Teflon vessel to centrifuge tube. Spin at 2500 revs for 10 minutes.
3) Remove and store supernatant.
4) Rinse samples 3 or 4 times with 1ml aliquots of 6M HCl until all yellow colouration is removed. Spin samples between washing as before. Recover washings and store.
5) Transfer residue to Teflon digestion vessel and dry on hotplate.

H.2.2 Sample decomposition (in scrubbed fume cupboard)

1) Add 5 drops of ARISTAR $HClO_4$ (perchloric acid), followed by 3ml of ARSITAR HF (hydrofluoric acid) to the samples. This volume is increased pro-rata if more than 200mg of sample is used.
2) Seal the vessels and leave to digest on a hotplate at 150°C for 24 hours or more.
3) Remove vessles from hotplate and allow to cool to room temperature. Remove screw-caps from vessels and inspect the contents. They should appear as anything from a clear solution to an opaque solution, which can be white to pale grey or pink. Provided there is no unreacted material (e.g., sulphides or organic carbon) evaporate solution to complete dryness on the hotplate.
4) Add 3ml of 6M ARISTAR HCl and wait for the sample to dissolve (15 mins to 24 hours), then add 3ml of milli-Q water.
5) Close the lid and replace on the hotplate for approximately 1 hour.
6) Check for complete dissolution of sample. If there is any solid material left, add a further 5ml of 6M ARISTAR HCl and heat until there is a true solution.
7) Evaporate to complete dryness. This stage ensures that the sample is converted to chloride.
8) Add the 6M HCl supernatant and washings from the pre-treatment procedure (H.2.1).
9) Add 6-10ml of 6M ARISTAR HCl, replace the lid and allow sample to dissolve.
10) Rinse the required number of 60ml Nalgene polyethene bottles with 6M ARISTAR HCl, folloed by several rinses with milli-Q water, and dry in the oven.
11) Tare bottle on a balance. Transfer the solution from the digestion vessel to the bottle, rinsing the bottle with 6M HCl until there is no more yellow colour. Make up to weight, depending on expected concentration of REEs (usually 50g).

NB: A reagent blank must be prepared alongside the samples.

H.2.3 Preparation of daughter solution

1) Rinse the required number of Azlon polyethene bottles with 2% ARISTAR HNO_3, followed by several rinses with milli-Q water and dry in the oven.
2) Weigh an aliquot of the mother solution into a clean PTFE beaker and evaporate to incipient dryness. Prolonged baking can result in the decomposition of some chlorides to oxides. Should this happen, redissolve the residue in a few drops of 6M ARISTAR HCl and try again.
3) Dissolve the residue in a few ml of:
   - 2% ARISTAR HNO_3 for blanks
   - 2% ARISTAR HNO_3 with 10ppb In and Re for samples and standards.

   Some warming may be required to dissolve the samples. Solutions should be colourless. Cover beakers with parafilm.
4) Transfer solutions to Azlon bottles or polyethene scintillation vessels and make up to weight depending on the final dilution factor required.

H.2.4 Sample preparation for TIMS Sr analysis

1) Boil down sufficient mother solution to give about 1microgram of strontium. This takes approximately 1 hour per 5ml of mother solution.
2) Dissolve in 2ml 6M ARISTAR nitric acic. Centrifuge samples prior to loading to remove any silica gel.

H.2.5 Column preparation

Commercially available resins are used for the column. Approximately 0.075 to 0.1g is used per column.

1) Mix the Sr specimen resin to a slurry with milli-Q. Do the same with the anion exchange resin.
2) Place clean, 4M nitric acid-soaked columns in the removable horizontal platforms from the small column stands, and place the platforms on a polyethene container to catch the unwanted wash.
3) Using a disposable polyethene pipe, load the Sr spec into the column at a bed depth of 6mm and allow to settle to this depth.
4) Load the anion exchange resin on top to a depth of at least 3mm.

H.2.6 Conditioning the columns

1) Wash the columns through with 10ml of milli-Q water, followed by 10ml of 6M ARISTAR nitric acid. Repeat. Ensure that the final wash is acid.
2) Slide the column-bearing platforms into the column stands and and place a 20ml scint vial under each column to catch the recoverable wash, which contains everything except lead and strontium, and can be used for other analyses.

H.2.7 Running the columns

1) Centrifuge the samples to remove any silica gel.
2) Load the 2ml solution with care, using a polyethene pipette and making sure that the surface of the resin is not disturbed much. Allow the liquid to run through until the resin surface is just dry again.
3) Wash down the inside of the column with 2ml 6M nitric acid using a polyethene pipette.
4) When resin surface is just dry again, elute the column with 9ml 6M nitric acid.
5) Place a PTFE beaker under each column and wash the strontium fraction from the column with 10ml of milli-Q water. Evaporate to dryness, cover beaker with parafilm and store ready for loading onto a tantalium filament.
6) The Sr spec resin is always discarded after use. The columns are washed with milli-Q water and left soaking in 4M nitric acid. New columns are always made up for each new set of samples.